

THE JOURNAL OF PHYSICAL CHEMISTRY

(Registered in U. S. Patent Office)

CONTENTS

B. Lovreček: Kinetics of the Electrode Processes Involving more than One Step.....	1795
T. M. Reed, III: The Polarizability of Molecules in Liquid Mixtures.....	1798
D. M. Himmelblau: Partial Molar Heats and Entropies of Solution for Gases Dissolved in Water from the Freezing to Near the Critical Point.....	1803
Dipti K. Chattoraj and Henry B. Bull: Electrophoresis and Surface Charge.....	1809
A. J. Darnell and S. J. Yosim: Some Thermodynamic Properties of Solid Bismuth Chlorides.....	1813
Cecil V. King and Sheldon Evans: Radiotracer Studies of Zinc-Zinc Ion Exchange.....	1816
Cecil V. King and Robert Skomoroski: Radiotracer Studies of Cadmium-Cadmium Ion Exchange.....	1819
Cecil V. King and Robert Skomoroski: Radiotracer Studies of Iron in Iron Salt Solutions.....	1822
James E. Cassidy and Wendell J. Whitcher: The Polarographic Characteristics of Furfurylidene-acetophenone and Some of its <i>para</i> Derivatives.....	1824
Arnulf Muan and W. C. Hahn, Jr.: Some Energy Relations in Solid State Reactions Involving Crystalline Phases of Variable Compositions.....	1826
O. W. Edwards and E. O. Huffman: Diffusion of Aqueous Solutions of Phosphoric Acid at 25°.....	1830
C. P. Fenimore and G. W. Jones: Consumption of Oxygen Molecules in Hydrocarbon Flames Chiefly by Reaction with Hydrogen Atoms.....	1834
R. W. Kilb: The Effect of Simultaneous Crosslinking and Degradation on the Intrinsic Viscosity of a Polymer.....	1838
Jack Milgrom: Inclusion Complexes of Methylanthralenes.....	1843
W. F. Wolf: Adsorption on Conducting Surfaces. Hydrolysis of Potassium on Active Carbon.....	1848
Arnim Henglein: Crosslinking of Polymers in Solution under the Influence of Gamma Radiation.....	1852
A. J. Majumdar and Rustum Roy: Experimental Study of the Polymorphism of AgI.....	1858
J. H. Beynon, G. R. Lester and A. E. Williams: Some Specific Molecular Rearrangements in the Mass Spectra of Organic Compounds.....	1861
Thomas J. Dougherty and Irvin M. Krieger: Potential Around a Charged Colloidal Sphere.....	1869
Reginald Mills: Tracer Diffusion of Sodium and Rubidium Ions in Aqueous Alkali Chloride Solutions at 25°.....	1873
J. D. Mackenzie: Structure of Liquid Boron Trioxide.....	1875
A. N. Webb and J. J. Mitchell: The Carbon Monoxide Exchange of Iron Carbonyls.....	1878
L. L. Brown and J. S. Drury: The Fractionation of Oxygen Isotopes Between Water and Sulfur Dioxide.....	1885
Clark J. Egan and W. C. Buss: Determination of the Equilibrium Constants for the Hydrogenation of Mesitylene. The Thermodynamic Properties of the 1,3,5-Trimethylcyclohexanes.....	1887
E. A. V. Eboworth and J. A. Weil: Paramagnetic Resonance Absorption in Peroxo-Dicobalt Complexes.....	1890
Kurt A. Kraus and Richard J. Raridon: Temperature Dependence of some Cation Exchange Equilibria in the Range 0 to 200°.....	1901
Edoardo Frasson, Carlo Panattoni and Luigi Sacconi: Studies in Coordination Chemistry. V. Structure of the Diamagnetic Bis-(N-methylsallylaldimine)-nickel(II) Complex.....	1908
Marianne K. Bernett and W. A. Zisman: Wetting of Low-Energy Solids by Aqueous Solutions of Highly Fluorinated Acids and Salts.....	1911
Arthur C. Thompson and J. L. Culbertson: Acidic Properties of Bentonite.....	1917
Rebecca A. Parker and Stanley P. Wasik: Diffusion Coefficient of Dodecyltrimethylammonium Chloride in Aqueous Solution at 23°.....	1921
S. Lindenbaum, C. F. Jumper and G. E. Boyd: Selectivity Coefficient Measurements with Variable Capacity Cation and Anion Exchangers.....	1924
A. Rothen: Enzymatic Reaction Across a Thin Membrane.....	1929
R. H. Wentorf, Jr.: Condensed Systems at High Pressures.....	1934
Takayuki Fueno, Taikyue Ree and Henry Eyring: Quantum-Mechanical Studies on Oxidation Potentials and Antioxidizing Action of Phenolic Compounds.....	1940
Earl J. Forman and David N. Hume: Heats of Neutralization and the Strengths of Amines in Acetonitrile.....	1949
O. J. Kleppa and C. E. Thalmayer: An E.m.f. Investigation of Binary Liquid Alloys Rich in Zinc.....	1953
D. R. Douslin, R. T. Moore and Guy Waddington: The Pressure-Volume-Temperature Properties of Perfluorocyclobutane: Equations of State, Vital Coefficients, and Intermolecular Potential Energy Functions.....	1959
J. T. Atkins and F. W. Billmeyer, Jr.: Long Chain Branching in Polystyrene Polymerized with Stannic Chloride.....	1966
Charles K. Hersh, Gerald M. Platz and Raymond J. Swehla: Dielectric Constant of Liquid Ozone and Liquid Ozone-Oxygen Mixtures.....	1968
NOTES	
D. E. Burge, H. Freund and T. H. Norris: The Formation of Tetrachloroborate Ion in Liquid Sulfur Dioxide Solution.....	1969
S. L. Bafna and V. M. Bhale: Catalysis by Ion Exchange Resins: Catalytic Behavior of Low-Cross-Linked Resins.....	1971
Sigmund Schuldiner: An Application of Vetter's Criterion for Determining Hydrogen Overvoltage Mechanism.....	1971
George H. Stewart and Hyung Kyn Shin: The Stationary Phase in Paper Chromatography.....	1972
L. A. Harris, G. D. White and R. E. Thoma: X-Ray Analyses of the Solid Phases in the System LiF-ThF.....	1974
George J. Ianz and Jerome Goodkin: Heat and Entropy of Fusion of Mercuric Bromide.....	1975
Harold A. Dewhurst: Chemical Reactions of Active Nitrogen.....	1976
William Fox: Fluid Phases in Mutual Contact: Further Experimental Considerations.....	1977
P. R. Wells: Kinetics of Consecutive Competitive Second Order Reactions.....	1978
J. S. Forrester and G. H. Ayres: Rhodium(III) in Aqueous Solutions.....	1979
Frank T. Eggertsen and Richard M. Roberts: Molybdenum Disulfide of High Surface Area.....	1981
Robert B. Anderson and H. L. Toor: Definition of the Differential Reaction Rate in Ammonia Synthesis Kinetics.....	1982
Robert Benz, Milton Kahn and J. A. Leary: Phase Equilibria of the Binary System $FuCl_2-KCl$	1983
M. H. Lietzke and R. W. Stoughton: The Solubility of Silver Sulfate in Electrolyte Solutions. V. Solubility in Magnesium Sulfate Solutions.....	1984
COMMUNICATION TO THE EDITOR	
F. W. Lampe: On the Radiation-Induced Polymerization of Isobutylene in the Liquid Phase.....	1986

THE JOURNAL OF PHYSICAL CHEMISTRY

(Registered in U. S. Patent Office)

W. ALBERT NOYES, JR., EDITOR

ALLEN D. BLISS

ASSISTANT EDITORS

A. B. F. DUNCAN

EDITORIAL BOARD

C. E. H. BAWN

S. C. LIND

G. B. B. M. SUTHERLAND

R. W. DODSON

R. G. W. NORRISH

A. R. UBBELOHDE

JOHN D. FERRY

W. H. STOCKMAYER

E. R. VAN ARTSDALEN

G. D. HALSEY, JR.

EDGAR F. WESTRUM, JR.

Published monthly by the American Chemical Society at 20th and Northampton Sts., Easton, Pa.

Second-class mail privileges authorized at Easton, Pa. This publication is authorized to be mailed at the special rates of postage prescribed by Section 131.122.

The *Journal of Physical Chemistry* is devoted to the publication of selected symposia in the broad field of physical chemistry and to other contributed papers.

Manuscripts originating in the British Isles, Europe and Africa should be sent to F. C. Tompkins, The Faraday Society, 6 Gray's Inn Square, London W. C. 1, England.

Manuscripts originating elsewhere should be sent to W. Albert Noyes, Jr., Department of Chemistry, University of Rochester, Rochester 20, N. Y.

Correspondence regarding accepted copy, proofs and reprints should be directed to Assistant Editor, Allen D. Bliss, Department of Chemistry, Simmons College, 300 the Fenway, Boston 15, Mass.

Business Office: Alden H. Emery, Executive Secretary, American Chemical Society, 1155 Sixteenth St., N. W., Washington 6, D. C.

Advertising Office: Reinhold Publishing Corporation, 430 Park Avenue, New York 22, N. Y.

Articles must be submitted in duplicate, typed and double spaced. They should have at the beginning a brief Abstract, in no case exceeding 300 words. Original drawings should accompany the manuscript. Lettering at the sides of graphs (black on white or blue) may be pencilled in and will be typeset. Figures and tables should be held to a minimum consistent with adequate presentation of information. Photographs will not be printed on glossy paper except by special arrangement. All footnotes and references to the literature should be numbered consecutively and placed in the manuscript at the proper places. Initials of authors referred to in citations should be given. Nomenclature should conform to that used in *Chemical Abstracts*, mathematical characters marked for italic, Greek letters carefully made or annotated, and subscripts and superscripts clearly shown. Articles should be written as briefly as possible consistent with clarity and should avoid historical background unnecessary for specialists.

Notes describe fragmentary or incomplete studies but do not otherwise differ fundamentally from articles and are subjected to the same editorial appraisal as are articles. In their preparation particular attention should be paid to brevity and conciseness. Material included in Notes must be definitive and may not be republished subsequently.

Communications to the Editor are designed to afford prompt preliminary publication of observations or discoveries whose value to science is so great that immediate publication is

imperative. The appearance of related work from other laboratories is in itself not considered sufficient justification for the publication of a Communication, which must in addition meet special requirements of timeliness and significance. Their total length may in no case exceed 500 words or their equivalent. They differ from Articles and Notes in that their subject matter may be republished.

Symposium papers should be sent in all cases to Secretaries of Divisions sponsoring the symposium, who will be responsible for their transmittal to the Editor. The Secretary of the Division by agreement with the Editor will specify a time after which symposium papers cannot be accepted. The Editor reserves the right to refuse to publish symposium articles, for valid scientific reasons. Each symposium paper may not exceed four printed pages (about sixteen double spaced typewritten pages) in length except by prior arrangement with the Editor.

Remittances and orders for subscriptions and for single copies, notices of changes of address and new professional connections, and claims for missing numbers should be sent to the American Chemical Society, 1155 Sixteenth St., N. W., Washington 6, D. C. Changes of address for the *Journal of Physical Chemistry* must be received on or before the 30th of the preceding month.

Claims for missing numbers will not be allowed (1) if received more than sixty days from date of issue (because of delivery hazards, no claims can be honored from subscribers in Central Europe, Asia, or Pacific Islands other than Hawaii), (2) if loss was due to failure of notice of change of address to be received before the date specified in the preceding paragraph, or (3) if the reason for the claim is "missing from files."

Subscription Rates (1959): members of American Chemical Society, \$8.00 for 1 year; to non-members, \$16.00 for 1 year. Postage free to countries in the Pan American Union; Canada, \$0.40; all other countries, \$1.20. Single copies, current volume, \$1.35; foreign postage, \$0.15; Canadian postage \$0.05. Back volumes (Vol. 56-59) \$15.00 per volume; (starting with Vol. 60) \$18.00 per volume; foreign postage, per volume \$1.20, Canadian, \$0.15; Pan-American Union, \$0.25. Single copies: back issues, \$1.75; for current year, \$1.35; postage, single copies: foreign, \$0.15; Canadian, \$0.05; Pan American Union, \$0.05.

The American Chemical Society and the Editors of the *Journal of Physical Chemistry* assume no responsibility for the statements and opinions advanced by contributors to THIS JOURNAL.

The American Chemical Society also publishes *Journal of the American Chemical Society*, *Chemical Abstracts*, *Industrial and Engineering Chemistry*, *Chemical and Engineering News*, *Analytical Chemistry*, *Journal of Agricultural and Food Chemistry*, *Journal of Organic Chemistry* and *Journal of Chemical and Engineering Data*. Rates on request.

THE JOURNAL OF PHYSICAL CHEMISTRY

(Registered in U. S. Patent Office) (© Copyright, 1959, by the American Chemical Society)

VOLUME 63

NOVEMBER 18, 1959

NUMBER 11

KINETICS OF THE ELECTRODE PROCESSES INVOLVING MORE THAN ONE STEP

BY B. LOVREČEK¹

John Harrison Laboratory of Chemistry, University of Pennsylvania, Penna.

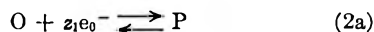
Received October 9, 1958

A method is developed for kinetics of electrode processes proceeding in more than one step and a theoretical expression is found for the slope of the Tafel line for cases in which one step is slow and rate determining. Using the experimental slope and this equation, it is possible to determine both the α -value and the step which is rate determining. As a further consequence of such treatment, a corrected theoretical interpretation of the experimental ($\eta - i$) curve is presented. The approach of this method is different from those published earlier by others^{2,3} and more general than a similar one by Vetter.⁴

There is evidence that many electrode processes proceed in more than one step.⁵ Thus the over-all reaction of an electrode process as represented by eq. 1



(where O is oxidized form, R reduced form and z the number of electrons used in the reaction according to eq. 1) may involve several steps



Every step represents an oxidation-reduction system, except in the case of electrochemical deposition or dissolution of a metal, where the last eq. 2c represents an electrochemical system Me/Me^{z+} , or with the symbols from eq. 2 R/a_Q , where a_Q is the activity of the respective ion.

If so, one can assume also that at the reversible potential V_{rev} for the over-all reaction 1, when no net current flows, electrochemical reactions (eq. 2a-2c) proceed simultaneously and the reversible potential for the over-all reaction 1 is under the given conditions the reversible potential for each "reaction step" (2a-2c). The rate of each "reaction step" at the reversible potential (and also

during the polarization, after a steady state is reached) must be equal.⁶

If a net cathodic or anodic current flows, an overpotential can be expected. Under the assumption that one of the steps is slow, *i.e.*, rate determining, the following changes will take place at the electrode. For increase of the potential of the electrode by 0.059 v. at 25° (or $2.303RT/F$), if every step involves 1 electron, a change in the ratio of activities, for every step which can be considered as reversible, will be one power of ten. If the step $Q + z_3e_0 \rightleftharpoons R$ is the electrochemical deposition or dissolution of a metal, the activity a_Q will also change by one power of ten. This does not apply for the slow, irreversible step, but a method will be shown later by which the change of activities of the ions involved in the rate-determining step can be evaluated.

If the activity of the starting ion a_0 in cathodic polarization is assumed constant,⁷ the activities of other ions, preceding the rate-determining step, will change in the manner given for the change of potential, -0.059 v. at 25° or $(-2.303RT/F)$. For the first two steps, if they are reversible

$$a'_P = 10a_P \quad (3)$$

$$a'_Q = 10^2a_Q \quad (3a)$$

(6) The differences in diffusion rates may cause some differences in rates of electrochemical reactions during polarization to maintain the steady-state concentrations.

(7) This is the usual assumption if the bulk concentration of the respective ion is high and diffusion can replace discharged ions sufficiently fast, so that no appreciable concentration overpotential develops. Also a high concentration of a foreign electrolyte is assumed to eliminate the ζ potential.

(1) University of Zagreb, Zagreb, Yugoslavia.
(2) R. Parsons, *Trans. Faraday Soc.*, **47**, 1332 (1951).
(3) J. O'M. Bockris, *J. Chem. Phys.*, **24**, 817 (1956).
(4) K. J. Vetter, *Z. Naturforsch.*, **7a**, 328 (1952); **8a**, 823 (1953).
(5) *E.g.*, W. Kangro and Fr. Weingartner, *Z. Elektrochem. Ber. Bunsenges.*, **58**, 505 (1954); **59**, 137 (1955).

(a' is the activity after the change of the potential and a is the activity before the change of the potential).

This will give the new activity ratios corresponding to the change of the potential

$$\frac{a'_P}{a'_Q} = 10^{-1} \frac{a_P}{a_Q} \quad (4)$$

and

$$\frac{a'_P}{a'_Q} = 10^{-1} \frac{a_P}{a_Q} \quad (4a)$$

The change in activity ratio for each reversible step is one power of ten. But the absolute change in activity of an ion depends on the step in which it is involved. *E.g.*

$a'_P = 10a_P$ (note that P will be reduced in the second step)

$a'_Q = 10^2a_Q$ (note that Q will be reduced in the third step)

or in general

$$a'_{n_c} = 10^{n_c-1} a_{n_c} \quad (5)$$

(n_c is the number of the step in which the respective ion will be reduced.) If n_c step is rate determining the activity of the ion reduced in this slow step (a'_{n_c}) is given by eq. 6

$$a'_{n_c} = 10^{n_c-1} a_{n_c} \quad (6)$$

The activity of any ion, involved in reduction after the rate-determining step, can be calculated in a similar way, starting from the constant activity a_R

$$a'_{n_c} = 10^{-(\bar{n}_c-1)} a_{n_c} \quad (7)$$

a' = activity after the change of the potential

a = starting activity of the same ion

\bar{n} = no. of the step (numbering starts from R)

And for the ion produced in the rate-determining step

$$a'_{\bar{n}^*c} = 10^{-(\bar{n}^*c-1)} a_{\bar{n}^*c} \quad (8)$$

\bar{n}^*c is the number of the rate-determining step (numbering starts from R).

From eq. 5 it follows that

$$\log a'_{n_c} = (n_c - 1) + \log a_{n_c} \quad (9)$$

for every change of potential of $-2.303RT/F$ volts, or for any change of potential (ΔV)

$$\log a'_{n_c} = -\frac{(n_c - 1)F\Delta V}{2.303RT} + \log a_{n_c} \quad (10)$$

also from eq. 7

$$\log a'_{n_c} = \frac{(\bar{n}_c - 1)F\Delta V}{2.303RT} + \log a_{n_c} \quad (10a)$$

or for the ions involved in the slow step

$$\log a'_{\bar{n}^*c} = -\frac{(\bar{n}^*c - 1)F\Delta V}{2.303RT} + \log a_{\bar{n}^*c} \quad (11)$$

and

$$\log a'_{\bar{n}^*c} = \frac{(\bar{n}^*c - 1)F\Delta V}{2.303RT} + \log a_{\bar{n}^*c} \quad (11a)$$

In anodic polarization the same reasoning can be applied so that

$$\log a'_{n_a} = \frac{(n_a - 1)F\Delta V}{2.303RT} + \log a_{n_a} \quad (12)$$

or

$$\log a'_{n_a} = \frac{(n^*_a - 1)F\Delta V}{2.303RT} + \log a_{n_a} \quad (12a)$$

(the numbering of the steps begins from R) and

$$\log a'_{\bar{n}^*a} = -\frac{(\bar{n}^*_a - 1)F\Delta V}{2.303RT} + \log a_{\bar{n}^*a} \quad (13)$$

or

$$\log a'_{\bar{n}^*a} = -\frac{(\bar{n}^*_a - 1)F\Delta V}{2.303RT} + \log a_{\bar{n}^*a} \quad (13a)$$

(the numbering of the steps begins from O). If z is not equal to 1 in all steps, appropriate changes should be made in equations 3 to 13a.

For metal electrodeposition and dissolution the same equations can be applied if R is replaced by Me.

The above considerations can now be applied to the usual equations for electrode kinetics.⁸ For a cathodic rate-determining step, if $z = 1$, and if anodic current can be neglected (in presence of excess of a foreign electrolyte)

$$i_- = Fk_- a_{n^*c} e^{-\Delta G_-/RT} e^{-(1-\alpha)FV/RT} \quad (14)$$

or

$$i_- = K_- a_{n^*c} e^{-(1-\alpha)FV/RT} \quad (14a)$$

(k_- and K_- are constants) and

$$\frac{\partial \log i_-}{\partial V} = \frac{\partial \log a_{n^*c}}{\partial V} - \frac{(1-\alpha)F}{2.303RT} \quad (15)$$

From eq. 11 it follows that

$$\frac{\Delta \log a_{n^*c}}{\Delta V} = -\frac{(n^*c - 1)F}{2.303RT} \quad (16)$$

i.e., the change of $\log a_{n^*c}$ with V is a linear function of n^*c and

$$\frac{\partial \log a_{n^*c}}{\partial V} = -\frac{(n^*c - 1)F}{2.303RT} \quad (16a)$$

Combining eq. 16a and 15

$$\frac{\partial \log i_-}{\partial V} = -\frac{(n^*c - 1)F}{2.303RT} - \frac{(1-\alpha)F}{2.303RT} \quad (17)$$

or

$$\frac{\partial \log i_-}{\partial V} = -\frac{F}{2.303RT} (n^*c - \alpha) \quad (17a)$$

For the anodic rate-determining step, if $z = 1$, when cathodic current can be neglected, analogous equations can be derived

$$\frac{\partial \log i_+}{\partial V} = \frac{(n^*_a - 1)F}{2.303RT} + \frac{\alpha F}{2.303RT} \quad (18)$$

or

$$\frac{\partial \log i_+}{\partial V} = \frac{F}{2.303RT} (n^*_a - 1 + \alpha) \quad (18a)$$

If z is not equal to 1 in the rate-determining step, appropriate changes in equations 14 to 18a should be made.

In the above expressions i_- and i_+ should be taken as that part of the whole current which is used in the rate-determining step. In a "many step" electrochemical reaction, after a steady state is reached, the part of the current used in each step is proportional to the number of electrons involved in the respective steps. But for the determination of the slope $\log i_-$ (or $\log i_+$) versus V the usual $\log i-V$ representation (i is the total measured current) can be applied, since the calculation and graphical representation of the true

(8) J. A. V. Butler, *Trans. Faraday Soc.*, **19**, 729 (1924); **19**, 734 (1924); T. Erdey-Gruz and M. Volmer, *Z. physik. Chem.*, **150A**, 203 (1930).

"step-current" would displace the curve in a parallel direction, but would not affect the slope. From eq. 15 to 18a one can see that on the basis of experimental relation $\log i-V$ the correct value of α can be calculated from an expression which differs from the usual one⁹ by a correction which takes into account changes in the activity of the ion which is to be reduced or oxidized in the rate-determining step. If the first step is rate determining the correction equals zero. Using this method the original physical meaning of α is preserved. Further this method offers the possibility to get a fair estimation on which step is rate determining in a "many step" electrode process. This is so because the value of n^* can only be a small integer and $0 < \alpha < 1$, so that in equations 17a and 18a the term in brackets, which can be evaluated from experiment, indicates the value of n^* and α , e.g., if the term in brackets is less than 1, $n^* = 1$; if the value is between 1 and 2, $n^* = 2$, etc.

With certain precautions also the usual equations

$$i_- = i_0 \exp\left(\frac{-(1-\alpha)zF\eta_a}{RT}\right) \quad (19)$$

and

$$i_+ = i_0 \exp\left(\frac{\alpha zF\eta_a}{RT}\right) \quad (19a)$$

can be applied, if care is taken that each term corresponds to its original definition:

(a) One must apply them for the electrochemical process of the rate-determining step only and consequently i_- or i_+ can represent only this part of the current which is used in this step.

(b) The activation overpotential is no longer simply the difference in potential at a certain current and in beginning of the measurement before polarization started. Because of the change of activities with polarization (eq. 10-13a) and in accordance with the essence of the definition of activation overpotential, η_a should represent the differences between the potential during polarization and that without net current flow, but in solutions of the same activity of corresponding ions. The starting reversible potential should therefore be corrected for every potential obtained during polarization. This correction can be made using equations 11, 11a and 12a, 13a. From the first two, for cathodic polarization, it follows that

$$\log \frac{a'_n{}^*c}{a'_n{}^*c} - \log \frac{a_n{}^*c}{a_n{}^*c} = -\frac{F\Delta V}{2.303RT} (n^*c + \bar{n}^*c - 2) \quad (20)$$

or

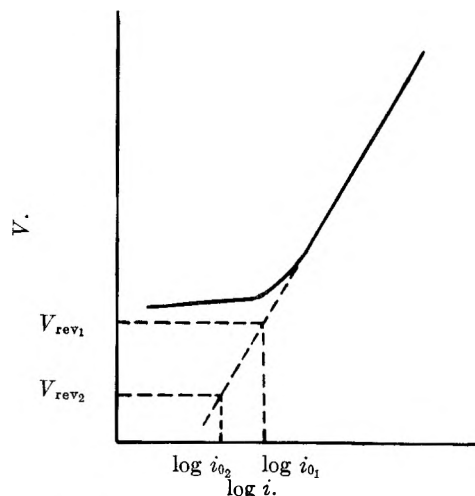


Fig. 1.

$$\frac{2.303RT}{F} \left(\log \frac{a'_n{}^*c}{a'_n{}^*c} - \log \frac{a_n{}^*c}{a_n{}^*c} \right) = -\Delta V (n^*c + \bar{n}^*c - 2) \quad (20a)$$

The term on the left-hand side of eq. 20a represents the shift of the reversible potential (ΔV_{rev}) for a change of polarization potential (ΔV)

$$\Delta V_{rev} = -\Delta V (n^*c + \bar{n}^*c - 2) \quad (21)$$

For anodic polarization analogous calculations (from eq. 12a and 13a) give

$$\Delta V_{rev} = \Delta V (n^*a + \bar{n}^*a - 2) \quad (22)$$

Using equations 21 and 22 the true η_a can be calculated from measured values. Finally the i_0 value which is by definition given by the equation

$$i_0 = zFk_- a_0 \exp\left[-\frac{\Delta G_- + (1-\alpha)zFV_{rev}}{RT}\right] = zFk_+ a_R \exp\left[-\frac{\Delta G_+ - \alpha zFV_{rev}}{RT}\right] \quad (23)$$

should also be calculated taking into account the change of both activity and V_{rev} . This can be done graphically in the usual way from experimental $\log i-V$ curves, but by extrapolating the straight portion of the curve for every measured potential to a new value of reversible potential, as schematically represented in Fig. 1.

With these precautions the usual kinetic equation for electrode processes can be applied also in a "many step" electrochemical reduction or oxidation.

The author wishes to thank Prof. J. O. M. Bockris for helpful discussion of this work.

(9) Derived from eq. 14 or its equivalent for anodic reaction, but without taking into account the changes in the activity of the ion which is to be reduced or oxidized in the rate-determining step.

THE POLARIZABILITIES OF MOLECULES IN LIQUID MIXTURES

BY T. M. REED, III

*College of Engineering, University of Florida, Gainesville, Florida**Received December 22, 1968*

The electron polarizabilities of molecules in liquid mixtures containing both a non-polar fluorocarbon and a non-polar hydrocarbon are different from the polarizabilities of the molecules as pure liquids. An explanation is presented which is based on a coupled oscillator model. Coupling through van der Waals forces in the liquid phase alters the polarizability of a molecule adjacent to another molecule of dissimilar species by a magnitude which is proportional to the number of peripheral bonds of the molecule and inversely proportional to the ionization potential of the dissimilar species. Equations based on the quantum theory of dispersion are applied to the polarizabilities and to thermodynamic data on mixtures of fluorocarbons with hydrocarbons. The theory explains the anomalous behavior of these mixtures in both phenomena.

In the classical theory and in the quantum theory of dispersion the polarizabilities of atoms are calculated by considering the interaction between a periodic external electromagnetic field and the charges composing an isolated atom. It is known from the theory concerning dispersion forces or van der Waals forces that there is an interaction between non-polar atoms. Because of these dispersion forces it should be expected that in general the interaction between an atom in the liquid state and an external periodic electromagnetic field will not be the same as that for the same atom in the gaseous state where it is more or less isolated from interactions with neighboring atoms. There exists already a part of the classical theory of normal dispersion of atoms (when the frequency of the external field is very different from the natural frequency of the dipole oscillators of the atom) which does not require that the polarizability of an isolated atom be the same as that in an external field. The calculation of polarizability in the liquid state can in general hardly be equivalent to a theoretical polarizability based upon a model for an isolated atom.

In the classical theory and in the quantum theory the frequency terms (characteristic of oscillators in the former theory and of differences in energy states in the latter theory) are approximately equal to the first ionization potentials divided by Planck's constant. If we examine a list of first ionization potentials for molecules, such as hydrocarbons and their derivatives and in fact many molecules which have boiling points above zero degrees centigrade, we see that these ionization potentials are within approximately 20% of 10 electron volts. Recently there have appeared some¹ data on the refractive indices of binary liquid mixtures (obtained for other purposes) which indicate that, when the ionization potentials, or characteristic molecular frequencies, differ greatly between the two species, the polarizability of a molecule in the mixture is different from its polarizability as a pure liquid, even though the periodic external field (visible light in this case) be the same in the mixture and in the pure liquid. The mixtures studied each contained a fluorocarbon and a hydrocarbon. Such solutions are unique in that the ionization potentials of fluorocarbons are 1.3 to 1.7 times those for hydrocarbons.^{2,3} The following is suggested as

a postulated model for the liquid phase to amend the existing theories of polarizabilities.

We imagine that the molecules in the liquid phase possess oscillating dipoles as usual in the classical theory. Arising from a coupling of adjacent molecules through the relatively weak dispersion force (compared to the force binding the positive and negative charges within a molecule) there exists a second frequency of motion for each molecular dipole. In the language of Slater and Frank where they discuss coupled oscillators,⁴ "each coordinate has two periods in its motion, or is doubly periodic."

The mechanical model for the coupled oscillators is shown in Fig. 1. Mass 1 is bound by a spring of constant k_1 and mass 2 is bound by a spring of constant k_2 and the two masses are coupled through a spring of constant k_3 , where $k_3 \ll k_1$ and k_2 . The equations of motion for free vibration of this system, in terms of the displacements X_1 and X_2 from equilibrium, are⁵

$$M_1 \ddot{X}_1 + (k_1 + k_3)X_1 - k_3 X_2 = 0 \quad (1)$$

$$M_2 \ddot{X}_2 + (k_2 + k_3)X_2 - k_3 X_1 = 0 \quad (2)$$

By free vibration it is meant that the energy of the system is constant. Taking as the solutions to 1 and 2

$$X_1 = A_1 \cos \omega t \quad (3)$$

$$X_2 = A_2 \cos \omega t \quad (4)$$

in which ω is 2π times the frequency of vibration of the system, it can be shown by substitution of equations 3 and 4 in 1 and 2 that

$$A_2/A_1 = (k_1 + k_3 - M_1\omega^2)/k_3 \quad (5)$$

and

$$A_2/A_1 = k_3/(k_3 + k_2 - M_2\omega^2) \quad (6)$$

From equations 5 and 6 ω is given by

$$\omega^4 - \left[\frac{k_1 + k_3}{M_1} + \frac{k_2 + k_3}{M_2} \right] \omega^2 + \frac{k_1 k_3 + k_1 k_2 + k_2 k_3}{M_1 M_2} = 0 \quad (7)$$

For the particular case of interest where k_3 is very small compared to k_1 and k_2 , equation 7 gives

$$\omega_+^2 \cong k_1/M_1 = \omega_1^2 \quad (8)$$

$$\omega_-^2 \cong k_2/M_2 = \omega_2^2 \quad (9)$$

ω_+^2 is obtained using the positive root of the dis-

(4) J. C. Slater and N. H. Frank, "Introduction to Theoretical Physics," 1st Ed., McGraw-Hill Book Co., Inc., New York, N. Y., 1933, p. 110.

(5) The following treatment is given in many texts on mechanical vibration; for example, L. S. Jacobson and R. L. Ayre, "Engineering Vibrations," McGraw-Hill Book Co., Inc., New York, N. Y., 1958, p. 324.

(1) T. M. Reed, III, and T. E. Taylor, *THIS JOURNAL*, **63**, 58 (1959).

(2) T. M. Reed, III, *ibid.*, **59**, 425 (1955).

(3) T. M. Reed, III, *ibid.*, **59**, 428 (1955).

criminant in 7 while ω_-^2 is obtained from the negative root of the discriminant. Equations 8 and 9 mean that the motion of each mass of the system of Fig. 1 may be described by two frequencies corresponding to ω_1 and ω_2 .⁶ That is, each one is doubly periodic. These two frequencies are approximately the natural frequencies of each mass vibrating freely as a single oscillator when $k_3 \ll k_1$ and k_2 . In the coupled system each oscillator will have two periods of vibration: one period at a frequency corresponding to ω_1 , the other at a frequency corresponding to ω_2 . Oscillator 2 will vibrate at ω_2 with an amplitude $A_{2(2)}$. It will also possess a small oscillation at ω_1 with an amplitude $A_{2(1)}$ given by equation 6⁷ in terms of $A_{1(1)}$

$$A_{2(1)} = k_3 A_{1(1)} / [k_3 + k_2 - k_2 \omega_1^2 / \omega_2^2] \quad (10)$$

$$\cong k_3 A_{1(1)} / k_2 [1 - \omega_1^2 / \omega_2^2]$$

A similar derivation for the small second oscillation of M_1 at frequency ω_2 , using equation 5, gives

$$A_{1(2)} \cong k_3 A_{2(2)} / k_1 [1 - \omega_2^2 / \omega_1^2] \quad (11)$$

In general then for the second oscillations

$$A_{i(j)} \cong k_3 A_{j(i)} / k_i [1 - \omega_j^2 / \omega_i^2] \quad (12)$$

The displacement corresponding to $A_{i(j)}$ is

$$X_{i(j)} \cong A_{i(j)} \cos \omega_j t = \frac{k_3 A_{j(i)} \cos \omega_j t}{k_i [1 - \omega_j^2 / \omega_i^2]} \quad (13)$$

If there is a charge $\beta_i e$ associated with this displacement, the field strength is $[k_3 A_{j(i)} \cos \omega_j t] / e$ and the displacement times $\beta_i e$ per unit field is the incremental polarizability $\alpha_{i(j)}$ of i arising from the oscillations of j

$$\alpha_{i(j)} \cong \beta_i e X_{i(j)} / [k_3 A_{j(i)} \cos \omega_j t / e] = \beta_i e^2 / k_i [1 - \omega_j^2 / \omega_i^2]$$

$$\alpha_{i(j)} \cong [\beta_i e^2 / M_i] / [\omega_i^2 - \omega_j^2] \quad (14)$$

Depending upon whether $\omega_j^2 >$ or $<$ ω_i^2 , $\alpha_{i(j)}$ is positive or negative.

The approximate equation 14 does not apply to systems in which $M_1 = M_2$ and $k_1 = k_2$ (in which the oscillators are essentially identical).⁶ In this case the amplitude ratio is either +1 or -1. "There is in this case a pulsation of amplitude and energy from one of the oscillators to the other."⁸ The average increment over many molecules is effectively zero on a macroscopic scale.

Equation 14 serves to define the algebraic sign on $\alpha_{i(j)}$ and to identify the frequency value associated with this incremental polarizability. The polarizability $\alpha_{1(2)}$ is associated with frequency ω_2 while $\alpha_{2(1)}$ is associated with frequency ω_1 . Equation 13 shows that dipole i oscillates at a small amplitude with frequency ω_j . The sign on $1 - \omega_j^2 / \omega_i^2$ determines whether this second oscillation of i is in phase or out of phase with main frequency of j .

From quantum theory an expression for the total polarizability of an atom is written as

$$\alpha_i = 2 \sum \frac{\mu_i^2 \nu_i}{h} \times \frac{1}{\nu_i^2 - \nu^2} \quad (15)$$

where μ_i is "the matrix component of electric moment associated with the transition from state

(6) For example, equation 7-6a, p. 326, in ref. 5.

(7) Equation 6 is obtained from equation 2 which describes the motion of M_2 .

(8) Ref. 4, p. 111. The treatment of this problem in ref. 4 gives conclusions identical to those obtained here.

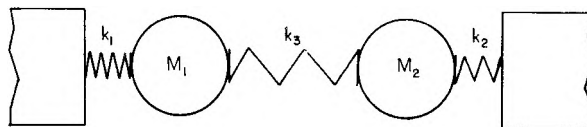


Fig. 1.—Model for coupled oscillators.

o to m ,"⁹ and ν_i is the frequency corresponding to the energy difference between these states. We will assume that there are only two terms in the summation, one corresponding to each frequency of motion of each mass in the mechanical model. One term gives the polarizability of an isolated molecule in an external field of frequency zero ($\nu = 0$)

$$\alpha_i^0 = 2(\mu_i^0)^2 p_i / h \nu_i \quad (16)$$

where p_i is the number of identical peripheral atoms attached to a central group composed of a second type of atom.³ The second term in Σ is $\alpha_{i(j)}$ in an external field of zero frequency

$$\alpha_{i(j)} = 2(\mu_{ij})^2 p_i / h \nu_j \quad (17)$$

The polarizability for a molecule in the liquid is then

$$\alpha_i = \alpha_i^0 + \alpha_{i(j)} = \frac{2(\mu_i^0)^2 p_i}{h \nu_i} + \frac{2(\mu_{ij})^2 p_i}{h \nu_j} \quad (18)$$

The form of equation 16 was established in ref. 3 for certain types of molecules such as the alkanes. In this reference (μ_i^0) was shown to be a constant for an homologous series and $h \nu_i$ is approximately given by the first ionization potential of the particular molecule i . In writing equation 17 it is assumed that an analogous situation applies to (μ_{ij}), the matrix component of the electric moment associated with the frequency ν_j in molecule i . The value of $h \nu_j$ is the ionization potential of the molecule j .

To establish the sign on $\alpha_{i(j)}$ and on $\alpha_{j(i)}$ by equation 14, we will say that $\omega_j >$ ω_i , so that $\alpha_i <$ α_i^0 and $\alpha_j >$ α_j^0 . The polarizability of one species (i) in a binary liquid mixture will be less than the polarizability of that species as a pure substance, while the reverse will be true for the polarizabilities of the second species (j).

The first approximation to Guggenheim's solution¹⁰ to the problem of computing the number of like and unlike pairs gives for the average polarizability α of a molecule in a binary mixture

$$\alpha = x_1 \alpha_1^0 + x_2 \alpha_2^0 + x_1 x_2 (2\Delta) \quad (19)$$

in which x is mole fraction and 2Δ is the sum of the incremental polarizabilities produced in each molecule by its proximity to an unlike molecule. Subtracting the linear mean polarizability $\alpha_m = x_1 \alpha_1^0 + x_2 \alpha_2^0$ from equation 19

$$\alpha - \alpha_m = x_1 x_2 (2\Delta) \quad (20)$$

Assuming that $\alpha - \alpha_m$ is approximately equal to $\alpha_e - \alpha_{em}$ obtained from refractive index data and plotted in Fig. 2 and 3, the data for fluorocarbon-hydrocarbon solutions require that $\alpha - \alpha_m$ be zero for three values of x_1 : $x_1 = 0$, $x_1 = 1$ and $0 <$ $x_1 <$ 1. Equation 20 can conform to this require-

(9) Ref. 4, p. 549.

(10) E. A. Guggenheim, "Mixtures," Clarendon Press, Oxford, 1952, Chapter IV, eq. 4.10.1. The interchange energy W is approximately 10^{-3} times kT for dispersion forces so that the exponential factor appearing in this equation is essentially unity.

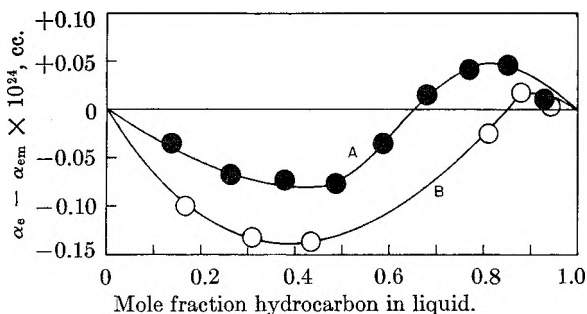


Fig. 2.—Deviation in polarizability from linearity in mole fraction for (A) $i\text{-C}_8\text{H}_{18}$ with $\text{C}_8\text{F}_{16}\text{O}$ and (B) $n\text{-C}_8\text{H}_{18}$ with $\text{C}_8\text{F}_{16}\text{O}$; from refractive index.

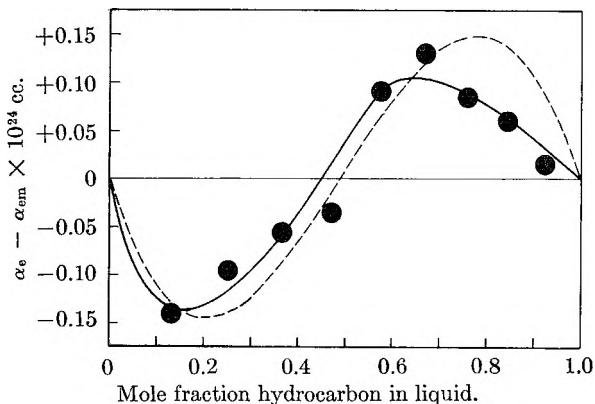


Fig. 3.—Deviation in polarizability from linearity in mole fraction for (C) $i\text{-C}_8\text{H}_{18}$ with C_7F_{16} . Points are from refractive index. Dashed curve is from free energy of mixing.

ment if 2Δ is a function of composition. The following considerations show the dependence of 2Δ on x .

For mixtures composed of molecules each of which contain several or many peripheral atoms it is to be expected that some of the peripheral atoms on a given molecule will be adjacent to like atoms on neighboring like molecules, while the remaining peripheral atoms will be adjacent to unlike atoms on neighboring unlike molecules. By applying Guggenheim's treatment to peripheral atom pairs we obtain an expression for the fraction θ_1 of peripheral atoms of molecules of kind 1 that are adjacent to peripheral atoms of kind 2. If there are in a mixture N_1 molecules of kind 1 and N_2 molecules of kind 2, possessing p_1 identical peripheral atoms and p_2 identical peripheral atoms per molecule, respectively, $\theta_1 N_1 p_1$ are the number of peripheral atoms of kind 1 that are adjacent to those of kind 2. From Guggenheim's treatment

$$\theta_1 N_1 p_1 = z_1 N_1 p_1 N_2 p_2 / (N_1 p_1 + N_2 p_2), \text{ or} \\ \theta_1 = y_2 z_1 \quad (21)$$

where y_2 is the peripheral atom fraction, $x_1 p_1 / (x_1 p_1 + x_2 p_2)$, and z_1 is the number of nearest neighbors to a peripheral atom of kind 1. The contribution of peripheral atoms of kind 1 to 2Δ is $\Delta_1 = \theta_1 \alpha_{1(2)} + (1 - \theta_1)(0)$. For atoms of kind 2, $\Delta_2 = \theta_2 \alpha_{2(1)} + (1 - \theta_2)(0)$. Thus

$$2\Delta = \Delta_1 + \Delta_2 = \theta_1 \alpha_{1(2)} + \theta_2 \alpha_{2(1)} = y_2 z_1 \alpha_{1(2)} + y_1 z_2 \alpha_{2(1)} \quad (22)$$

According to equation 22 the root of equation 20 for $0 < x_1 < 1$ is obtained from

$$(1 - y_1) z_1 \alpha_{1(2)} = -y_1 z_2 \alpha_{2(1)} \text{ as} \\ x_1 = R_p / (2 - R_z R_\alpha - R_p) \quad (23)$$

The R 's are defined as $R_p = p_2/p_1$, $R_z = z_2/z_1$ and $R_\alpha = \alpha_{2(1)}/\alpha_{1(2)}$.

At this point it might be well to digress a moment to see if equation 23 and the assumptions involved in equation 17 are consistent with the experimental data of Fig. 2 and 3. First it will be assumed that $z_1 = z_2$ so that $R_z = 1$. The value of R_α is not known explicitly at this point. However, we have in Fig. 2 two systems each of which contain $\text{C}_8\text{F}_{16}\text{O}$ as one of the components. For one of these systems A, [$i\text{-C}_8\text{H}_{18}(1):\text{C}_8\text{F}_{16}\text{O}(2)$], $x_1^A = 0.65$ for $\alpha_e - \alpha_{em} = 0$. $R_p^A = 0.89$ and $R_z = 1$ so that from equation 23, $R_\alpha^A = -0.26$. According to equation 17

$$R_\alpha^A = \mu_2^2 p_2 v_2 / \mu_1^2 p_1 v_1 \quad (24)$$

For the second system B, [$n\text{-C}_8\text{H}_{18}(3):\text{C}_8\text{F}_{16}\text{O}(2)$], $R_p^B = p_2/p_3 = 1.14$, $R_z = 1$ and

$$R_\alpha^B = \mu_2^2 p_2 v_2 / \mu_3^2 p_3 v_3 \quad (25)$$

Using the good assumption that $v_1 \cong v_3$ (since the ionization potentials of these hydrocarbons are approximately 10 e.v.), and noting that a postulate of the theory is that $\mu_1^2 = \mu_3^2$, equations 24 and 25 give $R_\alpha^B = R_\alpha^A (p_1/p_3) = -0.26(18/14) = -0.33$. The value of x_3^B calculated from equation 23 using $R_\alpha^B = -0.33$, $R_p^B = 1.14$, $R_z = 1$ is $x_3^B = 0.95$. Figure 2 shows that $\alpha_e - \alpha_{em} = 0$ when $x_3^B = 0.85$. The agreement is satisfactory, considering the inferiority of the refractive index data and the assumption regarding the equality of $\alpha_e - \alpha_{em}$ and $\alpha - \alpha_m$.

The third binary (Fig. 3) is C, [$i\text{-C}_8\text{H}_{18}(1):\text{C}_7\text{F}_{16}(4)$] for which $x_1^C = 0.45$ approximately. For reasons (based upon the thermodynamics of this mixture), which are discussed below, $R_\alpha = -0.936$. $R_p = 16/18 = 0.89$ and $R_z = 1$. From these R values x_1^C is calculated as 0.44. The theory gives a quantitative description of the polarizability of these mixtures as a function of composition.

Evaluation of $\alpha_{i(j)}$ from the Free Energy of Mixing

If we assume that the polarizability of each molecule required in the London expression for dispersion forces between a pair of unlike non-polar molecules is that given by equation 18, it is possible to calculate values for $2(\mu_i)^2$ and $\alpha_{i(j)}$ for each member of the pair from experimental free energies of mixing two compounds, using Hildebrand's theory of solutions.¹¹ With this assumption the theoretical expression for the cohesive energy density of 1-2 pairs, given as equation 16 in ref. 2, will contain a factor

$$f_\alpha = (\alpha_1^0 + \alpha_{1(2)})(\alpha_2^0 + \alpha_{2(1)}) / \alpha_1^0 \alpha_2^0 \quad (26)$$

in addition to the factors f_1 and f_d already described.² Excess free energy of mixing per mole, ΔF^E , is given by

$$\Delta F^E = (x_1 V_1 + x_2 V_2) \phi_1 \phi_2 K \quad (27)$$

$$K = \delta_1^2 + \delta_2^2 - 2\delta_1 \delta_2 f \quad (28)$$

$$f = f_\alpha f_1 f_d \quad (29)$$

Here ϕ is volume fraction and δ is the solubility parameter.¹¹ An experimental value for K may be obtained from experimental free energies of mixing

(11) J. H. Hildebrand and R. L. Scott, "Solubility of Non-electrolytes," 3rd Ed., Reinhold Publ. Corp., New York, N. Y., 1950.

TABLE I
 POLARIZABILITIES IN SOLUTION

System 1 2	T_c , °K.	x_{c1}	V , cc./mole		δ , (cal./cc.) ^{0.5}		K , cal./cc. Eq. 27 or 30	f Eq. 28	$q =$ I_2/I_1	f_I^{22}	f_{α}^{24} Eq. 29	f_{α} calcd., Eq. 31	$\alpha_{i(j)} \times 10^{24}$, cc. ²⁸	
			1	2	1	2							$i = 1$	$i = 2$
CH ₄ :CF ₄ ¹²	110.5 ²²	0.50	37.8	49.1	7.50	8.10	8.40	0.934	1.35	0.989	0.946	0.945	-0.32	+0.28
C ₂ H ₆ :C ₂ F ₆ ¹²	176 ²²	.50	53.6	82.0	7.87	6.75	9.82	.919	1.46	.982	.938	.959	-0.50	+0.49
<i>n</i> -C ₄ H ₁₀ :C ₄ F ₁₀ ¹⁴	232.2	.61	90.4	137.2	7.75	6.55	8.07	.935	1.51	.979	.956	.963	-0.87	+0.88
<i>n</i> -C ₆ H ₁₂ :C ₆ F ₁₂ ¹⁶	265.5	.63	110.5	168.6	7.50	6.23	7.50	.937	1.54	.977	.961	.970	-1.05	+1.08
<i>n</i> -C ₈ H ₁₄ :C ₈ F ₁₄ ¹⁶	295.7	.630	131.1	201.3	7.30	5.72	7.01	.946	1.56	.975	.971	.971	-1.22	+1.28
<i>n</i> -C ₁₀ H ₁₆ :C ₁₀ F ₁₆ ¹⁷	287.9	.593	126.8	176.1	7.40	5.81	7.53	.942	1.56	.975	.967	.971	-1.22	+1.09
<i>n</i> -C ₁₂ H ₁₈ :C ₁₂ F ₁₈ ¹⁸	302	.75	132.3	226.2	7.21	5.78	6.74	.944	1.54	.977	.968	.971	-1.22	+1.46
<i>n</i> -C ₇ H ₁₆ :C ₇ F ₁₆ ^{16,20}	328	.62	153.2	236.5	7.06	5.45	6.60	.948	1.55	.976	.973	.971	-1.41	+1.47
<i>n</i> -C ₈ H ₁₈ :C ₇ F ₁₆ ²¹	341	.59	172.2	242.0	7.05	5.29	6.55	.953	1.57	.975	.979	.973	-1.59	+1.49
<i>i</i> -C ₈ H ₁₈ :C ₇ F ₁₆ ^{20,21}	296.9	.614	165.8	224.2	6.86	5.85	6.01	.938	1.57	.975	.964	.973	-1.59	+1.49

by equation 27. From the critical unmixing temperature T_c and composition x_c an experimental value for K may also be obtained as

$$K = \frac{RT_c(x_{c1}V_1 + x_{c2}V_2)^3}{2x_{c1}x_{c2}(V_1V_2)^2} \quad (30)$$

Some data for ten systems taken from the literature are given in Table I. Each system contains a fluorocarbon and a hydrocarbon. Values of f and f_{α} were calculated from these data by equations 28 and 29 using δ 's, V 's and I 's obtained as described in the Appendix. From bond lengths and the van der Waals radii²⁶ f_d was computed as 0.998 for hydrocarbon-fluorocarbon mixtures.

Defining 1 for hydrocarbon and 2 for fluorocarbon, and $q = v_2/v_1 = I_2/I_1$, $r_1 = 2(\mu_1)^2/2(\mu_1^0)^2$, and $r_2 = 2(\mu_2)^2/2(\mu_2^0)^2$, and using equations 16 and 18 in equation 26

$$f_{\alpha} = 1 + r_1/q + qr_2 + r_1r_2 \quad (31)$$

Rearranging

$$q(f_{\alpha} - 1) = r_1 + q^2r_2 + qr_1r_2 \quad (32)$$

According to the hypothesis that the μ 's are characteristic constants associated with peripheral atom types, r_1 and r_2 are independent of the choice of the particular mixture of this series, since only alkanes and perfluoroalkanes are included. Values for r_1 and r_2 may be obtained by applying equation 32 simultaneously to any two of the ten binary mixtures listed, using the experimental values for f_{α} and the corresponding q values. For this purpose the two systems CH₄:CF₄ and C₇H₁₆:C₇F₁₆ were chosen. The result of this calculation is that $r_1 = -0.161$, $r_2 = +0.0535$. The algebraic signs on the r 's verify the expectations of the calculations leading to equation 14, since $I_2(=$

(12) M. Thorp and R. L. Scott, *THIS JOURNAL*, **60**, 670 (1956).

(13) M. Thorp and R. L. Scott, *ibid.*, **60**, 1441 (1956).

(14) J. H. Simons and J. W. Mausteller, *J. Chem. Phys.*, **20**, 1516 (1952).

(15) J. H. Simons and R. D. Dunlap, *ibid.*, **18**, 335 (1950).

(16) R. G. Bedford and R. D. Dunlap, *J. Am. Chem. Soc.*, **80**, 282 (1958).

(17) R. Dunlap, R. Digman and J. Vreeland, Abstract of Papers, 124th Meeting Am. Chem. Soc., Chicago, Sept., 1953.

(18) J. B. Hickman, *J. Am. Chem. Soc.*, **77**, 6154 (1955).

(19) B. G. Kyle and T. M. Reed, *ibid.*, **80**, 6170 (1958).

(20) J. H. Hildebrand, B. B. Fisher and H. A. Benesi, *ibid.*, **72**, 4348 (1950).

(21) D. N. Campbell and J. B. Hickman, *ibid.*, **76**, 2879 (1953).

(22) These temperatures are above T_c .

(23) $f_I = 2q^{0.5}/(1+q)$.

(24) $f_d = [2(d_2/d_1)^{0.5}/(1+d_2/d_1)]^2 = 0.998$.

(25) Equation 17, using $r_1 = -0.161$ and $r_2 = +0.0535$ determined from CH₄:CF₄ and C₇H₁₆:C₇F₁₆.

(26) L. Pauling, "The Nature of the Chemical Bond," Cornell University Press, Ithaca, N. Y., 1940.

$\omega_2h/2\pi) > I_1(=\omega_1h/2\pi)$ in all the hydrocarbon-fluorocarbon systems. These values of r_1 and r_2 were used to compute values for f_{α} by equation 31 for the remaining eight systems in Table I with the results to be compared with f_{α} obtained from the experimental free energy data in each case. Using $2(\mu_1^0)^2 = 8.8 \times 10^{-24}$ cc. \times e.v. and $2(\mu_2^0)^2 = 17.8 \times 10^{-24}$ cc. \times e.v. found in reference 3, $2(\mu_1)^2 = -1.42 \times 10^{-24}$ cc. \times e.v. and $2(\mu_2)^2 = +0.953 \times 10^{-24}$ cc. \times e.v. for hydrocarbons in fluorocarbons and fluorocarbons in hydrocarbons, respectively. Values for $\alpha_{i(j)}$ computed by equation 17 are shown in Table I for the compounds in each mixture. For binary mixtures of a perfluoroalkane with an alkane, each containing more than 4 carbon atoms per molecule, $f_I \cong 0.97$, $f_{\alpha} \cong 0.97$ and $f_d \cong 1$ so that $f \cong 0.94$.

To obtain values for β_i in the equation 14 for the mechanical model we may use the values for $\alpha_{i(j)}$, or in general equate the right-hand side of equation 14 to that of equation 17, knowing the value for $2\mu_i^2$

$$\beta_i = \left[\frac{2\mu_i^2 p_i}{h\nu_i} \right] (\nu_i^2 - \nu_i'^2) \left[\frac{M_i}{e^2} \right] (4\pi^2) \quad (33)$$

Converting ν 's to I 's and using the electronic charge for e and the electronic mass for M_i when $2\mu_i^2$ is in cc. \times e.v.

$$\beta_i = 9.14 \times 10^{21} (2\mu_i^2) p_i (I_i^2 - I_i'^2) / I_i \quad (34)$$

Using the above values for $2\mu_i^2$ for perfluoroalkanes (2) and alkanes (1) and $I_1 = 10$ e.v. and $I_2 = 16$ e.v. approximately for molecules containing more than four carbon atoms

$$\beta_1/p_1 \cong 0.13 \quad \beta_2/p_2 \cong 0.14 \quad (35)$$

That is, there is approximately 0.13 electronic charge involved in each bond in the secondary oscillation effect.

Since $(\beta_1/p_1)/(\beta_2/p_2)$ is approximately unity, from equation 34

$$2\mu_1^2/2\mu_2^2 \cong -I_2/I_1 \cong -q \quad (36)$$

Discussion

To complete the description of the properties of these systems the values of $\alpha_{i(j)}$ obtained from the free energy of mixing should reproduce the curves of $\alpha_e - \alpha_{em}$ vs. x , when 2Δ in equation 22 is evaluated from the $\alpha_{i(j)}$'s in Table I and $\alpha_e - \alpha_{em}$ is obtained by equation 20. The dash line drawn on Fig. 3 for the system *i*-C₈H₁₈:C₇F₁₆ was obtained in this way.

A similar calculation cannot be made for the two systems of Fig. 2 containing C₈F₁₆O until the ioni-

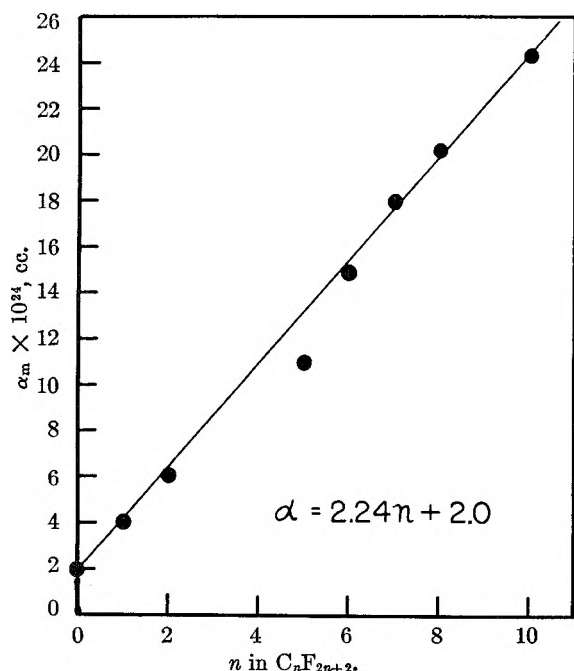


Fig. 4.—Total polarizabilities of perfluoroalkanes.

zation potential of this molecule and the thermodynamics of these mixtures are available. However, it was shown above that the intermediate intercepts of the experimental curves of $\alpha_m - \alpha_{em}$ vs. x are consistent with the requirements of the theory. As an alternative procedure the value of I_2 (the ionization potential of C₃F₁₆O) may be estimated from f_α values obtained from the critical unmixing temperatures of these two systems by the simultaneous solution of two equations 31 and two equations 23 (one for each system) using the intercepts obtained from accurate refractive index measurements. The four unknowns would be I_2 , r_1 , r_2 and R_α .

We could have used the mechanical expression equation 14 throughout and evaluated the β_i 's in a manner similar to that for the μ_i 's. The procedure followed, based on equation 15, is preferred because of the earlier findings concerning the constancy of μ_i^0 for an homologous series.

The value of f_α in the above examples is less than unity. An interesting feature of f_α is that it may be greater than unity in other mixtures. Neglecting the term $r_1 r_2$ in equation 31, f_α will be less than unity when $q^2 < -r_1/r_2$, and f_α will be greater than unity when $q^2 > -r_1/r_2$. Introducing the definitions of r_1 and r_2 , and assuming equation 36 to be true in all cases

$$f_\alpha < 1 \text{ when } q < (\mu_2^0)^2/(\mu_1^0)^2$$

$$f_\alpha > 1 \text{ when } q > (\mu_2^0)^2/(\mu_1^0)^2$$

For C-Cl bonds, C-F bonds and C-H bonds (all in saturated molecules), $(\mu_i^0)^2$ has been obtained.³ The ratios for binary mixtures of a fluorocarbon with each of the other are

1	2	$(\mu_2^0)^2/(\mu_1^0)^2$	Approx. q	f_α
C-Cl	C-F	17.8/30 = 0.6	1.5	>1
C-H	C-F	17.8/8.8 = 2.2	1.6	<1

(27) $r_1 r_2$ is of the order 0.01, while r_1/q and r_2/q are of the order 0.1.

Mixtures of carbon tetrachloride (1) with perfluoroheptane (2) have been studied.²⁰ The critical unmixing point is at 331.9°K. and 0.78 mole fraction CCl₄. Scott has pointed out²⁸ that the inclusion of $f_I = 0.982$ and $f_d = 0.976$ for this system does not appear to be necessary since $K = (\delta_1 - \delta_2)^2$ predicts the critical unmixing temperature fairly well without the term $2\delta_1\delta_2(1-f)$. Formerly² f included only f_I and f_d . The experimental facts actually mean that $f = f_I f_d f_\alpha$ is closer to unity than is $f_I f_d$ alone. That is, $f_\alpha > 1$ as required by the discussion in the preceding paragraph. Using the experimental values for T_c and x_c , and $\delta_1 = 8.15$, $\delta_2 = 5.50$ (cc./mole)^{0.5}, $V_1 = 101.4$ and $V_2 = 240$ cc. per mole in equations 28-30, f_α is obtained as approximately 1.08.

Conclusion

The model postulated to explain the polarizability of molecules in the liquid state produces values for the variation of the refractive index with composition of fluorocarbon-hydrocarbon solutions which are consistent with the thermodynamics of such solutions.

Appendix

The total polarizabilities of the fluorocarbon alkanes plotted in Fig. 4, were computed from the dielectric constants.²⁹

The ionization potentials were calculated from these polarizabilities by the method of ref. 3. The first ionization potential for CF₄ recently has been reported³⁰ as 17.81 e.v., which is the same as the value used in the original paper 3.

The values of δ for the fluorocarbon alkanes were estimated in the following manner. $d \ln \delta / d \ln V$ was found to be -1.49 for n -C₆F₁₄³¹ and -1.37 for C₇F₁₆.¹ A constant value of -1.4 was used for the homologous series. The entropy of vaporization for this series at the respective boiling points was found to be 20.5 ± 0.2 cal./°C. \times g. mole for CF₄,^{12,32} C₂F₆,³³ C₆F₁₄,³¹ and C₇F₁₆.¹ Since the energy of vaporization is approximately $(\Delta S - R)T$, the value of δ at any temperature T is

$$\ln \delta_t = \ln \delta_b - 1.4 \ln V_t + 1.4 \ln V_b \quad (37)$$

$$\ln \delta_b = 0.5 \ln \Delta E_b^{\text{vap}} - 0.5 \ln V_b = 0.5 \ln T_b + 0.5 \ln (\Delta S_b - R) - 0.5 \ln V_b \quad (38)$$

Combining equations 37 and 38 and using $\Delta S_b = 20.5$ cal. per mole per °K.

$$\delta_t = 4.30 T_b^{0.5} V_b^{0.9} V_t^{-1.4} \quad (39)$$

where T_b is the boiling point in °K., V_b is the molar volume of the liquid at the boiling point in cc. and V_t is the molar volume of the liquid at the temperature for which δ_t is desired. The values of δ_t so calculated are within about 2% of accurate calculations.

(28) R. L. Scott, *THIS JOURNAL*, **62**, 136 (1958).

(29) J. H. Simons, editor, "Fluorine Chemistry," Vol. I, Academic Press, Inc., New York, N. Y., 1950, p. 441.

(30) S. Stokes and A. B. F. Duncan, *J. Am. Chem. Soc.*, **80**, 6177 (1958).

(31) R. D. Dunlap, C. J. Murphy, Jr., and R. G. Bedford, *ibid.*, **80**, 83 (1958).

(32) O. Ruff, *Angew. Chem.*, **46**, 739 (1933).

(33) O. Ruff and O. Bretschneider, *Z. anorg. allgem. Chem.*, **210**, 173 (1933).

The molar volume at the boiling point for the fluorocarbon alkanes is given by $V_b(\text{cc./g. mole}) = 32.2n + 22.0$, in which n is the number of carbon atoms per molecule.

Values of δ and V for the hydrocarbons were obtained from "Selected Values of Physical and Thermodynamic Properties of Hydrocarbons,"

American Petroleum Institute Research Project 44, Carnegie Institute of Technology.

Acknowledgment.—This work was made possible by a grant from the National Science Foundation. Presented in part at Meeting in Miniature, Florida Section of the American Chemical Society, May 8, 1959.

PARTIAL MOLAL HEATS AND ENTROPIES OF SOLUTION FOR GASES DISSOLVED IN WATER FROM THE FREEZING TO NEAR THE CRITICAL POINT

By D. M. HIMMELBLAU

Department of Chemical Engineering, The University of Texas, Austin 12, Texas

Received January 12, 1959

Thermodynamic solubility functions for O_2 , N_2 , H_2 , He, Xe and CH_4 in water have been calculated by making use of a new solubility correlation and the principles of the ideal dilute solution. Partial molal heats and entropies of solution are presented from the freezing point of water to near the critical point. Partial molal heats of solution appear to correlate linearly best at 25° with force constants and at 4° with polarizability factors. Partial molal entropies of solution are considerably more negative than those of the same gases in the same standard state in non-polar solvents. Interpretation of partial molal heat capacities and entropies of solution reaffirms the "iceberg" concept of the structure of water, and this effect appears at higher temperatures than previously noted.

The solubility of gases in water has been the subject of innumerable experimental and theoretical papers. Extensive solubility data below 100° can be found in standard reference books and review articles; however, above the normal boiling point of water reliable data are rather scarce. Early workers in the field realized that gases exhibit a solubility minimum with respect to temperature, and it is clear that proper theoretical interpretation of solubility phenomena must account for the entire temperature range from the freezing point of water to the critical point.

There are so many aspects to solubility problems in water—the effect of temperature, pressure, association, dissociation—that this study had to be limited to a consideration of just one aspect, the effect of temperature. Thus the gases to be discussed were limited to those non-polar gases that do not combine chemically with water nor ionize or dissociate in water. In order to avoid consideration of systems which form multiple liquid phases at high pressures and have large deviations from ideality at low pressures, only gases whose critical temperatures lie below the freezing point of water were considered, namely: O_2 , N_2 , H_2 , He, Xe and CH_4 .

A number of pertinent measurements of solubility for these gases above the normal boiling point of water have been made at the Battelle Memorial Institute.¹⁻⁴ High temperature solu-

bility of methane has been reported by Culbertson and McKetta⁵ and Michels.⁶ A number of other references for O_2 , N_2 , H_2 , He, Xe and CH_4 at temperatures above 100° are given in Table I together with the approximate temperature range of the recorded data.

TABLE I

REFERENCES FOR SOLUBILITY OF GASES IN WATER AT ELEVATED TEMPERATURES

Gas	Lit. ref.	Year	Temp. range ($^\circ\text{C}.$)
O_2	1	1952	163-343
	2	1953	100-163
	7	1954	0-330
N_2	3	1956	100-288
	8 ^a	1931	0-169
	9	1934	50-240
	10	1951	76-240
H_2	1	1952	25-316
	1 ^a	1952	163-316
	4	1953	100-163
He	3	1956	100-163
	1	1952	33-316
Xe	3	1956	163-302
	3	1956	100-302
CH_4	6	1936	25-150
	5	1951	25-171

^a Data not used in generalized correlation.

(1) H. A. Pray, C. E. Schweickert and B. H. Minnich, *Ind. Eng. Chem.*, **44**, 1146 (1952). Identical to BMI-T-25 (May 15, 1950).

(2) H. A. Pray and E. F. Stephan, "The Solubility of Hydrogen in Uranyl Sulfate Solutions at Elevated Temperatures," BMI-840 (June 10, 1953).

(3) E. F. Stephan, N. S. Hatfield, R. S. Peoples and H. A. Pray, "The Solubility of Gases in Water and in Aqueous Uranyl Salt Solutions at Elevated Temperatures and Pressure," BMI-1067 (Jan. 23, 1958).

(4) H. A. Pray and E. F. Stephan, "The Solubility of Hydrogen in Uranyl Sulfate Solutions at Elevated Temperatures," BMI-870 (Sept. 25, 1953).

(5) O. L. Culbertson and J. J. McKetta, Jr., *J. Petrol. Technology*, **3**, 223 (1951).

(6) A. Michels, J. Gerver and A. Bijl, *Physica Grav.*, **3**, 797 (1936).

(7) L. M. Zoss, S. N. Suci and W. L. Sibbitt, *Trans. Am. Soc. Mech. Engr.*, **76**, 69 (1954).

(8) J. B. Goodman and N. W. Krase, *Ind. Eng. Chem.*, **23**, 401 (1931).

(9) A. W. Saddington and N. W. Krase, *J. Am. Chem. Soc.*, **56**, 353 (1934).

(10) M. J. Smith and D. L. Katz, "Physical Behavior of the H_2 - O_2 - H_2O System under Pressure," ORNL-1069 (September 24, 1951).

TABLE II
 CONSTANTS FOR THE GENERAL SOLUBILITY CORRELATION EQUATION^a

Gas	A	B	C	D	E	Av. dev. (%) ($\mathcal{C}_{\text{Calc}} - \mathcal{C}_{\text{Expt}}$)
O ₂	-0.0005943	-0.1470	-0.05120	-0.1076	0.8447	2.7
N ₂	-.1021	-.1482	-.01900	-.03741	.8510	4.3
H ₂	-.1233	-.1366	.02155	-.2368	.8249	1.3
He	.1216	-.1146	-.06702	-.3277	.8257	1.9
Xe	.0001156	-.1632	-.003025	-.2264	.8541	5.3
CH ₄	-.1173	-.1247	-.07629	.1959	.7413	1.4

^a In using the values in this table in equation 3, \mathcal{C} is multiplied by 10^{-4} and $(1/T)$ by 10^3 .

Since regular solution theory^{11,12} for a solute gas assumes that there are no orientation or chemical effects between solvent molecules and that there are no interactions between solvent and gaseous solute, for the gases chosen it was not convenient to predict the thermodynamic properties of the solution from the properties of the pure components (extrapolated in the case of the gas). Instead the concept of the ideal dilute solution was applied.

Treatment of Data.—For solutions of sparsely soluble gases in liquids Henry's law expresses the relationship between the partial pressure p of the solute in the vapor phase and the solubility (in terms of mole fraction x) in the liquid phase

$$p = \mathcal{C}x \quad (1)$$

where \mathcal{C} is the Henry's law constant in appropriate units, and is determined by experiment. Further extension of this type of relationship, equation 1, to include corrections for vapor phase non-idealities leads to

$$f = p\gamma = \mathcal{C}x \quad (2)$$

where γ is a correction factor obtainable from generalized charts of fugacity coefficients or specific experimental data where obtainable. The advantage of equation 2 is that it correctly predicts gas solubilities to considerably higher pressures than equation 1. As dictated by equation 2, all the solute gas partial pressures at high pressure were corrected to fugacities (in most instances the corrections were negligible), and these calculated fugacities were plotted vs. mole fraction. The least square slope of these plots in the apparent linear range gave the Henry's law constant at each temperature. All the data from the references listed in Table I except for the two indicated cases (which were in considerable disagreement with the remaining data) were correlated in the form of a general equation of the second degree which, although cumbersome, represents the experimental data quite well

$$A(\log \mathcal{C})^2 + B(1/T)^2 + C(\log \mathcal{C})(1/T) + D(\log \mathcal{C}) + E(1/T) - 1 = 0 \quad (3)$$

where \mathcal{C} is the Henry's law constant in units of atm./mole fraction and T is the absolute temperature in °K. Table II gives the constants and reliability for this equation for each gas. More detailed information concerning the treatment of data and the development of equation 3 can be found in reference 13.

The thermodynamic functions discussed below

(11) J. H. Hildebrand and R. L. Scott, "The Solubility of Non-Electrolytes," 3rd ed., Reinhold Publ. Corp., New York, N. Y., 1950.

(12) J. M. Prausnitz, *A.I.Ch.E. Journal*, **4**, 269 (1958).

have been derived with the assistance of equation 3. Other presentations of thermodynamic solubility functions for water, such as the work of Frank and Evans,¹⁴ Butler,¹⁵ Glew and Moelwyn-Hughes,¹⁶ Morrison and Johnstone,¹⁷ Eley,¹⁸ and earlier workers, have used less complex correlations that cannot be extended to high temperatures (above 100°).

Differential Partial Molal Heat of Solution.—The Henry's Law constant, \mathcal{C} , in units of atm./mole fraction, is related to the differential partial molal heat of solution as

$$\left(\frac{\partial \ln \mathcal{C}}{\partial T}\right)_P = -\frac{\bar{H}^0_L - \bar{H}^*_G}{RT^2} \quad (4)$$

where \bar{H}^0_L is the partial molal enthalpy of the solute gas in the standard state of an infinitely dilute solution and \bar{H}^*_G is the partial molal enthalpy of the ideal gas in the vapor phase. The quantity $(\bar{H}^0_L - \bar{H}^*_G)$ represents the partial molal heat of solution based on the standard state referred to infinite dilution. A more convenient form of equation 4 is

$$\frac{\partial \log \mathcal{C}}{\partial(1/T)} = \frac{\bar{H}^0_L - \bar{H}^*_G}{2.303R} \quad (5)$$

Figure 1 shows the quantity $(\bar{H}^0_L - \bar{H}^*_G)$ for 6 gases as a function of temperature, actually $1/T$, since the lines are more linear if the inverse of the absolute temperature is used as a parameter rather than T itself. The values at 25° listed in Table III are based on \mathcal{C} being expressed in the units of atm./mole fraction.

At first glance it would appear easy to extrapolate the heat of solution curve to $1/T_c = 1.545$, the inverse of the critical temperature for water, and thus obtain the heat of solution for each gas in water at the critical temperature. However, this extrapolation is improper because the gas solubility increases so rapidly as the critical point is approached that the basic assumptions relating to the ideal dilute solution no longer apply. Zero partial molal heat of solution represents the minimum in the solubility curve.

Figure 1 indicates clearly the tendency of the partial molal heats of solution for each gas to converge toward identical values as the temperature approaches the critical point. Because of in-

(13) D. M. Himmelblau, *J. Chem. Eng. Data*, in press.

(14) H. S. Frank and M. W. Evans, *J. Chem. Phys.*, **13**, 512 (1945).

(15) A. Butler, *Trans. Faraday Soc.*, **33**, 235 (1937).

(16) D. N. Glew and E. A. Moelwyn-Hughes, *Disc. Faraday Soc.*, **15**, 150 (1953).

(17) J. T. Morrison and N. B. Johnstone, *J. Chem. Soc.*, 3441 (1954).

(18) D. D. Eley, *Trans. Faraday Soc.*, **40**, 184 (1944).

TABLE III

PARTIAL MOLAL HEATS OF SOLUTION AND ENTROPIES OF SOLUTION AT 25°

Gas	Heat of soln. std. state: "infinite dilution" $-(\bar{H}_L^0 - \bar{H}^*_G)$, cal./g. mole	Entropy of solution $-(\bar{S}_L - \bar{S}^*_G)$, cal./g. mole, °K.		
		Std. state: $f = 1$ atm.	Std. state: ^b $x = 10^{-4}$	Std. state: ^b $x = 1.0$
He	390	1.34	6.70	25.0
H ₂	905	3.07	6.96	25.3
Ne ^a	1080	3.63	8.62	26.9
N ₂	2500	8.48	12.8	31.1
O ₂	2850	9.65	12.6	30.9
A ^a	3100	10.4	13.2	31.5
CH ₄	3170	10.7	13.6	31.9
Kr ^a	3440	11.5	13.2	31.5
Xe	4710	15.8	16.4	34.7

^a From data of ref. 17. ^b To convert from the standard state of $x = 10^{-4}$ to that of $x = 1.0$, add -18.30 cal./g. mole °K., i.e., $2.303R \log 10^{-4}$.

accuracies in the experimental data at high temperatures, this convergence is not as clear for Xe and N₂ as for the other gases, but it is believed that if additional reliable data were available above 300°, this trend would show up also for these two gases.

A comparison of our results with those of Morrison and Johnstone and Frank and Evans is in Table IV for 25 and 80° (the extreme of their work). The agreement at 25° is good but at 80° large discrepancies are apparent. Since 80° is in the vicinity of the minimum in the solubility curve for most of these gases, i.e., the curve is rapidly changing in direction, such deviations can be expected if 80° represents the highest temperature for which a continuous solubility curve can be fit. In differentiating a short range curve the extreme values frequently are erratic.

TABLE IV

COMPARISON OF PARTIAL MOLAL QUANTITIES WITH THE RESULTS OF OTHERS

Gas	$(\bar{H}_L^0 - \bar{H}^*_G)$, cal./g. mole					
	25°			80°		
	This work	Ref. 17	Ref. 14	This work	Ref. 17	Ref. 14
O ₂	-2850	-2950	-2990	-576	-380	
N ₂	-2500	-2640	-2140	-146	394	-180
H ₂	-905	-962	-1280	814	420	170
He	-390	-400	-840	1860	1840	-550
Xe	-4710	-4360	-4490	-1440	-2120	-720
CH ₄	-3170	-3210	-3180	-626	-336	

$(\bar{S}_L - \bar{S}^*_G)$, cal./g. mole °K, standard state $x = 10^{-4}$						
	This work	Ref. 17	Ref. 14	This work	Ref. 17	Ref. 14
O ₂	-12.6	-12.83	-13.0	-5.52	-4.95	
N ₂	-12.8	-13.13	-11.5	-5.41	-3.76	-5.5
H ₂	-6.96	-7.12	-7.7	-1.61	-2.87	-3.0
He	-6.70	-6.67	-8.2	+0.26	+0.22	-7.2
Xe	-16.4	-15.15	-15.3	-6.05	-8.25	-3.8
CH ₄	-13.6	-13.59	-13.5	-5.57	-4.72	

Correlation of Partial Molal Heats of Solution with Physical Properties of Gas.—Since only one solvent is under consideration, it is natural to look first at the physical characteristics of the gas to explain the differences in the partial molal heats of solution and solubility phenomena. Among the common methods used to correlate the partial molal heats of solution are (a) partial molal vol-

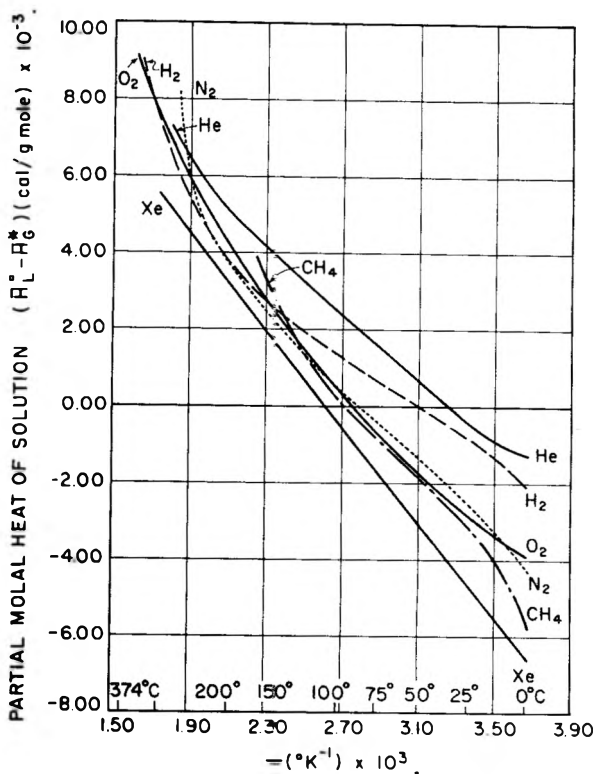


Fig. 1.—Partial molal heat of solution as a function of temperature.

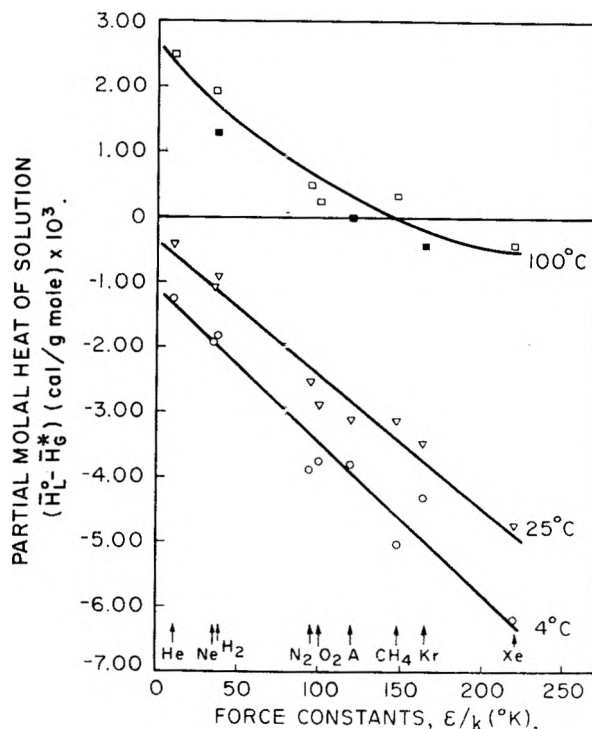


Fig. 2.—Correlation of partial molal heats of solution with force constants.

umes, (b) force constants and (c) polarizability. The latter two, since they are fundamental characteristics of a gas molecule, are utilized here.

Figure 2 indicates the relationship between the partial molal heats of solution and the force con-

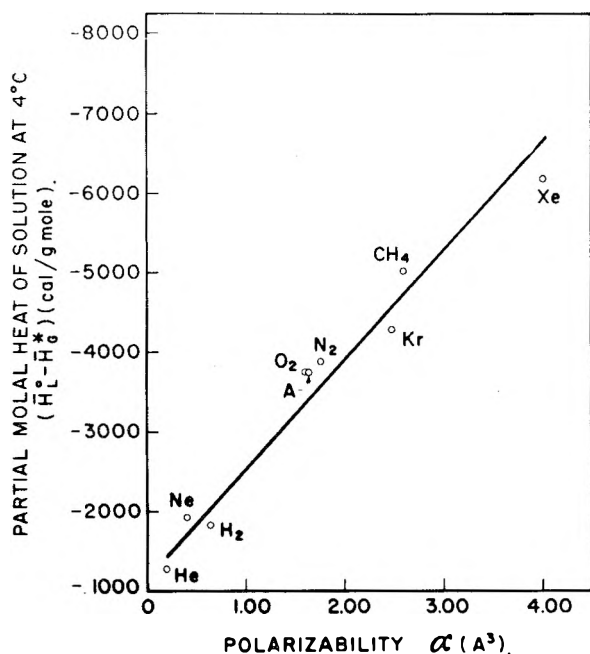


Fig. 3.—Partial molal heat of solution as influenced by polarizability (at 4°).

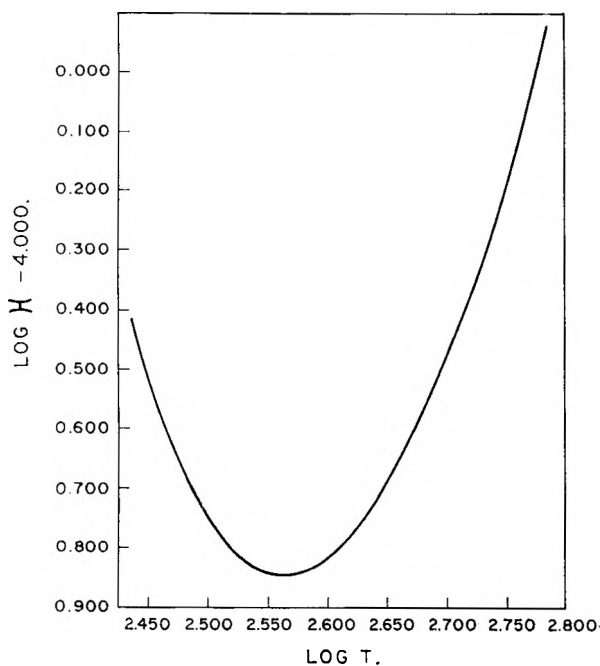


Fig. 4.—Smoothed solubility data for O₂.

starts ϵ/k in $^{\circ}\text{K}$. (from the second virial coefficient¹⁹) for 4, 25 and 100°. Data from reference 17 for Ne, A and Kr are included. Although comparisons such as this usually are made at 25°, Eley¹⁸ has suggested that it might be more significant to compare heats and entropies of solution at 4°, the temperature at which there is little or no energy or entropy change in forming cavities in the water. While the values at 25° appear to fit better a linear correlation than those at 4°, there is no question that at 100° a linear correlation is some-

(19) J. O. Hirschfelder, C. F. Curtiss and R. B. Bird, "Molecular Theory of Gases and Liquids," Appendix I-A, John Wiley and Sons, New York, N. Y., 1954, p. 1110.

what poorer than at lower temperatures. The solid points at 100° are extrapolated values from Morrison and Johnstone (whose data extended only to 80°) and probably are high. If at some high temperature, say above 300°, the partial molal heats of solution were approximately the same for each gas, then this situation would be represented by a horizontal line in Fig. 2 off the scale.

In Fig. 3 at 4°, the best temperature to obtain a linear fit, we can see the influence of polarizability on the partial molal heat of solution.

Differential Partial Molal Entropy of Solution.—Hildebrand²⁰ has derived an expression for the partial molal entropy of solution of gases in liquids which can be expressed as

$$\bar{S}_L - \bar{S}_G^* = R \left(\frac{\partial \ln a_L}{\partial \ln x_L} \right)_T \left(\frac{\partial \ln x_L}{\partial \ln T} \right)_{\text{Sat.}} \quad (6)$$

where $(\bar{S}_L - \bar{S}_G)$ is the entropy change for a differential process (per mole of gas) during solution. The value of $(\partial \ln a_L / \partial \ln x_L)$ approaches unity in the very dilute solutions we are considering. If Henry's Law applies, $f = \mathcal{K}x$, and if $f = 1$ atm., then

$$\left(\frac{\partial \ln x_L}{\partial \ln T} \right) = \left(\frac{\partial \ln 1/\mathcal{K}}{\partial \ln T} \right) = - \left(\frac{\partial \log \mathcal{K}}{\partial \log T} \right) \quad (7)$$

Hildebrand found for non-polar solvents that a plot of $\log x_L$ vs. $\log T$ for a given solvent gave an approximately straight line, and while this is true for water in some temperature regions (especially in the vicinity of 25°), as can be seen from Fig. 4 for O₂, the value of the slope $-(\partial \log \mathcal{K} / \partial \log T)$ varies widely in magnitude, though not in trend, for the entire temperature range from the freezing point of water to near the critical point. Like the partial molal heats of solution, the partial molal entropies of solution (Fig. 5) start in the low temperature range as negative values and change to positive values with increasing temperature.

It should be noted that the standard state for equation 6 is a solution above which the fugacity (partial pressure) of the solute gas is one atmosphere. This is a solution of different concentration for each gas and each temperature. To compare more clearly the partial molal entropies of solution for the six gases included in this study, the values determined by equation 6 have been converted to the uniform standard state of $x = 10^{-4}$. This was done by computing the entropy change in the ideal gas phase from $f = 1$ atm. to the f corresponding to an equilibrium solution at $x = 10^{-4}$, and adding this quantity (generally a negative amount) to the values in the second column of Table III. A concentration of $x = 10^{-4}$ is somewhat near the equilibrium concentration at a fugacity of one atmosphere. If it is desired to calculate the partial molal entropies of solution for the standard state of $x = 1.0$, this can be done easily by subtracting 18.30 cal./g. mole $^{\circ}\text{K}$. ($2.303 R \log 10^{-4}$) from the values given for the standard state of $x = 10^{-4}$.

Partial molal entropies of solution at 25° for each of these standard states are tabulated for convenience in Table III. Some of the entropy difference among the various gases is seen to be due to

(20) J. H. Hildebrand, *J. Chem. Phys.*, **20**, 190 (1952).

the entropy of dilution, but not all. Table IV compares the values calculated in this study with those of previous workers for 25 and 80°. Figure 5 illustrates the change with temperature of $(\bar{S}_L - \bar{S}^*_G)$ based on the standard state of $x = 10^{-4}$.

A comparison of the entropies of solution derived here with corresponding values²¹ based on the same standard states for gases in non-polar solvents at 25° shows that entropies of solution in water are all negative by large amounts relative to the same gas in a non-polar solvent. This is true whether the standard state is f equal to one atmosphere or whether it is a mole fraction of 10^{-4} in the liquid phase.

If the entropies of solution using the standard state of $x = 10^{-4}$ are examined, there appear to be two categories of gases at 25°, those in the range of -6.7 to -8.6 e.u. (He, H₂, Ne) and those in the range of -12.6 to -13.6 e.u. (O₂, N₂, CH₄, A, Kr), if we put Xe in a special class. Because of the fact we are dealing with a variety of types of bonding in water solutions and different numbers of nearest neighbors, the significance of this grouping is not entirely clear. However, if the sphere of influence of these gases in solution is presumed to bear some relation to their covalent bond distances, or atomic diameters in the case of the rare gases, it is possible to compare $(\bar{S}_L - \bar{S}^*_G)$ ratios as in Table V. The equivalent covalent diameters for the gases other than rare gases have been assumed to be the single, double or triple bond length, as the case may be, plus a single bond length representing the interaction between gas molecule and water. These data roughly indicate that the partial molal entropy of solution is influenced by the size of the cavity created by the gas molecules if the estimate of this cavity size is made by bond distances.

TABLE V

COMPARISON OF RELATIVE ORDER OF PARTIAL MOLAL ENTROPIES OF SOLUTION (STANDARD STATE = $x \times 10^{-4}$) AND MEASURES OF MOLECULAR SPHERES OF INFLUENCE

	Relative $(\bar{S}_L - \bar{S}^*_G)$ H ₂ = 1.00	Relative molecular covalent diameter ^a H ₂ = 1.00	Relative atomic radius for rare gas A = 1.90 ^b	Relative force constants σ (Å.) ^c H ₂ = 1.00
He	0.96			0.872
H ₂	1.00	1.00		1.00
Ne	1.24		1.60	0.940
O ₂	1.81	1.75		1.18
N ₂	1.84	1.80		1.26
CH ₄	1.95	2.04		1.30
A	1.90		1.90	1.16
Kr	1.90		1.99	1.23
Xe	2.34		2.19	1.36

^a Data from L. Pauling, "The Nature of the Chemical Bond," 2nd Ed., Cornell University Press, Ithaca, N. Y., 1943, Chapt. V. ^b Data from T. Moeller "Inorganic Chemistry," John Wiley and Sons, New York, N. Y., 1952, p. 375. ^c Ref. 19.

Structural Aspects of Solute-Water Interaction.

—Water as a liquid has certain microscopic physical characteristics which have been summed up in the word "ice-like-ness." The extent of this "ice-like-ness" can be altered by changes in (a) tempera-

(21) J. E. Jolley and J. H. Hildebrand, *J. Am. Chem. Soc.*, **80**, 1050 (1958).

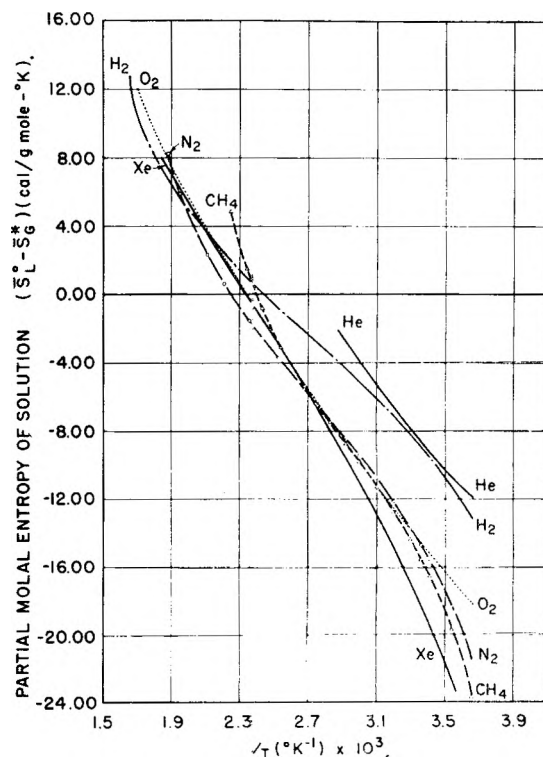


Fig. 5.—Partial molal entropy of solution as a function of temperature.

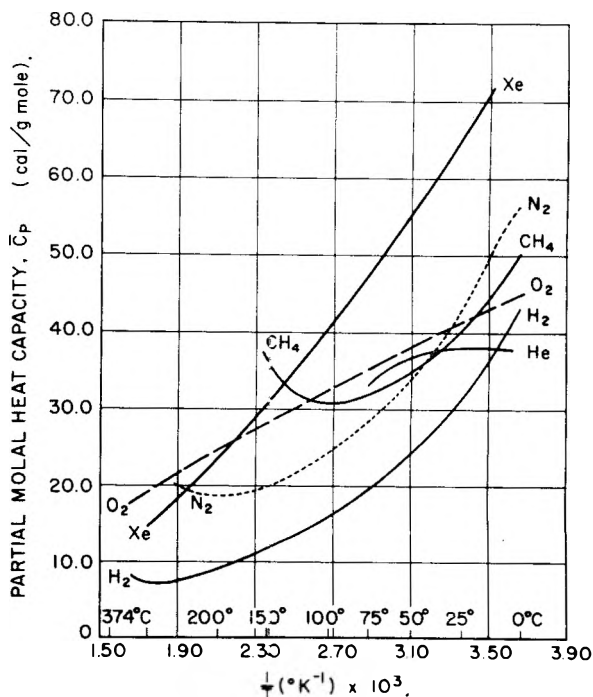


Fig. 6.—Partial molal heat capacities as a function of temperature.

ture, (b) pressure, and (c) addition of a solute. What inferences can be drawn from the previous thermodynamic data concerning the influence of a small amount of gaseous non-polar solute upon the structure of water?

Frank and Evans,¹⁷ Eley,¹⁸ and others²² have

(22) W. F. Claussen and M. F. Polglase, *ibid.*, **74**, 4817 (1952).

pointed out that the large negative values found for partial molal entropies of solution of non-polar gases in water (as compared with the same gases in non-polar solvents) can best be interpreted as the creation of a more highly ordered state in water, or of "icebergs." The larger the atom or molecule, the greater the effect. As the temperature increases these quasi-ice-like structures break up, and the entropy of solution becomes positive. Frank and Evans¹⁴ indicated that the relative order of this effect reversed with temperature, *i.e.*, Rn, Xe and the larger molecules gave more negative values of $(\bar{S}_L - S^*_G)$ at low temperatures (0°) than He, H₂, Ne, etc., while at higher temperatures (100°) the opposite was true. However, they had some reservations about the accuracy of the solubility data they used, and Fig. 5 here shows no such trend but indicates that the relative influence of molecular size is approximately constant with rising temperature although the differences among molecules becomes less and less significant as the temperature increases. Other than in this one aspect, the conclusions of previous workers concerning the quasi-ice-like structure of water in the vicinity of a solute molecule are reaffirmed. It would be interesting to compare the partial molal entropies of solution (if reliable data were available) for the reported gases in non-polar solvents with corresponding values in water at equal reduced temperatures of solvent to see how closely the partial molal entropies of solution approached each other at high temperatures.

Another characteristic of "ice-like-ness" in water is that as the more rigid structures around the gas solute molecule break up, large partial molal heat capacities are noted, larger than the absolute heat capacities of either solute or solvent. Claussen and Polglase²² have compared the "melting" of these "ice-bergs" to the stretching of a balloon and indicate that the stretching of the hydrogen bonds of the ice-like structure without breaking is the main contribution to the high values found for the partial molal heat capacities.

The expression $\bar{H}^0_L - \bar{H}^*_G$ as a function of temperature was determined with the assistance of equations 3 and 5, and then the value of ΔC_p computed as

$$\frac{\partial \bar{H}^0_L - \bar{H}^*_G}{\partial T} = \Delta C_p \quad (8)$$

There is not much use in comparing the values of ΔC_p obtained in this manner with those of previous workers for the following reason. If the equation of Valentiner,²³ as used by Glew and Moelwyn-Hughes, and Morrison and Johnstone is used to correlate the Henry's Law constant with respect to temperature

$$\log (P_2/c_2) = a - b \log T - C/T \quad (9)$$

(where P_2 is the pressure in millimeters and c_2 is the concentration in moles/l.), one can show easily that

$$\bar{H}^0_L - \bar{H}^*_G = 2.3Rc - RbT \quad (10)$$

and that

$$\Delta C_p = -Rb \quad (11)$$

These relations give the impression that ΔC_p is independent of temperature. In this work, by use of a more complicated solubility correlation, ΔC_p is found to vary substantially between 0 and 300°, although over a shorter temperature range such as 25 to 50° it does not vary very much. Furthermore, depending on the precise constants used to fit equation 9, quite wide variations in the value of b and therefore the value of ΔC_p can be obtained even though the correlation equation fits well.

Since ΔC_p represents the difference in the heat capacity of the solute gas in solution *versus* that in the ideal gas phase, if we subtract the heat capacity of the ideal gas, we obtain the partial molal heat capacity (\bar{C}_p) of the gas in solution

$$\bar{C}_p = \Delta C_p - C_p^* \quad (12)$$

The values of C_p^* used for O₂, N₂, H₂ and CH₄ were from Wagman.²⁴ Figure 6 shows the values of \bar{C}_p as a function of $1/T$. Even at temperatures above 200° it appears as if hydrogen bonds are being stretched and that the rigidity of structure found in water at low temperatures has not completely disappeared. Furthermore, the curves for \bar{C}_p have gradual trends without sharp breaks in agreement with the hypothesis of Claussen and Polglase.²² The slight up trends at high temperatures probably are due to errors in fitting the high temperature data by equation (3) which is differentiated twice by the time equation 8 is applied. It would seem likely that \bar{C}_p should only decrease as the temperature increases.

(23) S. Valentiner, *Z. Physik*, 42, 253 (1927).

(24) D. D. Wagman, "Selected Values of Chemical Thermodynamic Properties," National Bureau of Standards, 1953.

ELECTROPHORESIS AND SURFACE CHARGE

BY DIPTI K. CHATTORAJ¹ AND HENRY B. BULL*Biochemistry Department, State University of Iowa, Iowa City, Iowa**Received January 29, 1959*

The interfacial tension lowering produced by organic ions adsorbed at a paraffin oil-water interface and the electrophoretic mobility of isoelectric paraffin oil particles in the presence of organic ions have been studied and the charge density at the interface calculated from the two methods. Agreement is found as the concentration of the organic ion approaches zero. The shift of the apparent pK values of weak acids adsorbed at solid-paraffin surfaces as determined by electrophoresis have been compared with theory and satisfactory correspondence between theory and experiment is reported.

There has long been an interest in the distribution of counterions adjacent to a charged interface and the relation of this distribution to the potential of the interface. Recently Davies,² Philips and Rideal³ and Philips and Haydon⁴ have considered this problem anew and have published results of their measurements of the potential change at oil-water and air-water interfaces produced by monolayers of ionic detergents. They used the vibrating plate technique for their potential measurements and, accordingly, the total potential change from one phase to the adjacent phase has been determined. They also measured the film pressures exerted by the organic ions and have discussed their results in terms of equations of state of the ionic monolayers.

We have concerned ourselves with the potential of the electrical double layer as measured by electrophoresis (the zeta potential) and have thus confined the electrical effects to the water phase only. The interfacial tension lowerings produced by organic ions at oil-water interfaces have been compared under what we think are suitable conditions with the corresponding electrophoretic mobilities of emulsion particles of oil in the presence of solutions of the organic ions.

We have also considered the shifts of the apparent pK values of weak acids at paraffin-water interfaces and the relation of the observed shifts to the electrophoretic mobility of paraffin particles covered with the weak acids.

Experimental

The hydrocarbon oil was Nujol which was vigorously shaken with 40% sodium hydroxide and then washed exhaustively with distilled water until the washings were neutral. The solid paraffin wax was from Fisher Scientific Co. and had a melting point of 68–70°. It was melted in the presence of 40% sodium hydroxide, vigorously shaken and washed, while melted, with distilled water until the washings were neutral.

The stearic acid was from Eastman Organic Chemicals (lot no. 41) and used without further purification. The octadecylamine was from the Research Division of Armour and Co. (lot no. 4) and used without further purification. The sodium dodecyl sulfate was a special lot from Procter and Gamble Co. and was recrystallized from hot ethanol before use.

Interfacial tensions of the Nujol-water systems were measured at 25° by the drop-weight method. It was found that the time of formation of the drops had to be extended to 5 minutes to achieve constant values for the interfacial tensions. The corrections of Harkins and Brown⁵ have been applied.

Electrophoretic measurements were conducted in a micro-electrophoretic cell of flat design.⁶ Mobilities were observed at room temperature and corrected to 25° by multiplying the measured mobilities by the ratios of the viscosities of water at the temperature of the measurement to the viscosity of water at 25°.

The emulsions were manually prepared and the solid paraffin was melted and emulsified at an elevated temperature. The particles were in the neighborhood of 5 μ in diameter which at an ionic strength of 0.05, gives a κr value of about 1,000 (κ is the reciprocal Debye-Hückel distance and r is the radius of the particle). This value of κr permits the use of the Smoluchowski equation for the calculation of the zeta potential from the electrophoretic mobility.

Results

The electrophoretic mobilities of Nujol particles at an ionic strength of 0.05 have been measured as a function of pH . The aqueous solutions consist of mixtures of sodium chloride and hydrochloric acid. The mobilities of such particles decrease almost linearly with decreasing pH and become zero at a pH of 1.65. The pH of isoelectric Nujol particles has been adopted as our reference state for both interfacial tension measurements as well as for electrophoretic mobilities in the presence of organic ions.

Figures 1 and 2 show plots of the electrophoretic mobilities of Nujol particles as functions of the molar concentrations of octadecylamine and of sodium dodecyl sulfate, respectively. Figures 3 and 4 are plots of the interfacial tension lowering in dynes per centimeter produced by the indicated molar concentrations of octadecylamine and of sodium dodecyl sulfate, respectively, at the Nujol-water interface.

Figures 5 and 6 show the results of the study of the mobilities of various kinds of particles as functions of the pH of the solutions. The pH was adjusted by the addition of the appropriate amounts of hydrochloric acid or of sodium hydroxide and enough sodium chloride added to yield an ionic strength of 0.05. Figure 5 has curves for a suspension of micelles of pure octadecylamine, for paraffin particles containing 0.265 g. of octadecylamine in 25 ml. of the melted paraffin and emulsified at pH 2.0, for Nujol emulsified in 1×10^{-4} molar octadecylamine at the pH of the experiment. Figure 6 gives plots for micelles of sodium stearate-stearic acid, for paraffin particles containing 0.10 g. of stearic acid dissolved in 25 ml. of melted paraffin and emulsified at pH 10.5 and for Nujol containing 0.067 g. stearic acid dissolved in 25 ml. of the oil.

In a preliminary study of the mobilities of Nujol

(1) Chemistry Department, Jadavpore University, Calcutta, India.

(2) J. T. Davies, *Proc. Roy. Soc. (London)*, **A208**, 224 (1951).

(3) J. N. Philips and E. Rideal, *ibid.*, **A232**, 149 (1955).

(4) J. N. Philips and D. A. Haydon, *Trans. Faraday Soc.*, **54**, 698 (1958).

(5) W. D. Harkins and F. E. Brown, *J. Am. Chem. Soc.*, **41**, 503 (1919).

(6) H. B. Bull, *ibid.*, **80**, 190 (1958).

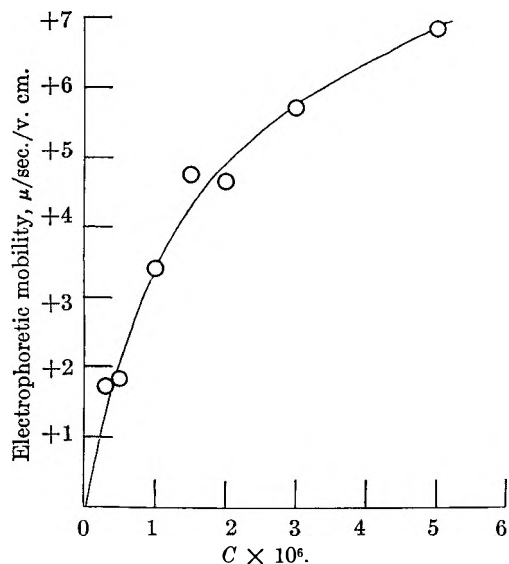


Fig. 1.—Electrophoretic mobilities of Nujol emulsion particles as a function of the molar concentration of octadecylamine at pH 1.65 and at an ionic strength of 0.05 (NaCl plus HCl) and at 25°.

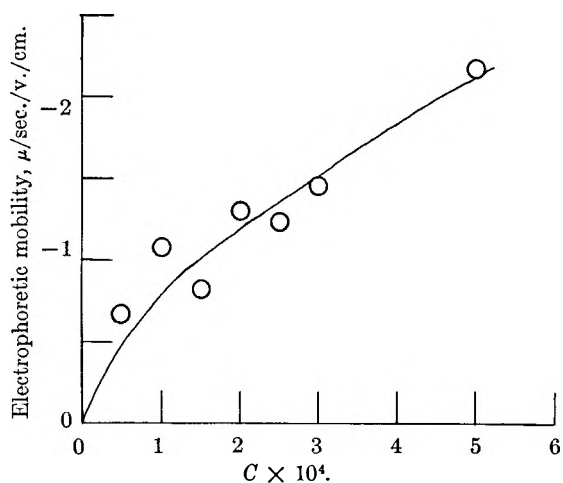


Fig. 2.—Electrophoretic mobilities of Nujol emulsion particles as a function of the molar concentration of sodium dodecyl sulfate at pH 1.65 and at an ionic strength of 0.05 (NaCl plus HCl) and at 25°.

and of paraffin emulsions as a function of the concentrations of octadecylamine and of stearic acid it was found that the amounts of these compounds employed in the experiments described in the paragraph above were sufficient to give the highest mobilities at a given pH.

Discussion

Since the radii of the emulsion particles are very much larger than is the thickness of the double layer, the electrical double layer of the non-conducting particles may be treated as a plane plate condenser and the Gouy equation can be used to calculate the electrostatic charge per unit area at the oil-water interface. For a uni-univalent electrolyte the Gouy equation may be written⁷

(7) H. A. Abramson, L. S. Moyer and M. H. Gorin, "Electrophoresis of Proteins," Reinhold Publ. Corp., New York, N. Y., 1942. See eq. 77, page 133 and substitute the value of κ .

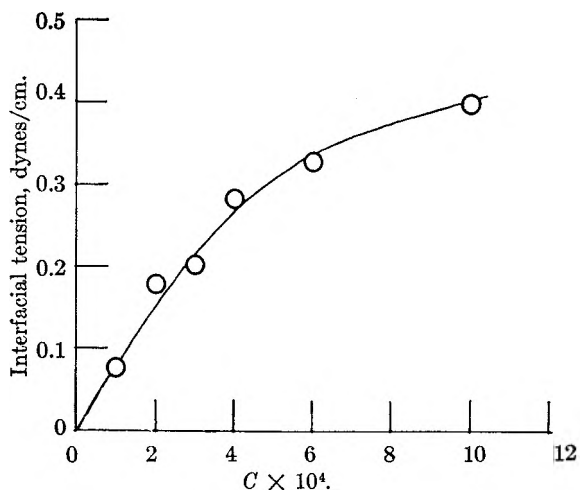


Fig. 3.—Interfacial tension lowering of Nujol-water system as a function of the molar concentration of octadecylamine at pH 1.65 and at an ionic strength of 0.05 (NaCl plus HCl) and at 25°.

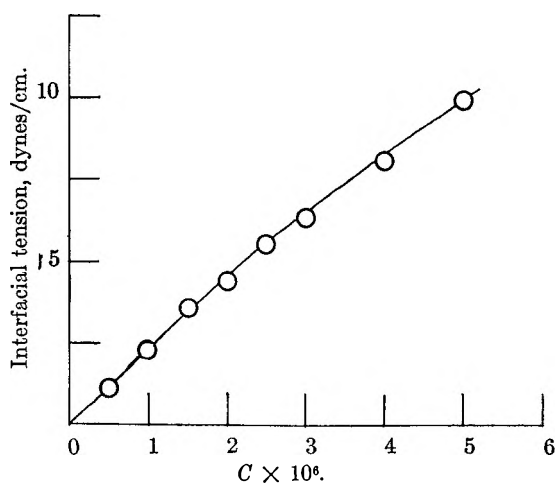


Fig. 4.—Interfacial tension lowering of Nujol-water system as a function of the molar concentration of sodium dodecyl sulfate at pH 1.65 and at an ionic strength of 0.05 (NaCl plus HCl) and at 25°.

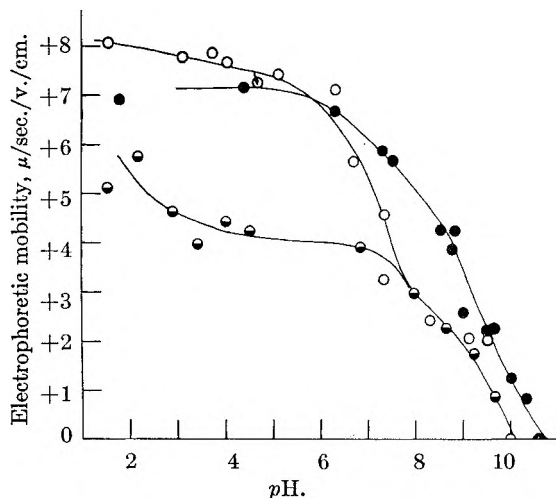


Fig. 5.—Electrophoretic mobilities as a function of pH at an ionic strength of 0.05 (NaCl plus HCl or NaOH) and at 25°; O, Nujol emulsion particles and octadecylamine; \ominus , micelles of octadecylamine; \bullet , solid paraffin particles and octadecylamine.

$$\sigma = \frac{\kappa DRT}{2\pi N\epsilon} \sinh \frac{\zeta e}{2\kappa T} \quad (1)$$

where σ is the electrostatic charge per unit area, κ the Debye-Hückel reciprocal distances, D the dielectric constant, R the gas constant, ϵ the elementary charge, κ the Boltzmann constant and ζ is the potential of the electrical double layer as obtained from electrophoresis.

Gorin⁸ applied a small ion correction to the electrophoretic mobilities of spherical particles. The physical basis for this correction lay in the fact that the small ions not being point charges cannot approach the larger colloidal particles closer than the radius of the small ion; this has the effect of increasing the radius of the colloidal particle by the radius of the ion. The Gorin correction has been discussed by Overbeek⁹ who, apparently, is of the opinion that the small ion correction is somewhat speculative in character. The correction factor⁹ for the finite size of the small ions is

$$f = \frac{1 + \kappa(\tau + a)}{(1 + \kappa\tau)(1 + \kappa a)} \quad (2)$$

Where f is the ratio of the charge on the spherical particle with the small ion correction to that without the small ion correction, τ is the radius of the spherical particle and a is the radius of the small ion. For very large values of $\kappa\tau$ such as employed in the present research eq. 2 reduces to

$$f = \frac{1}{(1 + \kappa a)} \quad (3)$$

According to this conclusion, the right side of eq. 1 should be multiplied by f and this is the form of eq. 1 that Bateman and Zellner¹⁰ use in their calculation of the surface charge of red blood cells. At an ionic strength of 0.05 and at 25° and with a small ion radius of 2.5×10^{-8} cm., f has the value 0.845 and is, therefore, a significant correction.

The electrostatic charge at the oil-water interface has been calculated from the electrophoretic mobilities of the oil droplets both with the use of uncorrected eq. 1 as well as with the aid of the correction factor for the finite size of the small ion (eq. 3).

At pH 1.65 octadecylamine would exist entirely as the ammonium ion and sodium dodecyl sulfate would be completely dissociated. The affinity of these organic ions for the hydrocarbon-water interface must be very much larger than it is for the inorganic ions present. We have, accordingly, assumed that the number of moles of organic ions present at the interface can be calculated directly from the charge per unit area as revealed by eq. 1 and also by a combination of eq. 1 and 3.

The concentrations of the organic ions in solution have been divided by the corresponding number of adsorbed mole ions (N_a) and this ratio plotted against the molar concentrations of the organic ion; this is a suitable procedure for linearizing a Langmuir adsorption plot. The best straight lines through the experimental points have been calculated by the method of least squares.

(8) M. H. Gorin, *J. Chem. Phys.*, **7**, 405 (1939).

(9) J. Th. G. Overbeek, *Advances in Colloid Sci.*, **3**, 125 (1950).

(10) J. B. Bateman and A. Zellner, *Arch. Biochem. Biophys.*, **60**, 44 (1956).

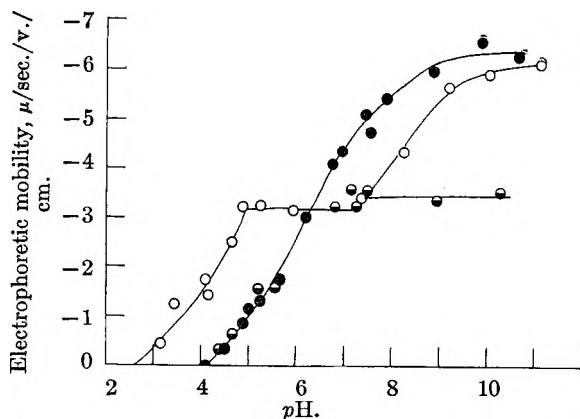


Fig. 6.—Electrophoretic mobilities as a function of pH at an ionic strength of 0.05 (NaCl plus HCl or NaOH) and at 25°; ○, Nujol emulsion particles and stearic acid; ●, micelles of stearic acid-stearate; ●, solid paraffin particles and stearic acid.

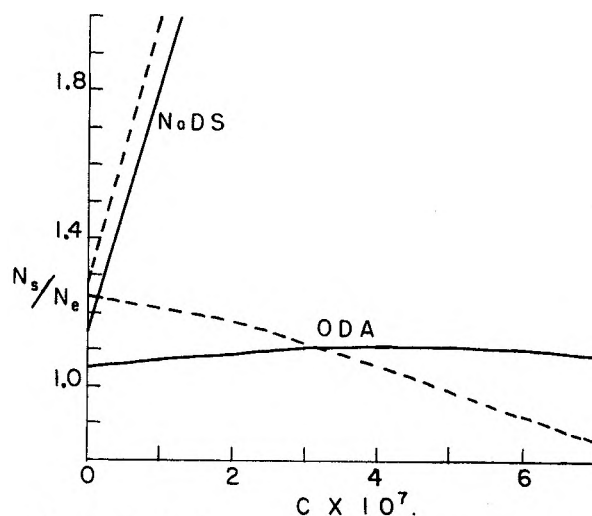


Fig. 7.—Ratio of organic ions per unit area from interfacial tension lowering (N_s) to the number calculated from electrophoresis (N_e) as a function of the molar concentration of sodium dodecyl sulfate (NaDS) and of octadecylamine (ODA) at pH 1.65, ionic strength 0.05 and at 25°. Broken lines include small ion corrections.

The interfacial tension lowerings in dynes per centimeter at the Nujol-water interface have been divided by the corresponding molar concentrations of the organic ions and these ratios have been plotted against the molar concentrations and the least square line calculated. The resulting equations have been differentiated (interfacial tension in respect to concentration). These differentials have been substituted in the Gibbs adsorption equation thus permitting the calculation of the number of moles of adsorbed organic ions (N_a) per unit area as a function of the molar concentration of the organic ions.

Combining the least square equations for N_s and for N_e , the ratio of N_s to N_e as a function of the concentration of octadecylamine and sodium dodecyl sulfate has been plotted in Fig. 7 both with and without the small ion correction. At zero concentration of octadecylamine the ratio N_s/N_e extrapolates to 1.053 ± 0.081 without the small ion correction and to 1.244 ± 0.081 with the small ion correction. The intercept at zero concentration

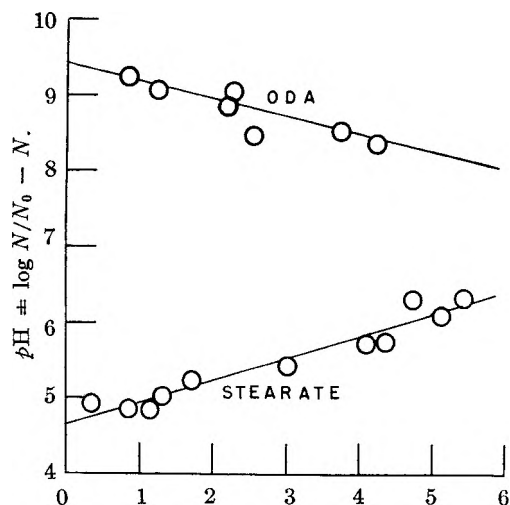


Fig. 8.—Apparent pK as a function of the electrophoretic mobilities of solid paraffin particles with octadecylamine (ODA) and with stearate; ionic strength 0.05 and at 25° .

of sodium dodecyl sulfate is 1.16 ± 0.31 without the small ion correction and is 1.28 ± 0.24 with the correction for the small ions. The results obtained with octadecylamine are much more satisfactory than are those with sodium dodecyl sulfate. The difficulty with the sodium dodecyl sulfate data arises from the erratic electrophoretic results (see Fig. 2). Whereas the interfacial data are certainly statistically consistent with the electrophoretic measurements with sodium dodecyl sulfate, the probable error associated with N_s/N_e at zero concentration is too large to inspire confidence.

Agreement between the techniques is best supported by the octadecylamine data. Here the ratio N_s/N_e approaches unity fairly closely as the concentration approaches zero with a much smaller probable error and furthermore the ratio remains near unity over an appreciable concentration range of the octadecylamine. It is to be noted that the ratio N_s/N_e is closer to unity both for sodium dodecyl sulfate and for octadecylamine if the surface charge is not corrected by including the small ion radii.

Hartley and Roe¹¹ proposed an equation relating the apparent pK of a weak acid at an interface to the electrophoretic mobility. This equation has been used and discussed on several occasions and the following simple derivation serves to illustrate the effect being considered.

The total free energy of ionization of an acid can be separated into two parts such that

$$\Delta F = \Delta F_i + \Delta F_e \quad (4)$$

where ΔF_i is the intrinsic free energy change and ΔF_e is the contribution made by the electrostatic interaction. The electrostatic contribution to the free energy change is simply

$$\Delta F_e = \epsilon \zeta \quad (5)$$

where ϵ is the elementary charge substituting eq. 5 into eq. 4, there results per molecule

$$-kT \ln K = -kT \ln K_i + \epsilon \zeta$$

or

(11) G. S. Hartley and J. W. Roe, *Trans. Faraday Soc.*, **36**, 101 (1940).

$$PK = PK_i + \frac{0.4343 \epsilon \zeta}{kT} \quad (6)$$

In analogy to the expression for the pH of a weak acid, we can write

$$PH = PK + \log \frac{N}{N_0 - N} \quad (7)$$

where N_0 is the number of mole ions per unit area of the surface of the particle at surface saturation and N is the number of mole ions for intermediate stages of ionization corresponding to the existing pH in solution.

Substituting eq. 7 into eq. 6 and introducing numerical values at 25°

$$PH - \log \frac{N}{N_0 - N} = pK_i + 0.217U \quad (8)$$

where U is the electrophoretic mobility in microns per second per volt per centimeter. The sign of the last term on the right of eq. 8 will depend on the sign of the electrostatic charge on the particle. For a negative particle the sign is positive whereas if the particle is positive the sign is negative (for the ionization of protons).

It is to be noted from Figs. 5 and 6 that the mobility- pH curves for micelles of the organic ions as well as those for Nujol particles have pronounced inflections in them; it is probable that phase changes have occurred in the surface layers in response to changes in state of ionization. The solid paraffin particles, however, appear to exhibit mobility- pH curves resembling titration curves. Assuming that the largest mobility observed corresponds in the case of stearic acid to complete ionization of the stearic acid at the interface and that the largest mobility for the octadecylamine-paraffin emulsion represents maximal formation of the ammonium ion, we have plotted in Fig. 8 the function $pH - \log [N/(N_0 - N)]$ (the apparent pK) for stearic acid and $pH + \log [N/(N_0 - N)]$ (the apparent pK) for octadecylamine against the electrophoretic mobilities. For convenience of plotting, we have neglected the sign of the electrophoretic mobility. By the nature of the function $N/(N_0 - N)$ is very sensitive to the value of N_0 when N is large and becomes very much less so as N decreases. Omitting the experimental points for large values of N , the least square line through the remaining experimental points give slopes of $+0.292 \pm 0.017$ and -0.224 ± 0.041 for stearic acid and for octadecylamine, respectively. The slope according to theory should be ± 0.217 . The intrinsic pK of stearic acid is 4.65 and that for octadecylamine is 9.41. It is clear that the equation of Hartley and Roe is in fairly close agreement with experiment.

The maximum charge density for both octadecylamine and for stearate surfaces is surprisingly small and corresponds to an area of about 300 sq. Å. per ion.

The results described above both in respect to the calculation of the charge density and to the work of charging the electrical double layer as expressed by the equation of Hartley and Roe tend to confirm the reality of the conception of the zeta potential and indicate that the values of the coef-

ficient of viscosity and of the dielectric constant in the electrical double layer are not greatly different from what they are in bulk solution.

Acknowledgment.—Financial support for this research was provided by the National Science Foundation for which we wish to express our thanks.

SOME THERMODYNAMIC PROPERTIES OF SOLID BISMUTH CHLORIDES¹

By A. J. DARNELL AND S. J. YOSIM

Atomics International, A Division of North American Aviation, Inc., Canoga Park, California

Received February 10, 1959

The thermodynamic stability of solid BiCl with respect to its disproportionation products, Bi(s) and BiCl₃(g), has been determined from 127 to 242°. This was accomplished by measuring the pressure of BiCl₃ gas over the solid subhalide and over pure BiCl₃ by the Knudsen technique. The pressures of BiCl₃ from the sublimation and disproportionation reactions are, respectively, $\log P_{\text{BiCl}_3} = (-6200 \pm 30)/T + 9.95 \pm 0.07$ and $\log P_{\text{BiCl}_3} = (-6360 \pm 60)/T + 9.29 \pm 0.14$. These results show that the subchloride is barely stable with respect to its solid disproportionation products. At 298°K. the ΔH^0 , ΔF^0 and ΔS^0 of formation of BiCl(s) are, respectively, -30.4 kcal./mole, -24.0 kcal./mole and -18.0 e.u. New values for ΔF^0_{form} , ΔS^0_{form} and S^0 of BiCl₃(s) were calculated and are, respectively, -73.6 kcal./mole, -57.1 and 36.4 e.u.

Introduction

The bismuth chlorides consist of bismuth trichloride, BiCl₃, and the subhalide, BiCl.² The dichloride, BiCl₂,³ appears to be unstable by disproportionation⁴ while the existence of the tetrachloride⁵ has not been confirmed.

Bismuth trichloride is a colorless salt, melting at 232° and boiling at 447°. Bismuth subchloride is not as well known. It was first isolated by Eggink⁶ who determined the compound to have a chlorine to bismuth ratio of unity. At 320°, the solid subchloride disproportionates to form two immiscible solutions, a black salt-rich phase with an over-all composition of 47 mole % bismuth and 53 mole % BiCl₃, and a metal-rich phase consisting of 99 mole % bismuth and 1 mole % BiCl₃.⁶ Some of the physical and chemical properties of BiCl have been described by Corbett.⁷

Recently there has been some question concerning the stability of BiCl. Brewer⁴ suggested that if BiCl exists in the solid form, it is just barely stable toward disproportionation and, therefore, has about the same free energy of formation per equivalent as the trichloride. However, Sokolova,⁸ who studied BiCl by X-ray techniques at room temperature concluded that it was unstable. This was based on the fact that after the compound was formed, predominant lines, which were attributed to BiCl, became quite weak in 20 minutes. Corbett⁷ determined that BiCl was inert in dry air, and attributed Sokolova's results to excessive impurities. Therefore, it was of interest to determine the thermody-

amic stability of BiCl with respect to its solid disproportionation products, Bi and BiCl₃.

An earlier experiment in this Laboratory showed that the gas phase over solid BiCl was essentially BiCl₃ gas. Thus, by studying the sublimation pressure of BiCl₃ and the pressure of BiCl₃ over solid BiCl, the stability of BiCl with respect to its solid disproportionation products could be determined. Therefore, a series of vaporization experiments was carried out to determine the thermodynamic stability of BiCl. In addition to the stability of BiCl, the heat and entropy of sublimation of BiCl₃ and the heat of fusion of BiCl₃ were obtained.

The absolute entropy, the entropy and free energy of formation of solid BiCl₃⁹ are based, in part, on the entropy of fusion of BiCl₃.¹⁰ Since, as will be shown later, this value may be in error, new values for S^0 , ΔS^0_{form} and ΔF^0_{form} of BiCl₃ were calculated from the sublimation data.

Experimental

Materials.—Reagent grade bismuth was melted under an inert atmosphere and filtered through Pyrex glass wool to remove bismuth oxide. Reagent grade bismuth trichloride was dried under a current of HCl gas, distilled under HCl and then under argon. The first and last eighths of the distillate were discarded. The salt had a melting point of 232.2°. A bismuth and chlorine analysis of the salt showed a 66.2 ± 0.1 weight % bismuth as compared to 66.27% theoretical.

Bismuth subchloride, free of BiCl₃, could not be synthesized simply by direct combination of BiCl₃ with excess bismuth, as was also noted by Corbett.⁷ Therefore, the excess BiCl₃ was removed by sublimation. The BiCl used in this investigation was prepared from a mixture originally consisting of 80 mole % bismuth and 20 mole % BiCl₃, heated in a sealed Pyrex tube with continuous mixing for two days at 305°. This process converted approximately 85% of the BiCl₃ into BiCl. Most of the unreacted bismuth "lumps" were mechanically removed. Since one of the products of the reaction studied was solid bismuth, it was not necessary to remove completely the unreacted bismuth.

Pressure Measurements.—The vapor pressure of solid BiCl₃ at the temperatures of interest is in the range where the effusion technique is applicable. The experimental apparatus was similar to that used by Farber and Darnell,¹¹ in their

(1) This paper was supported by the Atomic Energy Commission, and has been presented in part before the Division of Physical Chemistry at the National Meeting of the ACS in April, 1958.

(2) Solid bismuth subchloride is referred to, in this paper, as BiCl, although it is possible that, like Hg₂Cl₂, the cations of this subhalide are dimerized, or form higher polymers.

(3) R. Schneider, *Ann. Physik.*, **96** 130 (1855); R. Weber, *ibid.*, **107**, 596 (1859); P. Muir, *J. Chem. Soc.*, **29**, 144 (1876).

(4) L. Brewer, "The Chemistry and Metallurgy of Miscellaneous Materials—Thermodynamics," L. L. Quill, Ed., NNES IV-19B, McGraw-Hill Book Co., New York, N. Y., 1950.

(5) B. G. Eggink, *Z. physik. Chem.*, **64**, 449 (1908).

(6) S. J. Yosim, A. J. Darnell, W. G. Gehman and S. W. Mayer, *THIS JOURNAL*, **63**, 230 (1959).

(7) J. D. Corbett, *J. Am. Chem. Soc.*, **80**, 4757 (1958).

(8) M. A. Sokolova, G. G. Urazov and V. G. Kuznetsov, *Akad. Nauk, S.S.S.R. Inst. Gen. Inorg. Chem.*, **1**, 102 (1954).

(9) F. D. Rossini, D. D. Wagman, W. H. Evans, S. Levine and I. Jaffe, "Selected Values of Chemical Thermodynamic Properties," National Bureau of Standards, Circular 500, 1952.

(10) K. K. Kelley, U. S. Bureau of Mines, Bulletin 393, Washington, D. C. (1936).

(11) M. Farber and A. J. Darnell, *THIS JOURNAL*, **59**, 156 (1955).

study of the lower halides of titanium. In that and in this work, a small portable dry box was attached to the vacuum manifold. Thus, the material studied was never exposed to the atmosphere. The effusion cells in this study were made of Pyrex glass 1.5 cm. in diameter by 4.5 cm. in length. The lids were also of Pyrex except in the case where a very small orifice was desired, in which case a platinum lid, sealed to the cell with AgCl, was used. Orifice areas were measured with a microscope and were also calibrated by vaporization of mercury. Temperatures were measured with a chromel-alumel thermocouple inserted in a thermocouple well in the cell. The quantity of effused material was determined from the weight loss of the cell contents during each run.

Pressures of BiCl₃ were calculated by the Knudsen equation¹² which included a Clausing¹³ factor to correct for the non-ideality of the orifice. Since BiCl₃ gas is known to be essentially monomeric,¹⁴ 315 was used as the molecular weight.

Initially, due to the presence of excess BiCl₃, the vapor pressure of the mixture was equal to that obtained for pure BiCl₃. When about 15% of the material in the cell had effused, the pressure became constant at a value approximately one tenth that of pure BiCl₃. X-Ray diffraction patterns of the material remaining in the Knudsen cell showed a set of lines which agreed with the pattern of BiCl obtained by Corbett⁷ but disagreed with the pattern reported by Sokolova,⁸ *et al.* The assumption that BiCl₃ was the predominant gaseous species was verified by determining a Cl/Bi ratio of the effusate and by comparing the weight of the effusate with the weight loss of the sample. The results indicated that the gas consisted of more than 99% BiCl₃.

Within the experimental error, the pressures obtained for the disproportionation process were independent of orifice area indicating that equilibrium pressures were attained in the cell.

Results

The results for the pressures of BiCl₃ for the sublimation and disproportionation processes are shown in Tables I and II.

TABLE I
SUBLIMATION PRESSURE OF BiCl₃
BiCl₃(s) → BiCl₃(g)

Temp., °K.	Time int., sec.	Wt. loss, g.	Orifice	Pressure, atm.
371	4.10 × 10 ⁵	0.0247	a	1.90 × 10 ⁻⁷
394	5.76 × 10 ⁴	.0280	a	1.58 × 10 ⁻⁶
395	1.56 × 10 ⁵	.0776	a	1.62 × 10 ⁻⁶
415	7.25 × 10 ⁴	.2172	a	9.98 × 10 ⁻⁶
416	4.72 × 10 ⁴	.1548	a	1.09 × 10 ⁻⁵
416	7.50 × 10 ⁴	.2333	a	1.04 × 10 ⁻⁵
435	4.14 × 10 ³	.0589	a	4.85 × 10 ⁻⁵
435	3.90 × 10 ³	.0572	a	5.00 × 10 ⁻⁵
456	4.68 × 10 ³	.3110	a	2.32 × 10 ⁻⁴
457	4.08 × 10 ³	.2717	a	2.33 × 10 ⁻⁴
468	4.38 × 10 ³	.6446	a	5.21 × 10 ⁻⁴

^a Orifice area, 0.0152 cm². Clausing factor 0.51.

A least-squares analysis of the sublimation pressure ($P^0_{\text{BiCl}_3}$) data and of the disproportionation pressure (P_{BiCl_3}) data yielded, respectively

$$\log P^0_{\text{BiCl}_3} = \frac{-6200 \pm 30}{T} + 9.95 \pm 0.07 \quad (371-468^\circ\text{K.}) \quad (1)$$

$$\log P_{\text{BiCl}_3} = \frac{-6360 \pm 60}{T} + 9.29 \pm 0.14 \quad (400-515^\circ\text{K.}) \quad (2)$$

The heat and entropy of sublimation for solid BiCl₃ was calculated from equation 1 to be 28.4 ± 0.1 kcal./mole and 45.2 ± 0.3 e.u., respectively.

(12) M. Knudsen, *Ann. Physik*, **29**, 179 (1909).

(13) P. Clausing, *ibid.*, **12**, 961 (1932).

(14) D. Cubicciotti, F. Keneshea, Jr., and C. Kelley, *This Journal*, **62**, 463 (1958).

TABLE II

PRESSURES OF BiCl₃ FROM DISPROPORTIONATION OF BiCl(s)

Temp., °K.	Time int., sec.	Wt. loss, g.	3BiCl(s) → 2Bi(s) + BiCl ₃ (g)	
			Orifice	Pressure, atm.
400	2.36 × 10 ⁵	0.0178	a	2.47 × 10 ⁻⁷
412	4.54 × 10 ⁴	.0136	a	9.93 × 10 ⁻⁷
419	8.46 × 10 ⁴	.0359	a	1.42 × 10 ⁻⁶
419	8.01 × 10 ⁴	.0310	a	1.30 × 10 ⁻⁶
427	5.90 × 10 ⁴	.0775	b	2.16 × 10 ⁻⁶
429	5.58 × 10 ⁴	.0464	a	2.82 × 10 ⁻⁶
431	7.45 × 10 ⁴	.1299	b	2.89 × 10 ⁻⁶
437	6.11 × 10 ⁴	.2117	b	5.78 × 10 ⁻⁶
437	6.00 × 10 ⁴	.0919	a	5.24 × 10 ⁻⁶
446	4.82 × 10 ⁴	.1543	a	1.11 × 10 ⁻⁵
446	1.08 × 10 ⁴	.0299	a	9.56 × 10 ⁻⁶
449	5.40 × 10 ⁴	.0700	c	1.76 × 10 ⁻⁶
457	5.28 × 10 ⁴	.3968	a	2.62 × 10 ⁻⁶
458	4.56 × 10 ³	.0358	a	2.75 × 10 ⁻⁶
459	4.80 × 10 ³	.0366	a	2.67 × 10 ⁻⁶
461	8.70 × 10 ³	.0756	a	3.05 × 10 ⁻⁶
473	6.06 × 10 ³	.1281	a	7.15 × 10 ⁻⁶
474	2.40 × 10 ³	.0453	a	6.72 × 10 ⁻⁶
493	1.06 × 10 ⁴	.1933	c	2.59 × 10 ⁻⁴
515	3.54 × 10 ³	.2347	c	9.64 × 10 ⁻⁴

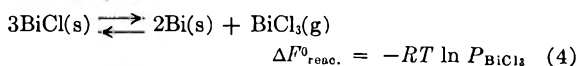
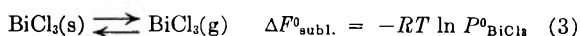
^a Orifice area = 0.0152 cm². Clausing factor 0.513.

^b Orifice area = 0.0227 cm². Clausing factor 0.700. ^c Orifice area = 0.00208 cm². Clausing factor 0.952.

In order to obtain the heat of fusion of BiCl₃, the heats of sublimation and vaporization were calculated at the melting point. Applying a ΔC_p estimate¹⁵ of -10.4 to the heat of sublimation obtained in this work (28.4 kcal. at the mid-temperature, 420°K.) yielded a value of 27.3 kcal. at the melting point. Applying a ΔC_p of -12.8¹⁶ to the heat of vaporization (20.4¹⁴ kcal. at 533°K.) resulted in a value of 20.8 kcal. Thus, the resulting heat of fusion of BiCl₃ is 6.5 kcal./mole.

The absolute entropy of solid BiCl₃ at 298°K. was calculated from the absolute entropy of the gas ($S^0 = 85.5$ e.u.)¹⁶ and the entropy of sublimation of BiCl₃ at 298°K. ($\Delta S_{\text{subl.}} = 49.1$). The latter was obtained by applying a ΔC_p correction of -10.4 to the entropy obtained from equation 1. Combining the value of the absolute entropy of solid BiCl₃ ($S^0_{\text{BiCl}_3} = 36.4$ e.u.) with the absolute entropy of solid bismuth and chlorine gas¹⁷ yields an entropy of formation of BiCl₃ of -57.1 e.u. The free energy of formation of solid BiCl₃ was calculated from Thomsen's¹⁸ value for the heat of formation of solid BiCl₃ ($\Delta H^0_{\text{form}} = 90.6$ kcal.) to be -73.6 kcal./mole.

Assuming no solid solution between Bi and BiCl, the stability of BiCl(s) with respect to Bi(s) and BiCl₃(s) can be determined from these considerations



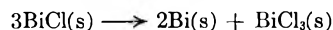
(15) O. Kubaschewski and E. Evans, "Metallurgical Thermochemistry," John Wiley and Sons, Inc., New York, N. Y., 1956.

(16) K. K. Kelley, U. S. Bureau of Mines, Bulletin No. 434, 1940.

(17) D. Stull and G. Sinke, "Thermodynamic Properties of the Elements," American Chemical Society, Washington, D. C., 1956.

(18) J. Thomsen, "Thermochemische Untersuchungen," Barth, Leipzig, 1882-1886.

Subtracting (3) from (4)



$$\Delta F^0_{\text{disprop}} = RT \ln \frac{P^0_{\text{BiCl}_3}}{P_{\text{BiCl}_3}} \quad (5)$$

Therefore, the standard free energy change per chlorine for (5), *i.e.*, the standard free energy of disproportionation ($\Delta F^0_{\text{disprop}}$) of $\text{BiCl}(s)$ to $2/3\text{Bi}(s)$ and $1/3\text{BiCl}_3(s)$, is

$$\Delta F^0_{\text{disprop}} = \frac{1}{3}\Delta F^0_{\text{form. BiCl}_3(s)} - \Delta F^0_{\text{form. BiCl}(s)} = 1.53T \log \frac{P^0_{\text{BiCl}_3}}{P_{\text{BiCl}_3}} \quad (6)$$

Substituting (1) and (2) in (6)

$$\Delta F^0_{\text{disprop}} = (0.245 \pm 0.102) + (0.00101 \pm 0.00024)T \text{ kcal./BiCl} \quad (7)$$

The enthalpy of the reaction of 1 mole of solid BiCl to yield solid Bi and solid BiCl_3 is obtained by the usual $\partial\Delta F/T/\partial 1/T$ and is 0.245 ± 0.102 kcal. while the entropy of the above reaction is obtained from the equation

$$\Delta S^0 = \frac{\Delta H^0 - \Delta F^0}{T} = -1.01 \pm 0.24 \text{ e.u.} \quad (8)$$

The thermodynamic values for the disproportionation reaction at the mid-temperature, $\sim 450^\circ\text{K}$., are

$$\Delta F^0_{450^\circ\text{K}} = 0.700 \pm 0.144 \text{ kcal./BiCl} \quad (9)$$

$$\Delta H^0_{450^\circ\text{K}} = 0.245 \pm 0.102 \text{ kcal./BiCl} \quad (10)$$

$$\Delta S^0_{450^\circ\text{K}} = -1.01 \pm 0.24 \text{ e.u./BiCl} \quad (11)$$

If the small heat capacity corrections ($\Delta C_p \sim 0.1$ cal./mole $^\circ$) are neglected, the values at 298°K . obtained are

$$\Delta F^0_{298} = 0.546 \pm 0.125 \text{ kcal./BiCl} \quad (12)$$

the other values being unchanged.

Using the above data for the formation of BiCl_3 , the formation of 1 mole BiCl from the elements at 298°K ., was calculated, and the results are compared with those of BiCl_3 in Table III.

TABLE III
THE FORMATION OF SOLID BISMUTH HALIDES

	$\Delta F^0_{\text{form. kcal.}}$	$\Delta H^0_{\text{form. kcal.}}$	$\Delta S^0_{\text{form. e.u.}}$
$\frac{1}{3}\text{BiCl}_3$	-24.5	-30.2	-19.0
BiCl	-25.0	-30.4	-18.0

Discussion of Results

The pure BiCl_3 sublimation pressure reported in this work is considerably lower than that of Maier,¹⁹

who measured the pressure of both liquid and solid BiCl_3 by a static method. However, his values for the vapor pressure of liquid BiCl_3 in the lower temperature region (below 340°) are considerably higher than those of other workers,^{14,20} and thus, it is reasonable to suspect that his sublimation pressures are too high. The vapor pressure obtained by extrapolation of equation 1 to the melting point (4.68×10^{-3} atm. at 232°) is in good agreement with the pressure obtained from the extrapolation of the data of Cubicciotti, *et al.*, for the liquid (4.80×10^{-3} atm. at 232°). The equation of Kelley²¹ gives 3.93×10^{-3} atm. at this temperature.

Since the heat of fusion of BiCl_3 was the difference of two large numbers, this value is admittedly inexact. Nevertheless, this number is considerably greater than the value of 2.6 kcal./mole accepted in the literature.^{4,10} However, the latter value was selected¹⁰ on the basis of phase diagrams of systems consisting of BiCl_3 and solutes, such as bismuth, ferric chloride and cuprous chloride. The heat of fusion of BiCl_3 was calculated with certain assumptions as to the identity of these species. Preliminary cryoscopic experiments with different solutes, carried out in this Laboratory, indicate that the heat of fusion of BiCl_3 lies between these extreme values.²²

It appears that BiCl , as Brewer⁴ suggested, is just barely stable toward disproportionation and has indeed about the same free energy of formation per chlorine as solid BiCl_3 . While the thermodynamic values for the disproportionation of BiCl have large uncertainties relative to the small values, these uncertainties are quite small relative to the values for the formation of the subhalide from the elements. Thus, the accuracy for the formation values for BiCl is limited to the accuracy of the formation values of BiCl_3 . A repeat of Thomsen's calorimetric determination or a determination of the ΔF^0_{form} of BiCl_3 by an independent method would be desirable.

Acknowledgment.—The authors wish to acknowledge the assistance of Mr. J. A. Rubin in carrying out the experimental work.

(19) C. G. Maier, U. S. Bureau of Mines, Tech. Paper No. 360, 1925.

(20) E. V. Evnevich and V. A. Sukhodskii, *J. Russ. Phys. Chem. Soc.*, **61**, 1503 (1929).

(21) K. K. Kelley, U. S. Bureau of Mines Bulletin No. 383, 1935.

(22) L. E. Topol and S. W. Mayer, Abstracts of Papers, ACS Meeting, Chicago, Ill., Sept. 1958.

RADIOTRACER STUDIES OF ZINC-ZINC ION EXCHANGE

BY CECIL V. KING AND SHELDON EVANS

*Department of Chemistry, New York University, New York, N. Y.**Received February 27, 1959*

Measurements have been made of the rate and extent of acquisition of radioactivity by zinc coupons when immersed in solutions of zinc perchlorate containing Zn^{65} as tracer. Air-saturated and deaerated solutions were used, as well as neutral and acid solutions containing dichromate as corrosion inhibitor. Activity pickup is much greater in the presence of air, due to the formation of solid corrosion products. Exchange is very small in the presence of dichromate, and even pretreatment with dichromate or chromic acid inhibits exchange. In deaerated solutions of $Zn(ClO_4)_2$ corrosion is very slow, and the continuing activity pickup is ascribed to self-diffusion within the metal. Calculated diffusion coefficients are too large, which may be the result of applying the theory of homogeneous diffusion to polycrystalline specimens.

Measurements of zinc-zinc ion exchange reported in the literature have been, for the most part, qualitative in nature, and have not solved the problems presented by dissolution and corrosion, crystal nature of the metal or possible adsorption of ions at the interface. Not much is known about the mechanism of exchange, or the relation of this mechanism to values of the exchange current. The present work is only semi-quantitative in nature and does not answer all these questions. However, it does show some of the factors which must be taken into account in future work if measurements are to be interpreted in terms of rates and mechanism.

It was first shown by Rollin¹ that zinc does exchange, by shaking zinc powder with $ZnCl_2$ solution containing Zn^{65} as tracer. The metal became radioactive; little more than this fact was shown. The experiments were done in the presence of air, and the metal corroded somewhat.

Haenny and Mivelaz² rotated zinc coupons at 900 r.p.m. in radioactive $ZnSO_4$ solutions, in the presence of air, and found that the activity acquired by the metal reached an apparent maximum in 2 or 3 hr. On reimmersing in inactive $ZnSO_4$ little or no activity was lost. The authors concluded that the activity was sealed in an oxide layer, which does not exchange with the solution. Dissolving a layer less than 25μ thick in HCl removed all the activity. The experiments do not really tell whether exchange is involved, or only precipitation of zinc ion from solution, due to corrosion.

Matsuura³ shook powdered zinc with active $ZnSO_4$ solution and showed that the activity of the solution decreased to a minimum in about 50 hr. In similar experiments with zinc sheet, the activity of the solution decreased 40-75% and apparent equilibrium was reached in 200 hours; a plot of $\log(1 - F)$ was linear with time, where F is the ratio of activity lost from the solution at time t , to activity lost during 200 hr. (However, the zinc metal had not come to true equilibrium with the solution, *i.e.*, the ratio of active to inactive zinc was not the same in the two phases. The experiments apparently were conducted with air present, so we do not know the relative importance of corrosion.)

Matsuura points out that self-diffusion within the metal is an important factor in the exchange.

He does not give details in the paper cited³ but states that from experiments with electropolished zinc specimens the value of D , the self-diffusion coefficient, was estimated to be about 10^{-12} cm.²/sec. The author says that such a large value, at room temperature, is only possible in a solid of extremely disordered crystal lattice.

A few experiments on $Zn-Zn^{++}$ exchange with single crystals have been carried out.⁴ After immersion in 0.03 M Zn^*SO_4 , it was found that the prism facets had acquired some 10% more activity than the base facets. There is a definite difference in electrical potential, the prism facets being more anodic.

The present work with zinc was undertaken to learn more about the metal-solution interface in the case of an active metal; the effect of corrosion with air present and the much slower corrosion in the absence of air; the effect of corrosion inhibitors and cathodic protection; the role of internal diffusion and possible adsorption on the metal. The possible mechanisms by which a metal can acquire activity in a labeled solution of its own ions have been discussed elsewhere⁵; other factors than simple exchange must be considered.

Experimental

Zinc disks 3.74 cm. in diameter were cut from 99.99% pure sheet, 0.05 cm. thick. A small hole in the center served to mount the disk on a motor shaft or to suspend it on a glass hook. The disks were usually polished with No. 600 silicon carbide paper, washed and dried with alcohol and ether. Some were annealed at 110° and etched as described later.

Zn^{65} was obtained as $ZnCl_2$ in HCl. Since preliminary experiments showed that $Zn(ClO_4)_2$ is less corrosive than the chloride, sulfate or acetate, HCl was expelled from the active solution by repeated evaporation. Small amounts of tracer were added to solutions of inactive $Cd(ClO_4)_2$ which were then diluted to final concentration. Measurements were made with a thin mica window GM tube, with conventional scaler and shielding. The activity was high enough to make counting errors small except as described below. Counts were converted to gram atoms of pickup per cm.² by comparison with evaporated samples of the solutions. Since appreciable radiation penetrated the disks (Zn^{65} is a positron- and γ -emitter), both sides of the calibration disks were counted and the sum taken, or solution was evaporated on both sides and the average count taken. Since both sides of the experimental disks were exposed to the solution, both sides were counted and the average taken. The disks were immersed in 100 ml. of 0.01 M $Zn(ClO_4)_2$ at room temperature (about 23°). To deaerate, nitrogen was passed over hot copper, then through water and through the solution cell for 1 hr. before introducing a coupon.

(1) B. V. Rollin, *J. Am. Chem. Soc.*, **62**, 86 (1940).
 (2) C. Haenny and P. Mivelaz, *Helv. Chim. Acta*, **31**, 633 (1948).
 (3) N. Matsuura, *Sci. Papers, Coll. Gen. Educ., Univ. Tokyo*, **5**, 97 (1955).

(4) B. N. Bushmanov and G. S. Vozdvizhenskii, *Doklady Akad. Nauk SSSR*, **114**, 1046 (1957); in English translation, *Proc. Acad. Sci. U.S.S.R., Sect. Phys. Chem.*, **114**, 397 (1957).

(5) C. V. King and N. E. McKinney, *Can. J. Chem.*, **37**, 205 (1959).

Air-saturated vs. Deaerated Solutions.—Figure 1 shows the activity pickup on single immersions up to 1 hr. in the two cases. Two to four disks were used for each point, and the vertical lines indicate the reproducibility. Multiple immersions gave similar results, *i.e.*, the activity acquired in air-saturated solution was 5 or 6 times as great as in deaerated solution. Long immersion in the presence of air (up to 280 hr.) led to weight gains of as much as 10 mg. per coupon (of 22 cm.² area). The disks became dull gray with many white spots, which proved to be corrosion products covering deep pits.

The pickup in deaerated solution was somewhat larger for repeated short immersions, with 2-minute cold water washing, than for a single immersion of the same total time. The behavior is much like that of silver.⁶ Complete exchange in one atomic layer corresponds to about 2.7×10^{-9} gram atoms/cm.², and the exchange in a single short immersion corresponds to about 3 apparent layers. This may indicate a roughness factor of 3, with rapid exchange in one layer. The exchange current evidently is large.

In deaerated solutions the coupons remained bright up to 48 hr. On immersion up to 250 hr. they became slightly dull, but the brightness was restored by dipping in 0.01 M K₂Cr₂O₇, which removed a few per cent. of the activity. In the range of 4–24 hours the measured activity became erratic ($\pm 50\%$). In the range 48–250 hr. the acquired activity varied as much in amount, but this was a smaller per cent. of the total.

If continuing pickup is due entirely to homogeneous diffusion within the metal, the activity should be linear with the square root of time. The actual plots show continuous upward curvature with slopes from 2×10^{-10} to 9.5×10^{-9} gram atoms cm.⁻² sec.^{-1/2}. This is analogous to the corresponding curves for silver.⁷

Re-exchange.—On immersion of active disks in inactive solution some activity is lost, the rate evidently depending on the previous depth of penetration within the metal. Given sufficient time, the active atoms obviously must distribute themselves in the same ratio (to inactive atoms) throughout the metal and the solution.

Effect of Dichromate.—Chromates and dichromates can inhibit the corrosion of zinc; for example, a zinc cylinder has been rotated for 48 hr. without weight loss, in 0.5 M acetic acid containing 0.06 M KNO₃ and 0.01 M K₂Cr₂O₇.⁸ The metal dissolves rapidly in the same solution of acid and nitrate, without dichromate. Zinc perchlorate does not destroy the protection, but other anions do, as shown in Table I. The potentials found are all polarized, since the reversible potential is about 1.03 volt; the values remained about the same in the least corrosive solutions but rose with time to about 1 volt in corrosive solutions. The solutions were not deaerated.

TABLE I

CORROSION OF ZINC DISKS ROTATED IN SOLUTIONS CONTAINING 0.5 M ACETIC ACID, 0.01 M K₂Cr₂O₇. *E* vs. SATD. KCL CALOMEL CELL

Zn salt 0.01 M	KNO ₃ , M	<i>E</i> , v.	Wt. loss, mg.	Time, hr.
...	...	0.65	0	48
ZnAc ₂ ^a	0.06	.70	0.4	5
ZnCl ₂	0.06	.74	31	3
ZnSO ₄88	45	7 min.
Zn(ClO ₄) ₂72	0	48
Zn(ClO ₄) ₂60	0	24

^a Acetate.

Zinc disks, polished with No. 600 silicon carbide paper, were immersed in solutions containing radioactive Zn(ClO₄)₂ and K₂Cr₂O₇, as shown in Table II. The disks remained bright and there was no weight loss in any of the runs. The radioactive counts were only 10–20 c.p.m. above background, corresponding to about 1/3 atomic layer. It is evident that the film which prevents corrosion, whatever its nature, also inhibits exchange.

(6) C. V. King and A. Simonsen, *J. Electrochem. Soc.*, **104**, 194 (1957).

(7) H. Gerischer and R. P. Tischer, *Z. Elektrochem.*, **58**, 819 (1954).

(8) C. V. King and E. Hillner, *J. Electrochem. Soc.*, **101**, 79 (1954).

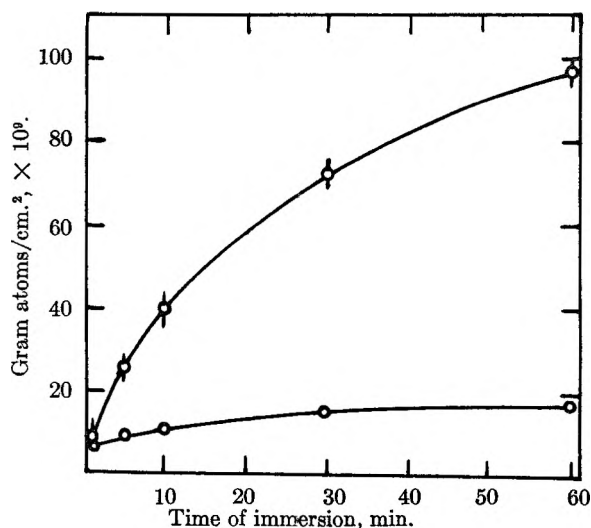


Fig. 1.—Activity acquired by zinc disks on single immersions in 0.01 M Zn(ClO₄)₂: upper curve, air-saturated solution; lower curve, deaerated solution.

TABLE II

PICKUP FROM 0.01 M Zn(ClO₄)₂, 0.01 M K₂Cr₂O₇, GRAM ATOMS $\times 10^9$ /CM.²

HAc, M	KNO ₃ , M	Time, hr.	Activity
...	...	1	0.86
...	...	12	0.90
...	...	24	1.02
0.5	...	1	0.90
.5	...	26	.90
.5	0.06	3	.90
.5	0.06	20	.90

A number of zinc disks were etched in a chromic acid solution used to show grain structure.⁹ Some of these disks had been annealed *in vacuo* at 110°, which resulted in the formation of large crystals around the edges and center holes. The etched disks were washed, dried and then immersed in active Zn(ClO₄)₂ solution. The activity picked up in 10–60 minutes corresponded to about 0.45×10^{-9} gram atoms/cm.², independent of the exact treatment or time. A brief dip in dilute HClO₄-KNO₃ solution restored the ability to pick up the normal 70×10^{-9} gram atoms/cm.² in 30 minutes (in air-saturated solution).

Similar inhibition to exchange was conferred by 30-minute immersion in 0.01 M K₂Cr₂O₇ alone, or in 0.5 M acetic acid containing 0.01 M K₂Cr₂O₇, followed by washing.

Other Experiments with Dichromate.—Coupons which had been made active by short immersion lost much of their activity on immersion in K₂Cr₂O₇ solution, as shown in Table III. The gases (O₂, H₂, N₂) were bubbled through the solutions for 1 hr. in advance. It is of interest that coupons activated in air or oxygen lost so much of their activity; while those treated in hydrogen acquired twice as much activity as those treated in nitrogen and also retained more. The point of main interest is that dichromate always dissolves some zinc, releasing it to the solution, and does this within a few seconds. When activated coupons were immersed in 0.01 M potassium chromate (which has a higher pH than the dichromate), much less activity was removed, even on standing several hours.

Cathodic Polarization.—To simulate conditions of cathodic protection, zinc disks were rotated in active 0.01 M Zn(ClO₄)₂ and polarized cathodically. A silver anode in KCl solution was separated from the cell by an agar bridge. Currents of even a few microamperes/cm.² led to weight gains and to greatly increased pickup. The weight gains were 3 to 5 times greater than the weight of zinc corresponding to the activity count; evidently the solution at the inter-

(9) C. J. Smithells, "Metals Reference Book," Interscience Publishers, Inc., New York, N. Y., 1949, p. 267.

TABLE III

COUPONS IMMERSSED 30 MIN. IN 0.01 M $Zn(ClO_4)_2$ IN VARIOUS ATMOSPHERES, THEN IN 0.01 M $K_2Cr_2O_7$, GRAM ATOMS $\times 10^9$

Atm.	Activity	Min. in $K_2Cr_2O_7$	Remaining activity
Air	76	30	1.2
	77	2	0.9
	69, 69	2	0.9, 0.7
O ₂	72	2	1.6, 1.6
	H ₂	36, 39	2
35		2.5	10
32		0.5	13
N ₂	17, 17	2	4.4, 3.7
	16	0.5	4.7
	18	5	4.8

face becomes alkaline and a hydrated oxide precipitates. Matsuura mentions similar results of cathodic polarization.⁸

Discussion

In the presence of air it is evident that corrosion takes place with oxygen reduction and that much of the activity pickup is due to precipitation of zinc ion from solution, on cathodic areas. This does not involve metal-metal ion exchange.

The lack of activity pickup in the presence of dichromate or after treatment with chromic acid or dichromate could indicate either that an impermeable oxide film is formed or that all adsorption sites are firmly occupied by a chromium compound. The metal does not become passive; in fact, after etching with chromic acid the potential in dilute $Zn(ClO_4)_2$ was close to 1 volt *vs.* the calomel cell. Dissolution of a trace of zinc by dichromate does not establish either mechanism, since ordinary oxide might dissolve in the slightly acid solution, dichromate might be reduced to form a different oxide film, or both processes might occur simultaneously. The smaller effect of the chromate may favor the adsorption mechanism, preceded by oxide dissolution.

In deaerated solutions it is evident that exchange in depth takes place and that the process is controlled by the rate of self-diffusion within the metal. If conditions were sufficiently simple, it would be possible to calculate the self-diffusion coefficient. The equations for homogeneous diffusion with boundary conditions as in the present case are discussed by Darken and Gurry.¹⁰ Total activity acquired as a function of time is given by the equation

$$a_t = 2a_0(Dt/\pi)^{1/2} \quad (1)$$

where a_t is the activity/cm.² at time t , D is the dif-

fusion coefficient and a_0 is the surface activity in gram atoms/cm.². (Of course, total gram atoms are used, being proportional to the a 's.) This equation is given by Gerischer and Vielstich¹¹ with the addition of a constant term for the rapid initial exchange shown by silver.

Inserting slopes of the plots of a_t *vs.* $t^{1/2}$ mentioned previously in equation 1, with $a_0 = 10^{-5}$ (moles Zn^{++} /cm.³ in the solution), values of D ranging from 1.3×10^{-10} to 7×10^{-8} cm.²/sec. are obtained. Equation 1 assumes that the surface is planar, that a_0 is constant and that the solid is homogeneous. The last condition is not met by a polycrystalline metal, since grain-boundary diffusion is usually faster than lattice diffusion at lower temperatures, and the total pickup depends on grain size; cold-rolled silver acquires activity more rapidly than annealed silver of larger grain size.⁵

There is no independent theory of grain-boundary diffusion, but this coefficient D_b and the lattice diffusion coefficient D_v are related by an equation derived by Fisher.¹² Values of D_v have been measured with zinc single crystals by the dry method between 75 and 200°, and using these, D_b has been calculated from measurements with polycrystalline zinc.^{13,14} The equation for D_b as a function of temperature is

$$D_b = 0.38 \exp(-14,600/RT) \text{ cm.}^2/\text{sec.} \quad (2)$$

which gives a value of 6.3×10^{-12} cm.²/sec. at 23°. There are of course uncertainties in this value, such as the extrapolation to room temperature.

This value of D could result from our measurements if a_0 were larger than the solution concentration, *e.g.*, if adsorption equivalent to a fraction of a monolayer of zinc ions were assumed. More plausibly, if exchange equilibrium is maintained in a surface monolayer, we believe that a_0 should be taken as the metal phase concentration, *i.e.*, 0.11 gram atoms/cm.³ but the area should be that of the exposed grain boundaries and not that of the entire specimen. The upward curvature of the a_t *vs.* $t^{1/2}$ plots probably is due to lattice diffusion in the surface of the specimen, which becomes appreciable with time; in short, equation 1 is unsatisfactory in this case. Similar experiments with single crystals should give more useful information concerning adsorption and diffusion, and these are in progress.

The authors gratefully acknowledge support of this investigation by the U. S. Army Office of Ordnance Research.

(11) H. Gerischer and W. Vielstich, *Z. Elektrochem.*, **56**, 380 (1952).

(12) J. C. Fisher, *J. Appl. Phys.*, **22**, 74 (1951).

(13) G. A. Shirn, E. S. Wajda and H. B. Huntington, *Acta Metallurgica*, **1**, 513 (1953).

(14) E. S. Wajda, *ibid.*, **2**, 184 (1954).

(10) L. S. Darken and R. W. Gurry, "Physical Chemistry of Metals," McGraw-Hill Book Co., New York, N. Y., 1953, Chapt. 18.

RADIOTRACER STUDIES OF CADMIUM-CADMIUM ION EXCHANGE

By CECIL V. KING AND ROBERT SKOMOROSKI

*Department of Chemistry, New York University, New York, N. Y.**Received February 27, 1959*

Measurements have been made of the rate and extent of acquisition of radioactivity by cadmium specimens when immersed in cadmium perchlorate solutions containing Cd^{115} as tracer. Good reproducibility of measurement was obtained with electropolished coupons in deaerated solutions. It is shown that the continuing activity pickup is due to self-diffusion within the metal, most of it presumably along grain boundaries. The diffusion coefficient calculated from pickup as a function of time is higher than expected from values in the literature unless adsorption of cadmium salt on the metal is assumed. The distribution of activity in depth in the specimens has been measured, to calculate diffusion coefficients at room temperature and at 98°.

We have found no quantitative studies reported in the literature, of exchange between cadmium metal and its ions in solution. Exchange with cadmium amalgam has been studied by the radio-tracer method by Fronaeus,¹ who found exchange to be so rapid from ordinary cadmium salts as to deplete the surface layer of solution of the tracer ions; the loss of activity from solution is then controlled by convection and diffusion. This indicates that the actual exchange is very rapid, and the "exchange current" is high. Measurements of exchange current with the amalgam have been made by a non-tracer method,² and found to be as large as 0.12 amp./cm.² for $10^{-3} M \text{Cd}(\text{NO}_3)_2$ in 1 $M \text{KNO}_3$.

The purpose of the present study was to see what could be learned about the metal-solution interface, by measuring the rate and extent of radioactivity pickup on cadmium specimens when immersed in a solution containing active cadmium ions. It was necessary to study the effects of corrosion in the presence and absence of air and the effect of surface preparation. It was expected that internal diffusion would be a rate-controlling factor, and it was hoped that diffusion coefficients could be estimated.

Experimental

Cadmium sheet, 0.07 cm. thick and of 99.99% purity, was cut into 2.54 cm. square coupons, and a 2 mm. hole was drilled in a corner of each in order to suspend it on a glass hook or a platinum wire. The actual area was 6.60 cm.² on each side.

Radiocadmium, $\text{Cd}^{115\text{m}}$ with half-life of 43 days, was obtained as the nitrate in HNO_3 solution. Since the experiments were to be carried out with $\text{Cd}(\text{ClO}_4)_2$ in the hope of minimizing corrosion, HClO_4 was added and the HNO_3 expelled by evaporation. Inactive $\text{Cd}(\text{ClO}_4)_2$ was prepared from reagent grade CdCO_3 and HClO_4 , and the stock solution was standardized by the sulfide method.³ Small amounts of tracer were added on diluting.

Counting and conversion to gram atomic amounts have been described.⁴ The coupons were thick enough to absorb nearly all radiation from the side away from the G.M. tube. Tests showed that about 4% of the radiation is absorbed in passing through 1.75×10^{-3} cm. of the metal (about 65,000 atomic layers). The counting time was chosen so that the counting error ordinarily was less than 2% at the nine-tenths probability level.

Immersion experiments usually were carried out with 250 ml. of 0.01 $M \text{Cd}(\text{ClO}_4)_2$ in a 500-ml. bottle. Purified nitrogen was used for deaeration. The temperature was $23 \pm 3^\circ$; for a few experiments at $98 \pm 2^\circ$ the immersion

vessel was placed in boiling water and equipped with a condenser.

Results

Table I shows the activity pickup in air-saturated solution; these results are of interest because comparison with the deaerated solution shows that the corrosion film blocks the surface and acts as an inhibitor. After the 13-hr. and 17-hr. immersions the coupons were covered with a colorless, gelatinous film, which was largely removed on rubbing with cleansing tissue and water. Activity in the film need not all represent exchange.

TABLE I

Air-saturated 0.01 $M \text{Cd}(\text{ClO}_4)_2$, 23°. A new coupon for each immersion.

Time immersed, hr.	Wt. loss, mg.	C.p.m. side 1	C.p.m. side 2	Gram atoms per cm. ² $\times 10^9$
1	0.3	187	253	87
1	.1	124	340	91
2	...	91	74	32
3	...	167	152	62
4	.2	240	196	84
5	.2	346	914	240
13	.3	2720	3140	1120
17	-.2 ^a	920	1350	410

^a Wt. gain.

The counts per minute columns of Table I give an idea of the divergence in counts between the two sides of a coupon in air-saturated and even in deaerated solutions when the surfaces were prepared by abrasion with fine paper.

In deaerated solutions the coupons corroded slowly, the greatest weight loss noted corresponding to about 10 atomic layers per hour. No visible solid films were formed, and the pH of the solutions (about 5.7) did not change appreciably. The activity pickup was much greater than with air present and increased regularly with time. With abraded coupons the reproducibility was no better than the values given in Table I, and various methods of polishing and etching were tried. The best results were obtained by electropolishing the coupons as described below.⁵ Table II shows some results for comparison. Not only was there usually (though not always) good agreement in counting, but the pickup was much smaller, no doubt due to a much smaller roughness factor.

The polishing solution was made with 20 g. of $\text{Cd}(\text{OH})_2$ and 120 g. of KCN per liter. The

(1) S. Fronaeus, *Acta Chem. Scand.*, **7**, 764 (1953); **8**, 412 (1954).
 (2) J. E. B. Randles and K. W. Somerton, *Trans. Faraday Soc.*, **48**, 951 (1952).
 (3) W. W. Scott, "Standard Methods of Chemical Analysis," D. Van Nostrand Co., Inc., New York, N. Y., 1946, p. 203.
 (4) C. V. King and S. Evans, *This Journal*, **63**, 1815 (1959).

(5) C. J. Smithells, "Metals Reference Book," Interscience Publishers, Inc., New York, N. Y., 1949, p. 240.

TABLE II

Deaerated 0.01 M $\text{Cd}(\text{ClO}_4)_2$ at 23°. A new coupon for each immersion. A, polished with No. 600 silicon carbide paper; B, electropolished.

Time immersed, hr.	A, g. atoms/cm. ² × 10 ⁹	B, g. atoms/cm. ² × 10 ⁹	B, c.p.m. side 1	B, c.p.m. side 2
30 min.	720
1	1430	200	332	329
2	1840	324	523	554
2	1460	336	540	522
4	2680	380	551	707
4	2820

cadmium coupon was suspended between 2 iron sheet cathodes in a 400-ml. beaker. After a number of experiments a current of 1 amp. (on 13.2 cm.²) for 5 minutes was chosen for all further work. This reduces the thickness of the coupons by about 0.01 cm.

Exchange as a Function of Time.—Three groups of coupons were prepared as follows: (a) abraded and electropolished; (b) stored in deaerated inactive $\text{Cd}(\text{ClO}_4)_2$ solution for several days, electropolished; (c) annealed *in vacuo* at 110° and electropolished. In all, 22 coupons were then immersed in deaerated, active 0.01 M $\text{Cd}(\text{ClO}_4)_2$ for periods from 15 minutes to 24 hours. On plotting the amount of exchange *vs.* the square root of time, all of the points could be represented within experimental error by a single straight line of slope 4.2×10^{-9} gram atoms cm.⁻² sec.^{-1/2}. The plot is in accordance with the theory of diffusion from an interface of constant composition into a homogeneous medium. The best straight line does not pass through the origin, however. The behavior is like that of zinc⁴ and silver.⁶ There is a very rapid pickup corresponding to complete exchange in 2 or 3 apparent atomic layers, followed by slow exchange with continual upward curvature of the plot *vs.* $t^{1/2}$, when this is examined in detail. Several coupons were immersed in active 0.1 M $\text{Cd}(\text{ClO}_4)_2$; the corresponding plot showed upward curvature with apparent linearity in the range 16–250 hours, the slope being 1.8×10^{-8} gram atoms cm.⁻² sec.^{-1/2}.

Depth of Penetration.—The extent of penetration of activity can be studied by etching the metal with a reagent which dissolves it uniformly and measuring the remaining activity as well as the weight lost. The reagent chosen was a solution of 0.02 M HCl, 0.06 M KNO_3 , which is known to dissolve several metals at a maximum, diffusion (or transport) controlled rate.⁷ This does not ensure uniform dissolution, but our experience has shown that the softer metals remain quite smooth.

Table III gives the results of preliminary experiments to determine the extent of penetration. The A and B coupons had undergone about the same amount of exchange, although the counts per minute are not the same. The B coupons show that inward diffusion continues on storage. The weight of cadmium dissolved can be expressed in distance since 1 mg. = 8.74×10^{-6} cm. on these coupons of 13.2 cm.² area. If more than 200 mg. were dissolved in a quantitative experiment, it should be

TABLE III

Coupons immersed in deaerated 0.01 M $\text{Cd}(\text{ClO}_4)_2$, etched in 0.02 M HCl, 0.06 M KNO_3 . A, etched immediately after immersion. B, etched 67 days after immersion.

A		B	
Wt. diss., mg.	C.p.m.	Wt. diss., mg.	C.p.m.
..	3080	..	2220
61	684	139	490
182	63	430	75
..	6480	..	3240
170	223	171	377
280	46	608	48

remembered that radiation from greater depths was originally subject to more than 4% self-absorption. (Calibration coupons were never stored so long that self-absorption of radiation was appreciable.)

Quantitative measurements were made with 14 coupons which were immersed until the activity had penetrated to a suitable depth and then were dissolved down a few milligrams at a time until 75–90% of the activity had been removed. Grain-boundary diffusion theory predicts that the logarithm of the activity, per unit volume at each penetration depth, should be a linear function of depth.

Plots of log activity remaining on some of the coupons, in c.p.m., *vs.* milligrams dissolved, are shown in Fig. 1. About 9 of the 14 curves showed a reasonably linear portion; the other straight lines were drawn as seemed best. It was expected that the first points would be high, because there must be appreciable diffusion into the surface grains, which is slower and follows a different law; however, this behavior was not shown uniformly. The last points on each plot become uncertain because the number of counts is small, self-absorption of the deeper radiation diminishes, and the assumption of uniform dissolution becomes uncertain.

Self-diffusion in Cadmium.—Lattice and grain-boundary self-diffusion in cadmium have been studied by Wajda, Shirn and Huntington,⁸ the latter in the temperature range 56–146°. Thin layers of active cadmium were electrodeposited on inactive specimens and, after storage at various temperatures, thin sections were milled off and dissolved to measure the activity. Single crystals were used in measuring lattice diffusion, and grain-boundary diffusion coefficients were derived from experiments with polycrystalline specimens, using the method of analysis developed by Fisher.⁹ The equations (1) to (3) summarize their results

$$\text{Lattice diffusion parallel to hexagonal axis} \\ D_v = 0.05 \exp(-18,200/RT) \quad (1)$$

$$\text{Lattice diffusion perpendicular to hexagonal axis} \\ D_v = 0.10 \exp(-19,100/RT) \quad (2)$$

$$\text{Grain-boundary diffusion} \\ D_b = 1.0 \exp(-13,000/RT) \quad (3)$$

The units of D are cm.²/sec., and the numbers in the exponentials are calories per gram atom. From equation 3, $D_b = 2.4 \times 10^{-10}$ cm.²/sec. at

(6) H. Gerischer and R. P. Tischer, *Z. Elektrochem.*, **58**, 819 (1954).

(7) C. V. King and P. Howard, *Ind. Eng. Chem.*, **29**, 75 (1937).

(8) E. S. Wajda, G. A. Shirn and H. B. Huntington, *Acta Metallurgica*, **3**, 39 (1955).

(9) J. C. Fisher, *J. Appl. Phys.*, **22**, 74 (1951).

23°, 2.2×10^{-8} cm.²/sec. at 98°, values about 10⁶ times as large as D_v .

The Fisher equation⁹ relates grain-boundary and lattice diffusion coefficients and is based on the analogy with heat conduction down thin sheets of a good conductor imbedded in a semi-insulating body. The relation may be put in the form

$$D_b = 2D_v^{1/2} (\log e)^2 \delta^{-1} (\pi t)^{-1/2} (d \log a_x/dx)^{-2} \quad (4)$$

where e is the log base, δ is the grain boundary thickness, a_x is the activity per unit volume at penetration depth x after the time t .

From equations 1 and 2, average values of D_v are 1.27×10^{-15} cm.²/sec. at 23° and 7.4×10^{-13} at 98°. Fisher suggested that δ be taken as 5×10^{-8} cm., and in the absence of better information other workers have used this value.⁸ Inserting numerical values in equation 4 we obtain

$$D_b = 0.152t^{-1/2} (\text{slope})^{-2} \text{ at } 23^\circ \quad (5)$$

$$D_b = 3.67t^{-1/2} (\text{slope})^{-2} \text{ at } 98^\circ \quad (6)$$

where the slopes ($\Delta \log a/\Delta x$) can be taken from plots like Fig. 1 with a in c.p.m. and x in cm. (= mg. $\times 8.74 \times 10^{-6}$).

Table IV gives details of the treatment of the 14 coupons used in these experiments and summarizes the calculated D_b values. All the coupons were electropolished except No. 8 and 9, and it was shown previously that abraded coupons acquire activity faster than electropolished ones. Coupon 7 probably was immersed too long in the more concentrated Cd(ClO₄)₂ so that diffusion into the surface grains was exceptionally large. In expt. 1 and 2, only the immersion time was used; the values are included to show that the calculation is rather insensitive.

TABLE IV
GRAIN-BOUNDARY DIFFUSION COEFFICIENTS

Expt.	23 ± 3°		Expt.	98 ± 2°	
	Immersion time, hr.	D_b , cm. ² /sec. $\times 10^{10}$		Immersion time, hr.	D_b , cm. ² /sec. $\times 10^8$
1	40 ^a	1.8	10	2	2.12
2	40 ^a	1.8	11	2	0.37
3	40	1.52	12	1	1.06
4	40	1.47	13	2	0.50
5	160.5	1.46	14	3	0.71
6	185	1.42			
7 ^b	258	0.34			
8 ^c	12	16			
9 ^c	14	28			

^a Etched 22 days after immersion. ^b In 0.1 M Cd(ClO₄)₂. All others in 0.01 M Cd(ClO₄)₂. ^c Abraded coupons. All others electropolished.

Discussion

The values of D_b in expt. 3-6 and 10-14 of Table IV are in satisfactory agreement with equation 3, considering the extrapolations and approximations made, the neglect of corrosion, etc. Similar experiments with silver¹⁰ did not agree as well with values

(10) C. V. King and N. E. McKinney, *Can. J. Chem.*, **37**, 205 (1959).

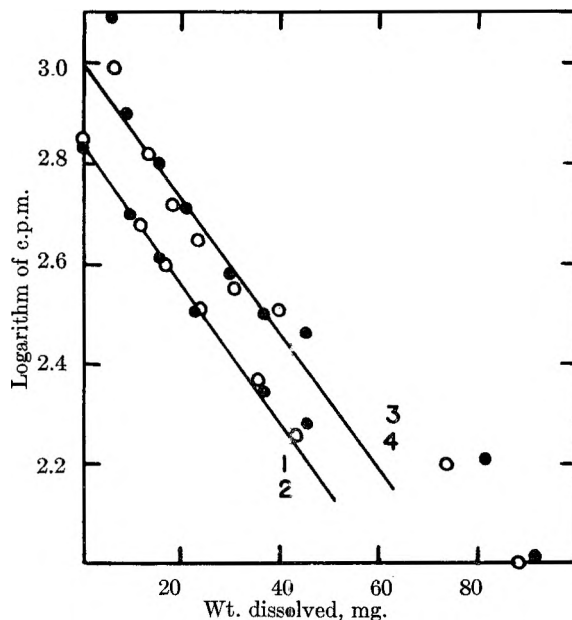


Fig. 1.—Coupons 1, 2, 3, 4 of Table IV.

from the literature, but in that case the numerical values are 10⁷ times smaller and D_v is obtained by extrapolation from much higher temperatures. Cold-rolled silver sheet, which presumably consists of very fine, distorted grains, gave linear plots of $\log a$ vs. x , while annealed silver, with much larger grains and a rough surface, did not.

There is no independent theory of grain-boundary diffusion, since the relative area and volume of grain boundaries is not known and varies with grain size. The Fisher relation assumes that diffusion takes place into the crystals from grain boundaries, but that lattice diffusion can be neglected at the specimen surface. The relation is independent of grain size, since only the ratio of activity at different depths is needed.

Exchange vs. Time.—When the slopes of the square root plots given above are inserted in the equation

$$a_t = 2a_0(Dt/\pi)^{1/2}$$

with $a_0 = 10^{-5}$ and 10^{-4} moles/cm.³, respectively (the solution concentrations), apparent values of the diffusion coefficient become 1.4×10^{-7} and 2.5×10^{-8} cm.²/sec. These are much larger than the values in Table IV; but if the surface concentration a_0 were taken as 3×10^{-4} and 1.3×10^{-3} moles/cm.³, corresponding to adsorption of a small fraction of a monolayer, the discrepancy would disappear. Since this is not a homogeneous diffusion, further speculation is unwarranted.

We are continuing the exchange studies with cadmium single crystals, since the homogeneous diffusion should be more amenable to simple interpretation.

The authors wish to thank the U. S. Army Office of Ordnance Research for its support of this investigation.

RADIOTRACER STUDIES OF IRON IN IRON SALT SOLUTIONS

BY CECIL V. KING AND ROBERT SKOMOROSKI

*Department of Chemistry, New York University, New York, N. Y.**Received February 27, 1959*

A study has been made of the behavior of pure iron, immersed in solutions of ferrous and ferric perchlorates, using radioactive iron ions as tracer. The results indicate that exchange in depth is negligible at room temperature and that most, if not all, of the activity acquired by the metal is incorporated in solid corrosion products. Dichromate reduces the rate of dissolution of the metal in $\text{Fe}(\text{ClO}_4)_3$, but activity is picked up in a corrosion film. Cathodic polarization also inhibits dissolution in $\text{Fe}(\text{ClO}_4)_2$ but deposits a non-adherent film which contains active ions. The results are in accord with the very low rate of self-diffusion in iron, the low exchange current, and the great susceptibility of the metal to local-cell corrosion.

This investigation was designed to find whether radiotracer studies could give any useful information concerning the nature of an iron surface in contact with solutions of its own salts, especially under conditions which minimize corrosion. The rate of self-diffusion in iron has been measured at high temperatures¹ and extrapolation to room temperature appears to give a negligible value. Consequently internal diffusion should not cause continued tracer pickup unless grain-boundary diffusion should prove to be important. The exchange current is small; values of 2×10^{-8} and 2.5×10^{-11} amp./cm.² have been reported in various solutions of FeSO_4 at room temperature.^{2,3} Radiotracer pickup, even in a surface monolayer, could not occur faster than the equilibrium exchange rate.

When the exchange current is very small, it is likely that an active metal will show a mixed potential rather than its reversible potential, and this is the case with iron. The effect of local-action corrosion currents on the potential of an iron electrode has been discussed by Uhlig.⁴ Unhindered exchange should be most probable under conditions of approach to the reversible potential, e.g., in deaerated solutions of pH 5 or higher, depending on the ferrous ion concentration.⁵ If solid corrosion products are formed, radioactive ions can be incorporated from the solution, without involving exchange.

Experimental

Disks 3.74 cm. in diameter and 0.05 cm. thick were cut from sheet reported as 99.92+ % iron.⁶ A small central hole was drilled for mounting. In some experiments smaller square coupons were used.

Radioactive iron powder was obtained, containing Fe^{59} , a weak β - and γ -emitter of 45 day half-life, and Fe^{56} , which emits 5.9 Kev. Mn X-rays and has a half-life of 2.94 years. Ferrous solutions were prepared by dissolving weighed amounts of the powder in deaerated HClO_4 and were kept under oxygen-free nitrogen or hydrogen at all times. Ferric solutions were made up with the proper amount of HClO_4 , allowing oxygen to be absorbed until all of the ferrous ion was oxidized. The pH was adjusted with HClO_4 . An iron disk was kept in each ferrous solution at all times, except in the double cell described later.

Counting was done with a thin-window argon-filled GM

tube, which was 3 times as efficient as a similar helium-filled tube. The counting time was usually long enough to give not more than 6% error at the nine-tenths level. Calibration coupons were prepared by evaporating small solution samples and were used to convert counts to apparent atomic layers (ca. 3.2×10^{-9} gram atoms/cm.²). The specific activity of the solutions was not high, 16-18 counts per minute above background on the larger disks being equivalent to complete exchange in a monolayer.

Coupons were polished with fine silicon carbide paper and washed with absolute ethanol. Immersion experiments, at room temperature ($23 \pm 3^\circ$), were carried out in a closed vessel equipped with a glass hook, a fritted bubbler and an outlet tube. After immersion, coupons were washed with absolute ethanol either (a) without rubbing or (b) by rubbing with paper tissue wet with ethanol. Water or other solvents caused visible rusting while drying.

Results

The detailed data are of little interest, and the results are summarized below. Each numbered paragraph represents a new solution.

Ferrous Solutions.—1. Different disks were immersed in deaerated 0.087 M $\text{Fe}(\text{ClO}_4)_2$ for various periods from 1 minute to 20 hours. The disks were washed in ethanol, counted, then rubbed with tissue and ethanol and counted again. The activity acquired was equivalent to the iron in 7-25 apparent layers but did not increase regularly with time. Rubbing removed 25-75% of the activity, much of which must have been in loosely adherent corrosion films even though these were not visible. The pH of the solution increased from 2.8 to 4.7 during the runs, and coupons immersed 10 hr. or longer lost weight equivalent to 80-200 atom layers.

2. Different disks were immersed in deaerated 0.01 M $\text{Fe}(\text{ClO}_4)_2$ of initial pH 4.5, for periods from 30 seconds to 41 hours and were washed by rubbing with tissue and ethanol at once after removal. The activity usually corresponded to 1-2 layers but was sometimes as high as 5-6 layers after 10 hr. or more. The coupons lost weight; the pH rose to 5.0 but did not go higher, and the solution became cloudy.

3. Two coupons were given repeated one-minute immersions in deaerated 0.087 M $\text{Fe}(\text{ClO}_4)_2$ and were rubbed with tissue and ethanol between immersions. The activity acquired increased regularly and corresponded to 55 layers after 100 immersions. The disks became covered with irregular brown films but remained very smooth and shiny because of the rubbing. The increasing activity pickup was due no doubt to the growing polished film of corrosion products rather than to penetration into the metal. The pH increased from 2.8 to 4.4 and the disks lost about 4.5 mg.

Disks treated in the same way in 0.01 M $\text{Fe}(\text{ClO}_4)_2$ with an initial pH of 5.2 acquired activity equivalent to 35 layers after 100 immersions. The pH did not change and the solution became cloudy. Similar experiments in which the coupons were not rubbed resulted in less adherent, dull films and visible rust spots.

4. For further experiments, square coupons with an area of 3.7 cm.² on each side were cleaned and polished, then annealed in a silica tube at 800° for 2 hr. in either hydrogen, argon or vacuum. The tube and coupons were cooled over a period of 7-8 hours.

In order to take more precautions in preventing access of air, a cell was prepared, having two compartments connected at the bottom by a tube and stopcock. Each compartment had a drainage stopcock. The tops had ground covers with

(1) C. E. Birchenall and R. F. Mehl, *Trans. Am. Inst. Mining Metallurg. Engrs.*, **188**, 144 (1950).

(2) W. A. Rojter, W. A. Juza and E. S. Polujon, *Acta physicochim.*, **10**, 389 (1939).

(3) T. P. Hoar and T. Hurlen, International Committee of Electrochemical Thermodynamics and Kinetics (CITCE), Eighth Meeting, Butterworth and Co., Ltd. (Toronto), 1958, p. 445.

(4) H. H. Uhlig, *Proc. Nat. Acad. Sci.*, **40**, 276 (1954).

(5) J. D'Ans and W. Breckheimer, *Z. Elektrochem.*, **56**, 585 (1952).

(6) Swedish Iron and Steel Co.

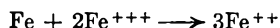
gas-bubbling and exit tubes. Air was displaced from one compartment by hydrogen, and 100 ml. of 0.01 M $\text{Fe}(\text{ClO}_4)_2$, prepared under hydrogen, was introduced. Purified wet hydrogen was passed through the solution continuously. In the meantime an iron coupon was suspended on a glass hook in the other compartment and was heated in hydrogen to 500° by means of a resistance coil surrounding the tube.

After cooling the cell and coupon slowly, the solution was forced over to cover the iron. After suitable immersion the solution was forced back, and the coupon was washed with deaerated water, always with hydrogen flowing through the cell. The iron was dried by evacuating the compartment and warming with the surrounding coil.

Neither the type of annealing nor the time of heating in hydrogen was significant. In all, about 25 coupons were treated in the one solution for periods of 1 minute to 40 hours. By that time only half the solution was left and the concentration had increased 10%. The pH rose from an initial 2.4 to 5.3, then dropped back and remained at 4.9 in succeeding runs. Little or no activity was acquired by coupons at the lowest pH; at pH 3, the activity corresponded to 1-1.5 layers. At pH 4.7-4.9 this value rose to 4-9 layers, reduced to 1-2 layers on rubbing with tissue. The solution became cloudy, and after this nearly all activity could be removed by rubbing. Even a platinum coupon acquired some activity, which could be removed with tissue and ethanol.

Since accepted values for the Fe/Fe^{++} potential have been obtained in FeSO_4 solutions, experiments with active FeSO_4 were carried out in the same cell. The results were similar; the pH rose steadily to 5.0, after which it did not change, and the solution became cloudy. In no case was there any clear relation between the amount of activity and the time of immersion.

Ferric Solutions.—5. Coupons were immersed in active 0.01 M $\text{Fe}(\text{ClO}_4)_3$ for periods from 10 seconds to 16.5 hr. Iron dissolves with reduction of ferric ion



The activity acquired corresponded to 2-4 layers and did not increase with time of immersion. Half of it was removed by rubbing with tissue. The pH increased during the runs, showing that corrosion not due to ferric reduction was occurring (the solution was not deaerated).

6. Coupons rotated at 2550 r.p.m. in 0.01 M $\text{Fe}(\text{ClO}_4)_3$ lost 30 mg. in weight in 30 minutes. With 0.01 M $\text{K}_2\text{Cr}_2\text{O}_7$ present they lost no more than 0.5 mg. and often gained a similar amount. Activity pickup corresponded to 1-1.5 layers, much of which was removed by rubbing, along with any weight gained. The coupons acquired orange streaks of corrosion products. At pH values above 2 the solution quickly became cloudy, and at pH 4.5 the iron became covered with a rusty film and acquired much more activity than usual.

7. Current was passed, with iron disks rotated at about 100 r.p.m., as cathodes in 0.01 M $\text{Fe}(\text{ClO}_4)_3$. Silver in NaCl solution served as anode (with an agar bridge). At a pH 2.2, less than 1 ma./cm.² prevented iron from dissolving and led to weight gains, with deposition of non-uniform yellow films, with a very large increase in activity pickup. Evidently an increase in pH at the cathode led to precipitation of hydrated oxide; the activity, if due to pure iron, would account for only half the weight gains. Runs with a platinum coupon as cathode showed that currents too small to prevent iron dissolution still deposited a film on the platinum.

Discussion

The obvious conclusion from these experiments is that iron does not exchange in any depth with its ions even on long immersion; there is no rapid grain-boundary diffusion. Corrosion of the metal under all conditions makes it impossible to say whether true exchange occurs even in the surface layers. An exchange current of 2×10^{-8} amp./cm.² corresponds to complete exchange in one atomic layer in 8 hours. Even with no deeper exchange, radioactive equilibrium with the solution would require a much longer time because of back-exchange. The low specific activity of the iron used and the inefficient counting method would make detailed investigation impossible, while the interference of corrosion with exchange measurements makes it worthless to improve the method.

The initial corrosion product in deaerated solution is probably $\text{Fe}(\text{OH})_2$. When iron samples are sealed in carefully deaerated water at 25°, they remain bright for a long time, but the water soon becomes slightly cloudy⁷ and the pH rises to 9.3. However, $\text{Fe}(\text{OH})_2$ is stable in contact with water only in the absence of a catalyst for its reaction with water; Linnenbom found that even a trace of air causes its transformation to magnetite. In none of our experiments was a film or precipitate resembling magnetite seen. The ferrous solutions became cloudy at pH about 5.0, and this could be due to $\text{Fe}(\text{OH})_3$, not in equilibrium with the metal. According to the potential-pH diagrams of Pourbaix,⁸ iron, magnetite and 0.01 M Fe^{++} could exist in equilibrium at pH 5 only if the iron potential were about that of the standard hydrogen electrode, and $\text{Fe}(\text{OH})_3$ would require a still more noble potential or a higher pH. The pH at the surface of corroding iron probably is considerably higher than that in the solution. In any case we do not believe that the precipitate seen in several solutions was caused by entrance of air into the cells.

Results somewhat like the present ones have been reported for tracer studies with cobalt and tantalum and their ions.⁹ The solutions were not deaerated and some were agitated with air. Probably little or no exchange was involved, the activity pickup being incorporated in oxide films.

The authors wish to thank the U. S. Army Office of Ordnance Research for its support of this investigation.

(7) V. J. Linnenbom, *J. Electrochem. Soc.*, **105**, 322 (1958).

(8) M. J. N. Pourbaix, "Thermodynamics of Dilute Aqueous Solutions," Edward Arnold and Co., London, 1949, p. 89.

(9) M. Cottin, *J. chim. phys.*, **47**, 231 (1950).

แผนกห้องสมุด ธรรมวิทยาสาสตร์
กระทรวงอุตสาหกรรม

THE POLAROGRAPHIC CHARACTERISTICS OF FURFURYLIDENEACETOPHENONE AND SOME OF ITS *para* DERIVATIVES

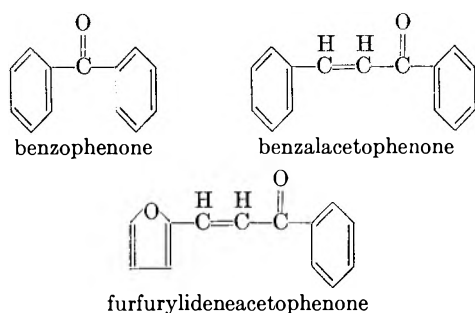
BY JAMES E. CASSIDY¹ AND WENDELL J. WHITCHER

Contribution from the Department of Chemistry, University of Vermont, Burlington, Vermont

Received March 17, 1959

Plots of the half-wave potentials of the furfurylideneacetophenones in a buffered acetate solution vs. Hammett's σ constants give essentially linear relationships. The slopes of these plots are similar to that of benzophenones, and indicate that an increase in the positivity of the carbonyl carbon facilitates the reduction.

Sigma values obtained from the Hammett function have been used to correlate quantitatively half-wave potentials of aromatic carbonyl compounds with the type of substitution present in the rings. In attempting any such comparison all substances and all operating conditions must be very similar due to the fact that organic reactions for the most part are irreversible and therefore the half-wave potentials are not directly related to the change of the free energy for the electrode process.² Benzophenone, benzalacetophenone and furfurylideneacetophenone are similar in nature with the exception that the first compound does not have a double bond in conjugation with the carbonyl.



Brockman and Pearson³ have completed a study of the derivatives of the benzophenones and Geissman and Friess⁴ have studied some of the benzalacetophenones. The reductions of these compounds yield dimeric compounds at a low pH, whereas at higher values the saturated ketone is mainly found.⁵ However, investigations⁶ have shown that a sharp delineation between the two processes does not exist. The purpose of this paper is to present polarographic characteristics of some of the furfurylideneacetophenones, to plot the half-wave potentials against the proper sigma values, and to show the similarity of the reduction of these compounds to those of benzalacetophenones and benzophenones.

Experimental

A manually operated polarograph, Sargent Model III, was used with a polarographic H cell with a saturated calomel cell as a reference. The calibration factor of the galvanometer was 0.0058 microampere per millimeter. With this

(1) American Cyanamid Co., Stamford, Conn., to whom inquiries should be directed.

(2) P. Delahay and W. Vielstich, *J. Am. Chem. Soc.*, **77**, 4955 (1955).

(3) R. W. Brockman and D. E. Pearson, *ibid.*, **74**, 4128 (1952).

(4) T. A. Geissman and S. L. Friess, *ibid.*, **71**, 3893 (1949).

(5) R. Pasternak, *Helv. Chim. Acta*, **31**, 753 (1948).

(6) H. J. Gardner, *Chemistry & Industry*, 819 (1948).

apparatus, the half-wave potential of zinc was found to be in good agreement with the values in the literature. No correction was made for the IR drop or the junction potential. All polarographic analyses were executed with the H cell placed in a bath at $25.0 \pm 0.5^\circ$. The capillary, when in the stock solution, had these characteristics at zero potential: drop time = 3.70 sec., $m = 2.46$ mg./sec., and $m^{2/3} t^{1/6} = 1.73$.

A stock solution (1 M, 3:7 ratio of acid to salt) was used as buffer, solvent and supporting electrolyte throughout this investigation. It was prepared by dissolving 57.40 g. of sodium acetate and 17.2 ml. of glacial acetic acid in an alcohol-water mixture and then diluting to a liter. The alcohol-water mixture was prepared by mixing equal volumes of distilled water and isopropyl alcohol. The apparent pH of the stock solution was 5.90 using a Beckman pH meter, Model G.

The *p*-bromo-, *p*-methyl-, *p*-methoxy- and the *p*-hydroxy-furfurylideneacetophenones were prepared by the conventional condensation⁷ of furfural and the substituted acetophenone in alcoholic sodium hydroxide (see Table I). With the exception of the *para*-hydroxy derivative, a yield of about 50% for each product was obtained when the reaction mixture was cooled in an ice-salt-water bath. For precipitation of the *para*-hydroxy compound, acetic acid had to be added to the cooled reaction mixture.

TABLE I

DERIVATIVES OF FURFURYLIDENEACETOPHENONE
Each product was recrystallized from hot ethyl alcohol

Compound	Color	M.p., °C.	
		Lit.	Found
<i>p</i> -Bromo	Yellow	80-81 ^a	78
<i>p</i> -Methyl	Yellow	67 ^b	63-64
<i>p</i> -Methoxy	Yellow	75-79 ^c	75-76
<i>p</i> -Hydroxy	Yellow	None	160-161

^a N. Maxim and J. Angelesco, *Bull. soc. chim.*, **51**, 1365 (1932).

^b N. Maxim and I. Popescu, *ibid.*, **58**, 89 (1939).

^c R. Robinson and W. M. Todd, *J. Chem. Soc.*, 1743 (1939).

Freshly prepared solutions in the range of 2×10^{-4} to 6×10^{-4} M gave polarograms which had total diffusion currents that were directly proportional to the concentrations. These colorless solutions, which became yellow on standing, showed an 8% decrease in the total diffusion currents after standing two days. In comparison no such changes were noted in benzalacetophenone solutions. The procedure for each polarographic run was standardized as follows: a 20-ml. sample of fresh solution was flushed with oxygen-free and solvent saturated nitrogen, and the voltage-current relationship immediately recorded. From the resulting plots, the half-wave potentials ($E_{1/2}$'s) and the diffusion currents (i_d 's) for each step were determined graphically. These results are given in Table II.

Discussion of Results

The polarograms of furfurylideneacetophenones and benzalacetophenones³ are very similar in that they all have three distinct waves. Of the two series, the furfurylideneacetophenones are the easier

(7) N. L. Drake and H. W. Gilbert, *J. Am. Chem. Soc.*, **52**, 4965 (1930).

TABLE II
POLAROGRAPHIC REDUCTIONS OF FURFURYLIDENEACETOPHENONE

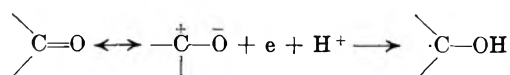
Substituents	Waves	$E_{1/2}$ vs. (S.C.E.), v.	Concn., mmoles	i_d , μ amp.	i_d/c	σ^a
Unsubstituted	1st	0.845	0.522	1.10	2.11	0
	2nd	1.18		1.25	2.39	
	3rd	1.35		0.580	1.11	
<i>p</i> -Bromo	1st	0.780	.500	1.09	2.34	.232
	2nd	1.12		0.957	2.49	
	3rd	1.31		0.943	1.64	
<i>p</i> -Methyl	1st	0.851	.500	1.09	2.18	— .170
	2nd	1.23		1.07	2.18	
	3rd	1.38		0.552	1.04	
<i>p</i> -Methoxy	1st	0.887	.518	1.10	2.13	— .268
	2nd	1.23		1.26	2.44	
	3rd	1.42		0.582	1.01	
<i>p</i> -Hydroxy	1st	0.96	.487	0.914	2.08	— .475
	2nd	1.30		1.28	2.42	
	3rd	None				

^a H. H. Jaffe, *Chem. Revs.*, **53**, 191 (1953).

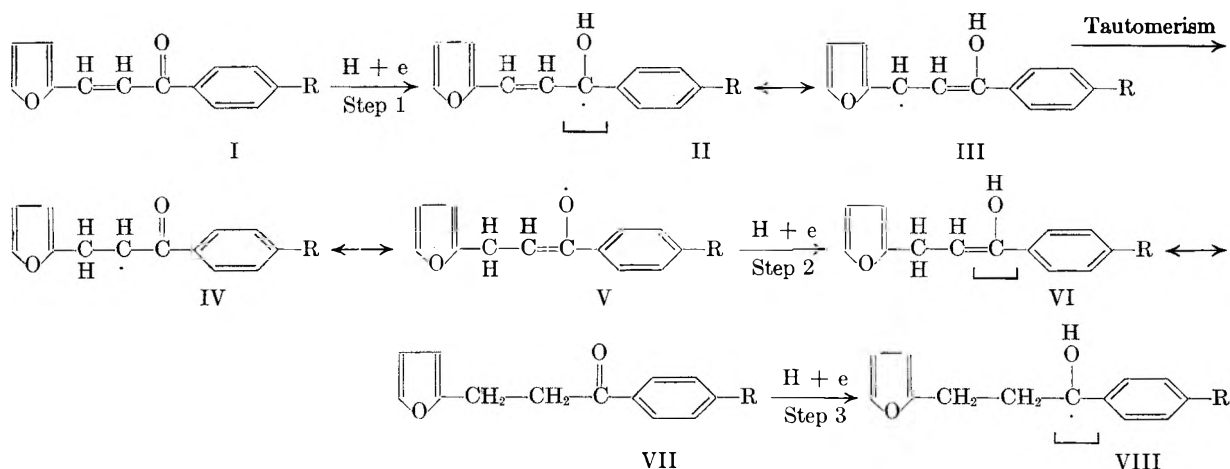
to reduce. The data for both series show that electron releasing groups decrease the ease of reduction at the electrode whereas the electron withdrawing groups increase it. The i_d/c values for both series are of the same order of magnitude; but when these values and those for benzophenone are compared, the latter are greater by a factor of about 2.

The most interesting results are those in Fig. 1 which relates Hammett's σ -values to half-wave potentials. That the plots of the furfurylideneacetophenones and benzophenones are not only linear but parallel indicates these waves are subject to the same type of structural influences and suggests that the rate-controlling electron transfer may occur at the same site for all steps. The plot of the three benzalacetophenones though linear is not parallel to the others. The reason for this difference may

probably a nucleophilic attack on the carbonyl by an electron resulting in the formation of a free radical.



In the case of the benzophenones, which give only one wave,^{2,9} the free radical is not stable and thus is reduced immediately to the carbinol; whereas the furfurylideneacetophenones can form a stable free radical which can undergo a subsequent reduction at the electrode. A possible explanation for this difference is that the double bond causes a decrease in the electron density at the carbonyl and results in a relatively stable free radical. The reduction sequence of the furfurylideneacetophenones may be represented as



be the higher pH and the change in buffer system; however, due to the limited data available, little significance can be attached to this slope.

In the case of the furfurylideneacetophenones each wave apparently corresponds to an one electron reduction process.^{4,5} Consistent with the views of others,^{3,5,6,3} the initial step in each case is

The mechanism as outlined above accounts for the three waves and for the parallelism of the slopes in Fig. 1. The latter observation may be due to the electron and proton transfers occurring at the same site for each reduction step. Another tautomeric form of

(8) J. W. Baker, W. V. Davies and M. L. Hemming, *J. Chem. Soc.*, 692 (1940).

(9) R. A. Day, Jr., and J. J. Kirkland, *J. Am. Chem. Soc.*, **72**, 2766 (1950).

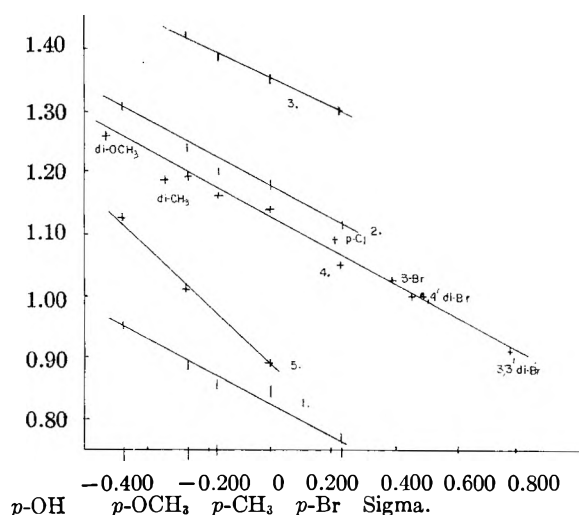
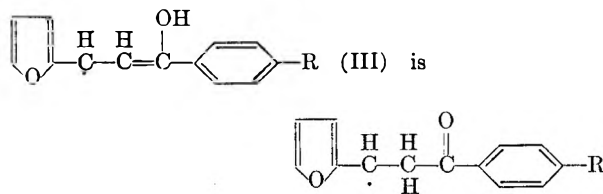


Fig. 1.—Half-wave potentials vs. σ -values: (1) 1st step, furfurylideneacetophenone; (2) 2nd step, furfurylideneacetophenone; (3) 3rd step, furfurylideneacetophenone; (4) benzophenone, 0.1 *N* acetate buffer pH 5.2 (R. W. Brockman and D. E. Pearson, *J. Am. Chem. Soc.*, **74**, 4128 (1952)); (5) 1st step, chalcone, $(\text{CH}_3)_4\text{NOH}$ -acetic acid buffer (T. A. Geissman and S. L. Fries, *J. Am. Chem. Soc.*, **71**, 3893 (1949)).



However, the electron attack and protonation in this case would not be at the carbonyl site. Though this reduction mechanism is not conclusive, the second wave does represent the formation of the saturated ketone VII at the electrode surface.

The first two waves are simple diffusion controlled reductions representing one electron transfers, whereas the third wave does not represent such a simple reduction. The i_a/c values for this wave are about half those for the first and second waves. In addition, a change in the concentration of the buffer used in this investigation results in decided differences in the heights of the third wave. The polarographic characteristics of this third wave as a function of the buffer are being investigated.

SOME ENERGY RELATIONS IN SOLID STATE REACTIONS INVOLVING CRYSTALLINE PHASES OF VARIABLE COMPOSITIONS

BY ARNULF MUAN AND W. C. HAHN, JR.

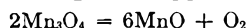
Contribution No. 58-101 from College of Mineral Industries,
The Pennsylvania State University, University Park, Pennsylvania

Received March 19, 1959

In a recent experimental study of the equilibrium between hausmannite and manganosite according to the approximate equation $2\text{Mn}_2\text{O}_4 = 6\text{MnO} + \text{O}_2$, it was observed that manganosite used as starting material reacted with oxygen of the atmosphere to form hausmannite as a metastable phase at conditions of temperature and O_2 partial pressure within the stability field of manganosite but close to the manganosite-hausmannite boundary curve. This apparently anomalous reaction is explained in terms of a free energy-composition diagram for the system Mn-O. Implications of this observation on criteria used for judging equilibrium in some solid state reactions are indicated.

Introduction

The equilibrium between hausmannite and manganosite according to the approximate equation¹



was studied recently by Hahn and Muan,² using an open system in which the desired O_2 partial pressures of the gas phase were attained by mixing CO_2 and O_2 or CO_2 and H_2 .

The method consisted in equilibrating two samples side by side at constant temperature and chosen constant O_2 partial pressure, the starting material in one sample being manganosite and in the other hausmannite. The manganosite had been prepared in advance from MnO_2 under strongly

reducing conditions ($p_{\text{O}_2} = 10^{-10}$ atm. at 1100°), and hausmannite had been prepared by thermal decomposition of MnO_2 in air at 1100° . After equilibrium was attained among gas and crystalline phases, the samples were quenched rapidly to room temperature and the phases present determined by using X-ray diffraction. In some cases, supplementary data were obtained by using only one starting material, either manganosite or hausmannite, and following the progress of the reaction by frequent weighing of the sample in a simple thermal balance setup.

The results of the investigation are summarized in Fig. 1, where the solid line represents conditions for coexistence of the two phases hausmannite and manganosite in stable equilibrium.

In preliminary experiments for determination of the equilibrium between the two crystalline phases, the transformations of manganosite to hausmannite and *vice versa* were studied under conditions of constant temperature and partial pressures of O_2 which were later found to be well within the regions

(1) Hausmannite has approximately stoichiometric Mn_2O_4 composition and occurs in two modifications, a low temperature ($<1160^\circ$) tetragonal and a high temperature ($>1160^\circ$) cubic form. Manganosite, with sodium chloride structure, has variable composition, Mn_{1-x}O .^{3,4}

(2) W. C. Hahn, Jr., and A. Muan, *Am. J. Sci.* (in press).

(3) M. LeBlanc and G. Wehner, *Z. physik. Chem.*, **A168**, 59 (1934).

(4) T. E. Moore, M. Ellis and P. W. Selwood, *J. Amer. Chem. Soc.*, **72**, 856 (1950).

of stability of the respective oxides. The complete transformations in both directions took place in 3 to 4 hr. in tests run at 1300°. (The transformations were called complete when the sample had reached a constant weight and consisted of only one phase according to X-ray analysis.)

It was later discovered that when the two starting materials, manganosite and hausmannite, were equilibrated side by side under conditions of temperature and O_2 partial pressure in the stability field of manganosite but close to the manganosite-hausmannite boundary curve, both quenched samples turned out to be mixtures of manganosite and hausmannite as determined by X-ray analysis. Experience showed that if both samples were a mixture the first time they were removed from the furnace, the amount of manganosite increased and that of hausmannite decreased in every case upon further time in the furnace. On the basis of this observation it was assumed that manganosite is the truly stable phase under these experimental conditions. Results of weighing experiments carried out in the thermal balance are shown in Fig. 2. Illustrated here is the weight change as a function of time for a sample of manganosite starting material, as it is kept in the furnace at 1443° in an atmosphere of O_2 partial pressure of $10^{-1.99}$ atm. A small part (0.230 g.) of the sample was removed after 130 hr. in order to check the progress of the reaction by X-ray analysis. The portion of the curve to the right of this point on the horizontal axis was obtained by allowing for the amount taken out and recalculating to the original weight of the sample. It can be seen from the curve that the weight increases rapidly at first, then it levels off and remains nearly constant for some time before finally decreasing. This weight decrease could not be accounted for by vaporization from sample and container. The X-ray observations showed peaks of hausmannite and manganosite of approximately equal intensities after 130 hr., whereas only traces of hausmannite peaks were present in the pattern of the sample at the conclusion of the experiment (215 hr.).

The presence of hausmannite in the quenched sample which originally was manganosite cannot be explained simply by assuming that exsolution of hausmannite from the oxygen-rich manganosite phase close to the boundary curve took place during quenching. The X-ray evidence as well as the weight-time curve indicate clearly that the content of hausmannite first increases and subsequently decreases with time at constant temperature and O_2 partial pressure. It is concluded that manganosite of low oxygen content does not transform directly to manganosite of higher, equilibrium, oxygen content, but first forms a mixture of manganosite and hausmannite.

Energy Relations.—The stability relations existing among phases in the system Mn-O can be illustrated in a free energy-composition diagram (1443°) such as shown in Fig. 3. (For a general discussion of free energy-composition diagrams, see for instance Darken and Gurry.⁵) In the

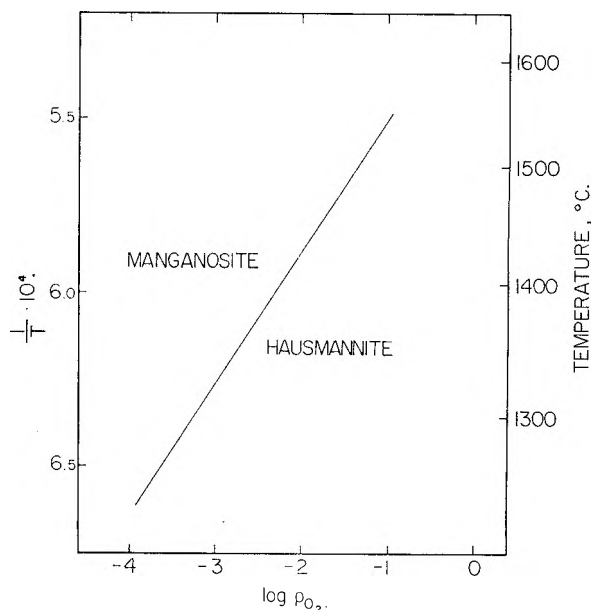


Fig. 1.—Diagram showing stabilities of the phases hausmannite and manganosite as a function of O_2 partial pressure (log scale in atm.) and temperature (inverse °K. scale), after Hahn and Muan.²

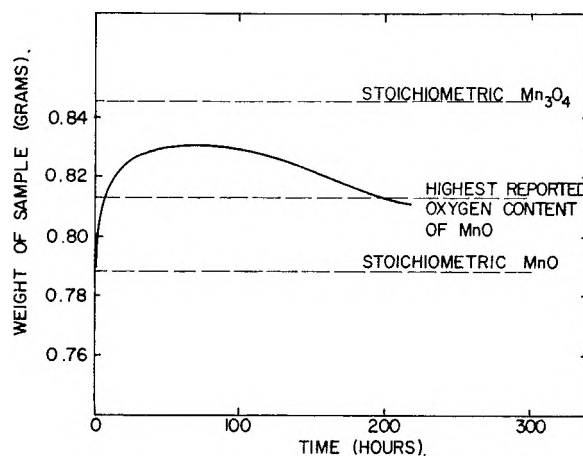


Fig. 2.—Diagram showing weight changes as a function of time as a sample of manganosite of low oxygen content transforms to manganosite of higher, equilibrium, oxygen content under conditions close to the manganosite-hausmannite boundary curve, as explained in detail in the text.

diagram in Fig. 3 are plotted atom fractions of O along the horizontal axis, and along the vertical axis free energy values $F^* = F - (N_1 \cdot F^0_{Mn} + N_2 \cdot F^0_O)$. Here F is the free energy per g. atom of material and F^0_{Mn} and F^0_O the free energies per g. atom of manganese and oxygen, respectively, in their standard states.⁶ We will choose as standard states metallic Mn and O_2 gas of 1 atm. pressure, respectively. Hence F^* will be zero for metallic Mn as well as for O_2 gas of 1 atm. pressure. The other free energy values used in the graph were taken from the data tabulated by Coughlin⁷ in

(6) The free energy-composition diagrams discussed by Darken and Gurry⁶ were constructed for closed systems. However, the relations apply equally well to a chosen part of an open system. In the present case we are dealing with a total amount of 1 g. atom of material (Mn + O).

(7) J. P. Coughlin, Bulletin 542, U. S. Bureau of Mines, Washington, D. C., 1954.

(5) L. S. Darken and R. W. Gurry, "Physical Chemistry of Metals," McGraw-Hill Book Co., Inc., New York, N. Y., 1953.

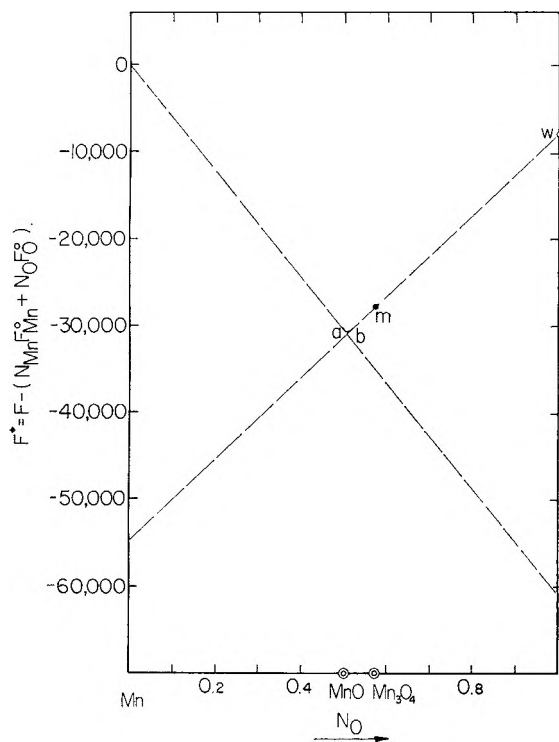


Fig. 3.—Diagram showing free energy as a function of composition for the phases manganosite and hausmannite in the system Mn-O at a constant temperature of 1443°. The meanings of the various lines and symbols used are explained in detail in the text. (Diagram based on data compiled by Coughlin⁷ as well as recent data by Hahn and Muan.²)

conjunction with data contained in Fig. 1. It will be noticed that hausmannite is represented in the diagram by a point (m) because the composition of this phase is essentially constant. The manganosite phase, on the other hand, is represented by a curve (a—b). The exact shape of this curve and the exact location of its end-points a and b are unknown. However, we know that the oxygen content of the manganosite phase increases with increasing O_2 pressure of the atmosphere. Hence, the curve must be concave upward and the slope of the tangent to the curve must vary continuously. Furthermore, the intercepts of this tangent with the two vertical axes measure the partial molal free energies of Mn and O, respectively, of the manganosite phase. Therefore, the shape of the curve must be such that its tangent at the extreme left end (a) (representing manganosite in equilibrium with metallic Mn) must go through the zero point on the left side vertical axis. Similarly, the tangent to the curve at its extreme right end (b), representing composition of manganosite in equilibrium with hausmannite, must pass through point m (and also through point w on the right side vertical axis corresponding to a value of F^* of $\frac{1}{2} RT \ln p_{O_2}$, where p_{O_2} is the O_2 partial pressure of the gas phase in equilibrium with hausmannite and manganosite).

In order to illustrate more clearly the relations probably causing the anomalous behavior of manganosite, a distorted free energy diagram in conjunction with a distorted temperature-com-

position-pressure diagram for the system Mn-O is presented in Fig. 4. In both diagrams in this figure the part of the diagram between the MnO and Mn_2O_4 composition points has been greatly enlarged for sake of clarity. The upper diagram shows qualitatively phase relations at subsolidus temperatures in a part of the system Mn-O. Attention is drawn to the dash lines representing O_2 isobars. (For a detailed discussion of the significance of such lines, see for instance a recent paper by Muan.⁸) These are horizontal lines through the two-phase (two condensed phases) regions, but traverse one-phase areas, such as that of manganosite, at an angle. Only two such O_2 isobars have been indicated in Fig. 4, one marked "high p_{O_2} " and the other marked "low p_{O_2} ."

It is obvious that the composition of manganosite made up at a chosen temperature will depend on the O_2 partial pressure of the atmosphere, the oxygen content of manganosite increasing with increasing O_2 partial pressures. Assume that the manganosite used as starting material in the investigation of the hausmannite-manganosite equilibrium² was made up at "low p_{O_2} " and at temperature t_1 shown in Fig. 4. The composition of this manganosite is therefore, assuming that equilibrium was reached, represented by point D₁. Now consider the situation when manganosite of this composition is introduced into the furnace under conditions of temperature and O_2 pressure close to the boundary conditions (the equilibrium curve shown in Fig. 1) for the hausmannite-manganosite equilibrium. Let this situation be represented by the "high p_{O_2} " isobar and temperature t_2 in Fig. 4. It is evident from the sketch that the equilibrium phase under these conditions is manganosite of composition represented by point C while the starting material is in a condition represented by point D₂, which is obtained by projecting the composition point D₁ to the higher temperature level t_2 . Hence the starting material is unstable in the new surroundings, and in order to obtain stability it must change its composition to C. This does not necessarily occur as a simple reaction between the manganosite starting material and oxygen of the atmosphere to form a manganosite phase increasingly rich in oxygen.

A demonstration of this is offered by the sketch in the lower half of Fig. 4. Here the free energy F^* , at constant temperature t_2 , is plotted along the vertical axis and composition along the horizontal axis. The free energy of hausmannite is represented by point m, whereas the free energy of the manganosite phase of varying composition is represented by the curve a—b. The dash line x'cx is the tangent corresponding to "high p_{O_2} ". Also shown is the straight line w'bmw which passes through point m and at the same time is tangent to the manganosite curve at point b.

The system has at least two alternative ways of reaching the equilibrium state of minimum free energy, characterized by the coexistence of manganosite (represented by point c) and gas (represented by point x). One possible way would be for manganosite to change composition continuously along the

(8) Arnulf Muan, *Amer. J. Sci.*, **256**, 171 (1958).

curved path a—b from d to c. The free energy of the system (condensed phase plus gas phase) at any instant would be represented by a point on a straight line anchored to point x and whose other end slides along the curve a—b from d to c. Another possibility is the following: Because point m, representing free energy of hausmannite, is located below the straight line connecting d and x, the system could also decrease its free energy from the original by forming hausmannite. It is easily recognized from the diagram that if manganosite of composition d and O₂ gas of partial pressure represented by point x react in the proportions required to form stoichiometric hausmannite, the free energy is lowered, as indicated by the arrow in the diagram. With manganosite, hausmannite and gas coexisting, the free energy of the system at any instant is represented by ε point in the triangle outlined by the straight line m—x and the two straight lines connecting some point on the a—b curve below d with points m and x, respectively. As the manganosite composition slowly changes along a—b during this process, the free energy gain caused by formation of hausmannite gradually diminishes and becomes zero as the manganosite composition reaches point e. From here on a reversal in the process is to be expected: The free energy of the system will be lowered by the hausmannite formed during the first stages of the reaction reverting to manganosite of compositions gradually changing from e toward c.

The weight *versus* time curve shown in Fig. 2 can be explained on this basis. The initial steep portion of the curve marked by relatively rapid weight increase corresponds to the situation where hausmannite forms while the manganosite composition is close to point d. The curve levels off as the manganosite composition moves toward point e. Here the weight reaches a maximum, and with increasing time the weight decreases slowly because of the very slow decomposition of hausmannite to manganosite of composition continuously changing from e toward c. The X-ray evidence also supports this interpretation.

It is evident from the sketch in Fig. 4 that the anomalous behavior of manganosite, that is, the intermediate formation of metastable hausmannite, is to be expected only at combinations of temperature and O₂ partial pressure close to the boundary conditions. At the chosen temperature (*t*₂) for which the sketch in Fig. 4 applies, point w represents O₂ partial pressure at the boundary curve where hausmannite and manganosite coexist in equilibrium. Point z, the intersection with the O axis of a line through point m drawn from the extreme left end of the manganosite composition curve (a), represents the largest distance from equilibrium at which the observed phenomenon should be expected. As the oxygen content of the manganosite used as starting material increases, this maximum distance from boundary conditions decreases. With point d representing the manganosite used in our experiments, the maximum distance from boundary conditions for observing the anomalous behavior is represented by point y. It is also evident that when the composition of the

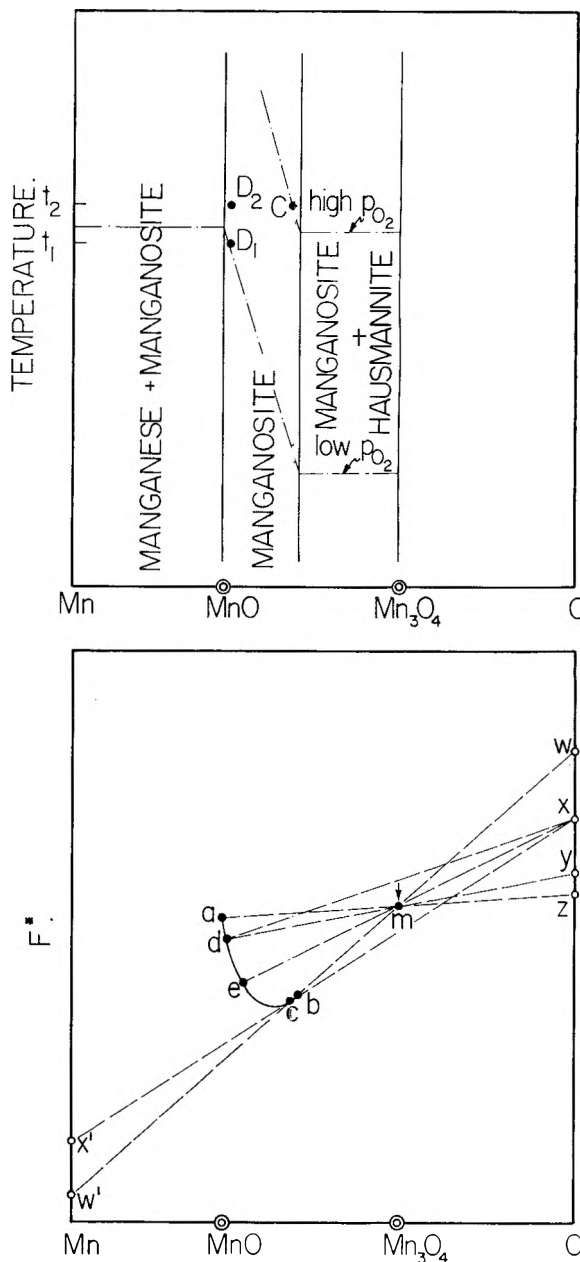


Fig. 4.—Diagrams presented in order to explain observations made as manganosite of low oxygen content transforms to manganosite of higher, equilibrium, oxygen content under conditions close to the manganosite—hausmannite boundary curve, as explained in text. The upper diagram is a distorted sketch of phase relations at subsolidus temperatures in the system Mn—O. Solid lines are boundary curves, and dash-dot lines are O₂ isobars. The lower diagram illustrates free energy relations of the manganosite and hausmannite phases at temperature *t*₂. Solid dots labeled D₁, D₂ and C in the upper diagram and a, b, c, d, e, m, in the lower diagram represent compositions of manganosite and hausmannite phases whose reactions are discussed in the text. Open circles labeled w, x, y, z, w', x', in the lower diagram are points pertaining to discussion in the text.

manganosite starting material is such that its free energy falls to the right of point e on the line a—b, the formation of hausmannite as a metastable phase should not take place at the “high *p*_{O₂}” and temperature *t*₂ used as an example in the present discussion.

The formation of metastable phases as intermediate products during heterogeneous chemical reactions is, of course, a well-known phenomenon expressed in "Ostwald's Stufenregel."⁹ However, the present case seems to be different from any observation reported previously in the literature. Our case is one in which a phase of one structure first transforms to a metastable phase of a different structure which then in turn reverts back to the original structure, all at a constant temperature and constant O₂ partial pressure. This is made possible because compositional variations occur in one of the structures involved in the equilibrium. The observation has a very significant bearing on criteria used for judging what the true equilibrium phase is in heterogeneous reactions. It is generally assumed that when a crystalline phase A of a certain struc-

(9) W. Ostwald, *Z. physik. Chem.*, **22**, 289 (1897).

ture is observed experimentally to convert to a second phase B of a different crystalline structure under a given set of experimental conditions, then structure B is stable relative to structure A under these conditions. The present investigation has shown that this is not necessarily so. Compositional variations in one of the phases may cause formation of the metastable phase B although A is the truly stable crystalline structure under the prevailing conditions. The present experience has shown that very critical evaluation of observations made in phase equilibrium studies is necessary in order to avoid wrong conclusions.

Acknowledgments.—The ideas presented in this paper resulted from experimental work carried out as part of a research project on phase equilibrium relations in oxide systems sponsored by the American Iron and Steel Institute.

DIFFUSION OF AQUEOUS SOLUTIONS OF PHOSPHORIC ACID AT 25°

BY O. W. EDWARDS AND E. O. HUFFMAN

Division of Chemical Development, Tennessee Valley Authority, Wilson Dam, Alabama

Received March 21, 1959

Diffusion coefficients of phosphoric acid solutions at 25° were measured with a two-lens Gouy diffusimeter over the concentration range 0.036 to 16 *M*. The coefficients decrease from 10.41×10^{-6} cm.² sec.⁻¹ at 0.036 *M* to 8.29×10^{-6} at 1 *M*, remain nearly constant between 1 and 5 *M*, and decrease from 7.84×10^{-6} cm.² sec.⁻¹ at 5 *M* to 1.32×10^{-6} cm.² sec.⁻¹ at 16 *M*. The precision of the *D* values is $\pm 0.3\%$. An extrapolation leads to 7.6×10^{-6} cm.² sec.⁻¹ for *D*_m⁰, the hypothetical limiting diffusion coefficient for undissociated phosphoric acid at 25°. This value, along with hydrodynamic considerations, suggests that a hydration shell surrounds the undissociated molecule. The ratio $D_{\text{H}_2\text{PO}_4^-}^0/D_m^0$ is 1.15.

Extensive inquiry¹⁻¹³ into the physicochemical properties of phosphoric acid has paralleled a remarkable growth in the industrial importance of the acid in recent years. Study of the diffusion of aqueous solutions of phosphoric acid offers means for gaining additional insight into the nature of this complex electrolyte. Of particular interest are the relative mobilities of the phosphate anion and the neutral molecular species—a comparison of the type recently reported for the weaker electrolytes acetic acid¹⁴ and citric acid.¹⁵

Here we describe measurements of diffusion coefficients of phosphoric acid at 25° over the concentration range 0.036 to 16 *M*. Made by means of a Gouy interferometer, the measurements led to a value for the limiting diffusion coefficient of undissociated phosphoric acid. The results expand greatly upon the few integral values heretofore available.¹⁶

Measurements

Apparatus.—A two-lens Gouy diffusimeter was constructed by modifying a diffractometer that was similar in design and dimensions to Buerger's apparatus.¹⁷ The light source, slit, filter and cell masks of the interferometer were essentially identical to those described^{14,18} for single-lens instruments, whereas the camera and the plate masks were modified for convenience of operation. The two lenses were almost identical plano-convex air-spaced doublets, 6 in. in diameter, corrected for chromatic and spherical aberration.

The components were mounted on an H-beam that was supported, through intervening cushions of cork and of rubber, by a continuous concrete pier.

The water-bath was mounted directly on the beam between the lenses by means of an adjustable foot assembly that fit holes in the beam. The windows of the bath were single optical flats in holders that were adjustable about the two axes perpendicular to the optic axis. The temperature of the bath was $25 \pm 0.005^\circ$.

The diffusion cell was a tall-form Tiselius cell whose top section extended above the bath liquid. The cell holder was of standard design^{18,19} with the usual cell masks and a rack-

(1) J. H. Christensen and R. B. Reed, *Ind. Eng. Chem.*, **47**, 1277 (1955).

(2) E. P. Egan, Jr., B. B. Luff and Z. T. Wakefield, *THIS JOURNAL*, **62**, 1091 (1958).

(3) K. L. Elmore, C. M. Mason and J. H. Christensen, *J. Am. Chem. Soc.*, **68**, 2528 (1946).

(4) N. N. Greenwood and A. Thompson, *Proc. Chem. Soc. (London)*, 352 (1958).

(5) E. O. Huffman, J. D. Fleming and A. J. Smith, *Ind. Eng. Chem., Chem. Eng. Data Series*, **3**, 17 (1958).

(6) O. W. Edwards and E. O. Huffman, *ibid.*, **3**, 145 (1958).

(7) C. M. Mason and J. B. Culvern, *J. Am. Chem. Soc.*, **71**, 2387 (1949).

(8) A. J. Smith and E. O. Huffman, *Ind. Eng. Chem., Chem. Eng. Data Series*, **1**, 99 (1956).

(9) C. M. Mason and W. M. Blum, *J. Am. Chem. Soc.*, **69**, 1246 (1947).

(10) R. Ripan and C. Liteanu, *Acad. Rep. Populare Române, Bul. Stiint.*, **A1**, 387 (1949).

(11) H. Sadok, *J. Indian Chem. Soc.*, **29**, 846 (1952).

(12) M. Kerker and W. F. Espenscheid, *J. Am. Chem. Soc.*, **80**, 776 (1958).

(13) K. N. Branscombe and R. P. Bell, *Disc. Faraday Soc.*, No. **24**, 158 (1957).

(14) V. Vitagliano and P. A. Lyons, *J. Am. Chem. Soc.*, **78**, 4538 (1956).

(15) G. T. A. Müller and R. H. Stokes, *Trans. Faraday Soc.*, **53**, 642 (1957).

(16) L. W. Öholm, *Finska Kemistsamfundets Medd.*, **30**, 69 (1921).

(17) M. J. Buerger, *J. Appl. Phys.*, **21**, 909 (1950).

(18) L. J. Gosting, E. M. Hanson, G. Kegcles and M. S. Morris, *Rev. Sci. Instr.*, **20**, 209 (1949).

(19) L. J. Gosting, Thesis, University of Wisconsin, 1947.

ing device for the boundary-sharpening siphon. The holder was supported by a separate bottom plate, adjustable about horizontal and vertical axes by means of screws. The components of the interferometer and the diffusion cell were optically aligned by the usual procedures.¹⁹

Calibration of the instrument against solutions of potassium chloride and of sucrose^{20,21} showed the optical lever arm ("b" distance) to be 232.25 cm.—a value reproducible within $\pm 0.05\%$. The "b" distance as determined by means of a wire grating^{22,23} agreed with the other calibration within $\pm 0.1\%$.

Preparation of Solutions.—Solutions of phosphoric acid were prepared from the triply crystallized hemihydrate. Duplicate determinations of density at 25°, with correction for the buoyancy of air, agreed to 1 part in 10,000. Concentrations were found from tables of density.¹

Procedure.—Procedures for photographing and analyzing the interference patterns have been described.^{20,21,24} Displacements of the Gouy fringes were measured with a micro-cathetometer (Gaertner M930-342), which had been calibrated against a standard scale. The usual starting time correction²⁴ Δt was applied to each determination.

Results.—Each diffusion coefficient reported in Table I is the average of values calculated from 14 to 19 patterns that were obtained within a 2- to 2.5-hr. period. The precision of D is about $\pm 0.3\%$. The deflection constant C_i did not drift significantly when the average concentration exceeded 0.15 M . A drift of 0.7 to 2.0% in C_i at concentrations below 0.14 M suggested that these boundaries were non-Gaussian, probably in the sense that they were skew. The concentration dependence of D in the concentration range 0.036 to 0.14 M (Table I) was about 10 times that at concentrations above 9 M , and was many times that at intermediate concentrations. Although generally small at low concentrations, Δc doubtless was high enough at concentrations (\bar{c}) below 0.14 to give skew boundaries because of the high concentration dependence of D .

TABLE I

GOUY DATA FOR PHOSPHORIC ACID SOLUTIONS AT 25° ^a				
\bar{c}	Δc	j_m	$D \times 10^6$	$(\Delta n/\Delta c) \times 10^4$
0.0360	0.0719	32.46	10.41	98.49
.0362	.0724	32.46	10.43	97.81
.0486	.0972	43.16	10.20	96.87
.0714	.1434	61.53	9.91 ₂	93.61
.0717	.1434	61.57	9.94 ₆	93.67
.1422	.1408	56.63	9.12 ₁	87.71
.2143	.1426	55.62	8.90 ₃	86.62
.3586	.1443	55.91	8.69 ₃	84.52
.4992	.1976	76.08	8.53 ₀	84.00
1.0846	.2115	79.40	8.29 ₇	81.90
1.9112	.1669	59.23	8.14 ₇	77.42
2.643	.1823	64.34	8.03 ₇	77.00
3.940	.2155	73.39	7.97 ₃	74.30
4.872	.1680	57.31	7.84 ₆	74.60
5.650	.2125	68.68	7.69 ₃	70.51
6.439	.2299	72.98	7.45 ₄	68.30
7.772	.1732	53.33	6.87 ₆	67.17
8.940	.2742	79.24	6.26 ₃	63.04
10.238	.1876	52.51	5.30 ₂	61.06
13.257	.2732	67.72	3.04 ₃	54.08
15.992	.2767	59.61	1.32 ₂	47.00

^a Symbols: \bar{c} = average concentration, moles/l.; Δc = difference in concentration across the boundary; j_m = total number of fringes in the Gouy pattern; D = diffusion coefficient at \bar{c} in $\text{cm}^2 \text{sec}^{-1}$; $\Delta n/\Delta c = (j_m/\Delta c)(\lambda/a)$, where a = length along optic axis of diffusion cell (2.503 cm.) and λ = wave length (5460.7 Å.).

(20) L. J. Gosting and M. S. Morris, *J. Am. Chem. Soc.*, **71**, 1998 (1949).

(21) L. J. Gosting, *ibid.*, **72**, 4418 (1950).

(22) E. Leibhardt, *J. Opt. Soc. Am.*, **43**, 1221 (1953).

(23) F. A. Jenkins and H. E. White, "Fundamentals of Optics," 2nd Ed., McGraw-Hill Book Co., Inc., New York, N. Y., 1950, p. 323.

(24) L. G. Longworth, *J. Am. Chem. Soc.*, **69**, 2510 (1947).

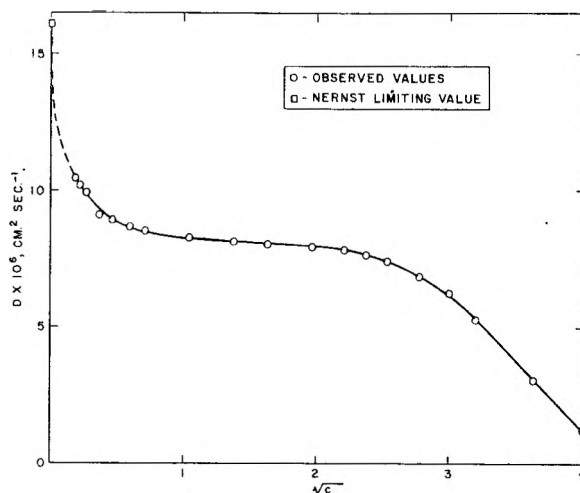


Fig. 1.—Diffusion coefficients for phosphoric acid at 25°.

With exclusion of the Δt corrections at the two highest concentrations, Δt averaged 22 sec. and ranged from 7 to 44 sec. Although Δt amounted to 75 and 144 sec. at the two highest concentrations, the precision of D at these points was $\pm 0.2\%$. The two high values of Δt may have reflected attack on the lubricant between the flanges.

A plot of D against \sqrt{c} is shown in Fig. 1.

Discussion

For a partially ionized electrolyte, Fick's first law leads to the equation

$$D = 1000RT \left(\frac{\bar{M}}{c} \right) \frac{d \ln a_u}{d \ln c} \quad (1)$$

where a_u , the activity of the undissociated species in solution, is equal to the solute activity, $a_2^{0.25} c$ is the solute concentration in moles per liter, and \bar{M} is the mobility. Activity data for phosphoric acid,³ together with the diffusion and other data, make possible an evaluation of the mobility term.

An important additional consideration, however, is how to account correctly for the effect of changing viscosity of the solution on the mobility. A correction for viscosity has been applied²⁶ as in the equation

$$D = 1000RT \left(\frac{\bar{M}}{c} \right)^* \left(\frac{d \ln a_u}{d \ln c} \right) \frac{\eta^0}{\eta} \quad (2)$$

where η^0 denotes the viscosity of the solvent and η that of the solution, and $(\bar{M}/c)^*$ is the mobility term at infinite dilution. The factor η^0/η is of limited applicability^{27,28}; it often tends toward overcorrection.²⁹⁻³¹ Stokes and Stokes^{29,32} proposed a new correction factor

$$R = \frac{\Lambda_s^0}{\Lambda_w^0} \quad (3)$$

where Λ_s^0 is the limiting equivalent conductance of an electrolyte in sucrose solution of specified viscosity and Λ_w^0 is the limiting equivalent conductance of the same electrolyte in water. The factor R generally provides less correction than does η^0/η and

(25) P. Van Rysselberghe, *This Journal*, **39**, 403 (1935).

(26) A. R. Gordon, *J. Chem. Phys.*, **5**, 522 (1937).

(27) A. R. Gordon, *J. Am. Chem. Soc.*, **72**, 4840 (1950).

(28) P. A. Lyons and C. L. Sandquist, *ibid.*, **75**, 3896 (1953).

(29) J. M. Stokes and R. H. Stokes, *This Journal*, **62**, 497 (1958).

(30) W. H. Green, *J. Chem. Soc.*, **93**, 2049 (1908).

(31) C. L. Sandquist and P. A. Lyons, *J. Am. Chem. Soc.*, **76**, 4641 (1954).

(32) J. M. Stokes and R. H. Stokes, *This Journal*, **60**, 217 (1956).

TABLE II
DIFFUSION COEFFICIENTS AND SUPPLEMENTARY DATA FOR PHOSPHORIC ACID SOLUTIONS AT 25^oa

\bar{c} , moles/l.	Density, g./ml.	$\frac{d \ln a_u}{d \ln c}$	η^0/η	R	$D_{\text{obsd}} \times 10^6$, cm. ² sec. ⁻¹	$f(D) \times 10^{19}$	$F(D) \times 10^{19}$
0.1	1.0026	1.0431	0.9734	0.970	9.392	3.731	3.745
.3	1.0130	1.1074	.9273	.938	8.734	3.431	3.392
.5	1.0234	1.1389	.8818	.902	8.514	3.420	3.343
1.0	1.0490	1.2393	.7776	.850	8.295	3.472	3.176
1.5	1.0744	1.3654	.6859	.782	8.195	3.530	3.096
2.0	1.0996	1.5219	.6049	.728	8.126	3.561	2.959
2.5	1.1246	1.7001	.5237	.660	8.061	3.652	2.898
3.0	1.1495	1.9059	.4641	.620	8.026	3.660	2.740
4.0	1.1987	2.4240	.3569	.540	7.956	3.710	2.144
5.0	1.2472	3.0465	.2752	.462	7.836	3.770	2.246
6.0	1.2953	3.8808	.2139	.399	7.597	3.692	1.977

^a Density from ref. 1; $d \ln a_u/d \ln c$ calculated from activity data in ref. 3; η^0/η from ref. 6; **R** derived from data for HCl, ref. 29.

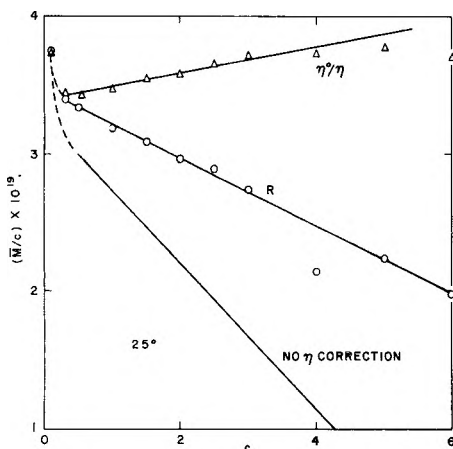


Fig. 2.—Effect of viscosity corrections on mobility term.

may more reliably represent the effect of viscosity on mobility.³³ Factor **R** varies somewhat with the electrolyte (10% difference between HCl and tetramethylammonium iodide in 20% sucrose) but is not a highly specific function of the electrolyte.²⁹ The hydrogen ion is considerably less affected by increase in viscosity than are other ions,²⁹ and we have assumed that the values of **R** for hydrochloric acid at a given value for η^0/η are applicable to phosphoric acid solution of the same viscosity.

Values for the limiting mobility ratio, represented as a function of diffusion coefficient, were calculated from the equations

$$f(D) = \frac{D_{\text{obsd}}}{1000RT \left(\frac{d \ln a_u}{d \ln c} \right) \frac{\eta^0}{\eta}} \quad (4)$$

$$F(D) = \frac{D_{\text{obsd}}}{1000RT \left(\frac{d \ln a_u}{d \ln c} \right) \mathbf{R}} \quad (5)$$

The data required and results of the calculations are shown in Table II. The importance of viscosity in the mobility of phosphoric acid is shown in Fig. 2, where mobility ratios from equations 4 and 5 are compared with the values derived from the experimental diffusion coefficients when no viscosity factor was used. Since η^0/η is more highly concentration-dependent than **R**, it has a much greater effect on the mobility term, as has been found for other materials.²⁹⁻³²

(33) J. C. M. Li and P. Chang, *J. Chem. Phys.*, **23**, 518 (1955).

In addition to the viscosity correction, a complete equation for predicting diffusion coefficients of a partially ionized electrolyte must reflect the influence of dielectric constant, hydration and degree of dissociation, α , in relation to concentration. A treatment has been advanced which incorporates corrections for α and for hydration,³⁴ but the data available on phosphoric acid are not adequate for a test.

The hypothetical diffusion coefficient of the undissociated phosphoric acid at infinite dilution, D_m^0 , may be estimated from somewhat less information. Phosphoric acid is too strong an electrolyte to permit confident use of the method that Vitagliano and Lyons¹⁴ used for acetic acid, however, because the method requires data at concentrations where $\alpha \cong 0$. Furthermore, the degree of dissociation of phosphoric acid, as calculated from either conductance or e.m.f., passes through a minimum at about 1 *M*—a phenomenon presumably attributable to association or hydration reactions of uncertain detail, although several complex species have been suggested.¹⁰⁻¹³ Thus, any use of α at concentrations above 1 *M* may lead to unreliable results.

Müller and Stokes¹⁵ evaluated D_m^0 for the undissociated citric acid molecule from data in a range of concentration where α varied from 0.06 to 0.09. They plotted a function of the observed and the Nernst limiting diffusion coefficients against concentration and extrapolated to zero concentration. The function may be written

$$D_m' = \frac{\left[\left(1 - \frac{\alpha}{2} \right) D_{\text{obsd}} \left(\frac{1}{\mathbf{R}} \right) - \frac{\alpha}{2} D_1^0 \right]}{d \ln a_u/d \ln c} / (1 - \alpha) \quad (6)$$

where D_1^0 is the Nernst limiting diffusion coefficient and $1/\mathbf{R}$ replaces the quantity η/η^0 . At zero concentration

$$\lim_{c \rightarrow 0} D_m' = D_m^0$$

The approximations and limitations inherent in equation 6 were discussed.¹⁵ As α approaches unity, the calculated value for D_m' will approach infinity. Even with this relationship, data should be used for concentrations corresponding to low values of α , and the extrapolation should be made from the linear portion of the curve corresponding

(34) B. F. Wishaw and R. H. Stokes, *J. Am. Chem. Soc.*, **76**, 2065 (1954).

TABLE III
QUANTITIES^a REQUIRED FOR ESTIMATING D_m^0

\bar{c} , moles/l	Density, g./ml.	η/η^0	1/R	Equiv. conductance, Λ , int. ohm ⁻¹ cm. ²	α	$D_{\text{obsd}} \times 10^6$, cm. ² sec. ⁻¹	$\frac{d \ln a_u}{d \ln c}$	$D_m' \times 10^6$, cm. ² sec. ⁻¹
0.0717	1.0009 ₇	1.0191	1.0081	117.71	0.33	9.946	1.047	8.16
.1422	1.0047 ₈	1.0382	1.0163	95.64	.27	9.121	1.062	7.55
.2143	1.0085 ₄	1.0555	1.0246	83.06	.24	8.90E	1.077	7.45
.3586	1.0160 ₃	1.0945	1.0452	66.51	.20	8.69E	1.108	7.41
.4992	1.0230 ₂	1.1323	1.0661	64.30	.20	8.530	1.138	7.23

^a Density from ref. 1; η/η^0 from ref. 6; R derived from data for HCl, ref. 29; equivalent conductance from ref. 8; limiting equivalent conductance ($\Lambda^0 = 382.74$) from ref. 7; α calculated from conductance data, ref. 8.

to the higher concentrations. The weaker the electrolyte, the more reliable will be the value derived for D_m^0 .

Calculation of D_m' for several concentrations of phosphoric acid in the concentration range 0.07 to 0.5 M yielded the results shown in Table III. The value of α at each concentration was calculated from conductance data by the method outlined by Wishaw and Stokes,³⁴ except that the factor R replaced the ratio η^0/η . Note that the values for α are relatively high—0.2 to 0.3. The Nernst limiting diffusion coefficient was found to be 16.05×10^{-6} cm.² sec.⁻¹ by use of the usual formula

$$D_i^0 = \frac{2RT}{F^2} \frac{\lambda_+^0 \lambda_-^0}{\lambda_+^0 + \lambda_-^0}$$

where R is in joules deg.⁻¹ mole⁻¹ and F is in absolute coulomb equivalent⁻¹.

Extrapolation of the linear portion of a plot of D_m' against concentration leads to the value 7.6×10^{-6} cm.² sec.⁻¹ at infinite dilution, which is taken as an approximate value for D_m^0 .

Values for D_m^0 based on classical hydrodynamical considerations are of interest, even though the phosphoric acid molecule may not fully meet the requirements of theory in regard to size and shape.³⁵ In spite of its inherent limitations, the Stokes-Einstein equation

$$D = \frac{kT}{6\pi\eta r} \quad (7)$$

often leads to values for D in surprisingly good agreement with values determined by more direct methods.³⁵ Equation 7 assumes no slip at the surface of the diffusing particle. With complete slip at the surface the equation becomes³⁵

$$D = \frac{kT}{4\pi\eta r} \quad (8)$$

A value of 3.41 Å. was calculated for r , the radius of

the diffusing particle, from intrinsic viscosity according to the method of Scheraga and Mandelkern.³⁶ Equation 7 leads to 7.2×10^{-6} cm.² sec.⁻¹ for D_m^0 , and equation 8 leads to 10.8×10^{-6} cm.² sec.⁻¹. Other modifications of hydrodynamic models^{33,37} lead to even higher, and less likely, values for D_m^0 .

The relatively good agreement between the values calculated from equations 6 and 7 suggests that the limiting diffusion coefficient of H_3PO_4 molecules is approximately 7.6×10^{-6} cm.² sec.⁻¹ and lends strength to the assumption of no slip at the surface of the diffusing phosphoric acid molecule—a condition indicating that the diffusing molecules are surrounded by an associated layer of solvent.³⁵ The value for D_m^0 is less than the limiting diffusion coefficient calculated for the anion $H_2PO_4^-$, 8.79×10^{-6} cm.² sec.⁻¹, from the relation

$$D_{H_2PO_4^-}^0 = \frac{RT\lambda^0}{F^2} \quad (9)$$

where λ^0 was taken as 33.0 (ref. 7). The ratio $D_{H_2PO_4^-}^0/D_m^0$ is 1.15. Finding ratios for limiting diffusion coefficients of anions to molecules ranging from 1.23 to 1.33, Stokes^{15,35} suggested that this relationship is accounted for by the charged particle breaking the water structure and thus giving a lubricating effect for the ions. On the other hand, Vitagliano and Lyons¹⁴ found for the much weaker electrolyte, acetic acid, a value of D_m^0 that is slightly greater than that of $L^0_{CH_3COO^-}$ calculated from equation 9.

Acknowledgment.—K. L. Elmore, Chief of the Research Branch, TVA, and H. S. Harned, Consultant to TVA, contributed guidance and encouragement during the study. P. A. Lyons, Consultant to TVA, gave helpful advice about the design and testing of the Gouy apparatus.

(36) H. A. Scheraga and L. Mandelkern, *J. Am. Chem. Soc.*, **75**, 179 (1953).

(37) B. Ottar *Acta Chem. Scand.*, **9**, 344 (1955).

(35) R. H. Stokes, *Australian J. Sci.*, **19**, P35 (1957).

CONSUMPTION OF OXYGEN MOLECULES IN HYDROCARBON FLAMES CHIEFLY BY REACTION WITH HYDROGEN ATOMS

BY C. P. FENIMORE AND G. W. JONES

General Electric Research Laboratory, Schenectady, N. Y.

Received March 21, 1959

The rate of consumption of O_2 is measured by probe sampling through low pressure, flat, premixed flames of CH_4 , O_2 , A or through flames with C_2H_2 or C_3H_8 fuels, all burnt on cooled porous burners with flame temperatures of 1300 to 1950°K. $[H]$ is also measured in the same flames by the rate of formation of HD from added D_2 or D_2O , and turns out to be the concentration required, within 30%, to account for the observed $-d[O_2]/dt$ according to the known rate of the reaction, $H + O_2 \rightarrow OH + O$. It is concluded that O_2 is consumed chiefly by reaction with H atoms in either lean or rich hydrocarbon flames.

Introduction

The rate constant for the reaction $H + O_2 \rightarrow OH + O$ is fairly well known,¹⁻³ so by measuring $[H]$, $[O_2]$ and $-d[O_2]/dt$ in hydrocarbon flames, one can tell whether this reaction is of major importance for the observed decay of O_2 . In the flames reported in this paper, with CH_4 , C_2H_2 or C_3H_8 fuels, O_2 is consumed much more by reaction with H atoms than in any other way.

Experimental

Water-cooled, flat-flame burners⁴ were used at reduced pressures to obtain moderately thick, flat flames. Any rich flames used were free from soot. Temperature traverses were made with quartz-coated thermocouples corrected for radiation,⁴ sampling was through fine quartz probes, and analyses were carried out on a mass spectrometer.

The composition traverses were recast as reaction rates through the flame as already described.³ Briefly, the mole fraction of each species was plotted *vs.* distance from the surface of the burner, X_1 *vs.* z . Using approximate binary diffusion coefficients,⁵ the diffusion velocity of the *i*th species was calculated through the flame, $V_i = -(D_i/X_i) dX_i/dz$; and then the fraction of mass flow due to the *i*th species

$$G_i = \frac{X_i M_i}{M} \left(\frac{v + V_i}{v} \right)$$

In these formulas, D_i = diffusion coefficient, M = average molecular weight, M_i = molecular weight of the *i*th species, v = gas velocity as calculated from the known mass flow ρv and the density ρ . Finally, the rate of appearance of the *i*th species due to chemical reaction was obtained, it is equal to $(\rho v/M_i) dG_i/dz$.

The concentrations of radicals were estimated by "indicator" reactions as already described. The estimates of $[H]$ are accurate to within a factor of two at least, because independent estimates by other methods have been found to agree at least this well.³ A few estimates of $[O]$ must be viewed more skeptically because the method used for this radical has not been checked against other methods.

The rate constants used to interpret the data are listed in Table I. The reverse constants for reactions (a) and (b) were calculated from the forward constants and from a tabulation of equilibria over the temperature range of interest.⁶ k_c is known from measurements of the rate of consumption of O_2 in the early parts of three H_2 , O_2 flames, with simultaneous measurements of $[H]$ via the formation of HD from added heavy water.³ The value of Table I lies between an estimate by Semenov¹; 6.7×10^6 at 793° which would become 1.8×10^8 at 1100°K. if one accepts his activation energy of 18.5 kcal.; and Baldwin's² estimate of 2.7×10^6 at 793°, which would become 0.7×10^8 at 1100°K. on the same basis.

(1) N. N. Semenov, *Acta Physicochim.*, **20**, 290 (1945).

(2) R. R. Baldwin, *Trans. Faraday Soc.*, **52**, 1344 (1956).

(3) C. P. Fenimore and G. W. Jones, *THIS JOURNAL*, **63**, 1154 (1959).

(4) W. E. Kaskan, "6th Symposium on Combustion," Reinhold Publ. Corp., New York, N. Y., 1957, p. 134.

(5) A. A. Westenberg, *Combustion & Flame*, **1**, 346 (1957).

(6) B. Lewis and G. von Elbe, "Combustion, Flames and Explosions of Gases," Academic Press, New York, N. Y., 1951.

TABLE I

RATE CONSTANTS IN L. MOLE⁻¹ SEC.⁻¹ AT FLAME TEMPERATURES

	$k_{forward}$	$k_{backward}$
(a) $H + H_2O = H_2 + OH$	$1 \times 10^{12} e^{-25,500/RT} \cdot 8$	$2.5 \times 10^{11} e^{-10,000/RT}$
(b) $H + CO_2 = CO + OH$	$3 \times 10^{12} e^{-33,300/RT} \cdot 9$	$2.3 \times 10^{10} e^{-10,300/RT}$
(c) $H + O_2 = OH + O$	1.5×10^8 at 1100°K. ¹ $E = 18 \pm 3$ kcal.	
(d) $H + N_2O = N_2 + OH$	$4 \times 10^{11} e^{-16,300/RT} \cdot 3$	
(e) $O + N_2O = 2NO$	$2 \times 10^{11} e^{-32,000/RT} \cdot 10$	
	or approximate values only	$0.9 \times 10^{11} e^{-27,800/RT}$

k_e in Table I is the unchecked constant used to determine $[O]$. The first value is the approximate estimate from our own work; the second is obtained from the assumption that NO decays at moderate temperatures *via* the reverse process, and from Kaufman and Kelso's accurate determination of this decay rate.⁷ For the rough estimates of $[O]$ made in this paper, it does not matter which expression is used.

It should be pointed out that a percentage comparison of $[H]$ as measured *via* reaction (a), $H + D_2O = HD + OD$, with $[H]$ required to destroy O_2 *via* reaction (c) depends on the ratio k_a/k_c rather than on the absolute value of either constant. This is all to the good, for k_b , k_c and k_d of Table I were determined relative to k_a and while these constants are only claimed to be correct to within a factor of two, their ratios are correct to perhaps 30%. This estimate is suggested because we find a 30% discrepancy between our data and a conclusion which we believe to be consistent with them. It would be very difficult to estimate separately the errors resulting from approximate diffusion corrections, sampling errors, etc.; but an earlier comparison of reaction rate ratios, k_a/k_b with the reverse constants, gave about the same discrepancy.³

Results from a Typical Run.—Some analyses and derived rates of reaction in CH_4 flames are plotted in Figs. 1 to 3, and numerical data are listed in Table II. The flame described by Fig. 1 is discussed in detail as an example. This had the reactant composition $CH_4 + 1.87 O_2 + 8A + H_2$, and was burnt with a mass flow of 8.65×10^{-3} g./cm.², sec. at a pressure of 7 cm. Small concentrations of C_2 hydrocarbons and perhaps H_2CO were formed in the strongly luminous zone, but did not persist into the post flame gas.

The concentration of H atoms was estimated by two different methods. First, heavy water was added to the reactants and the rate of formation of HD measured just beyond the main reaction zone.⁸ At 0.4 to 0.55 cm. from the burner surface,

(7) F. Kaufman and J. Kelso, *J. Chem. Phys.*, **23**, 1709 (1956).

(8) C. P. Fenimore and G. W. Jones, *THIS JOURNAL*, **62**, 693 (1958).

(9) C. P. Fenimore and G. W. Jones, *ibid.*, **62**, 1678 (1958).

(10) C. P. Fenimore and G. W. Jones, *ibid.*, **62**, 178 (1958).

this method gave $[H] = 50 \times 10^{-7}$ mole/l. in the post flame gas at 1780°K . Second, part of the H_2 in the fuel was replaced by D_2 and the rate of formation of HD measured early in the flame.³ In this second method, one must correct for the fact that the gross rate of formation of HD is larger than $[\text{HD}]$ observed because HD undergoes simultaneous oxidation at a rate which is approximated by

$$\left\{ \frac{[\text{HD}]}{[\text{H}_2]} \right\} \times (\text{rate of formation of water from } \text{H}_2)$$

The quantity (rate of formation of water from H_2) is about $8[\text{CO}_2][\text{H}_2]/[\text{CO}]$, see below, and then the gross rate of formation of HD at 1100°K . turned out to be 4 times the $[\text{HD}]$ observed. Equating this to $k'[\text{H}][\text{D}_2]$ where k' is the rate constant for $\text{H} + \text{D}_2 \rightarrow \text{HD} + \text{D}$,^{3,11} $[\text{H}] = 80 \times 10^{-7}$ at 1100° , $z = 0.137$ cm. Thus $[\text{H}]$ by the two methods agreed to $\pm 25\%$.

The $[\text{H}]$ found above is of the right order to account for the observed rate of consumption of O_2 . If O_2 is consumed only *via* reaction (c), $-\dot{[\text{O}_2]} = k_c[\text{O}_2][\text{H}]$. Introducing the measured $[\text{O}_2]$ and $[\text{O}_2]$ at 1100°K ., and taking k_c from Table I, we get $[\text{H}] = 60 \times 10^{-7}$ mole/l. This agrees very well with $[\text{H}]$ as measured directly. It can be shown that reaction (c) accounts for $-\dot{[\text{O}_2]}$ not only at 1100° but up to 1600° ; for a plot of $\log -\dot{[\text{O}_2]}/[\text{O}_2]$ vs. $1/T$ is linear and possesses a slope corresponding to 17 kcal. which is about the activation energy of reaction (c). At temperatures much above 1600°K ., toward the end of the reaction zone, $-\dot{[\text{O}_2]}/[\text{O}_2]$ decreases because the reverse of reaction (c) increases rapidly.¹²

Some additional information can be obtained from Fig. 1. Until CH_4 has fallen below 10% of its initial value, $[\text{CO}]$ is 70 to 85% of $-\dot{[\text{CH}_4]}$. This agrees with the common belief that CO is the only carbon oxide formed directly from CH_4 , and that CO_2 is formed only from the intermediate CO.

Now if the last sentence is accepted, it can be shown that H_2O is not formed directly from CH_4 either, but only from the H_2 present at any time. We have found previously that in the early parts of flames of mixed H_2 and CO fuel, a situation in which CO_2 is surely formed only from CO, $[\text{H}_2\text{O}][\text{CO}]/[\text{CO}_2][\text{H}_2] = 8$; and this was considered fair agreement with the ratio $k_a/k_{-b} = 12$ which would be expected if H_2O were formed from H_2 only *via* the reverse of reaction (a), and CO_2 from CO only *via* the reverse of reaction (b).³ Therefore, if H_2O were formed from CH_4 in the present flame as well as from H_2 , but CO_2 still formed only from CO, one must have $[\text{H}_2\text{O}][\text{CO}]/[\text{CO}_2][\text{H}_2] > 8$. But over the region $z = 0.125$ to 0.3 cm., we find this ratio only 5 ± 1 ; that is, the observed

(11) G. Boato, G. Careri, A. Cimino, E. Molinari and G. G. Volpi, *J. Chem. Phys.*, **24**, 783 (1956).

(12) The inhibition of (c) toward the end of the reaction zone cannot be a temperature effect because the reverse of (c) has practically zero activation energy. Rather, the build up of radicals by reaction (c) ultimately limits their own formation. The inhibition sets in rather sharply; possibly because (c) is a branching reaction, possibly in part because H atoms can diffuse upstream more readily than O or OH.

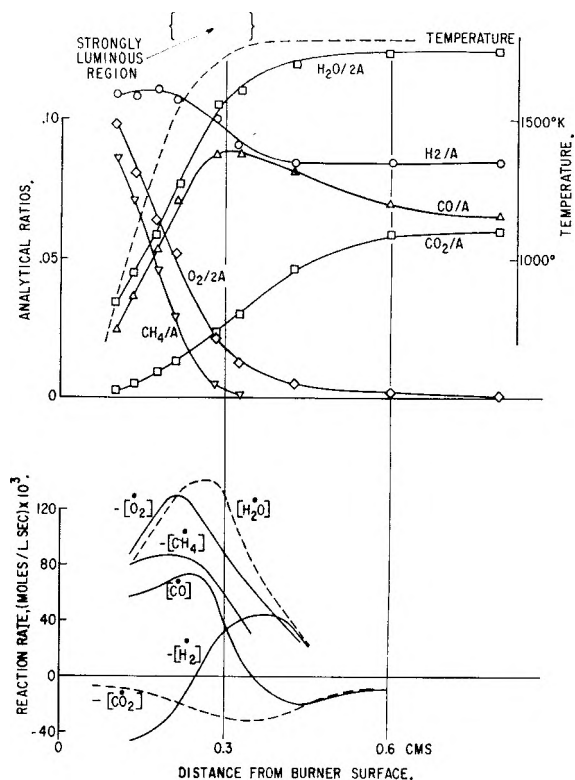


Fig. 1.—Analyses and derived reaction rates through a moderately rich CH_4 , H_2 , O_2 , A flame.

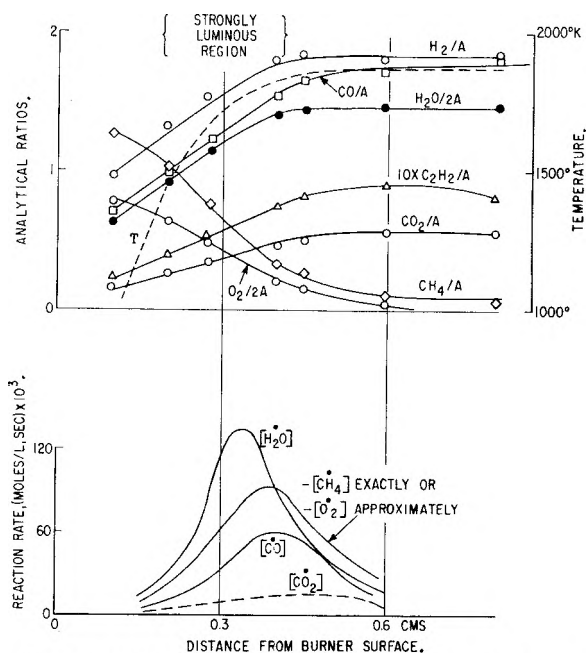
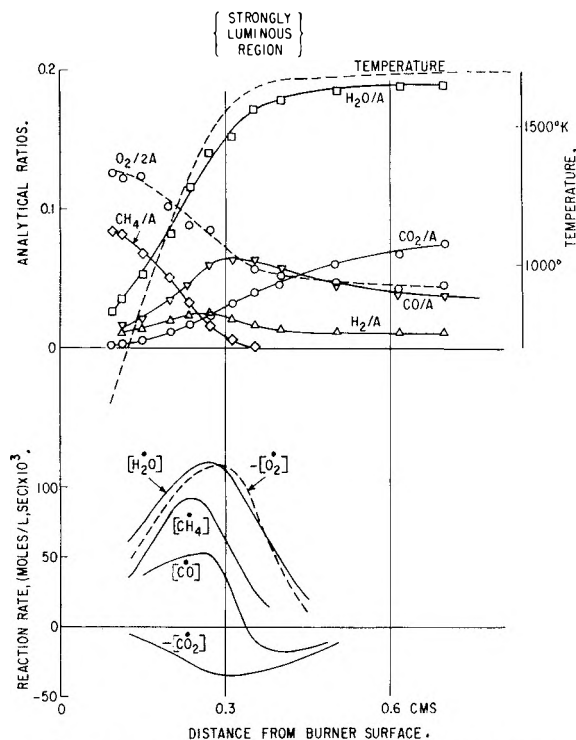
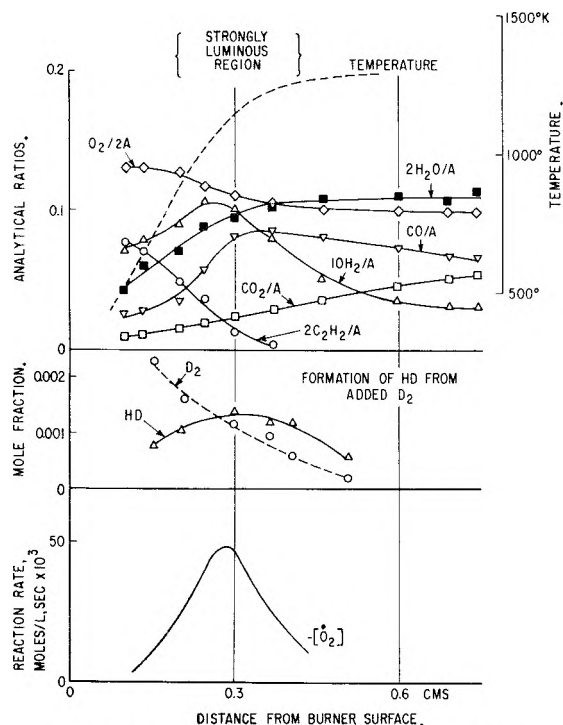


Fig. 2.—Results through a very rich CH_4 , O_2 , A flame.

rate of H_2O formation relative to CO_2 formation is surely no greater and probably even less than we expect only from the H_2 present. In other flames, $[\text{H}_2\text{O}][\text{CO}]/[\text{CO}_2][\text{H}_2]$ is sometimes larger, but never significantly greater than 8, and this rules out $\text{CH}_4 + \text{OH} \rightarrow \text{CH}_3 + \text{H}_2\text{O}$ as an important reaction in CH_4 flames; or at least admits it only if H_2O is consumed in some other step so that the

Fig. 3.—Results through a lean CH_4 , O_2 , A flame.Fig. 4.—Results through a lean C_2H_2 , O_2 , A flame.

net H_2O formation from decomposing CH_4 is zero or less than zero.

We sum up the discussion of Fig. 1. It has been shown that O_2 is destroyed chiefly *via* H atom attack just as in the H_2 , O_2 flame, and that no considerable net formation of CO_2 or of H_2O occurs directly in the decay of CH_4 .

Other CH_4 Flames.—Four other CH_4 flames were examined and are discussed briefly. Figure 2

shows some results for a very rich flame in which more than 10% of the carbon fed as CH_4 appears as C_2 hydrocarbons, mostly as C_2H_2 . $[\text{H}]$ is smaller in this than in the preceding flame and near the value appropriate to the equilibrium $\text{H}_2 = 2\text{H}$, for in the burnt gas the equilibrium $[\text{H}] = 6 \times 10^{-7}$ mole/l. Small as it is, however, $[\text{H}]$ is just about that required to destroy O_2 *via* reaction (c) at the observed rate.

Figure 3 gives results of a lean flame. In such flames, $[\text{H}]$ cannot be determined easily in the burnt gas by adding D_2O , but can be estimated roughly at least by the residual $[\text{H}_2]$. Because the reactions $\text{H} + \text{O}_2 = \text{OH} + \text{O}$, $\text{O} + \text{H}_2 + \text{OH} + \text{H}$, $\text{H} + \text{H}_2\text{O} = \text{H}_2 + \text{OH}$ are generally equilibrated in the post flame gas,¹³ the equilibrium $3\text{H}_2 + \text{O}_2 = 2\text{H}_2\text{O} + 2\text{H}$ is also generally satisfied. This consideration, with equilibrium constants, from ref. 6, gives the approximate $[\text{H}]$ titled "other" in Table II. Once again $[\text{H}]$ is just sufficient to react early in the flame with O_2 at the measured rate of $-\dot{[\text{O}_2]}$.

Finally, we replaced 10% of the O_2 in the reactants by an equivalent amount of N_2O in two flames, those described by Figs. 1 and 3, in order to get an estimate of $[\text{O}]$ by means of the reaction, $\text{O} + \text{N}_2\text{O} \rightarrow 2\text{NO}$. The effect of this partial replacement was to raise the final temperature by about 160°K. The general appearance of the curves for reaction rate *vs.* z was not greatly changed however. $[\text{H}]$ was reduced, see Table II, but remained the $[\text{H}]$ required by reaction (c) to give the $-\dot{[\text{O}_2]}$ observed early in the flame. Furthermore, over the temperature range 1000 to 1600°K., $-\dot{[\text{O}_2}]/[\text{O}_2]$ was within 30% the same as $-\dot{[\text{N}_2\text{O}]}/[\text{N}_2\text{O}]$; and since N_2O reacts with H atoms with a rate constant, k_d of Table I, about the same as k_c , it is evident that N_2O also is destroyed chiefly by attack of H atoms. The small amount of NO formed suggests that in the region of maximum rate of reaction, $[\text{O}] = 3[\text{H}]$ approximately in the fuel lean flame, and $[\text{O}] = [\text{H}]$ approximately in the rich flame. In both flames, $[\text{O}]$ decays rapidly as one moves downstream into the post flame gas. Thus $[\text{O}]$ behaves differently from $[\text{H}]$ which is about the same in the reaction zone and in the post flame gas. The result that $[\text{O}]$ is comparable to $[\text{H}]$ in these flames means that O atoms might be important in the decay of CH_4 . Our finding that $-\dot{[\text{O}_2]}$ is accounted for by reaction (c), however, is not affected by $[\text{O}]$ or $[\text{OH}]$ because these species cannot destroy O_2 molecules.

Since five times out of five tries we found reaction (c) proceeding at about the measured rate of $-\dot{[\text{O}_2]}$, we took the chief mechanism of O_2 destruction in either rich or lean CH_4 flames as known at this point.

Flames with Other Fuels.—The remainder of Table II shows that O_2 is destroyed chiefly by attack of H atoms in rich or lean flames of other hydrocarbon fuels also. Figures 4 and 5 will be discussed briefly.

(13) (a) E. M. Bulewicz, C. G. James and T. M. Sugden, *Proc. Roy. Soc. (London)*, **A235**, 89 (1956); (b) W. E. Kaskan, *Combustion & Flame*, **2**, 229 (1958).

TABLE II
DATA SHOWING THAT [H] IN FLAMES IS JUST SUFFICIENT TO CONSUME O₂ AT THE RATE OBSERVED

Figure Reactants	1	2	3 CH ₄ ^a C ₂ H ₂ ^a	4	...	5 C ₃ H ₈ ^a	...
O ₂	1.87	1.12	2.56	2.31 ^a	1.68 ^b	1.88	4.84	8.33	3.13	4.50
A	8	0.4	10	10	8	7.5	17.2	11.33	4.54	5.56
H ₂	1	0	0	0	1	0	0	0	0	0
Mass flow × 10 ³ , g./cm. ² × sec.	8.65	1.93	8.81	7.96	8.4	5.05	7.26	3.0	3.2	4.23
Flame T, °K.	1780	1860	1700	1860	1950	1818	1310	1500	1920	1940
Pressure, cm.	7	14	6	8	7	6	4	3	8	3
10 ⁷ [H] found <i>via</i>										
added D ₂ O	50	5	25	15	10	22
added D ₂	80	4	60	30	20	10	44	6	6	33
Other	30	30	50	10
10 ⁷ [H] required by -[O ₂]	60	3	40	30	14	10	35	4	7	23
[H ₂ O][CO]	5	5	9	8	8	7	9	8	5	7
[CO ₂][H ₂]										

^a Also had 0.51 N₂O per mole CH₄ in reactants. ^b Also had 0.40 N₂O per mole CH₄ in reactants.

It may be interesting to compare our lean C₂H₂ flame, Fig. 4, with a very lean C₂H₂, O₂ flame probed by Fristrom and co-workers.¹⁴ Their flat flame was C₂H₂ + 31O₂ burnt at 7.5 cm. Hg P with burning velocity 71 cm./sec. and calculated final flame temperature of 1451°K. Ours is C₂H₂ + 4.8 O₂ + 18 A at 4 cm. Hg P, 90 cm./sec. burning velocity, measured final flame temperature 1300°K. At our lower pressure, the strongly luminous zone is a little thicker (~0.22 cm. *vs.* their ~0.16 cm.). We agree in finding that the maximum CO occurs just about when C₂H₂ has fallen to zero, and in placing this point within but toward the downstream edge of the luminous zone. Also we agree in finding that the maximum H₂ occurs earlier in the luminous zone, about 0.1 cm. before the maximum CO, and when about 1/2 of the total fall of O₂ has occurred. In both flames, H₂O is near its final value at the downstream end of the luminous zone. The principal differences are: we find more residual H₂ in the post flame region than they do, and we find a much slower formation of CO₂. These differences are probably reasonable since their flame was much leaner.

Figure 4 also shows the course of HD formation and decay when a little D₂ is added to the reactants. Since HD goes through a maximum, it is easy to estimate [H] when d[HD]/dt = 0 on the assumption³ that

$$k'[H][D_2] = \frac{[HD]}{[H_2]} \times (\text{rate of formation of water from H}_2)$$

where *k'* is the rate constant for H + D₂ → HD + D.

Figure 5 gives some results for a very rich C₃H₈ flame which resembles the flame described by Fig. 2 in that [H] is near the calculated concentration in the burnt gas appropriate to the equilibrium H₂ = 2H; [H]_{equi} = 7 × 10⁻⁷. The flames described by Fig. 2 and 5 are the only ones in which the post flame gas contains hydrocarbons, and are also the only ones which contain just the equilibrium [H] in the post flame gas.

C₂H₂ or C₃H₈ flames resemble CH₄ flames in

(14) R. M. Fristrom, W. H. Avery and C. Grunfelder, "7th Symposium (International) on Combustion," Butterworths, London, 1959, p. 304.

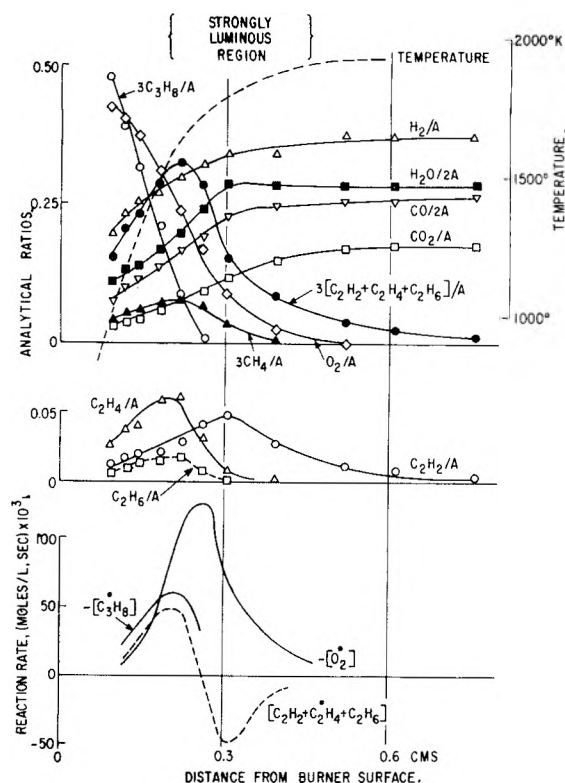


Fig. 5.—A very rich C₃H₈, O₂, A flame.

that CO₂ appears to be formed only from the intermediate CO. If this is really so, then the observed value for the ratio [H₂O][CO]/[CO₂][H₂] requires the conclusion that little direct net formation of H₂O occurs from these fuels either, but that H₂O is formed chiefly from the H₂ present at any time.

Conclusion

Ignoring the rough estimates of [H] entitled "other" in Table II, we find that [H] determined *via* added D₂ or D₂O is the same within an average deviation of 30% as the [H] required if O₂ decays solely by reaction (c), and this is true over a 20-fold change in [H].

There is little doubt that O₂ is destroyed more by reaction (c) than in any other way. A de-

struction of O_2 entirely *via* (c), that is, no considerable reaction between O_2 and any hydrocarbon or hydrocarbon radical at all, would be consistent with our results and with other observations on hydrocarbon flames. For it O_2 reacts only with H atoms, the large amount of CO formed in CH_2 flames would have to arise by reactions of O, OH, H_2O with species such as CH_3 , CH_2 , etc. But then all plausible reactions which form CO would also destroy free valences and the formation of CO and H_2 from the hydrocarbon fuel should have to be considered a chain terminating process which was fed by free radicals generated in reaction (c). This view would account for the fact that flames rich enough to contain hydrocarbon in the products possess only about the equilibrium [H] in the post flame gas, while fuel lean hydrocarbon flames or either rich or lean H_2 flames contain so many free radicals that [H] in the post flame gas is many times the concentration appropriate to the

equilibrium $H_2 = 2H$. It would also agree with experiments on the slow CH_4 , O_2 reaction in static systems at $900^\circ K$. or higher, where CH_4 inhibits its own oxidation presumably by the destruction of radicals.¹⁵ A destruction of O_2 only *via* reaction (c) would require that reactions between O_2 and hydrocarbon or hydrocarbon radicals, such as are presumed to occur in low temperature oxidations and in cool flames, be irrelevant to the main course of the reaction in hot flames; but many persons have believed the low temperature mechanisms to be irrelevant to hot steady flames.

It must be pointed out, however, that our data are not sufficiently precise to exclude some reaction of O_2 in other ways than *via* reaction (c). All we can claim is that (c) is more important than any other way.

(15) M. Vanpee and F. Gard, "5th Symposium on Combustion," Reinhold Publ. Corp., New York, N. Y., 1955, p. 484; D. E. Hoare and A. D. Walsh, *ibid.*, p. 474; and references cited by these authors

THE EFFECT OF SIMULTANEOUS CROSSLINKING AND DEGRADATION ON THE INTRINSIC VISCOSITY OF A POLYMER

By R. W. KILB

General Electric Research Laboratory, Schenectady, New York

Received March 25, 1959

The change in intrinsic viscosity $[\eta]$ is studied for a process during which a polymer is simultaneously degraded and crosslinked. An example of such a process is irradiation of polymers. It is possible to determine the relative amount of degradation and crosslinking by following the change of $[\eta]$ during the process. Qualitative agreement of theory with experiment is good. Quantitatively the method is limited to the range unity to ten for the ratio of degradations to crosslinks; outside these limits the shape of the $[\eta]$ curve is insensitive to this ratio. It is found that the best sensitivity is obtained when $[\eta]$ is determined in Θ solvents. By following the change in osmotic and light scattering molecular weight for silicone irradiated by an electron source, the ratio of degradations to crosslinks was found to be less than 0.5.

During certain processes, polymer molecules are simultaneously crosslinked and degraded. Typical examples are irradiation and oxidation. This leads to a polymer with long chain branching and either increased or decreased molecular weight, depending on the degree of degradation. We are interested here in determining the relative amount of crosslinking and degradation from a study of the change in intrinsic viscosity of the polymer. This problem has been treated in an approximate manner by Shultz, Roth and Rathmann.¹ Although most of their results are qualitatively correct, their quantitative calculations are inexact because of their use of the Stockmayer and Fixman² approximation for the effect of branching on the intrinsic viscosity of a polymer. Recently Zimm and Kilb³ have shown that previous theories seriously overestimate the effect of branching on intrinsic viscosity, and proposed a new theory which is in good agreement with the available data. We propose to use this theory in the present study. The quantitative results of Shultz, *et al.*, also suffer to some extent from the lack of use of a definite molecular weight distribution.

The problem of determining the relative amount of crosslinking and degradation has also been treated by Charlesby.⁴ His method involves following the amount of gel produced during the process.

It has perhaps not been sufficiently forcibly pointed out in previous studies that the quantitative calculations are rather sensitive to the assumed initial molecular weight distribution. Consequently, in the application of the calculations, it is necessary to determine if the experimental polymer actually has the assumed distribution. If this is not the case, the results must be viewed with some scepticism.

In this paper we shall make the assumptions: (1) the scissions are directly proportional to the crosslinks throughout the process and their distribution is "random"; (2) the crosslinks are tetrafunctional, *i.e.*, four branches radiate out from the crosslinked site; (3) the initial molecular weight distribution is assumed to be the "most probable" distribution (see below).

On the basis of these assumptions, we may combine the results of Zimm and Kilb with the distribution function given by Stockmayer⁵ to cal-

(1) A. R. Shultz, P. I. Roth and G. B. Rathmann, *J. Polymer Sci.*, **22**, 495 (1956).

(2) W. H. Stockmayer and M. Fixman, *Ann. N. Y. Acad. Sci.*, **51**, 334 (1953).

(3) B. H. Zimm and R. W. Kilb, *J. Polymer Sci.*, **37**, 19 (1959).

(4) A. Charlesby, *Proc. Roy. Soc. (London)*, **A224**, 120 (1954).

(5) W. H. Stockmayer, *J. Chem. Phys.*, **11**, 45 (1943); **12**, 125 (1944).

culate the change in intrinsic viscosity during the process.

The Distribution Function

In order to avoid needless repetition of details, it will be assumed that the reader is familiar with the papers of Stockmayer⁵ and the approximations introduced by Thurmond and Zimm.⁶ The discussion will be given in terms of an irradiation process. Other processes will be analogous. The initial molecular weight distribution is assumed to have a ratio of weight to number average degree of polymerization of two.

Stockmayer's distribution function deals with a random polymerization of difunctional monomers and multi-functional branch units, driven to extent of reaction p . We may use his results by viewing our crosslinks as randomly distributed tetrafunctional branch units. The scissions will be viewed as changing the extent of reaction p . Using his notation, we define

$$\begin{aligned} N &= \text{no. of tetrafunctional crosslink units} \\ L &= \text{no. of difunctional units} \\ M &= \text{no. of polymer molecules} \end{aligned}$$

Let us assume the following for an irradiation process of dose R : (1) αR difunctional units are crosslinked, yielding $\alpha R/2$ tetrafunctional units; consequently, αR difunctional units are simultaneously removed; (2) βR scissions are introduced; (3) α and β are constant throughout the process.

\therefore

$$N = \alpha R/2 \quad (1)$$

$$L = L_0 - \alpha R \quad (2)$$

$$M = M_0 - \alpha R/2 + \beta R \quad (3)$$

where L_0 and M_0 are the original number of difunctional units and polymer molecules present before irradiation.

We also define

$$\begin{aligned} \rho &= \frac{\text{functional groups on branch units}}{\text{all functional groups}} \\ &= 4N/(4N + 2L) \\ &= \alpha R/L_0 \end{aligned} \quad (4)$$

$$\begin{aligned} p &= \text{fraction of groups reacted} \\ &= 2(N + L - M)/(4N + 2L) \\ &= (L_0 - M_0 - \beta R)/L_0 \end{aligned} \quad (5)$$

$$\begin{aligned} y_{no} &= \text{original no. av. degree of polymer.} \\ &= L_0/M_0 \end{aligned} \quad (6)$$

$$\begin{aligned} y_{wo} &= \text{original wt. av. D.P.} \\ &= 2y_{no} \end{aligned} \quad (7)$$

$$\begin{aligned} y_{ni} &= \text{instantaneous no. av. D.P. of the polymer after dose } R \\ &\quad \text{if all the crosslinks were broken but scissions remained} \end{aligned}$$

$$= L_0/(M_0 + \beta R) < y_{no} \quad (8)$$

$$y_{wi} = 2y_{ni} < y_{wo} \quad (9)$$

After dose R , the number, weight and z -average D.P. (x_n , x_w and x_z) of the irradiated polymer are

$$x_n = L/M \quad (10)$$

$$x_w = 2(1 - \rho)p/(1 - p - 2p\rho) \quad (11)$$

$$x_z = 3(1 - \rho)p(1 - p)/(1 - p - 2p\rho)^2 \quad (12)$$

Using the approximations introduced by Thurmond and Zimm,⁶ the weight fraction W_{mk} of polymer consisting of m crosslinks and k difunctional units is

$$W_{ok} = \frac{2x}{y_{wi}} \exp\{-x(1 + \gamma'/2)\} \quad (13)$$

$$W_{mk} = \frac{\gamma' x^k}{2m(2m + 1)(2m + 2)} W_{m-1,k} \quad (14)$$

where

$$\gamma' = \rho y_{wi} = 2\alpha R/(M_0 + \beta R) \quad (15)$$

$$x = 2k/y_{wi} \quad (16)$$

The quantity

$$W_k = (y_{wi}/2) \sum_m W_{mk} \quad (17)$$

has been tabulated⁷ for $\gamma' < 1$.

The instantaneous number and weight average number of crosslinks per molecule (m_n and m_w) are given by

$$m_n = \gamma'/(4 - \gamma') \quad (18)$$

$$m_w = \gamma'/(1 - \gamma') \quad (19)$$

We comment that the number average number of crosslinks per original linear molecule is $m_n y_{no}/x_n$; per instantaneous linear molecule it is $m_n y_{ni}/x_n$.

We may also rewrite the respective D.P. averages

$$x_n \sim y_{ni}/(1 - \gamma'/4) \quad (20)$$

$$x_w \sim y_{wi}/(1 - \gamma') \quad (21)$$

$$x_z \sim 3y_{wi}/2(1 - \gamma')^2 \quad (22)$$

Stockmayer has shown that the critical extent of reaction, p_c , at which gelation occurs is given by

$$p_c = 1/(1 + 2\rho) \quad (23)$$

which implies that at initial gelation $\gamma' = 1$. From equation 15, one finds that the dose R^* at initial gelation is given by

$$(2\alpha - \beta)R^* = M_0 \quad (24)$$

This implies that gelation can occur only if $2\alpha > \beta$. Since $\alpha R/2$ is the number of crosslinks, and βR is the number of scissions, equation 24 shows that gelation is possible whenever there are less than four degradations per crosslink.

Case I. Gelation Is Possible ($2\alpha > \beta$)

If $2\alpha > \beta$, then gelation occurs at R^* as determined from equation 24. The quantity R^* is an important and readily determinable experimental parameter, and therefore it is desirable to restate the above molecular averages in terms of R and R^* , rather than R and γ' . This may be accomplished by use of equation 24. The results are

$$\gamma' = R/R^*[1 - (1 - R/R^*)\beta/2\alpha] \quad (25)$$

$$R/R^* = \gamma'(1 - \beta/2\alpha)/(1 - \gamma'\beta/2\alpha) \quad (26)$$

$$y_{wo}/y_{wi} = y_{no}/y_{ni} = 1 + R/R^*(2\alpha/\beta - 1) \quad (27)$$

$$y_{no}/x_n = 1 - \frac{(1 - 2\beta/\alpha) R}{(4 - 2\beta/\alpha) R^*} \quad (28)$$

$$y_{wo}/x_w = 1 - R/R^* \quad (29)$$

$$x_z = 3y_{wo}[1 - (1 - R/R^*)\beta/2\alpha]/2(1 - \beta/2\alpha)^2(1 - R/R^*)^2 \quad (30)$$

$$m_w = R/R^*(1 - R/R^*)(1 - \beta/2\alpha) \quad (31)$$

$$m_n = R/R^*[4 - R/R^* - (2\beta/\alpha)(1 - R/R^*)] \quad (32)$$

Equation 29 shows that the inverse of the weight average D.P., x_w , varies directly as the dose R ; x_w becomes infinite at gelation. Equation 28 shows that the inverse of the number average D.P., x_n , also varies directly as the dose R ; but x_n may

(6) C. D. Thurmond and B. H. Zimm, *J. Polymer Sci.*, **8**, 477 (1952).

(7) R. W. Kilb, *J. Polymer Sci.*, in press (1959).

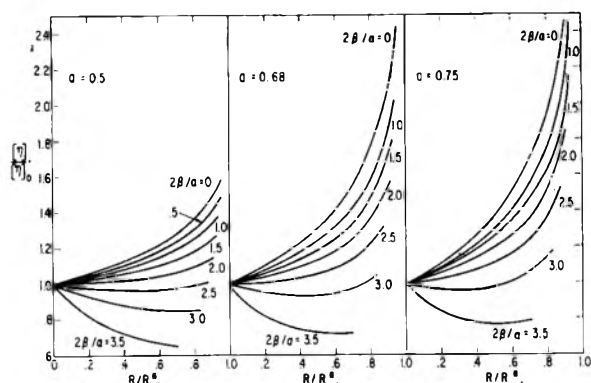


Fig. 1.—The ratio of $[\eta]$ after dose R to the initial $[\eta]_0$ versus R/R^* , where R^* is the dose needed for gelation. The plots are given for several values of the ratio of the number of scissions to crosslinks, $2\beta/\alpha$. The parameter a is the exponent in the intrinsic viscosity-molecular weight relationship for the linear polymer.

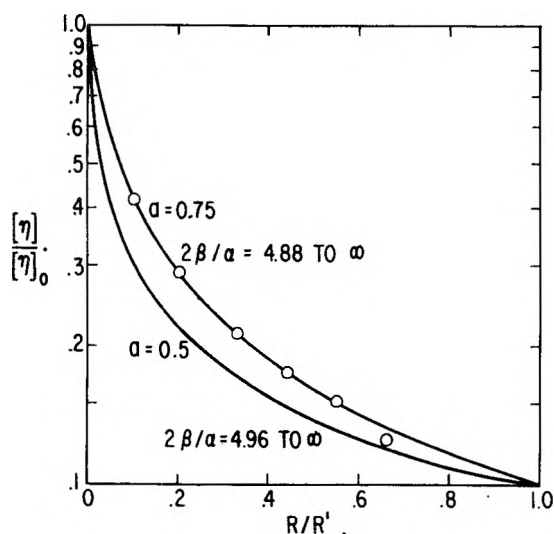


Fig. 2.—The ratio of $[\eta]$ after dose R to the initial $[\eta]_0$ versus R/R' , where R' is the dose needed to reduce $[\eta]$ to one-tenth of $[\eta]_0$. The curves are independent of $2\beta/\alpha$, and have a slight dependence on the exponent a in the intrinsic viscosity-molecular weight relationship for the linear polymer.

either increase (if $2\beta < \alpha$) or decrease (if $2\beta > \alpha$) during the process.

From equation 32 we see that at gelation there is one cross-link for every three molecules present. The quantity which Shultz, *et al.*,¹ refer to as "the number of crosslinked units per instantaneous primary weight average molecule" is given by $m_w y_{wi}/x_w$, which is unity at gelation.

To find the intrinsic viscosity after dose R , we note that the distribution function (equations 13 and 14) has the same mathematical form as that treated previously by Kilb.⁷ The only difference is that y_{wi} appears instead of y_{wo} , and γ' is defined differently. Consequently, the $[\eta]$ after dose R is

$$[\eta] = \kappa(y_{wi}/2)^a f(\gamma', a) \quad (33)$$

Here $f(\gamma', a)$ is a function dependent on the amount of branching in the polymer, a is the exponent in the intrinsic viscosity-molecular weight relationship for the polydisperse linear polymer, and κ is the corresponding coefficient

$$[\eta]_0 = \kappa(y_{wo}/2)^a f(0, a) \quad (34)$$

The ratio of $[\eta]$ after dose R , to the initial intrinsic viscosity is therefore

$$\begin{aligned} [\eta]/[\eta]_0 &= (y_{wi}/y_{wo})^a f(\gamma', a)/f(0, a) \\ &= (1 - \beta\gamma'/2\alpha)^a f(\gamma', a)/f(0, a) \end{aligned} \quad (35)$$

Values of $f(\gamma', a)/f(0, a)$ are given in Table I for various values of γ' and for $a = 0.5, 0.68$ and 0.75 . Other values may be obtained by graphical interpolation.

TABLE I

a/γ'	Values of $f(\gamma', a)/f(0, a)$						
	0.2	0.4	0.6	0.8	0.9	0.95	$f(0, a)$
0.5	1.06	1.13	1.22	1.36	1.48	1.58	1.29
.68	1.10	1.23	1.41	1.74	2.09	2.43	1.48
.75	1.11	1.27	1.51	1.95	2.46	3.00	1.56

By use of equations 26 and 35, one may construct plots of $[\eta]/[\eta]_0$ vs. R/R^* for various values of a and $2\beta/\alpha$. Typical plots are given in Fig. 1.

Examination of Fig. 1 confirms Shultz's¹ finding that the intrinsic viscosity may in some cases decrease almost up to the gel point. This occurs when there are about three scissions per crosslink ($2\beta/\alpha > 3$).

We also note from Fig. 1 that the better solvents ($a > 0.65$) give a greater absolute change in $[\eta]/[\eta]_0$. On the other hand, although one can determine intrinsic viscosities quite accurately, the value of R^* is difficult to determine experimentally to better than 5%. Consequently because of the steep slopes of the curves for the case of good solvents, the error R^* causes a greater uncertainty in finding the value of $2\beta/\alpha$ in good solvents than in the Θ solvent ($a = 0.5$). Thus in general, it is advisable to work with Θ solvents. We also comment that the theory is really developed only for Θ solvents, and its application to other solvents is an extrapolation.³

Comparison with experimental data is given below.

One can also determine how much greater R^* is than the dose R_0^* required to produce gel if there were no degradation. This is given by

$$R^* = (1 - \beta/2\alpha)R_0^* \quad (36)$$

Thus if one finds that an unexpectedly large dose is required for gelation, it indicates that there are nearly four scissions per crosslink.

Case II. No Gelation Occurs ($2\alpha < \beta$)

If no gelation occurs, there does not exist a definite point such as R^* , and so one cannot construct plots like Fig. 1. But it was hoped that similar figures could be constructed by plotting $[\eta]/[\eta]_0$ vs. R/R' , where R' is that value of dose for which $[\eta]/[\eta]_0$ is one-tenth. This would be convenient for interpretation of experimental data. Surprisingly, it was found that the curves were virtually independent of $2\beta/\alpha$ in the range of R/R' from 0.005 to 1. Consequently viscosity data alone is not sufficient to yield $2\beta/\alpha$. Plots are given in Fig. 2 for $a = 0.5$ and 0.75 . The experimental values of Shultz, *et al.*,¹ for irradiated poly-methyl methacrylate I (which has $a = 0.73$) follow the expected curve.

Casting about for other methods, we note from

equations 8, 15 and 20, that the ratio y_{no}/x_n of number average D.P. before and after dose R is

$$\begin{aligned} y_{no}/x_n &= 1 + (\beta - \alpha/2)R/M_0 \\ &= 1 + k_n R \end{aligned} \quad (37)$$

Similarly for the weight average D.P.

$$\begin{aligned} y_{wo}/x_w &= 1 + (\beta - 2\alpha)R/M_0 \\ &= 1 + k_w R \end{aligned} \quad (38)$$

Consequently by determining the slopes k_n and k_w of these straight-line plots, one finds that the ratio of scissions to crosslinks is given by

$$2\beta/\alpha = \frac{4 - k_w/k_n}{1 - k_w/k_n} \quad (39)$$

Another method, suggested by A. A. Miller, involves the use of a radical scavenger which is capable of completely suppressing crosslinking (so $\alpha = 0$) and yet presumably not affecting degradation (so β is unchanged). We also assume that the scavenger need be present in only small concentration (less than 5%). One then needs three intrinsic viscosities: (1) the $[\eta]_0$ of the original polymer; (2) the $[\eta]^*$ of the polymer irradiated in presence of the scavenger; and (3) the $[\eta]$ of the polymer irradiated to the same dose R in the absence of the scavenger.

For the ratio $[\eta]^*/[\eta]_0$ we have (since $\gamma' = 0$)

$$\begin{aligned} [\eta]^*/[\eta]_0 &= (y_{wi}/y_{wo})^a \\ &= [1/(1 + \beta R/M_0)]^a \end{aligned} \quad (40)$$

This may be solved for β/M_0 .

Equation 35 shows the $[\eta]/[\eta]^*$ is

$$[\eta]/[\eta]^* = f(\gamma', a)/f(0, a) \quad (41)$$

Use of Table I and the appropriate a value then yields γ' . The quantity $2\alpha/M_0$ may be obtained from equation 15 and the found value of β/M_0

$$2\alpha/M_0 = \gamma'(1 + \beta R/M_0)/R \quad (42)$$

A third method involves the use of light scattering techniques. One finds the dose R^+ needed to reduce the weight average D.P., x_w , to some fraction of the initial y_{wo} (e.g., $x_w = 0.1y_{wo}$). Then one plots $[\eta]/[\eta]_0$ versus R/R^+ .

The plots are constructed in the following manner. One chooses x_w/y_{wo} ; then from equations 9, 15 and 21 one finds

$$y_{wo}/x_w = 1 + R(\beta - 2\alpha)M_0 \quad (43)$$

If one take $x_w/y_{wo} = 0.1$ at R^+ , this yields

$$M_0 = R^+(\beta - 2\alpha)/9 \quad (44)$$

Substituting in equation 15 gives

$$R/R^+ = \gamma'(\beta/2\alpha - 1)/9(1 - \gamma'\beta/2\alpha) \quad (45)$$

The desired plots are obtained by choosing appropriate values of γ' and $2\beta/\alpha$, and using Table I with equations 35 and 45. The results are given in Fig. 3 and 4 for $a = 0.5$ and 0.75 . Once again it is found that solvents give better sensitivity for determining $2\beta/\alpha$ than better solvents.

The data of Shultz, *et al.*,¹ on irradiated PMMA I are also plotted in Fig. 4. This follows the curve for no crosslinking quite well, and confirms their result that there is very little crosslinking on irradiation of PMMA. Actually, they have $a = 0.73$, which would have the effect of raising all curves in Fig. 4 by a small amount, thus giving even better agreement.

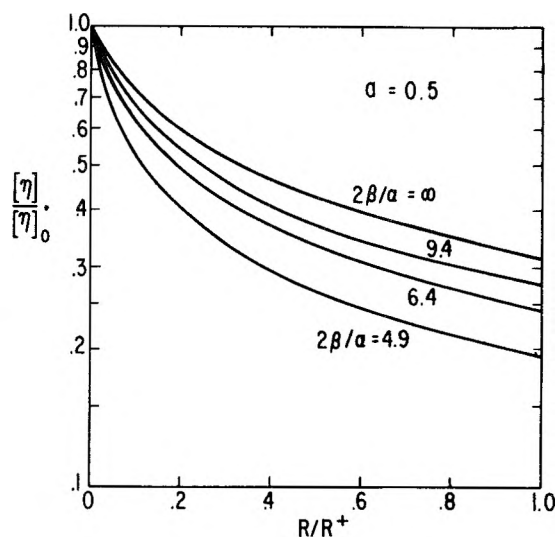


Fig. 3.—The ratio of $[\eta]$ after dose R to the initial $[\eta]_0$ versus R/R^+ , where R^+ is the dose needed to reduce the weight average molecular weight to one-tenth of the initial value. The exponent $a = 1/2$ (a θ solvent).

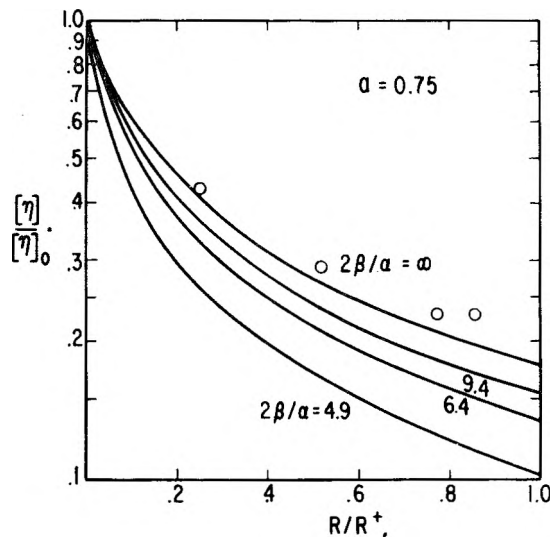


Fig. 4.—The ratio $[\eta]/[\eta]_0$ versus R/R^+ for a good solvent ($a = 0.75$).

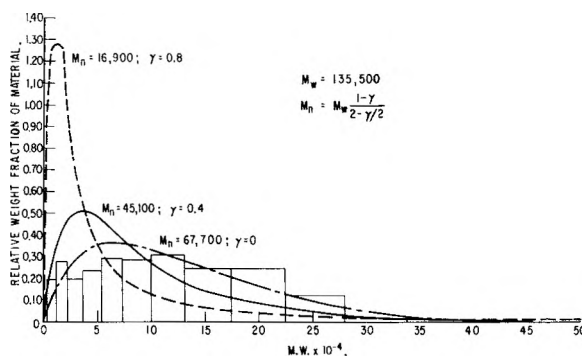


Fig. 5.—The experimental distribution for the silicone polymer. The curves for a polymer with no branching ($\gamma = 0$); a small amount of branching ($\gamma = 0.4$, weight average number of branches $m_w = 0.67$); and large amount of branching ($\gamma = 0.8$, $m_w = 4$).

Other methods (e.g., plots of $[\eta]/[\eta]_0$ vs. x_w/y_{wo} , etc.) might also be employed.

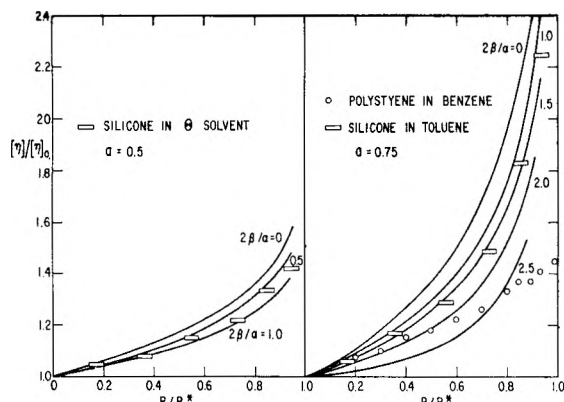


Fig. 6.—The experimental $[\eta]/[\eta]_0$ versus R/R^* for irradiated silicone polymer in a θ solvent, and in toluene. The data of Schultz, *et al.*,¹ of polystyrene in benzene are also plotted.

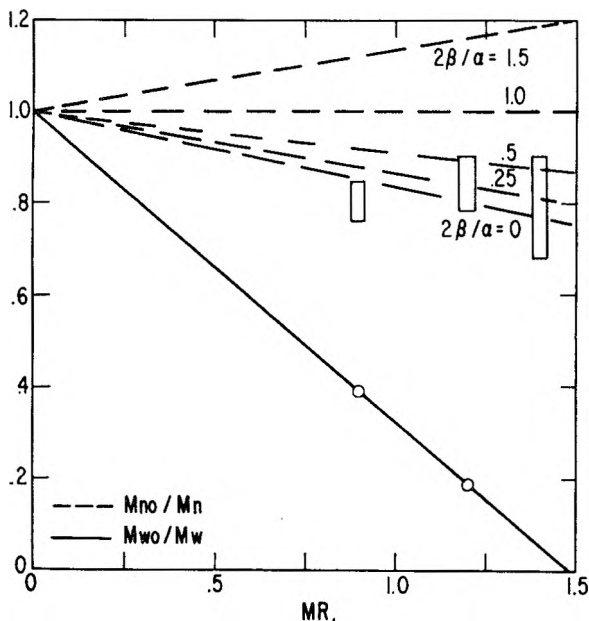


Fig. 7.—The ratios of initial light scattering and osmotic average molecular weights of the silicone polymer to the corresponding values for the irradiated samples. The dashed lines give the expected values of M_{n0}/M_n for various values of ratios of scissions to crosslinks ($2\beta/\alpha$) using the value of $R^* = 1.5$ MR. obtained from the M_{w0}/M_w data.

Each of the three above methods could also be used to determine $2\beta/\alpha$ if gelation were possible.

Experimental

A sample of dimethylsilicone oil (120,000 c.p.s.) was obtained from Dr. A. C. Martellock of the General Electric Silicone Products Dept., Waterford, N. Y. This sample had been decatalyzed and also devolatilized by heating at 200° in a vacuum oven for 24 hours.

To determine the molecular weight distribution, a 2.95-g. sample was fractionated in a one meter thermal gradient column of the Baker and Williams⁸ type; 2.8 g. was recovered.

The intrinsic viscosities of the fractions were determined in toluene solution, and the molecular weights were found from the equation

$$[\eta] = 4.37 \times 10^{-3} M^{0.79}$$

where the $[\eta]$ is in ml./g. This relationship has been determined recently in this Laboratory from data in the range $M = 85,000$ to 2,000,000. It differs rather considerably from Barry's⁹ equation

(8) C. A. Baker and R. J. P. Williams, *J. Chem. Soc.*, 2352 (1956).

$$[\eta] = 2 \times 10^{-2} M^{0.68}$$

The fractionation data are given in Table II. The light scattering M_w of the original sample was 142,500, which agrees quite well with $M_w = 135,500$ calculated from the fractionation data. The osmotic M_n was 63,500 which is also in good agreement with the calculated value of 62,800. This yields $M_w/M_n = 2.2$ which is reasonably close to the expected value of two for a linear random distribution. The found molecular weight distribution is compared to the expected random linear distribution ($\gamma = 0$) in Fig. 5. The agreement is reasonable, especially in view of the experimental accuracy. Distribution curves for branched polymers ($\gamma = 0.8$ and 0.4) of the same M_w are also given; the experimental distribution does not resemble these, and so one concludes that there is little or no branching in the original sample.

Samples (2 g.) of the polymer were irradiated in aluminum dishes of two inch diameter. Oxygen was removed from the samples by pumping under vacuum for 24 hr. The irradiations were done under N_2 with a 800 kv. (peak energy) source of electrons at a rate of 100 MR./hr.

The intrinsic viscosities of the irradiated samples were found in toluene, and in a mixture of diethylphthalate (21.5% by weight) and toluene, which is a θ solvent for dimethylsilicones.¹⁰

TABLE II
FRACTIONATION DATA OF ORIGINAL SAMPLE

Fraction	Wt. of material, mg.	$[\eta]$, ml./g.	Mol. wt.
1	65.4	4.2	6,000
2	130.7	9.0	16,000
3	120.1	14.5	29,000
4	160.2	20.9	46,000
5	235.4	26.7	62,000
6	313.5	34.3	85,000
7	418.2	43.0	115,000
8	431.5	54.0	150,000
9	514.1	67.6	200,000
10	300.7	81.5	250,000
11	109.7	96.3	315,000

The results are given in Table III.

TABLE III
VISCOSITY AND MOLECULAR DATA ON IRRADIATED SAMPLES

Dose, MR.	$[\eta]$ in toluene, ml./g.	k in toluene	$[\eta]$ in θ solvent	k in θ solvent	$M_w \times 10^{-3}$	$M_n \times 10^{-3}$
0	50.0	0.33	28.1	0.70	142.5	63.5
.3	52.5	.36	29.3	.66		
.6	59.0	.39	30.1	.70		
.9	64.5	.44	32.4	.68	370	77.6-85.5
1.2	73.5	.37	34.0	.80	780	75.3
1.4	91.8	.55	37.3	.82		70-95
1.6	112.5	.76	39.5	.90		

The viscosity was represented by

$$\eta_{sp}/c = [\eta] + k[\eta]^2 c$$

In the irradiated samples there was a slight tendency for k to rise with increasing dose, especially near the gel point. In the unirradiated fractionated samples, k remained essentially constant at 0.33 ± 0.02 in the mol. wt. range of 50,000 to 300,000.

Some difficulty was presented by filtration. Solutions of samples irradiated to dose 1.2 MR. and less could easily be filtered through fine fritted glass filters. A fraction of the 1.4 MR. sample would not filter through a fine filter, but would easily go through a coarse filter. In the 1.6 MR. dose sample, a fraction would not go through even a coarse filter. In the viscosity work, therefore, the solutions of dose 1.4 MR. and less were filtered through a coarse filter before viscosity determination, but the solutions of dose 1.6 MR. was not filtered. (In the toluene solution, the 1.6 MR sample

(9) A. J. Barry, *J. Appl. Phys.*, 17, 1020 (1946).

(10) F. P. Price and J. P. Bianchi, *J. Polymer Sci.*, 15, 355 (1955).

was found to give a $[\eta]/[\eta]_0$ value of 2.25 if unfiltered, while the filterable portion gave $[\eta]/[\eta]_0 = 2.04$.)

On close inspection of the calculations⁷ involved in the evaluation of $[\eta]/[\eta]_0$ from the distribution functions, it is found that for the 1.6 MR. sample more than one-third of the value of $[\eta]/[\eta]_0$ is contributed by that portion of the sample which has mol. wt. greater than 6,000,000. The sensitivity to filtration is therefore understandable.

Another problem was in fixing the gel point R^* . If one plots the light scattering M_{90}/M_w versus dose, one finds $R^* = 1.5$ MR. (see equation 29). On the other hand, if one allows the 1.6 MR. sample to swell in toluene for several hours and then shakes the flask vigorously, one finds no entrapment of air bubbles, thus indicating no gel.¹¹ A sample of dose 1.7 MR. does entrap minute air bubbles by this test. This indicates $R^* \sim 1.65$ MR. Since this value gives better over-all consistency in the viscosity analysis, it was adopted in the following calculations for purposes of illustrations.

Plots of $[\eta]/[\eta]_0$ versus R/R^* for measurements in the Θ solvent are given in Fig. 6. Comparison of these with theory yields $2\beta/\alpha \sim 0.5-1.0$. For the measurements in toluene, if we take $\alpha \sim 0.75$, one obtains $2\beta/\alpha \sim 1.0-1.5$. On the other hand, if Barry's value of $\alpha = 0.68$ is assumed, one finds $2\beta/\alpha = 0-1.0$. This lack of precision is disappointing; furthermore, studies by A. A. Miller¹² of this system by chemical techniques indicates that $2\beta/\alpha \sim 0.1$. The difficulty is the lack of sensitivity of $[\eta]$ to small amounts of degradation. Thus it appears that although the theory gives the correct qualitative features, the method is only useful in a quantitative manner when $2\beta/\alpha > 1$. It is also desirable to use Θ solvents to improve precision.

As an alternative method, the osmotic and light scattering molecular weights of several of the irradiated samples were determined. These are given in Table III. These data are plotted in Fig. 7. Using $R^* = 1.5$ as determined by equa-

(11) W. J. Barnes, H. A. Dewhurst, L. St. Pierre and R. W. Kilb, *J. Polymer Sci.*, **36**, 525 (1959).

(12) A. A. Miller, private communication.

tion 29, lines were constructed from equation 28 for various values of $2\beta/\alpha$. Although the precision of the osmotic pressure data is rather poor, it is clear that $2\beta/\alpha > 1/2$, in rough agreement with Miller's value.

In Fig. 6, there are also plotted the data of Shultz, *et al.*,¹ on irradiated polystyrene. At $R/R^* < 0.6$, $[\eta]/[\eta]_0$ follows the curve for $2\beta/\alpha \sim 2$ fairly well. At larger values of R/R^* , $[\eta]/[\eta]_0$ falls much below the expected values. Some possible experimental causes are: (1) filtration difficulties, (2) non-random initial molecular weight distribution, (3) incorrect value of the exponent α , and (4) the crosslinking is not purely tetrafunctional and so the theory developed here is not applicable. In any case, the apparent difference in the behavior silicones and polystyrene is unexpected and would be an interesting topic for further study.

Conclusion

The qualitative features of the change in intrinsic viscosity of a polymer with irradiation are predicted satisfactorily by the above model. Quantitatively, it is found that $[\eta]/[\eta]_0$ is not very sensitive to $2\beta/\alpha$ (the ratio of number of degradations to crosslinks) unless $1 < 2\beta/\alpha < 10$. Consequently viscosity studies by themselves are practically useful only in this range of $2\beta/\alpha$. Outside this range, other techniques—such as light scattering, osmotic pressure or chemical scavenging of radicals—must be employed to find the ratio of scission to crosslinking.

Acknowledgment.—The author is grateful to Mr. W. J. Barnes and Miss W. E. Balz for the light scattering and osmotic pressure measurements, and to Mr. J. S. Balwit for the irradiations. He also wishes to acknowledge the interesting discussions of the problem with Dr. A. A. Miller.

INCLUSION COMPLEXES OF METHYLNAPHTHALENES

BY JACK MILGROM

Contribution from the Research and Development Department, Standard Oil Company (Indiana), Whiting, Indiana

Received March 26, 1959

A chance observation of an unaccountably high melting point prompted investigation of the system 2-methylnaphthalene-*n*-heptane. To confirm complex formation, this system was studied by regular and differential thermal analyses, vapor-pressure measurement, solids separation and X-ray analysis. Data have been represented by the usual linear phase diagram and a special logarithmic one. Six different complexes of 2-methylnaphthalene and *n*-heptane were found at temperatures between 25 and -92° . Depending upon temperature, eight moles of 2-methylnaphthalene combine with one, three or eight moles of *n*-heptane to form three pairs of complexes. The members of each pair have different crystal modifications. Transitions do not proceed readily; some complexes must be cooled below 0° before they transform and one is metastable. These results suggest a mechanism for complex formation. At room temperature a void apparently exists in the 2-methylnaphthalene crystal lattice, which can accommodate guest molecules of a definite shape. Complexes form with both straight- and branched-chain hydrocarbons, although molecules as long as *n*-hexadecane fail to react. Complex formation is not limited to 2-methylnaphthalene. 1-Methylnaphthalene and perhaps other polycyclic compounds also adduct paraffins. Below room temperature, a new realm of inclusion complexes probably exists.

Introduction

During an attempted purification of 1-methylnaphthalene in our laboratories, a 30 mole % solution of 1-methylnaphthalene in *n*-pentane solidified unexpectedly at -70° . If an ideal solution had been formed, it would have solidified below -130° , the freezing point of *n*-pentane. Solutions of 2-methylnaphthalene and paraffins behaved similarly. These results suggested that both methylnaphthalenes form complexes with alkanes and led to further investigation.

Knowledge of solid-liquid equilibria of methylnaphthalene in binary systems is sparse. 2-Methylnaphthalene was observed to form a simple

eutectic mixture with triphenylmethane¹ and a solid solution with naphthol.² Complexes were formed between methylnaphthalene and acetone, phenol or hydrogen sulfide.³ A recent calorimetric study⁴ has revealed that both 1- and 2-methylnaphthalene undergo polymorphic transitions sluggishly, exhibiting supercooling and superheating.

The system 2-methylnaphthalene-*n*-heptane has

(1) V. M. Kravchenko, *Ukrain. Khim. Zhur.*, **18**, 36 (1952); *C. A.*, **48**, 3776f (1954).

(2) G. Nazario, *Rev. inst. Adolfo Lutz.*, **8**, 137 (1948); *C. A.*, **44**, 421f (1950).

(3) E. Terres and A. Doerges, *Brennstoff-Chem.*, **37**, 385 (1956).

(4) J. P. McCullough, H. L. Finke, J. F. Messerly, S. S. Todd, T. C. Kincheloe and G. Waddington, *THIS JOURNAL*, **61**, 1105 (1957).

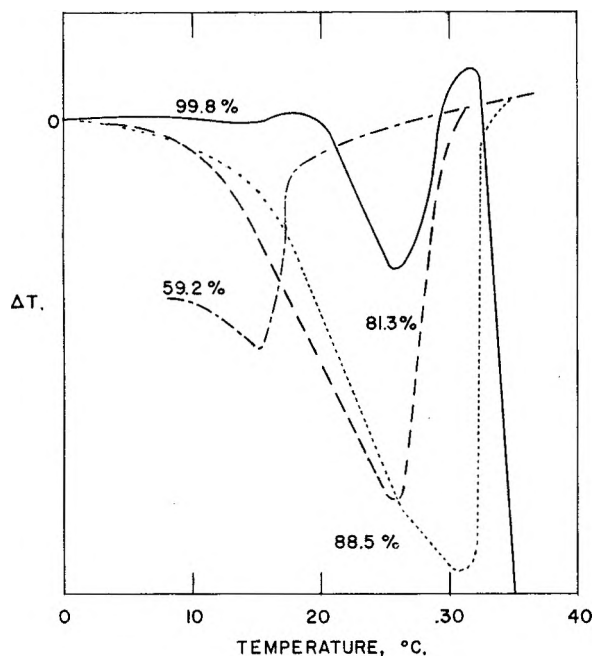


Fig. 1.—Differential thermal analysis of 2-methylnaphthalene-*n*-heptane mixtures.

been investigated to confirm the existence of methylnaphthalene-paraffin complexes. This system was selected because both materials are available in high purity, and the 2-methyl derivative is conveniently higher-melting than the 1-methyl. To prepare phase diagrams, the system was studied by regular and differential thermal analysis, vapor-pressure measurement and solids separation. Preliminary thermal analyses indicated that the solid precipitated first was metastable and, if cooled below 0° , it transformed to a stable solid. Therefore, mixtures were precooled before thermal analysis. To compute heats of fusion and transition temperatures, a plot of log mole-fraction against reciprocal temperature was also prepared. Data from the phase diagrams and X-ray studies provided a basis for a mechanism of complex formation in this system and perhaps in analogous ones.

Experimental

2-Methylnaphthalene was used without further purification if cryoscopic analysis showed a purity of 98% or higher. When purification was necessary, it was crystallized from an aqueous alcohol solution and dried at 100° at 1 mm. Material 99.8% pure was readily obtained. Crystallization of 2-methylnaphthalene from its own melt proved unsatisfactory. The cryoscopic purity of 1-methylnaphthalene was 96.0%; of *n*-heptane, 99.6%; and of *n*-hexane, 95.0%.

Five methods of analysis were used to determine the solid-liquid equilibria. The primary method, thermal analysis, defined the liquidus curve in the phase diagram and partially defined phase transitions; however, transitions were more readily and accurately determined by differential thermal analysis and vapor-pressure measurements. Analysis of isolated solids by refractive-index measurements determined their compositions and X-ray studies revealed their structures.

Thermal analyses were carried out in an apparatus similar to one used in cryoscopic analysis of pure materials.⁵ A ten-gram sample, weighed to 0.01 g., was charged to a special Dewar flask and the flask and sample were cooled with liquid

nitrogen or a mixture of acetone and Dry Ice. During cooling, a continuous stream of dry nitrogen covered the sample in the flask and prevented absorption of water. Agitation was maintained as long as a liquid phase remained, and cooling was continued through the eutectic temperature. Cooling curves were automatically plotted by a recorder linked to a platinum-resistance thermometer in the sample. Heating curves were similarly plotted after the cold bath surrounding the sample was replaced by a warm bath of acetone or water. Near the melting point, the heating rate was 0.05 to 0.10° per min. Melting points were easily read to 0.02° but duplicate analyses differed by as much as 0.05° . Supercooling made freezing-point values less accurate than melting-point values; therefore, only the latter were used to plot the liquidus curve. However, complete freezing and melting curves were used to determine solid-solid transitions.

Differential thermal analyses were carried out in a well-insulated bath equipped with a heater; a constant heating rate of 0.56° per min. was maintained by a controller. Samples were sealed in glass containers having a capacity of 3 ml., and temperature differences ΔT were measured by an iron-constantan thermocouple having a diameter of 0.065 in. An azelaic acid ester served as the reference material. An X-Y recorder, coupled with a preamplifier, automatically recorded the difference between temperatures of the reference and test samples as a function of time. A mercury thermometer was used to measure the bath temperature. Samples were precooled at -50° for at least 24-hr. and then placed in the bath, which was cooled to a temperature just below 0° . The samples were allowed to warm and equilibrate in the bath at 0° before heating was started and the melting curve was obtained. Melting curves for 2-methylnaphthalene and *n*-heptane mixtures containing 88.5, 81.3 and 59.2 mole % 2-methylnaphthalene are shown in Fig. 1.

Vapor-pressure measurements were made in an apparatus that consisted of a flask, an attached mercury manometer and a manifold connected to a series of traps on a high-vacuum line. A mixture of known composition was degassed in the flask until the vapor pressure remained constant. The volatile component was then incrementally distilled into the vacuum line. Before each pressure measurement, the residue in the flask was allowed to equilibrate at the temperature of the surrounding bath. Measurements were easily read to 0.05 mm.

Solids were separated in a Skau tube⁶ or a regular centrifuge tube. The Skau tube was placed in a large centrifuge bottle containing acetone and Dry Ice, which maintained a low temperature during filtration. This apparatus was especially suited to the separation of solids melting near or above 0° ; below 0° , the liquid bath surrounding the tube warmed too rapidly in the centrifuge.

X-Ray analyses were made by the powder-diffraction method. The apparatus was adapted to low-temperature work by using a stream of cold vapor from liquid nitrogen to cool the capillary tube containing the sample. The temperature of each sample was thus maintained between -20 and 0° . A cellophane box enclosing the sample holder prevented severe icing.

Phase Diagram for 2-Methylnaphthalene and *n*-Heptane.

—2-Methylnaphthalene has two crystal forms.⁴ Crystals I, stable at a temperature above 15.3° , can be supercooled below 0° before they transform into crystals II, and crystals II can be superheated 5° before transformation to I. In this investigation, polymorphism was confirmed by differential thermal analysis of pure 2-methylnaphthalene. It was first cooled at -50° for more than 24 hr., and then heated in the regulated-temperature bath. The heating curve shown in Fig. 1 has two peaks: one, beginning at 19° , corresponded to the heat absorbed in isothermal transition; the other, at about 34° , was the heat of fusion.

When mixtures of 2-methylnaphthalene and *n*-heptane were cooled in the thermal analysis apparatus, their cooling curves showed first a freezing point and then a long halt between -20 and -25° , as heat was evolved in a phase transformation. Mixtures freezing below -20° often froze and transformed simultaneously. Cooling curves of mixtures containing 50 mole % or less 2-methylnaphthalene also showed an additional long halt as the mixtures solidified between -90 and -92° . This halt no doubt corresponds to the eutectic transition.

(5) Am. Soc. Testing Materials, "ASTM Standards on Petroleum Fuels and Lubricants." Philadelphia, Pa., 1957. Designation D 1015-55.

(6) A. Weissberger, "Technique of Organic Chemistry," Vol. III, Second Edition, Interscience Publishers, Inc., New York, N. Y., 1956.

Melting curves of mixtures previously cooled through the transformation, in contrast to freezing curves, exhibited a series of halts. These halts apparently arise from isothermal phase transitions. The data obtained from the melting curves were used to plot the phase diagram in Fig. 2 which shows that five stable complexes having three different compositions are formed in this system. Two pairs of complexes have the same composition, but each member has a different crystal form and all melt incongruently.

According to vapor-pressure measurements and thermal analyses, horizontal transition lines in the phase diagram probably extend all the way across the diagram through points B, C, D, E and F. The vapor pressure of a mixture containing 36 mole % 2-methylnaphthalene was measured at 0° as heptane was removed in increments; at the composition of the complex, the vapor pressure dropped from 10.0 to 9.0 mm. and remained constant until the residue was solely 2-methylnaphthalene. Solid-solid transitions were often observed beyond the vertical solidus lines. However, in regions having a high concentration of methylnaphthalene, these transitions were difficult to see.

Along curve AB, solid 2-methylnaphthalene crystals I is in equilibrium with liquid compositions of 2-methylnaphthalene and *n*-heptane. This curve coincides almost exactly with the "ideal" solubility curve of 2-methylnaphthalene I, as calculated from the Clausius-Clapeyron equation.

A solid complex of 2-methylnaphthalene and *n*-heptane precipitates below 25°; the solubility curve is BC. Cooling and heating curves of a mixture containing 88.9 mole % 2-methylnaphthalene exhibited a halt between 23 and 26°. This mixture solidified as it cooled through the transition temperature. In contrast, a mixture containing 88.5%—only 0.4% less—did not solidify completely when cooled below 23°. Therefore, the solid stable between temperatures B and C corresponds closely to a combination of eight moles of 2-methylnaphthalene per mole of heptane or an 8:1 complex.

The stable solid in equilibrium with liquid along curve CD apparently has the same composition as the solid melting along BC, but the crystal form is different. Such dimorphism was suggested by results obtained from both regular and differential thermal analyses, which indicated that the solidus transition occurred at 6° rather than 15°. Curves obtained by differential thermal analyses of mixtures containing 88.5 and 81.3% 2-methylnaphthalene had peaks that began between 6 and 8° and ended at the melting point, as shown in Fig. 1. The beginning of the peak corresponds to the transition line going through point D in the phase diagram. Because the 88.5% mixture was warmed through the 25° transition, it absorbed more heat than the 81.3% mixture.

Solid melting along curve DE is probably an 8:3 complex. According to regular and differential thermal analyses, the solidus line in the diagram shifts from 6 to 1° at some composition between 75.6 and 59.2% 2-methylnaphthalene. For example, differential thermal analysis of a 59.2% mixture was started at about 0° but, as shown in Fig. 1, ΔT was displaced. This displacement occurs because heat is absorbed by the mixture as it is warmed through the 1° solidus transition. Continued slow heating produced a curve with a peak beginning between 6 and 8°, similar to the peaks produced by the other mixtures. Results from thermal analysis were more difficult to interpret because solidus transitions were not readily differentiated from solid-solid transitions.

Solid 1:1 complex is in equilibrium with liquid 2-methylnaphthalene and *n*-heptane at temperatures represented by curve EG. The solid phase isolated at -20 to -22° contained 50% 2-methylnaphthalene. All melting curves of mixtures containing 60% or less 2-methylnaphthalene exhibit a short halt between -18 and -22°. This halt apparently corresponds to a polymorphic change in the 1:1 complex, because the solidus line for these mixtures is at -90.8°.

The eutectic composition of this binary system at G, contains less than 1% 2-methylnaphthalene. Adding as little as 0.96% 2-methylnaphthalene to *n*-heptane raised the melting point from -90.70 to -90.00°. The heating curve of the dilute solution indicated that the melting point of the eutectic was -90.79°. A short halt between -94 and -96° was exhibited by melting and freezing curves of mixtures containing as much as 81% 2-methylnaphthalene. This effect could be the result of incomplete transformation at temperatures below 0°; however, the same halt occurred

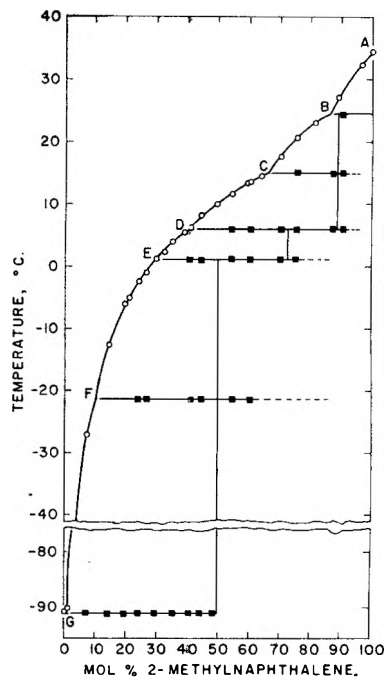


Fig. 2.—The phase diagram for the system 2-methylnaphthalene-*n*-heptane: open circles are melting points and full squares are transition temperatures. Both temperatures were determined from the heating curves obtained by thermal analysis.

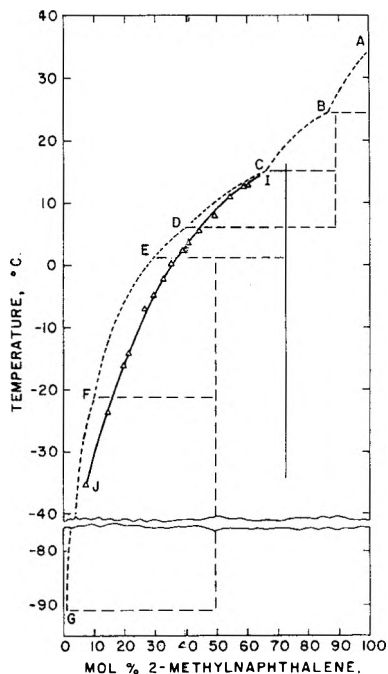


Fig. 3.—Metastable phase.

even after the sample was cooled at -30° for as long as 24 hr. Perhaps the halt corresponds to still another isothermal transition, if not to supercooling of the -22° transition.

Metastable Phase.—Each mixture freezing below 15° could have two melting points, as shown by Fig. 3. If the mixture was cooled to a temperature slightly lower than its freezing point and then allowed to warm, it melted not along curve CG but along curve IJ. The mixture melted at a higher temperature along curve CG only if it was cooled to -20°. Thus, 2-methylnaphthalene reacts with heptane to form one metastable and five stable complexes.

The metastable solid precipitated along curve IJ is a com-

plex containing eight moles of 2-methylnaphthalene and three moles of *n*-heptane. The solid was actually isolated at 5° and analyzed. However, pure metastable complex could not be isolated below 0°, because it transformed rapidly to the stable 1:1 complex. Existence of this metastable 8:3 complex supports the assumption that the solid stable between D and E in the phase diagram is also an 8:3 complex. Thus, this system has three pairs of complexes.

In the transformation from metastable to stable form, two effects were evident. Cooling curves showed a long halt as the mixture evolved heat. The crystals, which were transparent initially, became fine and opaque.

Temperature affected the rate of transformation. Between 2 and 0°, transformation was sluggish and complete only after six hours, but, between -20 and -30°, it was rapid and complete in a few minutes. Seeding had no effect; the rate was not increased when a 44% mixture was cooled just below its 5° freezing point and seeded with stable crystals. Therefore, the sluggish rate is not the result of supercooling.

Transformation did not always go to completion, particularly when the mixtures froze between 0 and -20°. If these mixtures were cooled slightly below the freezing point and then heated slowly, the solid began to transform but melted before the reaction was complete. These melting points were lower than those of mixtures containing 1:1 complex and heptane. Because the transformation was rapid below 0°, only freezing points were used to plot curve IJ below 0°. When the freezing point of the mixture was lower than -20°, transformation accompanied freezing.

Mixtures freezing at temperatures above 15° underwent the metastable-stable transformation when cooled below 0°, but the melting point remained unchanged. Apparently the transformation proceeds reversibly only if the mixture is heated through the transition temperature at 15°.

Logarithmic Diagram.—A plot of the logarithm of mole fraction against reciprocal temperature is often prepared for simple binary systems containing no complexes. Over a short concentration range, a straight line is then obtained with a slope that varies, according to the Clausius-Clapeyron equation, with the heat of fusion of the solute. The heat of fusion determined in this manner can be compared with that determined experimentally to measure the deviation of the solvent from "ideal".⁷

In this study, the Clausius-Clapeyron equation was applied to binary systems containing complexes having incongruent melting points. The modified equation is

$$-\log N = \frac{\Delta H_f}{2.303R} \left(\frac{1}{T} \right) - \left[\frac{\Delta H_f}{2.303RT_0} + \log x \right]$$

where *N* is the mole fraction of component A in the binary mixture melting at *T*, *x* is the mole fraction of A in the complex A₂B₃, Δ*H_f* is the heat of fusion of the complex, and *T*₀ is the theoretical melting point of the complex. This equation was derived, as given in the Appendix, by assuming that the amount of B was always more than required for the complex, Δ*H_f* was constant, and the solute formed an "ideal" solution with the solvent. A plot of log *N* against 1/*T* then gives a straight line for A and each complex formed by A, the slope varying with Δ*H_f* and the intercept varying with *x* and *T*₀.

Advantages of this graphic representation are manifold. Straight lines are useful for correcting small experimental errors and intersections between them give more accurate values for transition temperatures. Heats of fusion can be easily estimated and compared. If *x* is known, *T*₀ can be calculated; it cannot be determined experimentally because the complex decomposes before it melts.

Figure 4 shows such a logarithmic plot applied to the system 2-methylnaphthalene-*n*-heptane. For easy comparison with the composition-temperature phase diagram, the lettered solubility curves and lines refer to the same solid phases. The data points between C and F might be described by a single straight line; however, evidence indicates the points belong to three different lines having similar slopes that correspond to similar Δ*H_f* values for the solid phases. The broken line below 0° deviates from the line above 0°, because the metastable solid reacted in this temperature region.

Heats of fusion and incongruent melting points were computed by the least-squares method and are summarized in Table I. The values for the heats of fusion of the complexes

are only approximate, because the solutions of the complexes in *n*-heptane are not completely "ideal." Nevertheless, the straight-line correlation in Fig. 4 does suggest that the Δ*H_f* values are sufficiently valid for an internal comparison. The calculated Δ*H_f* of pure 2-methylnaphthalene agrees well with the value of 2.898 kcal. per mole determined by experiment.⁴ Thus, *n*-heptane probably forms an "ideal" solution with 2-methylnaphthalene when the heptane is present in low concentration.

A Mechanism for Complex Formation

According to X-ray diagrams, the two polymorphic forms of 2-methylnaphthalene belong to the monoclinic crystal system. Moreover, the unit-cell volume of crystals II is smaller than that of crystals I. Therefore, 2-methylnaphthalene crystals contract at the transition temperature. Crystals II do not form complexes; pure 2-methylnaphthalene cooled to a temperature of -30°, where the polymorphic transformation is complete, can be mixed with cold *n*-heptane without reaction. Apparently a void exists in the lattice structure at ordinary temperatures. But at low temperatures, where van der Waals forces become more important, a compact crystal lattice forms that prevents the inclusion of heptane.

The cavity in the 2-methylnaphthalene crystal lattice probably extends through two unit cells, because each cell has four molecules⁸ and the complexes involve units of eight. Furthermore, the complexes form in pairs; the 8:1 and 8:3 complexes that precipitate initially are less stable, according to the heats of fusion, than the 8:1 and 8:3 complexes that form after the low-temperature transformation. The complexes that precipitate first probably belong to the same structural family and those that form after the transformation belong to another.

TABLE I
RESULTS CALCULATED FROM LOG DIAGRAM

Solubility curve	Solid phase	Crystal form	Heat of fusion, kcal./mole	Incongruent m.p., °C.
AB	2-Methylnaphthalene	I	2.94	...
BC	8:1 Complex	I	4.7	B: 25.4
CD	8:1 Complex	II	8.7	C: 14.8
DE	8:3 Complex	II	9.6	D: 6.0
EF	1:1 Complex	I	7.2	E: 1.2
IJ	8:3 Complex	I	6.4	I: 15.4

A mechanism of complex formation is thus apparent. Molecules as large as *n*-heptane can be trapped in the void as methylnaphthalene begins to crystallize at temperatures below 25°. As the crystals are cooled through the 15° transition, the void in the lattice and the increased importance of van der Waals forces permit the inclusion of additional *n*-heptane. On further cooling, methylnaphthalene molecules try to move closer to conform to the arrangement of crystals II but are prevented by heptane already in the crystal lattice. The lattice structure becomes strained, such that the molecules realign into a stable—though expanded—unit cell. This rearrangement corresponds to the metastable-stable transformation

(7) F. S. Mortimer, *J. Am. Chem. Soc.*, **44**, 1416 (1922).

(8) Armour Research Foundation, *Anal. Chem.*, **20**, 1249 (1948).

observed during cooling of mixtures to temperatures below 0°.

X-Ray analysis of the 1:1 complex confirmed that the largest side of the unit cell expanded. These X-ray results, and the data showing formation of complexes containing an integral number of molecules, suggest that 2-methylnaphthalene behaves much like graphite⁹ or the clay minerals halloysite and montmorillonite,¹⁰ which form layer-type inclusion complexes.

During the transformation, therefore, 2-methylnaphthalene molecules form a structure with enough space to accommodate as much as one molecule of *n*-heptane per molecule of naphthalene. As the crystal is warmed, the void in the lattice remains, but the heptane escapes because van der Waals forces become less significant. Thus, melting curves show short halts as five molecules, and then two more molecules, of *n*-heptane are removed from the void in two unit cells.

Although the temperature of isothermal transition of pure 2-methylnaphthalene is the same as that of the 8:1 complex, the two transitions correspond to different arrangements of the crystal lattice. The heat of transition of 2-methylnaphthalene is 1.34 kcal. per mole,⁴ but that of the 8:1 complex is approximately four kcal. per mole, according to Table I. The transition of the 8:1 complex from crystals II to crystals I involves the largest energy change of any transition in the system 2-methylnaphthalene-*n*-heptane. This large absorption of heat probably corresponds to the collapse of the expanded crystal lattice to the normal lattice of crystals I.

The magnitude of the forces binding the methylnaphthalene complexes together is revealed by the large heats of fusion of the complexes. At low temperature, these forces are as strong as the dipole-dipole forces in urea complexes at room temperature. Thus, in a sense, the methylnaphthalene molecule probably becomes a dipole at low temperature, because the electrons are undoubtedly localized. The intensity of the cohesive forces in urea and methylnaphthalene complexes can also be compared by measurement of their respective dissociation pressures. At 0°, the dissociation pressure of heptane-urea is 3.3 mm.¹¹; that of heptane-2-methylnaphthalene is 9.0.

Other Complexes of Methylnaphthalenes.—If this mechanism is correct, formation of complexes should not be limited to *n*-heptane. A survey of binary systems containing 2-methylnaphthalene and other hydrocarbons, as well as compounds with a variety of functional groups, has demonstrated that complex formation is general. Complexes are formed with both straight-chain and branched hydrocarbons; however, molecules as long or longer than *n*-hexadecane do not fit into the cavity in the crystal I lattice of 2-methylnaphthalene.

Flat aromatic compounds, such as toluene, form complexes easily. Mixtures of 2-methylnaphthalene and toluene evolve heat below 0° and melt

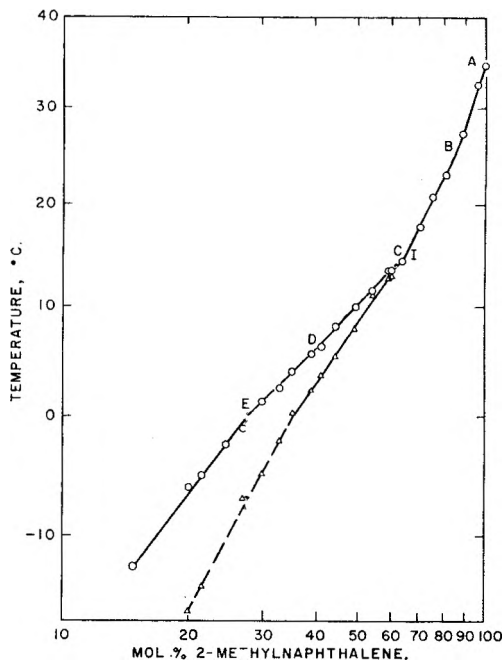


Fig. 4.—Log diagram.

at temperatures higher than theoretical. Although the binary system was not studied completely, initial results suggest that the phase diagram resembles the system 2-methylnaphthalene-*n*-heptane.

Molecules as large as phenylcyclohexane and decalin complex with 2-methylnaphthalene at temperatures below 0°, but above 0° 2-methylnaphthalene complexes only with decalin. Thus, the cavity in crystals I of 2-methylnaphthalene accommodates the compact decalin molecule and not the slightly larger phenylcyclohexane molecule. However, below 0°, where the crystal lattice can expand, even phenylcyclohexane is accommodated.

1-Methylnaphthalene behaves like the 2-methyl derivative; the complexes, as might be expected, are lower-melting. Preliminary thermal analysis of the 1-methylnaphthalene-*n*-hexane system indicates that it also is composed of incongruent-melting complexes. When a mixture was cooled below its freezing point, it transformed at -68° to a higher-melting form. Apparently the transformation is similar to that observed in the 2-methylnaphthalene-*n*-heptane system and corresponds to an expansion of the unit cell.

Formation of these novel inclusion complexes is not limited to methylnaphthalenes. Initial experiments indicate that other naphthalene derivatives and other polycyclic compounds react similarly. Future work will be directed toward determining the dimensions of the cavity in the methylnaphthalene lattice and delineating the scope of the reaction that occurs below room temperature.

Acknowledgment.—The author is indebted to Dr. George S. John for help and advice on the mathematical development of the logarithmic representation of the data.

Appendix

Application of Clausius-Clapeyron Equation to

(9) H. L. Riley, *Fuel in Science and Practice*, **24**, 1 (1945).

(10) W. Schlenk, *Fortschr. chem. Forsch.*, **2**, 92 (1951).

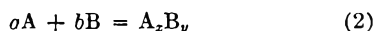
(11) W. Schlenk, *Ann.*, **565**, 204 (1949).

Binary Systems Containing Incongruent-Melting Complexes. General Equation.—If N_2 is the mole fraction of the solute in an ideal solvent

$$\ln N_2 = -\frac{\Delta H_f}{R} \left[\frac{1}{T} - \frac{1}{T_0} \right] \quad (1)$$

where ΔH_f is the heat of fusion of the solute, T_0 is the melting point of the solute and T is the melting point of the mixture.

Reaction.—



where A_xB_y is an incongruent-melting complex.

Definition.—

$$x + y = 1 \quad (3)$$

Derivation.—In a mixture of A_xB_y and B formed by reaction of “ a ” moles of A and “ b ” moles of B

$$\text{moles } A_xB_y = a/x \quad (4)$$

and

$$\text{moles of B} = b - ay/x \quad (5)$$

Therefore, when N_2 represents the mole fraction of complex A_xB_y in the solvent

$$N_2 = \frac{a/x}{a/x + (b - (ay/x))} = \frac{1}{1 + bx/(a - y)} \quad (6)$$

or, in terms of the logarithm

$$\ln N_2 = -\ln(1 + bx/(a - y)) \quad (7)$$

The value for y from equation 3 can be substituted into equation 7 to give

$$\ln N_2 = -\ln(1 + bx/a - (1 - x)) \quad (8)$$

which reduces to

$$\ln N_2 = -\ln x(1 + b/a) \quad (9)$$

But

$$1 + b/a = 1/\text{mole fraction A} = 1/N \quad (10)$$

Therefore, substitution of expression 10 into equation 9 gives

$$\ln N_2 = -\ln x(1/N) = -\ln x + \ln N \quad (11)$$

Substitution of this expression for $\ln N_2$ into the general equation 1 and rearrangement of terms leads to the new expression

$$-\ln N = \frac{\Delta H_f}{RT} - \left[\frac{\Delta H_f}{RT_0} + \ln x \right] \quad (13)$$

or, in terms of common logarithms

$$-\log N = \frac{\Delta H_f}{2.303RT} - \left[\frac{\Delta H_f}{2.303RT_0} + \log x \right] \quad (14)$$

ADSORPTION ON CONDUCTING SURFACES. HYDROLYSIS OF POTASSIUM ON ACTIVE CARBON

BY W. F. WOLFF

Research and Development Department, Standard Oil Company (Indiana), Whiting, Indiana

Received April 1, 1959

Recent work suggests that certain active carbons provide uniform, essentially graphitic surfaces suitable for use in studying adsorption phenomena. Compositions prepared by depositing potassium on active carbon have been studied by reacting them with water. Significant changes in the amounts of hydrogen evolved are observed as functions of potassium and carbon content. The results are interpreted in terms of the potassium being discretely adsorbed both atomically and ionically on a conducting surface, as has been proposed for cesium on tungsten. An extension of the mathematical treatment developed for cesium on tungsten seems to apply to potassium on active carbon, as well as to alkali and alkaline-earth metals on tungsten.

Recent work on the structure of gas-adsorbent carbons¹ suggests that active carbons of this type provide graphite-like surfaces suitable for use in the study of adsorption phenomena. If this is the case, electrons are presumably mobile within the small graphitic planes that make up such a surface. These carbons might be expected to show adsorption properties characteristic of metallic conducting surfaces.

A study of the behavior of potassium deposited on gas-adsorbent carbons should be of particular interest; the alkali metals are known to react with graphite and much attention has been given to the products obtained from potassium.²⁻⁷ Vapor-

pressure measurements and X-ray studies indicate that potassium, rubidium, and cesium penetrate the plane structure of graphite to give series of ordered sandwich compounds, with limiting compositions containing one metal atom per eight carbon atoms.³ Although the X-ray evidence has been interpreted in terms of the alkali metal being present in an atomic form,²⁻⁴ electrical studies favor ionic or partially ionic structures.^{5,7}

Little information is available in the literature on products obtained by the interaction of alkali metals with active carbons or other microcrystalline forms of carbon. X-Ray and conductance techniques are difficult to apply in such cases and the structures of the carbons are not known with certainty. However, vapor-pressure studies suggest that compositions similar to those obtained with graphite are formed.^{2,8}

To study the systems formed by potassium and gas-adsorbent carbons, three series of such compositions with different carbons were treated with water. Changes in hydrolytic activity associated

- (1) W. F. Wolff, *THIS JOURNAL*, **62**, 829 (1958); **63**, 653 (1959).
- (2) K. Fredenhagen and G. Cadenbach, *Z. anorg. Chem.*, **158**, 249 (1926).
- (3) H. L. Riley, *Fuel*, **24**, 8 (1945).
- (4) A. Hérol, *Bull. soc. chim. France*, 999 (1955).
- (5) F. R. M. McDonnell, R. C. Pink and A. R. Ubbelohde, *J. Chem. Soc.*, 191 (1951).
- (6) R. C. Asher and S. A. Wilson, *Nature*, **181**, 409 (1958).
- (7) G. R. Hennig, "Proceedings of the First and Second Conferences on Carbon," The Waverly Press, Baltimore, Md., 1956, pp. 103-112.

- (8) N. Platzer, *Compt. rend.*, **245**, 1925 (1957).

with changes in composition were measured by the volumes of hydrogen evolved. A quantitative interpretation of the results, based on the theory of adsorption on conducting surfaces, has been attempted.

Experimental

Commercial active carbons, designated A, B and C, were used without purification. Carbons A and B were separate batches of an 8-to-14-mesh coconut charcoal supplied by E. H. Sargent and Company. Carbon C was a 20-to-50-mesh coal-based carbon from Pittsburgh Coke and Chemical Company. Analyses of these carbons are given in Table I. Immediately before use, carbon samples were dried by heating to 300° under a stream of nitrogen.

Potassium was deposited on the carbon by a procedure conventionally used to disperse sodium on inert solids.⁹ Weighed amounts of potassium and carbon were heated with stirring to flask temperatures of 300°. Heating and stirring were continued for about one-half hour beyond the time required to obtain visually homogeneous products. All operations were carried out under an atmosphere of high-purity nitrogen.

Distilled water was slowly added to the cooled product at room temperature and atmospheric pressure. To ensure the exclusion of air and to avoid transfer errors, the total freshly prepared product was hydrolyzed in the preparation flask. The volume of gas released was measured with a gas buret or by water displacement. In order to determine the amount of hydrogen evolved the measured volume was corrected for the volume of adsorbed nitrogen. The volume of adsorbed nitrogen was determined separately by desorption with either *n*-heptane or *n*-dodecane.¹

TABLE I
ANALYSES OF ACTIVE CARBONS (WEIGHT %)

	A	B	C
Carbon	95.2	94.7	77.8
Hydrogen	0.91	1.07	1.62
Oxygen	0.94	2.12	2.25
Sulfur	0.09
Ash, total, as oxides	3.9	2.4	18.44

Results

Hydrolytic activities were determined for a series of compositions prepared from each carbon. The hydrogen volumes are plotted as a function of potassium concentration in Fig. 1. The dashed line represents the volumes that would be expected if there were no interaction between the potassium and the carbon.

Experimental points for carbon A appear to be best fitted by linear segments, rather than by a curved line. Compositions with a K/C atomic ratio below 0.03 give little or no hydrogen on hydrolysis. Potassium added beyond the 0.03 ratio leads to the formation of products that displace hydrogen from water. However, to a ratio of 0.12, the slope of the curve is less than that expected for pure potassium; only a fixed fraction of the incremental potassium added in this region displaces hydrogen from water. Beyond the 0.12 ratio, the curve parallels that of pure potassium; the incremental potassium reacts quantitatively with water.

The data for carbon B and C define incomplete hydrolytic curves of the type obtained for carbon A. All experimental points are satisfied by completed curves of this type, although they do not define them. The curves for carbon A and B ap-

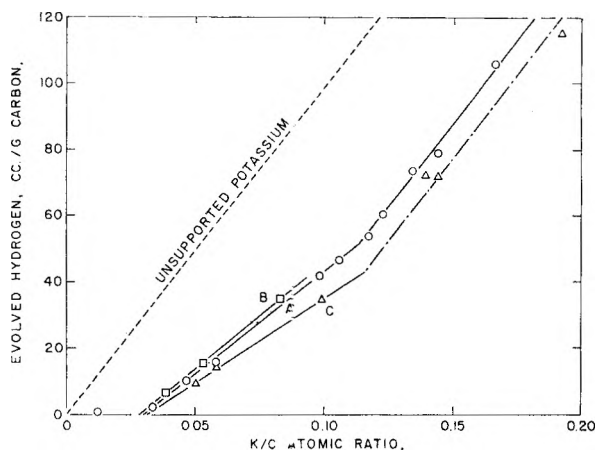


Fig. 1.—Hydrolytic activity of potassium on three carbons.

pear almost identical, as would be expected for carbons of similar source and composition. That for the dissimilar carbon C falls surprisingly close to those for carbon A and B.

Comparison of the experimental curves with that for pure potassium shows that much of the supported metal fails to release hydrogen from water. Four possible causes for this failure were examined.

There was no evidence that the activity loss was caused by reaction of potassium with impurities in the carbon or by attack on the preparation flask. Examination of analyses of carbon A and B showed insufficient impurities to account for more than a small fraction of the activity loss. Portions of carbon B were purified by extraction with hydrofluoric acid, followed by heat-treatment at 800° and 1,000° in a stream of nitrogen and then of hydrogen.¹⁰ Hydrolysis results for potassium on the original and purified carbon are given in Table II. Although the ash content was reduced from 2.4 to 0.15% and the oxygen from 2.1 to 0.4%, there was little change in the amounts of hydrogen evolved.

TABLE II
EFFECT OF CARBON PURITY ON HYDROLYTIC ACTIVITY

	K/C atomic ratio	Evolved hydrogen, cc./g. carbon
Carbon B	0.018	0.7
	.053	15.1
Purified carbon B	.018	0.6
	.053	16.5

Attempts to relate the loss in activity to degradative reactions of the potassium with carbon or hydrocarbon constituents were unsuccessful. Little or no gas evolution was observed under typical preparation conditions. In general, volumes of hydrogen evolved on hydrolysis were unaffected by changes in preparation temperature. Significant changes in activity were obtained only when the compositions were prepared at temperatures well above 300°. Analysis of the hydrogen evolved on hydrolysis showed only 0.1 mole % hydrocarbon from compositions prepared under

(9) National Distillers Chemical Co., "High-Surface Sodium on Inert Solids," New York, N. Y., 1953.

(10) Robert B. Anderson and P. H. Emmett, *THIS JOURNAL*, **51**, 1308 (1947).

the usual conditions. Samples prepared at higher temperatures gave up to 5% hydrocarbons.

To test the possibility that some of the potassium was physically inaccessible, several compositions of this type were repeatedly washed with distilled water at room temperature. In all cases, the alkali metal was quantitatively recovered as titrated base. Complete removal was confirmed by the spark spectrum of the leached carbon.

The possibility that the activity loss was caused by interaction of either the potassium or liberated hydrogen with unsaturated regions in the carbon was also investigated. In either case, potassium treatment followed by hydrolysis should lead to an increased hydrogen content of the carbon. The hydrogen content of untreated carbon B was compared with that of the carbon after potassium treatment, hydrolysis, leaching, and drying. The treated carbon showed a significantly higher hydrogen content, 1.34 weight %, on an ash-free basis, as compared with 0.97% for the original carbon. A slight increase in oxygen content, from 1.01 to 1.14%, was obtained, but the difference is less than the estimated experimental error.

The theoretical increase in hydrogen content was calculated from the K/C atomic ratio (0.083) and the amount of hydrogen released on hydrolysis (35.2 cc. per g. of carbon). The calculated increase in the hydrogen content of the carbon 0.40%, is in satisfactory agreement with the observed value 0.37%. Thus the data are consistent with a limited hydrogenation of the active carbon.

Discussion

A possible interpretation of the experimental data is that some of the potassium atoms give up their valence electrons to the surface, forming ions incapable of displacing hydrogen from water. The fraction of atoms transformed into ions presumably is determined by the extent of surface coverage. This type of adsorption has been proposed by Becker to account for the results of thermionic-emission studies with cesium on tungsten.^{11,12} Such a view represents one of the two principal approaches that have been used in developing the theory of the adsorption bond. In the other approach, the adsorption of identical particles on a uniform surface is generally treated as giving identical adsorption bonds.¹³

The properties of potassium on active carbon might be expected to be similar to those of cesium on tungsten. The graphitic adsorption surfaces postulated for active carbon¹ not only should show a metallic character but also should have electron affinities approaching those of tungsten. In both systems, the adsorbed species are alkali metals with low ionization potentials. Thus relationships valid for cesium on tungsten should be applicable to potassium on charcoal.

In developing a quantitative treatment of thermionic-emission data for cesium on tungsten, Becker¹²

calculated the number of alkali-metal ions per square centimeter of surface, N_p , by

$$N_p = \frac{\Delta\phi_s}{1.8 \times 10^{-6}L} \quad (1)$$

where $\Delta\phi_s$ is the reduction in the electron work function of the support caused by the adsorption of the alkali metal, in electron volts, and L is the distance in Å. between the nucleus of an adsorbed ion and the electronic surface of the tungsten.¹⁴ The number of adsorbed atoms per square centimeter, N_a , was determined from the N_p value

$$N_a = \gamma\theta - N_p \quad (2)$$

where γ is the number of sites available for alkali-metal adsorption per square centimeter of surface, and θ is the fraction of sites filled. The surface ionization potential, I_s , for a system of this type was defined as the energy required to convert an adsorbed alkali-metal atom to an adsorbed ion. Values of this variable can be calculated, by means of a Born cycle, from emission data for atoms, ions and electrons, or by the equation

$$\log(N_p/N_a) = \frac{-5050}{T} I_s \quad (3)$$

where T is the absolute temperature and I_s is measured in electron volts.¹²

Although the preceding equations are presumably valid for potassium on active carbon, Becker's approach must be extended if a significant interpretation of the hydrolytic results is to be obtained. Such an extension is suggested by the probable dependence of the surface ionization potential on the concentration of electrons within the support. If changes in the concentration of ions adsorbed on the surface—and thus of excess electrons in the support—are assumed to cause directly proportional changes in the surface ionization potential

$$dI_s = k dN_p \quad (4)$$

The postulate is in reasonable accord with both the free-electron and band theories for metals.¹⁵

Upon integrating from a clean surface to an ion concentration of N_p , the surface ionization potential is obtained as a function of N_p

$$I_s - (I_s)_0 = kN_p \quad (5)$$

where $(I_s)_0$ is the limiting value of the surface ionization potential as θ approaches zero. If $(N_p)_{el}$ is defined as the concentration of ions on the surface at a concentration such that $N_p = N_a$, equations 3 and 5 give

$$I_s = (I_s)_0 [1 - N_p/(N_p)_{el}] \quad (6)$$

and

$$\log(N_p/N_a) = \frac{-5050(I_s)_0}{T} [1 - N_p/(N_p)_{el}] \quad (7)$$

If these equations are valid, ion-distribution curves obtained by plotting $\log(N_p/N_a)$ against N_p should be linear. Thermionic-emission data for

(14) The constant in this equation may be in error by a factor of two. See G. E. Moore and H. W. Allison, *J. Chem. Phys.*, **23**, 1609 (1955).

(15) The fractional change in the $N(E)$ value of the electron-distribution curve is assumed to be small over the region in which electrons are introduced. Should this region include the completion or initial filling of a band, marked deviations from the linear relationship might be expected.

(11) J. A. Becker, *Trans. Am. Electrochem. Soc.*, **55**, 169 (1929).

(12) J. A. Becker, "Advances in Catalysis," Vol. VII, Academic Press, Inc., New York, N. Y., 1955, pp. 135-59.

(13) For a treatment of the adsorption of alkali and alkaline earth metals, see I. Higuchi, T. Ree and H. Eyring, *J. Am. Chem. Soc.*, **77**, 4069 (1955); **79**, 1330 (1957).

cesium on tungsten¹² and barium on tungsten¹⁶ have been plotted in this manner so as to test the equations; the plots are given in Fig. 2. Two distribution curves are given for cesium on tungsten. One is based on published N_p and N_a values corrected for the polycrystalline nature of the surface by adjusting the values of L in equation 1 as a function of θ .¹² If L is treated as a constant, the second plot is obtained. The plot for barium on tungsten is also uncorrected for polycrystallinity. With the possible exception of values calculated for low N_p values—hence, low surface coverages—the points fall on straight lines.

The applicability of equation 7 to the activity data for potassium on active carbon is readily tested. The experimental data give the ratio N_p/N_a directly, by the relationship

$$N_p/N_a = \frac{Va}{2Mg} - 1 \quad (8)$$

where V is the molar volume of hydrogen under the experimental conditions, a is the weight of metal deposited on the support, M is the atomic weight of the metal, and g is the volume of hydrogen released. The concentration of ions on the surface, N_p , is given by

$$N_p = \frac{N}{WA} \left(\frac{a}{M} - \frac{g}{V} \right) \times 10^{-4} \quad (9)$$

where N is the Avogadro number, W is the weight of the support in grams, and A is the surface area accessible to the metal, in square meters per gram. All factors except A are obtained directly from experiment. An error in A will displace the values of N_p by a constant factor but will not affect the linearity of a plot of $\log(N_p/N_a)$ vs. N_p .

By assuming an effective surface area of 1310 square meters per gram, equations 8 and 9 have been used to determine values of $\log(N_p/N_a)$ and of N_p for potassium on carbon A. The values for less than monolayer coverage are plotted in Fig. 3. Excluding values for low potassium concentration, the points define a straight line. The hydrolytic curve back-calculated from this line, and extended to greater than monolayer coverage, is shown in Fig. 4. With one possible exception, the composite curve fits all experimental points.

The agreement between the experimental and calculated values supports the hypotheses inherent in this treatment; however, other possibilities are not precluded. The data indicate that the potassium or hydrogen reacts with unsaturated regions in the carbon, but fail to define either the type of reaction or the nature of the unsaturation. Furthermore, interpretation of the results is complicated by the heterogeneity of the support and by its possible modification during the course of the hydrolysis. The hydrolysis results reflect an unknown distribution of graphitic plane sizes, and may indicate average atom-ion distributions significantly different than those existing before the water was added.

Conclusion

The major properties of potassium on active carbon appear to be explainable in terms of the hypotheses inherent in equation 7. However, the

(16) J. A. Becker, *Phys. Rev.*, **34**, 1323 (1929).

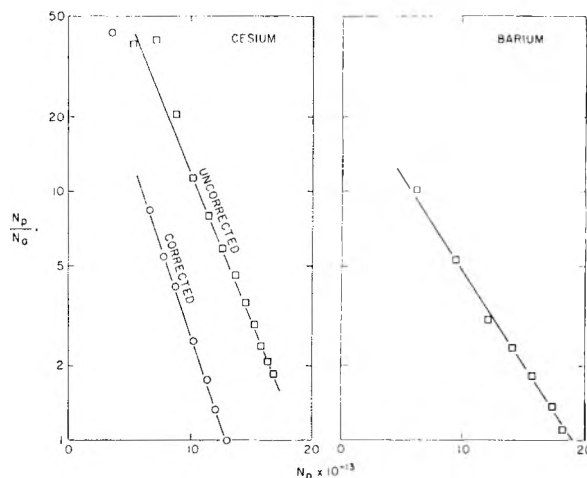


Fig. 2.—Ion distributions for metals on tungsten.

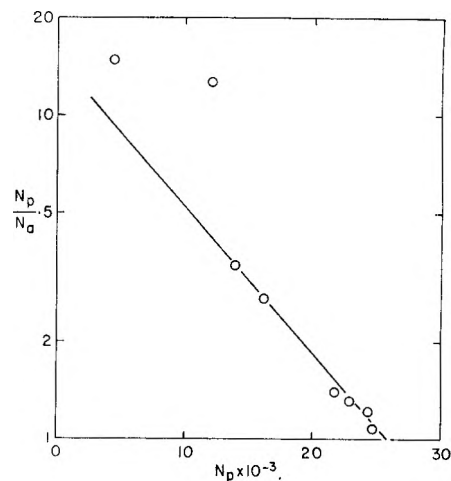


Fig. 3.—Ion distribution for potassium on carbon A.

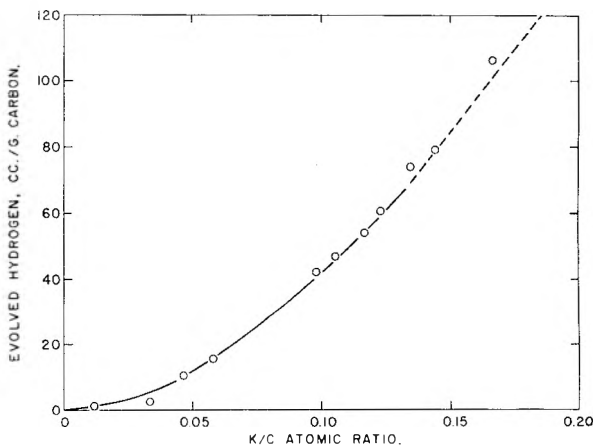


Fig. 4.—Calculated hydrolytic activity of potassium on carbon A.

equation fails to account for the apparent linearity of the principal segments of the experimental curves. Indications that this deviation is associated with the formation of compositions corresponding to the potassium graphites are being studied. Work with other metals on carbon is also in progress, to test the hypothesis that the observed changes in hydrolytic activity primarily reflect the electronic state of the metal. Data from this work

should permit direct testing of the exactness and validity of equations 4 and 7, and should provide a sound basis for studying the dependence of the constants $(I_s)_0$ and $(N_p)_{el}$ on the properties of the system.

The apparent similarities between potassium on active carbon, barium on tungsten, and cesium on

tungsten may apply to adsorption on metallic conducting surfaces in general. If such is the case, many effects that have been ascribed to surface heterogeneity could simply reflect the formation of adsorbed ions on essentially uniform surfaces.

Acknowledgment.—The author thanks G. S. John and C. E. Johnson for helpful discussions.

CROSSLINKING OF POLYMERS IN SOLUTION UNDER THE INFLUENCE OF γ -RADIATION¹

ARNIM HENGLEIN²

Contribution from the Radiation Research Laboratories, Mellon Institute, Pittsburgh, Pa.

Received April 4, 1959

Polyvinylpyrrolidone, polyvinyl acetate and polystyrene simultaneously undergo intermolecular crosslinking and degradation of their main chains when irradiated in solution. Below a critical concentration which depends on the solvent no continuous network is built up since degradation is the predominant reaction in dilute solutions. Only a few solvents or mixtures of solvents in which this critical concentration is smaller than 10 g./100 cc. have been found for each of these polymers. No relation exists between the radiation sensitivity of the solvent and the rate of crosslinking of dissolved polymers. However, crosslinking seems to be slightly favored in poor solvents. Observations on the gel dose show that this often increases with increasing polymer concentration in concentrated solutions. Radical scavengers inhibit crosslinking of these polymers and often are incorporated into the polymers. A mechanism is proposed in which the formation of macroradicals and low molecular weight radicals from the solvent by direct action of radiation are the primary steps. Crosslinks are formed by combination of macroradicals. The solvent radicals sensitize or retard crosslinking by attacking the polymer to form additional macroradicals or by deactivating macroradicals, respectively. The increase in gel dose in concentrated solutions is attributed to the decrease in the rate constant for the combination of the free macroradicals in viscous solutions as is well known from the autoacceleration observed in the bulk polymerization of a number of vinyl monomers.

Introduction

In recent years considerable research on the radiation chemistry of macromolecular substances has been devoted to changes which occur in polymers when they are irradiated in the solid state.³ Only a few investigations concerned with the effects of ionizing radiation on macromolecules in solution have been reported. These, however, have revealed that polymers in solution undergo changes similar to those observed in solid state irradiations, *i.e.*, degradation of their main chains,⁴⁻⁷ decomposition of side groups^{8,9} and also intermolecular crosslinking.^{10,11} However, the mechanisms responsible for these changes are more complex since they may result from either indirect or direct action of radiation or both.

In early investigations on the radiation chemistry of polymers in solution no attempts were made to study the dependence of the reactions on the

nature of the solvent. In recent communications^{8,9,12-15} it has, however, been shown that the rate as well as the nature of the chemical changes in the dissolved polymer depend strongly on the properties of the solvent. Certain generalizations for the various interactions that take place between the dissolved polymer and the solvent during irradiation have been established. Polymers such as polymethyl methacrylate and polyisobutylene which undergo a degradation of their main chains in the solid state are also degraded in solution.^{12,14} Alexander and Charlesby found that several water-soluble polymers crosslink when they are irradiated in aqueous solutions at concentrations above 0.5 weight %.^{10,11} Recent studies¹³ on the radiation chemistry of polystyrene in solution showed that this phenomenon is not limited to aqueous solutions. It appears that every polymer that crosslinks in the solid state may also be crosslinked in solution under suitable conditions.

The studies reported here are concerned with the radiation chemistry of polyvinylpyrrolidone and polyvinyl acetate in solution. Viscosity measurements were carried out to study the changes in these polymers. The results obtained are compared with earlier investigations on the crosslinking of polystyrene in solution. Each of these polymers

(1) This work was supported, in part, by the U. S. Atomic Energy Commission.

(2) Visiting fellow on leave from the University of Cologne, Cologne, Germany.

(3) See, for example, F. A. Bovey, "The Effects of Ionizing Radiation on Natural and Synthetic High Polymers," Interscience Publishers, New York, N. Y., 1958.

(4) P. Alexander and M. Fox, *Trans. Faraday Soc.*, **50**, 605 (1954).

(5) P. Alexander and M. Fox, *J. chim. phys.*, **50**, 415 (1953).

(6) L. A. Wall and M. Magat, *ibid.*, **50**, 308 (1953).

(7) A. Chapiro, J. Durup, M. Fox and M. Magat, International symposium in macromolecular chemistry, Milan-Turin, 1954, Supplemento a "la Ricerca Scientifica," 1955, p. 207.

(8) A. Henglein and M. Boysen, *Makromol. Chem.*, **20**, 83 (1956).

(9) A. Henglein, M. Boysen and W. Schnabel, *Z. physik. Chem. Neue Folge*, **10**, 137 (1957).

(10) P. Alexander and A. Charlesby, *J. chim. phys.*, **52**, 694 (1955).

(11) P. Alexander and A. Charlesby, *J. Polymer Sci.*, **23**, 355 (1957).

(12) A. Henglein, Ch. Schneider and W. Schnabel, *Z. physik. Chem. Neue Folge*, **12**, 339 (1957).

(13) A. Henglein and Ch. Schneider, *ibid.*, **18**, 56 (1958).

(14) A. Henglein and Ch. Schneider, *ibid.*, in press.

(15) A. Henglein, K. Heine, W. Hoffmeister, W. Schnabel, Ch. Schneider and H. Url, International Conference on the peaceful uses of atomic energy in Geneva, Sept. 1958 (United Nations), contribution No. 962.

can be crosslinked by radiation in the solid state. It will be shown that these polymers simultaneously undergo intermolecular crosslinking and degradation in their main chains when irradiated in solution. The rates of crosslinking as well as of degradation depend on the nature of the solvent and the concentration of the polymer. At suitable concentrations crosslinking in solution occurs at higher rates than in the solid state. This may be of interest in preparative macromolecular chemistry.

Experimental

The polyvinylpyrrolidone used for irradiation was an unfractionated product ($[\eta]$ in methanol: 2.0 g.⁻¹100 cc.) of the Badische Anilin and Soda Fabrik. The polyvinyl acetate was unfractionated Gelva V-800 ($[\eta]$ in benzene: 4.2 g.⁻¹100 cc.) of the Shawinigan Resins Corporation. The polystyrene used in the experiments shown by Fig. 1 was obtained from a product of the Badische Anilin and Soda Fabrik by rough fractionation. The fraction of highest mean molecular weight ($[\eta]$ in benzene: 4.6 g.⁻¹100 cc.) was used. The mean molecular weight of each of these polymers was in the range of 1×10^6 to 2×10^6 .

Irradiations were carried out in oxygen-free solutions at room temperature. The samples were exposed in the interior of a Brookhaven type cylindrical cobalt-60 source at an exposure dose rate of 7.1×10^4 r./h. (approximately 7.0×10^{15} e.v. g.⁻¹ min.⁻¹). The small test-tube like irradiation vessels contained 3–6 cc. of the solutions. Air was removed from the solutions by purging with pure argon before irradiation.

Viscosity measurements were carried out with a semi-micro viscometer of the Ostwald type at 25°. In order to compare the changes induced in the polymers when they were irradiated in different solvents all viscosity determinations were carried out in the case of polyvinylpyrrolidone in methanol solution and in the case of polyvinyl acetate and polystyrene in benzene solution. For the more dilute solutions the polymer was separated after irradiation by evaporation of the solvent and subsequently dissolved in the appropriate solvent. For the more concentrated solutions a high dilution was made with methanol or benzene. η_{sp}/c was determined at a polymer concentration of 0.5 g./100 cc.

Results and Discussion

The Interpretation of the Viscosity Changes in Irradiated Polymers.—The interpretation of the viscosity changes of polymers irradiated in solution has already been discussed briefly.¹³ Figure 1 illustrates typical data previously obtained for polystyrene solutions.¹⁵ The degradation of the main chain causes a decrease in the reduced viscosity whereas the formation of intermolecular crosslinks will increase the reduced viscosity of a polymer. When degradation of the main chain and intermolecular crosslinking occur simultaneously there exists a critical value, V_{crit} , of the ratio

$$V = \frac{\text{rate}_{\text{degradation}}}{\text{rate}_{\text{crosslinking}}} \quad (1)$$

above which no continuous network can build up in a particular polymer of given molecular weight. The ratio V depends on the nature of the solvent and on the concentration of the polymer. For $V \gg V_{crit}$ the intrinsic viscosity of the polymer gradually decreases with increasing dose. This case is illustrated in Fig. 1 for the irradiation of solutions of polystyrene in chloroform, benzene and toluene. The slope of these viscosity-dose curves decreases with increasing dose. In the case of $V \ll V_{crit}$ the intrinsic viscosity always increases with increasing dose. The crosslinking of

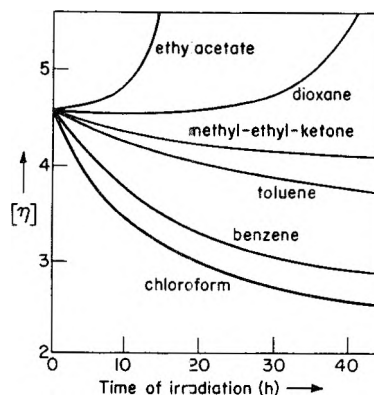


Fig. 1.—Irradiation of polystyrene in different solvents: concentration of the polymer, 50 g./l.; dose rate, 1.4×10^6 r./h. (from reference 15).

polystyrene in ethyl acetate and dioxane are examples of this case. The slope of these viscosity-dose curves after at first increases slowly with increasing dose. After prolonged exposure the viscosity suddenly increases sharply at a dose (gel dose) at which the polymer becomes insoluble. In methyl ethyl ketone the ratio V is only a little smaller than V_{crit} . Here the intrinsic viscosity at first decreases because of the greater influence of the degradation on the slope of the viscosity-dose curve at small doses. However, at much higher doses the viscosity increases again as a continuous network is built up. In the case that $V > V_{crit}$ no continuous network throughout the dissolved polymer will be formed, but essential changes may be expected not only in the mean molecular weight but also in the shape and the structure of the macromolecules by the formation of branched macromolecules and microgels and linear fragments of different chain lengths. The interpretation of the viscosity data must be handled with caution in this case. It seems noteworthy to mention that the formation of microgels can be explained by the simultaneous effects of degradation and intermolecular crosslinking. Berkowitch, Charlesby and Desreux¹⁶ explained microgel formation by intermolecular crosslinking. This, however, requires that two radical sites formed simultaneously on the same macromolecule.

Polyvinylpyrrolidone.—In Figs. 2 and 3 the reduced viscosity of polyvinylpyrrolidone is plotted as a function of the irradiation time for solutions having a concentration of 2.5 and 50 grams per liter. Figure 2 illustrates the cases of $V > V_{crit}$ or $V \gg V_{crit}$. At this low concentration the viscosity gradually decreases in all solutions studied. Apparently the rate of degradation of the main chain is dependent on the solvent. In general a degradation of the polymer by indirect action of radiation does not seem probable in organic solvents such as alcohols since the free radicals formed in these solvents are more likely to deactivate by reactions among themselves or with the solvent than with the polyvinylpyrrolidone present in low concentration. The degradation of the main chain therefore must be due to direct action of the radiation on the dissolved polymer.

(16) J. Berkowitch, A. Charlesby and V. Desreux, *J. Polymer Sci.*, **25**, 490 (1957).

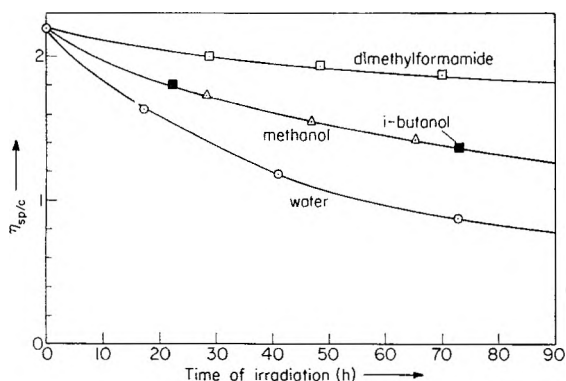


Fig. 2.—Irradiation of polyvinylpyrrolidone in different solvents: concentration of the polymer, 2.5 g./l.; dose rate, 7.1×10^4 r./h.

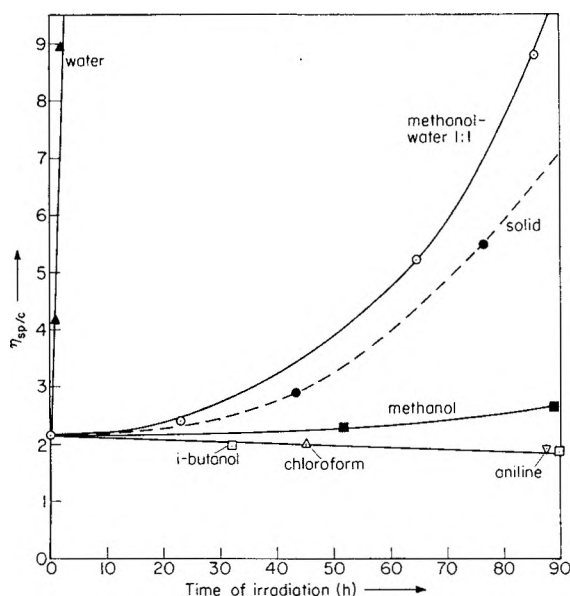


Fig. 3.—Irradiation of polyvinylpyrrolidone in different solvents: concentration of the polymer, 50 g./l.; dose rate, 7.1×10^4 r./h.

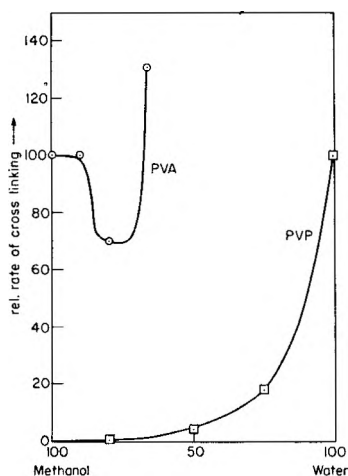


Fig. 4.—Relative rates of crosslinking of polyvinylpyrrolidone and polyvinyl acetate in mixtures of methanol and water: concentration of the polymers, 50 g./l.

The different rates of the degradation may be caused by energy transfer processes between the

polymer and the solvents as has already been found for other polymers.¹²⁻¹⁴

In aqueous solution however changes in the the polymer may be expected to be caused by indirect action of radiation. The H atoms and OH radicals formed in this solvent may easily abstract hydrogen atoms from the polymer thus forming reactive macromolecular free radicals which undergo a subsequent stabilization by breaking a bond in the main chain (see eq. 3) or which promote the formation of intermolecular crosslinks. In fact, the decrease in the reduced viscosity in Fig. 2 is most pronounced for the aqueous solution. Furthermore, this solution becomes strongly turbid during irradiation. This indicates changes in the structure of the polymer which are not due solely to a degradation of its main chain. The turbidity is explained by the formation of microgels as a consequence of simultaneous degradation and intermolecular crosslinking.

Figure 3 shows that at higher concentration of the polymer a continuous network is rapidly formed in the aqueous solution. In methanol solution a complete network is also built up after a very long time of irradiation. V is higher than V_{crit} for all the other solutions shown in Fig. 3 where the viscosity slowly decreases. During the irradiation of chloroform solutions the polymer separated from the solution to give a turbid sol of high viscosity. The amount of polymer precipitated was found to be proportional to the dose. This precipitation is due to the quaternization of the polyvinylpyrrolidone under the influence of the hydrogen chloride resulting from the radiolysis of the chloroform.

In Fig. 4 the rate of crosslinking is plotted for different mixtures of water and methanol. In every mixture the rate of crosslinking is much smaller than would be expected if it was a linear function of the composition of the mixture. Apparently methanol retards the crosslinking of polyvinylpyrrolidone in aqueous solution.

Tetranitromethane at a concentration of 10^{-3} mole/l. was found to inhibit the crosslinking of polyvinylpyrrolidone in solution. It has been shown earlier^{17, 18} that tetranitromethane is an effective radical scavenger for organic free radicals formed in the radiolysis of aqueous solutions of organic materials. The solutions, after irradiation, were colored yellow because of the nitroform formed.

Polyvinyl Acetate.—Figures 5 and 6 show similar data on the reduced viscosity of polyvinyl acetate as a function of the irradiation time. The concentrations of the polymer were 20 and 50 g./l., respectively. It can be seen from Fig. 5 that polyvinyl acetate in dilute solutions undergoes a degradation of its main chain. This degradation occurs at a high rate in chloroform solutions. Chloroform has been found to be an effective solvent for the degradation of other polymers such as polymethylmethacrylate and polystyrene also.^{12, 13} Experi-

(17) A. Henglein and J. Jaspert, *Z. physik. Chem. Neue Folge*, **12**, 324 (1957).

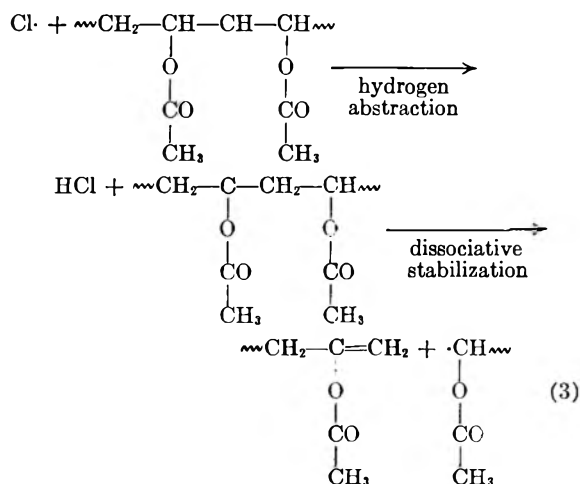
(18) A. Henglein, J. Langhoff and G. Schmidt, *THIS JOURNAL*, in press.

TABLE I
IRRADIATION OF POLYSTYRENE, POLYVINYLPYRROLIDONE AND POLYVINYL ACETATE IN DIFFERENT SOLVENTS
Concentration of the polymer, 50 g./l.

Polymer	Solvent	η_{sp}/c	Appearance of soln.		Relative rate of crosslinking
Polystyrene	Dioxane	5.42	Turbid	Crosslinks	30
	Chloroform	5.37	Clear	Degrades	
	Benzene	4.62	Clear	Degrades	
	Toluene	4.50	Clear	Degrades	
	Carbon tetrachloride	4.40	Clear	Degrades	
	Ethyl acetate ^a	2.62	Turbid	Crosslinks	
Polyvinylpyrrolidone	Methyl ethyl ketone	2.42	Turbid	Crosslinks	5
	Isobutyl alc.	2.46	Clear	Degrades	
	Methanol	2.26	Clear	Crosslinks	
	Aniline	2.10	Clear	Degrades	
	Chloroform	1.84	Clear	Degrades	
	Water ^a	1.64	Turbid	Crosslinks	
Polyvinyl acetate	Dimethylformamide	1.40	Clear	Degrades	100
	Aniline	7.30	Clear	Degrades	
	Chloroform	6.20	Clear	Degrades	
	Dioxane	6.10	Clear	Degrades	
	Acetone	4.95	Clear	Degrades	
	Ethyl acetate	4.90	Clear	Degrades	
	Dimethylformamide	4.74	Clear	Degrades	
	Benzene	4.60	Clear	Crosslinks	
	Toluene	4.20	Clear	Degrades	
	Propionitrile	4.18	Clear	Degrades	
Methanol ^a	1.90	Turbid	Crosslinks		

^a The rate of crosslinking in these solvents was made equal to 100.

ments on the photo-chlorination of these polymers showed that free chlorine atoms cause degradation of their main chains.¹⁹



The high rate of the degradation under the influence of γ -radiation is therefore explained by the action of free chlorine atoms resulting from the radiolysis of the solvent on the polymer. Possibly, for the other solvents in Fig. 5 the degradation of the polymer is caused more by direct than by indirect action of radiation.

At a concentration of 50 g./l. crosslinking predominates in methanol, water-methanol mixtures and benzene (Fig. 6).

All experimental results are compiled in Table I. It is seen that crosslinking of polymers in rather dilute solutions (50 g./l.) depends on the nature of the solvent in an extremely specific manner. For

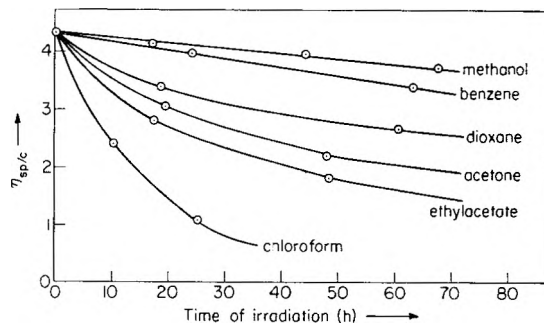


Fig. 5.—Irradiation of polyvinyl acetate in different solvents; concentration of the polymer, 20 g./l.; dose rate, 7.1×10^4 r./h.

each polymer studied only a few suitable solvents or mixtures of solvents have been found. No solvent exists which is generally suitable for crosslinking of all polymers. Similar observations have been reported by Wippler²⁰ for the crosslinking of polyvinyl chloride swollen to a high degree by different organic solvents.

In Table I there is also listed the reduced viscosity of the polymers in the different solvents. Some of the solutions were turbid even after filtration or centrifugation. Turbidity was preferentially observed for solutions in which η_{sp}/c of the polymer has a low value. This indicates that part of the polymer (branched structures or macromolecules of very high chain lengths) is poorly soluble in these solvents and that a certain aggregation took place. There is a slight but not unambiguous evidence in Table I that crosslinking occurs in these solutions preferentially.

(19) W. Hahn and F. Grafmüller, *Makromol. Chem.*, **21**, 121 (1956).

(20) C. Wippler, *J. Polymer Sci.*, **29**, 585 (1958).

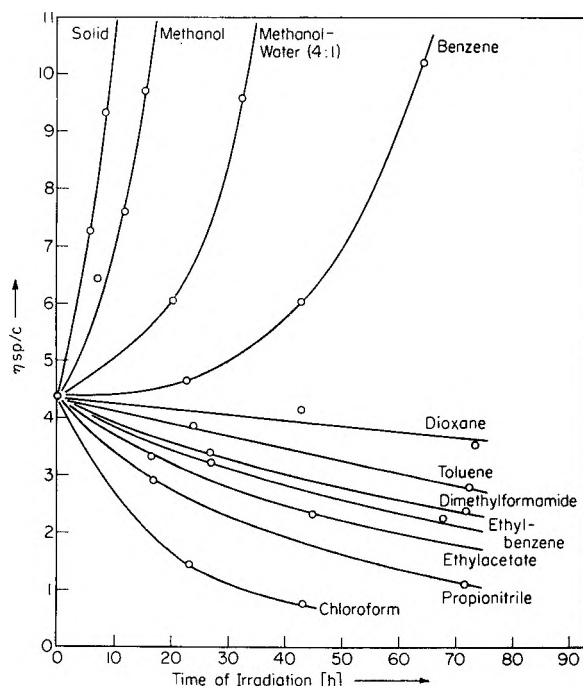


Fig. 6.—Irradiation of polyvinyl acetate in different solvents: concentration of the polymer, 50 g./l.; dose rate, 7.1×10^3 r./h.

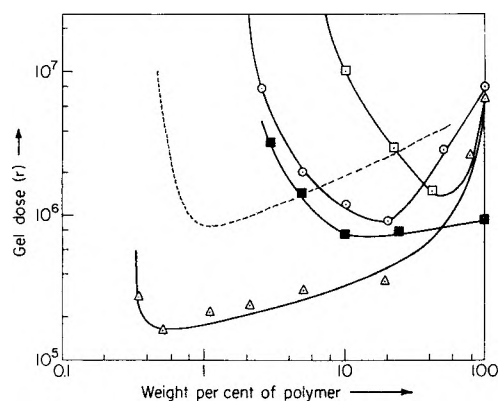


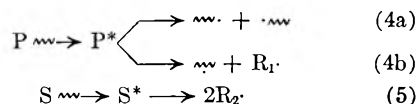
Fig. 7.—Gel dose as a function of polymer concentration: Δ , polyvinylpyrrolidone in water (dotted curve, data of Alexander and Charlesby¹⁰ for PVP of lower molecular weight); \square , polyvinylpyrrolidone in methanol; \blacksquare , polyvinyl acetate in methanol; \circ , polystyrene in ethyl acetate.

It seems, therefore, that the solubility or aggregation of a polymer in solution has some influence on the rate of crosslinking. An influence of the solubility has been reported earlier¹⁵ in the case of crosslinking of polystyrene in ethyl acetate. The turbidity and rate of crosslinking are strongly increased by adding methanol to such a solution up to a point just below precipitation. A similar effect has been observed for the crosslinking of polyvinyl acetate in mixtures of water and methanol. Water is known to increase the solubility of polyvinyl acetate in methanol when it is present in low concentrations. However, if water is present at concentrations higher than about 33 volume % precipitation occurs. Figure 4 shows that the rate of crosslinking at first decreases with increasing concentration of water and increases strongly again before precipitation occurs.

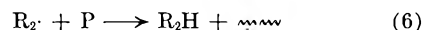
Radical scavengers such as tetranitromethane, iodine and diphenylpicrylhydrazyl at a concentration of 10^{-3} mole/l. were found to inhibit crosslinking of polyvinyl acetate in solution. In an earlier⁸ investigation it was observed that diphenylpicrylhydrazyl is incorporated into the polymer under the influence of radiation. The inhibiting action of the radical scavengers, therefore, is assumed to result from their reaction with macromolecular free radicals of the polyvinylpyrrolidone which are the reactive intermediates of crosslinking. Crosslinking of polystyrene in solution is already known to be inhibited by radical scavengers.¹³

Gel Dose and Polymer Concentration.—Figure 7 shows the dependence of the gel dose on the concentration of the dissolved polymer. Below the concentration where the ratio V passes through its critical value (the critical concentration) no continuous network can be built up in the dissolved polymer. This critical concentration was found to be 0.28, 4.0, 2.5 and 2.0 weight % for the systems polyvinylpyrrolidone in water, polyvinylpyrrolidone in methanol, polyvinyl acetate in methanol and polystyrene in ethylacetate, respectively. Above this concentration the gel dose at first decreases until it reaches a minimum which occurs at the concentrations of 0.5, 50, 10 and 20 weight %, respectively. Above these concentrations the gel dose increases again. This increase is especially pronounced for the solutions of polyvinylpyrrolidone and polystyrene. These two polymers need very high doses for network formation in their solid states. However, in the case of polyvinyl acetate the gel dose for the solid polymer is much lower and the minimum gel dose in solution is only slightly smaller than that in the solid state.

General Mechanism of Crosslinking in Solution.—The primary reactions occurring in the irradiation of a polymer in solution are the excitation and dissociation of both the polymer P and the solvent S by direct action of radiation

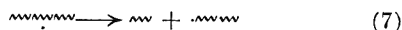


P^* and S^* being electronically excited or ionized molecules. Dissociation in the main chain of P leads to free "main chain" macroradicals (4a) while decomposition of a side group yields a free "side group" macroradical and a free radical R_1 of low molecular weight (4b). Dissociation in the main chain and in side groups may occur from the same or from different excited states P^* . A protection of the polymer occurs in the case that energy is transferred from the polymer to the solvent. Energy transfer in the opposite direction will result in a sensitization of the decomposition of the polymer. A sensitization also occurs when free radicals R_2 , resulting from the radiolysis (5) of the solvent, attack the polymer probably by hydrogen abstraction



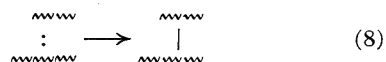
This process will enhance the formation of free side group macroradicals. Depending on the

nature of the polymer, degradation of the main chain may be increased by reaction (6) if some of the macroradicals formed stabilize spontaneously by breaking a bond in the main chain

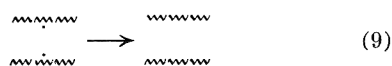


For example, this phenomenon occurs in polyvinyl acetate as illustrated by eq. 3.

The inhibition of crosslinking by radical scavengers and their incorporation into the dissolved polymer show clearly that crosslinking proceeds by a free macroradical mechanism. The formation of crosslinks, therefore, is attributed to the combination of side group macroradicals



Combinations between side group and end group macroradicals also may contribute to network formation. Many other reactions of the macroradicals are likely to compete with their combination (8). One of the competing reactions may be the mutual deactivation by disproportionation



However, most of the free macroradicals will be deactivated by their reactions with free radicals of low molecular weight R_2 resulting from the decomposition (5) of the solvent



The stationary concentration of R_2 , generally, will be much higher than that of the macroradicals because of the higher concentration of the solvent in the solutions.

Network formation in a polymer in solution, therefore, is favored if the rates of reactions 4b, 8 and 6 are high while it is retarded or inhibited if (4a,) (7), (9) and (10) are too fast. The rate of (5) depends on the radiation sensitivity of the solvent. Reaction 5 retards or sensitizes crosslinking depending on whether the following reactions 7 and 10 or 6 and 8 are fast.

The following considerations and explanations of the experimental results are derived from this general mechanism.

(a) The degradation of the main chain by reactions 4a and 7 is of lower order with respect to the polymer concentration than crosslink formation (8). A "critical" concentration of the polymer, therefore, must exist below which reactions 7 and 10 suppress the rate of crosslinking (8) so much that the ratio V (eq. 1) will become higher than the critical ratio V_{crit} . This critical concentration has been found in all cases where crosslinking of a polymer in solution occurs.

(b) Water is expected to be the most effective solvent for network formation in a dissolved polymer. The highly reactive H-atoms and OH-radicals formed here easily abstract hydrogen atoms from the dissolved polymer according to eq. 6. In aqueous solutions, therefore, free side group macroradicals will be formed by indirect action in a high yield. In fact, it can be seen from Figs. 3 and 7 that extremely fast crosslinking occurs in aqueous solutions. Furthermore, Fig. 7 shows

that the "critical" concentration of the polymer is much lower for crosslinking in water than in organic solvents.

Highly reactive radicals resulting from the radiolysis of organic solvents have little chance to react with the dissolved polymer. Most of these radicals will react with the solvent, present in much higher concentration, to give free radicals of lower reactivity which do not attack the polymer at all. A strong indirect action of radiation may be expected in a few special cases only, for example, in chloroform solutions (eq. 3). In organic solutions, therefore, there exists a rather high stationary concentration of free radicals R_2 resulting from the decomposition of the solvent. As a consequence, reaction 10 will be favored. The rate of crosslinking, therefore, will be much lower than in aqueous solutions and the critical concentration of the polymer will be much higher. In accordance with these considerations, the experiments show that the critical concentration in organic solutions is higher by a factor of at least ten.

The retardation of crosslinking of polyvinylpyrrolidone in aqueous solution by methanol (Fig. 4) can be understood easily by the mechanisms discussed. The reactive H-atoms and OH-radicals resulting from the decomposition of water are partly scavenged by the methanol before they abstract hydrogen atoms from the polymer to form free macroradicals according to eq. 6. The CH_2OH radicals thus formed²¹ in the methanol will scarcely abstract hydrogen atoms from the polymer. On the contrary, they can contribute to the decrease in the rate of crosslinking by deactivating macroradicals according to (10).

(c) The dose required to form a complete network in the dissolved polymer (gel dose) is expected to decrease with increasing polymer concentration in dilute solutions.

In the case of aqueous solutions, the suppression of reaction 10 by reaction 6 will strongly favor crosslink formation (8) with increasing polymer concentration. However, the number of macroradicals formed by reaction 6 per unit weight of the dissolved polymer will decrease when the concentration of the polymer is high enough to scavenge all free radicals R_2 . The gel dose, therefore, is expected to increase again with increasing polymer concentration. Figure 7 shows that this increase is already beginning at a very low concentration of the polymer.

In the case of non-aqueous solutions the decrease in the gel dose is attributed to the increased formation of free macroradicals by direct action of radiation (4a) with increasing polymer concentration. The number of macroradicals formed by direct action of radiation per unit weight of the polymer is constant. However, a higher stationary concentration of free macroradicals is built up during irradiation and this favors reaction 8 over the competing reactions 7 and 10.

(d) The gel dose, however, often increases again

(21) See for example M. Lefort in "Actions Chimiques et Biologiques des Radiations," edited by M. Haissinsky, Masson et Cie., Paris, 1955, serial No. 1, p. 174.

with increasing concentration of the polymer in concentrated non-aqueous solutions (Fig. 7). A very pronounced increase also occurs in aqueous solutions at high concentrations of the polymer. A plausible explanation is the decrease in the rate constant of combination (8) of the free macroradicals in concentrated solutions. Such a decrease is well known from the bulk polymerization of several vinyl compounds where autoacceleration occurs at high concentrations of the polymer formed.^{22, 23} This phenomenon is attributed to

(22) R. G. W. Norrish and R. R. Smith, *Nature*, **150**, 336 (1942).

(23) E. Trommsdorff, H. Kohle and P. Lagally, *Makromol. Chem.*, **1**, 169 (1948).

the high viscosities of these solutions in which the diffusion of the macroradicals is very low. The diffusion of species of low molecular weight, however, is not so strongly hindered in viscous solutions. As a consequence, reactions of the macroradicals with low molecular weight compounds become favored over macroradical combinations. In the case of autoacceleration of polymerizations the intermediate macroradicals do preferentially react with molecules of the vinyl monomer. In the irradiation of concentrated polymer solutions the deactivation of the macroradicals by low molecular weight radicals R_1 and R_2 (eq. 4b and 5) are favored.

EXPERIMENTAL STUDY OF THE POLYMORPHISM OF AgI

By A. J. MAJUMDAR AND RUSTUM ROY

Contribution No. 58-110, The College of Mineral Industries,
The Pennsylvania State University, University Park, Pennsylvania

Received April 10, 1959

Polymorphism in AgI has been studied in the temperature range between 25 and 200° and the pressure range between 1 and 1000 atm. Pressure dependence of the temperature of the transition that takes place at 146.5° at atmospheric pressure has been studied up to 1000 atmospheres, and the volume change has been determined by high temperature X-ray diffraction. From these parameters the enthalpy change at the transition temperature has been calculated. No evidence could be obtained for a definite transition temperature for the important cubic \rightleftharpoons hexagonal polytypic transition. It is concluded that there is no range of thermodynamic stability for the 3C polytype, if indeed it can be prepared at all.

Introduction

An examination of the literature¹⁻⁴ reveals the picture of the polymorphism of AgI. At least three forms are said to exist: i, a high temperature cubic form (I) which only forms (and is the stable form of AgI) above 146.5°; ii, a hexagonal form (II) with the wurtzite structure which forms reversibly upon cooling the high temperature cubic form below 146.5°; iii, a second cubic form (III) presumably with the sphalerite structure, which it has been claimed may be stable below 137°.

The transition between forms I and II is well authenticated and understood even though the high temperature structure is a very rare one in which the Ag^+ ions appear to be in random motion in the lattice. The transition between forms II and III is quite a different matter. It is a polytypic change from the hexagonal close-packing of II to cubic close-packing in III. However, a closer look at the experimental data shows that neither is it certain that an endmember sphalerite-structure form III exists, nor is there much justification for any equilibrium transition temperature being assigned for the $\text{II} \rightleftharpoons \text{III}$ reaction.

Our interest in the applicability of classical thermodynamics to solid phase transitions caused us to examine two phases of this problem. First, in the $\text{I} \rightleftharpoons \text{II}$ transition, in which we have an "ordered" arrangement changing to a "random" arrangement accompanied by a very large entropy

change, do the transition parameters fit the Clapeyron relationship. If not, would the equivalent expression for second-order phase transition fit it better?

Second, does AgI actually exist in a sphalerite III form and if so, what are the stability relations with the wurtzite II form. If a stable transition exists, one has a structural mechanism to explain a possible second-order transition, and the thermodynamic relations in such a case should be most interesting.

Experimental Procedure

I. Preparation of the Starting Materials.—Verwey, *et al.*,⁵ pointed out a long time ago that the structural nature of AgI depends to a large extent on its method of precipitation, and this has been the way in which "different" AgI structures have been usually made. Reagent grade AgNO_3 and KI (Fisher), in the present investigation, were used for the preparation of AgI. The following different methods of preparing the AgI starting material were used: (a) precipitated from solution by the addition of AgNO_3 to excess KI with constant stirring; (b) precipitated from solution by the addition of KI to excess AgNO_3 with constant stirring; (c) precipitated from solution, using aliquot amounts of AgNO_3 and KI; (d) previously precipitated AgI dissolved in KI, the solution filtered, and subsequently poured into a large excess of water. The precipitate now appearing filtered and washed free of I^- by repeated washing with water; (e) previously precipitated AgI melted in a sealed silica tube, quenched and pulverized carefully; (f) previously precipitated AgI treated with concentrated NH_4OH and evaporated to dryness at 110°; (g) formed by solid state reaction between metallic Ag powder and excess I_2 at 150° in a sealed silica glass tube; (h) formed by solid state reaction in a sealed tube between I_2 and excess metallic Ag powder at 300°; (i) previously precipitated AgI vaporized and redeposited on a glass plate; (j) previously precipitated AgI boiled with H_2O to dryness; (k) AgI powder melted in the

(1) L. W. Strock, *Z. physik. Chem. Bd.*, **25**, 441 (1934).

(2) L. W. Strock and V. A. Brophy, *Am. Mineralogist*, **40**, 94 (1955).

(3) M. L. Huggins, *Transition in Silver Halides*, in "Phase Transformation in Solids," ed. by Smoluchowski, *et al.*, John Wiley & Sons, New York, N. Y., 1951, Ch. 8.

(4) J. W. Mansen, *This Journal*, **60**, 806 (1956).

(5) E. J. W. Verwey and H. R. Kruyt, *Z. physik. Chem.*, **A167**, Spez. S. 142 ff. (1933).

presence of slight excess of I_2 in a sealed tube, quenched and powdered.

II. **Apparatus and Technique.**—For studying the sphalerite type \rightleftharpoons wurtzite type transition, samples of AgI with or without other reagents were placed in silica glass tubes and sealed. These sealed tubes were then heated to different temperatures for periods of time ranging from a few hours to a few months.

The transformation at 146.5° was studied in two different ways. (1) The pressure dependence of the transition temperature was determined by means of differential thermal analysis at high pressures. Nitrogen was used as the pressure transmitting medium. The pressure was generated by a laboratory pump described by Roy and Osborn.⁶ The sample holder was contained in a special "test-tube" bomb⁶ with four thermocouple leads "packed" in by means of a commercial "Conax" head.

(2) The crystallographic behavior of AgI was followed by means of X-ray diffraction on powdered samples at elevated temperatures. A high angle Norelco diffractometer was used throughout. By measuring precisely (at $1/8^\circ$ 2θ per min. scanning speed) the changes in the positions of a few reflections in the X-ray diffraction spectra as a function of temperature, the lattice parameters for the crystalline forms below and above the transformation temperature could be determined. The temperature of transition determined incidentally served as a check on the temperature of transformation obtained by thermal analysis.

Results and Discussion

None of the methods of preparation described above yielded a "pure" sphalerite structure, although methods a, d, and e appear to give what has been called, on the basis of peak intensities, a pure wurtzite structure. Verwey,⁵ trying various methods came to the conclusion that methods b and e give much more sphaleritic than wurtzitic structure. The main criterion used to distinguish between the two forms is that while the hexagonal wurtzite structure gives three X-ray reflections in the region of 22° 2θ for Cu $K\alpha$ ($d_{100} = 3.98 \text{ \AA}$; $d_{002} = 3.73 \text{ \AA}$; $d_{101} = 3.50 \text{ \AA}$), the cubic sphalerite structure gives only one reflection in the same region ($d_{100} = 3.72 \text{ \AA}$).

The results of the present investigation are summarized in a schematic diagram (Fig. 1). The letters a, b, c, etc., of the diagram refer to the methods of preparation referred to in the text with the corresponding letter. Results of all experiments have not been shown; the methods giving the most sphaleritic forms were repeated several times. The first general and surprising observation is, therefore, that AgI cannot be synthesized in the pure cubic sphalerite structure in any reproducible manner by methods previously suggested. Attention was then directed to the possibility that the direction of equilibrium could be indicated by converting one form to the other. Experiments were performed where samples of AgI made by different methods were placed on a glass slide for examination by X-rays. After having been examined at room temperature by X-ray the same slides were heated to 100° and 132° , respectively, and the results are also shown schematically in Fig. 1. As can be seen from the diagram (Fig. 1) a few of the many different preparations of AgI do appear to become more sphaleritic when heated to 110° . Attention is drawn to cases d and e. The claim of Mansen⁴ that in the presence of I_2 vapor AgI goes to the hexagonal form readily was not borne out by all the samples,

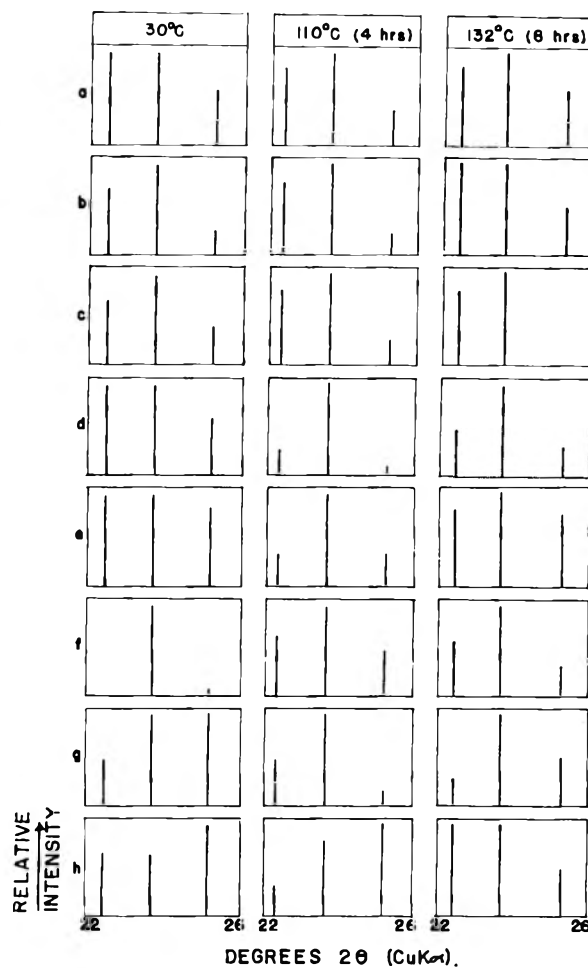


Fig. 1.—Schematic representation of diffractometer patterns of starting materials prepared by various methods (see text) shown in left-hand column. The effect of heat treatment also is illustrated for two temperatures 110° and 132° . No consistent pattern of conversion toward the sphalerite form can be detected.

i.e., there is no clear evidence that the sphaleritic material always converts to wurtzite at about 120° , although in cases b, d and h this seems to be the trend. All starting materials except d were heated to temperature ranges between 128 – 142° dry, as well as in the presence of H_2O , and NH_4OH for periods ranging from two weeks to three months. In no case was a pure sphalerite structure formed, while in most cases good wurtzite structures were formed.

Moreover, in ZnS Smith and Hill⁷ have shown that the effect of powdering sphalerite and wurtzite is to introduce disorder, making especially the hexagonal material look "more cubic" on cursory examination. AgI powder is very plastic and intensity measurements using "powdered" or ground samples are not likely to be reliable. Thus, although there was plenty of evidence for several other complex polytypes of AgI, it must be concluded that AgI does not exist stably in the sphalerite form. Hence, the 120° transition of Mansen⁴ and 137° reported by others as the transition temperature between sphalerite and wurtzite forms of AgI is without significance.

(6) R. Roy and E. F. Osborn, *Econ. Geol.*, **47** [7] 717 (1952).

(7) F. G. Smith and V. G. Hill, *Acta Cryst.*, **9**, 821 (1956).

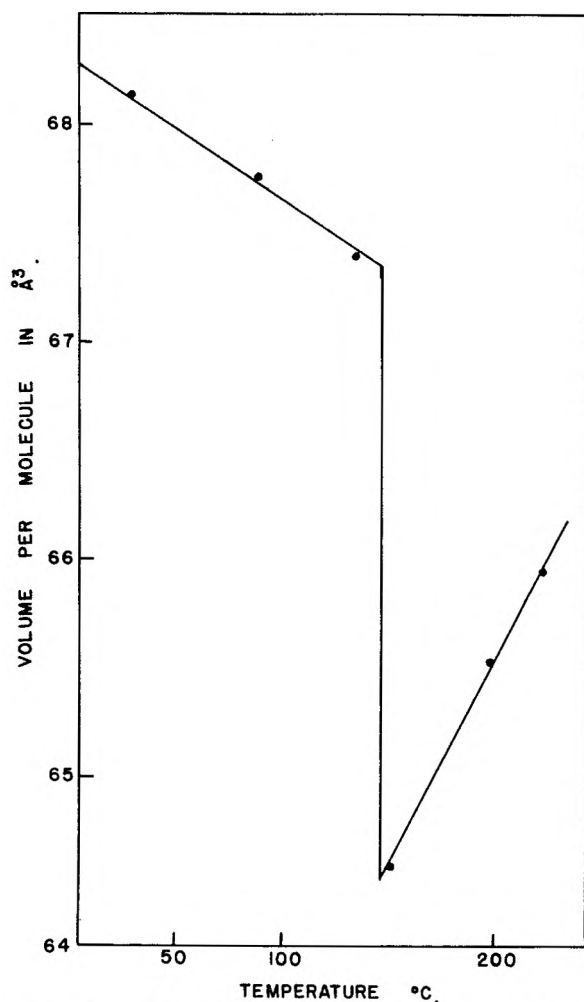


Fig. 2.—High temperature X-ray data on cell volume (converted to per "molecule" basis) of AgI as a function of temperature. Note negative thermal expansion of wurtzite and sharpness of volume change with no "second-order" behavior.

The volume of AgI per molecule as a function of temperature, as obtained by high temperature X-ray measurements, has been plotted in Fig. 2. It is interesting to note that the thermal expansion of the wurtzite form below 146.5° and the volume change for the transition both turned out to be negative. The temperature of transition was found to decrease with pressure. The data showing the dependence of the transition temperature for the 146.5° transformation on pressure are listed in Table I.

TABLE I
PRESSURE-TEMPERATURE DATA ON 146.5° TRANSITION IN AgI

Substance	Ref.	Pressure (atm. — ±2 atm.)	Temp., ±1°C. Heat-ing	Cool-ing
AgI (Iodyrite)	NaCl	1	146.5	146
		200	143	143
		400	140	140
		800	135	135
		1000	132	134

The thermodynamic quantities—enthalpy change (ΔH), volume change (ΔV)—of a substance undergoing transformation at a temperature T are related to the pressure dependence of the transition temperature (dp/dT) by the well known Clapeyron relationship as $dp/dT = \Delta H_{tr}/T\Delta V$. Taking dp/dT as 1000/−14.5 atm./°C. and ΔV as −1.727 cc./mole, the value of ΔH comes out to be 1208 cal./mole. Taking the maximum limits of error in the measurement of the experimentally determined quantities, the total uncertainty in the value of ΔH_{tr} is ± 140 cal./mole. Kelley⁸ quotes a thermochemically measured value of 1470 cal./mole, which in our experience may be considered as very good agreement in such work. Second-order behavior is ruled out by the markedly sharp volume change. This example also demonstrates that in cases of transitions where the volume change undergone by the substance at the transition temperature, and dp/dT are fairly large, the Clapeyron relationship can yield an accurate value of the other parameters associated with the transition.

Conclusions

There is no experimental proof of the existence of a true sphalerite form of AgI. Hence, the 137° transition temperature between the sphalerite and wurtzite form is meaningless and should be stricken from the records. Wurtzite is the stable form in the range 146.5–120° and probably from 146.5 to room temperature. The transition at 146.5° is clearly first order and takes place with a negative volume change (the transition temperature going down with pressure). The transition-enthalpy is 1208 ± 140 cal./mole.

Acknowledgment.—This work forms part of a study on the phase rule and polymorphism supported by the National Science Foundation under Grants G-1000 and G-4648.

(8) K. K. Kelley, Bur. of Mines Bull. 476, 1949.

SOME SPECIFIC MOLECULAR REARRANGEMENTS IN THE MASS SPECTRA OF ORGANIC COMPOUNDS

BY J. H. BEYNON, G. R. LESTER AND A. E. WILLIAMS

Contribution from Imperial Chemical Industries, Dyestuffs Divn., Manchester, 9, England

Received April 14, 1959

An important specific rearrangement process in oxygenated organic compounds has been found to involve the formation of carbon monoxide. A combination of accurate mass measurement and metastable peak analysis has provided in many cases unequivocal information on the course of the fragmentation processes involved. A fairly detailed study of the fragmentation of anthraquinone has shown that fresh bonds are formed to produce the ionized forms of fluorenone and *o*-diphenylene; in the case of hydroxy derivatives of anthraquinone the ion $C_{11}H_7^+$ appears to have high stability. Other compounds, mainly aromatic ethers and ketones, are discussed in a similar way and in a few cases suggestions are made regarding the nature of the transition states involved in these specific rearrangements. Analogously, HCN, NO and other groups are eliminated from nitrogen-containing compounds such as the nitroanilines. The theoretical implications of such specific low energy processes are considered briefly, with reference to the quasi-equilibrium theory of mass spectra.

In a recent paper, McLafferty¹ has surveyed the information available on rearrangement reactions in mass spectra and has subdivided the reactions observed into either "random" or "specific." The height of a peak in a mass spectrum depends both on the rates at which the ions which make up this peak are formed by fragmentation of parent ions and destroyed in further reactions. The reaction rates will depend² on the activation energies and entropies along any path leading to a particular ion. In the case of hydrocarbon molecules, there may be several competing decomposition paths of comparable energy requirements and several rearrangement reactions may occur. In such cases, the rearrangements are said to be "random." When the molecule contains a functional group, on the other hand, this group can dominate the fragmentation process and lead to only a single rearrangement process "specific" to that group. In the present paper, some of these "specific" rearrangements are considered. We have concentrated on a particular type of rearrangement in which the neutral fragment carbon monoxide is eliminated but have given a few examples of other rearrangements related to this involving, for example, the elimination of HCN. The implications of mass spectra of this type for existing theoretical interpretations, such as the quasi-equilibrium theory, are investigated. All mass spectra were measured on a double focusing high resolution mass spectrometer type M.S.8 made by Metropolitan-Vickers Electrical Co. Ltd., Trafford Park, Manchester, England.³ Where necessary samples were purified by zone melting.

An early example of mass spectral evidence for the elimination of carbon monoxide is given by Mariner and Bleakney.⁴ Here the neutral carbon monoxide is eliminated from the parent ion of formic acid with simultaneous formation of a water ion by rearrangement of a single hydrogen atom. Mariner and Bleakney were able to show that the presence of a peak due to H_2O^+ in the mass spectrum and also the presence of a peak due to CO^+ (formed by elimination of neutral water from the parent ion) were not due to thermal decomposition of the

formic acid followed by ionization of the products. They considered the energies of all possible forms of aggregation of 2 hydrogen atoms, 2 oxygen atoms and 1 carbon atom relative to their energy as formic acid, and obtained the result that the most stable arrangements are, respectively, $(CO_2 + H_2)$ and $(CO + H_2O)$, the energy of the latter arrangement being calculated to be 0.18 e.v. They found the appearance potential of the $(H_2O)^+$ ion to be 13.1 e.v., which is a value only 0.5 e.v. above the first ionization potential of water and is too low to be due to the reaction $[HCOOH]^+ \rightarrow H_2O^+ + C + O$, since the energy of the state of aggregation $(H_2O + C + O)$ is itself 9.33 e.v. relative to formic acid which would leave only 3.8 e.v. to remove an electron from the water molecule. Thus, the neutral fragment eliminated is in the form of carbon monoxide. The large peak due to $(H_2O)^+$ ions (15% of base peak) when formic acid is bombarded with 65 e.v. electrons and that of the peak at mass 28, formed in the complementary reaction (due to $(CO)^+$ ions for which the ionization potential is 13.9 e.v. and which is of height 9% of the base peak) suggest that the driving force behind the formation of these particular rearrangement reaction products is their over-all stability. The loss of neutral carbon monoxide from oxygen-containing organic molecules has been inferred to occur in a variety of cases by determination of the formula of the associated positive ion by accurate mass measurement. It should be noted that due to the relatively high first ionization potential of the carbon monoxide molecule, a smaller quantity of energy is required to form reaction products which include carbon monoxide from a parent ion if the charge does not lie in the CO fragment. However, as shown by Cummings and Bleakney⁵ in explaining some of the appearance potentials in methyl and ethyl alcohols, for most other modes of fragmentation of oxygenated molecular ions, the charge is likely to remain with the oxygenated fragment. This is because O^+ is trivalent, and the formation of ions such as $HO \cdot C \equiv O^+$ from, say, formic acid is thus favored by the energy difference between this triple bond and the $C=O$ bond energy (about 3 e.v.). Cases are, of course, known in which the loss of fragments other than CO is favored on the grounds of the stability of the products. Loss of H_2O is common and

(1) F. W. McLafferty, *Anal. Chem.*, **31**, 82 (1959).(2) H. M. Rosenstock, M. B. Wallenstein, A. L. Wahrhaftig and H. Eyring, *Proc. Natl. Acad. Sci. U. S. A.*, **38**, 667 (1952).

(3) R. D. Craig and G. A. Errock, "Advances in Mass Spectrometry," Pergamon Press, New York, N. Y., 1959.

(4) T. Mariner and W. Bleakney, *Phys. Rev.*, **72**, 792 (1947).(5) C. S. Cummings and W. Bleakney, *ibid.*, **58**, 787 (1940).

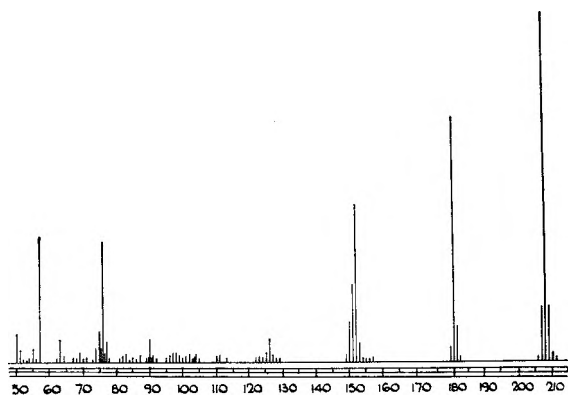


Fig. 1.—Anthraquinone.

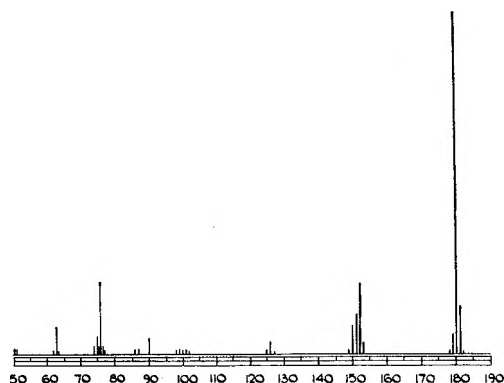


Fig. 2.—Fluorenone.

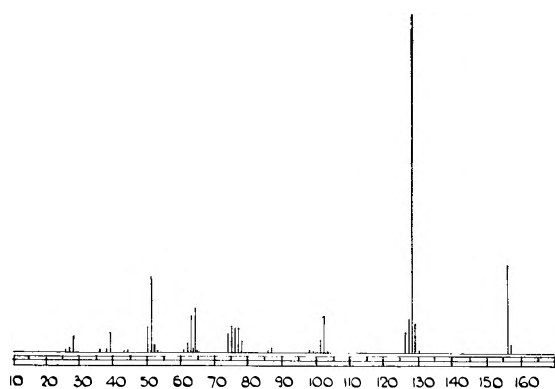
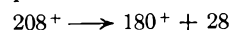


Fig. 3.—Benzotropone.

particularly so in the case of primary alcohols where the parent ion decomposes to give an olefinic ion. In other cases too the stability of the neutral fragment would seem to be the overriding consideration leading to a particular mode of breakdown, though it is the total energy of the particular state of aggregation of the constituent atoms which determines whether the reaction is energetically possible. In the spectrum of isopropyl alcohol the peak at mass 19 is particularly large (7% of base peak). It would seem that the reason for this lies in the fact that the neutral fragment simultaneously formed may be the allyl radical, but a further reason is the trivalency of the oxygen positive ion referred to above which enables $(\text{H}_3\text{O})^+$ to exist as a comparatively stable entity. In many cases, the fragments formed may be in a sterically favorable arrangement for an increase in stability by the formation of an extra bond, for example by ring

closure, and examples of cases in which this has, in fact, occurred are given below.

Accurate mass measurements on fragment ions are important in giving unequivocally the formula of each ion, and high resolution (of the order 10,000) is also important in that it ensures that any multiplets formed in the spectra can be resolved and measurements made on the individual components of which they are composed. Even when this has been done, the structural formula of the ion formed may not be apparent. Evidence as to one of the reaction paths by which a particular ion has been formed can sometimes be obtained from a study of the metastable ions. For example in the spectrum of anthraquinone shown in Fig. 1, obtained with an electron-bombardment ion source using 50 e.v. electrons, metastable peaks at masses 155.8 and 126.3 correspond to the transitions



and



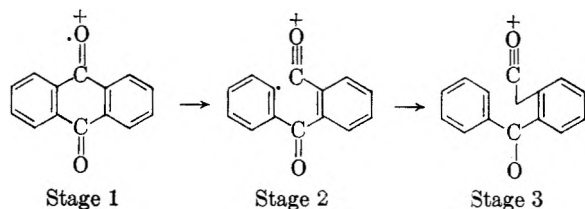
respectively. Accurate mass measurements show that the fragment ions have the formulas $[\text{C}_{13}\text{H}_8\text{O}]^+$ and $[\text{C}_{12}\text{H}_8]^+$. One can, therefore, infer that the neutral mass 28 fragment in each of the above reactions has the formula CO .⁶ It would seem reasonable to postulate the formation of an extra bond in the mass 180 ion, both to gain stability and to explain how the second carbon monoxide can be lost without separation of the remaining parts of the molecule. It is an obvious step to postulate the mass 180 ion to be a fluorenone molecular ion and it is interesting to compare the mass spectrum of fluorenone (see Fig. 2) with that of anthraquinone. It is found that from mass 180 downwards, the spectra are very similar⁶ which suggests strongly that such an ion is formed and that formation of this ion is the predominant fragmentation reaction of the anthraquinone ion. Further confirmation of the formation of neutral carbon monoxide and a fluorenone ion (presumably a very stable state of aggregation) is obtained by reducing the energy of the bombarding electrons. It is found that peaks at masses 180 and 152 remain prominent even at electron energies close to the first ionization potential of anthraquinone. This suggests the structure of the mass 152 ion to be that of the parent ion of *o*-diphenylene, and that another bond is formed when the second carbon monoxide molecule is eliminated. Thermochemical measurements made in these laboratories by G. R. Nicholson show that the formation of fluorenone and release of carbon monoxide from anthraquinone is endothermic to the extent of 21.3 kcal./mole. This measurement refers to anthraquinone and fluorenone in the solid state and to gaseous CO at 25°. The energy involved in the case of the ionized forms is likely to be smaller than this since the dissociation is accompanied by a transfer of positive charge from the carbonyl oxygen to a fluorenone link which is subject to strain. In the transition state this is probably a one-electron bond which has relatively small electron attracting power, so that the charge transfer provides a source of energy, helping to drive the reaction.

(6) J. H. Beynon, "Advances in Mass Spectrometry," Pergamon Press, New York, N. Y., 1959.

The spectrum of a sample of benzotropone (shown in Fig. 3) kindly supplied to us by Dr. R. I. Reed, Glasgow University, provides interesting additional evidence for the formation of an extra bond accompanying the elimination of CO. Except for the parent peak the spectrum of this compound is very similar to that of naphthalene taken from A.P.I. data sheets and shown in Fig. 4.

When the anthraquinone molecule is ionized, the most loosely-bound electron, which is, therefore, removed preferentially, is one of the lone-pair electrons on the oxygen atom. It has been men-

tioned above that $\overset{+}{O}$ has the capacity of trivalency, and as this is developed the electron pair in one of the C-C bonds adjacent to the carbonyl group will become uncoupled so as to provide an orbital which can give a π -bonding effect with the lone-pair oxygen orbital. Initially the direction of this bond orbital is not parallel to the orbital available on the oxygen, so that a complete π -bonding effect will not result. Nevertheless, to a first approximation the situation can be represented by stages 1 and 2 below



The positive charge on the oxygen will induce a polarity in the adjacent bonds and this will be a maximum in the remaining C-C bond. The direction of this polarity will be such that its negative end will be attached to the carbonyl group. If we consider the carbon hybridization, then the possibility of increasing the strength of the carbonyl bonds depends upon changing at least partially the trigonal hybridization for the digonal form, for this allows stronger σ - and π -bonds in the carbonyl group. The bond adjacent (α) to the carbonyl group is then "bent" and weakened (stage 3) but this is compensated by increase in the CO bonding. Moreover, the bent bond will be more readily polarized than the original stronger bond, and the electron pair may be regarded as almost entirely in the digonal orbital. This state of affairs corresponds exactly with the usual view of the electron distribution in neutral CO, lone pair electrons being accommodated at the carbon end of the molecule. In this state the carbonyl group is so weakly attached to the remainder of the molecule that the internal energy produced on impact will be sufficient to give amplitudes of vibration in the weak (vicinal) bonds beyond the dissociation limit. When this occurs we are left with stage 4

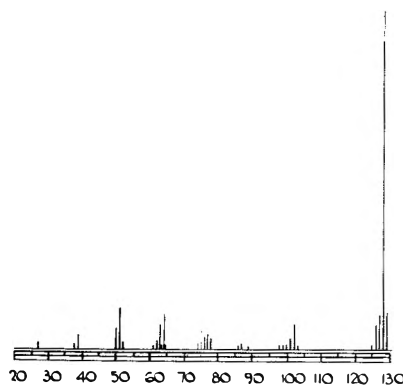
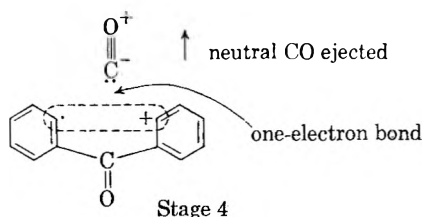
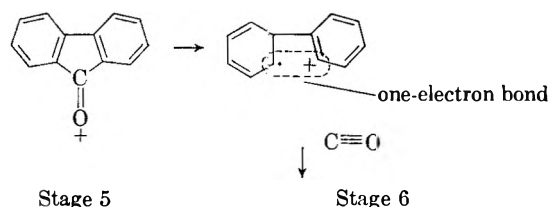


Fig. 4.—Naphthalene.

The remaining ion corresponds to a highly excited form of fluorenone having one bond stretched to $\sqrt{3} \times$ (normal bond length) and since this is virtually a one-electron bond it is quite reasonable that its length should be considerably greater than the normal bond length. Such a bond may be regarded as corresponding to a bond-order of about 0.5 and the order-length correlation for aromatic systems would suggest a bond-length as high as 1.65 Å. To reach the ground state of fluorenone, we must add one of the oxygen lone-pair electrons to the one-electron bond. This will be associated with release of vibrational energy since the one-electron bond will close up to the normal covalent distance. Not all the vibrational energy will be associated with the fluorenone ion, since we have omitted various intermediate stages in which the vibrational energy is being shared between the fluorenone and carbon monoxide and partly transferred into kinetic energy of the separating fragments. The fluorenone ion in which one of the oxygen lone-pair electrons has been removed can also break in an analogous fashion to that discussed above to eliminate a further neutral carbon monoxide molecule and give a highly excited ion of *o*-biphenylene as illustrated in stages 5 and 6



The energy regained by the charge transfer process during this rearrangement should be quite appreciable, since if we consider the isoconjugate hydrocarbon dibenzofulvene its least bonding π -orbital has energy 0.551 γ whereas the corresponding value for biphenylene is 0.400 γ (γ = resonance integral taking overlap into account).⁷ Now there are two additional features to take into account. One of these concerns the strain in the central bonds of biphenylene which is not taken into account in calculating the molecular orbital approximation to the energy since the assumption of equality of all resonance integrals is usually made in applying the semi-empirical theory. But in real-

(7) A. Pullman and B. Pullman, "Les Théories Electroniques de la Chimie Organique," Masson et Cie, Paris, 1952.

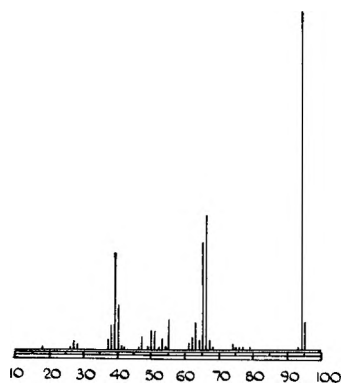
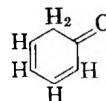


Fig. 5.—Phenol.

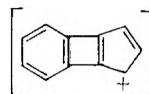
ity these central bonds are under strain and, therefore, much longer than typical aromatic bonds and correspondingly the electrons are held less firmly in this region. This would be expected to make the ionization potential unusually low. The second feature is the effect of the greater electron affinity of oxygen on all the term values for an oxygenated compound. The ionization potentials of the hybrid valence states of oxygen and carbon differ by several volts³ and this must increase appreciably the ionization potential of any compound containing oxygen. At the same time, if we are to accept the spectroscopic evidence,⁹ the non-bonding oxygen electrons are less firmly bound than any of the π -electrons. That is, of course, by no means inconsistent with the higher ionization potential of both of these in the oxygenated compound, and was the reason for our assumption that the initial ionization process led to a positively charged oxygen. Direct evidence for this greater ionization potential in oxygenated compounds is provided by pairs of compounds such as benzaldehyde (9.8 e.v.), styrene (8.9 e.v.).

Loss of carbon monoxide in this way also occurs in the mass spectra of many other quinones and occurs, for example in benzoquinone, naphthoquinone and all substituted anthraquinones which have been examined by us.¹⁰ Of particular interest are the spectra of hydroxyanthraquinones. The three major peaks in the spectrum of for example, 2-hydroxyanthraquinone occur at masses 196, 168 and 139 and correspond to successive loss of two carbon monoxide molecules followed by loss of a (CHO) radical. This is analogous behavior to that in phenol, the spectrum of which is shown in Fig. 5, and it would seem that in this latter stage the fact that (CHO) rather than CO is lost is partly associated with the exceptional stability of the ion $(C_{11}H_7)^+$ of mass 139 which is formed. An ion of this mass occurs widely in the mass spectra of aromatic hydrocarbons, and appears able to lose another electron without fragmentation; a peak of intensity 7% of the base peak occurs at a mass to charge ratio of 69.5.

Now phenol is known to behave in some of its chemical reactions (*e.g.*, Reimer-Tiemann condensation)¹¹ as though it had the structure



and it is easy to visualize a process by which such a molecule could lose CO, with simultaneous formation of a cyclopentadiene ion. Phenols and naphthols do, in fact, give spectral peaks at masses differing from the parent mass by that of CO (to be designated p-CO.) If one continues this analogy to the case of 2-hydroxyanthraquinone, one would be left with an ion

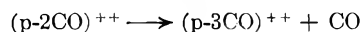


It seems unlikely that this is the final stable form of the 139 ion but it is not known what skeletal rearrangements of low activation energy are possible with such an ion.

The molecular ions postulated to take part in the first two stages of the above reaction are both odd-electron ions. Such ions are, in general, less stable than even-electron fragment ions which contain no unpaired electrons. The marginal gain in stability by pairing the electrons involves amounts of energy small compared with that needed to produce doubly-charged ions, but it is interesting to observe how the even-electron doubly-charged parent ions differ in their behavior from singly-charged ions. To continue with the example of 2-hydroxyanthraquinone which has been used above, peaks occur in its mass spectrum corresponding to $(p-CO)^{++}$ and $(p-2CO)^{++}$. A metastable peak at mass 58.2 corresponds, however, to the transition



i.e.



indicating a path to the even-electron ion of mass 140 rather than the ion of mass 139 formed from the singly-charged parent. The detailed manner in which the doubly-charged ion of mass 139 (which, as is mentioned above, is prominent in the spectrum) is formed is not indicated by any of the other metastable transitions which occur.

In many mass spectra, the first step in the fragmentation process is the loss of a free radical rather than a neutral molecule, leading immediately to an even-electron ion which can then break with loss of neutral molecules to give further even-electron ions. This is a common mode of breakdown in, for example, hydrocarbon spectra where the fragment first formed loses neutral ethylene molecules. Thus, the three most favored ions in the mass spectrum of phenyl styryl ketone (see Fig. 6) are p^+ , $(p-1)^+$ and $(p-29)^+$ where p^+ represents the "parent" or molecular ion. Accurate mass measurement shows the last of these ions to be a hydrocarbon fragment indicating that it is formed by a total loss of (CHO) from the parent. We suggest that in this case, the first step is the loss of a hydro-

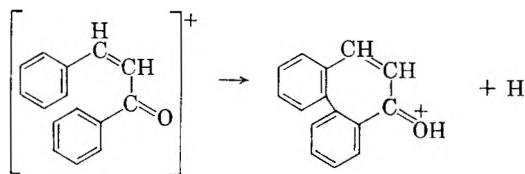
(8) W. Moffitt, *Proc. Roy. Soc. (London)*, **202A**, 534 (1950).

(9) H. L. McMurry, *J. Chem. Phys.*, **9**, 241 (1941).

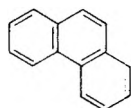
(10) J. H. Beynon and A. E. Williams, to be published.

(11) J. W. Baker, "Tautomerism," G. Routledge and Sons Ltd., London, 1934, p. 109.

gen atom and that CO is lost from the even-electron ion so formed. It seems at first sight surprising that the parent ion should lose a hydrogen atom so readily until one considers that this would make formation of an extra bond possible if the (p-1)⁺ ion assumed the structure given by the reaction



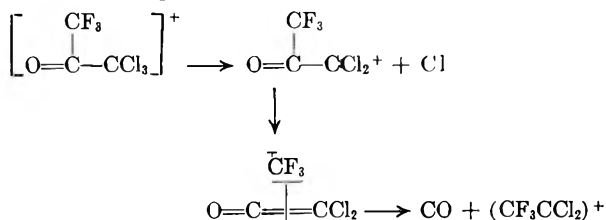
which is sterically favored by the number and arrangement of the atoms in the side-chain. Further loss of neutral CO from this molecule would then follow naturally, and would lead to a fused ring structure



having a protonated double bond.¹² Loss of a further H₂ is also a likely process.

Loss of CO also occurs in aliphatic ketones. A particularly striking case is that of acetyl acetone of molecular weight 100, which gives a prominent peak at mass 72 due to loss of CO (see Fig. 7). A peak at mass 51.8 shows the metastable transition 100⁺ → 72⁺ + 28 to be occurring, *i.e.*, that the fragment is lost in a single fragmentation.

Simple ketones such as acetone lose mass 28 from the parent ion with very low probability. Thus the peak at mass 30 in the acetone spectrum is only 0.2% the intensity of the base peak and is made up of almost equal amounts of (C₂H₆)⁺ and (CH₂O)⁺ ions. A large peak (4%) occurs at mass 29. This consists of (C₂H₅)⁺ and (CHO)⁺ in the ratio 9:11. The two fragments are complementary parts of the molecule. It is often noticeable that highly halogenated compounds undergo rearrangement reactions very similar to those of corresponding hydrocarbons. McLafferty¹³ has detected the analogous rearrangement process to that which leads to (C₂H₅)⁺ from acetone in the spectrum of CF₃.CO.CCl₃ and postulates that this is formed through an intermediate ion having the structure of an olefin coordinated¹⁴ with a cation of formula CF₃⁺. The process is



In other cases, where the structure of the molecule would seem to favor the ejection of CO from

(12) P. N. Rylander and S. Meyerson, *J. Am. Chem. Soc.*, **78**, 5799 (1956).

(13) F. W. McLafferty, *Appl. Spectroscopy*, **11**, 148 (1957).

(14) M. J. S. Dewar, "Electronic Theory of Organic Chemistry," Oxford University Press, New York, N. Y., 1949, p. 212.

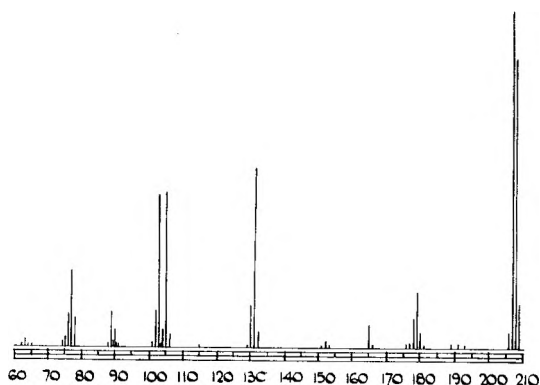


Fig. 6.—Benzalacetophenone.

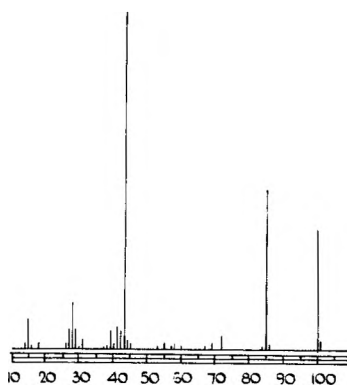
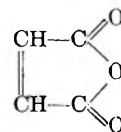


Fig. 7.—Acetylacetone.

the parent ion, the process is not particularly favored, and it is not yet possible to predict from a molecular formula whether or not loss of CO is likely to be a dominant fragmentation process. For example, in cyclopentanone, the major heavy ions in the spectrum are at masses 84, 56 and 55. These are due to the parent ion (22.8%) (p-C₂H₄)⁺ (12.7%) and (p-CO)⁺ (3.4%) and (p-C₂H₅)⁺ (94.4%) and (p-CHO)⁺ (5.6%), respectively. The loss of the isobaric hydrocarbons outweighs the loss of oxygenated fragments. Loss of ethylene is a feature of the fragmentation process in many hydrocarbons.

In the mass spectrum of maleic anhydride



a large peak in the spectrum is due to loss of carbon dioxide. The mass spectrum is shown in Fig. 8. The peak formed by loss of an oxygen atom from the parent ion is only of 1% intensity and that formed by loss of (CO) is only of 0.1% intensity. The parent peak is of height 49%. When doubly-charged ions are examined the peak (p-O)⁺⁺ is largest (7%) (p-CO₂)⁺⁺ is 6.5%, p⁺⁺ only 0.1% and there is no (p-CO)⁺⁺ peak. It seems that fully conjugated systems of double bonds are stable, and can accommodate a positive charge on each keto group without fragmentation.

Reaction intermediates can also be envisaged in the elimination of carbon monoxide from the parent ion of diphenyl ether, and lead to a postulated

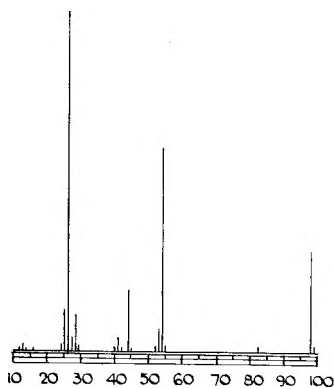


Fig. 8.—Maleic anhydride.

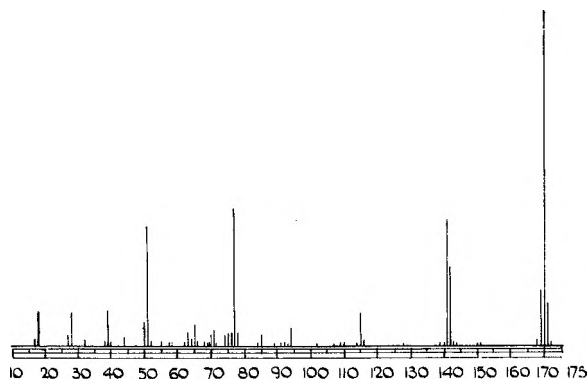
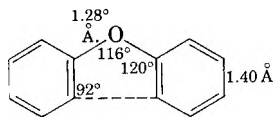


Fig. 9.—Diphenyl ether.

structure for the final ion species formed which may itself be of very high stability. A similar argument can be used to explain the corresponding reaction which takes place in the fragmentation of related compounds such as dinaphthyl ether. The mass spectrum of diphenyl ether is shown in Fig. 9.

In the neutral system of diphenyl ether



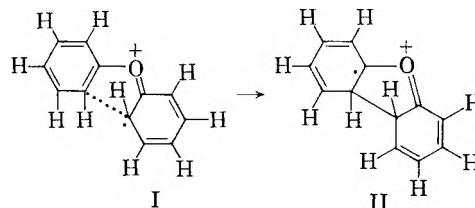
the distance between a pair of carbons in different rings is as much as $2.24 l_{cc}$ if their planes are at right angles but may be reduced to $1.48 l_{cc}$ in the coplanar configuration.

$$2(l_{cc} \sin 58^\circ - l_{cc} \sin 2^\circ) = 1.48 l_{cc}$$

There would seem, therefore, to be reason to suppose that the molecular ion adopts the planar configuration in order to facilitate the formation of a bond as in the case of anthraquinone. By closing up the COC bond angle to 90° it does in fact become possible for this distance to approach the CC bonding distance, although the positive charge on the oxygen atom would be expected to produce the opposite tendency of opening out this angle slightly. Since all these rearrangement processes take place at very low energy they can hardly proceed by any process of complete molecular disintegration followed by regrouping into stable products. They must, therefore, take advantage of any possible intramolecular processes providing a minimum of disturbance of the molecular skeleton. This fact is presumably the reason for the common occurrence

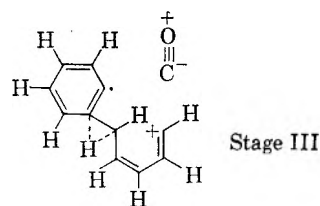
of hydrogen atoms in rearrangement processes since their small size and spherically symmetrical bond orbital enables them to change their allegiance within the molecule with a minimum of disturbance to the electron coupling arrangements.

The first step in the elimination of neutral CO is, therefore, probably

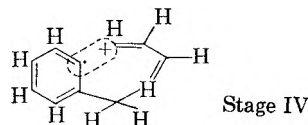


I is a possible resonance form of the molecule ion which has an odd number of electrons and presumably the odd electron will tend to the region of closest-contact where it can take part in some degree of secondary bonding across this region. In stage II an actual bond is shown existing in this region and the odd electron is then transferred to some other part of the system. On account of the inductive effect of the charged oxygen the bonds α to the carbonyl will be somewhat polarized with the negative end closest to the carbonyl group.

The third stage is then



in which a hydrogen atom from the ring transfers to the open chain. Since the first two bonds of the chain are single, rotation around them requires little energy. It is, therefore, easy to see that the chain can rotate successively around these two bonds to give stage IV.

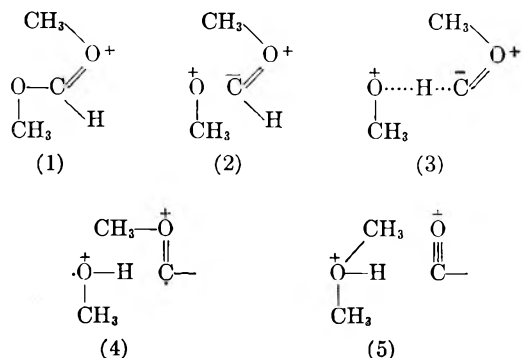


In this structure there appears a 1 electron bond inside the dotted region and various resonance forms with 1 electron bonds can be associated with this to stabilize the benzotropylium ion so formed.

Loss of neutral carbon monoxide can also be used to explain the formation of a peak at mass 47 due to ions of formula $(C_2H_7O)^+$ in the spectrum of dimethyl acetal (see Fig. 10). Empirical rules of breakdown would suggest that a very likely mode of fragmentation would involve loss of the methyl group attached to the $-CH$ carbon atom¹⁵ and it is postulated that the $(C_2H_7O)^+$ ion is, in fact, formed by a secondary breakdown of the $(p-CH_3)^+$ ion.

The sequence of low energy transition steps involved may be envisioned as

(15) J. H. Beynon, *Nature*, **174**, 735 (1954).



The positive oxygen in the initial form 1 induces polarity as shown in 2 and stabilizes this particular resonance structure. In 3 the central hydrogen transfers its allegiance partially to the oxygen atom in hydrogen bonding, and intramolecular rearrangement is achieved by rotation of the carbonyl segment (4 and 5).

Another element which has the capacity of increased valency in its ionized state is nitrogen and many of the fragmentation processes involving nitrogen-containing molecules closely parallel those of oxygenated compounds when one makes the assumption that $>NH$ is equivalent to $>O$. Thus, loss of HCN is a characteristic of many nitrogen containing molecules. For example, aniline loses HCN and should be compared in its behavior to phenol which loses CO. Loss of HCN is in fact, of very wide occurrence. Although we have not yet examined the kinetics of this fragmentation process in detail, the analogy with carbon monoxide would suggest that HNC, which is in tautomeric equilibrium with HCN,¹⁶ is liberated initially. Loss of HCN has been observed in such diverse compounds as dinaphthylamine (20% of base peak), benzotrile (35% of base peak), phthalonitrile (30% of base peak) and α -picoline (50% of base peak).

There is one important difference between nitrogen and oxygen. The nitrogen atom has an odd number of electrons in its outer shell, so that when a neutral molecule containing an odd number of nitrogen atoms is eliminated from a molecular ion (containing an odd electron) the fragment ion formed is in the stable even-electron form. Typical fragments eliminated, for example, from nitro-compounds are the molecules NO (by a rearrangement process) and NO_2 . Interesting examples of elimination of CO, HCN and NO by rearrangement occur in the spectra of the isomeric nitroanilines.

The *o*-isomer can be distinguished from the *m*- and *p*-isomers from the fact that it loses mass 17 rather than mass 16 to give the heaviest fragment ion. This is shown by mass measurement to be due to $(p-OH)^+$ and not $(p-NH_3)^+$. The complete mass spectrum is shown in Fig. 11. The formulas of the main peaks are illustrated in the scheme below. The fact that the peak at mass 80 is formed from that at mass 108 has been deduced by analogy with the breakdowns mentioned above. Masses 92 and 65 can be shown to be associated by the presence of a metastable peak at mass 46.

(16) N. V. Sidgwick, "The Organic Chemistry of Nitrogen," Oxford University Press, New York, N. Y., 1942, p. 320.

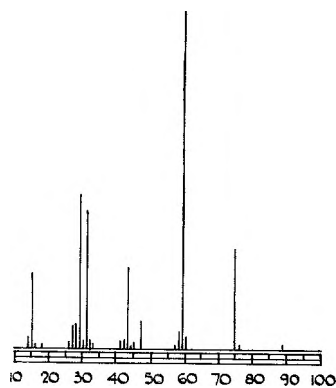


Fig. 10.—D-methyl acetal.

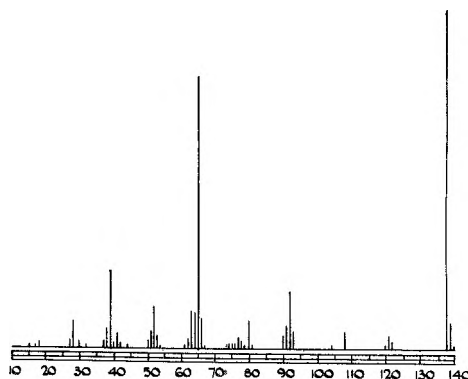
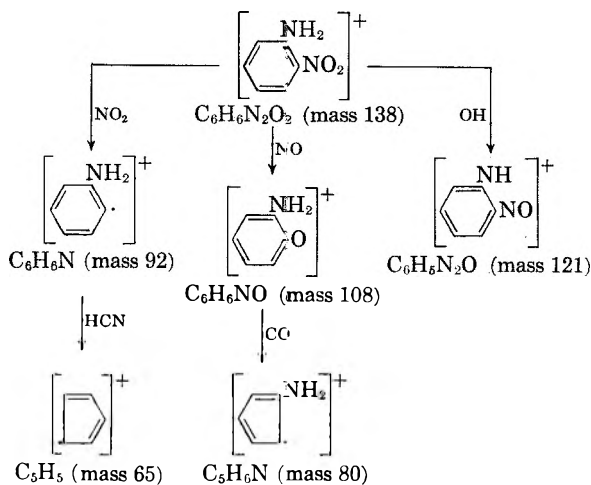


Fig. 11.—*o*-Nitroaniline.



It can be seen that most of the peaks involve rearrangement, but no attempt has been made to write structural formulas, except to indicate ring closure as a likely means of increasing stability. It should be noted that the presence of a single nitrogen atom in a fragment means that the even-electron ions will be of even mass in contrast to the ions containing hydrogen, carbon and oxygen only. Loss of neutral carbon monoxide is shown in the fragmentation of the rearrangement ion of mass 108. Many aromatic nitro-compounds give a similar rearrangement peak more suggestive of a nitrite than a nitro-structure. Loss of neutral HCN from $(p-NO_2)^+$ and of NO from the parent ion are examples of the loss of stable nitrogen-containing molecules analogous to the loss of carbon

monoxide from oxygenated organic compounds. Loss of HCN is particularly common especially from heterocyclic rings.

Theoretical Considerations

It is perhaps of interest to examine some of the implications of specific fragmentation processes of very low energy with regard to existing theories of mass-spectra such as the quasi-equilibrium theory.² Recently, King and Long¹⁷ have applied the theory to some organic esters and have shown that many of the secondary peaks are predicted to have much lower intensities than those observed. A sufficient exposition of the quasi-equilibrium theory for present purposes is given in the paper by King and Long, where the notation is fully explained. The relative yield of the parent is given by

$$f_p = \int_0^\infty e^{-\tau \sum_j k_j(E)} P(E) dE$$

and, with E_m as the maximum vibrational excitation energy

$$f_p = \frac{1}{E_m} \int_0^{E_m} e^{-\tau \sum_j k_j(E)} dE$$

Now a characteristic feature of the fragmentation processes in aromatic systems is the relatively high parent ion intensity which is many times larger than any other peak in the mass-spectrum. In fluorenone, for example, f_p is about 60%. For a specific fragmentation process such as the liberation of carbon monoxide, the activation energy is very small; in fact, it is found that the peak corresponding to mass 152 remains closely visible as the appearance potential of the parent ion is approached. It is also an inherently probable reaction involving the rupture of a carbon-carbon bond according to some scheme such as the one suggested earlier in this paper. It seems reasonable therefore to take the frequency factor as of the order $10^{14} \text{ sec.}^{-1}$ and consequently the exponential factor in the integrand approaches zero for an energy of approximately $2E_0$, where E_0 is the amount by which the appearance potential of the given ion exceeds that of the parent.

Hence

$$f_p \approx \frac{2E_0}{E_m} \text{ or } E_m \approx \frac{2E_0}{f_p}$$

Taking $f_p = 0.6$, it follows that, in fluorenone, $E_m = \frac{10}{3} E_0$ which is almost certainly less than a volt. This seems inconsistent with the fact that ions of activation energy larger than 1 e.v. appear, and agrees with the conclusion of King and Long that the predicted intensities of secondary ions are much too low if plausible values for the frequency

factors and activation energies for the primary fragmentations are used.

It is easy to put an upper limit to the relative yield of a secondary ion, since $1 - e^{-\tau \sum_j k_j(E)} \leq \tau \sum_j k_j(E)$

$$\therefore f_i \leq \frac{\tau}{E_m} \int_{E_0}^{E_m} k_i(E) dE$$

the equality sign being approached in the limit when the parent ion yield is 100%.

Now $k(E) = \nu(1-p)^m$, where $m = 3n - 7$ and $p = E_0/E$.

For many purposes the approximation $1 - p = e^{-p}$ is convenient and does not appear to lead to significant changes in the main conclusions. The number of uncertainties of a more fundamental kind which arise in applications of the quasi-equilibrium theory is usually so large that the convenience of this additional approximation would appear to be justified. It has the advantage that the expression reduces essentially to that familiar in ordinary chemical kinetics, namely $k(E) = \nu e^{-E_0/kT}$ if we define an effective temperature by the relation $E = mkT$. Essentially this assumption was made in a recent discussion of branched-chain paraffins.¹⁸

$$\therefore f_i \leq \frac{\tau \nu}{mp} e^{-mp} \text{ where } p = E_0/E_m$$

It follows that f_i approaches zero very rapidly for any ion with activation energy approaching E_m since e^{-m} (with m as large as 25 as in the case of fluorenone) is very small indeed. Thus, if our conclusion regarding the order of magnitude of E_m is correct, the quasi-equilibrium theory would predict negligible yields of all ions requiring more than about 1 e.v. activation energy.

The general appearance of these mass spectra, in which several peaks occur (including those for doubly charged ions) which disappear at lower energies, seems inconsistent with the low upper limit for such ions according to the quasi-equilibrium theory. In fact even the release of acetylene leads to an ion of just measurable intensity. In fluorenone its intensity is certainly very low, estimated at 0.06%, but for a high energy process this is much too large for agreement with theory. In anthracene, a molecule of similar size and shape, this release of acetylene occurs to about 4% and the activation energy from appearance potential measurements is 6 e.v. Since $E_m = (2/f_p)E_0$ a maximum energy of at least 12 volts is implied. It is difficult to see how a meaningful interpretation can be attributed to such large differences between the energies of similar molecules bombarded by electrons of the same energy.

(18) G. R. Lester, "Advances in Mass Spectrometry," Pergamon Press, New York, N. Y., 1959.

(17) A. B. King and F. A. Long, *J. Chem. Phys.*, **29**, 374 (1958).

POTENTIAL AROUND A CHARGED COLLOIDAL SPHERE

BY THOMAS J. DOUGHERTY AND IRVIN M. KRIEGER

*Department of Chemistry and Chemical Engineering, Case Institute of Technology, Cleveland, Ohio**Received April 17, 1959*

An approximation to the solution of the Poisson-Boltzmann equation in spherical symmetry was obtained by integrating a closely-related differential equation. The solution obtained reduces under proper limiting conditions to the familiar Debye-Hückel and flat plate approximations. The calculated potentials and surface charge densities compare favorably with those obtained by Hoskin by numerical integration of the Poisson-Boltzmann equation.

Introduction

Most lyophobic colloids are stabilized by the electrical repulsion between particles resulting from the surface charge on the particles. Since electrical forces determine the stability of the colloidal systems, it follows, *a fortiori*, that they play a dominant role in determining the thermodynamic and kinetic properties of the system. The exact calculation of these potentials presents a very difficult problem in statistical mechanics, but frequently the potentials can be calculated, to a satisfactory approximation, from the Poisson-Boltzmann equation. The derivation of this equation and discussions of the approximations involved in the derivation are available in several places^{1,2} so these subjects will not be considered here. Even with this approximation the problem remains formidable, since the Poisson-Boltzmann equation is a non-linear second-order partial differential equation.

Our treatment will be restricted to the case of spherical symmetry, in which case the problem is one-dimensional and we need deal only with an ordinary differential equation. Two well-known approximate solutions of this problem are the Debye-Hückel solution³ for "small potentials" and the flat plate approximation for very large spheres.⁴ In this paper we will develop a method for obtaining an approximate solution to the Poisson-Boltzmann equation which contains both the Debye-Hückel and the flat plate solutions as special cases.

Approximate Solution of the Poisson-Boltzmann Equation

The Poisson-Boltzmann equation can be written in the form

$$\nabla^2\psi(\bar{r}) = -\frac{4\pi}{D\bar{V}} \sum_i N_i z_i \epsilon \exp(-z_i \epsilon \psi/kT) \quad (1)$$

where ψ is the potential, D the dielectric constant of the solvent, \bar{V} the volume of solvent, ϵ the absolute magnitude of the electronic charge, N_i the number of ions of valence z_i , and other symbols have their usual meaning. In the case of spherical symmetry, equation 1 becomes

$$\frac{1}{\bar{r}} \frac{d^2 \bar{r}\psi}{d\bar{r}^2} = -\frac{4\pi}{D\bar{V}} \sum_i N_i z_i \epsilon \exp(-z_i \epsilon \psi/kT) \quad (2)$$

Introducing the quantities

(1) R. H. Fowler and E. A. Guggenheim, "Statistical Thermodynamics," The Macmillan Co., New York, N. Y., 1939, pp. 385-391.

(2) A. Münster, "Statistische Thermodynamik," Springer Verlag, Berlin, 1956, pp. 764-790.

(3) P. Debye and E. Hückel, *Physik. Z.*, **24**, 185 (1923); **25**, 97 (1924).

(4) E. J. W. Verwey and J. Th. G. Overbeek, "Theory of the Stability of Lyophobic Colloids," Elsevier Publishing Co., Inc., New York, N. Y., 1948, p. 25.

$$\phi = \epsilon\psi/kT, \kappa^2 = \frac{4\pi\epsilon^2}{D\bar{V}kT} \sum_i N_i z_i^2, \rho = \kappa r \quad (3)$$

we can write equation 2 in terms of dimensionless variables.

$$\frac{1}{\rho} \frac{d^2 \rho \phi}{d\rho^2} = - \sum_i N_i z_i e^{-z_i \phi} / \sum_i N_i z_i^2 \quad (4)$$

Letting $N = \sum_i N_i$, $x_i = N_i/N$, and $\langle z^2 \rangle = \sum_i x_i z_i^2$, equation 4 becomes

$$\frac{1}{\rho} \frac{d^2 \rho \phi}{d\rho^2} = - \frac{1}{\langle z^2 \rangle} \sum_i x_i z_i e^{-z_i \phi} \quad (5)$$

If a is the radius of the colloid particle and we let $\tau = \kappa a$ be the value of ρ at the surface of the particle, then the condition for the validity of the flat plate approximation is $a \gg 1/\kappa$ or $\tau \gg 1$, since $1/\kappa$ is essentially the distance from the particle surface beyond which the potential becomes small.

We make now the change of variable

$$y = \rho/(\tau + \alpha) \quad (6)$$

where α is a constant to be specified later. With this transformation, equation 5 becomes

$$\frac{d^2 y \phi}{dy^2} = - \frac{(\tau + \alpha)^2}{\langle z^2 \rangle} \sum_i x_i z_i y e^{-z_i \phi} \quad (7)$$

We now observe that if the variable y multiplying the exponential term in equation 7 could be shifted into the exponent to multiply ϕ , then we would obtain a new equation which would have the same form as the Poisson-Boltzmann equation for the flat plate problem, and hence solutions could be obtained by elementary means. Therefore we investigate next the possibility of commuting the two operations on ϕ in the product $y \exp(-z_i \phi)$ which appears in equation 7 to obtain the new equation

$$\frac{d^2 y \phi}{dy^2} = - \frac{(\tau + \alpha)^2}{\langle z^2 \rangle} \sum_i x_i z_i e^{-z_i y \phi} \quad (8)$$

Because of the boundary conditions on the potential, ϕ , $y\phi$ and $d(y\phi)/dy$ must all approach zero as y approaches infinity. Thus the boundary conditions force the solutions of equations 7 and 8 to agree at large y . In addition, they must agree for small ϕ , as can be shown by expanding the exponentials in both equations and retaining only the first power of ϕ . (We recall that electroneutrality requires that $\sum_i x_i z_i = 0$). Finally, the commutation is valid at the point $y = 1$; by suitable choice of α we may make this occur at any desired distance from the particle surface. An appropriate choice is $\alpha = 1/2$, which is in the region where the potential gradient is large. A first integral of equation 8 is

readily obtained. Multiplying both sides of equation 8 by $2 d(y\phi)/dy$ we obtain

$$\frac{d}{dy} \left[\frac{dy\phi}{dy} \right]^2 = -2 \frac{(\tau + \alpha)^2}{\langle z^2 \rangle} \sum_i x_i z_i e^{-z_i y \phi} \frac{dy\phi}{dy} \quad (9)$$

which integrates to

$$\left[\frac{dy\phi}{dy} \right]^2 = 2 \frac{(\tau + \alpha)^2}{\langle z^2 \rangle} \left[\sum_i x_i e^{-z_i y \phi} + C \right] \quad (10)$$

In the limit $y \rightarrow \infty$, ϕ approaches zero exponentially, so that ϕ , $y\phi$ and $dy\phi/dy$ all approach zero. These conditions determine C .

$$C = - \sum_i x_i = -1 \quad (11)$$

With this value for C , equation 10 becomes

$$\left[\frac{dy\phi}{dy} \right]^2 = 2 \frac{(\tau + \alpha)^2}{\langle z^2 \rangle} \left[\sum_i x_i e^{-z_i y \phi} - 1 \right] \quad (12)$$

On taking the square root of both sides of equation 12, we are faced with an ambiguity in sign. The sign is chosen which leads to a finite (actually zero) potential at infinity. Taking the square root and integrating from the surface out to an arbitrary point, we obtain

$$\int_{y_0\phi_0}^{y\phi} \frac{dy\phi}{\left(\sum_i x_i e^{-z_i y \phi} - 1 \right)^{1/2}} = - \left(\frac{2}{\langle z^2 \rangle} \right)^{1/2} (\tau + \alpha)(y - y_0) = - \left(\frac{2}{\langle z^2 \rangle} \right)^{1/2} (\rho - \tau) \quad (13)$$

Thus the problem has been reduced to quadratures; that is, to evaluating integrals of the form

$$I(\lambda) = \int_{\lambda_0}^{\lambda} \left(\sum_i x_i e^{-z_i \lambda} - 1 \right)^{-1/2} d\lambda \quad (14)$$

where $\lambda = y\phi$, $\lambda_0 = y_0\phi_0$. These integrals can be evaluated either graphically or numerically by standard methods. We will now examine some special cases for which solutions can be obtained in closed form.

Case 1: Symmetrical electrolyte (valencies of all ions having same absolute magnitude).—For this case, $z_1 = -z_2 = z$, $x_1 = x_2 = 1/2$, and $\langle z^2 \rangle = z^2$, so that

$$I(\lambda) = \sqrt{2} \int_{\lambda_0}^{\lambda} (e^{z\lambda} + e^{-z\lambda} - 2)^{-1/2} d\lambda = \frac{\sqrt{2}}{z} \ln \frac{\tanh(z\lambda/4)}{\tanh(z\lambda_0/4)} \quad (15)$$

In terms of our original dimensionless variables the result is

$$\tanh \left[\frac{z\rho\phi}{4(\tau + \alpha)} \right] = \tanh \left[\frac{z\tau\phi_0}{4(\tau + \alpha)} \right] e^{-(\rho - \tau)} \quad (16)$$

A form more convenient for computational purposes is

$$\phi = \frac{2(\tau + \alpha)}{z\rho} \ln \frac{1 + A_1 e^{-(\rho - \tau)}}{1 - A_1 e^{-(\rho - \tau)}} \quad (17)$$

where $A_1 = \tanh [\tau z \phi_0 / 4(\tau + \alpha)]$.

Case 2: Two to one electrolyte (valencies of ions of greater charge is numerically twice the valence of ions of opposite charge).—Here $z_1 = -2z_2 = -2z$, $2x_1 = x_2 = 2/3$, and $\langle z^2 \rangle = 2z^2$, and therefore equation 14 takes the form

$$I(\lambda) = \sqrt{3} \int_{\lambda_0}^{\lambda} (e^{2z\lambda} + 2e^{-z\lambda} - 3)^{-1/2} d\lambda = \frac{1}{z} \ln \frac{(1 - [3e^{z\lambda_0}/(e^{z\lambda_0} + 2)]^{1/2})(1 + [3e^{z\lambda_0}/(e^{z\lambda_0} + 2)]^{1/2})}{(1 - [3e^{z\lambda}/(e^{z\lambda} + 2)]^{1/2})(1 + [3e^{z\lambda}/(e^{z\lambda} + 2)]^{1/2})} \quad (18)$$

Returning to our original dimensionless variables and rearranging, we obtain for the final result

$$\phi = \frac{\tau + \alpha}{z\rho} \ln \frac{[1 + A_2 e^{-(\rho - \tau)}]^2}{[1 - A_2 e^{-(\rho - \tau)}]^2 - 2A_2 e^{-(\rho - \tau)}} \quad (19)$$

where

$$A_2 = \left\{ 1 - \left[\frac{1}{3} + \frac{2}{3} \exp \left(- \frac{z\tau\phi_0}{\tau + \alpha} \right) \right]^{1/2} \right\} / \left\{ 1 + \left[\frac{1}{3} + \frac{2}{3} \exp \left(- \frac{z\tau\phi_0}{\tau + \alpha} \right) \right]^{1/2} \right\}$$

Case 3.—A third case of considerable interest is the n to one electrolyte where $n \gg 1$. Physically this corresponds to the situation where the ions of valence z are the counterions and the ions of valence $-nz$ are the colloid particles themselves. Here $z_1 = -nz_2$, $nx_1 = x_2 = n/(n + 1)$ and $\langle z^2 \rangle = nz^2$, giving

$$I(\lambda) = \frac{1}{\sqrt{n + 1}} \int_{\lambda_0}^{\lambda} [ne^{z\lambda} + e^{-nz\lambda} - (n + 1)]^{-1/2} d\lambda \quad (20)$$

This integral cannot be evaluated exactly in closed form, but as long as $z\lambda \gg 1/n$ we can disregard the term $e^{-nz\lambda}$ in the integrand. With this approximation and neglecting one in comparison to n equation 20 becomes

$$I(\lambda) \simeq \int_{\lambda_0}^{\lambda} (e^{z\lambda} - 1)^{-1/2} d\lambda = \frac{2}{z} [\tan^{-1} (e^{-z\lambda} - 1)^{1/2} - \tan^{-1} (e^{-z\lambda_0} - 1)^{1/2}] \quad (21)$$

This result can also be expressed in the form

$$\phi = \frac{\tau + \alpha}{z\rho} \ln \left[1 + \left(\frac{A_n - \tan [(\rho - \tau) / \sqrt{2n}]}{1 + A_n \tan [(\rho - \tau) / \sqrt{2n}]} \right)^2 \right] \quad (22)$$

where

$$A_n = \left[\exp \left(\frac{\tau z \phi_0}{\tau + \alpha} \right) - 1 \right]^{1/2}$$

This approximation fails at large distances where the potential becomes very small. If this restriction were ignored then equation 22 would lead us to believe that the potential changes sign periodically as ρ increases, giving a rather peculiar damped oscillatory behavior. It is interesting to prove that the exact solutions of our approximate form of the Poisson-Boltzmann equation can never oscillate. To prove this we first note that from equation 12 it can be shown that the slope of the potential *versus* ρ curve can be zero only when the potential is zero. Now if we can show that the potential is zero only at $\rho = \infty$ the proof will be complete. To prove this we need only prove that

$$\lim_{\lambda \rightarrow 0} \int_{\lambda_0}^{\lambda} \left(\sum_i x_i e^{-z_i \lambda} - 1 \right)^{-1/2} d\lambda = -\infty \quad (23)$$

We divide the integral into two parts

$$\int_{\lambda_0}^{\lambda} = \int_{\lambda_0}^{\lambda^*} + \int_{\lambda^*}^{\lambda} \quad (24)$$

where λ^* is sufficiently small to allow us to neglect all powers of λ higher than the second in the expansion

sion of the exponentials in the second part of the integral. Recalling that $\sum_i x_i = 1$ and $\sum_i x_i z_i = 0$ (electroneutrality) and making the suggested expansion we obtain

$$\int_{\lambda^*}^{\lambda} \left(\sum_i x_i e^{-z_i \lambda} - 1 \right)^{-1/2} d\lambda = \left(2 / \sum_i x_i z_i^2 \right)^{1/2} \ln (\lambda / \lambda^*) \quad (25)$$

and thus

$$\lim_{\lambda \rightarrow 0} \int_{\lambda^*}^{\lambda} \left(\sum_i x_i e^{-z_i \lambda} - 1 \right)^{-1/2} d\lambda = -\infty \quad (26)$$

which is equivalent to equation 23; this completes the proof.

Properties of the Solution

We will now study some of the properties of our approximate solutions. We consider in particular the result for a symmetrical electrolyte which can be compared to the exact calculations of Hoskin⁵ who integrated the Poisson-Boltzmann equation numerically for this case. First we note that in the limits $\phi_0 \rightarrow 0$ and $\tau \rightarrow \infty$ we obtain the Debye-Hückel and the flat plate solutions, respectively, as we would expect. There is, however, an important difference between our solution for very large τ and the flat plate approximation. The flat plate solution predicts that the potential approaches zero as $e^{-\rho}$ whereas our solution predicts a Debye-Hückel form for the potential for large ρ . An interesting and somewhat unexpected result is that our solution predicts that the Debye-Hückel solution is correct in the limit $\tau \rightarrow 0$ even if ϕ_0 is large. (In fact, our result reduces to the Debye-Hückel result when $\tau\phi_0$ is small.) This result has been observed by Müller⁶ on the basis of more exact calculations than those presented here. It should be noted that it is the presence of the quantity α which enables us to obtain this result. This shows that the inclusion of this quantity improves the approximation at small values of τ .

To facilitate comparison with Hoskin's results, we define, following Hoskin, the function $C^*(\rho; \tau, \phi_0) = \phi / \phi_{DH}$ where ϕ_{DH} is the value of the potential calculated from the Debye-Hückel formula and ϕ is the value of the potential calculated from our solution. The function $C(\rho; \tau, \phi_0) = \phi_H / \phi_{DH}$ is defined similarly where ϕ_H is the value of the potential calculated by Hoskin. Figures 1 and 2 show comparisons of these two functions for the case of a symmetrical electrolyte (the only case treated by Hoskin) where we have taken $\alpha = 1/2$ in equation 17. Table I shows a comparison of the limiting values of these functions as $\rho \rightarrow \infty$. Values of $C^*(\infty; \tau, \phi_0)$ for $\alpha = 0, 1/2$ and 1 are presented to show the effect of the parameter α . The choice $\alpha = 1/2$ gives generally satisfactory agreement. Values of $C^*(\infty; \tau, \phi_0)$ for the two to one electrolyte with $\alpha = 1/2$ are also included in Table I to show the effect of valence type. These limiting values for C^* have been calculated from the relatively simple formulas $C^*(\infty; \tau, \phi_0) = [4(\tau + \alpha) - (\tau z \phi_0)] \tanh[\tau z \phi_0 / 4(\tau + \alpha)]$ for the symmetrical

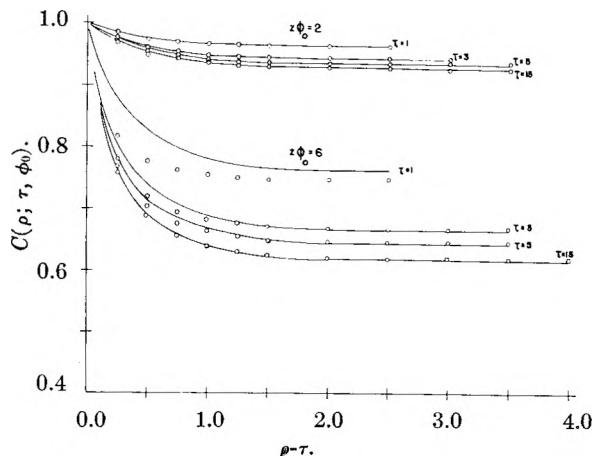


Fig. 1.—Comparison of the potentials calculated from equation 17 (solid lines) with those calculated by Hoskin (open circles). Continued in Fig. 2.

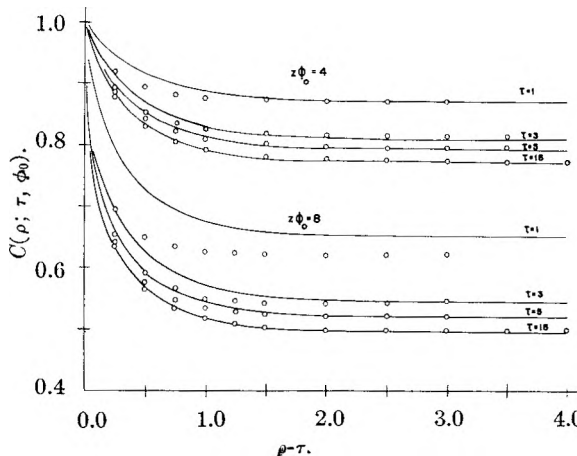


Fig. 2.—Continuation of Fig. 1. The data were plotted on two graphs to avoid confusion.

electrolyte and $C^*(\infty; \tau, \phi_0) = 6(\tau + \alpha)A_2 / \tau z \phi_0$ for the two to one electrolyte where A_2 is defined as in equation 19.

The approximation we have made introduces an error in the curvature of the potential versus ρ curve. The choice $\alpha = 1/2$ is made so that this error will be approximately as often negative as positive and, therefore, at large distances the error will be averaged out to some extent. However, if we were interested only in the region immediately adjacent to the surface of the particle, then we would want the error in the curvature to be small in this region. In this case, we would choose $\alpha = 0$. In the next section we will calculate the surface potential from the surface charge density. This calculation requires accurate values for the potential gradient at the particle surface, and so for this calculation we will choose $\alpha = 0$.

Evaluation of the Surface Potential

From equation 12 we obtain

$$\frac{dy\phi}{dy} = - \left(\frac{2}{\langle z^2 \rangle} \right)^{1/2} (\tau + \alpha) \left(\sum_i x_i e^{-z_i y \phi} - 1 \right)^{1/2} \quad (27)$$

which can be written in the form

(5) N. E. Hoskin, *Trans. Faraday Soc.*, **49**, 1471 (1953).

(6) H. Müller, *Kolloidchem. Beihfte*, **26**, 257 (1928).

TABLE I

COMPARISON OF VALUES OF $C^*(\infty; \tau, \phi_0)$ AND $C(\infty; \tau, \phi_0)$ FOR VARIOUS VALUES OF THE PARAMETERS τ AND $z\phi_0$

τ	$\alpha = 0$	Symmetrical electrolyte		$C(\infty; \tau, \phi_0)$	Two to one electrolyte $C^*(\infty; \tau, \phi_0)$ $\alpha = 1/2$
		$C^*(\infty; \tau, \phi_0)$ $\alpha = 1/2$	$\alpha = 1$		
$z\phi_0 = 1$					
1	0.9797	0.9908	0.9962	0.9915	0.8795
3	.9797	.9850	.9884	.9861	.8431
5	.9797	.9831	.9858	.9841	.8331
15	.9797	.9809	.9821	.9814	.8219
∞	.9797	.9757	.97578157
$z\phi_0 = 2$					
1	0.9242	0.9645	0.9797	0.9664	0.7524
3	.9242	.9430	.9555	.9466	.6833
5	.9242	.9364	.9458	.9395	.6652
15	.9242	.9286	.9327	.9299	.6453
∞	.9242	.9242	.92426346
$z\phi_0 = 4$					
1	0.7616	0.8742	0.9242	0.8734	0.5343
3	.7616	.8106	.8469	.8160	.4433
5	.7616	.7928	.8187	.7980	.4224
15	.7616	.7726	.7830	.7752	.4006
∞	.7616	.7616	.76163894
$z\phi_0 = 6$					
1	0.6034	0.7616	0.8460	0.7489	0.3894
3	.6034	.6673	.7477	.6695	.3095
5	.6034	.6433	.6786	.6470	.2926
15	.6034	.6173	.6305	.6202	.2754
∞	.6034	.6034	.60342668
$z\phi_0 = 8$					
1	0.4820	0.6526	0.7616	0.6220	0.2989
3	.4820	.5467	.6034	.5435	.2340
5	.4820	.5218	.5586	.5218	.2208
15	.4820	.4956	.5088	.5001	.2075
∞	.4820	.4820	.48202009

$$\frac{d\phi}{d\rho} = -\phi/\rho - \left(\frac{2}{\langle z^2 \rangle}\right)^{1/2} (\tau/\rho) \left(\sum_i x_i e^{-z_i \phi/\tau} - 1\right)^{1/2} \quad (28)$$

where we have set $\alpha = 0$ for the reasons mentioned at the end of the previous section. Setting $\rho = \tau$ in equation 28 we obtain for the potential gradient at the surface

$$\frac{d\phi}{d\rho}|_{\rho=\tau} = -\phi_0/\tau - \left(\frac{2}{\langle z^2 \rangle}\right)^{1/2} \left(\sum_i x_i e^{-z_i \phi_0} - 1\right)^{1/2} \quad (29)$$

The requirement that the normal component of the electric induction be continuous at the surface yields

$$\frac{d\phi}{d\rho}|_{\rho=\tau} = -\frac{4\pi\sigma\epsilon}{D\kappa kT} \quad (30)$$

where σ is the surface charge density. The corresponding expressions for the Debye-Hückel approximation are

$$\frac{d\phi}{d\rho}|_{\rho=\tau} = -\phi_0(1 + \tau)/\tau \quad (31)$$

$$= -\frac{4\pi\sigma_{DH}\epsilon}{D\kappa kT} \quad (32)$$

Equations 29 and 30 can be used to calculate the surface potential if the surface charge density is known. This calculation can be performed either graphically or by some appropriate numerical technique. From equations 29, 30, 31 and 32 we can calculate the ratio of the surface charge density calculated from our approximation to that calculated from the Debye-Hückel approximation for the same surface potential.

$$\frac{\sigma}{\sigma_{DH}} = -\frac{\tau}{(1 + \tau)\phi_0} \times \frac{d\phi}{d\rho}|_{\rho=\tau} = \frac{1}{1 + \tau} \left[1 + \left(\frac{2}{\langle z^2 \rangle}\right)^{1/2} \left(\frac{\tau}{\phi_0}\right) \left(\sum_i x_i e^{-z_i \phi_0} - 1\right)^{1/2} \right] \quad (33)$$

For the case of a symmetrical electrolyte, equation 33 becomes

$$\frac{\sigma}{\sigma_{DH}} = \frac{1}{1 + \tau} \left[1 + \frac{\sinh(z\phi_0/2)}{(z\phi_0/2)} \right] \quad (34)$$

Table II shows a comparison of the values of this ratio computed from equation 34 to those obtained by Hoskin. The maximum error, which occurs when $z\phi_0 = 6$ and $\tau = 1$, is less than 8%. Hoskin's value for $z\phi_0 = 8$ and $\tau = 15$ (marked with a question mark) we believe to be too large since our solution should become exact when τ becomes very large and Hoskin's value does correspond to our result for $\tau = \infty$. With this point excluded, we see that our approximation always gives higher values for the surface charge density, (the difference in the two values for $z\phi_0 = 6$ and $\tau = 15$ is probably meaningless) and thus we have an upper limit for this quantity.

TABLE II

COMPARISON OF THE VALUES OF σ/σ_{DH} CALCULATED FROM EQUATION 34 TO THOSE CALCULATED BY HOSKIN

τ		$z\phi_0 = 1$	$z\phi_0 = 2$	$z\phi_0 = 4$	$z\phi_0 = 6$	$z\phi_0 = 8$
		$\tau = 1$	Hoskin	1.015	1.063	1.317
	Eq. 33	1.021	1.088	1.407	2.170	3.911
$\tau = 3$	Hoskin	1.027	1.116	1.557	2.686	5.311
	Eq. 33	1.032	1.131	1.610	2.754	5.367
$\tau = 5$	Hoskin	1.032	1.135	1.641	2.914	5.843
	Eq. 33	1.035	1.146	1.678	2.949	5.852
$\tau = 15$	Hoskin	1.039	1.160	1.751	3.202	6.823 (?)
	Eq. 33	1.039	1.164	1.763	3.193	6.459
$\tau = \infty$	Hoskin
	Eq. 33	1.042	1.175	1.813	3.339	6.822

TRACER DIFFUSION OF SODIUM AND RUBIDIUM IONS IN AQUEOUS ALKALI CHLORIDE SOLUTIONS AT 25°

BY REGINALD MILLS

Contribution from the Department of Radiochemistry, Research School of Physical Sciences, Australian National University, Canberra, A.C.T., Australia

Received April 27, 1959

Diffusion coefficients for two cations, Na^+ and Rb^+ , have been measured over the concentration range 0.1–4 *M* in KCl, NaCl and LiCl solutions. The diffusion pattern in concentrated solutions shows similar viscosity relationships to those obtained with anions. At low concentrations, however, the separation between cation coefficients is much more marked, and this difference may be reconciled with the anion case by reference to the Onsager limiting law with an extension for ion size.

Introduction

Diaphragm-cell measurements of trace-ion diffusion coefficients can now be regarded as sufficiently accurate and precise to justify accumulation of data for various ions. The best evidence for this reliability is the agreement between two groups of workers¹ for the tracer diffusion of I^- ion in the three supporting electrolytes KCl, NaCl and LiCl. These studies were carried out in separate laboratories and with distinctly different analytical techniques, yet agreement to within an average precision of 0.4% was obtained for all measurements. Data from this study and a parallel one,² have allowed comparisons to be made between the trace-diffusion of the two anions, I^- and Cl^- in the above three supporting electrolytes. No comparable data exist for cation diffusion in these media beyond those for Na^+ in KCl³ and Na^+ in NaCl⁴ solutions. Since cations might be expected to exhibit wider divergencies than anions in diffusional behavior, because of their stronger degrees of hydration, such a comparison seems warranted. In this study, Na^+ ion diffusion in LiCl has been measured to complete the series for a hydrated ion and Rb^+ ion diffusion in the three electrolytes, KCl, NaCl and LiCl, to afford comparison with an unhydrated species.

Experimental

Diffusion Technique.—All diffusion measurements were made with magnetically-stirred diaphragm cells of the general pattern prescribed by Stokes.⁵ The cells were calibrated at regular intervals by diffusing 0.5 *M* KCl into water and analyzing the compartment solutions by conductance measurements with a Leeds and Northrup Jones bridge. All diffusion measurements were made in water thermostats maintained at $25 \pm 0.01^\circ$.

Sodium and potassium chloride solutions were made by accurately weighing the dried A.R. grade salts and diluting to volume. Lithium chloride solutions were made by a method described by Stokes and Stokes⁶ and their concentrations determined by conductance measurements with the Jones bridge using the data of Shedlovsky.⁷

Radioactive Analyses.—The radiotracers Na^{22} and Rb^{86} were obtained as their aqueous chlorides from the Radiochemical Centre, Amersham, England. One sample of Rb^{86} tracer as RbCl in HCl solution was obtained from the Isotopes Division, Oak Ridge National Laboratories, Oak Ridge,

Tennessee, U.S.A. The radioactive solutions were counted in the liquid phase in a well-type scintillation counter using a sodium iodide crystal as detector. Integral bias curves were obtained for each isotope to select suitable voltage and bias settings for good counting stability.

No trouble was experienced using the Na^{22} tracer but anomalous results were obtained using Rb^{86} tracer from both sources. These anomalies varied from batch to batch of tracer but had the common feature that low coefficients were obtained after several half-lives of the tracer had elapsed. Rb^{86} has a half-life of 19 days and it was suspected that there was a radioactive impurity with a much longer half-life present in the tracer solutions. Tracer solutions from each of the above sources of supply, were therefore examined with a scintillation spectrometer which was coupled to a multi-channel analyzer. In well-decayed specimens, the γ spectrum of 2.3 year Cs^{134} was plainly exhibited with energy peaks at 0.605, 0.80 and 1.37 Mev. The probable presence of cesium impurity in rubidium salts plus the comparatively high slow neutron capture cross-section of Cs^{133} reinforce these conclusions. Further, the anomalous diffusion coefficients were ca. 1% lower than the measurements made with fresh tracer and this is consistent with recent data obtained by Mills and Woolf⁸ which shows that the Cs^+ diffusion rate is on the average 1% lower than Rb^+ values in the same system.

Provided measurements were made before the elapse of three to four half-lives of the tracer, however, reproducibility to within 0.3% could be obtained with all tracer solutions and only data recorded in this period has been given. It is recommended that future diffusion measurements with Rb^{86} be made within this period or alternatively, spectroscopically pure rubidium salts be sent for neutron irradiation.

Results

The diffusion coefficients for Na^+ in LiCl and for Rb^+ in KCl, NaCl and LiCl are reported in Tables I and II. Values of $\mathcal{D}/\mathcal{D}^0$ are also given since this ratio allows direct comparison of the diffusional behavior of the two ions. The limiting diffusion coefficients \mathcal{D}^0 have been calculated by the Nernst equation using $\lambda^0 \text{Na}^+ = 50.10$ and $\lambda^0 \text{Rb}^+ = 77.81$ from Robinson and Stokes.⁹ The root-mean-square error in the Na^+ measurements averages 0.3% but because of the factors outlined in the experimental section, the error for the Rb^+ measurements has been arbitrarily doubled to 0.6%.

Discussion

The results are plotted in Fig. 1, together with data for Na^+ in KCl and NaCl which have been reported in previous papers in this series.^{3,4}

Comparison with the anion diffusion curves² shows no real divergencies in moderate to high concentrations, in that viscosity-related effects again appear to have the predominant influence and the

(8) R. Mills and L. A. Woolf, *THIS JOURNAL*, **63**, in press (1959).

(9) R. A. Robinson and R. H. Stokes, "Electrolyte Solutions," Butterworth Scientific Publications, London, England, 1955, p. 452.

(1) R. H. Stokes, L. A. Woolf and R. Mills, *THIS JOURNAL*, **61**, 1634 (1957).

(2) R. Mills, *ibid.*, **61**, 1631 (1957).

(3) R. Mills, *ibid.*, **61**, 1258 (1957).

(4) R. Mills, *J. Am. Chem. Soc.*, **77**, 6116 (1955).

(5) R. H. Stokes, *ibid.*, **72**, 763 (1950).

(6) J. M. Stokes and R. H. Stokes, *THIS JOURNAL*, **60**, 217 (1956).

(7) D. A. MacInnes, "The Principles of Electrochemistry," Reinhold Publ. Corp., New York, N. Y., 1939, p. 339.

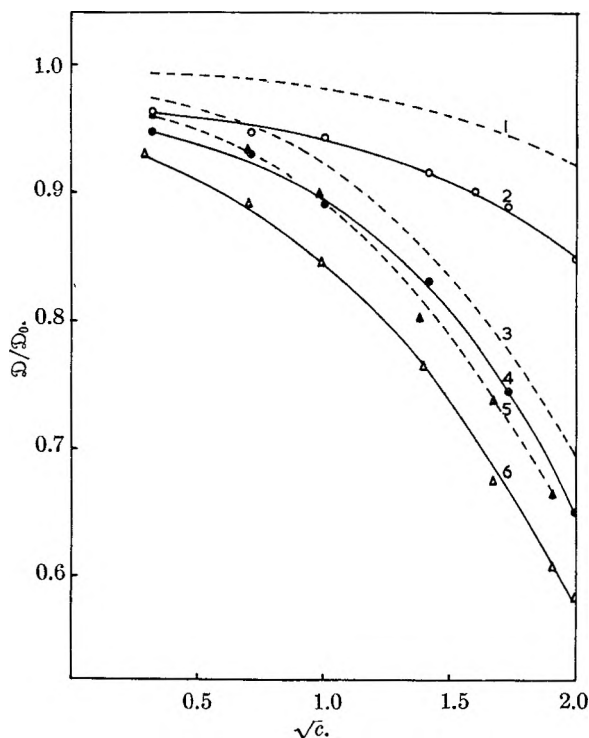


Fig. 1.—Cation diffusion curves in KCl, NaCl and LiCl: (1) Na⁺ in KCl³; (2) Rb⁺ in KCl; (3) Na⁺ in NaCl⁴; (4) Rb⁺ in NaCl; (5) Na⁺ in LiCl; (6) Rb⁺ in LiCl.

TABLE I
TRACER-DIFFUSION COEFFICIENTS OF Na⁺ IN LiCl (Aq.) AT 25°

<i>c</i> , moles/l.	<i>D</i> , cm. ² /sec. (±0.3%)	<i>D</i> / <i>D</i> ⁰ , (<i>D</i> ⁰ = 1.334)
0.1023	1.280	0.960
.4817	1.244	.933
.9621	1.186	.889
1.902	1.070	.802
2.813	0.983	.737
3.648	0.886	.664

simplest viscosity correction in which (*D*/*D*⁰) (*η*/*η*⁰) is plotted against \sqrt{c} , exhibits the over-correction effect previously observed. The cation curves are roughly parallel along their entire length and do not progressively converge in going from KCl, through NaCl to LiCl. This is in part, due to the rather large differences in the values of the coefficients for the two ions in each electrolyte at *ca.* 0.1 *M* concentrations. This separation between coefficients for the various ions in the same electrolyte can be examined by dilute solution theory which is sometimes applicable to concentrations of this order.

The two important equations, formulated for tracer of self-diffusion at very low concentrations, are the Onsager limiting law¹⁰ and the Nernst expression.¹¹ The Onsager law based on the relaxation effect as derived from interionic attraction theory takes the form for aqueous 1:1 electrolytes at 25°

$$D_i = D_i^0 [1 - 0.7816 (1 - \sqrt{d(u_i)})\sqrt{c}] \quad (1)$$

(10) L. Onsager, *Ann. N. Y. Acad. Sci.*, **46**, 209 (1945).

(11) W. Nernst, *Z. physik. Chem.*, **2**, 613 (1888).

TABLE II
TRACER-DIFFUSION COEFFICIENTS OF Rb⁺ IN AQUEOUS ALKALI CHLORIDE SOLUTIONS AT 25°

<i>c</i> , moles/l.	<i>D</i> , cm. ² /sec.	<i>D</i> / <i>D</i> ⁰ (<i>D</i> ⁰ = 2.071)
KCl		
0.1	1.994	0.963
0.5	1.961	.947
1.0	1.952	.943
2.0	1.897	.916
2.56	1.865	.901
3.0	1.842	.889
4.0	1.759	.849
NaCl		
0.1	1.961	0.947
0.5	1.927	.930
1.0	1.845	.891
2.0	1.721	.831
3.0	1.543	.745
4.0	1.348	.651
LiCl		
0.0805	1.921	0.928
.4931	1.844	.890
.9812	1.749	.845
1.962	1.582	.764
2.813	1.395	.674
3.648	1.260	.608
4.011	1.208	.583

where *i* refers to the trace ion and *d*(*u*_{*i*}) is a function depending on the valencies and mobilities of all the ions present. At zero concentration, this law reduces to the Nernst expression

$$D_i^0 = RT\lambda_i^0 / |z_i| F^2 \quad (2)$$

where *R* is the gas constant in joule/mole/deg., λ_i^0 and *z*_{*i*}, the limiting conductance and valency, respectively, of ion *i*, and *F* the faraday.

It will be realized that diaphragm-cells cannot be used below concentrations of 0.1 *M* owing to surface diffusion effects. However, data for the diffusion of Na⁺ in very dilute NaCl solution is being accumulated in this Laboratory by the continual monitoring capillary technique.¹² These results indicate that the limiting law as given by equation 1 is valid to a concentration of 0.005 *M* in this system. Further, by substituting the factor $\sqrt{c}/1 + \kappa a$ for \sqrt{c} in the above equation, the data can be represented up to at least 0.05 *M*. Introduction of the $\sqrt{c}/1 + \kappa a$ term is a device which makes allowance for ion size through the parameter "*a*" and has been used in an analogous manner to extend the applicability of the limiting law in conductivity studies. In view of the above experimental evidence, the comparison of cation and anion data in 0.1 *M* solution in terms of the extended equation seems justified.

Examination of the data for diffusion of Na⁺, Rb⁺, Cl⁻ and I⁻ in the three electrolytes shows that whereas *D*/*D*⁰ (Na⁺) is considerably higher than *D*/*D*⁰ (Rb⁺), *D*/*D*⁰ (Cl⁻) is only slightly more than *D*/*D*⁰ (I⁻) at 0.1 *M*. These differences can be attributed to two factors. The first is the fact that the value of the Onsager limiting slope, for *D*/*D*⁰.

(12) R. Mills and E. W. Godbole, *Aust. J. Chem.*, **11**, 1 (1958).

(Na⁺) is much higher than that for $\mathcal{D}/\mathcal{D}^0(\text{Rb}^+)$. The actual calculated values are -0.193 and -0.261 , respectively. In the anion case, however, the slopes for I⁻ and Cl⁻ are practically identical and so there is no differentiation at this stage. The second factor is involved in the use of the $\sqrt{c}/1+ka$ term. Use of this term will clearly reduce $\mathcal{D}/\mathcal{D}^0(\text{Rb}^+)$ relative to $\mathcal{D}/\mathcal{D}^0(\text{Na}^+)$ since "a" for NaCl is greater than for RbCl. The "a" values have been obtained from Harned and Owen.¹³ It will be noted that "a" has been given the value corresponding to the distance of closest approach between the tracer ion and the solution ion of opposite charge. This would seem the more appropriate figure since it can be assumed that the potential immediately surrounding the trace ion will be the main influence on its diffusion rate. Similarly, $\mathcal{D}/\mathcal{D}^0(\text{Cl}^-)$ will be reduced relative to $\mathcal{D}/\mathcal{D}^0(\text{I}^-)$ by the operation of this factor, but the lowering is much less proportionately than that effected by the slope values.

Comparison of the observed and calculated differences between anions and cations are shown in

(13) H. S. Harned and B. B. Owen, "Physical Chemistry of Electrolytic Solutions," 2nd Ed., Reinhold Publ. Corp., New York, N. Y., 1950, p. 380.

Table III. It will be observed that, within the error of measurement, the differences are consistent and the figures indicate that their comparative separation can be correlated with dilute solution theory at this concentration. In the anion case, good agreement is obtained between theory and experiment but in the cation case the observed differences whilst comparable are greater than the calculated values.

TABLE III

Electrolyte (0.1 M)	$\Delta\mathcal{D}/\mathcal{D}^0$ (Na ⁺ -Rb ⁺)		$\Delta\mathcal{D}/\mathcal{D}^0$ (Cl ⁻ -I ⁻)	
	Calcd.	Obsd.	Calcd.	Obsd.
KCl	0.017	0.030	0.000	0.003
NaCl	.021	.027	.001	.001
LiCl	.020	.032	-.005	-.004

Two further points of interest, arise from comparison of the diffusion of Rb⁺ with ions of similar type such as Cs⁺ and I⁻ ions. As would be expected, the $\mathcal{D}/\mathcal{D}^0$ curves for Cs⁺ ion in the three electrolytes,⁸ are indistinguishable from the Rb⁺ ones over this concentration range. However, the I⁻ data exhibit a different dependence and the coefficients fall off more rapidly with concentration than do the Rb⁺ values.

STRUCTURE OF LIQUID BORON TRIOXIDE*

BY J. D. MACKENZIE

General Electric Research Laboratory, Schenectady, New York

Received April 28, 1959

The viscosity, electric conductivity and density of liquid B₂O₃ have been measured over the temperature range 800–1350° and the effects of small amounts of residual H₂O examined. The structure of the liquid is temperature dependent. Viscous flow data indicate that the degree of association decreases with increasing temperature. However, the molar volume exhibits negative departure from linearity with rising temperature. The very low specific conductance of 7×10^{-6} ohm⁻¹ cm.⁻¹ at 900° above the melting point is not compatible with a structural variation which involves ionic dissociation. A tentative model is postulated to explain these results.

Introduction

The structure of liquid and vitreous B₂O₃ has been a subject of much controversy. Earlier concepts range from that of a molecular liquid consisting of B₄O₆ molecules,¹ an ionic melt involving complex boron-oxygen ions,² to that of a highly associated network of interlinking BO₃ triangles.³ Recently,⁴ studies of viscosity, electric conductivity and density suggested that the structure of the liquid is temperature dependent but that ionic dissociation is negligible, even at temperatures up to 1000° (m.p. 450°). However, in a concurrent X-ray diffraction study,⁵ extensive dissociation of the melt to give free oxygen ions was postulated to occur at 1200–1600°. Electric

conductivity data are not available at these elevated temperatures. Further, the specific conductances reported by various workers up to 1000° differ widely. The effects and the concentration of residual H₂O have not been determined. The present work was therefore undertaken with liquid B₂O₃ containing varying amounts of H₂O. Viscosity, conductivity and density have been re-determined and extended to 1350° to ascertain the validity of the interpretations from both the X-ray and the author's previous measurements.

Experimental

Mallinckrodt A. R. grade H₂BO₃ was first dehydrated by gradual heating of the charge in a Pt-20% Rh crucible to about 1000° until a bubble-free melt was obtained. The crucible containing 50 cc. of liquid B₂O₃ was then transferred to a vertical Pt resistance furnace for subsequent measurements. The apparatus was essentially the same as that used in a previous study of liquid germanium dioxide.⁶ Viscosity was measured by the counterbalance technique employing two Pt-20% Rh bobs of different dimensions. Electric conductivity was determined over the frequency range 1000–10,000 c./sec., the central suspension being adopted as one electrode and the crucible containing the melt as the other.

* This research was supported by the U. S. Air Force under Contract No. AF33 (616)-5699, monitored by the Aeronautical Research Laboratory, Wright Air Development Center.

(1) K. Fajans and S. W. Barber, *J. Am. Chem. Soc.*, **74**, 2761 (1952).
 (2) S. Anderson, R. L. Bohon and D. D. Kimpton, *J. Am. Ceram. Soc.*, **38**, 370 (1955).
 (3) B. E. Warren, H. Krutter and O. Morningstar, *ibid.*, **19**, 202 (1936).
 (4) J. D. Mackenzie, *Trans. Faraday Soc.*, **52**, 1564 (1956).
 (5) J. Zarzycki, *Proc. IV Intern. Cong. on Glass, Paris, VI*, 323 (1956).

(6) J. D. Mackenzie, *J. Chem. Phys.*, **29**, 605 (1958).

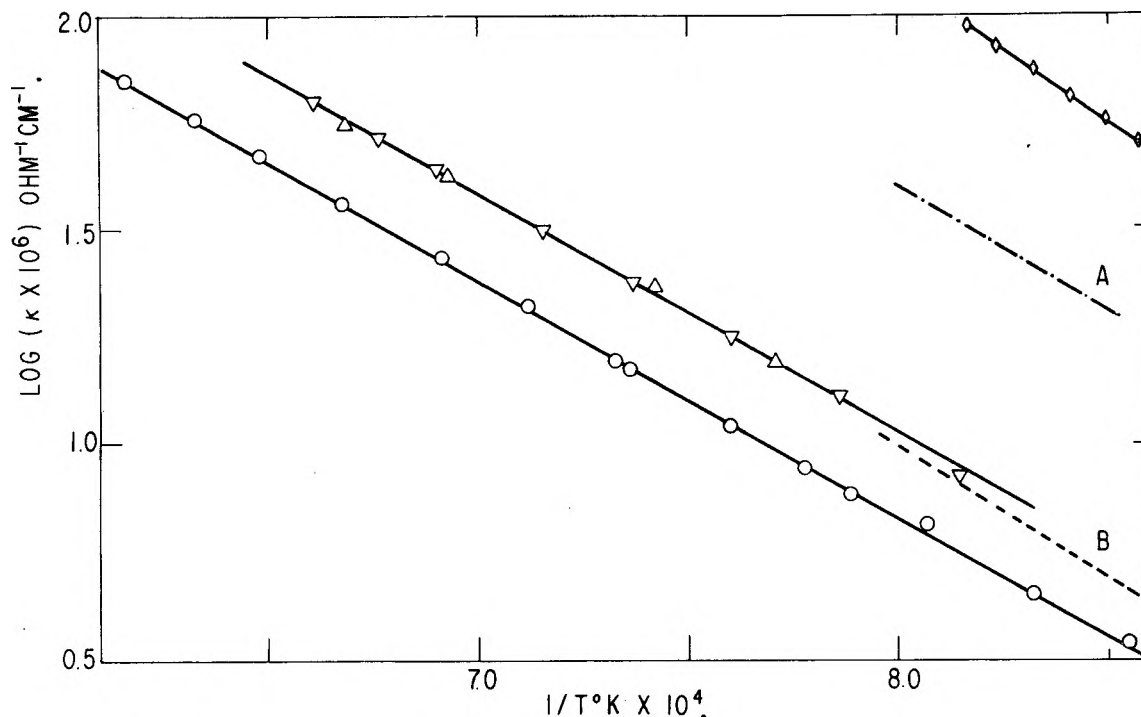


Fig. 1.—Relation between log specific conductivity and $1/T$ for liquid B_2O_3 : O, N_2 treated; Δ , 1250° and 5 mm. pressure for 8 hr.; ∇ , 1250° for 1 week; \diamond , Shartsis⁸ and Mackenzie⁴; A, Arndt and Gessler⁹; B, Phelps and Grace.¹⁰

By the use of two bobs and a similar suspension wire for the simple Archimedean method, the corrections due to surface tension were eliminated. The details, calibrations, and the determination of cell constants have been described elsewhere.⁷

Three different final dehydration treatments were employed. The first series of measurements were made after the melt had been kept at 1250° , with occasional stirring, for a week in an atmosphere of dry N_2 . The furnace was then evacuated to a pressure of about 5 mm. at 1250° for 8 hr. and the measurements repeated. Finally, the temperature was raised to 1300° and dry N_2 (~ 2 p.p.m. H_2O) allowed to bubble rapidly via a $1/8''$ i.d. Pt tubing through the melt for 4 hr. with constant stirring and the last series of measurements taken. Samples were withdrawn at the conclusion of each set of measurements for analysis. Spectroanalysis indicated that the upper limits for Li, Na, Ca, Pt, Pb, Sn and Fe were 0.001%, for K, Rb, Sr and Ba, 0.01%, and for Cs 0.1%. For the estimation of residual H_2O , thin glass discs were formed between Pt foils in an electric furnace with a dry N_2 atmosphere. Infrared analysis was made in a Beckman IR 7 spectrophotometer. OH absorption was observed only at 3580 cm.^{-1} if the ambient atmosphere was dry N_2 . In air, however, surface absorption of moisture occurred rapidly and the OH band at 3240 cm.^{-1} became increasingly evident. The OH concentrations in the B_2O_3 of the first two experiments were of the same order of magnitude but that in the last sample was clearly reduced by about 50%. Assuming that two OH corresponds to one H_2O , the residual H_2O contents in the melts were approximately 0.2, 0.2 and 0.1%, respectively.

Temperature measurements were made with a Pt-10% Rh thermocouple, the hot junction being placed adjacent to the crucible at the same level as the immersed bob. The temperature gradient along the crucible was less than 3° and measurements were accurate to $\pm 1^\circ$. The maximum overall errors in the viscosity, conductance and density results are estimated to be ± 8 , ± 10 and $\pm 0.4\%$, respectively. Reproducibles in the respective least favorable cases were ± 4 , ± 4 and $\pm 0.2\%$.

Results

Results obtained for the liquid B_2O_3 of minimum H_2O content, taken at 50° intervals from the

(7) J. D. Mackenzie, *Rev. Sci. Instr.*, **27**, 297 (1956).

smooth viscosity (η), specific conductivity (κ), and density against temperature curves, are presented in Table I. In Fig. 1, $\log \kappa$ is shown to be a linear function of $1/T$ for all three samples. From the simple Arrhenius equation

$$\kappa = A_\kappa \exp(-E_\kappa/RT)$$

the activation energy for electric conduction, E_κ , is 26 kcal./mole, being independent of the dehydration treatments. Over the range 1000–10000 c./sec., conductance is independent of the frequency. The specific conductances of the first two melts are similar but that of the N_2 -treated sample are about 35% lower. Although κ measured

TABLE I
VISCOSITY, ELECTRIC CONDUCTIVITY AND DENSITY OF LIQUID B_2O_3 CONTAINING APPROXIMATELY 0.1% H_2O

Temp., °C.	Viscosity, poise	Sp. conductivity $\times 10^6$, ohm ⁻¹ cm. ⁻¹	Density, g. cm. ⁻³
800	363 ^a		1.540 ^a
850	257	0.19	1.533
900	182	.35	1.525
950	133	.53	1.517
1000	103	.80	1.510
1050	82.2	1.19	1.505
1100	66.4	1.70	1.500
1150	54.7	2.34	1.496
1200	46.2	3.16	1.493
1250	40.1	4.17	1.491
1300	35.1	5.37	1.489
1350	31.0 ^a	7.05	

^a Extrapolated values.

by different workers^{1,8-10} shown in Fig. 1 differ

(8) L. Shartsis, W. Capps and S. Spinner, *J. Am. Ceram. Soc.*, **36**, 319 (1953).

(9) K. Arndt and A. Gessler, *Z. Elektrochem.*, **14**, 662 (1908).

(10) W. C. Phelps, Jr., and R. E. Grace, *J. Metals*, **9**, 1447 (1957).

widely, E_κ is similar, being 25 ± 2 kcal./mole. In Fig. 2, $\log \eta$ is shown plotted against $1/T$. The empirical equation

$$\eta = A_\eta \exp(E_\eta/RT)$$

is not obeyed over the entire temperature range studied. The energy of activation for viscous flow, E_η , at 1100° is approximately 15 kcal./mole. The viscosity of the nitrogen-treated liquid is about 7% greater than the other two samples. Although the estimated maximum experimental error is $\pm 8\%$, this observed difference is probably real on account of the consistency and reproducibility of the results. The author's previous measurements⁴ are lower by about 20%.

The non-linear variation of molar volume with temperature is shown in Fig. 3. No difference is detectable between the three samples. Between 850 and 1000° , the present and previous⁴ data are, within experimental error, identical. The expansivity, $(1/v)(\partial v/\partial T)_p$, varies from 1.06×10^{-4} per degree at 900° to 0.60×10^{-4} per degree at 1100° .

Discussion

The present work indicates that the complete removal of H_2O from liquid B_2O_3 is extremely difficult and that the conductance measured is sensitive to the small amounts of residual H_2O . The energies of activation for conduction from the present and five previous studies are all similar, being 25 ± 2 kcal./mole over the wide temperature range of 500 – 1350° . Although there are disagreements in the conductivity measured by various workers, all the κ values are low, e.g., between 10^{-5} – 10^{-6} ohm⁻¹ cm.⁻¹ at 1000° . For the melt containing about 0.1% H_2O , κ was only 7×10^{-5} ohm⁻¹ cm.⁻¹ at 1350° . Small amounts of alkali metal oxides may also cause a large increase of electric conductance in B_2O_3 .⁸ These facts strongly suggest that the conductances measured were primarily due to the small amounts of residual H_2O and metal oxide impurities in the melt. Ionic dissociation of the B_2O_3 is probably negligible even up to 1350° . From recent X-ray studies, Zarzycki⁵ estimated the coordination of oxygen around boron to be 3.3, 2.3 and 2.2 at 20, 1200 and 1600° , respectively. No error limits are given for these coordination numbers although it has been pointed out elsewhere¹¹ that the uncertainty can be as much as $\pm 30\%$. This decrease of the coordination was attributed to increasing ionic dissociation of the B_2O_3 with rising temperature, giving rise solely to free O^{--} ions. At 1200° , 30% of the B–O bonds are ruptured. The concentration of free O^{--} ions in the melt is thus 15%. This interpretation is not compatible with the observed conductance results discussed above.

According to the classical theory of the vitreous state,¹² pure B_2O_3 , SiO_2 and GeO_2 glasses are made up of disordered three-dimensionally continuous networks rigidly held together by the strong B–O, Si–O and Ge–O bonds. At elevated temperatures, therefore, these oxides constitute a special class

(11) O. Borgen, K. Grijotheim and J. Krogh-Moe, *Kgl. Norske Videnskab. Selskabs Forh.*, **27**, 17 (1954).

(12) W. H. Zachariassen, *J. Am. Chem. Soc.*, **54**, 3841 (1932).

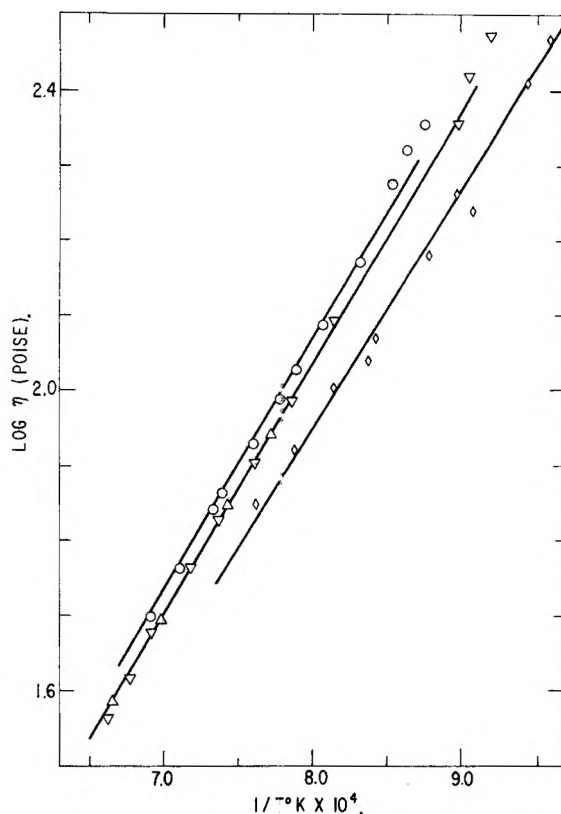


Fig. 2.—Relation between \log viscosity and $1/T$ for liquid B_2O_3 . Notations as for Fig. 1.

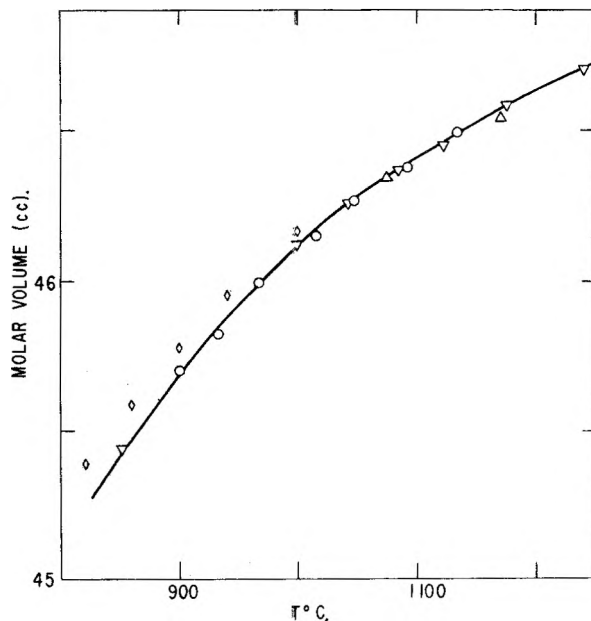


Fig. 3.—Relation between molar volume and temperature for liquid B_2O_3 . Notations are as for Fig. 1.

of highly associated liquids, where electric and viscous transport will necessitate the rupture of these strong bonds. A comparison of some relevant parameters is made in Table II. The low conductivity and high values of η and E_η at and above the melting temperatures suggested that at least for SiO_2 and GeO_2 , the random network concept is applicable.⁶ The flow parameters for B_2O_3 are

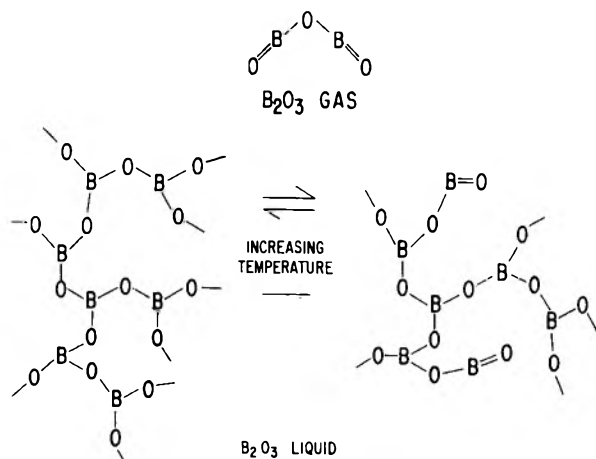


Fig. 4.—Schematic representation of possible structural variation with temperature in liquid B_2O_3 .

very different, both η and E_η being much lower. From previous viscosity and molar volume data, a structure in which adjacent BO_3 triangles only share corners has been shown to be untenable.^{13,14} This work shows that the viscosity results are far less sensitive to the small amounts of residual H_2O than conductivity. Further, the variation of viscosity with temperature is not noticeably affected. In Fig. 3, the negative deviation of the molar volume from linearity with increasing temperature is also confirmed up to 1350° . These results are thus in support of the previous interpretations.

The high viscosity and the low conductivity of B_2O_3 at the melting point is indicative of extensive association. The decrease of E_η from about 40 kcal./mole at the melting point to 10–15 kcal./mole at 1300° shows that the degree of association decreases with rising temperature. The variation of the structure of the liquid with temperature is also evident in the anomalous variation of the

(13) J. D. Mackenzie, *J. Chem. Phys.*, **24**, 925 (1956).

(14) J. D. Mackenzie, *ibid.*, **25**, 187 (1956).

TABLE II

COMPARISON OF LIQUID B_2O_3 , SiO_2 AND GeO_2

	B_2O_3	SiO_2	GeO_2
M-O bond energy, kcal.	110	106	104
T_m ($^\circ\text{C}.$)	450	1720	1115
κ ($\text{ohm}^{-1} \text{cm.}^{-1}$)	$<10^{-6}$	$<10^{-6}$	$<10^{-6}$
η (poise)	10^5	10^7	10^7
E_η (kcal./mole)	40	180	180
$T_m + 200^\circ : \eta$ (poise)	10^3	10^5	10^5
E_η (kcal./mole)	30	150	160

molar volume. However, from the conductance data, ionic dissociation is unlikely. These observations may be satisfactorily explained by a previous hypothesis⁴ that some adjacent boron atoms in the melt are bonded through two oxygen atoms instead of one. An alternative model involving the formation of $\text{B}=\text{O}$ in liquid B_2O_3 is also compatible with the present results. The structure of B_2O_3 molecules in the vapor state suggested by White, *et al.*,¹⁵ is shown in Fig. 4. The infrared emission maximum observed at 2041 cm.^{-1} was attributed to the $\text{B}=\text{O}$ stretchings. In liquid B_2O_3 , the formation of $\text{B}=\text{O}$ with increasing temperature is schematically represented in Fig. 4. This model does not involve ionic dissociation. Negative departure of the molar volume from linearity is explained by the shorter $\text{B}=\text{O}$ bonds. Decreasing association in the liquid is evident as some parts of the continuous network are terminated at every $\text{B}=\text{O}$. Preliminary examination of the infrared spectra of glassy B_2O_3 chilled from about 1000° has indeed revealed the presence of a maximum at about 2050 cm.^{-1} . Confirmation of this hypothesis must, however, await further measurements on the liquid.

Acknowledgments.—The author is grateful to Dr. J. E. Burke for his interest, Drs. W. L. Roth and B. H. Zimm for helpful discussions and Dr. R. S. McDonald for the infrared analysis.

(15) D. White, P. N. Walsh and D. E. Mann, *ibid.*, **28**, 508 (1958).

THE CARBON MONOXIDE EXCHANGE OF IRON CARBONYLS

BY A. N. WEBB AND J. J. MITCHELL

Texaco Research Center, Beacon, New York

Received May 7, 1959

Exchange of CO with $\text{Fe}(\text{CO})_5$ at low temperatures (25° or less) does not occur without a catalyst. Platinum and Ni are very active catalysts; Fe_3O_4 , Cu, Fe, $\gamma\text{-Al}_2\text{O}_3$ and $\alpha\text{-Fe}_2\text{O}_3$ are less active in descending order. Complex exchange rates, observed in some cases, are treated according to two three-compartment system models. In such cases a slow rate of transport is involved but the two calculated rates are assigned to exchange processes on more and less active catalyst sites. The mechanism of catalysis is postulated to be an associative one in which the catalyst functions as an electron acceptor. The solid iron carbonyls apparently exchange CO without a catalyst.

Introduction

In an investigation of the exchange between gaseous carbon monoxide and carbon monoxide chemisorbed on iron¹ multiple exchange rates were always observed. The fact that there were only a few discrete rates or a continuous range with a few

sharp maxima is taken as an indication of surface heterogeneity of a discontinuous type perhaps representing different exposed crystal planes. From the similarity of the $\text{Fe}-\text{CO}$ bond in iron carbonyls to that visualized between iron and chemisorbed CO it was considered that the equivalent (with respect to CO exchange) of a homogeneous iron surface covered with a layer of chemisorbed CO

(1) R. P. Eischens, *J. Am. Chem. Soc.*, **74**, 6148 (1952).

could be prepared by adsorbing iron pentacarbonyl on an inert carrier such as porous glass.²

For the system $\text{Fe}(\text{CO})_5\text{-CO}$, exchange means the replacement of one of the CO groups of the carbonyl molecule with a CO molecule from the gas. The progress of exchange was followed by using C^{14} as a tracer, initially present in the CO molecules of the gas phase. As exchange occurs the specific activity of the gas decreases by replacement with non-radioactive CO from the carbonyl phase.

There was no detectable CO exchange with the carbonyl adsorbed on porous glass at temperatures up to -33° . An attempt to observe exchange under what were considered more favorable conditions, using unadsorbed iron pentacarbonyl vapor at room temperature also failed. However, when reduced iron (similar to that used for the exchange between gaseous and chemisorbed CO) was introduced the carbonyl exchange occurred even at -78° .

Various metals and metal oxides were substituted for the iron catalyst in an attempt to explain the role of the catalyst in the carbonyl exchange.

Experimental Methods

Apparatus and Procedure.—The essential parts of the apparatus are shown in Fig. 1. The reactor contained in most cases an amount of catalyst sufficient to provide surface area to accommodate the iron carbonyl as a monolayer (allowing 30 \AA^2 per molecule). For supported catalysts this amount was usually 8 g. but up to 100 g. were used for unsupported metals. Reduction and degassing pretreatments were carried out with the catalyst in place.

Iron carbonyl³ (approximately 0.5 g.) was measured by micropipet or by weighing into a small bulb. A tube containing the small bulb was attached to the apparatus by a ground joint. The carbonyl was degassed by successive freezing and pumping periods and then distilled into the reactor.

The carbon monoxide labeled with C^{14} was prepared from C^{14}O_2 by reduction over zinc at 425° .⁴ The C^{14}O_2 was prepared by the reaction of perchloric acid on $\text{BaC}^{14}\text{O}_3$. The activity of the final gas, prepared by mixing with appropriate amounts of non-radioactive carbon monoxide, was in all cases in the range 3 to 4 counts per second per centimeter (of Hg gas pressure) measured by the end window G.M. counter. The CO gases were measured with the gas buretmanometer system and mixed by circulating the gas through the system, by-passing the reactor. The total amount of gas used was between 200 and 250 cc. or approximately equal to the carbonyl CO.

The circulating pump is a piston type made double acting by a set of four glass check valves. The steel piston within a brass tube is lifted by an external solenoid in a steel case. A relaxation oscillator using a neon glow tube switches the solenoid on and off at an adjustable frequency of 5 to 27 cycles per minute. With about 30 cc. displacement the pumping rate is variable between 300 and 1500 cc. per minute.

The radioactivity of the gas is measured by an end-window Geiger counter tube, Mark 1, Model 45 of Radiation Counter Laboratories. Gas passing through a small chamber adjacent to a window of thickness less than 2 mg. per cm^2 is counted with an efficiency of approximately 10%. Tracerlab Autoscaler and Superscaler circuits were used. At least 10,000 counts were measured so that the standard error of counting is 1% or less. If in a given run the pressure of the gas varied, corrections were made for self absorption.⁵ No dead time corrections were made because at the counting rates used, always less than 200 counts per second, these are negligible.

(2) 96% Silica Glass, No. 7930, Corning Glass Works.

(3) General Aniline and Film 99.5% $\text{Fe}(\text{CO})_5$.

(4) R. B. Bernstein and T. I. Taylor, *Science*, **106**, 498 (1947).

(5) Self absorption correction: $I = I_0(1 - e^{-\mu x})/\mu x$, μ = mass absorption coefficient for the radiation, x = sample thickness in mg./ cm^2 .

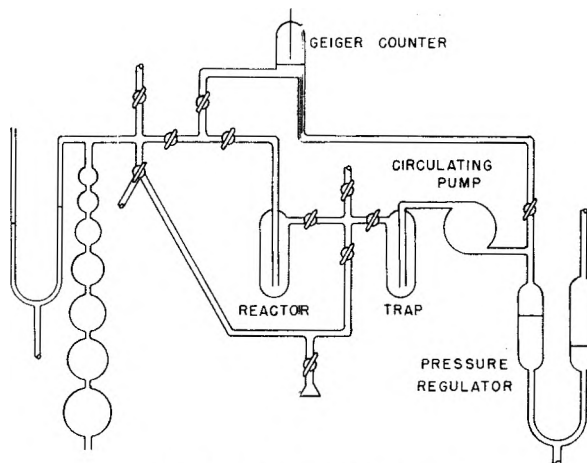


Fig. 1.—Exchange apparatus.

Nearly all of the exchange were carried out at 0° . The reactor containing catalyst and iron carbonyl was kept at this temperature overnight before each run to obtain uniform or equilibrium distribution of the carbonyl on the catalyst. The pressure of the CO was adjusted in most cases to 40 or 50 cm. by raising or lowering the mercury in the pressure regulator. The total volume of the system is thus variable but always remains large (300–400 cc.) compared to the small dead space of the reactor.

At 0° the vapor pressure of iron pentacarbonyl is 16 mm. (or less with adsorbents present) so that although most of the material remains in the reactor some circulates in the gas phase. This makes it advisable to do the experiment in subdued light to avoid photochemical decomposition. It also requires that the $\text{Fe}(\text{CO})_5$ be removed from the gas before counting. This was done by opening the by-pass, closing the stopcock to the reactor and circulating the gas through a trap immersed in liquid nitrogen. After determining the activity of the gas the trap was warmed up before resuming circulation to the catalyst. This procedure and the limitation of gas circulation make it difficult to secure significant data at intervals of less than five minutes. The small amount of exchange occurring in the closed off reactor during a counting interval was ignored.

A blank experiment carried out with glass wool in the reactor showed that after 20 hours, the maximum time for any run, there was no detectable exchange. During this or any run there was no detectable increase in pressure which would have indicated carbonyl decomposition.

Catalysts. Iron Oxides.— Fe_2O_3 , $5/32$ inch pellets were prepared from the precipitated hydroxide by calcination in air at 540° . The specific surface area of this material measured by B.E.T. N_2 adsorption is $25 \text{ m}^2/\text{g}$. Prior to the exchange run the sample was degassed at 150° . The magnetite sample, Fe_3O_4 , was prepared from the above by heating at 400° under vacuum. The specific surface area is estimated as approximately $20 \text{ m}^2/\text{g}$.

Iron.—Iron catalyst samples were prepared by reduction of the iron oxide pellets in a stream of purified hydrogen⁶ for ten days at 400° . A specific surface area of $4.25 \text{ m}^2/\text{g}$. was determined by B.E.T. nitrogen adsorption measurement after a preliminary reduction period of six days. The sample was degassed for six hours at 400° .

Copper.—Unsupported Cu with a specific surface area of $1.7 \text{ m}^2/\text{g}$. was prepared by heating pelleted CuCO_3 in H_2 at 240° for six hours. A final reduction in H_2 for six hours at 260° was followed by evacuation for 18 hours at 260° .

Supported Copper.—A catalyst calculated to contain 10% Cu was prepared by impregnating 8–14 mesh Alcoa F-10 alumina with aqueous $\text{Cu}(\text{NO}_3)_2$ drying at 100° and heating at 316° for 3 hours to decompose the nitrate. Before use the catalyst was reduced in flowing hydrogen for 73 hours at $450\text{--}550^\circ$ and evacuated 18 hours at 500° . X-Ray diffraction line breadth indicates 1000 \AA . or larger crystallites so that the maximum surface area per gram of metal is calculated to be 6.7 m^2 .

(6) Cu at 450° followed by charcoal and glass wool traps in liquid N_2 .

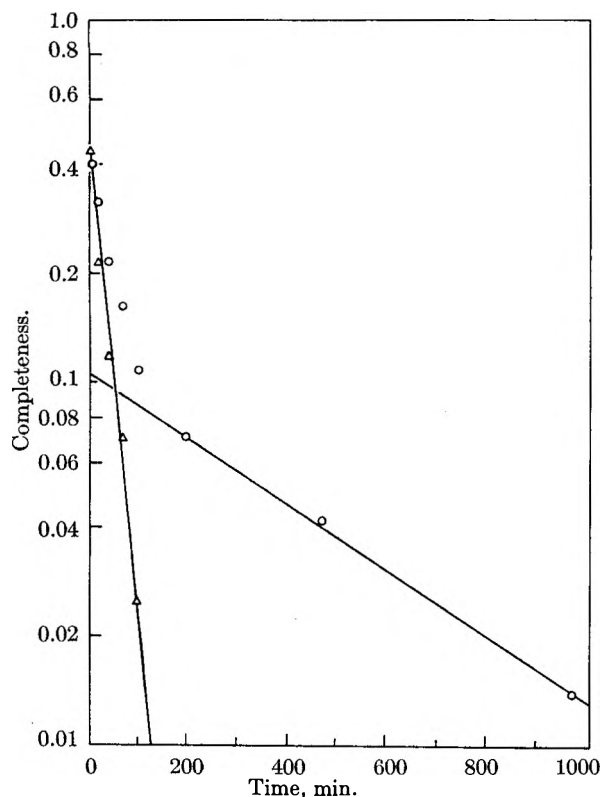


Fig. 2.— $\text{Fe}(\text{CO})_5$ -CO exchange, Fe catalyst.

Supported Nickel.—A catalyst calculated to contain 10% Ni was prepared in a similar manner and X-ray diffraction again indicated 1000 Å. or larger crystallites equivalent to a maximum area of 6.8 m^2/g . Ni. The sample used for exchange was reduced with H_2 for 153 hours at 480° and evacuated for 20 hours at 480°.

Supported Platinum.—Catalysts containing 0.5% Pt were prepared with 8-14 mesh Alcoa F-10 alumina which after calcination for 3 hours at 316° had a specific surface of 118 m^2/g . The alumina was impregnated with aqueous chloroplatinic acid solution, dried and reduced with various organic reducing agents.⁷ The reducing agents were hydrazine; alkaline (K_2CO_3) pyrogallol, hydroquinone and resorcinol, respectively, for the samples used in experiments 10 through 13. After thorough washing and drying the catalysts were again reduced in place with H_2 at 470° for 1.5 hours and evacuated for 18 hours at 470°. The specific surface of the Pt was determined by chemisorption of oxygen.⁸

The 0.3% Pt catalyst used for experiments 14 and 15 was prepared with alumina calcined at 700° for 22 hours to a specific surface of 64 m^2/g . This catalyst was reduced with hydrogen only.

Alumina Samples.—Uncalcined samples used in experiments 16 and 17 are 8-14 mesh Alcoa F-10 alumina as received except for in place H_2 treatment at 470° for 1.5 hours and evacuation at 470° for 18 hours. The sample of F-10 alumina used in experiment 18 was calcined at 790° for 16 hours and had a specific surface of 44 m^2/g . as determined by B.E.T. N_2 adsorption. For experiment 19 the alumina had been calcined for 10 hours at 760° to a specific area of 64 m^2/g . For experiment 20 ammonia was chemisorbed on this sample at 175°.⁹

Solid Carbonyls.—Iron pentacarbonyl adsorbed on porous glass chips was exposed to an ultraviolet lamp. (Cenco lamp output unknown) for 36 hours. The color changed from bright yellow to the deep orange of $\text{Fe}_2(\text{CO})_9$. Development of a blue-green color indicates that some $\text{Fe}_3(\text{CO})_{12}$ was also present. Evolution of CO was insufficient to account for complete conversion of $\text{Fe}(\text{CO})_5$ to $\text{Fe}_2(\text{CO})_9$.

Thus some $\text{Fe}(\text{CO})_5$ remained and all three iron carbonyls were present. No analysis of the solid phase was made.

Treatment of Experimental Data

In these experiments the labeled carbon was all initially in the observed, gaseous CO phase. The experimentally determined data were: S , the total amount of CO (in cc. at STP) in the system; S_{CO} , the amount of CO in the gas phase; $a_{\text{CO}}(0)$, the initial radioactivity in the gas phase, measured as already described; and $a_{\text{CO}}(t)$, the radioactivity in the gas phase at time t . If simple exchange of CO between the gas phase and the adsorbed carbonyl were the case, then one would expect¹⁰ a plot of the logarithm of the function $[a_{\text{CO}}(t)/a_{\text{CO}}(0)] - [S_{\text{CO}}/S]$ against the time to give a single straight line.

If the exchange is complex, such a plot will give a curve. A typical case is shown in Fig. 2 of the kind of complex exchange encountered in this work. These data for experiment 2, Fe catalyst, lie on a curve which can be resolved into the sum of two straight lines. The resolution process is the familiar one of extrapolating the straight-line portion of the curve that appears at long times back to short times and subtracting these extrapolated values from the early portion of the curve to obtain the second straight line. For all the experiments done in this work in which a complex exchange occurred the data could be fitted within experimental accuracy to a semi-logarithmic plot made up of the sum of two straight lines.

By adopting a modification of the notation of Sheppard and Householder¹¹ and using their analysis of exchange kinetics, one can state that the data therefore fit the relation

$$\frac{a_{\text{CO}}(t)}{a_{\text{CO}}(0)} - \frac{S_{\text{CO}}}{S} = X_1 e^{\lambda_1 t} + X_2 e^{\lambda_2 t}$$

$$X_1 = (S - S_{\text{CO}})(\lambda_1 + B)/S(\lambda_1 - \lambda_2)$$

and

$$X_2 = (S - S_{\text{CO}})(\lambda_2 + B)/S(\lambda_2 - \lambda_1)$$

are the ordinate intercepts of the straight lines in Fig. 2, each defining the same parameter B . Since it is obvious that $X_1 + X_2 = 1 - (S_{\text{CO}}/S)$, X_1 cannot carry any information not already included in X_2 . The values for S_{CO} , S , X_1 , X_2 , λ_1 and λ_2 , as determined from the experimental data, are given in Table I.

In the language of Sheppard and Householder, the data showing complex exchange indicate that one has observed exchange of CO between three compartments. No clue is given as to how the compartments are connected. If one assumes that each of the three is connected to the other two, he can define, in Sheppard and Householder's notation, the system parameters $S_2 = S_{\text{CO}}$, $\alpha_1 = \rho_{12}/S_1$, $\alpha_2 = \rho_{23}/S_3$, and $\alpha_3 = \rho_{13}/S_3$ where S_i is the amount of CO (in cc. at NTP) in the i th compartment and ρ_{ij} is the rate (in cc./min.) at which CO flows from compartment i to compartment j . Since the experiments were carried out under steady-state conditions, then $\rho_{ij} = \rho^{ji}$ and the total amount S of CO in the system was $S =$

(7) C. Paal and E. Windisch, *Ber.*, 4010 (1913).

(8) A. N. Webb, unpublished work.

(9) A. N. Webb, *Ind. Eng. Chem.*, 49, 261 (1957).

(10) H. A. C. McKay, *Nature*, 142, 997 (1938).

(11) C. W. Sheppard and A. S. Householder, *J. Applied Phys.*, 22, 510 (1951).

TABLE I
EXPERIMENTAL DATA

Expt. no.	Catalyst	Weight, g.	Spec. surface area, ^d m. ² /g.	S ₀ , cc.	S, cc.	X ₁	X ₂	-λ ₁	-λ ₂
1	Fe	82.0	4.23	225	522	0.513	0.056	0.1156	0.001
2	Fe	35.1	4.25	241	521	.433	.105	.0306	.0020
3	α-Fe ₂ O ₃	25.0	25	187	354	.445	.025	.0812	.000344
4	Fe ₃ O ₄	12.6	~20	211	492	.539	.0356	.723	.000554
5	Fe	1.8	4.25
6	α-Fe ₂ O ₃	2.2	25
7	10% Cu-Al ₂ O ₃	8.0	<6.7	188	434	.332	.236	.06076	.00826
8	Cu	111.1	1.7	152	248	.294	.0959	.036	.00091
9	10% Ni-Al ₂ O ₃	8.0	<6.8	177	436	.574	.015	.593	.0077
10	0.5% Pt-Al ₂ O ₃	8.0	9.26	184	427	.330	.240	.0625	.0163
11	0.5% Pt-Al ₂ O ₃	8.0	227	212	454	.533242	...
12	0.5% Pt-Al ₂ O ₃	8.0	77	219	467	.514	.017	.243	.0077
13	0.5% Pt-Al ₂ O ₃	8.0	164	215	468	.541311	...
14	0.3% Pt-Al ₂ O ₃	8.0	...	180	450	601404	...
15 ^a	0.3% Pt-Al ₂ O ₃	4.0
	γ-Al ₂ O ₃	4.0	...	238	465	.488416	...
16	γ-Al ₂ O ₃	8.0	120	213	465	.543133	...
17	γ-Al ₂ O ₃	8.0	120	154	405	.619169	...
18	γ-Al ₂ O ₃ calcd.	15.2	44	224	527	.425	.150	.0138	.0024
19	γ-Al ₂ O ₃ calcd.	5.8	64	161	366	.5610145	...
20 ^b	Cat. 19 + Ads. NH ₃	8.0	64	158	39600074	...
21 ^{b,c}	Solid carbonyls0127	.00034

^a Mechanical mixture of equal parts of catalyst 14 and calcined alumina of 19. ^b Exchange not followed to equilibrium mixing. ^c Mixture of Fe₂(CO)₉, Fe₃(CO)₁₂ and possibly Fe(CO)₅. ^d Specific surface area of the metal is given in cases of supported catalysts.

TABLE II
EXCHANGE RESULTS

Expt. no.	Catalyst	Mammillary				Catenary			
		S ₁ , cc.	S ₂ , cc.	^{α1} (cc./mm.)/cc.	^{α2} (cc./mm.)/cc.	S ₂ , cc.	S ₃ , cc.	^{α1} (cc./mm.)/cc.	^{α2} (cc./mm.)/cc.
1	Fe	236	61	0.056	0.00088	238	59	0.053	0.0036
2	Fe	175	105	.017	.0016	191	89	.021	.0036
3	α-Fe ₂ O ₃	149	18	.045	.00033	149	18	.057	.0027
4	Fe ₃ O ₄	246	35	.33	.00052	246	35	.29	.0036
5	Fe	299	0	0	0	299	0	0	0
6	α-Fe ₂ O ₃	283	0	0	0	283	0	0	0
7	10% Cu-Al ₂ O ₃	79	167	.042	.0052	124	23	.049	.0065
8	Cu	63	33	.025	.00079	65	32	.059	.0017
9	10% Ni-Al ₂ O ₃	238	21	.25	.0073	240	19	.19	.092
10	0.5% Pt-Al ₂ O ₃	61	182	.044	.0099	148	96	.038	.022
11	0.5% Pt-Al ₂ O ₃	242	0	.11	...	242	0	.11	...
12	0.5% Pt-Al ₂ O ₃	231	18	.12	.0074	233	15	.11	.11
13	0.5% Pt-Al ₂ O ₃	253	0	.14	...	253	0	.14	...
14	0.3% Pt-Al ₂ O ₃	253	0	.14	...	253	0	.14	...
15 ^a	0.3% Pt-Al ₂ O ₃
	γ-Al ₂ O ₃	227	0	.21	...	227	0	.21	...
16	γ-Al ₂ O ₃	253	0	.061	...	253	0	.061	...
17	γ-Al ₂ O ₃	251	0	.064	...	251	0	.064	...
18	γ-Al ₂ O ₃ calcd.	134	169	.0083	.0017	202	102	.0077	.0040
19	γ-Al ₂ O ₃ calcd.	206	0	.0064	...	206	0	.0064	...
20 ^b	Cat. 19 + Ads. NH ₃	23800030	...	23800030	...
21 ^{b,c}	Solid carbonyls	544	31	.011	.0001

^a Mechanical mixture of equal parts of catalyst 14 and calcined alumina of 19. ^b Exchange not followed to equilibrium mixing. ^c Mixture of Fe₂(CO)₉, Fe₃(CO)₁₂ and possibly Fe(CO)₅.

S₁ + S₂ + S₃. Following Sheppard and Householder's analysis of the kinetics, one can write four equations in the five unknowns α₁, α₂, α₃, S₁ and S₃

$$-(\lambda_1 + \lambda_2) = [(S - S_3)\alpha_1/S_2] + [(S - S_1)\alpha_2/S_2] + [(S - S_2)\alpha_3/S_1]$$

$$\lambda_1\lambda_2 = [\alpha_1S(\alpha_2 + \alpha_3/S_2)] + [S\alpha_2\alpha_3/S_1S_2]$$

$$S = S_1 + S_2 + S_3$$

$$B = [S_3\alpha_1/(S - S_2)] + [S_1\alpha_2/(S - S_2)] + [(S - S_2)\alpha_3/S_1]$$

Since there are no more such relations available,

this set of equations is insoluble, and so this model was considered no further.

If $\alpha_3 = 0$, one has what Sheppard and Householder call a mammillary case and one can solve the four equations for the system parameters: S_1, S_3, α_1 , and α_2 . If, on the other hand, one sets $S_1 = S_{CO}, \alpha_1 = \rho_{12}/S_2, \alpha_2 = \rho_{23}/S_3$ and $\alpha_3 = 0$, one has what Sheppard and Householder call a catenary case. Once again, the four equations can be solved for the system parameters. Table II shows these system parameters calculated for the mammillary and catenary models from the experimental data in Table I. In the solutions actually carried out, the value for B was the average of the values obtained from X_1 and X_2 .

This discussion has been restricted to three-compartment models because at most two simultaneous exchange processes were observed. However, it should be pointed out here that this observation actually infers only that there are at least three compartments in the system. If an ordinate intercept is less than 0.1 for the faster exchange or less than 0.05 for the slower exchange, experimental difficulties will prevent its observation.

This inability to detect data which would give rise to small values of X_i makes possible the situation shown in Table III. The many-compartment mammillary model in Table III was deliberately chosen so as to simulate the three-compartment one. The S_i and α_i are based on approximations to Gaussian distribution functions, $\rho(\alpha)$, which would give $dS(\alpha) = \rho(\alpha)d\alpha$, the amount of material having specific flow rates between α and $\alpha + d\alpha$. The parameters on which these functions were based were, respectively, an average α of 0.0133 cc./min./cc. and a standard deviation of 0.0010 cc./min./cc. and an average α of 0.00040 cc./min./cc. and a standard deviation of 0.00001 cc./min./cc.

As Table III shows the simulation was quite

TABLE III

COMPARISON OF A 3-COMPARTMENT MODEL AND A 15-COMPARTMENT MODEL DEvised TO SIMULATE IT

i	S _i , cc.	cc./min./ cc.	Calcd. ^a	
			Intercept X _i	Slope -λ _i , min. ⁻¹
2	15	0.013 3	0.471	0.000 552
3	25	.000 4	.529	.017 38
2	0.07	.010 3	.000 06	.000 370
3	0.81	.011 3	.000 36	.000 381
4	3.63	.012 3	.000 83	.000 393
5	5.98	.013 3	.000 93	.000 406
6	3.63	.014 3	.000 52	.000 419
7	0.81	.015 3	.000 12	.000 430
8	.07	.016 3	.468 34	.000 553
9	.11	.000 37	.000 52	.010 30
10	1.35	.000 38	.003 54	.011 36
11	6.05	.000 39	.009 95	.012 55
12	9.97	.000 40	.014 85	.013 86
13	6.05	.000 41	.013 64	.015 13
14	1.35	.000 42	.008 32	.016 26
15	0.11	.000 43	.478 02	.017 68

^a The calculations, all based on $S_1 = 50$ cc., were carried out by J. H. Matheny on the IBM CPC calculating equipment at the Texaco Research Center.

successful. One would be able to observe only X_8, λ_8 and X_{15}, λ_{15} from a semi-logarithmic plot of $F[a_1(t)] = 1 - [a_1(t)/a_1(\infty)]$ against t for the many-compartment model.¹² In addition, the values for X_3 and λ_3 are experimentally indistinguishable from X_2 and λ_2 in the three-compartment model, and X_{15} and λ_{15} differ from X_3 and λ_3 only by 10 and 1.5%, respectively.

It is also possible to construct models in which flow rates are too rapid to be detected or models which lead to straight lines the slopes of which are so nearly equal that the lines cannot be resolved from the composite curve. All of these possibilities show that one cannot rule out the presence of more than three compartments.

There are several points that can be made concerning the data in Table II. For some exchange runs the sizes of the carbonyl phases and α_i are nearly the same whether calculated according to the mammillary or catenary system models. These cases are those in which a large fraction of the carbonyl CO, approximately equal to the gaseous phase, exchanges at a rapid rate. This result is logical considering that the two models are identical for three phases except for the labeling of the phases and the identity of the observed phase. In general the values of the slow rate calculated for the catenary or "phases in series" model are much greater than the corresponding values for the mammillary or "common central phase" model.

In 10 cases a complex rate of exchange was observed which was resolved into two parts. In seven of the experiments exchange reached equilibrium at a simple rate. In experiment 20 with alumina poisoned by ammonia the reaction was followed only half-way to equilibrium with only a single slow rate apparent. The solid carbonyl exchange was also not followed to complete mixing as the bulk of the carbonyl CO appeared to be exchanging at a very slow rate. In two experiments, 5 and 6, there was no detectable exchange. Relatively small amounts of catalysts were used in these cases and the surface area provided is less than that required to accommodate the $Fe(CO)_5$ as a monolayer (allowing 30 Å. per molecule). The absence of exchange when the catalyst is thickly covered may be explained by restriction of mobility in the adsorbed layer or exclusion of CO from active surface sites.

The activities of the four Pt-Al₂O₃ catalysts used in experiments 10-13 are not more than two to three times greater than that of the uncalcined alumina from which they were prepared (experiments 16 and 17). However, the catalyst used in experiments 14 and 15 was prepared with calcined alumina of 64 m.²/g. Experiment 19 demonstrates the very low activity of this alumina and indicates that a high catalytic activity should be assigned to platinum.

The very low activity of the calcined aluminas and especially of the NH₃ poisoned catalyst used in experiment 20 shows that activity is not formed on any surface by traces of iron from decomposi-

(12) This is the function one would use on the basis of Sheppard and Householder's equation for the n -compartment mammillary model (see ref. 11).

tion of the carbonyl. Additional evidence on this point is that decomposition of as little as 2% of the iron carbonyl during the overnight contact with the catalyst preceding the exchange, would have been easily detectable both from the pressure of CO produced and as an apparent very fast initial exchange. Neither of these effects were observed. Iron from such decomposition if deposited in monolayer form would yield less than one square meter of area and only a negligible amount of exchange activity based on the specific activity of Fe from experiments 1 and 2.

Discussion

There are two aspects of the experimental results that appear to be significant. One is the appearance, in some cases, of two exchange rates, and the second is the variation in catalytic activity of different substances.

Significance of Complex Rates.—Neither the mammillary or catenary system models upon which the calculations of rates have been based fully describe the physical system. A transport process is certainly involved and, at least in the case of alumina-supported catalysts, there are two kinds of catalytic sites present. Unfortunately the equations corresponding to a complete model including all the possibilities of exchange and transport cannot be solved.

Whenever a complex rate is observed relatively slow transport is involved. Otherwise only a single exchange rate characterizing the most active portion of the catalyst would be apparent. Both of the calculated rates may apply to exchange processes or one may be associated with transport. In the mathematical treatment it is assumed that the transport process can be regarded as exchange. This assumption is valid if transport occurs by desorption and readsorption or by diffusion across a thin barrier.

The various possible systems are outlined below:

A. Systems with a single kind of catalytically active sites. 1. Exhibiting one rate. Exchange is slow compared to transfer to active sites and the rate measured is that of exchange itself. 2. Exhibiting two rates. Exchange is fast compared to transfer to active sites. Catenary model exactly applies.

B. Systems with two kinds of catalytically active sites. 1. Exhibiting one rate. Transfer between sites is fast compared to either exchange rate. The rate measured is that for the most active sites. 2. Exhibiting two rates. Transfer is as slow or slower than exchange over either kind of active site. The faster of the two exchanges is significantly faster.

The rate represented by α_1 , calculated on either the mammillary or catenary system models, is the exchange rate for that portion of the iron carbonyl which rapidly becomes available to the most active exchange sites. The second exchange rate or transport rate α_2 applies to a portion of the iron carbonyl which cannot be rapidly transferred to the active sites and is forced to exchange at a slower rate on less active sites, case B2, or is held up by slow transport, case A2.

Although the results of treating the experimental

data according to the two limited system models do not clearly indicate the correctness of one or the other there are several criteria which can be applied.

Examining the values of the specific exchange rates, α 's, calculated on the mammillary model there is agreement between the slow rate α_2 for alumina supported catalysts and the faster rate α_1 for the alumina used as support. (Catalyst pretreatments were equivalent to calcination of alumina.)

The values of α_2 for similar catalysts when calculated for the catenary model vary more than would be expected of a transport process under similar conditions.

These criteria argue in favor of the mammillary model in which both rates are concerned with exchange between CO and carbonyl phases. The first argument also places the heterogeneity of the exchange with the catalyst. The only possible source of heterogeneity in $\text{Fe}(\text{CO})_5$ itself is the distribution of $-\text{CO}$ groups between 2 polar and 3 equatorial positions. The exchange results do not differentiate between these positions.

The importance of the extent of active surface area on exchange kinetics is demonstrated by the series of experiments 10 to 13 inclusive. The catalysts are all 0.5% Pt on the same Al_2O_3 ; however as shown in Table I the Pt areas are quite different. The rates of slow exchange and transport should be closely the same.

For the two cases with a relatively large platinum surface area, experiments 11 and 13, exchange occurs at a single fast rate. In experiment 10 with a very small amount of platinum area 75% of the exchange occurs at a slow rate. Experiment 12 is an intermediate case. Other conditions being similar the available surface of active material appears to be the determining factor in whether or not two rates are observed. A larger active surface reduces the requirement on rapidity of transfer so that one rate rather than two is exhibited.

The Pt area of the catalyst used in experiment 14 is not known but must be high since all of the carbonyl exchanged at a single fast rate. Even when half the amount of this catalyst was mixed with an equal amount of alumina without Pt, experiment 15, exchange still occurred rapidly at a single rate. A separate experiment showed that there is no strong preferential adsorption of $\text{Fe}(\text{CO})_5$ on platinized alumina. Transport of carbonyl between catalyst granules is sufficiently rapid in this case that a second rate is not apparent.

The mode of transport is most probably desorption and readsorption. Iron carbonyl is always present in the vapor phase as shown by its appearance in the cold trap each time an activity measurement was made. The concentration is much less than the equilibrium vapor pressure at 0° , 16 mm., but the frequency of collisions which may lead to adsorption-desorption even at 1 mm. would be $3.3 \cdot 10^7$ (cc./min.)/cc., many times greater than the measured rates.

The solid carbonyl exchange is a separate case with several possibilities for heterogeneity of the carbonyl: (a) presence of different carbonyls, (b) bridged and linear-CO groups and (c) surface and

bulk exchange. The mammillary model fits (a) and (b); (c) corresponds to the catenary model.

Mechanism of Catalytic Action.—Exchange rate data obtained with a single set of concentration values provide no information on the underlying reaction mechanism, however, the relative activities of the catalytic materials do give some indication of the type of catalytic action involved.

Two possible mechanisms are to be considered: (a) an associative one represented by $\text{Fe}(\text{CO})_5 + \text{Catalyst} \rightleftharpoons \text{Fe}(\text{CO})_5 \cdot \text{Catalyst}$ and (b), a dissociative or replacement reaction represented by $\text{Fe}(\text{CO})_5 + \text{Catalyst} \rightleftharpoons \text{Fe}(\text{CO})_4 \cdot \text{Catalyst} + \text{CO}$. Whether or not the complex formed in (a) contains a sixth CO group from the gas phase or exchanges CO with the gas as a result of weakened Fe-CO bonds will not be examined and both possibilities are included under the associative case.

For the purpose of comparing catalyst activities values of α_1 calculated for the mammillary model are used. The correctness of this model or of the catenary model is not important since the values are essentially the same and in either case represent the direct exchange over the active catalyst.

The activities of the catalysts are put on a unit area basis by dividing the values of α_1 by the area of the catalyst or of the active constituent in the case of supported catalysts. Table IV shows the

TABLE IV

SPECIFIC ACTIVITIES			
Catalyst	$(\alpha_1/m.^2) \times 10^4$	Catalyst	$(\alpha_1/m.^2) \times 10^4$
Pt-Al ₂ O ₃	660	Fe	1.4
Ni-Al ₂ O ₃	470	γ -Al ₂ O ₃	0.7
Cu-Al ₂ O ₃	77	α -Fe ₂ O ₃	.7
Fe ₃ O ₄	13	γ -Al ₂ O ₃ calcd.	.2
Cu	1.8	γ -Al ₂ O ₃ calcd. + NH ₃	.006

specific activities of the different catalysts arranged in order of decreasing activity. Median values are used in cases of more than one run with similar catalyst compositions. These specific activities vary over the considerable range of 10⁶. Only Pt and Ni may be considered to show high activity for the exchange. The unsupported Cu catalyst is probably more representative of this metal than the supported sample considering the known influence of the support on metal catalysts. The high activity of Pt and Ni suggests that d band vacancies may be uniquely important. The activity of these metals and of all the catalysts in an associative mechanism may be explained by the notion that they function as electron acceptors. By removing electrons from the central Fe atom it is possible for an exchange complex containing a sixth CO group to be formed. The trigonal bipyramidal structure of Fe(CO)₅ indicates that the bonding orbitals involved are the 4s, three 4p and one 3d. These are all occupied by electron pairs from the five-CO groups and the remaining four 3d orbitals are filled by unshared pairs. Without a catalyst to withdraw electrons there is no available low energy orbital for association of an additional CO. In contrast to this the cobalt and nickel carbonyls, which do have 3d or 4p vacancies, exchange rapidly without a catalyst.¹³ The solid

iron carbonyls, which apparently do not require a catalyst, also have incompletely filled bonding orbitals.

In relation to the concept of catalytic function as an electron acceptor the relative positions of Cu and Fe and especially the low specific activity of Fe are anomalous. However the low activity of Fe may be due to excessive stability of the catalyst-carbonyl complex which would approach the more complex iron carbonyls in structure.

An inverse effect of CO concentration on the underlying exchange reaction rate could be considered as evidence against the dissociative mechanism. In the absence of information on this point it must be considered especially in the cases of Pt and Ni which chemisorb CO actively. There is a strong possibility that wherever allowed the dissociative mechanism operates in addition to a general associative one.

Complex rates do not require two mechanisms and, if equally probable for each molecule, several mechanisms in operation would still give a simple exchange. However, in a heterogenous system two mechanisms would probably give rise to complex exchange because the different kinds of sites involved would not be equally available to all carbonyl molecules.

The dissociative mechanism is not well suited to the oxide catalysts which lack a surface function which could replace one of the five -CO groups of Fe(CO)₅ leading to Fe(CO)₄·Catalyst + CO. However, electron acceptor properties can be assigned to the Lewis acid sites of Al₂O₃.¹⁴ The number of these sites is reduced more rapidly than is surface area by calcination and they are effectively neutralized by chemisorption of ammonia.⁹

Summary

1. One or both of the solid iron carbonyls exchange CO without a catalyst (subject to Fe or iron oxides not being a contaminant).

2. Iron pentacarbonyl exchanges CO with gaseous CO only in the presence of a catalyst at 25° or below.

3. The following are catalysts for the exchange of CO with Fe(CO)₅ in descending order of activity at 0°: Pt, Ni, Fe₃O₄, Cu, Fe, Al₂O₃, Fe₂O₃.

4. The exchange reaction is completely stopped by covering the catalyst surface with more than a monolayer of iron carbonyl.

5. In some cases part of the iron carbonyl is available for exchange on the most active portions of the catalyst surface and a second part is restricted to exchange on less active sites or must reach the active sites by a relatively slow transport process. Whether two rates or one is observed depends on the relative rates of the various processes involved. The evidence favors the interpretation of both observed rates in the complex case as exchange rates of carbonyl phases with a common gaseous CO phase, according to the mammillary system model.

6. All of the active catalysts have electron acceptor properties and the most active ones have

(13) D. F. Keeley and R. E. Johnson, private communication.

(14) J. F. Mapes and R. P. Eischens, *THIS JOURNAL*, **58**, 1059 (1954).

incompletely filled d bands. On this basis an associative mechanism is suggested rather than a dissociative mechanism of exchange.

Acknowledgment.—The authors wish to thank R. P. Eischens, L. C. Roess and Irving Wender for their interest and suggestions.

THE FRACTIONATION OF OXYGEN ISOTOPES BETWEEN WATER AND SULFUR DIOXIDE¹

By L. L. BROWN AND J. S. DRURY

Chemistry Division, Oak Ridge National Laboratory, Oak Ridge, Tennessee

Received May 8, 1959

The isotopic fractionation of oxygen between water and sulfur dioxide was measured at 21°. The experimental value (1.016) agreed well with a theoretical value calculated from Urey's data (1.014). Oxygen-18 concentrated in the gas phase.

Introduction

The literature has no experimental values of the fractionation factor for oxygen isotopes for the reaction



From Urey's data² the factor may be calculated to be 1.012 at 25°. Halperin and Taube³ showed that the exchange of oxygen between liquid water and SO₂ was fast. Hoering and Kennedy⁴ also observed that the exchange was rapid and called attention to the unsuitability of SO₂ for O¹⁸ analyses in mass spectrometers. A modification of the method of Gregg and Lauder⁵ for reduction of SO₂ to water has provided a practical way to assay SO₂ for O¹⁸, and made feasible the determination of the single stage fractionation factor (α) for oxygen isotopes between SO₂ and liquid H₂O.

Experimental

Materials.—The Matheson Company purified H₂S and anhydrous SO₂ were used after being purified further by two vacuum distillations in which only the center fractions were retained.

Laboratory-distilled water was vacuum distilled into the reaction vessels following several cycles of freezing and pumping to remove dissolved gases.

Water, containing 1.5% O¹⁸, was obtained from Stuart Oxygen Company.

Methods.—The sulfur dioxide and water were equilibrated by two different procedures in order to minimize systematic errors. In one equilibration, oxygen-18 enriched water was used so that a relatively large isotopic change would occur in the SO₂. In the other equilibration, the isotopic composition of both reactants was normal. The pressure of SO₂ in each case was approximately one atmosphere.

The isotopic composition of all water samples was determined indirectly from the mass analysis of CO₂ with which the water samples were equilibrated previously. In the first experiment average peak heights of masses 44 and 46 were obtained with a modified General Electric 60° sector, 6 in. radius spectrometer. In the second experiment measurements of the 46/44 mass ratio were obtained directly with a dual collector, ratio spectrometer constructed by Nuclide Analysis Associates. The SO₂ samples from each experiment were reduced to H₂O with H₂S and then were treated as described above.

Equilibration A.—The first equilibration was made in a 1 liter, round-bottom flask. The flask was connected through

a vacuum stopcock and a standard taper joint to a manifold for evacuation and filling. Diametrically opposite the filling port was a second vacuum stopcock which shut off a 20-ml. bulb from the main reaction volume. The entire container was evacuated and 0.998 g. of H₂O¹⁸ (about 1.10 × normal) was distilled into the small bulb where it was isolated. Then 2.443 g. of SO₂ was added to the large flask. Exact weights of reagents were determined by weighing the tared flask after each addition of reagent. The H₂O was transferred to the larger container by turning the flask on its side in an evaporating dish of liquid nitrogen and opening the connecting stopcock to the small bulb. This action froze both the SO₂ and H₂O on the wall of the large flask and voided the small bulb which was isolated by turning the stopcock to its closed position. The flask was put in a room thermostated at 21° for 48 hours, during which interval it was occasionally shaken to break up the liquid phase. At the end of the equilibration time, the gas and liquid phases were separated by draining the water into the small bulb and closing the stopcock. With the phases thus separated, the SO₂ was subjected to reduction as described below. Later the H₂O was distilled out of the small bulb and portions were pipetted into small bulbs for analysis by equilibration with CO₂.

Equilibration B.—The reaction vessel for the second equilibration was a 500-ml. round flask to which a three-way stopcock was attached. The two external arms of the stopcock were fitted with standard taper joints; one connected the apparatus to the vacuum manifold, the other accepted the product water receiver. The flask was evacuated and 0.466 g. of normal water and 1.245 g. of sulfur dioxide were added directly to the reaction flask by cooling with liquid nitrogen. The exact amounts of reagents were obtained by weighing after each addition. The equilibration was continued with occasional shaking of the flask for 44 hours in a room thermostated at 21°. Sampling of the liquid was done by collecting the water above the stopcock and diverting it into an evacuated bulb of 5-ml. capacity. The water was removed by pipet into another bulb for the CO₂ equilibration. The SO₂ was retained for further processing as described below.

Analyses of SO₂ for O¹⁸.—Gregg and Lauder⁶ reduced SO₂ to H₂O by using H₂S with catalytic amounts of water. Their isotopic measurements were done by density determinations of the product water. In the present instance, greater precision and convenience were obtained by analyzing the water samples by means of a mass spectrometer. This was done indirectly by equilibrating the water with CO₂ and calculating the isotopic composition of the water from that of CO₂. The latter method requires a weighable amount of water and necessitates reducing more SO₂ than is required for the ordinary mass spectrometer sample. The reduction reaction is



The stoichiometry requires a 2/1 mole ratio of H₂S/SO₂ and it was found that a 2.2/1 ratio gave 100% conversion. The reduction would not go if both reagents were anhydrous even with prolonged heating at 500°. Matthews⁶ studied various inorganic and organic solvent catalysts which pro-

(1) This paper is based on work performed for the U. S. Atomic Energy Commission by Union Carbide Corporation.

(2) H. C. Urey, *J. Chem. Soc.*, 562 (1947).

(3) J. Halperin and H. Taube, *J. Am. Chem. Soc.*, **74**, 375 (1952).

(4) T. C. Hoering and J. W. Kennedy, *ibid.*, **79**, 57 (1957).

(5) E. M. C. Gregg and I. Lauder, *Trans. Faraday Soc.*, **46**, 1039 (1950).

(6) E. Matthews, *J. Chem. Soc.* 2270 (1926).

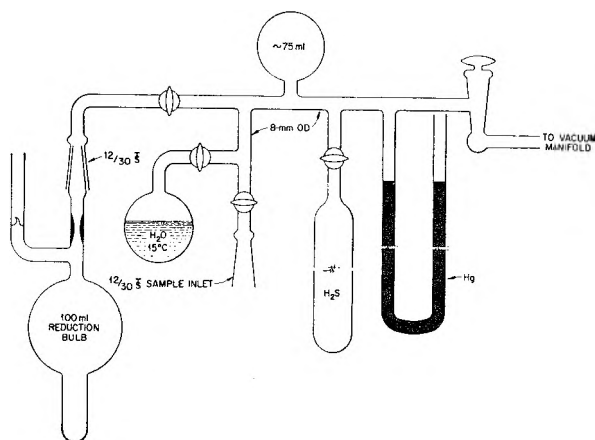


Fig. 1.—Sample preparation manifold.

mote (or prevent) the reaction; from his data, water was selected as the least likely to yield spurious side products.

The manifold for preparing samples is shown in Fig. 1. The total volume confined inside the stopcocks was approximately 90 ml. The SO_2 sample pressure was determined first, then the gas was condensed in a reduction bulb of 100-ml. size. SO_2 at a pressure of about 50 cm. yielded a satisfactory amount of water. Hydrogen sulfide now was measured into the evacuated manifold in two increments, each of which was about 1.1 times the original SO_2 pressure. The catalytic water reservoir was kept in a bath at 15° . An indefinite increment of water vapor was added to the reaction vessel by a rapid 180° turn of the confining stopcock. At most 1 mg. (100 ml., 13 mm.) of water could be added, and likely much less, since the water reservoir had only 75 ml. of gas instantaneously available above 25 ml. of water. The catalytic water was normal in O^{18} , and no corrections were made for its presence in the sample. The amount of water added was small and nearly equal for every sample. Its presence would not affect the ratio of isotopic ratios in a pair of samples.

The loaded reduction tube was sealed off with the contents at liquid nitrogen temperature. It then was allowed to warm to room temperature. As it warmed most of the SO_2 was reduced, leaving a coat of sulfur on the wall of the bulb. At this point water equivalent to 75% conversion could be recovered; the remainder of the oxygen probably was present in the sulfur as SO_2 or H_2O . A 100% recovery of water was obtained by heating the flask overnight at 350° . The excess H_2S was removed by repeatedly freezing the sample in a Dry Ice-acetone bath and pumping off the gas above the solid. The purified water was distilled into a tared receiver, then a known amount of CO_2 was added and the weight of water was determined. After equilibrating the mixture of water and CO_2 for three days at 25° , the isotopic composition of SO_2 was calculated from analysis of the CO_2 using the equation⁷

$$N_{\text{obs}} = \frac{1}{KR_0 + 1} + Q \left[\frac{1}{R_0 + 1/2} - \frac{1}{R_0 + 1/2} \right]$$

where

N_{obs} = atom fraction O^{18} in sample

R_0 = $\text{CO}^{18}\text{O}^{16}/\text{CO}_2^{16}$ for the sample (R_0 = reference CO_2)

Q = $\text{CO}_2/\text{H}_2\text{O}$ mole ratio in sample equilibration

K = 2.076 at 25°

Results

The isotopic data from both equilibrations are summarized in Table I. Data from equilibration A were obtained in the usual manner from measure-

ments of mass 44 and 46 peak heights. Data from equilibration B were arrived at differently since the results of the mass analysis were of the form $R = (46/44)_{\text{sample}}/(46/44)_{\text{standard}}$. The $\text{O}^{18}/\text{O}^{16}$ for the standard was taken as 0.00204. A calculation showed that a 4.1% increase in this ratio would cause the separation factor to appear only 0.0004 greater. Since this quantity is less than the confidence interval of the assays, it may be seen that the experimental α is not strongly dependent on the concentration chosen for O^{18} in the standard CO_2 .

The average value of the single stage separation factor [$\alpha = (\text{O}^{18}/\text{O}^{16})_{\text{SO}_2}/(\text{O}^{18}/\text{O}^{16})_{\text{H}_2\text{O}}$] is 1.016 and is probably correct to ± 0.003 . The uncertainty in the analyses of the samples from the second equilibration is known to be less than 0.003, and the agreement between the results of the two experiments makes that value a reasonable limit. The difference in the average experimental value, and the value calculated from Urey's² data extrapolated to 21° is less than the uncertainties in the experimental measurements. For both equilibrations the experimental α is greater than the calculated. The heavy isotope of oxygen enriches in the gas phase.

TABLE I

MASS ASSAY DATA AND SEPARATION FACTORS					
Equilibration	Sample	R^a	H_2O^b (g.)	$\text{O}^{18}/\text{O}^{16}$	α^c
A	$\text{H}_2\text{O}-1$	223.7	0.0751	0.002159	1.0157
	$\text{H}_2\text{O}-2$	223.1	.0812	(av.)	
	SO_2	219.9	.1072	.002193	
	CO_2	238.1 (ref. value)			
B	H_2O	1.0203 ± 0.0003 (95% C.I.)	.2762	.0020059	1.0159
	SO_2	1.0365 ± 0.0001 (95% C.I.)	.5050	.0020377	
	CO_2			.00204 ^d	

^a For equilibration A, $R = \text{CO}_2^{16}/\text{CO}^{16}\text{O}^{18}$. For equilibration B, $R = (46/44)_{\text{sample}}/(46/44)_{\text{standard}}$. ^b Weight of water equilibrated with 1.228×10^{-3} mole CO_2 . ^c $\alpha = (\text{O}^{18}/\text{O}^{16})_{\text{SO}_2}/(\text{O}^{18}/\text{O}^{16})_{\text{H}_2\text{O}}$. ^d Assumed value for standard CO_2 .

A chemical exchange reaction having a separation factor as large as that observed in this work is of interest as a possible method of separating isotopes. If the SO_2 - H_2O reaction were used to separate oxygen-18, the critical reflux would be the reduction of SO_2 to H_2O since the desired isotope is concentrated in this species. SO_2 reduction might be accomplished by the reaction already described for isotopic sample preparation. Similar work has been done on a large scale by Nishimori⁸ to remove H_2S from a gas stream.

(8) T. Nishimori, Japan Patent 2362 (1955); *C. A.*, **51**, 12453 (1957).

(7) I. Dostrovsky and F. S. Klein, *Anal. Chem.*, **24**, 414 (1952).

DETERMINATION OF THE EQUILIBRIUM CONSTANTS FOR THE HYDROGENATION OF MESITYLENE. THE THERMODYNAMIC PROPERTIES OF THE 1,3,5-TRIMETHYLCYCLOHEXANES

BY CLARK J. EGAN AND W. C. BUSS

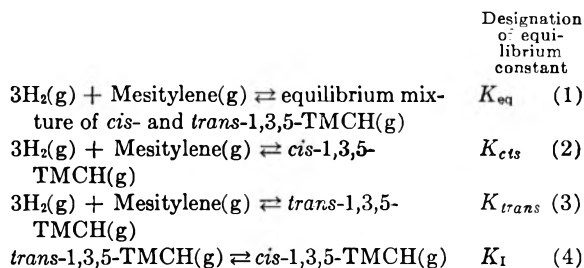
Contribution from the California Research Corporation, Richmond, California

Received May 9, 1959

The equilibria for the hydrogenation of mesitylene to an equilibrium mixture of *cis*- and *trans*-1,3,5-trimethylcyclohexanes were determined experimentally over the temperature range of 200 to 300°. The data were used to calculate (for the temperature range 298 to 1000°K.): values of the heat, free energy and equilibrium constant of the reactions, mesitylene + 3H₂ = *cis*-1,3,5-trimethylcyclohexane, and mesitylene + 3H₂ = *trans*-1,3,5-trimethylcyclohexane; values of the heat, free energy and equilibrium constant of formation and the entropy of the *cis*- and *trans*-1,3,5-trimethylcyclohexanes.

Although mesitylene is known to react with hydrogen to form 1,*cis*-3,*cis*-5-trimethylcyclohexane and 1,*cis*-3,*trans*-5-trimethylcyclohexane,¹ the equilibrium constant for the reaction has not been determined. Equilibrium constants for the hydrogenation of benzene, toluene and the xylenes can be calculated from thermodynamic data.² Such free energy data are available for mesitylene but not for the trimethylcyclohexanes. The hydrogenation equilibrium constants have also been determined experimentally for benzene,^{3,4} toluene⁵ and *m*-xylene.⁶ The data on the equilibrium for benzene hydrogenation have been summarized by Janz.⁷

We determined the equilibrium constants for the hydrogenation of mesitylene over the temperature range 200 to 300°. The equilibrium constants for the *cis*-*trans* isomerization were determined also over the same temperature range. It is concluded that the hydrogenation product is an equilibrium mixture of 1,*cis*-3,*cis*-5-trimethylcyclohexane (hereafter called *cis*-1,3,5-TMCH) and 1,*cis*-3,*trans*-5-trimethylcyclohexane (hereafter called *trans*-1,3,5-TMCH). From these data the equilibrium constants for the following reactions were calculated



Experimental

Materials.—The mesitylene used in these experiments was Eastman White Label product purified by distillation through 3 feet of Penn State packing to give a product boiling from 164.4 to 165° and having a purity of 98% by gas-liquid chromatography. The 2% impurity appeared to be

- (1) G. Chirudoglu, *Bull. soc. chim. Belges*, **60**, 39 (1951).
- (2) Selected Values of Properties of Hydrocarbons, American Petroleum Institute Research Project 44, National Bureau of Standards, Washington, 1948.
- (3) G. H. Burrows and Carl Lucarini, *J. Am. Chem. Soc.*, **49**, 1157 (1927).
- (4) V. R. Zharkova and A. V. Frost, *J. Gen. Chem. U.S.S.R.*, **2**, 534 (1932).
- (5) A. A. Vredenskii, S. G. Vinnikova, V. R. Zharkova and B. M. Funduiler, *ibid.*, **3**, 718 (1933).
- (6) A. A. Vredenskii and N. K. Takhtareva, *Zhur. Obschei Khim.*, **19**, 1083 (1949).
- (7) G. J. Janz, *J. Chem. Phys.*, **22**, 751 (1954).

unaffected upon contact with the hydrogenation catalyst. The *cis*-1,3,5-TMCH (99.92 ± 0.07 mole % purity) and the *trans*-1,3,5-TMCH (99.85 ± 0.07 mole % purity) were American Petroleum Institute standard samples. The hydrogen purity exceeded 99.5 mole %.

Apparatus.—The catalyst was supported inside a 0.46-inch i.d. by 43-inch long stainless steel tube, which was surrounded by a heavy walled steel block inside an electrically heated oven. The catalyst temperatures were measured by a chromel-alumel thermocouple located in a thermowell in the catalyst bed. A Celectray controller was used to control the temperature. Hydrocarbon feed rates were measured by means of a Microfeeder pump (Proportioners, Inc.). The hydrogen rate was measured by oil displacement in a reservoir.

A rhodium catalyst was tried in preliminary studies but gave considerable side reaction products including *m*-xylene.

The catalyst used in the present experiments was 12 ml. of Baker's 5% platinum on carbon (4-8 mesh). It was pre-reduced with approximately 0.3 mole of hydrogen before each run. In different runs the hydrocarbon feed rates were between 2.0 to 0.75 ml. per hour, and the mole ratio of hydrogen to hydrocarbon at the start was in the range 4 to 13.

The temperature variation through the catalyst bed was less than 1° with no reaction taking place. During a run, the temperature rise due to the heat of reaction was less than 2°, depending on the flow rate and the extent of reaction. The maximum variation in temperature through the catalyst bed during a run was usually of the order of 1°. The temperature used in calculations was the average temperature of the last half of the catalyst bed. The chromel-alumel thermocouple was calibrated against a Bureau of Standard's platinum resistance thermometer at 195° and 213°. The temperature of the catalyst bed is known within an estimated accuracy of ±1°.

A mercury manometer in conjunction with a barometer was used to measure the pressure at the end of the catalyst bed for the runs made at approximately atmospheric pressure.

In order to allow time for representative samples to be taken, the first 10% of the product was discarded.

Analysis.—The products were analyzed by gas-liquid chromatography (g.l.c.) using a Perkin-Elmer Model 154B with a dioctylterephthalate column at 130°. This technique separated the *cis*-isomer from the *trans*-isomer sufficiently for analysis. This chromatographic method was checked by analyzing known mixtures of mesitylene and the 1,3,5-TMCH's. Two g.l.c. analyses were made of each product and the results were averaged.

The products were analyzed also by refractometry. The g.l.c. analysis for the amount of the *cis*- and *trans*-isomers in the product was used to calculate the refractive index of the nonaromatic fraction. The method was checked by measuring the refractive index of known mixtures of mesitylene and the 1,3,5-TMCH isomers.

The standard deviation between the two methods of analysis for the mesitylene content of the product is less than 2% of the amount present.

Equilibria for Hydrogenation and Isomerization

Table I summarizes the experimental results and gives the equilibrium constants K_{eq} and K_I calcu-

TABLE I
EXPERIMENTAL DATA AND EQUILIBRIUM CONSTANTS
(Catalyst, 12 ml. of Baker's 5% platinum on carbon)

Run no.	Compn. of hydrocarbon feed, mole %	Av. mol. wt. of feed	Feed rate, ml./hr.	Temp., °C.	Pres- sure, mm.	Initial mole ratio H ₂ /feed	Product, mole %			K _I $\frac{cis-1,3,5-TMCH}{trans-1,3,5-TMCH}$	K _{eq}
							Total TMCH	Mesitylene	% Side reac- tion		
M-14	98% Mesitylene	120.2	2.65	227.8	762.5	8.77	56.3	41.2	0.0	2.59	
M-15	98% Mesitylene	120.2	1.57	223.8	760.2	8.53	68.6	28.9	0.0	2.68	3.65
M-16	98% Mesitylene	120.2	0.78	225.2	763.1	8.92	68.5	28.7	0.0	2.75	3.54
M-17	98% Mesitylene	120.2	1.55	251.4	762.2	10.53	20.4	77.3	0.0	2.47	0.349
M-18	98% Mesitylene	120.2	1.55	270.6	761.1	10.61	4.50	93.6	0.6	^b	0.063
M-19	57.1% <i>cis</i> -1,3,5-TMCH 19.5% <i>trans</i> -1,3,5-TMCH 22.2% Mesitylene	124.9	1.58	225.6	760.0	3.93	63.5	35.3	0.0	2.66	3.37
M-20	57.1% <i>cis</i> -1,3,5-TMCH 19.5% <i>trans</i> -1,3,5-TMCH 22.2% Mesitylene	124.9	0.79	207.2	761.0	11.95	92.8	6.2	0.0	2.83	19.13
M-21	98% Mesitylene	120.2	2.04	298.4	3280	10.46	29.5	68.9	1.0	2.00	0.0072
M-22	98% Mesitylene	120.2	1.04	243.4	761.3	13.49	31.6	67.3	0.0	2.39	0.588
M-23	43.2% <i>cis</i> -1,3,5-TMCH 55.6% Mesitylene	122.8	1.55	241.7	760.4	12.48	35.4	64.5	0.0	2.46	0.687

^a Hydrogenation equilibrium not established. ^b Amount of TMCH was too small for a satisfactory analysis.

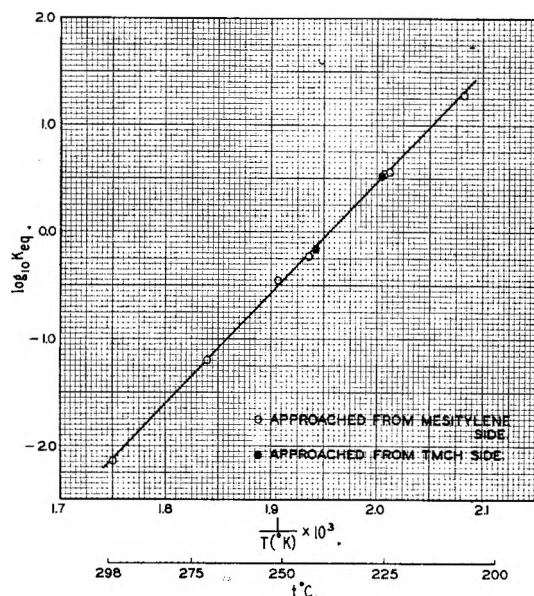


Fig. 1.—Logarithm of equilibrium constants for hydrogenation of mesitylene to an equilibrium mixture of *cis*- and *trans*-1,3,5-trimethylcyclohexanes.

lated from the data. In Figs. 1 and 2 the values of K_{eq} and K_I , respectively, are plotted against $1/T^\circ K$. K_{eq} is given by the equation

$$K_{eq} = \frac{N_{TMCH}}{N_{MES}} \left[\frac{(R - 3x + 1)760}{(R - 3x)P_{mm.}} \right]^3$$

where

- N_{TMCH} = mole fraction of total 1,3,5-TMCH in product
- N_{MES} = mole fraction of mesitylene in product
- R = mole ratio H₂/feed at the start
- x = fraction of feed converted from mesitylene to trimethylcyclohexane. In runs wherein the equilibrium is approached from the trimethylcyclohexane side, $-x$ is the fraction of feed converted from trimethylcyclohexane to mesitylene
- $P_{mm.}$ = pressure at end of catalyst bed, mm. of mercury

Most of the runs were made with a mesitylene feed, the equilibrium being approached from the

mesitylene side. In Runs M-19 and M-23, the equilibrium was approached from the trimethylcyclohexane side. The same results were obtained regardless of the side from which equilibrium was approached, thus proving that true equilibrium was established.

Runs M-14 to M-16 prove that the hydrogenation product is an equilibrium mixture of the *cis*- and *trans*-isomers of trimethylcyclohexane. In these runs the same ratio of *cis*- to *trans*-isomers was obtained within experimental error when the feed rate was progressively lowered. As a further proof, Run M-23 was made in which the equilibrium was approached from the trimethylcyclohexane side using a feed containing *cis*-1,3,5-TMCH but no *trans*-1,3,5-TMCH. The *cis* to *trans* ratio obtained in this experiment is in good agreement with other results. Because the *cis* to *trans* ratio does not change with longer contact time on the catalyst nor with the composition of the feed, it is concluded that the product contains an equilibrium mixture of the *cis* and *trans* isomers.

The following equations (including the standard deviations) for the best straight lines of $\log K_{eq}$ and $\log K_I$ against $1/T^\circ K$. were obtained by the least squares method

$$\log K_{eq} = \frac{10,328}{T} - 20.20 \pm 0.03 \quad (480 \text{ to } 571^\circ K.)$$

$$\log K_I = \frac{463.0}{T} - 0.505 \pm 0.015 \quad (480 \text{ to } 571^\circ K.)$$

Extension of these data to a wider temperature range is given later.

From these equations the values of ΔH^0 over the above temperature range for reactions 1 and 4 were calculated to be -47.3 ± 0.5 and -2.1 ± 0.25 kcal./mole, respectively.

Thermodynamic data for the temperature range 298.16 to 1000°K. were obtained as follows.

(a) The value of ΔH^0 of -47.93 ± 0.06 kcal./mole, given by Dolliver, *et al.*,⁸ was taken for the hydrogenation of mesitylene to a mixture of 68%

(8) M. A. Dolliver, T. L. Gresham, G. B. Kistiakowsky and W. E. Vaughan, *J. Am. Chem. Soc.*, **59**, 831 (1937).

TABLE II

HEAT (ΔH^0) AND FREE ENERGY (ΔF^0) (IN KCAL./MOLE) AND LOGARITHM OF THE EQUILIBRIUM CONSTANT (K) OF REACTIONS 1, 2, 3 AND 4

$T, ^\circ\text{K.}$	Mesitylene(g) + 3H ₂ (g) = equil. 1,3,5-TMCH(g)			Mesitylene(g) + 3H ₂ (g) = cis-1,3,5-TMCH(g)			log K
	ΔH^0	ΔF^0	log K	ΔH^0	ΔF^0	log K	
298.16	-47.46	-20.11	14.74	-47.64	-20.05	14.70	
300	-47.49	-19.94	14.52	-47.66	-19.88	14.48	
400	-48.39	-10.60	5.79	-48.77	-10.44	5.71	
500	-48.88	-1.09	0.48	-49.44	-0.77	0.34	
600	-49.04	8.48	-3.09	-49.72	8.99	-3.28	
700	-48.93	18.05	-5.63	-49.67	18.78	-5.86	
800	-48.60	27.59	-7.54	-49.36	28.54	-7.80	
900	-48.10	37.07	-9.00	-48.84	38.25	-9.29	
1000	-47.47	46.51	-10.16	-48.15	47.89	-10.47	

$T, ^\circ\text{K.}$	Mesitylene(g) + 3H ₂ (g) = trans-1,3,5-TMCH(g)			trans-1,3,5-TMCH(g) = cis-1,3,5-TMCH(g)			
	ΔH^0	ΔF^0	log K	ΔH^0	ΔF^0	K	% cis at equil.
298.16	-45.53	-18.64	13.66	-2.11	-1.41	10.9	91.6
300	-45.55	-18.47	13.45	-2.11	-1.41	10.7	91.5
400	-46.68	-9.26	5.06	-2.09	-1.18	4.43	81.6
500	-47.40	+0.19	-0.08	-2.04	-0.96	2.63	72.4
600	-47.76	9.74	-3.55	-1.96	-0.75	1.87	65.2
700	-47.82	19.34	-6.04	-1.85	-0.56	1.49	59.9
800	-47.64	28.92	-7.90	-1.72	-0.38	1.27	55.9
900	-47.26	38.47	-9.34	-1.58	-0.22	1.13	53.1
1000	-46.75	47.97	-10.48	-1.40	-0.08	1.04	51.0

cis-1,3,5-TMCH and 32% *trans*-1,3,5-TMCH at 381°K. From the relationship $\Delta H^0_{cis} - \Delta H^0_{trans} = -2.1$ kcal./mole values of ΔH^0_{cis} and ΔH^0_{trans} were calculated to be -48.6 and -46.5 kcal./mole, respectively, at 381°K.

(b) An equation was obtained for the change in ΔH^0_{cis} and ΔH^0_{trans} with temperature as follows. The heat capacities of *cis*-1,3,5-TMCH and *trans*-1,3,5-TMCH were estimated as

$$C_p^0(\text{cis-1,3,5-TMCH}) = C_p^0(\text{cis-1,3-DMCH}) + [C_p^0(\text{cis-1,3-DMCH}) - C_p^0(\text{methylcyclohexane})]$$

and

$$C_p^0(\text{trans-1,3,5-TMCH}) = C_p^0(\text{trans-1,3-DMCH}) + [C_p^0(\text{trans-1,3-DMCH}) - C_p^0(\text{methylcyclohexane})]$$

Values for the heat capacities of methylcyclohexane and dimethylcyclohexane are known.² Combining the above values with the heat capacities of mesitylene² and hydrogen,² one obtains the following equations for ΔC_p^0 for reactions 2 and 3 over the temperature range 298.16 to 1000°K.

$$\Delta C_p^0 \text{ cis (cal./deg. mole)} = -31.10 + 0.0673T - 2.88 \times 10^{-5}T^2$$

$$\Delta C_p^0 \text{ trans (cal./deg. mole)} = -29.90 + 0.0629T - 2.74 \times 10^{-5}T^2$$

The constant in each of the following equations was evaluated from the known values of ΔH^0 at 384°K.

$$\Delta H^0_{cis} = -41,105 - 31.10T + 0.03365T^2 - 0.960 \times 10^{-5}T^3$$

$$\Delta H^0_{trans} = -39,168 - 29.90T + 0.03145T^2 - 0.913 \times 10^{-5}T^3$$

(c) The free energy data obtainable from the experimental points in Table I were used to solve for the integration constant in the equation for the change of free energy with temperature. The average of the integration constants (-96.99 ± 0.21 for ΔF^0_{cis} and -92.52 ± 0.22 for ΔF^0_{trans}) appear in the equations

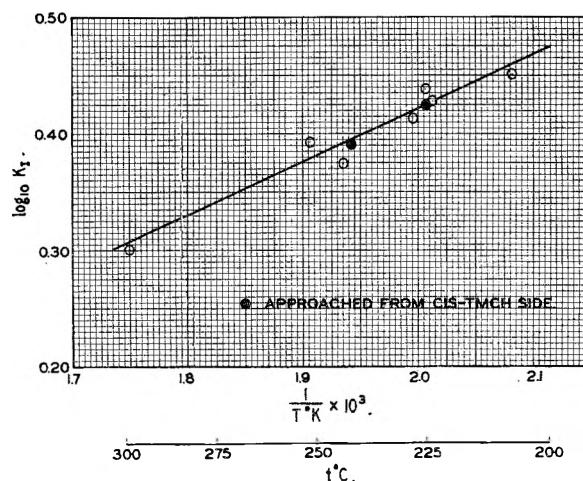


Fig. 2.—Logarithm of equilibrium constants for *trans*-1,3,5-trimethylcyclohexane = *cis*-1,3,5-trimethylcyclohexane.

$$\Delta F^0_{cis} = -41,105 + 31.10T \ln T - 0.03365T^2 + 0.480 \times 10^{-5}T^3 - 96.99T$$

$$\Delta F^0_{trans} = -39,168 + 29.90T \ln T - 0.03145T^2 + 0.457 \times 10^{-5}T^3 - 92.52T$$

(d) For extrapolation to 298.16°K. and to 1000°K. values of $\Delta F^0_{I^0}$ (and subsequently K_I) were taken from the above equations.

(e) Values for ΔH^0_{eq} , $\log K_{eq}$, and ΔF^0_{eq} were calculated from the above values of K_I and the relationships

$$\Delta H^0_{cis} = \Delta H^0_{eq} + \frac{\Delta H^0_{I^0}}{1 + K_I}$$

$$\Delta H^0_{trans} = \Delta H^0_{eq} - \frac{K_I \Delta H^0_{I^0}}{1 + K_I}$$

$$\log K_{cis} = \log K_{eq} - \log \left(1 + \frac{1}{K_I} \right)$$

$$\log K_{trans} = \log K_{eq} - \log (1 + K_I)$$

Table II summarizes the calculations.

TABLE III

HEAT (ΔH_f°), FREE ENERGY (ΔF_f°) (IN KCAL./MOLE), LOGARITHM OF THE EQUILIBRIUM CONSTANT OF FORMATION (K_f) AND ENTROPY (IN CAL./DEG. MOLE) OF THE 1,3,5-TRIMETHYLCYCLOHEXANES IN THE IDEAL GAS STATE

T, °K.	Equilibrium mixture				<i>cis</i> -1,3,5-TMCH				<i>trans</i> -1,3,5-TMCH			
	ΔH_f°	ΔF_f°	$\log K_f$	S°	ΔH_f°	ΔF_f°	$\log K_f$	S°	ΔH_f°	ΔF_f°	$\log K_f$	S°
298.16	-51.30	8.07	-5.91	94.0	-51.48	8.12	-5.95	93.3	-49.37	9.54	-6.99	95.6
300	-51.37	8.43	-6.14	94.3	-51.55	8.49	-6.18	93.5	-49.44	9.90	-7.21	95.8
400	-54.57	28.95	-15.82	109.2	-54.96	29.12	-15.91	107.8	-52.86	30.30	-16.55	110.1
500	-56.99	50.13	-21.91	124.1	-57.55	50.45	-22.05	122.4	-55.50	51.41	-22.47	124.5
600	-58.73	71.72	-26.12	138.6	-59.42	72.23	-26.31	136.6	-57.45	72.98	-26.58	138.6
700	-59.89	93.56	-29.21	152.4	-60.64	94.27	-29.43	150.3	-58.78	94.83	-29.61	152.2
800	-60.53	115.52	-31.56	165.6	-61.29	116.44	-31.81	163.5	-59.57	116.82	-31.91	165.1
900	-60.74	137.56	-33.40	178.0	-61.48	138.69	-33.68	175.9	-59.91	138.91	-33.73	177.4
1000	-60.56	159.60	-34.88	189.8	-61.25	160.93	-35.17	187.8	-59.85	161.01	-35.19	189.1

The calculated value of ΔH_{eq}^0 at 525°K. (an average temperature for the present experiments) is -48.95 kcal./mole. This is to be compared with -47.3 ± 0.5 kcal./mole derived from the equation of $\log K_{eq}$ versus temperature.

Thermodynamic Properties of the Trimethylcyclohexanes

By combining the values of ΔH^0 , ΔF^0 and $\log K$ for the hydrogenation equilibria with the values of ΔH_f^0 , ΔF_f^0 , and $\log K_f$ for the formation of mesitylene (as tabulated in the API tables²), one obtains the corresponding values for the formation of the 1,3,5-trimethylcyclohexanes shown in Table III. Included also are the entropy values of each 1,3,5-trimethylcyclohexane isomer calculated by combining ΔS^0 for the hydrogenation reaction with the entropy values of mesitylene and hydrogen.² The calculated value of the entropy of mesitylene at 298.16°K. is in excellent agreement with the experimental value of Taylor and Kilpatrick.⁹

Discussion

The structural analysis of the dimethylcyclohexanes given by Pitzer and Beckett^{10,11} is extended

(9) R. D. Taylor and J. E. Kilpatrick, *J. Chem. Phys.*, **23**, 1232 (1955).

readily to the 1,3,5-TMCH's. *cis*-1,3,5-TMCH exists only in the equatorial form because of the large strain energy in the axial form. *trans*-1,3,5-TMCH, at the lower temperatures, exists in the equatorial, equatorial, axial form (with a predicted strain energy of 1.94 kcal./mole¹²) in preference to the equatorial, axial, axial form (with a predicted strain energy of about 5.4 kcal./mole¹¹).

The heat of isomerization of *trans*-1,3,5-TMCH to *cis*-1,3,5-TMCH in the gaseous state at 0°K., calculated from the equations in the previous section, is -1.9 kcal./mole. This is in excellent agreement with the above predicted value.

The corresponding entropy of isomerization at 298.16°K. is -2.3 cal./deg. mole. This is in good agreement with the calculated difference of $-R \ln 3$, or -2.18 cal./deg. mole, due to the difference in symmetry numbers of the isomers.

Acknowledgments.—The authors gratefully acknowledge helpful discussions with Drs. G. E. Langlois and J. D. Kemp and Professor Kenneth S. Pitzer during this work.

(10) K. S. Pitzer and C. W. Beckett, *J. Am. Chem. Soc.*, **69**, 977 (1947).

(11) C. W. Beckett, K. S. Pitzer and R. Spitzer, *ibid.*, **69**, 2488 (1947).

(12) E. J. Prosen, W. H. Johnson and F. D. Rossini, *J. Research Natl. Bur. Standards*, **39**, 173 (1947).

PARAMAGNETIC RESONANCE ABSORPTION IN PEROXO-DICOBALT COMPLEXES

BY E. A. V. EBSWORTH*^a AND J. A. WEIL*^b

Department of Chemistry, Princeton University, Princeton, New Jersey

Received May 9, 1959

The paramagnetic resonance spectra of the ions $[(\text{NH}_3)_5\text{Co}-\text{O}-\text{O}-\text{Co}(\text{NH}_3)_5]^{+6}$ and $[(\text{NH}_3)_4\text{Co} \begin{array}{c} \diagup \text{O} \diagdown \\ \diagdown \text{O} \diagup \\ \text{NH}_2 \end{array} \text{Co}(\text{NH}_3)_4]^{+4}$ have been studied using various solvents. Under appropriate conditions, 15 hyperfine lines can be resolved in the spectrum of each, showing that the single unpaired electron must interact equally with both cobalt nuclei. The derivative spectra were not in general symmetric, and varied with changes in the acidity, viscosity and temperature of the solvent. These variations are interpreted in terms of anisotropy and relaxation effects.

Introduction

We have prepared salts of a number of paramagnetic peroxo-dicobalt cations, including the

* (a) University Chemical Laboratory, Lensfield Road, Cambridge, England; (b) Chemistry Division, Argonne National Laboratory, Lemont, Illinois.

monobridged $[(\text{NH}_3)_5\text{Co}-\text{O}-\text{O}-\text{Co}(\text{NH}_3)_5]^{+6}$ (to be denoted by M_1) and the dibridged

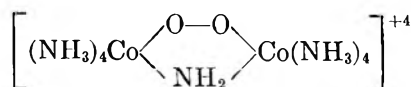


TABLE I
COMPOSITIONS OF THE PEROXO-DICOBALT COMPLEXES, AS DETERMINED BY ANALYSIS

Salt	Cobalt		Nitrogen		% composition Hydrogen		Other	
	Found	Calcd.	Found	Calcd.	Found	Calcd.	Found	Calcd.
$M_1(SO_4)_2 \cdot HSO_4 \cdot 3H_2O$	17.74	17.74	20.6	21.1	5.56	5.62	43.29	43.38 (SO ₄ ⁻)
$M_1(NO_3)_5$	18.60	18.70	33.1	33.3	4.86	4.80
$M_1(ClO_4)_5$	14.28	14.41	17.1	17.1	3.70	3.70	20.98	21.68 (Cl)
$M_2(NO_3)_4$	21.58	21.43	32.9	33.1	4.88	4.76
$M_2(ClO_4)_4$	16.97	16.84	17.7	18.0	3.70	3.74	20.26	20.25 (Cl)
$M_2'(NO_3)_4$	17.58	18.02	27.7	27.8	5.36	5.24	14.70	14.68 (C)

(to be denoted by M_2), in order to study their paramagnetic resonance absorption. As was discussed in a previous communication,¹ the spectrum of M_1 dissolved in concentrated H_2SO_4 was found to consist of 15 poorly resolved lines, with the two sides of the derivative absorption curve showing definite asymmetry. This spectrum was interpreted as arising from a single unpaired electron interacting identically with the two cobalt atoms, thus demonstrating their equivalence. It was concluded that the electronic structure could not be properly represented as including two cobalt atoms with different formal valences of +3 and +4, respectively, and that another possible structure consisting essentially of two cobalt +3 ions bridged by an O_2^- group was insufficient to explain the spectrum observed. No attempt was made to account for the asymmetry of the spectrum. In the present paper, we describe a more detailed investigation of the paramagnetic resonance spectra of various peroxo-dicobalt complexes.

Experimental

1. Preparation of Compounds. (a) $M_1HSO_4(SO_4)_2 \cdot 3H_2O$ (to be denoted by I).—This salt was prepared in the way described by Gleu and Rehm.² Cobalt^{II} sulfate was oxidized in ammoniacal solution with hydrogen peroxide and ammonium persulfate. Approximately equimolar amounts of hydrogen peroxide and ammonium persulfate were taken; no I was precipitated when a 2:1 molar ratio of peroxide to persulfate was taken, while with a molar ratio of less than 0.9 a quantity of yellow-orange solid was formed as well. This was tentatively identified from its elemental analysis and ultraviolet spectrum as a cobalt^{III} derivative, possibly the sulfate-persulfate described by Jorgensen.³

The dark green salt I was purified by recrystallization from 2 N sulfuric acid, care being taken to keep the temperature of the solution below 75°; with more concentrated acid, or at higher temperatures, the mother liquor tended to turn blue, indicating decomposition. The purified salt was washed with ethanol and diethyl ether until the washings were neutral. The elemental analysis for this and the other salts were carried out as follows: cobalt—by evaporation of the salt with concd. H_2SO_4 to constant weight; nitrogen—by the Dumas method; hydrogen and carbon—by combustion; sulfate—by precipitation as barium sulfate; perchlorate—by reduction and titration of total chloride. The results of the elemental analyses are listed in Table I. Washing the salt with water rather than with ethanol apparently converted it into a normal sulfate,⁴ as indicated by low sulfate (41.7%) and high cobalt (19.4%) contents. The yield of I was ca. 60 g. of crude salt per 140 g. of hydrated cobalt sulfate taken.

(b) $M_1(NO_3)_5$ (to be denoted by II).—The nitrate was made by Werner's method⁶ (blowing oxygen through an ammoniacal solution of cobalt^{II} nitrate at room tempera-

ture) and was recrystallized from 2% nitric acid as described by him. After washing the salt with alcohol and ether, it was found to have the composition shown in Table I.

(c) $M_1(ClO_4)_5$ (to be denoted by III).—It was found that a perchlorate could be made by adding a solution of 2 g. of I in 80% phosphoric acid to 70% perchloric acid.⁶ No perchlorate of this cation has been described before. The fine precipitate formed was filtered and recrystallized from 10% perchloric acid (or acetone) to yield fine, pale blue needles. After washing the complex with alcohol, it was found to have the composition given in Table I, showing that the salt has the above formula. The yield of this salt was 2.2 g.

(d) $M_2(NO_3)_4$ (to be denoted by IV).—The dibridged nitrate was prepared by Werner's method,^{7,8} with minor modifications. The best yield was obtained when the ammoniacal solution of cobalt^{II} nitrate was oxidized with a slow stream of air at 30–32° for 8 hr., allowed to stand for 18 hr. and neutralized at 5° ($\pm 3^\circ$) over a total period of 5–8 hr. After allowing the solution to stand for a further 36 hr., the precipitated solid was separated by filtering and the green nitrate IV isolated from it as described by Werner.⁸ The salt was recrystallized from 5% HNO_3 and, after it had been washed with ethanol, it was found to have the composition shown in Table I. We obtained 5 g. of salt for each 100 g. of hydrated cobalt nitrate taken.

(e) $M_2(ClO_4)_4$ (to be denoted by V).—This salt was made in exactly the same way as compound III (see above), by mixing a solution of IV in phosphoric acid with 72% perchloric acid. The fine, olive-brown solid precipitated was filtered and recrystallized from acetone and was found to have the formula given above (see Table I). The low yield, ~50%, may be accounted for by the appreciable solubility of this salt in perchloric acid.

(f) $[(en)_2Co \begin{matrix} O_2 \\ \diagdown \\ NH_2 \end{matrix} Co(en)_2](NO_3)_4$, where "en" means ethylenediamine, (to be denoted by VI).—Four grams of IV was dissolved in 60 ml. of water, 25 ml. of a solution of 10 ml. of ethylenediamine in 90 ml. of water was added, and the mixture was heated on a water-bath for 1.5 hr. After the solution had cooled to room temperature, concentrated nitric acid was added until the color of the reaction-mixture turned from red to olive-green; the addition of a little ethanol precipitated a mass of green crystals which were filtered and recrystallized from the minimum amount of water by adding concentrated nitric acid.⁹ About 3 g. of the pure salt was obtained; this, after it had been washed with ethanol and diethyl ether, was found to have the composition set out in Table I.

2. Solubilities.—The first of these substances to be investigated by us was the sulfate I. The difficulty in finding a suitable solvent for it, and the asymmetry of its EPR spectrum when dissolved in 80% phosphoric acid, led us to make a qualitative survey of the solubilities of some of the salts in various solvents. The solubilities in water and various mineral acids are summarized in Table II.

Compounds I and IV dissolved readily in 40% hydrofluoric acid in polythene vessels, but these solutions of I

(1) I. Bernal, E. A. V. Ebsworth and J. A. Weil, *Proc. Chem. Soc.*, 57 (1959).

(2) K. Gleu and K. Rehm, *Z. anorg. Chem.*, **237**, 79 (1938).

(3) S. M. Jorgensen, *ibid.*, **17**, 459 (1898).

(4) G. Vortmann, *Monatsh.*, **6**, 439 (1885).

(5) A. Werner and A. Mylius, *Z. anorg. Chem.*, **16**, 252 (1898).

(6) It was found that several M_1 salts could be made by precipitation. Solutions of I in 40% phosphoric acid were found to give precipitates when added to solutions of various salts in water—among them ammonium bromide, potassium ferricyanide and potassium permanganate. These solids all show paramagnetic resonance spectra and ultraviolet absorption bands corresponding to those of the known M_1 salts and seem to be M_1 salts of the appropriate anions.

(7) A. Werner, *Ber.*, **40**, 4600 (1907).

(8) A. Werner, *Ann.*, **375**, 6 (1910).

(9) A. Werner, ref. 8, p. 70.

TABLE II
SOLUBILITIES OF THE PEROXO-DICOBALT SALTS IN VARIOUS ACIDS

Salt	H ₂ O	H ₂ SO ₄	H ₃ PO ₄	HF 40%	HCl 35%	HClO ₄ 70%	HNO ₃ 70%
M ₁ (SO ₄) ₂ ·HSO ₄ ·3H ₂ O	Sl. sol.	Sol. in acid stronger than ~50%	Sol. in acid stronger than ~50%	V. sol.	Insol.	Insol.	Insol.
M ₁ (NO ₃) ₅	Sol., dec.	Sol. in acid stronger than ~50%	Sol., incr. as acid concn. increases	Sol.	Insol.	Insol.	Insol.
M ₁ (ClO ₄) ₅	Sol., dec.	Sol. in acid stronger than ~50%	Sol., decr. as acid concn. increases	Sol.	Insol.	Insol.	Insol.
M ₂ (NO ₃) ₄	Sol., dec.	Sol.	Sol., decr. as acid concn. increases	Sol.	Sl. sol., dec.	Sl. sol.	Insol.
M ₂ '(NO ₃) ₄	Sol.	Sol.	Sol.	Sol.	Sol.	Sol.	Sol.

when poured into a glass beaker gave a green precipitate which showed the ultraviolet and EPR spectra typical of derivatives of M₁ and may have been a fluorosilicate. All the salts were decomposed by base, giving brown solutions or precipitates. The various compounds were insoluble in organic solvents, with the exception of the perchlorates III and V; these were very soluble in acetone and slightly soluble in tetrahydrofuran, nitrobenzene and acetonitrile.

All the solutions of M₁ salts were an intense, deep green. Solutions of compounds IV and V were brown, and those of salt VI were olive-green; these colors appeared considerably less intense than those of the M₁ salts. The ultraviolet absorption spectra of all the compounds are described elsewhere.¹⁰

3. Stabilities.—We have used the ultraviolet and the magnetic resonance spectra as criteria of stability. None of the compounds was stable indefinitely as a solid under normal laboratory conditions. The perchlorate III, when pure and dry, decomposed in the open air in a day or two, giving a greenish-brown powder. The other compounds were more stable in the solid state; nonetheless, the shapes and widths of the resonance lines of the powders changed markedly in each case over a period of a month.

Solutions of compounds II, III and IV in pure water decomposed in times which depended on the anion and on the concentration of the solution. Solutions of II were the least stable, decomposing in a matter of minutes at room temperature. Strong solutions of III [$\sim 0.1 M$] also decomposed in a few minutes at room temperature, but dilute solutions [$\sim 0.01 M$] could be kept without apparent change for several days. Solutions of IV of comparable strength were rather more stable. In each case, decomposition was rapid once it had begun; the solution turned brown and ammonia was evolved. The process could be inhibited by one drop of phosphoric acid. Solutions in strong acid were stable indefinitely; a sample of I dissolved in 80% phosphoric acid gave an EPR spectrum which did not change in three months.

4. Apparatus.—The magnetic resonance spectrometer used was the Varian model V-4500, operated at 9500 Mc./sec. with a rectangular reflection cavity. The solutions were held in glass capillaries for the EPR measurements, and powders were studied in 5 mm. glass tubes. Derivative curves of the absorption lines were traced out with a Varian G-10 recorder.

Results

The magnetic resonances of the peroxo-dicobalt complexes studied here were intense at room temperature, in contrast to the resonances in Co²⁺ compounds. The powdered M₁ salts gave roughly symmetrical derivative spectra, with constant *g*-factor but with line widths which varied with the anion. Salts of dibridged cations (IV-VI) gave spectra with unsymmetrical derivatives, the low field side being the broader; the line widths also depended on the anion. The observed line widths (between points of maximum slope) for the powders are set out in Table III.

TABLE III

APPROXIMATE WIDTHS OF THE MAGNETIC RESONANCE LINES OF THE PEROXO-DICOBALT SALTS AS POWDERS, MEASURED BETWEEN POINTS OF MAXIMUM SLOPE

Salt	Line width, oersted
M ₁ (SO ₄) ₂ ·HSO ₄ ·3H ₂ O	170
M ₁ (NO ₃) ₅	150
M ₁ (ClO ₄) ₅	120
M ₂ (NO ₃) ₄	90
M ₂ (ClO ₄) ₄	260
M ₂ '(NO ₃) ₄	150

Solutions of the monobridged perchlorate III in water gave spectra which showed no hyperfine structure and were slightly asymmetric, the high field side being slightly the broader (see Fig. 1a). Addition of phosphoric acid caused marked changes in the spectrum. As the acid concentration increased, hyperfine structure developed on the low-field side and the center of the derivative curve; definite structure could be detected at a minimum acid concentration of about 20%. At a concentration of 50–60% phosphoric acid, the spectrum showed optimum resolution, with the hyperfine structure present on both sides of the derivative but with the low-field side much the more clearly resolved. At higher acid concentrations, the spectrum became slightly less well resolved. The other M₁ salts I and II gave spectra indistinguishable from these within their solubility ranges in phosphoric acid. The spectra for various phosphoric acid concentrations are shown in Fig. 1. Solutions in sulfuric acid gave similar results, but with somewhat better resolution of the hyperfine structure. At optimum resolution, fifteen equally spaced lines could clearly be distinguished (see Fig. 2a). The over-all line width and shape (disregarding the structure) did not vary much over the whole range, and the *g*-factor remained at 2.025. The spacing between the peaks was 11.4 ± 0.3 oe., and no significant change in this value was detected for any of the M₁ salts in any solvent. For a fixed acid-water ratio, the spectrum changed very little as the concentration of the complex was varied.

Although salt I is insoluble in water, it could be brought into solution by aqueous KF and gave spectra like that shown in Fig. 1a. Solutions of III in acetone at room temperature gave symmetrical spectra with hyperfine structure just visible near the center of the line (Fig. 3a).

(10) I. Bernal, unpublished work.

In order to see how the EPR spectra were affected by viscosity, solutions of constant acidity were studied in which the macroscopic viscosity was altered in different ways. When activated silica was added to aqueous solutions of III, slightly acidified to stabilize the complex, no change in the spectrum was observed over the range of viscosity from water to almost solid jelly. When gelatin was used, hyperfine structure became visible near the center of the line at the highest (jelly-like) viscosity, but there was little other change.

The EPR spectra of solutions of the dibridged salts differed from those of the M_1 complexes. Aqueous solutions of IV gave a slightly asymmetric spectrum of 15 almost completely resolved hyperfine lines with intensity ratios of 1:2:3:4:5:6:7:8:7:6:5:4:3:2:1, as shown in Fig. 4a. When phosphoric acid was added, the individual lines became less sharp and blurred together on the low field side as the acid concentration increased (see Fig. 4). Thus the asymmetry of these spectra is just opposite to that of the M_1 series. In concentrated phosphoric acid, only vestiges of the structure remained at the high field end of the curve (Fig. 4e). Similar spectra were obtained in sulfuric acid, except that the resolution was better at any given acid concentration. In concentrated sulfuric acid, more structure remained at the high field end, as shown in Fig. 2b. Both nitric acid and perchloric acid had similar but less prominent effects than phosphoric or sulfuric acid. A solution of IV in 70% perchloric or nitric acid had lost much of the resolution on the low field side, but 15 peaks were still distinguishable; the resolution was somewhat better in nitric acid. The over-all line width remained fairly constant and was the same as that of the M_1 salts, as was the g -factor. The spacing of the hyperfine components was slightly larger (12.7 ± 0.3 oe.).

Solutions of IV in heavy water gave spectra that were indistinguishable from those in ordinary water. A solution of the M_2 perchlorate V in acetone gave a spectrum very similar to that of IV in water (Fig. 3c); so did an aqueous solution of the ethylenediamine (M_2') nitrate (VI).

The M_2 spectra were studied as a function of macroscopic viscosity in water slightly acidified with phosphoric acid. No change was found with silica content up to jelly-like consistency, but gelatin did cause the individual lines to broaden, blurring resolution especially on the low field side. These asymmetric spectra looked very much like those in intermediate acid concentrations pictured in Fig. 4. A sample of IV in silica jelly which had been dehydrated to powder form by pumping showed a broad line (165 oe.) with no structure.

The changes in the spectra with temperature were also studied. Solutions were heated or cooled in the microwave cavity by a stream of nitrogen gas which was first passed through either a furnace or a suitable cooling-bath (such as Dry Ice-acetone or liquid nitrogen). Aqueous solutions of M_1 at temperatures just above their freezing point gave spectra in which hyperfine structure was quite well resolved and which were slightly asymmetric; these were similar to the curve of M_1 in 40% phos-

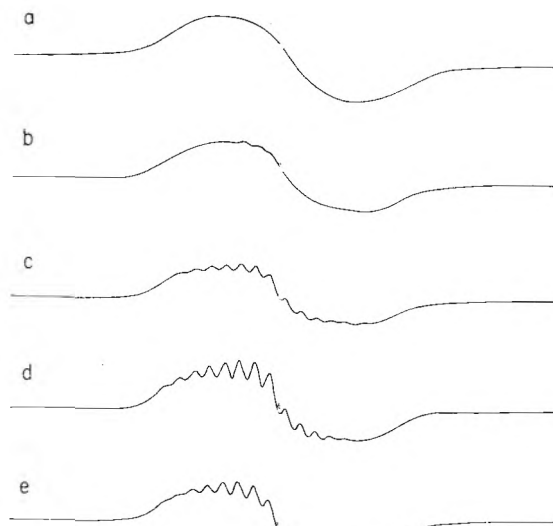


Fig. 1.—EPR spectra of $[(\text{NH}_3)_6\text{Co}-\text{O}-\text{O}-\text{Co}(\text{NH}_3)_6]^{+6}$ in aqueous phosphoric acid, as a function of acid concentration at room temperature. The approximate acid concentrations are: for curve (a), 0%; for curve (b), 20%; for curve (c), 40%; for curve (d), 60%; for curve (e), 80% H_3PO_4 .

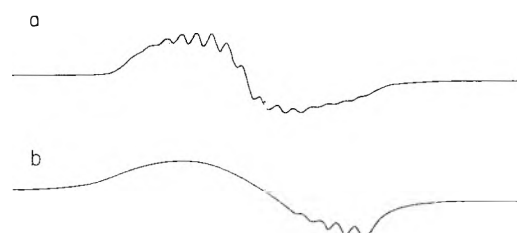


Fig. 2.—EPR spectra of $[(\text{NH}_3)_6\text{Co}-\text{O}-\text{O}-\text{Co}(\text{NH}_3)_6]^{+6}$ (curve a) and $[(\text{NH}_3)_4\text{Co}-\text{NH}_2-\text{Co}(\text{NH}_3)_4]^{+4}$ (curve b) in 95% sulfuric acid, both at room temperature.

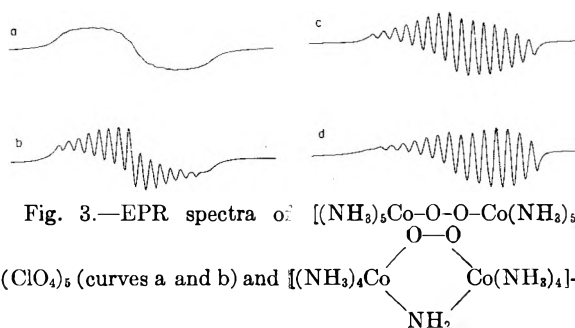


Fig. 3.—EPR spectra of $[(\text{NH}_3)_5\text{Co}-\text{O}-\text{O}-\text{Co}(\text{NH}_3)_5]^{+6}$ (ClO_4)₆ (curves a and b) and $[(\text{NH}_3)_4\text{Co}-\text{NH}_2-\text{Co}(\text{NH}_3)_4]^{+4}$ (ClO_4)₄ (curves c and d) dissolved in acetone. Curves (a) and (c) at room temperature, curves (b) and (d) at ca. -50° .

phoric acid shown in Fig. 1c. Heating solutions of M_1 in concentrated acid to $50-60^\circ$ caused peaks to broaden, with resulting loss of resolution. Cooling these solutions in concentrated acid gave spectra which lost their resolution on the low field side but gained greatly in the resolution of the structure on the high field side. The hyperfine spacing remained unaltered. In concentrated acid cooled all the way to the glassy state, M_1 showed a very complicated and poorly resolved spectrum which appeared to be composed of more than one set of

hyperfine lines with different spacings. One set of peaks could be distinguished with spacing of about the value observed at room temperature, and another with spacing almost twice as large. Solutions of M_1 perchlorate III in acetone were cooled to *ca.* -70° and showed well resolved and asymmetric spectra as shown in Fig. 3b.

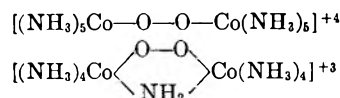
Aqueous solutions of M_2 cooled to just above their freezing temperature showed spectra very much like those obtained at room temperature except for increased asymmetry which caused the low field peaks to be somewhat less prominent and the high field peaks to be more distinct than at room temperature. These solutions when heated to $50-60^\circ$ gave spectra which again resembled the room temperature curves except that they were more symmetric and the individual peaks were slightly broader. For liquid solutions of M_2 in concentrated sulfuric acid, the peaks remaining at the high field side (Figs. 2b and 4e) became better resolved as the temperature increased; solutions in the same acid cooled to glassy consistency gave complicated, poorly resolved spectra which in many ways resembled those of M_1 . Solutions of M_2 perchlorate V in acetone at *ca.* -70° gave spectra (Fig. 3d) which were even more asymmetric than those of the cooled aqueous solutions. Aqueous solutions of both M_1 and M_2 below their freezing points gave very broad spectra with essentially no structure.

NOTE ADDED IN PROOF.—Solutions of $M_1(\text{NO}_3)_5$ and $M_2(\text{NO}_3)_4$ in liquid ammonia at *ca.* -50° gave spectra which were affected by the ammonium acid NH_4NO_3 very much as the spectra of aqueous solutions were affected by aqueous acids.

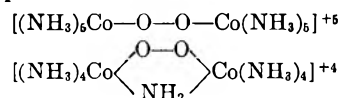
The behavior of the M_1 and M_2 spectra were studied as a function of microwave power within the limited range afforded by the Varian-6315/V-153 klystron, which furnished a maximum of approximately 90 milliwatts at the resonant cavity. It was found that most of the spectra showed evidence of saturation effects at the highest powers, as could be most easily seen by improved resolution when the power was lowered. The solutions in acid showed the strongest effects. With 20 and 40% solutions of M_2 in phosphoric acid, decreasing the power from its maximum by a factor of 10 resulted in blurring of the low field side and enhancement of the high field resolution. The structure remaining at the high field end in solutions of M_1 in concentrated acid was enhanced by lowering the power. For the M_1 complexes in water, very little effect was observable, whereas solutions in concentrated acid gave improved resolution at lower powers, with no blurring of some peaks such as occurred in M_2 . The structure of the spectra in acetone solutions of III also became more prominent as power decreased.

Discussion

When the peroxo-dicobalt complexes are considered from the viewpoint of electronic structure, they fall into two classes. Compounds of the first type have cationic charges which can be understood if the two cobalt atoms are regarded as both trivalent; the complexes are diamagnetic, as would be expected. Examples of this type are



Compounds of the second type contain cations with the same atomic skeletons as those of the first but have charges greater by one unit. These complexes are paramagnetic; the observed magnetic moments lie between 1.60 and 1.69 Bohr Magnetons,^{2,11,12} consistent with the presence of one unpaired electron. In several cases, these compounds have been prepared by direct oxidation of the corresponding members of the first type.¹³ We are concerned with complexes of this second type, examples of which are



Here the valence structure is more difficult to understand in conventional terms. Werner¹⁴ suggested that one cobalt atom is trivalent and the other is tetravalent. Malatesta¹¹ extended this idea by proposing that a resonance process could make the two cobalt atoms equivalent and of valency intermediate between three and four. It has also been suggested^{2,15,16} that the structures and many of the reactions of these salts can be understood if the two cobalt atoms are considered to be of valency three, coordinated to an O_2^- bridge.

These proposed structures differ essentially in the location of the unpaired electron. In Werner's structure, it would be localized on one cobalt, whereas in Malatesta's structure it would be delocalized over the bridge and both cobalt atoms. In the O_2^- structure, the electron would be confined to the oxygen atoms. Since the common isotope of cobalt (Co^{59} , 100% abundance) has a nuclear spin $I = 7/2$, observation of the hyperfine structure in the paramagnetic resonance absorption of a magnetically dilute sample offers a way of distinguishing between these structures. As will be discussed in more detail below, one would expect to find $2I + 1 = 8$ lines if the electron spends its time on only one cobalt, $2(I_a + I_b) + 1 = 15$ lines if it spends its time equally on both cobalt atoms and $(2I_a + 1)(2I_b + 1) = 64$ lines if it interacts with both cobalt atoms, but with unequal intensity. The oxygen atoms would not contribute hyperfine lines, since O^{16} has no nuclear magnetic moment.

The presence of hyperfine structure with 15 equally-spaced components in the paramagnetic resonance spectra of these ions in solution indicates clearly that the unpaired electron spends equal fractions of time on the two cobalt nuclei. The same fact has been adduced from the anisotropy and intensity of the ultraviolet absorption bands.¹⁷

(11) L. Malatesta, *Gazz.*, **72**, 287 (1942).

(12) V. I. Belova and Ya. K. Syrkin, *Izvest. Sekt. Plat. y Drug. Blag. Metal Inst. Obshch. i Neorg. Khem. Akad. Nauk S.S.S.R.*, **30**, 109 (1955).

(13) L. R. Thompson and W. K. Wilmarth, *THIS JOURNAL*, **56**, 5 (1952).

(14) A. Werner, *Ann.*, **375**, 9 (1910).

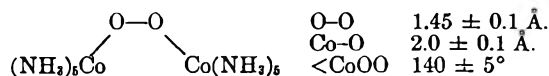
(15) J. D. Dunitz and L. E. Orgel, *J. Chem. Soc.*, 2594 (1953).

(16) W. Jakob and M. Ogorzalek, *Roz. Chem.*, **30**, 1064 (1956).

The over-all line width, the spacing between the hyperfine peaks when they are distinct and the g -factor vary little for all the complexes studied and for all solvents and concentrations used. This indicates that the unpaired electron is not very much affected by the changes in the ligand properties or in the solvent characteristics. The fact that no additional splittings are seen shows that the unpaired electron density on any ligand hydrogen or nitrogen atoms must be very small. Furthermore, since no dependence on the concentration of the complex in solution was observed for the ranges available, it is reasonable to dismiss dipolar interactions and exchange between solute molecules as unimportant. The line width of the individual hyperfine components is therefore caused by anisotropy broadening, by small hyperfine splittings from the ligands or by lifetime effects.

As can be seen in Figs. 1-4, the EPR spectra of M_1 and M_2 differ and have unusual line shapes which depend on the solvents used. In order to discuss these features, it is necessary to consider the electronic structures of the two cations in more detail.

Recent X-ray work by Okaya¹⁸ has shown that in single crystals of monobridged M_1 nitrate (II) the cation has the structure



The cobalt and oxygen atoms are co-planar; the ligands from each cobalt atom are octahedrally arranged around it, and the two octahedra are "cis" to one another. Mellor and Stephenson¹⁹ have made an X-ray study of the sulfates of this cation. No structure for any M_2 salt has yet been published.

Dunitz and Orgel¹⁶ have discussed the electronic structures of the two cations $[(\text{NH}_3)_5\text{Co}-\text{O}-\text{O}-\text{Co}(\text{NH}_3)_5]^{+4}$ and $[(\text{NH}_3)_5\text{Co}-\text{O}-\text{O}-\text{Co}(\text{NH}_3)_5]^{-5}$ from the molecular orbital point of view, using group theory. They considered a linear $\text{Co}-\text{O}-\text{O}-\text{Co}$ structure; the σ -orbitals involved may be regarded as built from cobalt orbitals and sp-hybrids of oxygen. There are two degenerate sets of four π -orbitals; the electronic structure of this part of the diamagnetic, tetrapositive ion may be represented as $(\sigma_b)^6(\pi_b)^4(\pi_b')^4(\pi_a)^4(\pi_a')^4$, where the subscripts "a" and "b" describe antibonding and bonding orbitals, respectively.²⁰ They concluded that there should be little resistance to bending the atomic skeleton; hence the $\text{Co}-\text{O}-\text{O}$ angles will be determined largely by steric and electronic repulsions.

For the paramagnetic ion $[(\text{NH}_3)_5\text{Co}-\text{O}-\text{O}-\text{Co}(\text{NH}_3)_5]^{+5}$ the situation is different. Here, if the skeleton were linear, the unpaired electron would be in an antibonding π -orbital, and the

ground state therefore degenerate. According to the Jahn-Teller theorem,²¹ the ion must distort in order to destroy this degeneracy and so bending of the atomic skeleton is to be expected. We shall for simplicity consider that the cobalt and oxygen atoms remain coplanar and that the two $\text{Co}-\text{O}-\text{O}$ angles are equal, as in the compound studied by Okaya. In that case, the set of π -orbitals with lobes projecting out of the $\text{Co}-\text{O}-\text{O}$ plane will be relatively little affected; as the $\text{Co}-\text{O}-\text{O}$ angles decrease, the π -orbitals in the plane of bending will become more like orbitals localized on the cobalt and oxygen atoms. The bending itself involves rehybridization of the σ -orbitals of the oxygen atoms; the sp-orbitals which gave linear σ -bonds will become intermediate between sp and sp²-, the s-character decreasing as the $\text{Co}-\text{O}-\text{O}$ angles approach 120°. At the same time, those orbitals (derived from the in-plane π -system) which are more or less localized on the oxygen atoms will change from p- to sp²- in character. At a $\text{Co}-\text{O}-\text{O}$ angle of 120°, the σ -bonds from oxygen can be regarded as formed from sp²-orbitals, with a third sp²-orbital on each oxygen atom directed at 120° from the $\text{Co}-\text{O}$ and $\text{O}-\text{O}$ directions and containing a lone pair of electrons. Hence it is clear that the lone pair orbitals will be definitely directed in space when the $\text{Co}-\text{O}-\text{O}$ angles are 120°.

This discussion has neglected all refinements of the crudest model. Nonetheless, the general trends which it brings out should give some idea of the change in electronic character of the $\text{Co}-\text{O}-\text{O}-\text{Co}$ system with $\text{Co}-\text{O}-\text{O}$ angle. The factors which will determine the precise $\text{Co}-\text{O}-\text{O}$ angle in the M_1 cation are very complicated. The Jahn-Teller principle suggests that it will bend; the extent of the bending will be decided by the competing influences of orbital overlap and steric and interelectronic repulsions. Hydrogen bonding is yet another factor which must be considered; such bonding is almost certainly responsible for the "cis" arrangement of the cobalt atoms in the crystalline M_1 nitrate. There is no reason to suppose that this "cis" arrangement will persist in solution, where steric repulsion is likely to lead to a "trans" configuration; since in the "cis" arrangement the distance between the nearest nitrogen atoms bound to different cobalt centers is between 2 and 4 Å., such repulsions must be considerable. However, if the cobalt groups are free to rotate relative to one another, unless there is very strong intramolecular hydrogen bonding (which is sterically unlikely) it seems improbable that the $\text{Co}-\text{O}-\text{O}$ angles will be less than they are in the solid state.

In the M_2 ion, if the $\text{Co}-\text{O}$ and $\text{O}-\text{O}$ distances are assumed to be the same as they are in $M_1(\text{NO}_3)_5$ and reasonable values are taken for the $\text{Co}-\text{N}$ distances, the geometry of the ring system makes the $\text{Co}-\text{O}-\text{O}$ angles likely to be about 120°. Moreover, the two cobalt atoms are rigidly held "cis" to one another. Hence in this ion the lone pair orbitals are both strongly directed away from the ring, giving rise to a region of high electron density.

(17) S. Yamada, Y. Shimura and R. Tsuchida, *Bull. Chem. Soc. Jap.*, **26**, 72 (1953).

(18) Y. Okaya, unpublished and preliminary results of experiments under Contract AF 1(600)-1556, Air Force Office of Scientific Research, ARDC—Chemistry Branch.

(19) D. P. Mellor and N. C. Stephenson, unpublished.

(20) There is a non-bonding d-orbital on each cobalt atom, containing an electron-pair and of energy probably comparable with π_b' and π_a' . These orbitals have been neglected in the discussion, since they take no direct part in bonding.

(21) H. A. Jahn and E. Teller, *Proc. Roy. Soc. (London)*, **A161**, 220 (1937).

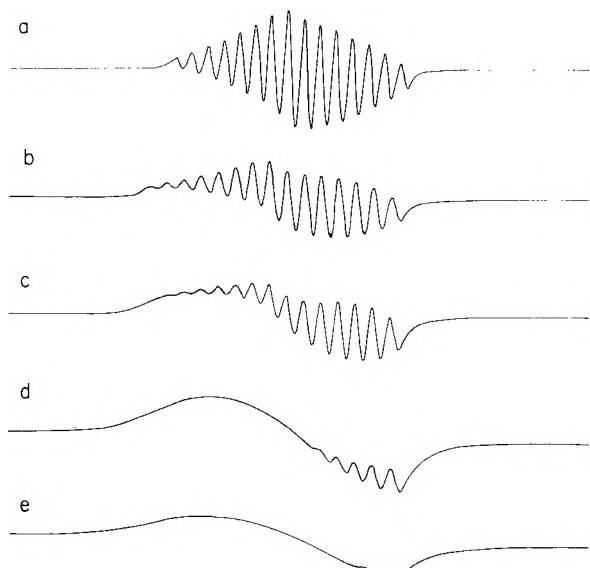


Fig. 4.—EPR spectra of $[(\text{NH}_3)_4\text{Co}(\text{O}-\text{O})\text{Co}(\text{NH}_3)_4]^{+4}$ in aqueous phosphoric acid, as a function of acid concentration at room temperature. The approximate acid concentrations are, for curve (a), 0%; for curve (b), 20%; for curve (c), 40%; for curve (d), 60%; for curve (e), 80% H_3PO_4 .

The bond lengths observed in $\text{M}_1(\text{NO}_3)_6$ have some relevance to the question of electronic structure. If the anti-bonding π -orbital containing the unpaired electron were largely located on the oxygen atoms, the O—O distance might be expected to be close to that observed in the O_2^- ion (1.28 Å).²² Our magnetic resonance measurements show that the electron interacts strongly with both cobalt nuclei and that therefore it cannot be in an orbital concentrated on the peroxo-bridge; the antibonding π -orbital must extend over the cobalt atoms as well. This leads us to expect an O—O distance closer to that observed in hydrogen peroxide (1.49 Å).²³ Okaya's value of 1.45 Å. agrees well with this. At the same time, any direct cobalt-cobalt bonding¹⁴ is most unlikely; the two cobalt atoms are at least 4 Å. apart in $\text{M}_1(\text{NO}_3)_6$.

The behavior of an unpaired electron moving in a molecule in the presence of an externally applied magnetic field H_0 is described in a first approximation by a Hamiltonian of the form

$$H = g\beta\vec{H}_0\vec{S} + (\sum_j A_j \vec{I}_j) \cdot \vec{S}$$

Here g is the spectroscopic splitting factor, β is the Bohr Magneton and \vec{S} is the electron spin operator, which is taken here for spin $1/2$. The interaction of the electron with nuclei having angular momentum operators \vec{I}_j is given by the second term. It can be shown²⁴ that for molecules tumbling freely in space, the quantity A_j essentially

measures the probability density of the unpaired electron near nucleus j . The second term of the Hamiltonian causes the magnetic resonance spectrum to exhibit a maximum of $\prod_k (2I_k n_k + 1)$

hyperfine components, where the product is taken over all non-equivalent groups, each containing n_k equivalent nuclei. Equivalence of two nuclei is defined to mean that they have the same value of A_j and of I_j . In our case, the only nuclei of importance are the two cobalt atoms, so that we obtain the number of lines discussed previously. Since each line is of finite width and since lines may overlap, it may happen that not all of these lines are resolved.

The relative areas under the hyperfine components arising from n equivalent nuclei are determined by the possible configurations of their independent nuclear spins, and are given by the coefficients in the series $(\sum_m x^m)^n$ (each coefficient is the sum of all the multinomial coefficients $n!/\pi_j n_j!$ for which $\sum_m m \cdot n_m$ equals the total nuclear spin component labelling the line in question). Here m is the spin component of the individual nucleus, ranging from $-I$ by integers to $+I$, and n_m is the number of nuclei with component m . In our case $n = 2$ and $I = 7/2$, and we arrive at the ratios quoted previously.

The hyperfine spectrum arising from equivalent nuclei will consist of equally spaced lines occurring at applied magnetic fields $(h\nu - A \sum_j m_j)/g\beta$, providing that the value of A is small compared to $g\beta H_0$.²⁵

The presence of the hyperfine structure in the EPR spectra shows that the unpaired electron must have finite probability near both cobalt nuclei. It follows that the molecular orbital in which the electron moves may be built partly from cobalt s orbitals. Abragam and Pryce²⁶ have discussed a possible mechanism, invoking configurational interaction with an excited state in which s electrons are unpaired and have shown that the amount of s character required need not be large. It is difficult to estimate quantitatively the relative fractions of the electron density on the cobalt atoms and on the oxygen bridge. Magnetic resonance experiments using O^{17} could shed more light on this question.

The changes in the resolution, and the marked asymmetry of the spectra under some conditions, can be at least partly understood if one makes the additional assumption that the spin energy levels are not isotropic. This can come about because the direction of quantization of the electron spin will to some extent be determined by the nature of the local electromagnetic field. The

(25) In the next higher approximation, the expression derived by Bleaney [*Phil. Mag.*, **42**, 441 (1951)] indicates that there will be 36 lines rather than the 15 expected in first approximation. This further splitting is largest for the center peak, which breaks up into 4 components; the splitting between the outermost of these is only ~ 0.15 oe., which is small compared to the line width. Therefore we would not expect to observe this secondary effect.

(26) A. Abragam and M. H. L. Pryce, *Proc. Roy. Soc. (London)* **A205**, 135 (1951).

(22) S. C. Abrahams and J. Kalnajs, *Acta Cryst.*, **8**, 503 (1955).

(23) S. C. Abrahams, R. L. Collin and W. N. Lipscomb, *ibid.*, **4**, 15 (1951).

(24) S. I. Weissman, *J. Chem. Phys.*, **22**, 1378 (1954).

electric fields caused by the nuclei and electrons making up the molecule in question, and by its immediate surroundings, do not in general affect the spin of the electron directly. However, they will tend to line up the spin indirectly *via* their influence on the orbital motion of the electron; this in turn will affect the spin because of the magnetic spin-orbit coupling. When an external magnetic field H_0 is present, there will therefore be competition between the local electric field and H_0 . If H_0 is large enough, the local field effects can be treated as a perturbation of the Zeeman states; they are conveniently taken into account by re-writing the main term of the Hamiltonian in the form $\beta \bar{S} \cdot \bar{g} \cdot H_0$. Here \bar{g} is a second-order symmetric tensor, with principal values which will deviate from the free electron value of 2.0023 according to the strength and symmetry of the local field effects.

Furthermore, when there is interaction of nuclear magnetic moments with the electron in question, the hyperfine interaction may also become anisotropic, because the axis of quantization of each nucleus is determined by both the orbital magnetic moment and the spin magnetic moment and to a much smaller extent by direct interaction with H_0 . The second term in the Hamiltonian previously written will then be taken as $\sum_j \bar{I}_j \cdot \bar{A}_j \cdot \bar{S}_j$, where \bar{A}_j is also a second rank tensor and j is summed over all nuclei with non-zero spin \bar{I}_j which contain appreciable unpaired electron density, *i.e.*, $\bar{A}_j \neq 0$.

For a stationary molecule, the local field configuration is at a fixed orientation relative to the applied magnetic field and the energies are constant with time. If, however, the molecule vibrates or tumbles, the two terms will be functions of time and can lead to paramagnetic relaxation effects. Thus if \bar{g} and \bar{A} are not isotropic, the energy eigenvalues will be a function of time, and there will be transitions between the spin energy levels, with energy interchanging with the molecular motions. Furthermore, the various possible orientations of the molecules lead to a whole spectrum of possible resonant applied fields H_c and hence give rise to line broadening. The actual line width (measured by $1/T_2'$) will be determined by the competing mechanisms of this anisotropy broadening (described by the reciprocal of the transverse relaxation time T_2') and lifetime broadening (associated with the spin-lattice relaxation time T_1); an approximate relationship between these quantities is

$$\frac{1}{T_2} \approx \frac{1}{T_1} + \frac{1}{T_2'}$$

and hence the smaller of T_1 and T_2' will determine the width, in the absence of other effects. When a line is broadened because of anisotropy effects, it will usually become asymmetric, causing this relationship to lose its exact meaning. A very approximate treatment of these effects has been published by McConnell,²⁷ who limited himself to axial symmetry for both \bar{g} and \bar{A} . With this

assumption, McConnell's expressions for our case are

$$1/T_1 \geq (8\pi^2/15)[\Delta g \beta H_0 + \Delta A(m_a + m_b)]^2 h^{-2} \tau_c / (1 + 4\pi^2 \nu_0^2 \tau_c^2)$$

$$(1/T_2')^2 \geq (32\pi/45)[\Delta g \beta H_c + \Delta A(m_a + m_b)]^2 h^{-2} \tan^{-1}(2\tau_c/T_2')$$

Here τ_c is the correlation time given by $\tau_c = 4\pi \eta R^3/3kT$, where η is the viscosity of the medium restricting the motions of the molecule, and R is an effective radius of the molecule. The terms Δg and ΔA are defined, respectively, to mean $g_{||} - g_{\perp}$ and $A_{||} - A_{\perp}$. The subscripts a and b here label the two cobalt atoms. The inequality sign serves as a reminder that other physical processes can cause shorter relaxation times and can thus be more effective. When ν_0 is a microwave frequency, we will expect that $4\pi^2 \nu_0^2 \tau_c^2 \gg 1$. These expressions indicate that the observed width and relaxation time of each hyperfine component can depend both on the temperature and viscosity of the solvent. At low viscosities and high temperatures, the tumbling is rapid and the anisotropy effects tend to average out, so that only the mean values of the three principal values of \bar{g} and of \bar{A} are observed. As the molecular motions decrease, the factor $1/T_1$ goes through a maximum, whereas $1/T_2'$ becomes continuously larger, leading to very broad lines in the upper limit of stationary, randomly oriented molecules. Furthermore, the widths and relaxation times depend on the value and sign of the nuclear spin component m , so that different hyperfine components can have different line shapes. Such effects have been observed in solutions of certain copper complexes.^{28,29} In our case, where the hyperfine lines overlap more or less strongly, the anisotropy effects can lead to the rather strange asymmetric line shapes observed.

Because of the difficulties involved in resolving the observed spectra, we have calculated line shapes by synthesis from 15 suitably chosen curves. These were taken equally spaced, with areas in the ratios 1:2:3:4:5:6:7:8:7:6:5:4:3:2:1. The total derivative curve for gaussian lines can therefore be written as

$$f(x) = \sum_{m=-7}^{m=+7} (8 - |m|) \frac{x + md}{(c_0 + mc)^6} \exp \left[-\frac{(x + md)^2}{(c_0 + mc)^4} \right]$$

Here x is proportional to the applied field H_0 , and d is the spacing of the components. The quantity $(c_0 + mc)^2$ is just the width between points of maximum slope of the Gaussian, divided by $2^{1/2}$. The parameters c_0 and c therefore determine, respectively, the basic width and the change in width with component peak. This choice of function for the width is consistent with the form of the above equations for the relaxation times. The function $f(x)$ for Lorentzian lines can be written in a completely analogous form, involving the same parameters. We can distinguish between the cases

$$d \gg (c_0 + mc)^2 > c \quad \text{components resolved}$$

$$(c_0 + mc)^2 \gg d > 0 \quad \text{components unresolved}$$

where

(28) B. R. McGarvey, *This Journal*, **60**, 71 (1956).

(29) B. R. McGarvey, *ibid.*, **61**, 1232 (1957).

(27) H. M. McConnell, *J. Chem. Phys.*, **25**, 709 (1956).

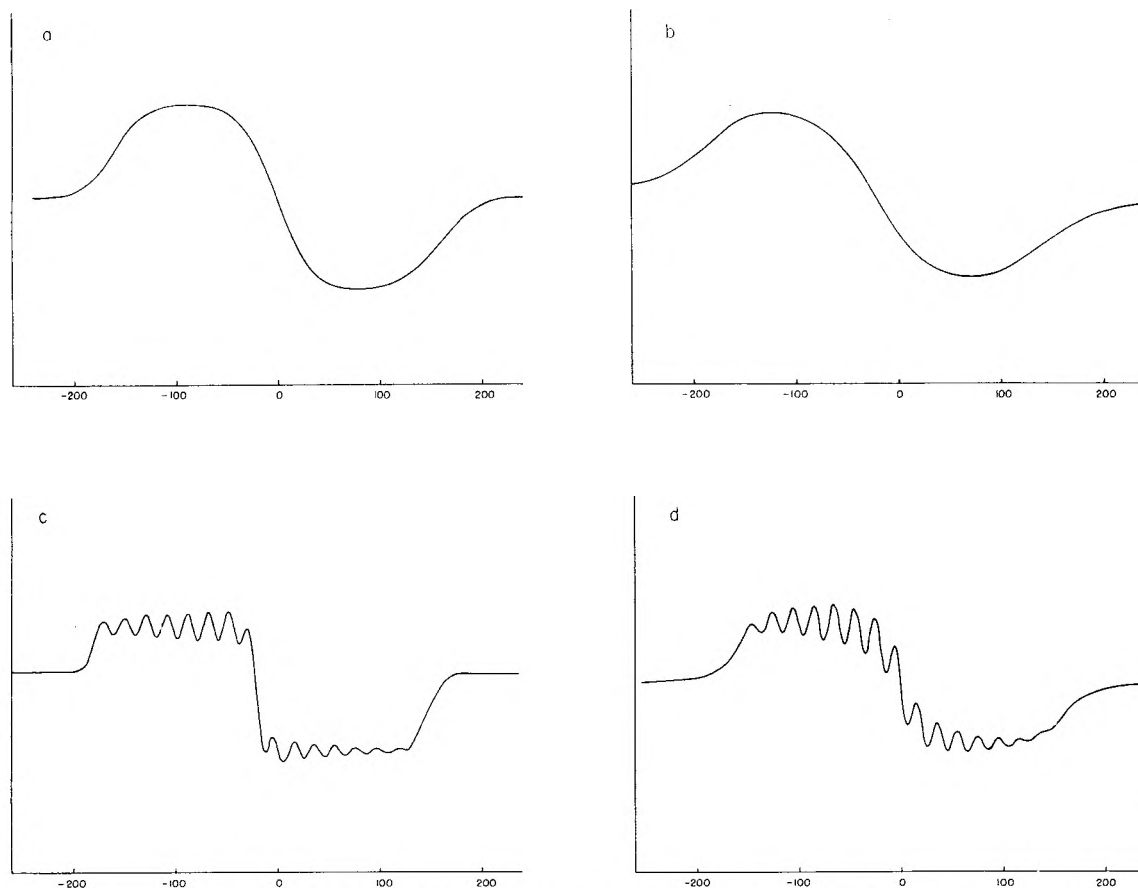


Fig. 5.—Calculated line shapes with spacing $d = 20$, and where (a) components are Gaussian, with $c_0 = 6.4$ and $c = 0.04$; (b) components are Lorentzian, with $c_0 = 6.4$ and $c = 0.04$; (c) components are Gaussian, with $c_0 = 3.9$ and $c = 0.02$; (d) components are Lorentzian, with $c_0 = 3.9$ and $c = 0.04$.

- (a) $|c_0| \gg c = 0$ produces no asymmetry, peaks of equal width
 (b) $|c_0| \gg |c| \neq 0$ produces small asymmetry
 (c) $|c_0| \sim |c|$ produces large asymmetry
 (d) $0 \neq |c_0| \ll |c|$ produces small asymmetry
 (e) $0 = c_0 \ll |c|$ produces no asymmetry, width of peaks increases from the center peak (which has "zero" width)

The function $f(x)$ was calculated, for suitably chosen d , for a variety of values of c_0 and c with the help of an IBM 650 computing machine. Selected curves are shown in Figs. 5 and 6. In a first approximation, the various line shapes observed can be reproduced quite accurately, and the asymmetric forms of the spectra can be synthesized for the entire range of acidity. The calculated line shapes, however, do not fit exactly for either Lorentzian or Gaussian curves; in general, the former furnished the better approximation, since the Gaussians gave curves with wings which returned to the baseline considerably faster than those observed experimentally. On the other hand, the spectrum of M_2 in water was reproduced almost exactly by a set of Gaussian components. The curves in Figs. 5 and 6 have been chosen as giving about the best correlation. No attempt has been made to find exact values of c and c_0 , because of the uncertainty in the individual line shapes; the parameters quoted give only an approximate indication of the actual width parameters.

Since the hyperfine components in the spectrum of M_1 broaden, whereas those of M_2 become narrower, as the applied magnetic field increases (see Figs. 1 and 4), it seems probable that the sign of $\Delta g/\Delta A$ is positive for M_1 and negative for M_2 . The factors which affect the anisotropy of \bar{g} and \bar{A} are the spin-orbit coupling and the strength and symmetry of the local electric fields; these fields can arise not only from within the molecule itself but also from interactions with the solvent. Moreover, the "cis" arrangement of the cobalt octahedra of M_1 in $M_1(\text{NO}_3)_6$ crystals is not likely to persist in solution. Values of \bar{g} and \bar{A} from single crystals^{30,31} should not therefore be used in discussions of the solution spectra, and we have no other data from which the values of \bar{g} and \bar{A} in solution may be deduced. From the geometry of the M_2 ion, it is clear that the lone pairs of electrons on the oxygen atoms will give rise to a local electric field perpendicular to the Co-Co axis. On the other hand, if the octahedra in M_1 are "trans" to one another, or rotate more or less freely about the O-O axis, the field due to the lone pairs will have a much smaller component perpendicular to the Co-Co axis, while the component along this axis will not vanish. It is possible that differences

(30) A preliminary account of \bar{g} measurements by E. E. Schneider for compound I has been presented at the Ampere Conference (Paris, 1958)—see also E. E. Schneider and J. Weiss, *Proc. Chem. Soc.*, 130 (1959).

(31) J. A. Weil and E. A. V. Ebsworth, unpublished results.

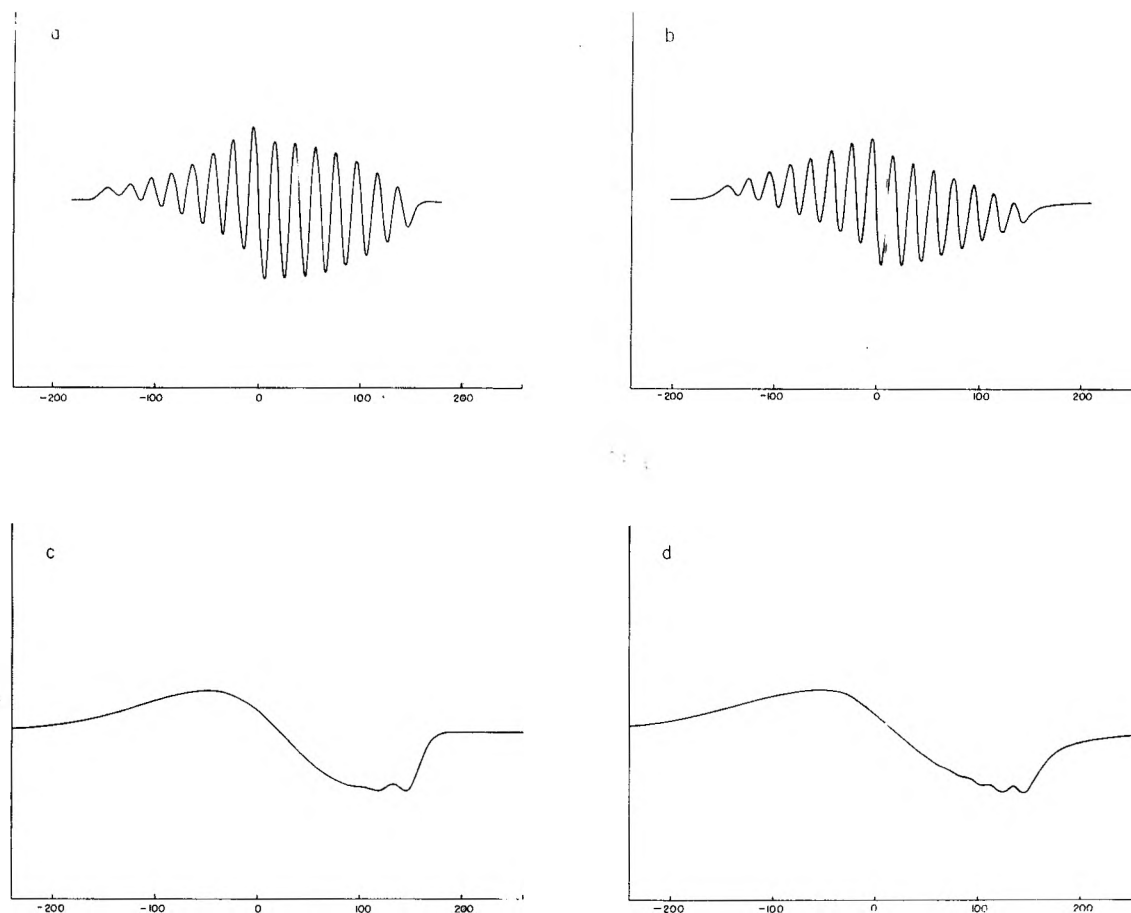


Fig. 6.—Calculated line shapes taken with spacing $d = 20$ and where (a) components are Gaussian, with $c_0 = 3.2$ and $c = 0.04$; (b) components are Lorentzian, with $c_0 = 2.9$ and $c = 0.02$; (c) components are Gaussian, with $c_0 = 7.5$ and $c = 0.48$; (d) components are Lorentzian, with $c_0 = 6.1$ and $c = 0.32$.

such as these will give rise to a change in the sign of the ratio $\Delta g/\Delta A$.

The solution spectra of M_1 and M_2 are affected in different ways by changes in acidity, viscosity and temperature. It is extremely difficult to separate these three variables even qualitatively from one another; for example, a change in the temperature of any solution is always accompanied by a change in its viscosity. An attempt was made to study the effect of changes in viscosity at constant temperature and acidity by using activated silica or with gelatin, but even large changes in macroscopic viscosity may give no real indication as to how the motions of the solute are affected on the molecular level. Since M_2 salts are somewhat soluble in 70% nitric and perchloric acids, whose viscosities are close to that of water, we have some idea of the changes in the M_2 spectra with acidity. Unfortunately, the solubility of M_1 salts in these acids is negligible. Acetone is both less viscous and less acidic than water, but the nature of the species present in solutions of M_1 and M_2 perchlorates in acetone is uncertain. From the complicated and inter-related set of facts observed, some deductions may be made about the relative importance of the various parameters in influencing the observed spectra.

Since hyperfine structure can be distinguished in the room temperature spectra of M_1 in acetone

but not in water, it appears that a relaxation mechanism is operating in aqueous solutions which is not effective in acetone. The improved resolution of hyperfine structure in sulfuric and phosphoric acids suggests that this involves acidity. Viscosity seems less important; when a solution of M_1 in strong phosphoric acid was heated to 50–60°, the resolution did not change very much, nor did the addition of gelatin to the aqueous solutions affect the spectra appreciably. It has already been shown that in both M_1 and M_2 there are lone pairs of electrons concentrated near each oxygen atom; these lone pairs are sites to which protons could readily become attached.^{13,16} In the M_1 ion, the large Co–O–O angle, the high cationic charge and the flexibility of the atomic skeleton all make it unlikely that such proton-oxygen bonding will be strong, and hence a rapid exchange of protons with the solvent would be expected; if such exchange were fast it could well provide a relaxation mechanism efficient enough to broaden the lines.

This relaxation mechanism, however, ought to become more efficient as the acidity of the environment increases; if the relaxation involves exchange of protons between the peroxy-bridge and anions or water molecules, the rate of exchange must increase with the concentration of protons.

On the other hand, it is known that NH_3 -groups

in cobalt ammines will exchange protons with water; the rate of this exchange depends on the concentration of hydroxyl ion in the solution and so drops as the acidity increases.³² Moreover, the rate at which ammonium ions exchange protons with the water in which they are dissolved has been shown by high resolution n.m.r. measurements to drop as the acid concentration increases³³; the single peak of the proton resonance spectrum in pure water splits into a triplet in acid solution, as a result of spin-spin interaction with the nitrogen atom.

It therefore seems possible that the acid-dependent relaxation mechanism may be connected with the lone pairs of electrons on the peroxy-bridge, with ionization of the NH_3 -groups bound to cobalt or with both of these. In any case, exchange must be rapid enough to maintain the equivalence of both cobalt atoms. In the *trans*-configuration, the oxygen atoms of the bridge could accept protons from the NH_3 -groups as well as from the solvent; hence relaxation might be affected by viscosity through restriction of the cation's internal motions.

The spectra of M_2 in acetone and water are almost indistinguishable at room temperature. Solutions in strong acids of low viscosity give spectra which are less symmetrical than those in water, but the over-all appearance is not very different. On the other hand, gelatin causes marked asymmetry and general broadening of the lines. In solutions which are both very viscous and strongly acidic, the asymmetry and broadening is pronounced; heating such solutions leads to much better resolution. It seems from this that viscosity is the more important factor for M_2 .

The different behavior of M_2 as compared with M_1 can be explained in part by the different proton affinities of the two ions. The smaller bond angle of M_2 , taken with the ring structure (which con-

centrates the lone-pair density) and the lower cationic charge would be expected to lead to much stronger oxygen-hydrogen and nitrogen-hydrogen bonding in M_2 than in M_1 . The proton exchange rate would be greatly reduced, and the contribution of such processes to relaxation could well become negligible. It may be noted that the diamagnetic analog of M_2 , which has a lower cationic charge, forms "acid" salts whose unusual stability has been interpreted as resulting from protolysis of the peroxy bridge.¹⁴

There is another important difference between the two cations; the atoms in M_2 are held in a comparatively rigid configuration because of the five-membered ring structure, while in M_1 there is no cross-linking to prevent internal motions. Such oscillations can afford another relaxation mechanism, which is likely to depend strongly on viscosity and temperature.

The spectra of solutions in water or acetone below room temperature show more asymmetry, probably because the increased viscosity brings out the anisotropy effects inherent from the molecular structure. The changes observed when strongly acidic solutions are cooled suggest that protons bind to the oxygen atoms for relatively long periods of time at low temperatures. The details of these spectra remain unexplained.

To summarize, the main features in the spectra of these complexes appear to be clearly understood and, taken with the other information available, form a reasonably consistent picture of their electronic structures. Some of the details of the spectra, although consistent with the proposed model, require further clarification; it is hoped that this work will provide a basis for such an elucidation in the future.

Acknowledgments.—We are most grateful to Prof. D. F. Hornig for the encouragement he has given us, and for several stimulating discussions. We are also indebted to Prof. H. Taube and to Prof. W. Kauzmann, who made a number of helpful suggestions. This work was supported in part by the Office of Naval Research.

(32) F. Basolo and R. G. Pearson, "Mechanisms of Inorganic Reactions," John Wiley and Sons, Inc., New York, N. Y., 1958, p. 130.

(33) S. Meiboom, A. Loewenstein and S. Alexander, *J. Chem. Phys.*, **29**, 969 (1958).

TEMPERATURE DEPENDENCE OF SOME CATION EXCHANGE EQUILIBRIA IN THE RANGE 0 TO 200°¹

BY KURT A. KRAUS AND RICHARD J. RARIDON²

Contribution from the Oak Ridge National Laboratory, Chemistry Division, Oak Ridge, Tenn.

Received May 11, 1959

The temperature dependence of a number of cation-exchange equilibria (tracers of Na⁺, K⁺, Rb⁺, Cs⁺, Be⁺⁺, Ba⁺⁺, Co⁺⁺, Zn⁺⁺, La⁺³, Eu⁺³ vs. H⁺; tracers of K⁺, Rb⁺, Cs⁺ and Ba⁺⁺ vs. Na⁺) was studied in dilute aqueous electrolyte solutions. The temperature range was 0 to 150° for exchanges with the H⁺-form of the resin and 0 to 200° for those with the Na⁺-form. The upper temperature limits were imposed by the stability of the resin (H⁺-form) and the "safe" operating range of the equipment (Na⁺-form). Apparent heat ($\Delta\bar{H}'$), entropy ($\Delta\bar{S}'$) and heat capacity ($\Delta\bar{C}_p'$) changes were computed for the ion-exchange equilibria. In all cases $\Delta\bar{C}_p'$ was positive; in a few cases it was quite large (up to 20 cal./deg./equiv.). Good agreement between calculated and observed selectivity coefficients could be obtained by assuming $\Delta\bar{C}_p'$ to be constant which leads to a linear variation of $\Delta\bar{H}'$ with temperature T , and of $\Delta\bar{S}'$ with $\log T$. In many cases $\Delta\bar{H}'$ becomes zero in or near the temperature range studied (minima in the selectivity coefficient vs. temperature curves); this appears to be one reason why values of $\Delta\bar{H}'$ for ion-exchange reactions are often small.

We have recently described³ a "pre-loaded" column method and equipment suitable for measurement of ion-exchange equilibria as a function of temperature in pressurized systems. In view of the paucity of available information regarding temperature coefficients of ion-exchange equilibria, particularly at temperatures above the boiling point of water, we have studied a number of representative cation-exchange systems (hydrogen form resin vs. tracers of Na⁺, K⁺, Rb⁺, Cs⁺, Be⁺⁺, Ba⁺⁺, Co⁺⁺, Zn⁺⁺, La⁺³ and Eu⁺³; sodium form resin vs. tracers of K⁺, Rb⁺, Cs⁺ and Ba⁺⁺) and the present paper summarizes our results. Most measurements were carried out between 0 and 150° though in a few cases, involving the Na⁺-form of the resin the measurements were extended to 200°, the upper limit of the apparent safe operating range of the equipment.

Experimental

1. **Method.**—The method which was described earlier,³ involves passage of eluting solution over a uniformly loaded bed of exchanger, analysis of the effluent and computation of the distribution coefficients (D) with the known initial composition of the bed. Metal analyses were carried out radiometrically and concentrations of the supporting electrolyte determined by standard titrations.

2. **Resin.**—The measurements were carried out with Dowex-50 \times 12 (W) of mesh size 200 to 325. Capacity (4.67 moles/kg. dry H⁺-form resin) was determined by titrating a known weight of resin with standard NaOH in the presence of 0.1 M NaCl. Measurements of pH were made on the supernatant after allowing the resin particles to settle. Resin was used in the air-dried form, although samples were occasionally dried over "Anhydron" in a vacuum desiccator at 60° to establish the water content and hence permit calculation in terms of dry weight of resin. All distribution coefficients (D) and concentration quotients (K^m) have been computed on this basis.

3. **Tracers.**—The radioactive tracers (Na²⁴($T_{1/2}$ = 15h); K⁴²($T_{1/2}$ = 12h); Rb⁸⁶($T_{1/2}$ = 20d); Cs¹³⁴($T_{1/2}$ = 2.3y); Be⁷($T_{1/2}$ = 53d); Ba¹³³($T_{1/2}$ = 9.5y); Co⁶⁰($T_{1/2}$ = 5.3y); Zn⁶⁵($T_{1/2}$ = 250d); La¹⁴⁰($T_{1/2}$ = 40h); Eu¹⁵²($T_{1/2}$ = 13y)) were obtained from the Radioisotopes Division of ORNL. These tracers were received in dilute acid solutions, usually HCl, and were of high specific activity (from

0.1 to 10 curies per g. of element). The stated radiochemical purities were greater than 98%, except for Na²⁴ and K⁴² which were stated to be more than 95% pure. No further purifications were carried out. The radiochemical purity of the shorter lived isotopes was checked by following the decay rates. Samples of Na²⁴, K⁴², Rb⁸⁶ and La¹⁴⁰ were each counted for several half-life periods, with no appreciable deviations from the accepted values for the half-lives.

4. **Solutions.**—An approximately 1 M stock solution of HClO₄ was prepared from C.P. reagents and standardized by the usual methods. A stock 1 M NaClO₄ solution, prepared from the salt, was standardized by a cation-exchange technique. A known volume of the solution was passed through a column of Dowex-50 in the H⁺-form. The capacity of the bed was in excess of that needed to replace the Na⁺ ions of the solution by H⁺ ions from the resin. The concentration of Na⁺ (and hence of NaClO₄) could thus be established by acid-base titration of the effluent.

Conversions from molarity (M) to molality (m) were made using appropriate density values from the literature.

5. **Procedure.**—Resin samples (air-dried) were uniformly loaded with the "trace" metal; the resin was agitated with appropriate solutions of the radioactive tracers in a supporting electrolyte whose cation was the same as that on the resin (H⁺ or Na⁺). The electrolyte concentration of the solutions was chosen so that most of the tracer would be adsorbed in a few hours. From analysis of the solution before and after agitation the amount of adsorbed tracer was determined. Concentration of the trace ion in the resin, $m_{B(r)}$, was calculated as amount/kg. of dry resin. The usual weight of resin loaded into the column was ca. 0.5 g., with a total capacity of ca. 2 meq. The average amount of activity used was 0.1 millicuries (mc.). Since all traces had specific activity larger than 100 mc./g., the tracer contributed <0.02 meq.; or <1% of the capacity.

The resin was added to the column as a slurry and the apparatus assembled. Pressure was applied from a nitrogen tank after the reservoir had been filled with the eluting solution. The recorder was adjusted to regulate the temperature and the column allowed to come to thermal equilibrium. The flow rate through the column was usually ca. 3 cm. per minute. Measurements as a function of flow rate showed that this rate was easily within the range where effluent concentration is independent of flow rate, *i.e.*, where at least the lower layers of the bed are in equilibrium with the effluent.

Samples for measurement of effluent concentration, m_B , were collected in 4-ml. (glass stoppered) vials, which had been weighed and checked to be free from radioactive contamination. Each sample (ca. 1 g.) was weighed and counted to establish the tracer concentration (c.p.m./g.). The distribution coefficient D (amount per kg. of resin/amount per kg. of water) could then be calculated with the known densities of the solutions. Samples were collected at each equilibration point until the values of D for successive samples agreed to better than $\pm 2\%$. After each temperature or solution change a 2-ml. sample was discarded, an ample volume for sweeping out the solution in the interstitial space of the bed and in the capillary leading to the letdown valve.

To permit measurement of distribution coefficients D

(1) This document is based on work performed for the U. S. Atomic Energy Commission at the Oak Ridge National Laboratory, Oak Ridge, Tennessee, operated by Union Carbide Corporation.

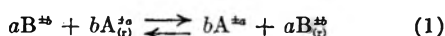
(2) Based on work submitted by R. J. Raridon to Vanderbilt University in partial fulfillment of the requirement for a Ph.D. degree. Work carried out at the Oak Ridge National Laboratory under sponsorship of the Oak Ridge Institute of Nuclear Studies.

(3) K. A. Kraus, R. J. Raridon and D. L. Holcomb, *J. Chromatography* (in press).

throughout the whole temperature range without reloading the resin, large distribution coefficients are needed. On the other hand, it is desirable not to operate at so high a value of D that at a reasonable tracer concentration in the effluent the concentration of tracer in the resin becomes so large as to require special shielding. Measurement at distribution coefficients of the order of 10^3 to 10^4 seems a satisfactory compromise. Suitable electrolyte concentrations could be selected in most cases to achieve these values of D . With the rare earths (La^{+3} , Eu^{+3}) however, measurements were carried out at values of D between 5×10^2 and 4×10^3 because otherwise the supporting electrolyte concentration would have been so high as to leave serious doubt regarding the validity of the activity coefficient corrections for the aqueous phase. The following concentrations of supporting electrolyte were used: Na-H, K-H, Rb-H and Cs-H exchange: $m_{\text{HClO}_4} = 0.00451$; Be-H: $m_{\text{HClO}_4} = 0.120$; Ba-H: $m_{\text{HClO}_4} = 0.224$; Co-H: $m_{\text{HClO}_4} = 0.0722$; Zn-H: $m_{\text{HClO}_4} = 0.0902$; La-H and Eu-H: $m_{\text{HClO}_4} = 0.180$; K-Na, Rb-Na and Cs-Na: $m_{\text{NaClO}_4} = 0.00504$; Ba-Na: $m_{\text{NaClO}_4} = 0.256$.

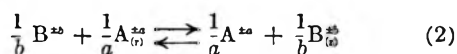
Results and Discussion

1. **Thermodynamic Relationships.**—A typical ion-exchange reaction may be represented by the equation



where A and B are ions with charges $\pm a$ and $\pm b$, respectively. The subscript (r) denotes the resin phase; no subscript is used for the aqueous phase.

Equation 1 can be rewritten in terms of equivalents as



with the equilibrium constant

$$K \equiv 1 = \frac{m_{\text{B}_{(r)}}^{1/b} m_{\text{A}}^{1/a} \gamma_{\text{B}_{(r)}}^{1/b} \gamma_{\text{A}}^{1/a}}{m_{\text{B}}^{1/b} m_{\text{A}_{(r)}}^{1/a} \gamma_{\text{B}}^{1/b} \gamma_{\text{A}_{(r)}}^{1/a}} = K^m \Gamma \quad (3)$$

where m is the stoichiometric concentration, γ the activity coefficient of the ions, K^m the concentration quotient and Γ the activity coefficient quotient. The ion-exchange equilibrium constant K has been set identical to unity at all temperatures which implies that the same standard states are taken for each distributable component in the resin and aqueous phases.

It is often convenient to write Γ as the product $\Gamma = \Gamma_{(r)} \Gamma_{(\text{aq})}$ where

$$\Gamma_{(r)} = \gamma_{\text{B}_{(r)}}^{1/b} / \gamma_{\text{A}_{(r)}}^{1/a} \quad (4)$$

and

$$\Gamma_{(\text{aq})} = \gamma_{\text{A}}^{1/a} / \gamma_{\text{B}}^{1/b} \quad (5)$$

Equation 3 may then be written as

$$\frac{1}{\Gamma_{(r)}} = K^m \Gamma_{(\text{aq})} = \frac{m_{\text{B}_{(r)}}^{1/b} m_{\text{A}}^{1/a} \gamma_{\text{A}}^{1/a}}{m_{\text{B}}^{1/b} m_{\text{A}_{(r)}}^{1/a} \gamma_{\text{B}}^{1/b}} = K' \quad (6)$$

where K' may be called the selectivity coefficient.

Thus with this definition of standard states ($K \equiv 1$), the activity coefficient quotient ($\Gamma_{(r)}$) of the ions in the resin phase may be estimated from measurement of the concentration of A and B in both phases (K^m) and from an estimate of the activity coefficient quotient of the ions in the aqueous phase ($\Gamma_{(\text{aq})}$).

Evaluation of K^m is simplified if one ion ($\text{B}^{\pm b}$) occurs at trace concentrations and if the supporting electrolyte concentration is sufficiently small so that resin invasion by the electrolyte is negligible compared with the capacity $C_{(r)}$ of the resin. Under these conditions $m_{\text{A}_{(r)}}$ becomes equal to

$C_{(r)}$ which may be determined in separate experiments. Estimation of changes in K^m then reduces to the determination of changes in the distribution coefficient

$$D = m_{\text{B}_{(r)}} / m_{\text{B}} \quad (7)$$

at a known and preferably constant supporting electrolyte concentration m_{A} .

In an ionic strength region where the Debye-Hückel theory can be used as a good approximation, $\Gamma_{(\text{aq})}$ may be computed. The mean activity coefficient γ_{\pm} of a component is given by

$$\log \gamma_{\pm} = -z_i z_j S \frac{\sqrt{(1/2) \sum_k c_k z_k^2}}{1 + A \sqrt{(1/2) \sum_k c_k z_k^2}} \quad (8)$$

where z_i and z_j are the charges on the ions, c the concentration in moles per liter, S the "limiting" slope (equal to 0.509 at 25° but varying with temperature) and A a term containing the "distance of closest approach."

Equation 8 is in an inconvenient form for evaluation of ($\log \gamma$) as a function of temperature, since in addition to S and A , c is also temperature dependent. Equation 8 was therefore rewritten as⁴

$$\log \gamma_{\pm} = -z_i z_j S f(\mu) \quad (9)$$

where

$$S = S \rho^{1/2} = 1.8252 \times 10^6 \left(\frac{\rho}{\epsilon^3 T^3} \right)^{1/2} \quad (10)$$

and

$$f(\mu) = \frac{\sqrt{(1/2) \sum_k m_k z_k^2}}{1 + A' \sqrt{(1/2) \sum_k m_k z_k^2}} = \frac{\sqrt{\mu}}{1 + A' \sqrt{\mu}} \quad (11)$$

Here μ is the ionic strength, m the concentration in moles per kg. of water (molality), T the absolute temperature, ρ the density and ϵ the dielectric constant of water. The term A' was taken as 1.5, independent of temperature, so that $(\rho/\epsilon^3 T^3)^{1/2}$ remains as the only temperature dependent term. The values of ρ were taken from the literature and the values of ϵ calculated from the Åkerlöf equation⁵ in view of the range of temperatures required.⁶

For a typical exchange reaction, $\text{B}^{\pm b} - \text{H}^+$, in the presence of a univalent anion X^- , $\log \Gamma_{(\text{aq})}$ can be written in terms of mean activity coefficients as

$$\Gamma_{(\text{aq})} = \frac{\gamma_{\text{H}}}{\gamma_{\text{B}}^{1/b}} = \frac{\gamma_{\text{H}} \gamma_{\text{X}}}{\gamma_{\text{B}}^{1/b} \gamma_{\text{X}}} = \frac{\gamma_{\pm \text{HX}}^2}{\gamma_{\pm \text{BX}}^{(1/b+1)}} \quad (12)$$

Combining eq. 9 and 12 yields

$$\begin{aligned} \log \Gamma_{(\text{aq})} &= 2 \log \gamma_{\text{HX}} - \left(\frac{1}{b} + 1 \right) \log \gamma_{\text{BX}} \\ &= 2 (-Sf(\mu)) - \left(\frac{1}{b} + 1 \right) (-Sbf(\mu)) = (b-1) Sf(\mu) \end{aligned} \quad (13)$$

which was used for calculation of $\log \Gamma_{(\text{aq})}$ as a function of temperature.

(4) We are indebted to Professor George Scatchard for suggesting to us this modification of the Debye-Hückel equation.

(5) G. C. Åkerlöf and H. I. Oshry, *J. Am. Chem. Soc.*, **72**, 2844 (1950).

(6) We are indebted to Dr. Milton Lietzke for computing the Debye-Hückel slopes and activity coefficients as a function of temperature with the Oak Ridge National Laboratory digital computer (ORACLE). The results of Dr. Lietzke's computations are available as report ORNL-2628, issued November, 1958.

Measurement of either K^m or K' as a function of temperature permits evaluation of an apparent partial molal heat (enthalpy) change for the ion-exchange reaction through the relationships

$$\frac{d \ln K^m}{d(1/T)} = - \frac{\Delta \bar{H}^m}{R} \quad (14)$$

and

$$\frac{d \ln K'}{d(1/T)} = - \frac{\Delta \bar{H}'}{R} \quad (15)$$

The enthalpy change $\Delta \bar{H}^m$ refers to the heat of transfer of the ions from and into the aqueous solution which was used in the measurements. The enthalpy change $\Delta \bar{H}'$ on the other hand refers to the heat of transfer of the ions from and into an ideal aqueous solution with unit activity coefficients. Thus $\Delta \bar{H}'$ appears to be the more useful quantity when the objective is comparison of various exchange reactions. Through combination of $\Delta \bar{H}'$ and $\ln K'$ the concordant entropy change $\Delta \bar{S}'$ may be computed, and through a second differentiation ($d \Delta \bar{H}'/dT$) the heat capacity change $\Delta \bar{C}'_p$.

2. Resin Stability.—The upper temperature limit for measurement of ion-exchange equilibria with Dowex-50 is determined by the thermal stability of the exchanger. This limit is considerably lower for the hydrogen form of the exchanger than for the sodium form.⁷ For the former, drifts in the distribution coefficients with time become serious above 150°, while with the latter no significant drifts were found even at 200°.

In the range 150 to 200° the principal decomposition reaction of the hydrogen form of the resin is probably desulfonation according to the equation $\text{RSO}_3\text{H} + \text{H}_2\text{O} \rightleftharpoons \text{RH} + \text{H}_2\text{SO}_4$, although some changes in cross-linking might also occur. The rate of loss of acid from the exchanger can be measured at elevated temperatures from the increase in acidity of the effluent. Presence of substantial amounts of sulfate in the effluent can readily be shown qualitatively (BaSO_4) though for quantitative measurements we elected to measure conductivity of the effluent.

A known weight of resin in the column was treated with water, slightly acidified (HClO_4) to avoid possible carbonate errors. The effluent was passed through a specially constructed micro conductivity cell (volume ca. 0.25 cc.) which was thermostated at $25 \pm 0.1^\circ$. The cell was calibrated with H_2SO_4 solutions of known concentration. Differences in conductivities between in-flowing and out-flowing solutions were ascribed to throw-off of sulfuric acid from the resin. Knowing also the rate of flow of solution through the bed, the sample weight and the (initial) capacity of the resin, the percentage of sulfonic acid lost from the resin per minute of contact time could be calculated. The losses per min. were 0.012% at 145°, 0.038% at 170° and 0.15% at 195°. The logarithm of the rate of acid loss varies approximately linearly with $1/T$ and an apparent heat of activation of ca. 20 kcal. may be calculated for the desulfonation reaction. There is no "apparent thresh-

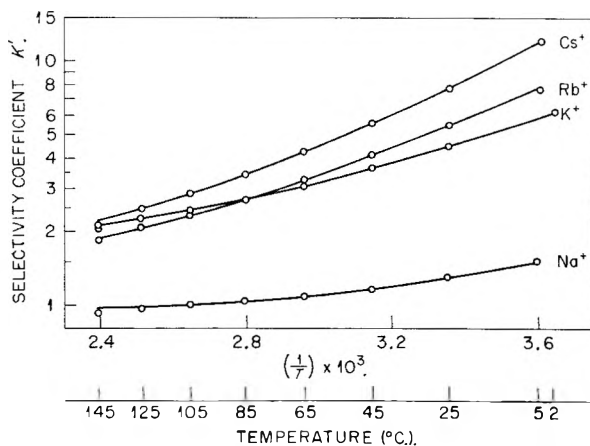


Fig. 1.—Temperature dependence of cation-exchange equilibria (metal tracers on Dowex-50 $\times 12$, H^+ form).

old near 180° for the desulfonation reaction as stated by Boyd and co-workers.⁸

The desulfonation rate observed here, although still modest, is considerably larger than the rate implied by the work of Bauman and co-workers.⁷ The capacity of their resin decreased by ca. 30% in 16 hours at 200°. Assuming a logarithmic decrease of capacity with time this implies a desulfonation rate of ca. 0.7% per minute which may be compared with our (extrapolated) value of 0.175% per minute.

An attempt was made to correlate the change in capacity through desulfonation with possible changes in selectivity coefficients using the Co^{++} (tracer)- H^+ reaction as an example. The observed decrease in D with time at 200° was ca. 0.2% per minute as measured during a 70 minute interval. According to eq. 3, distribution coefficients in this case ($b = 2$, $a = 1$) should be proportional to the square of the capacity (here $m_{\text{H}(r)}$) provided the electrolyte concentration of the solution (m_{H}) and the activity coefficients in the aqueous and resin phases are constant. Since the capacity change is 0.175% per minute one would thus expect a decrease of D of approximately 0.35% per minute. The observed rate of decrease of D is much less (0.2% per minute) and a substantial increase in the selectivity coefficient ($K' = 1/\Gamma_{(r)}$) on desulfonation is implied since under the conditions of the experiment activity coefficients in the aqueous phase as well as m_{H} are essentially constant. Similar increases in the selectivity coefficients with desulfonation have been reported by Boyd, Soldano and Bonner⁸ though they also show that in other cases ($\text{Na}^+ - \text{H}^+$) a decrease in selectivity coefficients may occur on desulfonation.

3. Selectivity Coefficients as a Function of Temperature.—With the hydrogen form exchanger measurements were carried out with some alkali metals (Na^+ , K^+ , Rb^+ and Cs^+), some alkaline earths (Be^{++} and Ba^{++}), divalent transition elements (Co^{++} and Zn^{++}) and two rare earths (La^{+++} and Eu^{+++}). With the sodium form exchanger measurements were limited to the alkali

(7) See e.g., W. C. Bauman, J. R. Skidmore and R. H. Osmun, *Ind. Eng. Chem.*, **40**, 1350 (1948).

(8) G. E. Boyd, B. A. Soldano and O. D. Bonner, *THIS JOURNAL*, **58**, 456 (1954).

TABLE I
 SELECTIVITY COEFFICIENTS AS A FUNCTION OF TEMPERATURE

A. Hydrogen-form resin													
t (°C.)	Na ⁺		K ⁺		Be ⁺⁺			Ba ⁺⁺			La ⁺⁺⁺		
	K^m	K'^{calcd}	K^m	K'^{calcd}	K^m	K'	K'^{calcd}	K^m	K'	K'^{calcd}	K^m	K'	K'^{calcd}
2	6.17	6.16	4.97	6.79	6.78
5	1.51	1.50	1.55	2.03	2.04	3.10	5.58	5.57
25	1.29	1.30	4.46	4.47	1.68	2.19	2.18	4.09	5.66	5.65	3.17	5.82	5.82
45	1.15	1.16	3.62	3.61	1.77	2.34	2.34	3.64	5.10	5.13	3.34	6.30	6.31
65	1.08	1.08	3.04	3.05	1.88	2.52	2.52	3.40	4.85	4.86	3.63	7.03	7.03
85	1.03	1.02	2.69	2.68	2.00	2.71	2.71	3.30	4.77	4.77	4.02	7.96	8.00
105	0.997	0.987	2.42	2.42	2.12	2.92	2.93	3.28	4.85	4.81	4.48	9.27	9.23
125	.958	.969	2.25	2.25	2.25	3.16	3.16	3.28	4.96	4.96	5.05	10.9	10.8
145	.915	.964	2.04	2.13	2.38	3.41	3.41	3.28	5.19	5.21	5.61	12.6	12.7
t (°C.)	Rb ⁺		Cs ⁺		Co ⁺⁺			Zn ⁺⁺			Eu ⁺⁺⁺		
	K^m	K'^{calcd}	K^m	K'^{calcd}	K^m	K'	K'^{calcd}	K^m	K'	K'^{calcd}	K^m	K'	K'^{calcd}
2	1.44	1.78	1.77	1.22	1.54	1.54
5	7.65	7.68	12.2	12.1	2.89	5.20	5.18
25	5.44	5.40	7.71	7.83	1.41	1.76	1.77	1.20	1.54	1.54	3.05	5.61	5.63
45	4.05	4.06	5.50	5.55	1.43	1.80	1.81	1.22	1.57	1.57	3.33	6.27	6.29
65	3.23	3.23	4.24	4.21	1.47	1.87	1.87	1.25	1.63	1.63	3.70	7.17	7.15
85	2.68	2.68	3.41	3.38	1.52	1.97	1.96	1.30	1.71	1.71	4.14	8.27	8.25
105	2.31	2.31	2.88	2.85	1.59	2.08	2.07	1.36	1.82	1.82	4.63	9.58	9.62
125	2.06	2.06	2.46	2.49	1.64	2.18	2.20	1.43	1.95	1.95	5.30	11.4	11.3
145	1.81	1.87	2.09	2.25	1.74	2.35	2.35	1.51	2.09	2.09	5.90	13.3	13.4
B. Sodium-form resin													
t (°C.)	K ⁺		Rb ⁺		Cs ⁺			Ba ⁺⁺					
	K^m	K'^{calcd}	K^m	K'^{calcd}	K^m	K'	K'^{calcd}	K^m	K'	K'^{calcd}	K^m	K'	K'^{calcd}
2	2.36	2.47	
5	3.00	3.02	4.40	4.37	...	2.92	4.04	4.08	
25	2.17	2.17	2.68	2.65	3.69	3.70	...	2.96	4.14	4.13	
45	1.97	1.97	2.36	2.37	3.18	3.20	...	3.03	4.31	4.27	
65	1.82	1.82	2.14	2.15	2.81	2.83	...	3.13	4.52	4.49	
85	1.69	1.69	1.97	1.97	2.53	2.53	...	3.27	4.80	4.78	
105	1.60	1.59	1.82	1.82	2.29	2.30	...	3.42	5.12	5.13	
125	1.51	1.51	1.70	1.70	2.12	2.11	...	3.61	5.52	5.55	
145	1.44	1.44	
150	1.58	1.58	1.94	1.92	...	3.85	6.09	6.17	
175	1.80	1.77	...	4.18	6.86	6.90	
200	1.61	1.64	...	4.59	7.87	7.75	

metals (K⁺, Rb⁺ and Cs⁺) and the alkaline earth Ba⁺⁺. Measurements with a few other polyvalent elements were abandoned since interference from hydrolytic reactions seemed to occur at high temperatures.

The results of the measurements are summarized in Table I in the form of concentration quotients K^m (note that for 1:1 exchange reactions in the Debye-Hückel range $K' = K^m$). The concentration quotients were computed from average values of the distribution coefficients obtained with increasing and decreasing temperatures. Agreement between the two types of measurements was usually within $\pm 1\%$ and in all cases, within $\pm 2\%$. Values of K^m were computed from the distribution coefficients according to eq. 3 using the known capacity of the resin and the known molality of the eluting solutions (see Experimental Section). All concentration units are molality for the aqueous phase and moles/kg. dry resin for the resin phase.

The changes of K^m over this wide temperature range are quite modest. This of course could have been anticipated from the considerable number of previous studies on temperature coefficients and enthalpy changes of ion exchange equilibria, all of which agree that the enthalpy changes for ion-exchange reactions are usually small.⁹⁻²⁰

It may be noted (Table I) that K^m decreases with temperature for some reactions (Na⁺, K⁺, Rb⁺, Cs⁺ vs. H⁺; K⁺, Rb⁺, Cs⁺ vs. Na⁺); for others it increases with temperature (Be⁺⁺, La⁺⁺⁺, Eu⁺⁺⁺ vs. H⁺; Ba⁺⁺ vs. Na⁺); and for still others K^m goes through a minimum (Ba⁺⁺, Co⁺⁺, Zn⁺⁺ vs. H⁺). In addition, the changes in K^m with temperature even within a group may differ substantially and as a result inversions of selectivity occur. Thus, as shown in Fig. 1, while the relative selectivity of the alkali metals vs. H⁺ is in the usual order near room temperature (Na⁺ < K⁺ < Rb⁺

(9) G. E. Boyd, J. Schubert and A. Q. Adamson, *J. Am. Chem. Soc.*, **69**, 2829 (1947).

(10) T. R. E. Kressman and J. A. Kitchener, *J. Chem. Soc.*, 1190 (1949).

(11) J. D. Cosgrove and J. D. H. Strickland, *ibid.*, 1845 (1950).

(12) H. P. Gregor and J. I. Bregman, *J. Colloid Sci.*, **6**, 323 (1951).

(13) K. A. Kraus and R. A. Plane, ORNL-1260, Chemistry Division Quarterly Report for the period ending December 31, 1951.

(14) N. T. Coleman, *Soil Sci.*, **74**, 115 (1952).

(15) G. Dickel and L. V. Nieciecki, *Z. Elektrochem.*, **59**, 913 (1955).

(16) J. F. Duncan, *Australian J. Chem.*, **8**, 1 (1955).

(17) O. D. Bonner and L. L. Smith, *THIS JOURNAL*, **61**, 1614 (1957).

(18) E. H. Cruickshank and P. Meares, *Trans. Faraday Soc.*, **53**, 1289 (1957), **54**, 174 (1958).

(19) G. Jangg, *Österr. Chemiker Ztg.*, **58**, 40 (1957).

(20) S. P. Surls, Jr., and G. R. Choppin, *J. Am. Chem. Soc.*, **79**, 855 (1957).

< Cs⁺), near 150° Rb⁺ is less strongly adsorbed than K⁺, while Cs⁺ is still slightly more strongly adsorbed than either K⁺ or Rb⁺. As another example (see also Fig. 3) consider the rare earths La⁺³ and Eu⁺³. Near room temperature La⁺³ is more strongly adsorbed than Eu⁺³ while at 145° the reverse is the case. One must thus conclude that correlations of ion exchange selectivities with such temperature insensitive properties as ionic radii, "hydrated" radii or "distances of closest approach" are untenable. Rather, interpretations must be based on more subtle properties of the resin phase. This reduces interpretation to properties of concentrated electrolyte and polyelectrolyte solutions whose detailed theoretical description at present has not been achieved.

As described in Section 1, selectivity coefficients K' were computed from the concentration quotients K^m on the assumption that the Debye-Hückel equation describes the ratio of the activity coefficients for the aqueous phase ($\Gamma_{(aq)}$). Plots of $\log K'$ vs. $1/T$ (see e.g. Figs. 1 to 3) are not straight lines as might be expected if $\Delta\bar{H}'$ were constant. Rather, the plots are concave upward which implies that the heat capacity change $\Delta\bar{C}'_p$ for the ion-exchange reactions is positive. Assuming that $\Delta\bar{C}'_p$ is constant one obtains the relationship

$$\log K' = \log K'_t + \alpha \log (T/T_t) + \beta [1 - (T_t/T)] \quad (16)$$

where α and β are constants and subscript "t" refers to a reference temperature, here taken as 75° (348.1° K.).

TABLE II

TEMPERATURE DEPENDENCE OF ION-EXCHANGE EQUILIBRIA—PARAMETERS FOR FITTING FUNCTIONS

A. Hydrogen-form resin

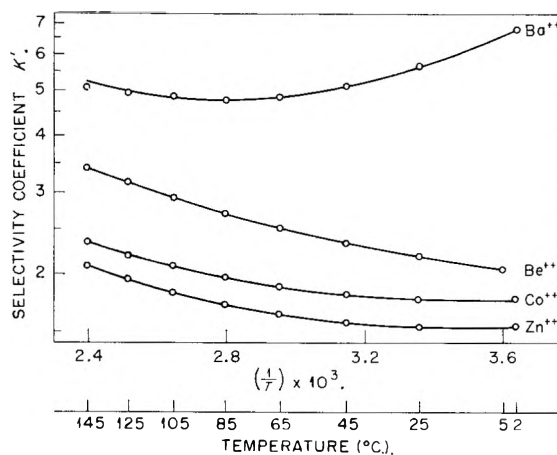
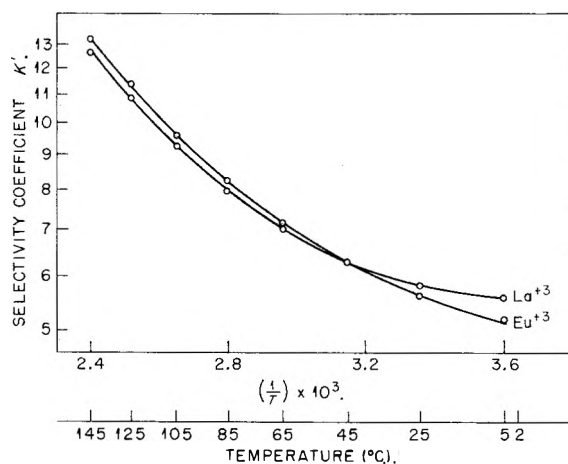
Ion	$\log K'_t$	α	$-\beta$	$\frac{\Delta\bar{C}'_p}{\text{equiv.}/^\circ\text{C.}}$	$T_{\text{min.}}$ (°C.)
Na ⁺	0.019	4.683	2.437	9.3	144
K ⁺	.454	5.735	3.474	11.4	213
Rb ⁺	.467	5.694	3.868	11.3	271
Cs ⁺	.574	7.811	5.042	15.5	244
Be ⁺⁺	.417	2.884	0.686	5.7	-82
Ba ⁺⁺	.681	8.687	3.914	17.3	89
Co ⁺⁺	.281	4.572	1.638	9.1	14
Zn ⁺⁺	.223	5.058	1.818	10.0	15
La ⁺³	.874	9.833	3.299	19.5	-4
Eu ⁺³	.885	8.699	2.694	17.3	-25

B. Na-form resin

K ⁺	0.244	0.564	0.777	1.1	ca. 800
Rb ⁺	.312	.209	0.745	0.4	>1000
Cs ⁺	.427	.441	1.020	0.9	>1000
Ba ⁺⁺	.665	5.380	1.865	10.7	5

By fitting ("least squares"²¹) the experimental data to eq. 16, the parameters (α , β , K'_t) listed in Table II were obtained. The solid lines in Figs. 1 to 3 represent the curves computed from these parameters. The deviations between observed and calculated values of K' (see also Table I) appear to be within experimental error except in a few cases at the extremes of the temperature range. For this reason, the first point in the K⁺-Na⁺ exchange series was not included in the least square

(21) The "least square" fitting was carried out with the ORNL digital computer, the ORACLE; we are indebted to Dr. Miron Lietzke for providing the code and assisting in the computations.

Fig. 2.—Temperature dependence of cation-exchange equilibria (metal tracers on Dowex-50 × 12, H⁺ form).Fig. 3.—Temperature dependence of cation-exchange equilibria (metal tracers on Dowex-50 × 12, H⁺ form).

fitting of the data. Neither were the last points (145°) in the alkali metal-hydrogen exchange series included. For the latter the observed values of K^m are expected to be low since through decomposition of the resin an amount of sulfuric acid would have been added to the solutions which is significantly large at the low supporting electrolyte concentrations used in these measurements. The corresponding error is estimated to be ca. 10%, i.e., ample to explain the observed deviations from the smooth function eq. 16. In the other exchange reactions where much higher supporting electrolyte concentrations had been chosen the error from this source should be negligible.

4. Enthalpy, Entropy and Heat Capacity Changes.—Differentiation of eq. 16, which was used to fit the ion-exchange equilibrium data, leads to the relationships

$$\Delta\bar{H}' = R d \ln K' / d(1/T) = \alpha RT + 2.303\beta RT_t \quad (17)$$

$$\Delta\bar{C}'_p = d(\Delta\bar{H}')/dT = \alpha R \quad (18)$$

$$\Delta\bar{S}' = (\Delta\bar{H}' - \Delta\bar{F}')/T \quad (19)$$

$$= \alpha R + 2.303\beta RT_t/T + R \ln K'$$

$$= \Delta\bar{C}'_p + 4.576\beta + R \ln K'_t + \Delta\bar{C}'_p \ln (T/T_t)$$

through which the partial molal enthalpy ($\Delta\bar{H}'$), entropy ($\Delta\bar{S}'$) and heat capacity changes ($\Delta\bar{C}'_p$) (all per/equiv.) may be computed from the parameters α , β and K'_t . As implied by the fitting

TABLE III
 THERMODYNAMIC FUNCTIONS OF CATION-EXCHANGE EQUILIBRIA

Exchange	Function	Temperature (°C.)								
		0	25	50	75	100	125	150	175	200
Na-H	$-RT \ln K'$	-0.244	-0.154	-0.083	-0.031	0.005	0.025	0.031	0.022	0.001
	$\Delta\bar{H}'$	-1.34	-1.11	-0.88	-0.64	-0.41	-0.18	0.06	0.29	0.52
	$\Delta\bar{S}'$	-4.0	-3.2	-2.5	-1.8	-1.1	-0.5	0.1	0.6	1.1
K-H	$-RT \ln K'$	-1.004	-0.887	-0.794	-0.723	-0.673	-0.642	-0.628	-0.631	-0.651
	$\Delta\bar{H}'$	-2.42	-2.14	-1.85	-1.57	-1.28	-1.00	-0.71	-0.43	-0.14
	$\Delta\bar{S}'$	-5.2	-4.2	-3.3	-2.4	-1.6	-0.9	-0.2	0.5	1.1
Rb-H	$-RT \ln K'$	-1.161	-0.999	-0.860	-0.743	-0.647	-0.570	-0.510	-0.467	-0.440
	$\Delta\bar{H}'$	-3.07	-2.79	-2.51	-2.22	-1.94	-1.66	-1.37	-1.09	-0.81
	$\Delta\bar{S}'$	-7.0	-6.0	-5.1	-4.2	-3.5	-2.7	-2.0	-1.4	-0.8
Cs-H	$-RT \ln K'$	-1.419	-1.219	-1.052	-0.914	-0.805	-0.722	-0.663	-0.627	-0.612
	$\Delta\bar{H}'$	-3.79	-3.40	-3.02	-2.63	-2.24	-1.85	-1.46	-1.08	-0.69
	$\Delta\bar{S}'$	-8.7	-7.3	-6.1	-4.9	-3.8	-2.8	-1.9	-1.0	-0.2
Be-H	$-RT \ln K'$	-0.377	-0.461	-0.557	-0.665	-0.782	-0.910	-1.046	-1.190	-1.343
	$\Delta\bar{H}'$	0.47	0.62	0.76	0.90	1.05	1.19	1.33	1.48	1.62
	$\Delta\bar{S}'$	3.1	3.6	4.1	4.5	4.9	5.3	5.6	5.9	6.3
Ba-H	$-RT \ln K'$	-1.050	-1.026	-1.038	-1.084	-1.161	-1.267	-1.400	-1.558	-1.741
	$\Delta\bar{H}'$	-1.52	-1.09	-0.66	-0.22	0.21	0.64	1.07	1.50	1.93
	$\Delta\bar{S}'$	-1.7	-0.2	1.2	2.5	3.7	4.8	5.8	6.8	7.8
Co-H	$-RT \ln K'$	-0.311	-0.338	-0.384	-0.448	-0.528	-0.623	-0.732	-0.855	-0.990
	$\Delta\bar{H}'$	-0.13	0.10	0.33	0.55	0.78	1.01	1.23	1.46	1.69
	$\Delta\bar{S}'$	0.7	1.5	2.2	2.9	3.5	4.1	4.6	5.2	5.7
Zn-H	$-RT \ln K'$	-0.236	-0.255	-0.295	-0.354	-0.432	-0.526	-0.637	-0.762	-0.901
	$\Delta\bar{H}'$	-0.15	0.10	0.35	0.60	0.85	1.11	1.36	1.61	1.86
	$\Delta\bar{S}'$	0.3	1.2	2.0	2.8	3.4	4.1	4.7	5.3	5.8
La-H	$-RT \ln K'$	-0.929	-1.044	-1.199	-1.392	-1.620	-1.881	-2.173	-2.493	-2.841
	$\Delta\bar{H}'$	0.08	0.57	1.06	1.55	2.04	2.52	3.01	3.50	3.99
	$\Delta\bar{S}'$	3.7	5.4	7.0	8.4	9.8	11.1	12.3	13.4	14.4
Eu-H	$-RT \ln K'$	-0.884	-1.024	-1.200	-1.409	-1.649	-1.919	-2.215	-2.537	-2.883
	$\Delta\bar{H}'$	0.43	0.86	1.29	1.73	2.16	2.59	3.02	3.45	3.89
	$\Delta\bar{S}'$	4.8	6.3	7.7	9.0	10.2	11.3	12.4	13.4	14.3
K-Na	$-RT \ln K'$	-0.497	-0.458	-0.422	-0.388	-0.356	-0.326	-0.298	-0.271	-0.246
	$\Delta\bar{H}'$	-0.93	-0.90	-0.87	-0.85	-0.82	-0.79	-0.76	-0.73	-0.71
	$\Delta\bar{S}'$	-1.6	-1.5	-1.4	-1.3	-1.2	-1.2	-1.1	-1.0	-1.0
Rb-Na	$-RT \ln K'$	-0.618	-0.577	-0.537	-0.497	-0.459	-0.421	-0.383	-0.346	-0.310
	$\Delta\bar{H}'$	-1.07	-1.06	-1.05	-1.04	-1.03	-1.02	-1.01	-1.00	-0.99
	$\Delta\bar{S}'$	-1.7	-1.6	-1.6	-1.6	-1.5	-1.5	-1.5	-1.5	-1.4
Cs-Na	$-RT \ln K'$	-0.825	-0.775	-0.726	-0.679	-0.634	-0.590	-0.548	-0.507	-0.467
	$\Delta\bar{H}'$	-1.38	-1.36	-1.34	-1.32	-1.30	-1.28	-1.25	-1.23	-1.21
	$\Delta\bar{S}'$	-2.1	-2.0	-1.9	-1.8	-1.8	-1.7	-1.7	-1.6	-1.6
Ba-Na	$-RT \ln K'$	-0.763	-0.840	-0.939	-1.059	-1.199	-1.356	-1.530	-1.720	-1.925
	$\Delta\bar{H}'$	-0.05	0.22	0.48	0.75	1.02	1.29	1.55	1.82	2.09
	$\Delta\bar{S}'$	2.6	3.5	4.4	5.2	5.9	6.6	7.3	7.9	8.5

function, $\Delta\bar{C}_p'$ is constant, $\Delta\bar{H}'$ a linear function of T and $\Delta\bar{S}'$ a linear function of $\log T$. Representative values of $\Delta\bar{H}'$ (kcal.), $\Delta\bar{S}'$ (e.u.) as well as of the excess free energy $\Delta\bar{F}' = -RT \ln K'$ (kcal.), computed at 25° temperature intervals for the various ion-exchange equilibria, are listed in Table III.

At a temperature $T = T_{\min}$, $\Delta\bar{H}'$ becomes zero and the curves such as in Figs. 1 to 3 have minima. This temperature may be computed by rearranging eq. 17 to

$$T_{\min} = -2.303T_i\beta/\alpha = -801.7\beta/\alpha \quad (20)$$

Values of T_{\min} are included in Table II. A surprisingly large number of ion-exchange equilibria have T_{\min} in or near the range 0 to 200° and hence the fact that so many ion-exchange equilibria have

small values of $\Delta\bar{H}'$ near room temperature is not necessarily significant. For the alkali metal-Na⁺ reactions, however, curvature of plots of $\log K'$ vs. $1/T$ is very small, T_{\min} hence extremely large, and the low values of $\Delta\bar{H}'$ appear characteristic. Further, for these reactions the pattern of selectivities (K < Rb < Cs) persists from 0 to 200° and is reflected in a similarly regular pattern for the enthalpy and entropy changes. For these reactions the excess free energy change in kcal. is considerably smaller than $\Delta\bar{H}'$ and further, $\Delta\bar{S}'$ for these reactions is approximately the same. Hence the relative selectivities for these systems seem to be primarily determined by the changes in heat content.

We are hesitant to make other generalizations regarding the comparative values of $\Delta\bar{F}'$, $\Delta\bar{H}'$ or

$\Delta\bar{S}'$ of the various ion-exchange reactions. Thus, while near room temperature $\Delta\bar{H}'$ for the alkali metal-H⁺ exchange reactions becomes increasingly negative as the atomic number of the alkali metal increases, this simple relationship does not hold at high temperatures. A similarly smooth relationship between $\Delta\bar{S}'$ and atomic number of the alkali metals near room temperature is destroyed at high temperature. For these reasons of course some of the many previously proposed generalizations are also untenable. Thus for example, Boyd and co-workers⁹ state that "ions of smaller hydration displace those of higher hydration or entropy, so that an over-all entropy decrease occurs." While it is true that frequently $\Delta\bar{S}'$ is negative this is by no means universally correct and indeed $\Delta\bar{S}'$ is a temperature dependent function, which in some cases changes sign in the temperature range studied.

Detailed comparison of our values of $\Delta\bar{H}'$ and $\Delta\bar{S}'$ with those previously reported⁹⁻²⁰ does not appear fruitful at this time. There is clearly qualitative agreement between our results at the lower temperatures and those described in the literature and not much more than qualitative agreement could in general be expected. Some authors have used different resins (*e.g.*, phenol-formaldehyde) or resins of different (or unspecified) cross-linking. Further, most data were obtained at substantial loading rather than the tracer loading used here. In those cases where data in the literature pertain to, or can be extrapolated to "zero loading," agreement is gratifying. The calorimetric data of Cruickshank and Meares¹⁸ give $\Delta\bar{H}' = -1.25, -2.05, \text{ and } -0.73$ kcal. for the Na⁺-H⁺, K⁺-H⁺ and K⁺-Na⁺ systems at 25° which may be compared with our values of $-1.11, -2.14$ and -0.90 kcal., respectively; they find $\Delta\bar{S}' = -3.02, -4.57$ and -1.31 e.u. for these systems, while we find $-3.2, -4.2$ and -1.5 e.u. Similarly agreement is good between the data reported here and those of Plane and Kraus¹³ for the Zn⁺⁺-H⁺ exchange for which we find $\Delta\bar{H}' = 0.10$ kcal. at 25° while the earlier work gives 0.15 ± 0.15 . Interestingly Plane and Kraus find for the Cd⁺⁺-H⁺ exchange reaction $\Delta\bar{H}' = 1.4$ kcal. which, if confirmed, would imply that even relatively similar transition elements may show large differences in the heats of adsorption. Extrapolation of the data of Bonner and Smith¹⁷ to zero loading yields $\Delta\bar{H}' = -0.3$ kcal. at 0° and 1.1 kcal. at 100° for the Cu⁺⁺-H⁺ reaction in good agreement with our values of -0.13 and 0.78 kcal. for the Co⁺⁺-H⁺ reaction at these temperatures. However, agreement is poor for the Na⁺-H⁺ reaction where one computes from Bonner and Smith -4.4 and -1.0 kcal. at 0 and 100°, respectively, while we find -1.34 and -0.41 kcal.

Description of the temperature dependence of the equilibria has been in terms of a constant heat

capacity change $\Delta\bar{C}_p'$. Unfortunately $\Delta\bar{C}_p'$ is the least accurately known of the thermodynamic properties discussed since it is obtained by an implied double differentiation. In spite of the large temperature range covered and the generally close agreement between calculated and observed values, $\Delta\bar{C}_p'$ is probably not known to better than ± 0.5 cal./degree and frequently is uncertain by ± 1 cal./degree. It is thus surprising that in the one example where comparison with the literature is feasible, agreement is very close. Surls and Choppin²⁰ studied temperature dependence of adsorption of some lanthanides and actinides and found $\Delta\bar{C}_p' = 18.2$ cal./equiv./degree²² for Pm⁺³ which is intermediate between our values of 19.5 for La⁺³ and 17.3 for Eu⁺³, as one might expect from the relative position of these lanthanides. Since Surls and Choppin used a 4% DVB resin and we a 12% resin, this agreement may be fortuitous; otherwise it would imply a remarkable insensitivity of $\Delta\bar{C}_p'$ to cross-linking.

Examination of Table II shows that $\Delta\bar{C}_p'$ for trace metal-H⁺ exchange reactions is large and there is a trend of increasing $\Delta\bar{C}_p'$ with increasing radius of the metal ion. Values of $\Delta\bar{C}_p'$ for exchanges involving the sodium form of the resin are substantially smaller than those for the hydrogen form resin. The difference amounts to 7 to 11 cal./deg./equiv. which presumably reflects possible partial association of the hydrogen ions with the sulfonate groups of the network.

In conclusion, we might mention that one of the main objectives of this study was delineation of some of the problems which one might encounter in ion-exchange processes at temperatures far from room temperature. Since the enthalpy changes for so many typical, though uncomplicated, ion-exchange reactions is small at room temperature and remains small at high temperature one may conclude that ion-exchange behavior at high temperature should not differ drastically from that at room temperature. For chromatographic separations, however, some allowance has to be made for possible reversals of selectivity with temperature.

In the present study cations were selected for which there was little likelihood of hydrolytic reactions and the anion (ClO₄⁻) was chosen to decrease the probability of complications from complexing reactions. One may anticipate that heats of hydrolysis and of complexing are usually large and positive. Hence such reactions may become important at high temperatures and for these systems large changes in ion-exchange behavior with temperature are to be expected. Conversely, the techniques described should prove useful for elucidation of these reactions at high temperatures.

Acknowledgment.—The authors are greatly indebted to Mr. Frederick Nelson for valuable advice.

(22) Their values are given on a per mole basis. They were divided by three to convert to the per equiv. basis used here.

STUDIES IN COÖRDINATION CHEMISTRY. V. STRUCTURE OF THE DIAMAGNETIC BIS-(N-METHYLSALICYLALDIMINE)-NICKEL(II) COMPLEX

BY EDOARDO FRASSON, CARLO PANATTONI AND LUIGI SACCONI

Contribution from the "Centro di Strutturistica Chimica del C.N.R.," Padova and the "Istituto di Chimica Generale dell'Università," Palermo, Italy

Received April 27, 1959

The present paper reports the results of an X-ray structural investigation on the diamagnetic form of bis-(N-methylsalicylaldimine)-nickel(II). The crystals belong to the space group $P2_{1/c}$ and have the following lattice constants: $a = 11.94$, $b = 7.00$, $c = 8.30$ Å., $\beta = 92^\circ 30'$, $Z = 2$. The nickel atoms are required to be at symmetry centers and the bonds around the nickel atom are in a *trans*-planar arrangement. The chelate ring does not lie in a plane. It is found that the shortest Ni-Ni distances are 5.32 Å. In the molecule the methyl-carbon is at 2.68 Å. from the oxygen atom. This leads to the possibility of some degree of hydrogen bonding between these two atoms.

The anomalous complexes of nickel(II) with N-alkylsalicylaldimines have been the object of various studies, both experimental and theoretical. In fact these complexes, diamagnetic in the solid state, becomes paramagnetic in solutions of organic (even inert) solvents and in the molten state.¹

The first member of the series, bis-(N-methylsalicylaldimine)-nickel(II), when heated to temperature above 150° , turns into a stable paramagnetic crystalline complex compound with a magnetic moment corresponding to that of two unpaired electrons.² This fact and the insolubility of this paramagnetic form in "inert" organic solvents has brought us to the conclusion that this complex possesses a polymeric octahedral sp^3d^2 configuration. Therefore both the diamagnetism and the paramagnetism of the two forms of the complex appear to be linked to a particular crystalline state.

On this account it was of interest to carry out an X-ray analysis of the two isomers. Unfortunately only the diamagnetic form of the complex can be obtained in crystals suitable for structural investigation. Consequently a complete X-ray analysis has been performed only on the green diamagnetic form, and the results are reported here.

Experimental

Preparation of Compound.—Bis-(N-methylsalicylaldimine)-nickel(II) was prepared according to Klemm and Raddatz.³ Single crystals of the complex were obtained by slow evaporation of a saturated chloroform solution at room temperature.

Anal. Calcd. for $C_{16}H_{16}O_2N_2Ni$: N, 8.56; Ni, 17.95. Found: N, 8.62; Ni, 17.90.

Procedure and Crystal Data.—From precession camera photographs it has been found that the crystal belongs to the space group $P2_{1/c}$. The unit cell has the lattice constants

$$\begin{aligned} a &= 11.94 \pm 0.05 \text{ \AA.} \\ b &= 7.00 \pm 0.03 \text{ \AA.} \\ c &= 8.30 \pm 0.04 \text{ \AA.} \\ \beta &= 92^\circ 30' \pm 20' \end{aligned}$$

The picnometric density is $d = 1.534$. The density determined by X-rays is $d = 1.550$ with two molecules in the unit cell. Owing to the presence of only two molecules in the elementary cell it was necessary to locate the two Ni-atoms in positions 000 and $0\frac{1}{2}\frac{1}{2}$, and therefore at crystallographic symmetry centers. Under these conditions, the entire molecule must be centrosymmetrical with respect to the nickel atom and the four coördinate bonds from the nickel atom must lie in the same plane.

Weissenberg equatorial photographs by oscillation about the three axes of the cell were taken with Cu $K\alpha$ radiation using bidimensional integration of the diffractions and multiple film technique. Intensities were measured by galvanometer readings of the integrated reflections using a photometer.

Owing to the flat shape of the crystal, the difference of the absorption power was significantly large for the $h0l$ and $hk0$ reflections notwithstanding the low linear absorption coefficient (for Cu $K\alpha$ radiation $\mu = 24.62$ cm.⁻¹). The $h0l$ and the $hk0$ intensities were therefore corrected by using a factor calculated by integration with a speed graphic method proposed by one of us.⁴ This approximate method gives very good results for small values of the optical path and eliminates the very tedious work which is usually necessary. The intensities were also corrected with the usual Lorentz and polarization factors for the Weissenberg camera.

Electron Density Maps.—From Patterson projections on the (100), (010) and (001) planes, the approximate orientation of the molecule was determined.

The projection of electron density on the same planes were then calculated. The structure factors F_0 , which contain the contribution of the Ni atom, were taken as positive, and the structure factors that contained no contribution from the nickel atom were given the signs calculated from the approximate coördinates of the other atoms derived from the orientation of the molecule.

From the projection on (010) a very clear picture of the molecule was obtained and this confirmed that the molecule lies fundamentally in this plane. The projection on (001) contains the major dimension of the molecule aligned on the axis a , but the molecule is viewed in profile. On the electron density projection on (100) the molecule appears in profile along its minor dimension; therefore this projection was discarded for further refinement owing to the impossibility of locating the maxima of electron density.

The direct location of all the atoms of the organic part of the molecule was carried out on the projection on (010). On the projection on (001) the location of some atoms required the aid of a molecular model owing to the considerable overlapping of the maxima on this electron density map. The structure factors F_0 were calculated using the atomic form factors of Berghuis, *et al.*⁵ for C, N, O atoms and the atomic

(1) (a) J. B. Willis and D. P. Mellor, *J. Am. Chem. Soc.*, **69**, 1237 (1947); (b) F. Basolo and W. R. Matoush, *ibid.*, **75**, 5663 (1953); S. Fujii and M. Sumitani, *Sci. Repts. Tôhoku Imp. Univ., First Series*, **37**, 49 (1953); H. C. Clark and A. L. Odell, *J. Chem. Soc.*, 3431 (1955); 520 (1956); L. Sacconi, R. Cini and F. Maggio, *J. Am. Chem. Soc.*, **79**, 3933 (1957); L. Sacconi, P. Paoletti and G. Del Re, *ibid.*, **79**, 4062 (1957); C. J. Ballhausen and A. D. Liehr, *ibid.*, **81**, 538 (1959); Gilda Maki, *J. Chem. Phys.*, **29**, 1129 (1958).

(2) L. Sacconi, P. Paoletti and R. Cini, "Proceeding Internl Symposium on the Chemistry of the Coördination Compounds," Rome, September 1957, *Supplemento La Ricerca Scientifica*, **28**, 492 (1958) in *J. Inorg. Nuclear Chem.*, **8**, 492 (1958); L. Sacconi, P. Paoletti and R. Cini, *J. Am. Chem. Soc.*, **80**, 3583 (1958); C. M. Harris, S. L. Lenzer and R. L. Martin, *Australian J. Chem.*, **11**, 331 (1958).

(3) W. Klemm and K. H. Raddatz, *Z. anorg. allgem. Chem.*, **250**, 207 (1942).

(4) E. Frasson and S. Bezzi, *Gazz. chim. ital.*, (to be published); E. Frasson, *ibid.*, (to be published).

(5) J. Berghuis, I. M. Haanappel, M. Potters, B. O. Loopstra, C. H. McGillivray and A. L. Veenendaal, *Acta Cryst.*, **8**, 478 (1955).

form factors of Viervoll and Ogrim⁶ for the Ni atom. This calculation imposed some changes in the previous signs for the F_o . The comparison of the F_o and F_c of a few strongest reflections revealed the presence of secondary extinction. Therefore a correction coefficient was calculated using the method proposed by Housty and Clastre⁷ on the basis of the slope of the graph

$$F_o/F_c = \exp(-\phi I_o)$$

The new electron density maps calculated on this basis on the (100), (010) and (001) are represented in Figs. 1, 2 and 3. At this stage the values of the reliability index were $R = 0.22$ for the $h0l$ reflections and $R = 0.28$ for the $hk0$ reflections. For the $0kl$ zone the calculation of the F_o was not carried out. The following calculation of new structure factors in the course of further refinement imposed no significant variations of sign.

Refinement of the Structure.—On the projections on (010) and (001) the atomic coordinates were corrected with a number of $F_o - F_c$ syntheses. For the projection on (010) the final coordinates were rapidly obtained. On the projection (001) the refinement required the calculation of several Fourier $F_o - F_c$. From such difference syntheses on both projections it was found either that the atomic form factor used for the Ni was not satisfactory for this structure, or that the thermal factor for this atom is a little larger than those of the light atoms. The Fourier transformation of the electron density of the Ni atom was calculated and a new atomic form factor including the thermal factor was introduced into the calculated structure factors.

In the last $F_o - F_c$ syntheses the residual maxima were interpreted as the locations of the hydrogen atoms. The observed and calculated structure factors are shown in a table available upon request to the authors. The final values of the reliability index are 0.10 for the $h0l$ reflections and 0.14 for the $hk0$ reflections. Table II lists the atomic coordinates for the bis-(N-methylsalicylaldehyde)-nickel(II).

TABLE I

FINAL ATOMIC COORDINATES FOR BIS-(N-METHYL-SALICYLALDIMINE)-N:(II)

	x/a	y/b	z/c
Ni	0.000	0.000	0.000
C ₁	+ .198	+ .040	+ .175
C ₂	+ .250	+ .102	+ .322
C ₃	+ .365	+ .080	+ .350
C ₄	+ .428	- .010	+ .238
C ₅	+ .375	- .080	+ .096
C ₆	+ .260	- .053	+ .066
C ₇	+ .220	- .086	- .100
C ₈	+ .095	- .112	- .326
N	+ .116	- .055	- .145
O	+ .093	- .071	+ .164
H ₂	+ .243	+ .136	+ .354
H ₃	+ .393	+ .129	+ .424
H ₄	+ .499	+ .040	+ .261
H ₅	+ .417	- .173	.000
H ₇	+ .264	- .079	- .176
H ₈	+ .115	- .196	- .408
H ₉	+ .038	- .117	- .369
H ₁₀	+ .064	- .208	- .249

TABLE II

ATOMIC COORDINATES IN A DIRECTION NORMAL TO THE MEAN PLANE OF THE TWO BENZENE RINGS OF THE MOLECULE (ÅNGSTRÖM UNITS)

C ₁	-0.034	C ₇	-0.332
C ₂	+ .017	N	- .460
C ₃	+ .001	C ₈	- .737
C ₄	- .003	O	- .032
C ₅	+ .016	Ni	.000
C ₆	- .006		

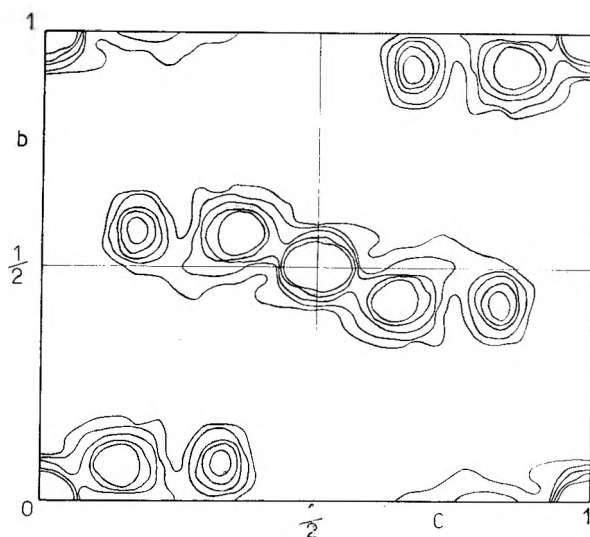
(6) H. Viervoll and O. Ogrim, *Acta Cryst.*, **2**, 277 (1949).(7) J. Housty and J. Clastre, *ibid.*, **10**, 695 (1957).

Fig. 1.—Electron density projection on (100). Contours at equal but arbitrary intervals.

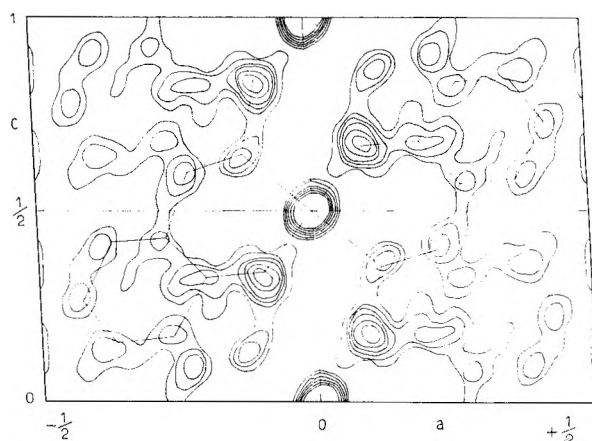
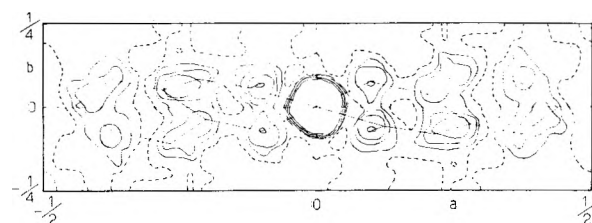
Fig. 2.—Electron density projection on (010). Contours at 3, 4, 5, 6, 7, 8 e.A.⁻¹. Upper levels are omitted.

Fig. 3.—Electron density projection on (001). Contours at equal but arbitrary intervals.

TABLE III

DISPLACEMENT OF THE ATOMIC POSITION FROM THE MEAN PLANE OF THE ATOMS C₆-C₇-C₈-N PASSING THROUGH THE Ni ATOM (ÅNGSTRÖM UNITS)

C ₆	+0.008	C ₈	+0.032
C ₇	+0.019	N	-0.082

Estimation of Accuracy.—The standard deviation of the atomic coordinates on the (010) projection were estimated by the Cruickshank's method.⁸ The extensive application of this method to the projection on (001) is ruled out by the overlapping of some atoms which occurs in that projection. Therefore the values of the mean error on the y coordinates were calculated only on the resolved maxima.

(8) D. W. J. Cruickshank, *ibid.*, **2**, 65 (1949).

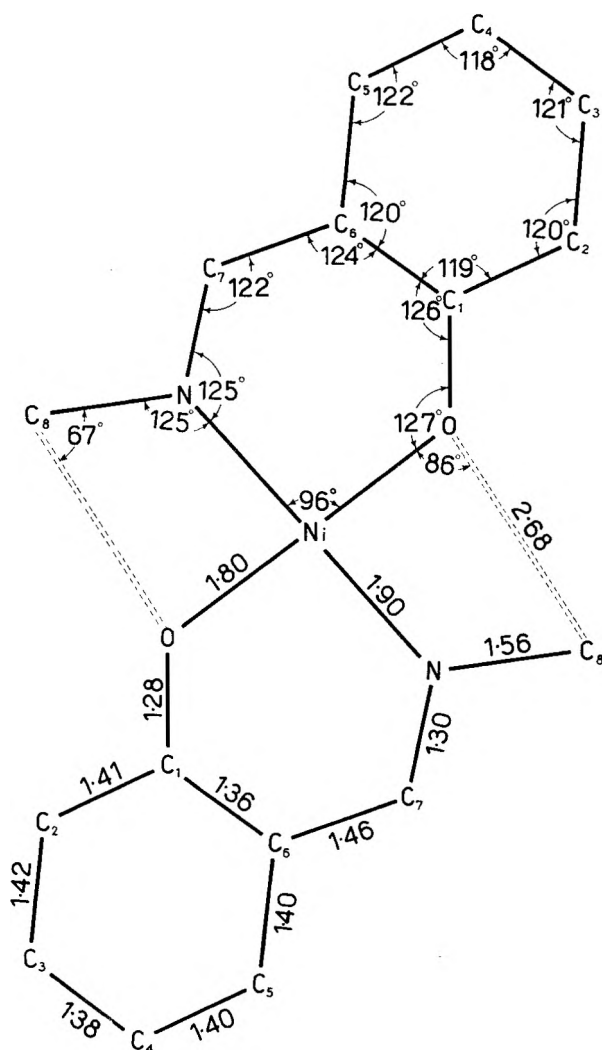


Fig. 4.—Molecular dimensions of the bis-(N-methyl-salicylaldimine)-Ni(II).

Using the symbols $\sigma(x)$, $\sigma(y)$ and $\sigma(z)$ to indicate the standard deviation of the x , y , and z coordinates, the values obtained were

For the C atoms: $\sigma(x) = 0.010 \text{ \AA.}$; $\sigma(y) = 0.050 \text{ \AA.}$; $\sigma(z) = 0.010 \text{ \AA.}$

For the N atoms: $\sigma(x) = 0.007 \text{ \AA.}$; $\sigma(y) = 0.030 \text{ \AA.}$; $\sigma(z) = 0.007 \text{ \AA.}$

For the O atom: $\sigma(x) = 0.020 \text{ \AA.}$; $\sigma(y) = 0.040 \text{ \AA.}$; $\sigma(z) = 0.010 \text{ \AA.}$

Description of the Structure of Bis(N-methylsalicylaldimine)-nickel(II).—In order to evaluate the planarity of the molecule the mean plane of the molecule was first calculated. The equation of this plane is

$$0.1233x - 0.3233z = y$$

The deviations of some atoms from this mean plane was found to be very strong and certainly greater than the calculated standard error. The mean plane of the benzene ring was then calculated (assuming a fundamentally planar structure for it). The equation of the mean plane of the benzene ring is

$$0.2119x - 0.5022z = y$$

From the coordinates of all the atoms in a direction normal to this plane the planarity of the benzene ring is confirmed within the limits of experimental error. Table II shows the coordinates of all the atoms in a direction normal to the mean plane of the benzene ring.

A mean plane for the zone C₆-C₇-C₈-N-Ni was then calculated. From the following equation of this plane

$$0.1543x - 0.2062z = y$$

and from the equation of the mean plane of the benzene ring passing through the Ni atom, it was found that the two planes make an angle of 12° to one another. The deviations of the atoms C₆-C₇-N-C₈ from the mean plane of this zone are listed on Table III. Figure 4 represents the projection of the molecule on its mean plane; bond lengths and angles are also shown. Table IV lists the intramolecular distances and angles.

TABLE IV
INTERATOMIC DISTANCES AND ANGLES IN THE MOLECULE OF
BIS-(N-METHYLSALICYLALDIMINE)-Ni(II)

Distances (Å)		Angles (°)	
Ni-O	1.80	N-Ni-O	96
O-C ₁	1.28	Ni-O-C ₁	127
C ₁ -C ₂	1.41	O-C ₁ -C ₂	126
C ₂ -C ₃	1.42	C ₁ -C ₂ -C ₃	124
C ₃ -C ₄	1.38	C ₆ -C ₇ -N	122
C ₄ -C ₅	1.40	C ₇ -N-Ni	125
C ₅ -C ₆	1.40	C ₈ -N-Ni	125
C ₁ -C ₆	1.36	C ₁ -C ₂ -C ₃	120
C ₆ -C ₇	1.46	C ₃ -C ₄ -C ₅	121
C ₇ -N	1.30	C ₃ -C ₄ -C ₆	118
Ni-N	1.90	C ₄ -C ₅ -C ₆	122
N-C ₈	1.56	C ₅ -C ₆ -C ₁	120
C ₈ -O	2.68	C ₆ -C ₁ -C ₂	119
		N-C ₈ -O	67
		Ni-O-C ₆	86

Discussion

The structure of the bis-(N-methylsalicylaldimine)-nickel(II) complex is strictly related to that of bis-salicylaldoxime-nickel(II) investigated by Merritt, *et al.*⁹ The two complexes are also similar with regard to the behavior in inert solvents. In fact the salicylaldoxime complex, as well as the bis-(N-methylsalicylaldimine)-nickel(II), are diamagnetic in the solid state but exhibit paramagnetism when dissolved in an inert solvent as chloroform.^{1a} For this reason it is interesting to compare the results of the two structural investigations.

In our complex the average length of the benzene ring bonds (1.39 Å) is in good agreement with the accepted value of 1.39-1.40 Å. The interatomic C-C and C-O distances in the six-membered chelate ring are 0.08-0.15 Å. shorter than those expected for single bonds. The C-C and C-N distances, 1.28 and 1.30 Å., respectively, are shorter than those observed in the oxime complex (1.40 Å.) and very close to the values of 1.24 and 1.28 Å., respectively, for the isolated double bonds. This could be taken as an indication that these bonds have greater double bond character in the aldimine than in the oxime complex. In the present case too the distance (1.36 Å.) of the C₁-C₆ bond which belongs both to the benzene and the chelate rings is the shortest of the bonds in the benzene ring. The Ni-O bond (1.80 Å.) is smaller than that calculated from the sum of the covalent radii (1.92 Å.) when one assumes the value of 1.15 Å. for the covalent radius of Ni.¹⁰ These facts lead to the assump-

(9) L. L. Merritt, Jr., C. Guare and A. E. Lessor, Jr., *Acta Cryst.*, **9**, 253 (1956).

(10) T. Moeller, "Inorganic Chemistry," John Wiley and Sons, New York, N. Y., 1952, p. 135.

tion of the existence of a "crossed" resonance in the chelate rings and consequently of the presence of π -bondings from the central nickel atom. This hypothesis was already brought forth on the basis of spectrophotometric measurements in the case of some nickel(II) complexes containing chelate rings of the same species.¹¹ The present results, therefore, seem to corroborate such a view.

The chelate ring in bis-(N-methylsallyaldimine)-nickel(II), unlike that in the oxime complex, is not planar. The N_1-C_6 axis bisects the chelate ring into two parts which are not co-planar. This distortion allows the C_3 atom to move away from the O atom. This effect is facilitated by the fact that the C_8-N-Ni angle is larger than the C_7-N-C_8 one. It should be noted that the three bonds from the N atom lie practically on the same plane, while the three bonds from the C_6 atom are not co-planar because the C_6-C_7 bond makes an angle of 13° with the plane of the other two.

(11) L. Sacconi, P. Paoletti and F. Maggio, *J. Am. Chem. Soc.*, **79**, 4067 (1957).

The C_8-O distance of 2.68 Å. is much shorter than a normal van der Waals distance and this may be due to the existence of a hydrogen bond between the two atoms. This hydrogen bond could arise from a $\delta+$ charge induced on the methyl carbon by the nitrogen atom carrying a positive charge.

It may be noted that the C_3 atom lies between two O atoms of two neighboring molecules at 3.21 and 3.79 Å., respectively. The direction $O-CH_3-O$ is approximately parallel to the axis b of the cell.

A very interesting datum is the distance between two neighboring nickel atoms. Actually the diamagnetism of this complex in the solid state could be explained on the assumption of spin-pairing between two nickel atoms, but the structure of the complex shows clearly that this is not the case. In fact the shortest Ni-Ni distance is found to be 5.32 Å.

Acknowledgment.—The authors are indebted to the Italian "Consiglio Nazionale delle Ricerche" for the support of this work.

WETTING OF LOW-ENERGY SOLIDS BY AQUEOUS SOLUTIONS OF HIGHLY FLUORINATED ACIDS AND SALTS¹

BY MARIANNE K. BERNETT AND W. A. ZISMAN

Contribution from the U. S. Naval Research Laboratory, Washington 25, D. C.

Received May 21, 1959

Wettability studies of aqueous solutions of several series of pure, highly fluorinated, aliphatic acids and salts were carried out on two low-energy organic solids, polyethylene and Teflon. As anticipated, the fluorinated compounds were able to depress the surface tension of water below the critical surface tension (γ_c) of Teflon, and were therefore capable of completely wetting it. In contrast, conventional hydrocarbon wetting agents do not depress the surface tension of water to this extent. Whenever possible, wettability curves were obtained for each solid surface by plotting the cosine of the contact angle *versus* the surface tension of the solution. The value of γ_c , 19 dynes/cm., thus obtained for Teflon is in reasonable agreement with the value of 18 dynes/cm. established from previous studies. With polyethylene a value of γ_c of 20 dynes/cm. was obtained, which is much lower than the established value of 31 dynes/cm. This led to experiments demonstrating that the phenomenon resulted from adsorption of the fluorinated compounds on the polyethylene surface, thereby altering its wetting characteristics to those of a fluorinated surface. As expected from the difference in their surface energies, greater and more tenacious adsorption was observed on polyethylene than on Teflon.

Introduction

In a recent study² on the wettability of low-energy solids by aqueous solutions of conventional surface-active agents, it was shown that the equilibrium contact angle (θ) and the ability of the solution to spread on the surfaces of polyethylene and polytetrafluoroethylene are rather simply related to the value of the critical surface tension (γ_c) of the solid surface and the surface tension (γ_{LV}) of the solution. Such solutions were found incapable of spreading freely on the clean, smooth surface of Teflon; this was expected because no single, pure, conventional, wetting agent lowers the surface tension of water below about 26 to 27 dynes/cm.³; the surface tension, therefore, cannot be decreased to the critical surface tension of about

18 dynes/cm.⁴ Aqueous solutions of certain highly fluorinated aliphatic acids and salts, however, can depress the surface tension of water lower than 18 dynes/cm.; such solutions should spread on Teflon. Solutions of a selected group of such compounds were investigated to examine further the relation of cosine θ to γ_{LV} and γ_c . In selecting fluorinated compounds for study, a variety of functional molecular end groups were desired, but choices were limited because each compound had to be sufficiently soluble in water and yet able to attain its surface tension minimum.

Materials and Experimental Procedures

Nearly all the fluorinated acids and salts used in these studies were preparations of unusual purity. The perfluoro acids (hereafter designated as ϕ -acids) were made available through the courtesy of the Minnesota Mining and Manufacturing Company. The ϕ -butyric acid was a water-white liquid with a reported boiling point of 170° (at 735 mm.), and the ϕ -octanoic, ϕ -decanoic and ϕ -dodecanoic acids were each recrystallized from carbon tetrachloride and toluene

(1) Presented before the Division of Colloid Chemistry, 135th Meeting, American Chemical Society, April 5-10, 1959, Boston, Massachusetts.

(2) M. K. Bennett and W. A. Zisman, *THIS JOURNAL*, **63**, 1241 (1959).

(3) E. K. Fischer and D. M. Gans, *Ann. N. Y. Acad. Sci.*, **46**, 371 (1946).

(4) H. W. Fox and W. A. Zisman, *J. Colloid Sci.*, **5**, 514 (1950).

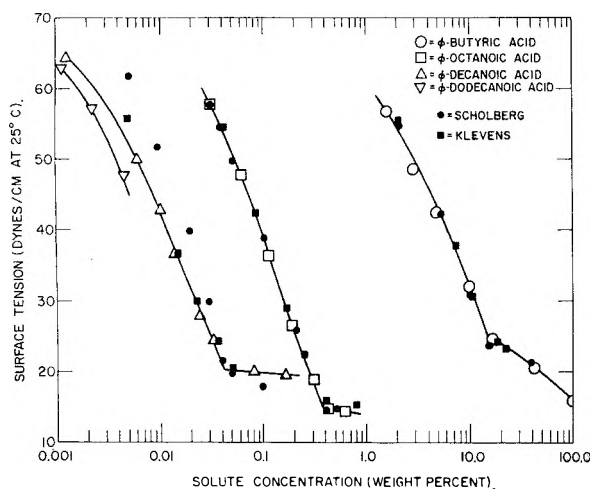


Fig. 1.—Surface tensions of perfluoro acids in aqueous solutions.

resulting in melting points of 54.9–55.6°, 87.4–88.2° and 112.6–114.7°, respectively. The potassium salt of ϕ -dodecanoic acid was prepared by dissolving the acid in water and alcohol, followed by neutralization with KOH. Salts of the ω -monohydroperfluoro acids (hereafter designated as ψ -acids) and the free ψ -heptanoic acid were kindly donated by the Jackson Laboratory of the du Pont Company. By decomposing the ammonium salt in aqueous solution and extracting with toluene, the free ψ -nonanoic and ψ -undecanoic acids were obtained. Recrystallization from toluene produced white solids with melting points of 67.5–68.5° and 96–97°, respectively.

Aqueous solutions of each fluorinated compound were prepared as described previously² using triply distilled water having a conductivity of 1.0×10^{-6} ohm⁻¹. Contact angles of the solutions were observed on a clean degreased square of platinum foil. Since the solutions completely wetted the clean platinum, surface tensions were measured by the ring method with a Cenco du Nouy interfacial tensiometer, using the Harkins and Jordan correction tables⁵; the precision was ± 0.1 dyne/cm. Surface tensions of several solutions were measured also by the pendant drop method,⁶ which is independent of the contact angle; the values obtained by the two methods were well within the margin of experimental error of $\pm 1\%$.

The source and surface preparation of the polyethylene and Teflon used have been described previously.² Contact angles were measured on a number of sites on three separate specimens of each plastic using an improved goniometer telescope⁴ and the drop buildup method.⁷ All measurements were carried out at $25 \pm 1^\circ$ and at 50% R.H. $\pm 2\%$.

Experimental Results

Figure 1 shows the surface tension (γ_{LV}) vs. concentration (c) curves of each of the ϕ -acids in aqueous solution. As Kauck and Diesslin⁸ have shown, acids containing as many as 10 carbon atoms per molecule were sufficiently soluble to depress appreciably the surface tension of water. However, ϕ -dodecanoic acid was too insoluble to reach the minimum surface tension. Our results agreed well with those obtained by Hendricks,⁹ Klevens¹⁰ and Scholberg, *et al.*¹¹ except those

(5) W. D. Harkins and H. F. Jordan, *J. Am. Chem. Soc.*, **52**, 1751 (1930).

(6) J. M. Andreas, E. A. Hauser and W. B. Tucker, *THIS JOURNAL*, **42**, 1001 (1938).

(7) E. G. Shafrin and W. A. Zisman, *J. Colloid Sci.*, **7**, 166 (1952).

(8) E. A. Kauck and A. R. Diesslin, *Ind. Eng. Chem.*, **42**, 2332 (1951).

(9) J. O. Hendricks, *ibid.*, **45**, 99 (1953).

(10) H. B. Klevens and M. Raison, *J. Chem. Phys.*, **51**, 1 (1954).

(11) H. M. Scholberg, R. A. Guenther and R. I. Coon, *THIS JOURNAL*, **57**, 923 (1953).

obtained by the latter on ϕ -decanoic acid. The higher surface tension values they obtained in the more dilute solutions may be due to errors caused by not allowing for the adsorption of the solute on the walls of the vessels. Table I shows that the discontinuities in the slopes of the graphs of Fig. 1 occur at approximately the same concentrations established by these previous investigators and correspond to the respective critical micelle concentration (c.m.c.) determined by them using the surface tension method. It is remarkable that the surface tensions at which the c.m.c. of these perfluoro acids occur do not decrease with increasing chain length as could usually be expected, but increase again starting with the ϕ -decanoic acid. Unfortunately, ϕ -dodecanoic acid is too insoluble in water to be useful in determining whether this upward trend would continue.

Figure 2 represents the γ_{LV} vs. c curves of the ψ -acids and ψ -ammonium salts in aqueous solution. Although the salts of the C_7 and C_9 acids were sufficiently soluble, the C_{11} acid and salt and higher homologs were too insoluble for the purposes of this study. The ψ -heptanoic acid was quite soluble but not quite enough to reach its minimum surface tension. Surface tensions of the ψ -NH₄-nonanoate in a series of concentrations had been previously investigated by Arrington and Patterson¹²; their much lower surface tensions, especially at the lowest concentrations, could have been caused by traces of a higher homolog. The c.m.c. they obtained by the dye titration technique for various ψ -compounds are somewhat higher than the concentration at which the breaks occurred in the surface tension vs. concentration curves obtained in this study and in their own experiment, as can be seen in Table I. This variation in the c.m.c. obtained by various methods has been observed by many investigators.

Surface tension vs. $\cos \theta$ curves obtained with aqueous solutions of each of the above-mentioned fluorinated compounds on clean, smooth Teflon and polyethylene surfaces are given in Figs. 3 and 4, respectively. In our earlier study of aqueous solutions of conventional wetting agents,² the discontinuities in slope in the $\cos \theta$ vs. γ_{LV} curve of each solution occurred approximately at the c.m.c. of the solute. However, a different result was obtained with the highly fluorinated wetting agents. Table II demonstrates that, although the surface tension corresponding to the c.m.c. in Figs. 1 and 2 varied from compound to compound, the discontinuities in slope in Figs. 3 and 4 fell within the narrow surface tension range of 35 to 42 dynes/cm. Evidently, such discontinuities in slope must relate to phenomena other than the c.m.c.

Figure 3 reveals that the critical surface tension γ_c falls within the previously established region of 17–19 dynes/cm.^{2,4} As anticipated, some of the ϕ -acids depressed the surface tension of water below the critical surface tension of wetting of Teflon and, therefore, completely wetted it (*e.g.*, ϕ -butyric acid and also a 0.4 and 0.6% solution of ϕ -octanoic acid). The contact angles formed on

(12) C. H. Arrington and G. D. Patterson, *ibid.*, **57**, 247 (1953).

TABLE I
C.M.C. AND CORRESPONDING SURFACE TENSION FOR AQUEOUS SOLUTIONS OF HIGHLY FLUORINATED COMPOUNDS^a

Solute	Surf. tens. at the c.m.c. (dynes/cm.)		C.m.c. (moles/l.)			
	This study	Lit. Ref.	By surf. tens.		By conduct. Lit. Ref.	By dye titr. Lit. Ref.
			This study	Lit. Ref.		
ϕ -Butyric acid	25.5	24.0 (10) 24.0 (11)	7.4×10^{-1}	7.1×10^{-1} (10) 7.5×10^{-1} (11)	4.2×10^{-1} (10)	
ϕ -Octanoic acid	15.3	16.8 (10) 15.0 (11)	9.1×10^{-3}	8.7×10^{-3} (10) 8.7×10^{-3} (11)	5.5×10^{-3} (10)	
ϕ -Decanoic acid	20.5	20.4 (10) 20.0 (11)	7.8×10^{-4}	8.9×10^{-4} (10) 8.5×10^{-4} (11)		
ψ -Nonanoic acid	21.8		9.0×10^{-3}			3.0×10^{-2} (12)
ψ -NH ₄ -Heptanoate	26.9		1.1×10^{-1}			2.5×10^{-1} (12)
ψ -NH ₄ -Nonanoate	27.5	25.5 (12)	2.8×10^{-2}	3.2×10^{-2} (12)		3.8×10^{-2} (12)

^a Values of references 10 and 11 are estimated from the cited graphs.

TABLE II

COMPARISON OF SURFACE TENSIONS AND CONCENTRATIONS AT THE BREAKPOINTS OBTAINED FROM γ_{LV} vs. c AND $\cos \theta$ vs. γ_{LV} CURVES

Solute	γ_{LV} at discontinuity (dynes/cm.)			Concn. at discontinuity (wt. %)		
	From γ_{LV} vs. c (at c.m.c.)	From $\cos \theta$ vs. γ_{LV} PE	γ_{LV} Teflon	From γ_{LV} vs. c (c.m.c.)	From $\cos \theta$ vs. γ_{LV} PE	γ_{LV} Teflon
ϕ -Butyric acid	25.5	34.5	34.5	14.8	8.0	8.0
ϕ -Octanoic acid	15.3	39.5 ^a	39.5 ^a	0.38	0.1 ^a	0.1 ^a
ϕ -Decanoic acid	20.5	42.0 ^a	40.0 ^a	0.042	0.011 ^a	0.012 ^a
ψ -Nonanoic acid	21.8	...	38.0	0.5	...	0.19
ψ -NH ₄ -Heptanoate	26.9	39	37.5	4.0	1.6	1.7
ψ -NH ₄ -Nonanoate	27.5	38	36	1.3	0.78	0.70

^a Determined from areas of adsorbed solution.

Teflon by drops of the ϕ -octanoic and the ϕ -decanoic acid solutions, however, were so erratic and difficult to reproduce that meaningful data could not be obtained. A modified method for obtaining contact angles was therefore used. Even with the dilute solutions exhibiting reproducible contact angles, the values observed were either higher or lower than would be expected from the value of the surface tension at such low concentrations. In short, there was a large spread of the $\cos \theta$ vs. γ_{LV} curves at the higher surface tensions and only a few curves actually converged at the graphical point for pure water.

Inspection of Fig. 4 will show that these difficulties were also observed with the solutions on polyethylene. Drops of some very dilute solutions exhibited contact angles which were the same or only a little less than that of pure water. When slightly higher concentrations were used, the contact angle varied by as much as 15°. Solutions of ϕ -butyric acid and of the ψ -ammonium salts exhibited reproducible contact angles. In working with the higher ϕ -acids, reproducible angles were obtained only by using the same modified method used on Teflon. All contact angles were found to be much larger than would be expected from the solution surface tensions. Graphs of $\cos \theta$ vs. γ_{LV} obtained with these solutions intercepted the line $\cos \theta = 1$ at values between 19.0 and 21.5 dynes/cm. Such intercepts should correspond to the critical surface tension of polyethylene approximating 31 dynes/cm.^{2,13} In the present investigations, however, solutions having surface tensions as low as 20.4 dynes/cm. still exhibited appreciable contact angles on polyethylene. It was surmised that these unusual

(13) H. W. Fox and W. A. Zisman, *J. Colloid Sci.*, **7**, 428 (1952).

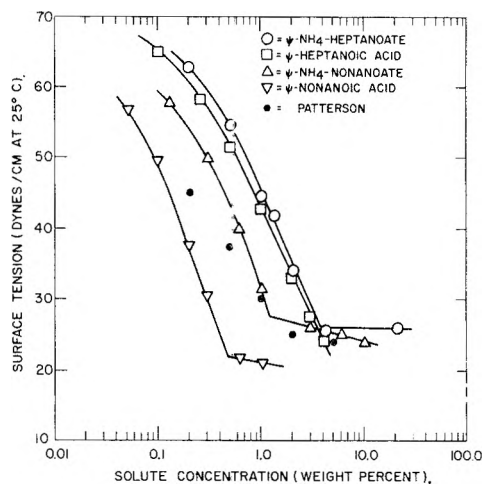


Fig. 2.—Surface tensions of ω -monohydroperfluoro compounds in aqueous solutions.

results were caused by adsorption of the fluorinated solute on both of these low-energy solids.

Experiments were therefore devised to ascertain whether adsorption of the solute had occurred at the interface of solid and solution. First, a large drop of the most concentrated solution of the wetting agent under investigation was placed on the clean organic solid. Then, after a two minute interval, the optimum length of time for avoiding either excessive evaporation of water or any associated precipitation of the solute, the drop was blotted up with clean filter paper, care being taken that no visible liquid or solid residue remained on the surface. Any solution remaining on the surface after blotting would not amount to more than 1% of the original amount of solution deposited. The drop having a volume of about

TABLE III

EVIDENCE OF SOLUTION ADSORPTION OF ϕ -K-DODECANOATE ON TEFLON AND POLYETHYLENE FROM CONTACT ANGLES WITH VARIOUS REFERENCE LIQUIDS

Ref. Liq.	θ on Teflon			θ on polyethylene			θ on close-packed monolayer	
	On clean surface	After contact with ϕ -soln. ^a	After subsequent contact with H ₂ O ^b	On clean surface	After contact with ϕ -soln. ^a	After subsequent contact with H ₂ O ^b	-CF ₂ groups	-CF ₂ H ^d groups
Methylene iodide	83	94-96	83-85	50	78-82	56-60	103	..
Aroclor 1248	78	88	78	37	64-68	48	96	83
Hexachlorobutadiene	64	66	64	<5	54-56	26	81	69
Dicyclohexyl	59	<5	56-60	25-29
Hexadecane	46	56-60	47	Spreads	50	15	78	67

^a Surface after contact with ϕ -K-dodecanoate solution. ^b Surface after contact with ϕ -K-dodecanoate solution, followed by H₂O. ^c Close-packed monolayer of ϕ -dodecanoic acid (ref. 14). ^d Close-packed monolayer of ψ -undecanoic acid (ref. 15).

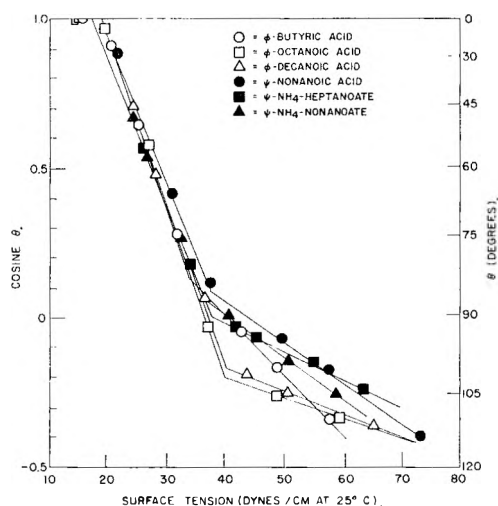


Fig. 3.—Wettability of Teflon by aqueous solutions of highly fluorinated compounds.

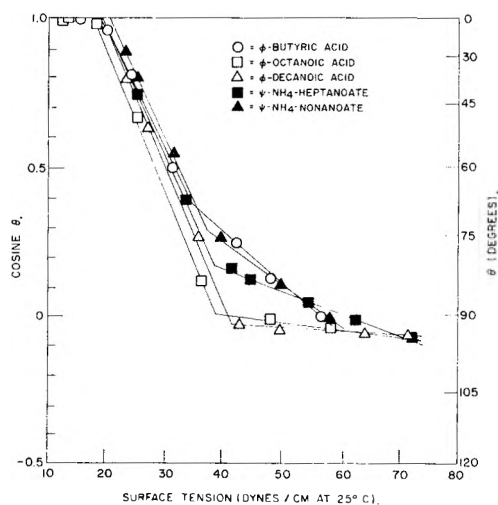


Fig. 4.—Wettability of polyethylene by aqueous solutions of highly fluorinated compounds.

0.05 ml. and a contact area of about 0.2 cm.² would, because of the low solute concentrations used, leave no more than a monolayer of solute on the polymer surface upon evaporation of the water. Finally, a drop of a reference liquid known not to dissolve these highly fluorinated compounds was

placed on the same area and its contact angle was measured. Reference liquids used were the carefully purified compounds given in Table III. When adsorption of the solute had occurred, the contact angle observed was larger than that on the clean surface, since the atoms on the exposed surface then consisted partially of -CF₂ or -CF₂H groups (according to the nature, packing and orientation of molecules of the adsorbed solute) rather than only of -CF₂- or -CH₂- groups which dominate the surface composition of Teflon or polyethylene. If no adsorption had occurred, the contact angle of the reference liquid remained the same as on the clean surface. By this approach it was demonstrated that solute adsorption was often occurring. The same experiment, when carried out with solutions of conventional wetting agents, showed no change in the values of the contact angles.

The erratic contact angle values obtained earlier from the solution of ϕ -octanoic and ϕ -decanoic acids were therefore caused by uncontrolled variables arising from the adsorption of the solute leaving a drop of a higher surface tension resting upon the adsorbed film. As the adsorption correction varied with the solute as well as the volume and concentration of the drop, it caused the contact angle to vary in repeat experiments. Consequently, a modified method was employed for determining the correct contact angles. A large drop of each solution was allowed to remain undisturbed for two minutes on the clean low-energy surface and was then blotted up. Immediately afterwards another drop of fresh solution was placed on the same area. This time a stable and reproducible contact angle was observed. Blotting up the second drop and adding a third did not cause a further change in the contact angle. Hence, the value obtained with the second drop was used in plotting the wettability curves of Figs. 3 and 4.

Desorptivity of the film previously adsorbed on each plastic was studied by placing a large drop of the solution on the clean, solid plastic surface and subsequently blotting it up; next a large drop of pure water was placed on the same area and allowed to remain for two minutes. Immediately afterwards, the drop was absorbed with clean filter paper and the contact angle was again determined on the same site using one of the organic reference liquids; if the same value was observed as after the adsorption experiment, the fluorinated monolayer had not desorbed. If the contact angle reverted back to the same value as on the

(14) E. F. Hare, E. G. Shafrin and W. A. Zisman, *THIS JOURNAL*, **58**, 236 (1954).

(15) A. H. Ellison, H. W. Fox and W. A. Zisman, *ibid.*, **57**, 622 (1953).

TABLE IV

EVIDENCE OF SOLUTION ADSORPTION OF VARIOUS FLUORINATED COMPOUNDS ON TEFLON AND POLYETHYLENE FROM CONTACT

Solute (wt. % in water)	ANGLES WITH HEXADECANE ^a			Contact angle on polyethylene, degree		
	Contact angle of Teflon, degree		After subse- quent contact with H ₂ O	On clean surface	After contact with adsorb- ing soln.	After subse- quent contact with H ₂ O
	On clean surface	After contact with adsorb- ing soln.				
<i>φ</i> -Compounds						
<i>φ</i> -Butyric acid (30%)	46	46	46	Spreads	Spreads	Spreads
<i>φ</i> -Octanoic acid (0.6%)	46	62-65	46	Spreads	52-56	Spreads
<i>φ</i> -Decanoic acid (0.024%)	46	64-67	46	Spreads	57-61	Spreads
<i>φ</i> -Dodecanoic acid (0.0055%)	46	51-52	46	Spreads	32-38	Spreads
<i>φ</i> -K-dodecanoate	46	56-60	47	Spreads	50	15
<i>ψ</i> -Compounds						
<i>ψ</i> -Nonanoic acid (0.6%)	46	56-60	47	Spreads	40	15
<i>ψ</i> -NH ₄ -Heptanoate (4%)	46	52-56	46	Spreads	60	Spreads
<i>ψ</i> -NH ₄ -Nonanoate (10%)	46	62-65	46	Spreads	62-64	Spreads

^a Contact angle of hexadecane on reference monolayer of -CF₃ = 78°¹⁴; of -CF₂H = 67°.¹⁵

original clean surface, complete desorption had occurred.

Since *φ*-dodecanoic acid was too insoluble in water to be of value in the adsorption studies, the potassium salt of the acid was used. Contact angles were measured for each of the various reference liquids on the areas of Teflon and polyethylene which had previously been treated with this salt solution; the results are given in Table III. After adsorption of each fluorinated compound, a drop of pure water was placed on the film-covered surface and later removed. The surface now exhibited the contact angles given in Table III. The results demonstrate that adsorption of the potassium *φ*-dodecanoate took place on polyethylene and Teflon. Since the contact angles in columns 3 and 6 were definitely much higher than on the original clean surfaces (columns 2 and 5), adsorption is clearly indicated. In fact, considerable adsorption of steeply-inclined oriented molecules on Teflon is suggested, since each contact angle is more than half way between that on a surface of close packed CF₃- groups and that on any of -CF₂- groups (see columns 8 and 2). On polyethylene the fluorinated molecules may be adsorbed nonuniformly with some in inclined position or may be adsorbed more extensively with all lying in the surface; however, adsorption was not sufficient to result in a close-packed monolayer. By comparing columns 4 and 7 with columns 3 and 6, respectively, it can be seen that after contact with the drop of water the contact angle of each organic reference liquid was lowered. In the experiments with Teflon the contact angles of column 4 are the same as on the original clean surface (see column 2), demonstrating complete desorption from Teflon by brief contact with water. In the experiments with polyethylene, the contact angles were somewhere between the two extremes, suggesting only partial desorption. It is thus evident that the fluorinated solute molecules adsorb more weakly on Teflon than on polyethylene.

By using the same procedures, the adsorption of each of the other fluorinated solutes on Teflon and polyethylene were observed using hexadecane as the reference liquid. The results, given in Table IV, also confirm the above conclusions and extend them to all of the fluorinated solutes studied.

It can be seen in Table IV that no change in contact angle occurs when a solution of *φ*-butyric acid had been placed on either surface. Increasingly larger contact angles indicated increasingly more efficient adsorption of the higher homologs of the perfluoro acids up through *φ*-dodecanoic acid. The apparent decreased adsorption in going from *φ*-octanoic to *φ*-dodecanoic acid reflects its insufficient solubility in water precluding maximum possible adsorption of solute molecules. Large increases in the contact angles resulting from adsorption of the *φ*-octanoic and *φ*-decanoic acids are evidence of considerable adsorption of fluorinated molecules at the solid/solution interface. Short-chain acids are believed to be adsorbed in an essentially flat configuration because of the weak adhesion of the polar-end group, and thus exhibit a heterogeneous surface. Longer-chain compounds, however, through the effect of intermolecular cohesion and adlineation, may adsorb with the long axes of the molecules in a more nearly upright orientation; the contact angles indicate that the outermost surface behaves as if composed of over 50% of the highly-fluorinated methyl groups.

An independent demonstration of the adsorption of *φ*-acids on polyethylene was made by vigorously shaking a 0.12% solution of *φ*-octanoic acid with clean, finely powdered polyethylene (Super Dylan 6600). The surface tension of the solution after contact with the polyethylene was raised by 5.0 dynes/cm., corresponding to a final concentration of 0.09%. This 25% decrease in solute concentration is caused by adsorption of molecules of *φ*-acid on the surface of the particles of polyethylene.

One would expect the solution adsorption of fluorinated compounds on polyethylene to be stronger than on Teflon, since the change in free surface energy in going from a surface consisting of -CH₂- groups to one consisting of CF₃- groups is much larger than in going from a surface comprised essentially of -CF₂- groups. It can now be understood why aqueous solutions of highly fluorinated compounds having a surface tension lower than the critical surface tension of polyethylene may not be able to wet its surface completely. Unless sterically or otherwise hindered from so doing, the fluorinated compound can

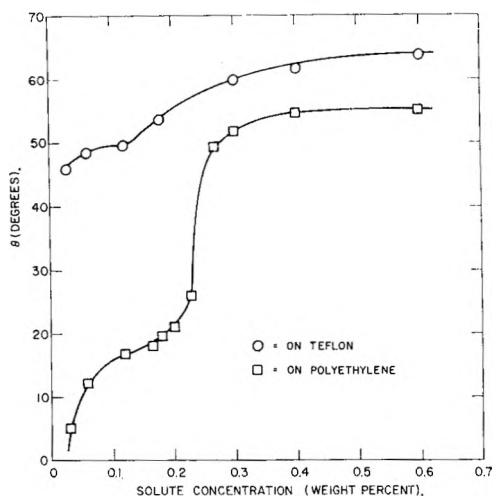


Fig. 5.—Hexadecane contact angles on polymer surfaces with ϕ -octanoic acid adsorbed from aqueous solutions of various concentrations.

adsorb at the solid/solution interface to change the constitution of the solid surface from a hydrocarbon to a more or less completely fluorinated surface with much lower surface energy. An analogous adsorption of the conventional hydrocarbon wetting agents on polyethylene would not be expected to occur, since little or no lowering of the surface energy would result.

Earlier it had been shown in Figs. 3 and 4 and Table II that for each fluorinated solute the discontinuity in slope of the γ_{LV} vs. c curve occurred at a much lower concentration than that of the $\cos \theta$ vs. γ_{LV} curve. For example, whereas the discontinuity in the γ_{LV} vs. c curve for ϕ -octanoic acid occurred at a concentration of 0.38 wt. % that in the $\cos \theta$ vs. γ_{LV} curve for either polyethylene or Teflon occurred at about 0.1 wt. %. The discontinuities in the wettability curves for Teflon and polyethylene occur at nearly equal solution concentrations for a given solute; also, the corresponding surface tensions all range between 35 and 42 dynes/cm. It was inferred, therefore, that the adsorption of the fluorinated solute was occurring at the solid/solution interface at such low concentration as to cause a considerable lowering in the critical surface tension of wetting of the solid. To verify this, contact angles of hexadecane were measured on Teflon and polyethylene using the same procedure as for the

previous adsorption experiments. Drops of ϕ -octanoic acid solution of different concentrations were placed on the respective solid and blotted up after a two-minute interval. Plots of the contact angle of hexadecane obtained on those areas vs. the ϕ -octanoic acid concentration are given in Fig. 5. Each curve shows two remarkable changes in the slope, one at a concentration of about 0.1% and one at 0.3%. It may be concluded from the first change in slope that significant adsorption at the solid/solution interface was occurring at concentrations of 0.1%, the concentration at which there was a discontinuity in the slope of the $\cos \theta$ vs. γ_{LV} curves (Table II). The phase change occurring at the 0.1% concentration is presumed to be due to a change in either the orientation or packing of the film adsorbed at the solid/solution interface, resulting in conversion of the gaseous film to a more condensed one.

The abrupt increase in contact angle with increasing concentration above 0.1% can be explained by another phase change occurring at the solid/solution interface, this time resulting in a highly condensed film. This effect reaches its maximum at a concentration of about 0.3 to 0.4%, the second change in slope apparent in the curves. Concurrently, solute adsorption also increases at the air/solution interface and reaches its maximum at a concentration of 0.3–0.4%, as evidenced by the formation of micelles. Table II shows that the c.m.c., as determined from the γ_{LV} vs. concn. curve, occurs at just this concentration, 0.38%. It can then be assumed that the second change in slope in Fig. 5 indicates the phase change to a highly condensed film at the solid/solution interface, coinciding with the maximum solute adsorption at the solution/air interface.

Thus, it may be concluded that the wettability behavior of the fluorinated wetting agents differs at low concentrations from that of the conventional wetting agents. In the former case, the pronounced adsorption of solute causes the maximum in the adsorption vs. concentration curve of the Gibbs isotherm to occur at a much lower concentration at the solid/solution interface than at the solution/air interface. In the latter case, the low adsorptivity of the solute causes the adsorption at both interfaces to occur at about the same concentration. Complete wetting, however, does not occur in any system until γ_{LV} is less than γ_c of the clean solid.

ACIDIC PROPERTIES OF BENTONITE¹BY ARTHUR C. THOMPSON² AND J. L. CULBERTSON*Contribution from the Department of Chemistry, State College of Washington, Pullman, Washington and of the Department of Physical Sciences, University of Idaho, Moscow, Idaho**Received May 22, 1959*

An investigation of the acidic properties of dibasic acid Wyoming bentonite was undertaken to determine the effects of aging of suspensions in the hydrogen form and at various degrees of saturation of H-bentonite with sodium ion. The effects of suspension concentration, neutral salt addition and the cation of the titrating base on the dibasic acid property are described. Polyelectrolyte theory in particular is applied to account for the weak acid function of bentonite titration curves. Methods of modifying the acidic character of the Wyoming bentonite by processing bentonite suspensions on ion-exchange resin columns are described.

Introduction

The dibasic acid titration behavior of Wyoming H-bentonite has been reported by various investigators. Characteristic of these titration curves is a first inflection at pH values 4.6–5.0 and a second inflection at pH 7.8–8.4. Where the pH is plotted as a function of the meq. (M) of base per 100 grams of H-bentonite oven-dried at 110°, the position of the first inflection, M_1 , is found around 45 meq. The " M " value for the second inflection, M_2 , corresponds to the titrated base exchange capacity of the bentonite; it is often found at about 90 meq.

Slabaugh³ has stressed the importance of the aging effect on the titration properties of H-bentonite suspensions. On titration of H-bentonite that has been allowed to stand a few months, the first equivalence point appears farther to the left on the abscissa of the pH versus " M " plot, the more so the older the suspension in the hydrogen form before titration. This effect is thought to be due to an auto-degradation of the clay structure by the adsorbed hydrogen ions according to Low⁴ and Coleman and Harward.⁵ This apparent degradative process is presumed to occur in the process of preparation by electro dialysis or acid leaching and continues slowly when hydrogen saturated suspensions are allowed to stand. Low⁴ and Coleman and Harward⁵ have prepared H-Al-bentonites in various H/Al ratios and have correlated the proportion of dibasic titration character to these ratios. In order to determine more precisely the conditions under which this autodegradation occurs, the effect of aging H-bentonite suspensions and of suspensions partially neutralized with sodium hydroxide and in the presence of varying amounts of added neutral salt were investigated. Also, titration curves on pure H-bentonite suspensions were determined after varying periods of aging.

The appearance of some H-bentonite titration curves suggests that for the weak acid function the pH values are linearly related to the function, $\log \frac{\alpha_2}{1 - \alpha_2}$, where α_2 is the degree of neutralization of the weak acid function. It is of interest to consider the titration curves from the point of view of polyelectrolyte theory. In this connection it should be possible to relate the pH values of H-

bentonite suspensions at various degrees of neutralization and at various suspension concentrations. Also, in this connection, the effect of saturation of the bentonite with aluminum ion is of interest.

Since the apparent dibasic acid character of H-bentonite titration curves is affected by aging, it is of interest to determine if the effect of aging could be reversed by substitution of hydrogen ion for exchange site substituted aluminum. In this connection, Low⁴ has reported titration curves of Wyoming H-bentonite obtained by addition of sufficient hydrochloric acid to silver saturated bentonite to convert all the ion-exchange site substituted silver ion to silver chloride. The H-bentonite obtained by this method is essentially monobasic and strongly acidic.

Experimental

The Wyoming bentonite used in this investigation was supplied by the National Lead Company, Baroid Division. A fine particle bentonite was dispersed to a 3% suspension and allowed to settle for several days. The settled portion was rejected. H-bentonite was prepared by forcing the 1% solids bentonite suspension through a deionizing resin column by application of an aspirator vacuum. A monobed resin performed the function of electro dialysis by exchanging the small cations for hydrogen ion and the anions present for hydroxyl ion.

The titrations were carried out with carbonate-free, approximately 0.1 *N* NaOH. The pH measurements were made with a model "G" Beckman pH meter. The bentonite suspension was stirred at a constant rate during a given titration, using a magnetic stirrer. Frequently, a conductance titration was carried out simultaneously using a dipping conductance cell. The H-bentonite suspensions were titrated after various periods of standing at room temperature. The pH values at various standing times were measured for a series of partially neutralized samples which were prepared by addition of the requisite volume of base to 25 ml. of a 1.27% solids suspension of H-bentonite already 60 days aged. Each sample was diluted to 40 ml., making the suspension concentration 0.79% for all samples.

It is possible to saturate bentonite with a given cation by passing the sodium or hydrogen bentonite through the cation saturated resin several times. Aluminum bentonite, however, was prepared by shaking the H-bentonite with sulfonic acid resin particles saturated with aluminum ion. Slow centrifugation of this mixture, followed by washing of the settled resin with distilled water, was sufficient to separate the resin particles from the Al-bentonite.

Results and Discussion

Conductance and pH titration curves were run on suspensions of H-bentonite prepared by sulfonic acid ion-exchange resin after aging periods of 3 days, 60 days, 5 months and 18 months. The pH titration curve (Fig. 1, curve E) of a freshly prepared suspension is similar to that of an approximately 1:1 mixture of a strong acid and a weak acid. The

(1) In partial fulfillment of the requirements for the Ph.D. degree at the State College of Washington, Pullman, Washington.

(2) Nalco Chemical Co., 6216 W. 66th Place, Chicago 38, Ill.

(3) W. H. Slabaugh, *J. Am. Chem. Soc.*, **74**, 4462 (1952).

(4) P. F. Low, *Soil Sci. Chem. Proc.*, **19**, 135 (1955).

(5) N. T. Coleman and M. E. Harward, *J. Am. Chem. Soc.*, **75**, 6045 (1953).

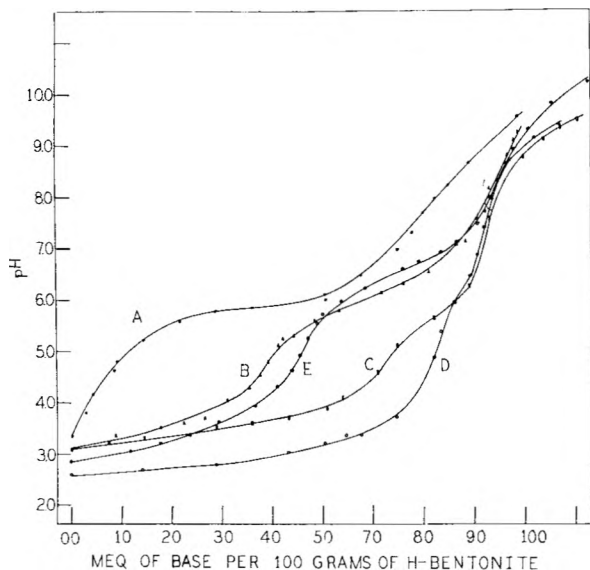


Fig. 1.—Effect of aging Wyoming H-bentonite and of recycling aged sample on H-sulfonic and Na-carboxylic ion exchange resins: (A) H-bentonite 1.27%, aged 18 months; (B) same as "A," aged 60 days; (C) sample "A" after 10 Na-H resin cycles; (D) sample "A" after 24 Na-H resin cycles; (E) titration curve of 0.76% H-bentonite suspension from monobed resin column.

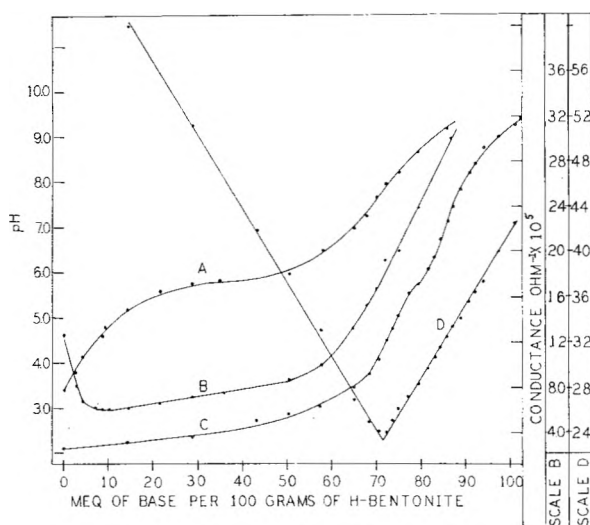


Fig. 2.—Conductance and pH titrations of aged and resin cycled H-bentonite: A and B, 1.27% solids, aged 18 months; C and D, titration of aged sample after many Na-carboxylic and H-sulfonic resin cycles.

effect of aging of H-bentonite suspensions for 60 days resulted in a decrease of only 4 meq. in the titrated exchange capacity, M_2 . The position of the first inflection, M_1 , shifted from 46 to 37 meq. The effect of aging is much more apparent for H-bentonite suspensions that were aged 18 months (Fig. 1, curve A, Fig. 2, curves A and B); the pH rises sharply on the addition of a few meq. of base and M_2 is reduced from 88 to 57 meq. The conductance curve for H-bentonite suspensions aged 18 months, which was obtained simultaneously with the pH curve, shows a steep decline in the conductance on addition of a few meq. of base to a minimum, which corresponds to the position and pH of the first equivalence point. The conduct-

ance at first slowly, and then abruptly, increases on titration to the second equivalence point.

The titration curves of the H-bentonite suspension aged 5 months or more resemble the titration curves of electrodyalized H-bentonite reported by Marshall⁶ and Low.⁴ Electrolysis requires considerable time; it may be presumed that this process contributes to the degradation of the clay on aluminum ion saturated bentonite rather than H-bentonite being formed. However, the titration curve of an H-bentonite obtained by the rapid ion exchange process (Fig. 1, curve E) is almost identical with the titration curve reported by Slabaugh and Culbertson⁷ for electrodyalized H-bentonite. It is concluded that electrolysis or ion-exchange resin treatment is not responsible for any special degradation of Wyoming bentonite. It seems likely that the weak acid property is inherent in the particular sample; electrolysis or processing the bentonite suspensions on ion-exchange resins will not remove exchange site substituted aluminum ion.

The effect of aging partially neutralized H-bentonite suspensions is shown in Fig. 3. For samples neutralized up to the first inflection, there is a very slow pH rise on aging. The pH curve of the suspensions aged for various periods of time cross the pH curve of suspensions aged for 3 days at the position of the first equivalence point. From this point to about 80% neutralization of the weak acid function, there is a pH drop of 0.25–0.35 pH unit. The pH drop for suspensions to which excess base was added was much greater. There is a tendency for all the higher pH values to drop down to pH values of 7.5–8.0. The exchange capacity obtained from the position of the second inflection is somewhat larger than obtained in the usual titration.

Varying amounts of neutral salt were added to partially neutralized suspensions of H-bentonite. The effect of salt addition is to decrease the pH . If sufficient salt is added, it is difficult to identify the position of the first equivalence point; the position of the second equivalence point is more sharply defined. The effect of aging these partially neutralized suspensions, 0.002 and 0.032 N in NaCl is shown in Fig. 4. The pH changes are qualitatively similar to suspensions to which no salt is added. The curves for fresh and aged suspensions cross near the first equivalence point. If sufficient neutral salt is present as in the case of the suspensions in curves C-1 and C-2, autodegradation of the clay due to hydrogen ion probably does not occur to an appreciable extent. Most of the hydrogen ion associated with the clay micelle is dissociated into the "outside solution" and does not participate in the autodegradative process. The concentration of hydrogen ion at the surface of the bentonite particles ("inside solution") is much greater in those suspensions to which no neutral salt was added than in suspensions in curves C-1 and C-2.

These results indicate that the marked decrease in osmotically active hydrogen ion as indicated by

(6) C. E. Marshall, "The Colloidal Chemistry of Silicate Minerals," Academic Press, Inc., New York, N. Y., 1949.

(7) W. H. Slabaugh and J. L. Culbertson, *THIS JOURNAL*, **55**, 705 (1950).

pH and conductance measurements continues in samples of H-bentonite not neutralized beyond the first equivalence point and this process can occur at fairly high solution pH (up to pH 4.5). These results again suggest the involvement of adsorbed aluminum ion in the weak acid segment of the titration curve. The weak acid function may be due to the hydrolysis of exchange site adsorbed aluminum. The strong acid function is possibly due to the hydrogen ion that balances the negative sites not covered by aluminum ion.

The bentonite particle may be considered to be an assembly of negative charges distributed on its surface to which hydrogen ions are bound as counterions. The dissociation of hydrogen ion from a given charge site increases the net charge on the particle from i to $i+1$. An intrinsic dissociation constant can be assigned to each undissociated hydrogen ion. For the special case of no interaction between charged sites the intrinsic dissociation constant k is the same regardless of the position of the particular ionization site with respect to a previously ionized state. Similarly, the dissociation constant for the ionization of the i th $+1$ hydrogen ion is the same regardless of the particular position of the dissociating site with respect to neighboring dissociated or undissociated sites. The ionization constant k_i differs from the ionization constant, k_{i+1} , by statistical factors only. An analysis of the neutralization of such an acid according to this simple model, using the statistical method outlined by Pauli and Valko⁸ and by Veiss⁹ leads to the derivation of a modified Henderson-Hasselbach equation such as has been proposed by Kern¹⁰ and Kachalsky.¹¹ For a given concentration of polyacid; where the pK_m is called the "mean" pK and

$$pH = pK_m - n \log \frac{\alpha}{1 - \alpha}$$

where α corresponds to the half neutralization pH at a given concentration of acid; the slope factor n is equal to unity for a polyacid having the properties previously described. Such an analysis was carried out on the titration curve for the specially prepared series in which the concentration is 0.79% and the suspension already 60 days old. If the pH versus the function $\log \alpha_1 / (1 - \alpha_1)$ is plotted for the strong acid function, the slope approaches one and is equal to one for $\alpha_1 \geq 1/2$. The Henderson-Hasselbach plots are given for both neutralizations of a fresh 0.76% solids H-bentonite in Fig. 5. For the weak acid function the slope n_2 is found to be unity within experimental error. This is found to be true for the titration of fresh samples of H-bentonite when the base is simply added to the pH measured after stirring. For aged H-bentonite, the slope n_2 decreases to lower values. ($n_2 = 0.85$ for the instantaneous titration of the 60 day old sample). For samples aged 5 months or more, the Henderson-Hasselbach plot is linear only over a short range and the slope is less than one. Apparently, one of the effects of the aging is a modi-

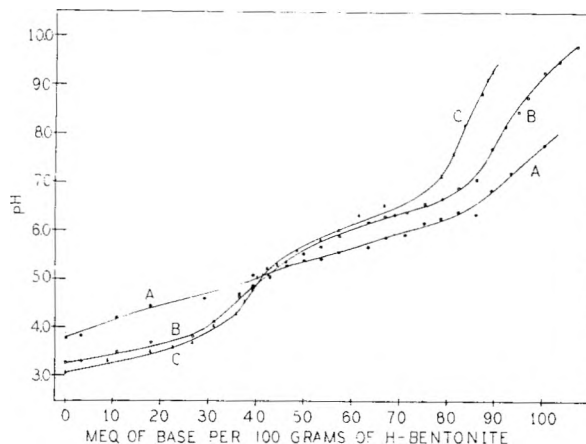


Fig. 3.—Effect of aging partially neutralized samples of H-bentonite: (A) 0.79% H-bentonite + base, samples from (B) aged one year; (B) 0.79% H-bentonite, aged 60 days before addition of base; (C) titration of 1.27% H-bentonite, aged 60 days.

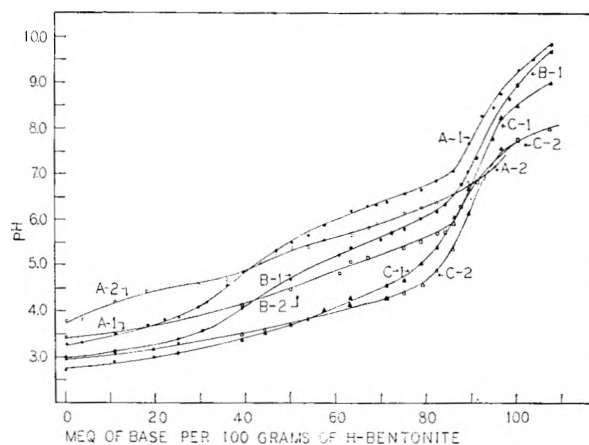


Fig. 4.—Effect of addition of NaCl and aging on the pH of H-bentonite suspensions, 0.76% solids, prepared samples neutralized to various extents: A-1, no salt, aged 3 days; A-2, aged 18 months; B-1, 0.002 N NaCl, aged 3 days; B-2, 0.002 N NaCl, aged 18 months; C-1, 0.032 N NaCl, aged 3 days; C-2, 0.032 N NaCl, aged 18 months; all samples prepared from 1.27% stock suspension of H-bentonite aged 60 days.

fication in the character of the weak acid function. The apparent pK value, the pH at $\alpha = 1/2$ for an approximately 0.5% suspension of Al-bentonite was 6.76, or 2 to 3 times as great as the apparent k_2 observed for any of the fresh or aged H-bentonite of comparable concentration. For the titration curve the slope n_2 was found to be unity.

An empirical relationship between the pH values at a given degree of neutralization can be derived by plotting the pH versus the logarithm of concentration in arbitrary units, the concentration of the most concentrated suspension being equal to 16A and the concentration of the most dilute suspension being equal to A. For the neutralization of the H-bentonite suspension to the first equivalence point, a linear relationship is found with slope $\theta = 0.85$ at $\alpha_1 = 0$ and $\theta = 1.25$ at $\alpha_1 = 0.5$. For the neutralization of the weak acid function the slope θ is equal to 1.25 between degrees of neutralization $\alpha_2 = 0.1$ to $\alpha_2 = 0.9$. The pH is thus related to the logarithm of the concentration according to

(8) W. Pauli and E. Valko, "Electrochem. Kolloide," 114, 115, Julius Springer, Vienna (1929).

(9) A. Veiss, THIS JOURNAL, 57, 169 (1953).

(10) W. Kern, Macromol. Chem., 2, 299 (1948).

(11) A. Kachalsky and J. Gillis, Rev. trav. chim., 68, 379 (1949).

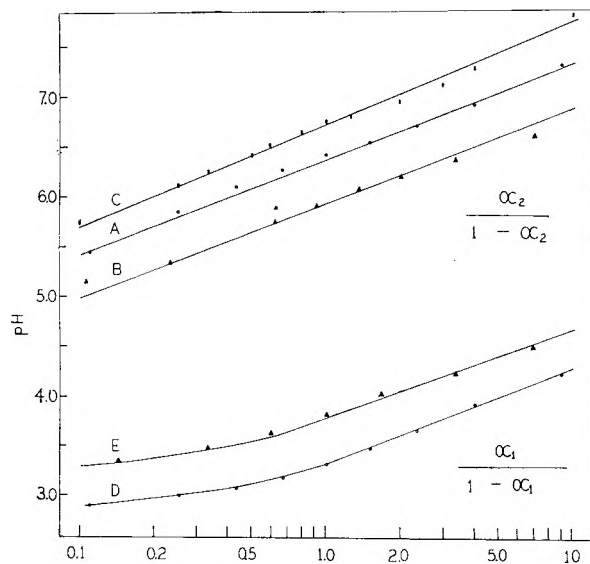


Fig. 5.—Plot of pH versus $\log \alpha/(1 - \alpha)$, for the neutralization of the weak acid (A, B, and C) and the strong acid (D and E) segments of the pH titration curves of Wyoming H-bentonite: A and D, 0.76% monobed resin processed (see curve E, Fig. 1); B and E, 0.79% partially neutralized samples (see curve C, Fig. 2); C, neutralization of Al-bentonite (no strong acid function).

$$pH = pK' - n \log \frac{\alpha}{1 - \alpha} - \theta \log Ac \quad (1)$$

when $Ac = 1$ and $\alpha = 1/2$. Then, $pH = pK'$. The apparent pK at a given concentration would then be

$$pK = pK' - \theta \log Ac \quad (2)$$

It is well known that the addition of neutral salt will lower the pH values of titration curves of polyelectrolytes and ion exchangers. A series of titrations on a freshly prepared 0.76% sample of H-bentonite was run in the presence of varying amounts of neutral salt. A slightly higher exchange capacity is obtained in this way. In general, the Henderson-Hasselbach plot is linear with unit slope. A unit slope at $\alpha_1 \geq 1/2$ is obtained for the strong acid titrations. The position of the equivalence points is not affected by the addition of neutral salt, though the pH values at the inflections and at corresponding degrees of neutralization are lowered. Even a very small salt addition such that the salt concentration is $3 \times 10^{-4} N$ will decrease the pH values throughout the titration. Except for the two solutions having the highest concentration of added salt the pH plotted against $\log \alpha_2/(1 - \alpha_2)$ is linear with unit slope.

It has been shown that long aging of the H-bentonite suspensions results in an almost complete loss of the strong acid character of the titration curves. It was thought that this strong acid property might be regenerated by repeated processing of the aged H-bentonite suspension on a

strong acid cation-exchange resin. It is evident from Fig. 3 that only a slight effect on the titration curve and exchange capacity of the H-bentonite resulted from such treatment. However, when an H-bentonite suspension aged 18 months was titrated with base and then regenerated to the hydrogen form by processing on a strong acid resin column, the position of the first equivalence point on the $pH-M$ scale was shifted 5–6 meq. to the right. Then, this same suspension was processed successively on sodium saturated carboxylic resin¹² and sulfonic resin (H-IR 120) for 5, 10, 15 and 25 cycles. The effect of this treatment of the bentonite suspension after 10 and 25 recycles is shown in Fig. 1, curves C and D. By this method, an H-bentonite was produced which titrated very much like a strong monobasic acid. The processing of an H-bentonite suspension on the sodium saturated carboxylic resin was equivalent to titration to the second equivalence point. The pH of the eluate was 7.6, which is the pH of the second equivalence point in the H-bentonite titration. However, when an H-bentonite suspension was passed through a column of sodium saturated sulfonic acid resin, the pH of the eluate was only 5.2. Apparently, the weak acid sites on the bentonite were not saturated with hydrogen ion in this case since the weak acid protons are not readily exchanged by the sodium ion of the sulfonic acid resin. The sulfonic acid groups of the strongly acidic resin have a lesser affinity for protons than the carboxylic anionic groups of the weak acid resin. The results for this series of titrations are shown in Fig. 1 and 2. In this process, the weak acid property is almost entirely removed; the exchange capacity of the titrated fresh sample is recovered. Apparently, the aging effect does not result in a permanent loss of titrated exchange capacity.

It seems likely that the weak acid function, apparently due to exchange site adsorbed aluminum, of the H-bentonite prepared by electro dialysis, acid leaching, or ion-exchange column processes, does not necessarily result from an autodegradation during the preparation. This property is not removed by any simple application of these processes, though the acid-leaching process might be expected to remove some of the adsorbed aluminum ion. This work suggests that the weak acid property is dependent on the past history of the sample and can be modified by aging in the past history of the sample and by aging in the hydrogen state or, in the opposite way, by repeated recycling on ion-exchange resin as previously described.

Acknowledgment.—The authors wish to acknowledge Dr. W. H. Cone and Mr. C. C. Cowin of the Department of Physical Sciences of the University of Idaho for their cooperation in providing materials for the experimental work.

DIFFUSION COEFFICIENT OF DODECYLTRIMETHYLAMMONIUM CHLORIDE IN AQUEOUS SOLUTIONS AT 23°

BY REBECCA A. PARKER AND STANLEY P. WASIK

Contribution from the National Bureau of Standards, Washington, D. C.

Received May 22, 1959

The diffusion coefficient of the colloidal electrolyte dodecyltrimethylammonium chloride has been measured as a function of concentration in aqueous solutions at 23° at concentrations up to 1.5 g./100 ml. The diffusion coefficient is approximately a step function of the concentration; it decreases from a value of about 8.2×10^{-1} cm.²/sec. at concentrations below the critical micelle concentration (cmc.) to about 2.2×10^{-6} cm.²/sec. above the cmc. This behavior is consistent with other properties of the solutions.

Introduction

The diffusion of paraffin-chain salts in aqueous solution might be expected to be unusual. These salts are generally thought to dissolve in water in the form of two different species¹: a strong monomeric electrolyte and a micellar electrolyte containing highly charged colloidal aggregates of the paraffin-chain ions. Since the two species are in equilibrium, their relative concentrations vary as a function of the concentration of the solution. Hence, the diffusion coefficient of the salt would be expected to be dependent on concentration.

The approximation generally made concerning the relative concentrations of the monomeric and micellar species is that the salt dissolves in water as a strong monomeric electrolyte until the concentration is equal to the critical micelle concentration (cmc.); at this concentration, the solution is saturated with monomeric ions and any further added salt dissolves to form micelles. (This is equivalent to assuming that the micelles are composed of an infinite number of monomeric ions¹). If this approximation is valid, the diffusion coefficient should be a step function of the concentration with the step from the higher value corresponding to the monomeric electrolyte to the lower value corresponding to the micellar electrolyte occurring at the cmc.

The general differential equation for a uni-directional diffusion process is Fick's Second Law²

$$\frac{\partial c}{\partial t} = \frac{\partial}{\partial x} \left(D \frac{\partial c}{\partial x} \right) \quad (1)$$

where

- c = concentration
- t = time
- x = distance in the direction of diffusion
- D = diffusion coefficient

If diffusion is studied at a liquid junction between two solutions of different concentrations, the boundary conditions which are imposed upon the solution of the diffusion equation are that at $t = 0$, for $x < 0$, $c = c_1$ and for $x > 0$, $c = c_2$ where $c_1 < c_2$. It is assumed that the concentrations at large values of x in the diffusion cell are unaltered during an experiment. With these restrictions, no general solution for equation 1 has been obtained. However, if it is assumed in addition that $x/$

$\sqrt{t} = \theta$, where θ is a function of c only,³ equation 1 can be transformed and integrated at constant time to give

$$D = - \left(2t \frac{dc}{dx} \right)^{-1} \int_{c_1}^c x dc \quad (2)$$

D in this case is a differential diffusion coefficient corresponding to the definite concentration c rather than an integral coefficient appropriate to the range of concentrations, c_1 to c . The integral in equation 2 must be evaluated from the experimental data. This calculation is valid only if $(x/\sqrt{t})_c$ is constant during the experiment.

Dodecyltrimethylammonium chloride was chosen for these experiments because the properties of its aqueous solutions have been studied extensively. Measurements of the viscosity of the solutions^{4,5} indicate that the micelles are approximately spherical. Other properties of the solutions which have been measured are turbidity,⁴ electromotive force of concentration cells,⁶ micellar electrophoretic mobility⁷ and electrolytic conductivity.⁸

Experimental

The quaternary salt, dodecyltrimethylammonium chloride, was obtained from Armour and Co. It was purified by recrystallization from anhydrous mixtures of ethanol and diethyl ether. A chemical analysis of the carbon, hydrogen, nitrogen and chlorine content of the salt gave the theoretical values for its composition within the error of the determinations.

Dextrose, National Bureau of Standards Standard Sample No. 41, was dried and used without further purification.

The cell used for the diffusion experiments and the experimental technique have been described in detail by Longworth.⁹ A sharp, plane, horizontal boundary between two solutions of different concentrations was formed in a rectangular cell. The subsequent concentration distribution at the boundary was observed with a Rayleigh interference optic system. The temperature of the water-bath in which the cell was immersed during the measurements was controlled at $23 \pm 0.003^\circ$. The water-bath and optic system were those of a modified Aminco Model B Electrophoresis Apparatus. Photographs of the interference patterns⁹ were taken on glass plates. With a two-dimensional comparator, about fifty measurements of the refractive index of the solution as a function of distance in the cell were made for each pattern. The relation between the refractive index and the concentration of the solutions was determined with a differential refractometer. For dextrose, the rate of change of the refractive index with concentration (dn/dc)

(3) L. Boltzmann, *ibid.*, **289**, 959 (1894).

(4) L. M. Kushner, W. D. Hubbard and R. A. Parker, *J. Research Natl. Bur. Standards*, **59**, 113 (1957) RP 2778.

(5) R. A. Parker and S. P. Wasik, *THIS JOURNAL*, **62**, 967 (1958).

(6) L. M. Kushner and R. A. Parker, *ibid.*, **61**, 822 (1957).

(7) R. A. Parker and S. P. Wasik, manuscript in preparation.

(8) Unpublished data, this Laboratory.

(9) L. G. Longworth, *J. Am. Chem. Soc.*, **74**, 4155 (1952).

(1) G. S. Hartley, "The Colloidal State. II. Aqueous Solutions of Paraffin-Chain Salts: A Study in Micelle Formation," Hermann et Cie., Paris, 1936.

(2) A. Fick, *Ann. Physik*, **170**, 59 (1855).

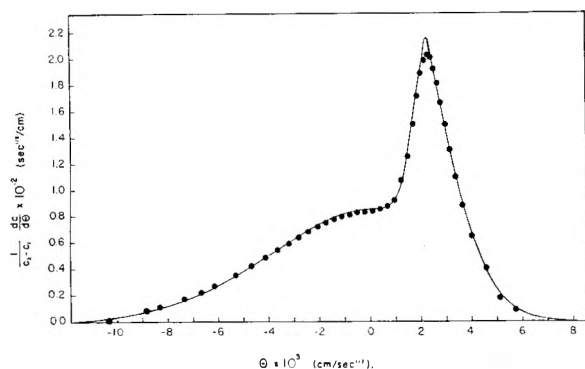


Fig. 1.—A comparison between experimental and theoretical values for $dc/d\theta$ as a function of θ . $\theta = x/\sqrt{t}$; $c_1 = 0$; $c_2 = 1.027$ g./100 ml. The points represent values for $dc/d\theta$ calculated by differentiation of the experimental data. The line represents values for $dc/d\theta$ obtained by a numerical solution of the diffusion equation, if the diffusion coefficient as a function of concentration (see Fig. 2) is approximated by three straight lines.

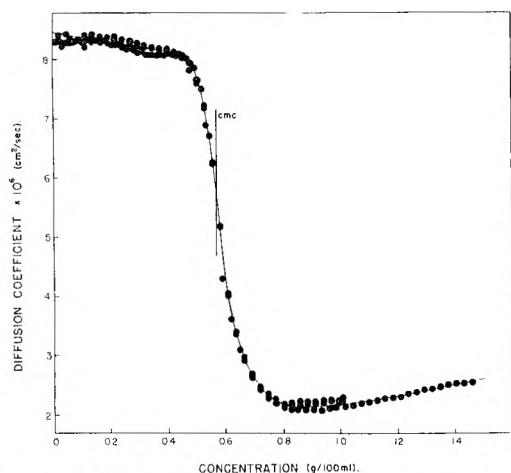


Fig. 2.—Diffusion coefficient of dodecyltrimethylammonium chloride in aqueous solutions at 23°. The points represent the values for the diffusion coefficient calculated from four different experiments: $c_1 = 0$, $c_2 = 0.560$ g./100 ml., $t = 8$ hours; $c_1 = 0.570$ g./100 ml., $c_2 = 1.567$ g./100 ml., $t = 24$ hr.; $c_1 = 0$, $c_2 = 1.027$ g./100 ml., $t = 15$ hr.; $c_1 = 0$, $c_2 = 1.027$ g./100 ml., $t = 20.25$ hr. The value for the cmc. was obtained from measurements of the turbidity of the solutions.

was found to be 0.144 ml./g. For dodecyltrimethylammonium chloride at concentrations below the cmc., $dn/dc = 0.165$ ml./g.; at concentrations above the cmc., $dn/dc = 0.157$ ml./g. From these data, the concentration distribution was calculated.

In order to check the calibration of the apparatus, measurements were made of the diffusion coefficient of dextrose in aqueous solutions at 25°. The experiments performed by Longworth^{9,10} were duplicated. Since the diffusion coefficient of this sugar is constant, it may be calculated from the properties of the probability function and data for c as a function of x at a particular value for t .^{9,11} These calculations were performed on the National Bureau of Standards IBM-704 electronic computer. The diffusion coefficient of dextrose in a solution of concentration 0.380 g./100 ml. obtained in six separate measurements was $6.729 (\pm 0.006) \times 10^{-6}$ cm.²/sec., compared with the value of $6.728 (\pm 0.006) \times 10^{-6}$ cm.²/sec. measured by Longworth.¹⁰ The zero time correction¹² in these experiments, *i.e.*, the correction to the observed time due to the fact that

the initial boundary is not infinitely sharp when $t = 0$, was less than ± 10 seconds.

The evaluation of the diffusion coefficient with equation 2 requires a simultaneous determination of c , x and dc/dx . This may be done conveniently by measuring two of the quantities and calculating the third. In these experiments, data for c as a function of x were differentiated to obtain dc/dx as a function of c and x ; these calculations were also performed on the National Bureau of Standards IBM-704

computer. The integral $\int_{c_1}^c xdc$ in equation 2 was evaluated graphically for each of the experimental points. In order to estimate the error in the calculation, values for the diffusion coefficient of dextrose were calculated from the data used previously to check the calibration of the instrument. The error in the evaluation of the diffusion coefficient by equation 2 was found to be $\pm 0.5\%$ except for concentrations near c_1 and c_2 . In these regions the error is much larger because of the relatively large error in the integration and because of a peculiarity in the differentiation program for the computer which results in less accurate values for dc/dx . The value for t used in these calculations was the actual elapsed time from the start of the experiment. Since for all the experiments considered, t was greater than 6 hours, the error caused by neglecting the zero time correction was less than ± 10 sec/6 hours or $\pm 0.05\%$.

Results

A number of diffusion experiments were performed at 23° with aqueous solutions of dodecyltrimethylammonium chloride of various concentrations up to 1.5 g./100 ml. Regardless of the values of c_1 and c_2 chosen, θ was a function of c only. Therefore, equation 2 could be used to calculate the diffusion coefficient. The circles in Fig. 1 represent a typical set of values for $dc/d\theta$ calculated from the data for an experiment in which $c_1 = 0$ and $c_2 = 1.027$ g./100 ml. If the diffusion coefficient were constant, the shape of this curve would be Gaussian. The experimental curve is highly asymmetrical and bears slight resemblance to a Gaussian curve.

Values calculated for the diffusion coefficient of the salt are shown in Fig. 2. The data, the results of four different experiments, agree within $\pm 0.05 \times 10^{-6}$ cm.²/sec. The value for the cmc. shown in Fig. 2 was obtained from measurements of the turbidity of the solutions.⁴

In Fig. 2 the diffusion coefficient is seen to be approximately a step function of the concentration. If the diffusion coefficient at concentrations below the cmc. is assumed to be constant, the best value for the integral diffusion coefficient, calculated by the method described by Longworth⁹ from data for repeated experiments in which $c_1 = 0$ and $c_2 = 0.560$ g./100 ml., is $8.12 (\pm 0.01) \times 10^{-6}$ cm.²/sec. This is close to the value of 8.22×10^{-6} cm.²/sec. calculated with equation 2 for $c = 0.560/2$ g./100 ml. If the diffusion coefficient at concentrations above the cmc. is assumed to be constant, the best value for the integral diffusion coefficient, calculated from data for repeated experiments in which $c_1 = 0.570$ g./100 ml. and $c_2 = 1.567$ g./100 ml., is $2.22 (\pm 0.01) \times 10^{-6}$ cm.²/sec. This is close to the value of 2.24×10^{-6} cm.²/sec. calculated with equation 2 for $c = (0.570 + 1.567)/2$ g./100 ml. The discrepancies may be attributed to the fact that the calculation described by Longworth is strictly applicable only when D is a constant.

A further check on the calculation of the diffusion coefficient from equation 2 was obtained by solving

(10) L. G. Longworth, *THIS JOURNAL*, **58**, 770 (1954).

(11) "Tables of the Error Function and Its Derivative. National Bureau of Standards Applied Mathematics Series. 41," U. S. Government Printing Office, Washington, D. C., 1954.

(12) L. G. Longworth, *J. Am. Chem. Soc.*, **69**, 2510 (1947).

the non-linear diffusion equation (equation 1) numerically for given values for D as a function of c . The values for the diffusion coefficient used in these calculations were obtained by approximating the data shown in Fig. 2 by three straight lines. The results of a typical calculation¹³ are shown in Fig. 1 as the solid line. In both the experiment and the calculation compared in Fig. 1, the values chosen for c_1 and c_2 were 0 and 1.027 g./100 ml. The agreement between the experimental data and the numerical solution is seen to be very good.

Discussion

According to a theory proposed by Hartley¹ to explain the behavior of colloidal electrolytes, the diffusion coefficient at infinite dilution would be expected to correspond to that of the monomeric electrolyte. A value for the diffusion coefficient of the monomeric ions, D_m , at infinite dilution may be calculated from the Nernst equation¹⁴ as extended by Hartley¹⁵

$$D_m = \frac{2RT \times 10^{-7}}{F^2} \left(\frac{uv}{u+v} \right) \left(1 + \frac{c \ln f}{c \ln c} \right)$$

where

- u = equiv. conductance of the cation
- v = equiv. conductance of the anion
- f = mean activity coefficient of the ions

The limiting equivalent conductance of the electrolyte is approximately 95.8 ml. (mole ohm cm.)⁻¹.⁸ Assuming independent ionic conduction, $v = 73.3$ ¹⁶ and $u = 22.5$. The quantity $d \ln f/d \ln c = 0$ when $c = 0$. The calculated value for D_m at infinite dilution is 9.05×10^{-6} cm.²/sec. The value obtained by extrapolation of D as a function of c in Fig. 2 is 8.45×10^{-6} cm.²/sec. This discrepancy is not surprising since the lowest concentration at which D could be determined in these experiments was 0.01 g./100 ml. Below this concentration, u , v and $d \ln f/d \ln c$ would be expected to be strongly dependent on concentration. The value for D_m when $c = 0.01$ g./100 ml. is $8.3 (\pm 0.2) \times 10^{-6}$ cm.²/sec. The quantity $d \ln f/d \ln c$ at this concentration was calculated from values for the concentration potential.⁶ The equivalent conductance at this concentration is 93.6.⁸ If it is assumed that this decrease in the equivalent conductance from the value at infinite dilution may be attributed to a 2.3% decrease in the equivalent conductance of each ion, D_m is calculated to be 8.35×10^{-6} cm.²/sec., in good agreement with the experimentally determined value at this concentration.

If the approximation generally made concerning the relative concentrations of the monomeric and micellar species is valid, the diffusion coefficient at concentrations above the cmc. would be expected to correspond to that of the micellar electrolyte. A value for this diffusion coefficient, D_M , may be estimated from Hartley's equation¹⁷ for the

diffusion coefficient of a cationic colloid of concentration c in the presence of a strong supporting electrolyte of concentration c'

$$D_M = \frac{RT \times 10^{-7}}{F^2} \frac{U}{n_+} \left[1 + \frac{n_+ \left(\frac{V}{n_-} - \frac{U}{n_+} \right)}{U + V + \lambda c'/c} \right] \left(1 + \frac{d \ln f}{d \ln c} \right)$$

where

- U = equiv. conductance of colloidal cations
- n_+ = their valence in solution
- V = equiv. conductance of negatively charged gegenions
- n_- = their valence in solution
- λ = equiv. conductance of supporting electrolyte

If the supporting electrolyte is considered to be the monomeric salt and if the diffusion coefficient of the micelles is extrapolated to infinite dilution of micelles (*i.e.*, the cmc.), the second term in the brackets is zero. D_M may then be calculated from the electrophoretic mobility of the micelles extrapolated to the cmc. (32.5×10^{-5} cm.²/volt sec.), the charge (14) and degree of ionization (36%) of the micelles in solution,⁷ and values for the concentration potential.⁶ The value for D_M calculated from these data is 1.86×10^{-6} cm.²/sec., compared with 1.80×10^{-6} cm.²/sec. obtained by a linear extrapolation of the data in Fig. 2. Also, since $V/n_- > U/n_+$, this equation predicts an increase in the diffusion coefficient with increasing concentration, as is observed.

Thus, the magnitude of the diffusion coefficient of the salt is consistent with other properties of the solutions. The agreement between theoretical and experimental values for the diffusion coefficient is very good considering the assumptions made in the derivation of the equations and the approximations made in the calculations.

The change in the diffusion coefficient from the value corresponding to the monomeric electrolyte to that for the micellar electrolyte would be expected to occur at the cmc. If the micelles were very much larger than the monomeric ions, the diffusion coefficient would be an infinitely sharp step function of the concentration. The step in Fig. 2, however, occurs over a change in concentration of about 0.3 g./100 ml. Thus, even though a micelle of this salt is an aggregate of about 40 paraffin-chain ions⁴ the assumption that the micelle is composed of an infinite number of monomeric ions is a very rough approximation in considering the behavior of the salt in solution. It may be noted in this connection that the region above the cmc., in which the diffusion coefficient decreases rapidly with increasing concentration, is the region in which the viscosity and turbidity of the solution deviate from the behavior expected, if all of the salt added at concentrations above the cmc. dissolved in the form of micelles of constant size and charge.⁴

If the cmc. is defined as the concentration at which dD/dc is a maximum, the data for the diffusion coefficient indicate a cmc. of 0.583 g./100 ml. ± 0.01 compared with the value of 0.570 g./100 ml. ± 0.01 determined by measurements of the turbidity of the solutions.⁴

The radius of large spherical particles may be calculated from the value for their diffusion coef-

(13) Private communication, W. C. Rheinboldt, Applied Mathematics Division, National Bureau of Standards, 1958.

(14) W. Nernst, *Z. physik. Chem.*, **2**, 613 (1888).

(15) G. S. Hartley, *Phil. Mag.*, **12**, 473 (1931).

(16) B. E. Conway, "Electrochemical Data," Elsevier Publ. Co., Houston, Texas, 1952.

(17) G. S. Hartley and C. Robinson, *Proc. Roy. Soc. (London)*, **A134**, 20 (1931).

ficient in solution by means of the Stokes-Einstein relation

$$D = kT/6\pi\eta r$$

where

k = Boltzmann's constant
 η = viscosity of the solution
 r = radius of the particle

This equation is applicable to uncharged spheres or to charged spheres in the presence of swamping concentrations of electrolyte. From the value for the diffusion coefficient of the micelles, extrapolated to the cmc., the radius is calculated to be 13 Å. A value of 18.6 Å. is calculated from the micellar weight⁴ by assuming that the micellar density is 0.75 g./ml.⁵ and that a monomolecular layer of water is bound to the surface of the micelle. If the concentration of monomeric electrolyte at the cmc. is not sufficient to swamp the effects of the high micellar charge, the radius calculated from the diffusion coefficient would be expected to be the lower of the two, as is observed. The agreement between the two values would then be expected to improve as the concentration of supporting electrolyte is increased. Preliminary measurements of the diffusion coefficient of the micelles in the

presence of 0.04 M NaCl⁸ give a value of 19 ± 1 Å. for the micellar radius, compared with 19.1 calculated from the micellar weight.⁴

Conclusions

The diffusion coefficient of dodecyltrimethylammonium chloride at 23° in aqueous solutions at concentrations up to 1.5 g./100 ml. is approximately a step function of the concentration. The diffusion coefficient decreases from a value of about 8.2×10^{-6} cm.²/sec. at concentrations below the cmc. to 2.2×10^{-6} cm.²/sec. at concentrations above the cmc. These values are consistent with other properties of the solutions. The behavior of the electrolyte may be explained by the usually accepted theory of colloidal electrolytes.

Acknowledgment.—The authors thank Dr. Werner C. Rheinboldt and John P. Menard of the Applied Mathematics Division for writing the programs for the NBS IBM-704 electronic computer used in the calculations. The authors also thank Mrs. Rita Y. Cowan of the Chemistry Division, who performed the graphical integrations and many other essential calculations, and Erle R. Deardorff of the Chemistry Division, who performed the chemical analysis of dodecyltrimethylammonium chloride.

SELECTIVITY COEFFICIENT MEASUREMENTS WITH VARIABLE CAPACITY CATION AND ANION EXCHANGERS¹

BY S. LINDENBAUM, C. F. JUMPER AND G. E. BOYD

Contribution from the Oak Ridge National Laboratory, Oak Ridge, Tennessee

Received May 22, 1959

Measurements at 25° of equilibrium selectivity coefficients for the exchange of Na⁺ with H⁺, with NH₄⁺, Cs⁺ and Zn⁺⁺ ions, and for Cs⁺ with NH₄⁺ ions in dilute aqueous mixed electrolyte solutions were conducted with specially synthesized variable exchange capacity polystyrenesulfonic acid type cation exchangers. Coefficients also were measured for the exchange of Br⁻ with Cl⁻ ions using variable capacity quaternary ammonium type strong-base anion exchangers. In all exchanges the selectivity coefficient for the preferred ion decreased as the capacity per gram dry increased when the cross-linking was held constant. This behavior does not agree with the predictions made by a recent statistical thermodynamic theory of ion-exchange gels which states that increased exchange capacity increases the ion binding and therewith the selectivity.

A renewed interest in the capacity dependence of the selective uptake of different ions by organic ion exchangers has arisen as a consequence of the recent appearance of an attractive statistical thermodynamic theory of ion binding and exchange in polyelectrolyte solutions and gels.² A molecular model for linear and cross-linked polyelectrolytes is proposed in this theory, and it has been argued,³ "Since ion pairing only occurs when necessary to reduce strong electrostatic fields, we may understand why resins of high exchange capacity should be more selective than resins of lower capacity."

A limited amount of data is available for comparison with this prediction. With variable capacity, divinylbenzene (DVB) cross-linked poly-

styrene sulfonates, for example, it was found^{4a} that the selectivity coefficient^{4b} for the exchange of sodium and hydrogen ions, $D_{H^+}^{Na^+}$, increased with exchange capacity, E (meq. g.⁻¹ dry), but, in disagreement with the theory, the coefficient for the exchange of silver and sodium ions, $D_{Na^+}^{Ag^+}$, decreased with increasing E . Independent researches⁵ with nominal 14–15% DVB cross-linked monofunctional, variable capacity cation exchangers likewise showed that $D_{H^+}^{Na^+}$ increased with E and that a selectivity inversion occurred when the exchange capacity diminished below approximately three meq. g.⁻¹. An increase of $D_{H^+}^{Na^+}$ with E , and

(4) (a) G. E. Boyd, B. A. Soldano and O. D. Bonner, *ibid.*, **58**, 546 (1954). (b) The usual definition of selectivity coefficient is followed; thus, for the sodium-hydrogen ion exchange: $D_{H^+}^{Na^+} = (m_{Na^+}/m_{H^+})_r / (m_{Na^+}/m_{H^+})_w$ where the m_{Na^+} and m_{H^+} are the molalities of these ions in the exchanger, r , and in the equilibrium mixed electrolyte phase, w , respectively.

(5) I. H. Spinner, J. Ciric and W. F. Graydon, *Can. J. Chem.*, **32**, 143 (1954).

(1) Presented before the Division of Colloid Chemistry, 134th National Meeting, American Chemical Society, Chicago, Illinois, September 7–12, 1958.

(2) S. A. Rice and F. E. Harris, *Z. physik. Chem., N. F.*, **8**, 207 (1956).

(3) F. E. Harris and S. A. Rice, *THIS JOURNAL*, **61**, 1360 (1957).

an inversion for capacities below about 3.2 meq. g.⁻¹ also has been observed in unpublished work in this Laboratory⁶ with variable capacity sulfonated chlorostyrene-styrene copolymers cross-linked with nominal 8% DVB. The apparent concurrence of the sodium-hydrogen ion-exchange reaction with the Rice and Harris theory, however, cannot be accepted because of the selectivity reversal in this system. In such cases the preferred ion cannot be specified uniquely; the data may be interpreted with equal validity by stating that the coefficient, $D_{Na^+}^{H^+}$, for the selective uptake of hydrogen decreases with increasing capacity.

Measurements of the exchange of ammonium with lithium, sodium, hydrogen, calcium and barium ions using variable capacity, cross-linked polyacrylic and pectinic acid exchangers have been reported.⁷ With the former exchangers, selectivity inversions were absent and the selectivity coefficient for the uptake of the preferred ion increased with the exchange capacity in conformity with the theory. With the pectinic acid exchangers, however, selectivity reversals were observed in the exchange of ammonium with lithium and sodium ions, and the uptake of the preferred ions, H⁺, Ca⁺⁺ and Ba⁺⁺, decreased with increasing capacity. It was suggested that the presence of hydroxyl groups in the structure of the latter exchanger may have caused the difference in behavior. A subsequent report by Hutschneker and Deuel⁸ has described exchange equilibrium measurements with the same cation pairs using dilute solutions of variable capacity linear polystyrene sulfonic and polyacrylic acids. For these polyelectrolyte solutions the selectivity coefficient for the preferred ion increased with increasing exchange capacity.

In view of the apparently conflicting experimental findings on the capacity dependence of selectivity coefficients and because of the disagreements with theory, further measurements have seemed desirable particularly with cross-linked cation and anion exchangers in which only the number of ionogenic groups was varied keeping the composition and structure of the copolymer as nearly constant as possible. Fortunately, methods for the synthesis of such materials have been developed recently and measurements on exchange equilibria with some of them now can be described.

Experimental

Variable capacity sulfonic acid cation exchangers synthesized by three different procedures were examined. Initially, exchangers prepared by sulfonating copolymers containing differing amounts of styrene and chlorostyrene nominally cross-linked with 0.5 and 10% divinylbenzene (DVB) were studied.⁹ Nominal compositions and some of the properties of these preparations are given in Table I. The chlorine contents found by chemical analysis were in

agreement with the indicated amounts of chlorostyrene monomer used in the synthesis. If in the sulfonation step only those benzene rings not containing a chlorine atom in the "para" position had reacted, the capacity of the 70/20 preparation would have been 4.49, while that of the 30/60 exchanger would have been 3.42 meq. g.⁻¹, respectively. Probably a partial sulfonation of the divinylbenzene cross-links occurred in the 90/0 and 70/20 exchangers. In the 30/60 preparation, however, not even all the available styrene and *o*-chlorostyrene were sulfonated.

The second set of variable capacity cation exchangers employed was prepared by the sulfonation of a porous polystyrene-DVB copolymer.¹⁰ Using carefully controlled reaction conditions, the copolymer beads could be sulfonated uniformly to give cation exchangers of almost any desired capacity. Thus, using a nominal 5.5% DVB cross-linked copolymer, exchangers showing capacities of 1.90, 2.01, 2.99, 5.16 and 5.61 meq. g.⁻¹ were prepared. The homogeneity of the sulfonation of these preparations was checked by fractionating them into three particle size ranges and determining the capacity of each fraction. The highest capacity exchangers appeared to be uniform, but some variation of capacity with particle diameter occurred with the lowest capacity preparations. Again, because of the possible sulfonation of DVB cross-links, these preparations may not have been monofunctional.

TABLE I

PROPERTIES OF VARIABLE CAPACITY CHLOROSTYRENE-STYRENE COPOLYMER CATION EXCHANGERS

Monomer ratio ^a	Nominal % DVB	Capacity (meq./g. H-form)	Equiv. water content (NH ₄ R) (g. H ₂ O/eq.)	Equiv. vol. (NH ₄ R) (ml./eq.)	Exchange site density (equiv./l.)
100/0	0.5	5.32	1259	1397	0.72
50/50	0.5	4.44	1104	1269	0.79
20/80	0.5	2.74	778	1050	0.95
90/0	10	5.17	142	287	3.5
70/20	10	4.74	158	316	3.15
30/60	10	2.94	159	427	2.35

^a Mole % styrene to chlorostyrene.

The majority of the cation-exchange selectivity coefficient measurements were performed with cross-linked exchangers synthesized by copolymerizing *p*-sulfonamidostyrene and styrene with and without added di-(*p*-vinylphenyl) sulfone as a cross-linking monomer followed by a treatment of the copolymer with HNO₂ to convert the sulfonamido to sulfonic acid groups.¹¹ Strong acid cation exchangers prepared in this way should be monofunctional as only *p*-sulfonate groups are expected in the structure. If the reactivity ratios of the monomers and the cross-linking agent are practically equal, copolymers may be produced in which the distribution of ionogenic groups along the chain can be controlled with some degree of predictability and conformity. Information on the preparations employed in this work is summarized in Table II. The preparations probably were completely monofunctional; however, it is to be remembered that they contained variable numbers of sulfone cross-linking groups.

Two series of variable capacity anion exchangers were studied. The first was prepared¹² by copolymerizing differing amounts of dimethylaminostyrene and styrene with nominal 10% divinylbenzene. Subsequently, the tertiary amine groups of the copolymer were quaternized with methyl iodide or dimethyl sulfate at room temperature to give a strong-base, trimethylphenylammonium type anion exchanger. The capacities of these preparations, measured

(6) B. A. Soldano, private communication, December, 1958.

(7) H. Deuel, K. Hutschneker and J. Solms, *Z. Elektrochem.*, **57**, 172 (1953).

(8) K. Hutschneker and H. Deuel, *Helv. Chim. Acta*, **39**, 1039 (1956).

(9) The authors are indebted to Dr. C. Calmon of The Permutit Co., New York, N. Y., for these preparations. The chlorostyrene employed was an equimolar mixture of the *ortho*- and *para*-isomers. The synthesis of similar exchangers has been described by R. Feinland, D. E. Baldwin and H. P. Gregor, *J. Polymer Sci.*, **10**, 445 (1953).

(10) I. M. Abrams, *Ind. Eng. Chem.*, **48**, 1469 (1946). The authors are indebted to Drs. I. M. Abrams and J. Patterson of the Chemical Process Company, Redwood City, California, for making these novel exchangers, designated as Duolite C-25, available for our work.

(11) (a) R. H. Wiley and J. M. Schmitt, *J. Am. Chem. Soc.*, **78**, 2169 (1956); (b) R. H. Wiley and S. F. Reed, *THIS JOURNAL*, **60**, 533 (1956). The authors are indebted to Prof. R. H. Wiley of the University of Louisville, Louisville, Kentucky, for supplying us with these and the variable capacity anion exchangers described below.

(12) R. H. Wiley and J. M. Schmitt, *J. Am. Chem. Soc.*, **80**, 1389 (1958).

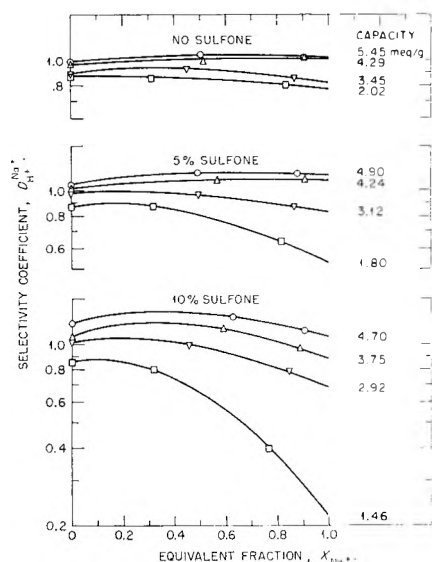


Fig. 1.—Dependence of selectivity coefficients (log scale) for the sodium-hydrogen ion exchange on the equivalent fraction of sodium ions x_{Na^+} in variable capacity sulfone cross-linked sulfostyrene exchangers.

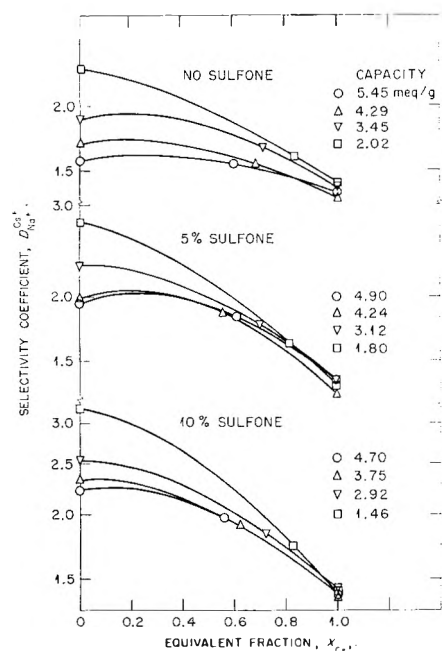


Fig. 2.—Variation of selectivity coefficients (log scale) for the cesium-sodium ion exchange with the equivalent fraction of cesium ion x_{Cs^+} in variable capacity sulfone cross-linked sulfostyrene exchangers.

by argentometric titration of the chloride salt-forms, were 1.62, 2.69, 3.40 and 3.96 meq. g.⁻¹ dry Cl-form, respectively. Variable capacity strong-base anion exchangers in which the structurally bound cation was a trimethylbenzylammonium group were examined also.¹³ These preparations, which were cross-linked with nominal 8% DVB, were reported¹³ to be the same chemically as Dowex-1, and to possess a uniform distribution of exchange sites throughout their spherical particles (Table III).

Selectivity coefficient measurements were conducted at room temperature by equilibrating a pre-determined number of milliequivalents of cation or anion exchanger with a known

(13) The authors are indebted to R. M. Wheaton and R. E. Anderson of the Physical Research Laboratory, Dow Chemical Company, Midland, Michigan, for making these preparations available for use in this research.

TABLE II
PROPERTIES OF VARIABLE CAPACITY SULFONAMIDOSTYRENE-STYRENE COPOLYMER CATION EXCHANGERS^a

Monomer ratio ^b	% Added sulfone	Capacity (meq./g. H-form)	Equiv. water content (g. H ₂ O/eq. H-form)
100/0	0.0	5.45	4030
75/25	.0	4.29	4050
50/50	.0	3.45	1740
25/75	.0	2.02	671
100/0	5.0	4.90	544
75/25	5.0	4.24	493
50/50	5.0	3.12	445
25/75	5.0	1.80	319
100/0	10.0	4.70	325
75/25	10.0	3.75	(366)
50/50	10.0	2.92	337
25/75	10.0	1.46	324

^a See ref. 11 also. ^b Mole % *p*-sulfonamidostyrene to styrene.

volume of 0.1 *N* mixed aqueous electrolyte solution for a period (usually two hours) sufficiently long to establish an equilibrium. The radio-tracers 2.6 y Na²², 30 y Cs¹³⁷, 245 d Zn⁶⁵ and 38.5 h Br⁸² were used in estimating the extent of exchange of Na⁺, Cs⁺, Zn²⁺ and Br⁻ ions, respectively. Hydrogen and chloride ion were determined by acidimetric and argentometric titrations, respectively, while ammonium ion was measured using a modified Kjeldahl method.¹⁴ The precision of the selectivity coefficient measurements was better than ±3.0%.

TABLE III
PROPERTIES OF VARIABLE CAPACITY TRIMETHYLBENZYL-AMMONIUM TYPE STRONG-BASE ANION EXCHANGERS (NOMINAL 8% DVB)

Capacity (meq. g. ⁻¹ Cl-form)	Equiv. water content (g. H ₂ O/eq. Cl-form)	Equiv. Br-form	Equiv. vol. (ml. eq. ⁻¹ Cl-form)	Exchange site density (equiv. l. ⁻¹)
4.10	255	186	465	2.15
2.43	268	264	631	1.6
1.46	243	245	876	1.1

Equivalent water contents (g. H₂O/equiv.) of several of the homo-ionic salt-forms of the variable capacity cation and anion exchangers when in equilibrium with 0.1 *N* electrolyte solutions also were determined. Unfortunately, because of their porosity, existing techniques could not be applied to find values for the Duolite C-25 cation exchangers. The centrifugation technique^{15,16} was utilized to find the water contents of the sulfostyrene exchangers. However, because of the aggregate character of the particles of these preparations difficulty was experienced in obtaining reliable values (Table II). The values reported for the chlorostyrene (Table I) and the trimethylbenzylammonium (Table III) type exchangers were found by shaking these preparations with an excess of 0.1 *N* electrolyte solution, blotting the spherical particles dry after filtering them from solution, and finally bringing them into a vapor equilibrium with 0.1 *N* electrolyte in a thermostated, evacuated isopiestic vapor pressure apparatus.¹⁷ Equivalent volume measurements were conducted with several of the equilibrated exchanger salt-forms using generally accepted displacement techniques.

Experimental Results

Variable Capacity Cation Exchangers.—Selectivity coefficients for the exchange equilibria of

(14) W. Rieman, III, J. D. Neuss and B. Naiman, "Quantitative Analysis," McGraw-Hill Book Co., Inc., New York, N. Y., 1951, p. 166.

(15) H. P. Gregor, K. M. Held and J. Bellin, *Anal. Chem.*, **23**, 620 (1951).

(16) K. W. Pepper, D. Reichenberg and D. K. Hale *J. Chem. Soc.*, 3129 (1952).

(17) G. E. Boyd and B. A. Soldano, *Z. Elektrochem* **57**, 162 (1953).

H^+ , Na^+ , NH_4^+ and Cs^+ measured with the sulfone crosslinked variable capacity sulfostyrene cation exchangers are plotted as functions of the equivalent fraction, x_{M^+} , of the preferred ion taken up by the exchanger in Figs. 1-4, inclusive. In the sodium-hydrogen exchange (Fig. 1) the values of $D_{H^+}^{Na^+}$ shown are consistent with previous studies on this equilibrium with desulfonated DVB cross-linked polystyrene sulfonates⁴ and with polychlorostyrene-styrene sulfonates⁶ in that the selectivity for Na^+ ion decreased with a decrease in capacity at constant cross-linking. It is to be noted that the selectivity increased with increasing cross-linking when the capacity was constant, and that a selectivity inversion occurred in each of the three cross-linked exchangers when the capacity decreased below about three meq. g.⁻¹. Interestingly, the greater the cross-linking the more pronounced the dependence of the selectivity coefficient on the exchange capacity. The variable capacity sulfonated porous polystyrene-DVB exchangers showed variations of $D_{Na^+}^{NH_4^+}$ with capacity and x_{Na^+} quite similar to those in Fig. 1.

Selectivity coefficients for the Cs^+ - Na^+ ion exchange (Fig. 2) increased with decreasing capacity for all three degrees of cross-linking of the exchanger in contrast to the coefficients for the Na^+ - H^+ ion-exchange using the same preparations. The convergence of the $D_{Na^+}^{Cs^+}$ values for equivalent fractions of cesium ion, x_{Cs^+} , of unity indicates, however, that the selectivity for Cs^+ ion becomes independent of capacity as the exchanger is converted to the cesium-form. The measurements also show for constant exchange capacity that $D_{Na^+}^{Cs^+}$ becomes virtually independent of cross-linking when $x_{Cs^+} = 1.0$. This result has been observed previously¹⁸ with this pair of cations using variously cross-linked Dowex-50 type exchangers of constant capacity where a value $D_{Na^+}^{Cs^+} = 1.33$ was found which, interestingly, is nearly identical with the value of 1.38 plotted in Fig. 2. For strongly bound cations the selectivity appears to become independent of exchanger capacity and cross-linking.

In the exchange of ammonium with sodium (Fig. 3) and of cesium with ammonium ions (Fig. 4) an increase in the selectivity coefficient again followed a decrease in exchanger capacity. Moreover, in the former system the value of $D_{Na^+}^{NH_4^+}$ fell to values below unity when the capacity exceeded 4.2 meq. g.⁻¹, suggesting, as with the Na^+ - H^+ ion-exchange system, that a selectivity inversion with increasing capacity may be found when selectivity coefficients close to unity occur.

Measurements with the variable capacity chlorostyrene exchangers showed that the selectivity for cesium in the cesium-ammonium ion exchange was only slightly dependent on the capacity. The variation of $D_{NH_4^+}^{Cs^+}$ with the equivalent fraction of cesium taken up, however, was different from that exhibited in Fig. 4 in that the curves were concave rather than convex toward x_{Cs^+} and that selectivity inversions occurred for $x_{Cs^+} > 0.8$. Measurements of the selective uptake of zinc on

(18) G. E. Myers and G. E. Boyd, *THIS JOURNAL*, **60**, 521 (1956).

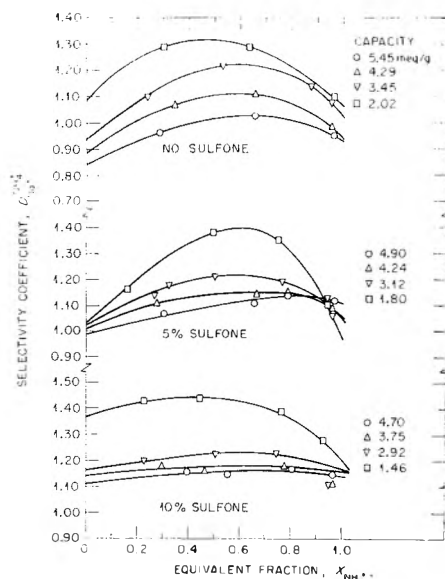


Fig. 3.—Variation of selectivity coefficients for the ammonium-sodium ion exchange with the equivalent fraction of ammonium ion $x_{NH_4^+}$ in variable capacity sulfone cross-linked sulfostyrene exchangers.

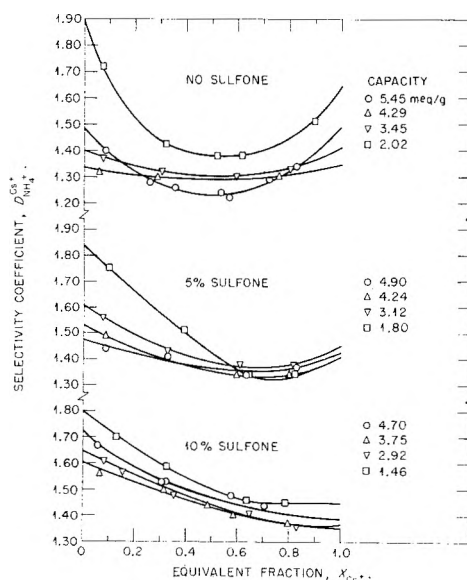


Fig. 4.—Variation of selectivity coefficients for the cesium-ammonium ion exchange with the equivalent fraction of cesium ion x_{Cs^+} in variable capacity sulfone cross-linked sulfostyrene exchangers.

the Zn^{++} - Na^+ ion exchange (Fig. 5) also showed that $D_{Na^+}^{Zn^{++}}$ increased with decreasing capacity and with increasing cross-linking.

The data of Figs. 1-4 show that the selectivity coefficient variation is dependent on the equivalent fraction of the preferred ion in the exchanger (*i.e.*, on the "loading") as well as on the exchange capacity. The former complication may be removed by finding the average value of D over the complete range of composition for a given exchanger through an application of the Gibbs-Duhem equation assuming that the exchanger behaves as a binary mixture. Such averages, which give thermodynamic equilibrium constants, were computed using the relation^{19,20}

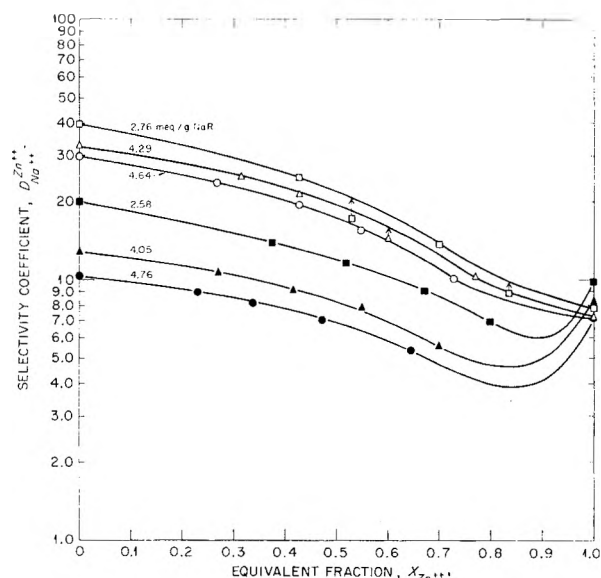


Fig. 5.—Dependence of the selectivity coefficients (log scale) for the zinc-sodium ion exchange on the equivalent fraction of zinc ions in variable capacity polychlorostyrene-styrene sulfonate exchangers. (Open symbols indicate 10% DVB, closed symbols, 0.5% DVB.)

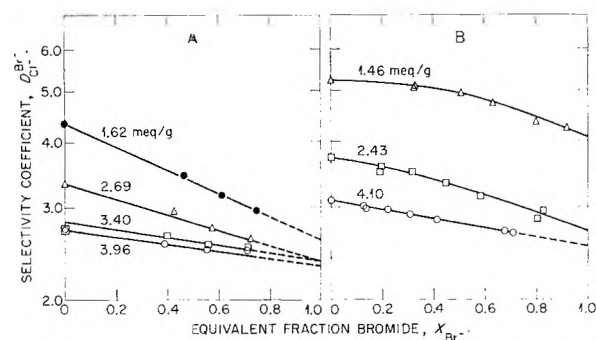


Fig. 6.—Dependence of the selectivity coefficients for the bromide-chloride ion exchange on the equivalent fraction of bromide ions for variable capacity trimethylphenylammonium anion exchangers A and trimethylbenzylammonium type anion exchangers B.

$$\log K = \int_0^1 \log D_0 dx_2 \quad (1)$$

The integration is performed over all values of the equivalent fraction, x_2 , of the preferred ion in the exchanger. The quantity D_0 is related to the measured selectivity coefficient, D , for the exchange of like, singly-charged ions by $D_0 \equiv D(\gamma_1/\gamma_2)w^2$, where γ_1 and γ_2 are the mean molal activity coefficients for the salts in the mixed aqueous electrolyte solution in equilibrium with the exchanger. The latter quantities were estimated for 0.1 N solutions using the Harned relations for electrolyte mixtures and assuming for the interaction coefficients, α_{12} and α_{21} , that $\alpha_{12} = -\alpha_{21}$. Numerical values for α_{12} were estimated using the equation²¹ $\alpha_{12} = (b_2' - b_1')$ and the empirical quantities b_1' and

(19) W. J. Argersinger, Jr., A. W. Davidson and O. D. Bonner, *Trans. Kansas Acad. Sci.*, **53**, 404 (1950).

(20) E. Ekedahl, E. Högfeltd and L. G. Sillén, *Acta Chem. Scand.*, **4**, 556, 828 (1950).

(21) R. A. Robinson and R. H. Stokes, "Electrolyte Solutions," Butterworth's Scientific Publications, London, 1955, p. 439ff.

b_2' tabulated by Guggenheim.²² The factor $(\gamma_1/\gamma_2)w^2$ in no case exceeded 1.05.

The calculated values of K are given in Table IV for the cation exchanges measured using the variable capacity sulfone cross-linked sulfostyrene resins, for the $\text{Na}^+ - \text{H}^+$ and $\text{Cs}^+ - \text{Na}^+$ exchange values derived from measurements with the sulfonated porous, polystyrene-DVB exchanger (Duo-lite C-25) and for the $\text{Cs}^+ - \text{NH}_4^+$ ion exchange in the chlorostyrene-styrene-DVB exchanger. It may be seen immediately that in all systems, excepting possibly those involving Cs^+ and NH_4^+ ions, where the capacity effect was extremely small, the equilibrium constants diminished as the capacity increased.

TABLE IV
VARIATION OF THE INTEGRATED CATION EXCHANGE SELECTIVITY COEFFICIENTS WITH CAPACITY

Exchanger	Capacity, meq./g. H^+ form				
	$K_{\text{Na}^+}^{\text{H}^+}$	$K_{\text{Na}^+}^{\text{NH}_4^+}$	$K_{\text{NH}_4^+}^{\text{Cs}^+}$	$K_{\text{Na}^+}^{\text{Cs}^+}$	$K_{\text{Na}^+}^{\text{Na}^+}$
Sulfonamidostyrene-styrene copolymers					
0% Sulfone	5.45	0.97	0.97	1.32	1.55
	4.29	1.00	1.04	1.31	1.60
	3.45	1.11	1.13	1.33	1.75
	2.02	1.22	1.24	1.49	1.91
5% Sulfone	4.90	0.87	1.09	1.39	1.83
	4.24	0.93	1.12	1.39	1.82
	3.12	1.06	1.16	1.43	1.94
	1.80	1.30	1.26	1.49	2.09
10% Sulfone	4.70	0.81	1.15	(1.51)	1.95
	3.75	0.92	1.17	1.45	1.97
	2.92	1.08	1.20	1.46	2.07
	1.46	1.64	1.40	1.54	2.33
Sulfonated styrene-divinylbenzene copolymers (Duo-lite C-25)	5.61	1.62
	5.16	0.81	1.64
	4.96	0.82
	4.20	0.89
	2.99	1.81
	2.01	1.28
Sulfonated polychlorostyrene-styrene-divinylbenzene copolymers	1.90	1.29	1.87
	4.75	1.24	...
	4.30	1.22	...
2.80	1.18	...	

Variable Capacity Anion Exchangers.—Selectivity coefficients measured for the exchange of bromide with chloride ions using variable capacity dimethylaminostyrene exchangers are shown in Fig. 6A; it may be seen that $D_{\text{Cl}^-}^{\text{Br}^-}$ increased as the capacity decreased. Analogous results were obtained with the variable capacity Dowex-1 anion exchangers (Fig. 6B).

Discussion

The foregoing data have shown that the selectivity coefficient for the uptake of a preferred ion by either a cation or anion exchanger decreased with an increase in the capacity of the exchanger on a dry basis, and that when the capacity was held constant the selectivity uniformly increased with cross-linking. The first of these observations is in

(22) E. A. Guggenheim, *Trans. Faraday Soc.*, **51**, 747 (1955).

striking apparent disagreement with the explicit prediction in the theory of Rice and Harris^{2,3} that the higher its capacity the more selective an exchanger should be. A careful examination of this theory, however, reveals that it is the exchange site density in the wet, swollen exchanger rather than the number of equivalents of exchange groups per gram of dry exchanger that is actually the governing variable. The site density, which is proportional to the exchange group normality (*i.e.*, equivalents of exchange groups per liter of exchanger), does not of necessity increase directly with the dry capacity as may be seen from Tables I and III. For example, in the weakly cross-linked exchangers an increase in normality accompanied a decrease in dry capacity because of the marked decrease in the equivalent water contents of these preparations. With these preparations, then, the observed selectivity coefficient increase was consistent with the theory. In contrast, the equivalent water contents of the highly cross-linked exchangers were found nearly independent of the dry capacity so that the site density decreased, yet the selectivity coefficients increased in contradiction to the theory. Such behavior

may, however, be a consequence of the fact that in the more highly cross-linked exchangers the ratio of organic to aqueous content of the gel increased as the number of exchange groups per dry gram decreased. A consequent decrease in the macroscopic dielectric constant inside the exchanger would be anticipated leading to stronger ion binding and, therefore, to an increased selectivity as observed. The usual increase in selectivity coefficient observed with increasing cross-linking would, according to the interpretation here suggested, be the result of both increased site density and of decreased dielectric constant. It is concluded, in agreement with the Rice and Harris model of ion-exchange gels, that factors which increase ion binding act to increase ionic selectivity. However, contrary to this theory, with all but the most weakly cross-linked exchangers increases in exchange site density cause a decrease in selectivity.

Acknowledgment.—It is a pleasure to acknowledge the assistance of A. C. Thompson, ORINS 1956 Summer Research Participant, in the measurements with the variable capacity Duolite C-25 exchangers.

ENZYMATIC REACTION ACROSS A THIN MEMBRANE

By A. ROTHEN

The Rockefeller Institute, New York, N. Y.

Received June 2, 1959

Experiments are described concerning the interaction of trypsin with protein layers deposited on solid slides and protected by a plastic blanket. It is shown that the trypsin molecules are carried across the blanket provided there are enough protein layers under the blanket. In the absence of protein layers a very thin blanket of Formvar offers an impermeable barrier and no trypsin molecules can cross the blanket. The passage of the trypsin through the blanket is determined not only by the number of protein layers located directly under it but also by the number of layers of long chain fatty acids or amines to which the protein is attached. It is suggested that some interaction between trypsin molecules and protein takes place across the blanket with the result that the trypsin molecules are pulled through it.

It was reported previously from this Laboratory that monolayers of protein (8 Å. thick per monolayer) formed at an air-water interphase and transferred onto a solid slide were capable of adsorbing antibodies from a dilute solution of a homologous antiserum.¹

The thickness of the adsorbed layer of antibodies was highly dependent on the nature of the antigenic films. A layer of antibodies 50 Å. thick could be adsorbed on ovalbumin multilayers, whereas the layer adsorbed on bovine albumin multilayers increased with the number of underlying antigenic layers and could be as thick as 200 Å.

Multilayers of protein deposited on solid slides were found to be very sensitive to proteolytic enzymes. A drop of a dilute solution of trypsin (0.1% in veronal buffer pH 7.5) deposited on a slide coated with protein films, altered the layers in a fraction of a minute so that they became incapable of adsorbing homologous antibodies.² Thus the action of proteolytic enzymes on protein

multilayers could be followed by measuring the amount of antibodies capable of being adsorbed on the protein layers after they had been submitted to enzymatic action. The over-all thickness of the layers was measured optically with a precision of a fraction of one Ångström unit.³

It also was reported² that the presence of a protective blanket made of plastic material or of long chain fatty acids deposited on the protein layers and thus separating the enzyme solution from the layers, did not completely prevent an enzymatic action from taking place. The enzymatic action was detected after washing off the enzyme solution by dissolving the blanket in the appropriate solvent (ethylene dichloride in the case of a Formvar blanket) and treating the slide with a dilute immune serum. The thickness of the blanket necessary to prevent an enzymatic action was found highly dependent on the mode of deposition and the number of underlying layers of protein. Its thickness varied from 50 Å. to well above 600 Å.

The bulk of the experiments could not easily be explained in terms of ordinary diffusion forces (the

(1) A. Rothen, *J. Biol. Chem.*, **168**, 75 (1947).

(2) A. Rothen, *J. Am. Chem. Soc.*, **70**, 2732 (1948).

(3) A. Rothen, *Rev. Sci. Instr.*, **16**, 26 (1945).

term "free" or "ordinary" diffusion means a diffusion which takes place under the influence of a gradient of concentration only), and it was concluded at the time that a Long Range Interaction might take place between the antigenic layers located on one side of the blanket and the enzyme molecules located on the other side. Other investigators came to the conclusion that free diffusion of the interacting entities took place across the blanket and that it was unnecessary to invoke a Long Range Mechanism.⁴⁻⁷

It will appear from the newer data that, whenever the protein layers were acted upon by trypsin, this action took place because trypsin had broken the barrier offered by the blanket. The experiments were so devised as to find out the conditions under which trypsin would or would not go through the blanket.

Experimental

The technique used in this work is essentially the one described previously.^{1,2} More recent improvement, however, will be mentioned.

Langmuir Spreading Trough.—A Plexiglas trough, 85 cm. long, 23 cm. wide and 1 cm. deep, provided with a well at one end to permit the dipping of the slides, was used for the formation of the films of the different fatty acids and long chain amines which were compressed mechanically at constant pressure (18 dynes) for their transfer to the slides. The surface pressure was measured by the Wilhelmy vertical pull method. A simple automatic device was used to maintain the pressure constant. This consisted in sending a pencil of light, reflected from a mirror located at the pivoting axis of the beam of the balance, onto a photoelectric cell the circuit of which controlled a motor driving the barrier.

Slides for Film Transfer.—Glass slides 1.5 cm. X 6 cm. and 0.2 cm. thick were used throughout. They were coated with a thin layer of either Cr, Rh, TiO₂ or TiO. The layer was just thick enough to ensure appropriate reflecting properties.

Thickness of Surface Films.—All measurements were carried out optically with the ellipsometer. The instrument has been greatly improved and the half shadow device described previously is not required any more to ensure the greatest sensitivity. Optical thicknesses could be appreciated within $\pm 0.1 \text{ \AA}$.⁸

Bovine albumin and ovalbumin layers formed from crystalline serum bovine albumin and crystalline ovalbumin were spread on an acetate buffer containing 0.047 g. of ammonium acetate per liter and adjusted to pH 5.9 with acetic acid. The protein solutions were 0.1% in water. The layers formed at the air-liquid interphase were compressed to 5 dynes per cm. before their transfer to the glass slides. The layers were transferred by successive immersion and emersion of the slide (\downarrow), or by successive emersions (\uparrow), as described previously.

Sera.—The sera were diluted 1 to 10 in veronal buffer adjusted to pH 7.5 with HCl (0.05 M in veronal).

Trypsin.—Crystalline trypsin was used in concentrations of 0.05 to 0.1% in the same buffer used for the dilution of the sera.

Blanket.—The plastic material used for the blanket was usually Formvar or Parlodion. Formvar was dissolved in ethylene dichloride and Parlodion in amyl acetate. The blankets were formed directly *in situ* by smearing a few drops of the plastic solution on the slide and letting the solvent evaporate with the slide in a vertical position, or they were first formed on a glass slide, floated on water and then transferred onto the slides under investigation. No differences in the results were obtained by the use of "deposited" or "transferred" blankets.

The results obtained when the experiments were carried out with blankets of Parlodion were qualitatively the same

as those obtained with Formvar but thinner blankets were required for the protection of a given assembly of protein layers against tryptic action.

Experiments on the porosity of Formvar blankets in the dry state previously reported⁹ were extended and confirmed the view that the mesh of a blanket is a tight one. These experiments consisted in measuring the rate of sublimation of stearic acid through a blanket and in comparing the rate of inactivation of protein layers by α particles in the presence or in the absence of a blanket.

Inactivation.—The term "inactivation" of the protein layers or protein films means the action of any proteolytic enzyme which abolishes or diminishes a subsequent adsorption of homologous antibodies.

Steps.—A slide was not always coated uniformly with a given number of layers of the fatty acid or protein. The layers often were deposited in a stepwise fashion, by immersing the slide to a lesser degree for each successive deposition. For short hand notation the expression "step one," "step three," etc., will designate that part of the slide upon which, one, three, etc., monolayers of fatty acid or of protein have been deposited.

Conditioning.—Conditioning was the treatment for a few minutes of a slide coated with fatty acid layers with a solution of uranyl acetate (0.424 g. per l.) mixed with veronal buffer (1.73 g. of barbital sodium per l. plus 0.45 cc. of concentrated HCl to bring the pH to 7.5). The purpose of the treatment was to permit the transfer of a great number of bovine albumin layers onto a slide. Without conditioning, only a few layers could be transferred. It was found that the smaller the ratio of uranyl acetate to the veronal solution, the greater the resistance of the protein layers to trypsin action and consequently the thinner the blanket necessary for protection. Unless otherwise indicated, the ratio 9 cc. of uranyl acetate to 5 cc. of veronal solution was used throughout.

Breath Figure Test.—Langmuir and Schaefer¹⁰ have reported that a sensitive indication of the uniformity of an initial layer of Ba stearate may be obtained by cooling the slide and breathing on it in order "to form a fog-like deposit of minute water drops. Lack of uniformity is made apparent by this "breath figure." This test proved very useful for detecting whether an assembly of protein layers protected by a blanket had been inactivated by the enzyme. The test did not require the removal of the blanket or the use of antiserum. After the drop of enzyme had been washed away, on breathing, the water vapor condensed in larger droplets on that part of the slide where inactivation had taken place. The inactivated part of the slide appeared shiny and the intact part appeared "milky." As testing with antiserum has shown, there was an excellent correlation between shininess and degree of inactivation.

Influence of the Age of the Water in the Trough Used for Spreading the Protein.—In all the new experiments reported in the present paper, protein layers were spread on water buffered at pH 5.9 (acetate buffer). It was indeed found that when the protein layers were formed on a freshly redistilled water, the blanket necessary to protect them from trypsin, after they had been transferred onto slides, was much thinner than the blanket needed when the layers were formed on water which had stayed overnight or even a few hours in the trough.

Influence of the Number of Underjacent Protein Layers on the Thickness of the Blanket Necessary to Prevent any Tryptic Action.—Most of the work previously reported was carried out with layers of serum bovine albumin. It was observed that after tryptic action through the blanket, the layers were hydrolyzed sometimes into fragments small enough to diffuse out during the inactivation period. After removal of the blanket an appreciable decrease in thickness was observed on that part of the slide upon which the trypsin solution had been deposited. The question then could be asked whether the protein layers had been detached from their anchorage and had diffused out through the blanket to be in-

(4) H. J. Trurnit, *Science*, **111**, 1 (1950).

(5) H. J. Trurnit, *ibid.*, **112**, 329 (1950).

(6) S. J. Singer, *J. Biol. Chem.*, **182**, 189 (1950).

(7) S. McGavin and J. Iball, *Trans. Faraday Soc.*, **49**, 984 (1953).

(8) A. Rothen, *Rev. Sci. Instr.*, **28**, 283 (1957).

(9) A. Rothen, *Helv. Chim. Acta*, **33**, 834 (1950).

(10) I. Langmuir and V. J. Schaefer, *J. Am. Chem. Soc.*, **59**, 2400 (1937).

activated on emerging from it, in spite of the fact that the veronal buffer used for the preparation of the enzyme solution was incapable by itself of detaching the layers.

In sharp contrast to the behavior of multilayers of bovine albumin, for which the thickness of adsorbed antibodies was proportional to the number of layers, the amount of specific antibodies adsorbed on ovalbumin layers was more or less independent of the number of layers. It was found that ovalbumin layers could be completely inactivated through a blanket, with no loss of thickness after removal of the blanket. The inactivation took place under the blanket. The following experiments were also very suggestive. One double layer of ovalbumin anchored to three layers of Ba stearate was not inactivated through 40 Å. of Formvar. However, if two "up" layers of bovine albumin were deposited on top of the ovalbumin double layer, the whole assembly of protein could be inactivated with trypsin through an even thicker blanket as subsequent treatment with anti-ovalbumin and antibovine albumin sera have shown in duplicate experiments. The presence of one double layer of bovine albumin on top of the ovalbumin did not interfere with the immunological reaction ovalbumin-antibody. In this example the anchorage of the ovalbumin was the same in both experiments, but the presence of the bovine albumin layers permitted the inactivation of the ovalbumin as well as that of the bovine albumin.

The inactivation of ovalbumin layers through a blanket ran parallel to the inactivation of bovine albumin layers. In both cases, the greater the number of layers the thicker the blanket necessary to prevent inactivation; in both cases the blanket needed to protect "up" layers was thicker than the one sufficient to protect the same number of "down-up" layers. For instance, 40 Å. of Formvar was sufficient to protect one double layer of ovalbumin whereas 300 Å. of Formvar were needed to protect 10 double layers and 500 Å. to protect an assembly of one double layer plus 18 monolayers ((↓↑)(↑)₁₈). The main difference between the behavior of these two albumins was the fact that many more layers of ovalbumin could be present under a given thickness of Formvar without being acted upon by trypsin.

Eight double layers of bovine albumin were not inactivated through 800 Å. of Formvar but 15 double layers were inactivated through 1500 Å. An assembly of one double layer plus 19 up layers of protein was inactivated through 2000 Å. of Formvar but not through 4000 Å. A solution of trypsin brought to a boil had no influence on the layers. For instance 12 double layers of bovine albumin were unaffected by a boiled solution of enzyme through 260 Å. of Formvar whereas they were completely inactivated if the trypsin was active.

Inactivation of Multilayers of Bovine Albumin in the Presence or in the Absence of a Protective Blanket.—The results summarized in Table I are a good illustration of the fact that the rate of inactivation of layers as a function of their number proceeds in opposite direction in the presence and

in the absence of a blanket, which is one of the strongest evidences against an ordinary diffusion process. The trypsin solution was diluted 1 to 50, when the inactivation was carried out without a blanket, in order to make the time of inactivation comparable to those measured when a blanket was present. The results seen in Table I were obtained by depositing 3, 6 and 9 double layers of bovine albumin in a stepwise fashion on slides coated uniformly with an anchorage of 3 monolayers of the fatty acid with 23 carbon atoms. It is apparent that when the slides were partially inactivated in the absence of a blanket, the steps corresponding to the greatest number of protein layers retained a greater capacity for adsorbing antibodies than the steps with fewer layers, which is what could have been expected. The situation, however, was reversed when the inactivation was carried out in the presence of a blanket. The step with 3 double layers was not inactivated at all whereas the step with 6 or 9 double layers was nearly completely inactivated. This is a very important result; its significance will be discussed later on.

TABLE I
INFLUENCE OF A BLANKET ON THE RATE OF INACTIVATION OF BOVINE ALBUMIN LAYERS

No. of double layers of bovine albumin	3	6	9
Antibody thickness, Å. (no trypsin)	127	222	318
Antibody thickness, Å. (trypsin through 600 Å. for 3 min.)	127	60	40
Antibody thickness, Å. (trypsin directly for 3 min.)	70	112	161

It also became evident that the action of trypsin was highly dependent upon the number of layers of fatty acid located under the protein. There was a periodicity in the inactivation of the protein as a function of the number of underlying monolayers of fatty acid especially marked when the slides were heated at 70 or 75° for five minutes before the deposition of the blanket. The most marked periodicity was observed when the anchorage consisted of steps made with layers of the straight chain fatty acid with 23 carbon atoms. Table II

TABLE II
INFLUENCE OF THE NUMBER OF UNDERJACENT LAYERS OF FATTY ACID ON THE INACTIVATION THROUGH A BLANKET

No. of underjacent monolayers of the C ₂₃ acid	1	3	7	11	15	17
Thickness of antibodies adsorbed after inactivation through 150 Å. Formvar	79	128	61	110	135	29

reproduces some typical results. Slides were coated with a series of steps consisting of 1, 3, 7, 11, 15 and 17 monolayers of the Ba salt of the acid deposited at pH 7.5. Four double layers of bovine albumin were transferred on top, the slides were heated for 5 minutes at 75° and finally were coated with a protective blanket 150 Å. thick. After a 3 minute trypsin treatment the blanket was dissolved and the slides treated with antiserum. The

second row of Table II corresponds to the amount of antibodies in Å. units adsorbed on each step. The results obtained with even numbers of fatty acid layers in the anchorage fell in line with those obtained with odd numbers. The first maximum in the amount of antibodies adsorbed occurred when the anchorage consisted of 3 monolayers of fatty acid. The thickness of the layer of antibodies decreased with the increase in the number of monolayers of the anchorage from 3 to 4, and 5 to reach a minimum at 7.

When the anchorage was made of steps of octadecylamine deposited at pH 7.5, similar results were obtained with heated slides. The periodicity in the inactivation as a function of the number of underlying layers of fatty acid which is so clearly evident from Table II, disappeared nearly completely when the reaction was carried out with dilute solution of trypsin without a protective blanket.

Detection of Material with Tryptic Activity Transported across a Blanket.—The experimental proof of the transport of a trypsin activity carrier across a blanket was obtained in two ways: (1) by the "strip" method; (2) by the use of trypsin labelled with tritium. All experiments with tritium trypsin will be described in a subsequent article.

The "Strip" Method.—When a piece of Scotch tape was pressed down on a slide coated with layers of protein anchored to fatty acid layers, on "stripping" the tape, all the layers deposited on the slide were detached from it, with the exception of the first layer of fatty acid which stayed firmly anchored to the slide. This could easily be demonstrated with the ellipsometer. If a slide coated with protein layers was treated for a few seconds with a trypsin solution, some trypsin molecules became attached to the slide. (There was an increase in the total thickness of the layers if the trypsin treatment was very short, otherwise a decrease was observed on account of the hydrolysis of the protein layers.) This was shown by stripping the layers with a narrow piece of Scotch tape which was then placed on another slide called "recipient" slide coated with fatty acid and bovine albumin layers prepared in the usual way. The Scotch tape was not in contact with the slide but separated from it by a thin film of veronal solution pH 7.5 (about 0.1 mm. thick or less). After 6 minutes, the strip was removed, and the slide treated with an antiserum solution. It could then be seen that the bovine albumin layers located directly under the strip were either completely or largely inactivated. In a control experiment performed in a similar way but using a tape stripped from a slide which had not been treated with trypsin, the bovine albumin layers of the recipient slide were not inactivated. The best results were obtained when the "recipient" slides were heated to 70° for 5 minutes before the transfer of the strip, which increased the adhesion of the layers to the slide.

When the protein covered slides were treated by trypsin for 3 minutes instead of a few seconds, the layers were completely hydrolyzed and trypsin activity could not be recovered from the slide by

the stripping method. No trypsin activity could be recovered either from tapes stripped from slides coated with multilayers of fatty acid and conditioned upon which trypsin molecules were adsorbed directly. The adsorption took place very rapidly and the thickness of the adsorbed layer was 16 Å. and independent of the number of underlying fatty acid layers. In both of these last cases the anchoring forces were too strong and the adsorbed trypsin molecules could not be released from the strip under the influence of the veronal buffer.

Similar experiments, where trypsin molecules could be transferred from one slide to another, were performed by stripping slides coated with protein layers which had been inactivated through a protective blanket. The stripping was usually done after dissolving the blanket. It was invariably found that, *if the blanket had been thin enough to permit the inactivation of the layers, the strip could inactivate the layers of a recipient slide whereas if no inactivation had taken place on the first slide, no action could be transferred to the recipient slide.* For instance, a strip carrying tryptic activity could be obtained by stripping a slide coated with nine double layers of bovine albumin which had been inactivated through a blanket of Formvar 500 Å. thick, whereas no transfer of activity took place if the strip came from a slide coated with three double layers of protein protected by 470 Å. of Formvar during the trypsin treatment.

As mentioned earlier, slides, coated with four double layers of protein deposited on steps consisting of one, three and five monolayers of fatty acid, upon heating at 75° and after treatment with trypsin through a blanket, showed that the proteins deposited on step three were inactivated much less than the protein on step one or five. The most striking results were observed when tapes, stripped from slides prepared and inactivated in this fashion, were placed on recipient slides coated uniformly with 5 layers of fatty acid (for instance the acid with 23 carbon atoms), plus protein layers. After removal of the strip and treatment with antibodies, the protein layers of the recipient slide located under the part of the strip corresponding to the step three of the first ("donor") slide was seen to be inactivated much less than the protein located under the strip corresponding to either step one or five. The lines of demarcation corresponding to these three different areas of the recipient slide were practically as sharp as the demarcation lines of the steps of the "donor" slide. The thicknesses of the antibody layers adsorbed on the "recipient" slide and corresponding to the steps 1, 3 and 5 of the strip were in one experiment 41, 103 and 60 Å., respectively. This pattern of inactivation of the recipient slide is what we shall call a "transferred" pattern.

Further experimenting showed that many factors affecting the anchorage, to which the protein layers are attached, have a major influence on the inactivation of the protein layers through a blanket. To the effect of the number of layers of fatty acid mentioned above should be added the influence of a

film of Formvar located under the anchorage of fatty acid. The protein layers deposited on five monolayers of Ba stearate, after heating at 70°, were inactivated much less than those deposited on three monolayers in the presence of a film of Formvar, thinner than 140 Å., and located under the fatty acid. When, however, the bottom film of Formvar was thicker than 140 Å., the protein layers deposited on 3 monolayers of stearate were less inactivated as in the absence of a bottom Formvar film (Table III). The range of Formvar thickness of the bottom film, within which the protein deposited on three layers of stearate was either more or less inactivated than those deposited on five layers, was extremely narrow. The change occurred within 10 Å. at about 130 Å. of Formvar. If, however, sudan black (a diazo dye with two diazo groups in the molecule) was incorporated in the bottom Formvar film, the proteins deposited on step 5 were always more inactivated than those on step 3, even with the thinnest bottom film. The results are summarized in Fig. 1.

TABLE III

INFLUENCE OF A BOTTOM FORMVAR FILM ON THE INACTIVATION THROUGH A BLANKET

Slide	Thickness of bottom film of Formvar, Å.	Thickness of top blanket of Formvar, Å.	Antibody thickness, Å., when anchorage consisted of				
			1	3	5	7	9
1	70	85	32	60	144	30	14
	No film	85	55	102	83	2	5
2	127	115	78	137	92	41	11
	No film	115	53	118	86	65	24

Summary of the Results

Two main facts clearly emerge from the experiments just described. First, whenever protein layers had been inactivated through a blanket, it invariably was found, with the help of the strip technique, that trypsin had gone through the blanket. Secondly, the number of protein layers as well as the number of fatty acid layers constituting the anchorage had a very large influence on the minimum thickness of the blanket necessary to prevent any tryptic action.

The results summarized in Table I illustrate the fact that in the presence of a blanket, the greater the number of protein layers the larger the inactivation, whereas without a blanket a few layers are completely inactivated in a time shorter than it takes to inactivate a larger assembly of layers. Table II shows the quasi periodic inactivation of the protein layers through a blanket as a function of the number of fatty acid layers in the anchorage. Many other factors were found that affect the rate of inactivation only in the presence of a blanket. For instance, progressively thicker blankets were needed for protection when the number of carbon atoms in the molecule of the fatty acid was increased from 18 to 20, 23 and 24. A given assembly of fatty acid layers and protein needed a thinner blanket for protection when the glass slide used for a support was coated with TiO or TiO₂ instead of Cr or Rh. Inactivation took place more readily with an anchorage of Sr stearate than Ca stearate and even more so with Ba stearate. The age of the water in the trough used for the for-

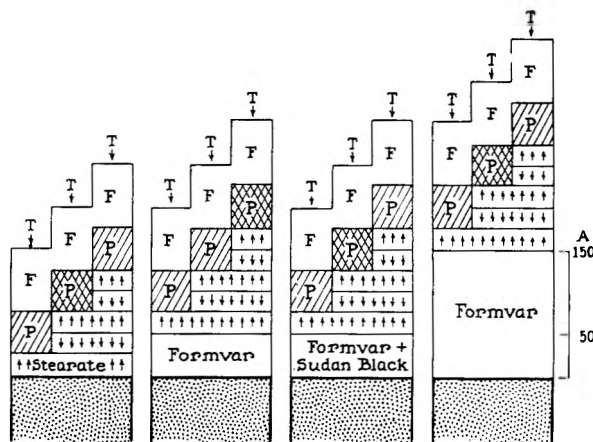


Fig. 1.—Schematic illustration of the inactivation of protein layers through a blanket as a function of the anchorage. The dotted areas represent the solid slides. The barium stearate monolayers are represented with arrows which indicate whether the layer was deposited by immersion (↓) or emersion (↑). P, stands for 4 double layers of bovine albumin. The cross hatched area in each slide indicates which "step" is the least inactivated. The protein on step "3" (3 underlying monolayers of barium stearate in the anchorage) has been least inactivated on slide 1, 3 and 4, and most inactivated on slide 2. A Formvar blanket marked F was present on all slides during the inactivation by trypsin marked T.

mation of the protein film as well as the washing of the protein layers with water after their transfer onto the slides also had an effect on the minimum thickness of the blanket needed for protection.

Thus, it is presumably the rate of diffusion of the enzyme through the blanket which is affected by all the factors just mentioned and not the reactivity of the protein layers themselves. This interpretation appears confirmed by the results obtained by the strip technique whereby the pattern of inactivation of a "donor" slide as a function of the number of fatty acid layers in the anchorage could be transferred to a "recipient" slide coated uniformly over its whole area.

It thus seems logical to assume that there is a Long Range Interaction across a blanket between protein layers and enzyme molecules, resulting in an attraction which could force the enzyme molecules through the blanket.¹¹ In such a "forced" diffusion, the diffusing molecules could go through the rather tight structure of the blanket which they could not cross if the forces of diffusion were only due to a gradient of concentration. An alternate hypothesis would be that all the factors which affect the rate of inactivation of the protein layers, affect primarily the porosity of the blanket, a rather unlikely hypothesis, in view of the fact that essentially the same results are obtained whether the blankets are formed directly on the slides or transferred to them. The most obvious and simplest of all interactions would be a coulombic interaction. Many facts, however, seem difficult to explain in such simple terms. Among them could be cited the influence of a bottom Formvar film or the rough periodicity in the inactivation of the protein layers as a function of the number of layers in the

(11) A. Rothen, *Science*, **112**, 330 (1950).

anchorage. It seems futile for the time being to speculate as to the nature of the interaction which takes place between the highly condensed phase of the protein layer and the trypsin molecules. It is likely, however, that mechanisms analogous to

those controlling the experiments described, play a role in the permeability of the living cell, the membrane thickness of which is of the order of magnitude of the thickness of the blankets which have been used in this investigation.

CONDENSED SYSTEMS AT HIGH PRESSURES AND TEMPERATURES

BY R. H. WENTORF, JR.

General Electric Research Laboratory, Schenectady, N. Y.

Received June 3, 1959

Considerations of the internal pressures of solids indicate that tangible products of superpressure processes will be hard, strong, refractory materials. A brief study showed that boron nitride melts at about 3500° at 80,000 atmospheres and is a good electrical conductor while molten. Some of the minerals associated with natural diamond (quartz, garnet, olivine) indicate that some natural diamonds probably formed at pressures of at least about 55,000 atmospheres and temperatures of at least about 1300°. It is expected that future studies of diamonds and their inclusions will yield information about the deeper layers of the earth's crust.

This paper will treat briefly three subjects which are united by virtue of their common connection with high pressure: first, a few remarks on the rules for recovering unchanged any new substances which may be prepared at high pressure; second, some recent exploratory work on the high temperature, high pressure behavior of boron nitride and carbon; third, some comments on the geological applications of the laboratory studies of high pressure minerals.

As you know, the field of high pressure has been receiving increasing attention during the past few years, a state of affairs which must be gratifying to Professor P. W. Bridgman and other pioneers in this field. Much of this new interest rests upon the preparation of interesting or valuable substances at high pressure and the subsequent recovery and use of these substances at low pressure. Of these substances, diamond, and coesite, a dense form of silica, are probably the best known, although many others have been prepared. Before very long many more undoubtedly will be discovered, and it is interesting to try to see what these substances will be like.

In Fig. 1 one can see the phase diagram of bismuth as determined by Dr. Francis Bundy of our laboratory.¹ Let one begin with bismuth at room temperature and compress it. At first it merely becomes denser, but at about 24,800 atmospheres, it changes abruptly into another allotropic crystalline form, known as "Bismuth II." This change is easily detected by the sudden increase in density or by the sudden increase in electrical conductivity. As the bismuth is compressed further, it changes into a third crystalline form, and so on. At about 125,000 atmospheres one reaches the most recently discovered form, and by then it is time to turn back. As one reduces the pressure the bismuth steadily expands, transforming from one form into another, until by the time we have reduced the pressure on it to one atmosphere we again have the ordinary kind of bismuth. Too bad. All that squeezing for nothing. Yet the majority of substances, when subjected to pressure, behave in a

similar fashion. They may change into new, interesting forms willingly enough, but they carelessly revert to their ordinary forms as soon as the pressure is reduced, long before one can get a good look at them. Diamond, on the other hand, is a much more friendly crystal, at least to scientists, and it faithfully preserves at one atmosphere the crystalline form which it acquired at a high pressure.

As a beginning toward understanding why some high pressure phases can be recovered at one atmosphere, let us consider the internal pressures of substances. By "internal pressure" one refers to the cohesive or attractive pressures which hold substances together in the solid or liquid form against the disruptive forces of thermal agitation and mechanical tearing.

The notion of internal pressure can be given more precise form if one defines it as $(\partial E/\partial V)_T$, where E is the internal energy, V is volume and T is the absolute temperature. Thus the internal pressure of a perfect gas is zero at any pressure. If one evaporates a liquid at constant temperature, one overcomes the internal pressure of the liquid by thermal agitation so that the energy of evaporation divided by the volume change gives one a measure of the internal pressure of the liquid. The internal pressures of most liquids are surprisingly high, between 2000 and 6000 atmospheres—perhaps good glues have even higher internal pressures. The internal pressure inside a crystal is probably not the same in all directions but varies with direction. However, a suitable averaging process could always yield a value for the internal pressure which had thermodynamic significance.

A few more remarks on the nature of internal pressure are worthwhile. From the definition of internal pressure as $(\partial E/\partial V)_T$ it follows that it can be expressed in terms of other thermodynamic quantities as

$$P_i = \left(\frac{\partial E}{\partial V}\right)_T = T \left(\frac{\partial P}{\partial T}\right)_V - P$$

where P , T and V are connected by the equation of state of the substance. If the equation of state has the general form

(1) F. P. Bundy, *Phys. Rev.*, **110**, 314 (1958).

$$P = \frac{RT}{V + b(v)} - a(v)$$

so that the pressure exerted by the substance is regarded as the sum of thermal agitation plus the interatomic forces of attraction and repulsion, then it follows that

$$\left(\frac{\partial E}{\partial V}\right)_T = a(v)$$

The term $a(v)$ is a function of volume and is positive for attraction and negative for repulsion. Clearly substances can have negative internal pressures, but the sum of the internal and external pressure can never be less than zero, since this would correspond to an explosion.

If one compresses a liquid or solid at constant temperature, its internal pressure would be expected to fall as the external pressure increases, for the atoms of the substance tend to repel each other more strongly as they are moved closer together from the equilibrium separations which they had at low external pressures.

In Fig. 2 the internal pressure of a substance is plotted as a function of the external pressure to which it is exposed. Because the internal pressure of a substance decreases with external pressure, but can never fall so low that the internal repulsion exceeds the external pressure, the internal pressure approaches the negative of the external pressure asymptotically. At a very, very high pressure the internal pressure must very nearly equal the negative of the external pressure. This implies that in the absence of phase changes the curve of internal pressure *versus* external pressure is concave upward or, in other words, the change of internal pressure with external pressure becomes less negative as the density of the substance increases. This is physically reasonable and corresponds to a decrease of compressibility with increasing pressure or density.

Suppose now that the substance undergoes a phase change at high pressure. The density of the new phase will certainly not be lower than that of the original phase, and in most cases the new, high pressure phase will have a higher density. Hence the rate of change of internal pressure with external pressure will be less negative for the new phase than for the old. Because the internal pressure must approach the negative of the external pressure at very, very high pressures, we can conclude that the internal pressure of the newly formed high pressure phase is less than the internal pressure of the old phase from which it was formed.

This seems reasonable, because one would expect the atoms of a substance to repel each other more strongly in a denser phase produced by the application of external pressure.

If the new phase is compressed further, its internal pressure will of course decrease, and perhaps other new phase changes will occur, each accompanied by a decrease in internal pressure. The shape of the curve suggests that phase changes would be more numerous at lower external pressures, because there is a larger internal pressure change available there. This seems borne out by experience; phase changes become relatively

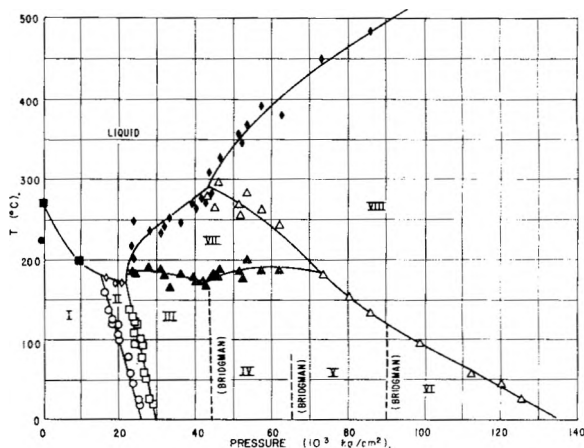


Fig. 1.—Phase diagram for BN.

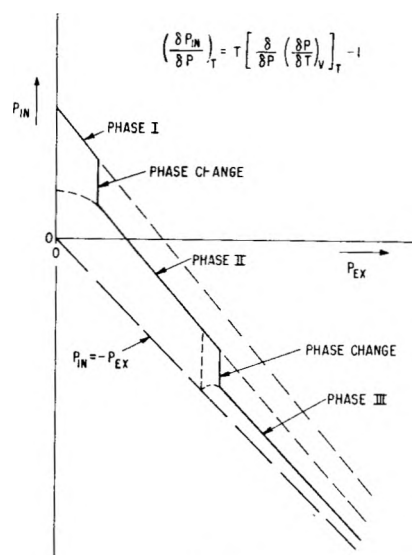


Fig. 2.

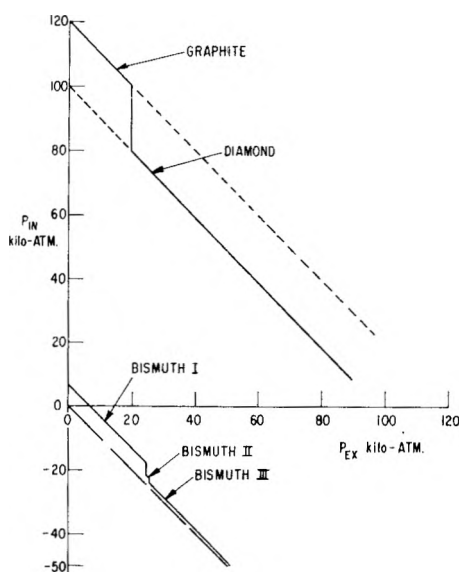


Fig. 3.

scarcer at higher pressures, both for substances in general and for any one substance in particular.

If starting from a high pressure, one reduces the

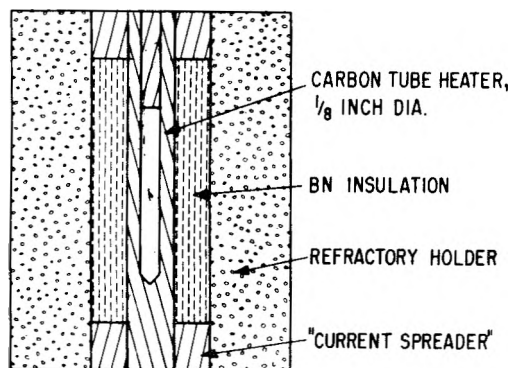


Fig. 4.

external pressure on a new high pressure phase, the internal pressure of this phase will increase. However, as the external pressure approaches the pressure at which this new phase first formed, this phase may become unstable enough to transform back into a lower pressure phase. As one reduces the external pressure upon a metastable high pressure phase, the internal pressure of this phase may rapidly decrease to the negative of the external pressure; *i.e.*, only the external pressure preserves the crystal structure against thermal agitation. If the external pressure is decreased further, the substance "explodes" into a lower-pressure phase. The closer the internal pressure of the high pressure phase lies to the negative of the external pressure, the more likely such a transformation becomes. This reverse transformation is indicated by appropriate dashed lines in Fig. 2. Some phase transformations take place reversibly in a narrow pressure interval, but others are more reluctant. The width of the pressure interval depends on the proximity of the internal pressure to the negative of the external pressure, and on the value of $(\partial P_{in}/\partial P_{ex})_T$.

From the expression for $(\partial P_{in}/\partial P_{ex})_T$, shown in Fig. 2, we can see that the ruling factor affecting this quantity will be the change in the "thermal expansion pressure," $(\partial P/\partial T)_V$, with pressure. Clearly this will increase much faster with decreasing pressure when the phase is unstable than when it is stable. It is also clear that this "thermal expansion pressure" will change less with pressure when the internal pressure is high than when it is low. For the lower the internal pressure, the more the lattice is at the mercy of the thermal agitation which tends to swell and disrupt it.

Thus, if at high pressure a new phase forms, the best criterion for determining in advance whether or not this phase will persist at atmospheric pressure is the internal pressure of the new phase. The higher its internal pressure, the less likely it will be to become negative, not only because the internal pressure has farther to drop before it can become negative, but also because the internal pressure falls less rapidly with decreasing external pressure when the internal pressure is high.

Since the internal pressure invariably falls as the external pressure increases, the best way to have a high pressure phase with a high internal pressure is to start at a low pressure with a parent phase which has a high internal pressure, and then

quench the high pressure phase before reducing the pressure upon it. Of course the higher the pressure at which the phase change takes place, the more important it will be to have a parent phase which has a high internal pressure.

Thus if we compare the internal pressures of bismuth and carbon as a function of the external pressure at room temperature, we would have something similar to that shown in Fig. 3. The values given for internal pressures are only approximate and were estimated from the mechanical properties of these solids. But it is clear why the two substances respond to pressure as they do. The internal pressure of carbon is quite high—some graphite "whiskers" have measured tensile strengths² of 200,000 atmospheres. Thus at the room temperature hypothetical transformation of graphite to diamond at 20,000 atmospheres, the internal pressure of diamond is still in no danger of becoming negative. However, the internal pressure of bismuth is already so low at one atmosphere, that when it changes into the bismuth II form its internal pressure is already negative. Naturally by heating a diamond one can reduce its internal pressure until the diamond changes to graphite.

The internal pressure of a substance increases as its temperature is decreased, but not indefinitely. Thus even at 0.1°K. the internal pressure of a high pressure phase might become negative as the external pressure is reduced. If the reversion to the low pressure phase involved an increase of entropy or volume, which seems possible, then the process might be useful as an adjunct to other cooling methods used to reach low temperatures.

From these considerations it seems to the author that most of the new substances which will be found as the products of high pressure, high temperature processes will be fairly hard, strong substances, whose parents are refractory materials which have high internal pressures at one atmosphere. Probably carbon has the highest internal pressure of any substance known today, so that the synthesis of a new substance substantially harder than diamond would be important not only for industrial reasons but also because its existence would substantially increase the range of both pressures and substances which might be expected to yield interesting new high pressure phases which could be quenched and recovered at low pressure. The internal pressure of carbon being what it is, about 200,000 atmospheres, it probably would not be worthwhile at this time to attempt to prepare substances at pressures much higher than about 400,000 atmospheres, for the new substances probably would not survive the decompression to one atmosphere. Fortunately this pressure is well above the static pressures currently available for high temperature synthesis, and we still have much to look forward to. Of course, the study of matter while it is under high pressure will continue to be fascinating.

The next topic is a brief description of some recent exploratory work on the high temperature, high pressure behavior of boron nitride and carbon,

(2) R. Bacon, *Nature*, **182**, 297 (1958).



Fig. 5.—Photograph of zirconia melted at 65,000 atm. in a carbon tube.

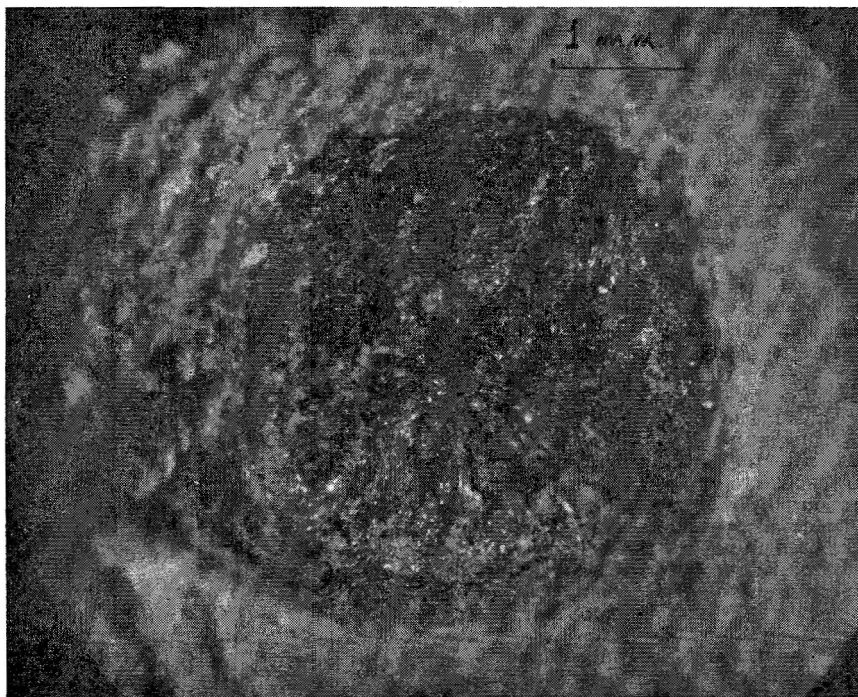


Fig. 6.—Photograph of boron nitride melted at 65,000 atm. in a carbon tube.

two very refractory substances. As one might expect, there are certain advantages in using high pressure for some high temperature studies. The main advantage is that many chemical reactions are more or less suppressed, particularly those in which a gas is ordinarily a product.

A typical reaction chamber arrangement for these high temperature studies is shown in Fig. 4. The zone of highest temperature is at the mid-length of the carbon heater tube. Various materials may be placed inside the tube. An electric current heats the tube, and the ends of the tube fit into carbon rings to reduce the current density and heat generation at the ends. The tube is electrically and thermally in-

sulated by a shell of rammed boron nitride powder, which is in turn contained within a refractory cylinder of lower thermal conductivity than the boron nitride. When the heater tube is at its hottest, the refractory next to the boron nitride does not quite melt and its electrical conductivity remains very low. Solid boron nitride is also a very poor conductor of electricity. As long as the carbon heater tube carries 99% of the current, one can obtain a fairly good measure of its temperature from the electric power dissipated in it.

Such a reaction chamber was subjected to high pressure in a suitable apparatus and then heated and cooled under pressure. Any changes in electrical resistance during the course of the experiment were noted as useful indicators of changes occurring in the high temperature zone. The re-

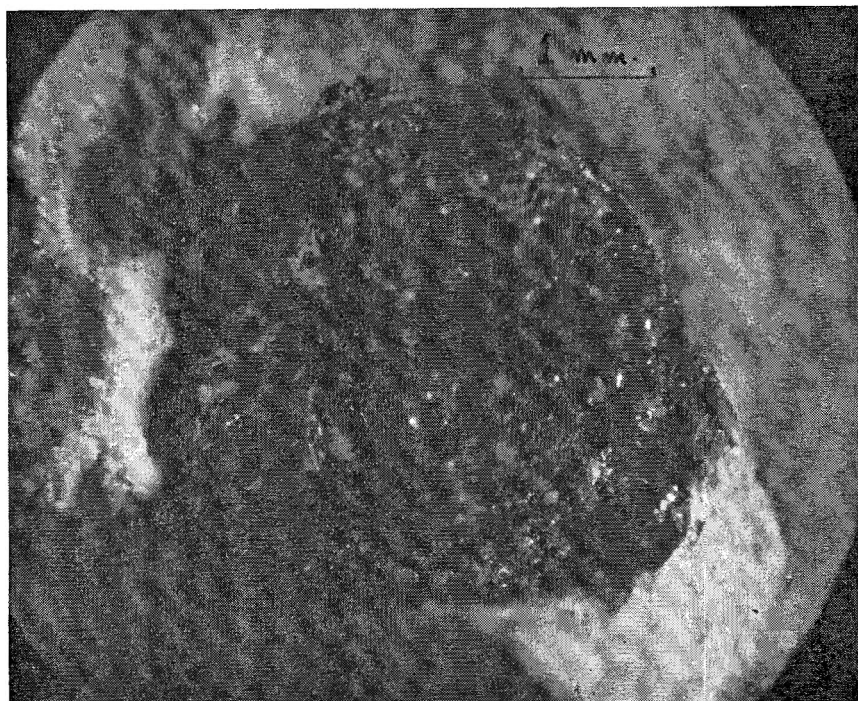


Fig. 7.—Photomicrograph of boron nitride which melted at 80,000 atm.

action chamber could be examined in detail after it was removed from the apparatus.

The temperature of the central part of the carbon tube was assumed to be proportional to the heating power dissipated in it. This is a good assumption because the refractories are already well consolidated by the high pressure, and so their thermal conductivity does not change much because of further sintering or compacting at high temperature. For purposes of calibration one observed the power required to melt various refractories, such as magnesia (melting temperature 2800° at one atmosphere), zirconia (m.p. 2600° at 1 atm.) and the tantalum carbide-carbon eutectic (m.p. 3300° at 1 atm.). The pressures used in these experiments probably do not increase these melting temperatures by more than 200°, Strong having found that the melting temperature of nickel is increased by 150° at 80,000 atmospheres.³

A photomicrograph of a cross section of the hottest part of the chamber after zirconia had been melted in it at 65,000 atmospheres is shown in Fig. 5. It is interesting that the zirconia did not react with the carbon tube. Presumably the pressure was high enough to suppress any such reaction, which would have produced carbon monoxide.

Figure 6 shows a photomicrograph of a cross section of the chamber in which boron nitride had just melted at 65,000 atmospheres. The large, dark radially arranged crystals in the center are frozen boron nitride. Surrounding them is the wall of the carbon tube heater. The boron nitride did not extensively attack the wall of the carbon tube because it was held in this molten condition for only about a minute. However, enough carbon has been absorbed into the boron nitride to color it black. The maximum temperature of the boron nitride was estimated to be about 3400° in this experiment.

Figure 7 shows a photomicrograph of a cross section of the chamber in which boron nitride has melted and attacked all the nearby carbon heater. This experiment was done at 80,000 atmospheres and the temperature was estimated to be about 3500°. One can see the large flakes of the frozen melt. These large flakes sharply indicate the extent of the molten zone. Their radial arrangement is the result of the radial temperature gradient which existed as the melt froze. The outer portions of the melt were the coolest and were the first to freeze. The inner portions were the last to freeze, and were often visibly richer in boron nitride than the outer parts. A Debye-Scherrer pattern of part of the melted zone showed the presence of graphite, hexagonal

boron nitride and a trace of boron carbide. No diamond or cubic boron nitride was detected, which indicates that these substances probably are not stable at 80,000 atmospheres and 3500°. There was no strong evidence for a mixed crystal of boron nitride and carbon in either the hexagonal or cubic form.

Experiments similar to this one, but carried out at different temperatures, showed that solid boron nitride is a good electrical insulator but that molten boron nitride conducts electricity about as well as graphite.

The melting temperature of boron nitride increases with pressure, as shown in Fig. 8, and is estimated to be 3200° at 30,000 atmospheres, 3400° at 65,000 atmospheres and 3500° at 80,000 atmospheres. The uncertainty in these temperatures is probably 100°. The literature value for the melting temperature of boron nitride at low pressure is 2730°. The increase of its melting temperature with pressure implies that molten boron nitride has a lower density than the solid hexagonal form or the solid cubic form. This is interesting because Hall⁴ found the density of molten germanium to be greater than the density of the solid at all pressures up to about 180,000 atmospheres, and solid germanium has a cubic structure like diamond or cubic boron nitride.

It would be interesting to determine the melting curve for carbon at high pressures, but there does not seem to be any material which can hold molten carbon without reacting with it or contaminating it. Perhaps this problem can be solved during the next several years.

The third and last portion of this paper has to do with some studies carried out in our laboratory on certain so-called "high pressure minerals."

The best known and most studied of these naturally occurring minerals is diamond, but plain

(3) H. M. Strong, *Phys. Rev., J. Geophys. Res.*, in press.

(4) H. T. Hall, *THIS JOURNAL*, 59, 1144 (1955).

diamonds are not nearly as interesting as the diamonds which contain inclusions of other minerals. These minerals can be olivine, diopside, magnetite, zircon and certain types of garnet, as well as less common minerals.^{5,6} Quartz has been reported occasionally as an inclusion in diamonds, particularly in some from Brazil,⁵ but a careful investigation by us has so far shown that all such diamonds do not carry quartz entirely surrounded by diamond, but instead the quartz merely adheres to or has been deposited in fissures in these diamonds. This is an interesting point which bears on the synthesis of natural diamond, because we have found that in the range of pressure and temperature at which it is now possible to form diamond, quartz is not stable. A piece of quartz next to a growing diamond invariably changes into a denser form of silica known as coesite. If natural diamonds could form where quartz was stable, then they could have formed at pressures and temperatures far below those now found necessary in the Laboratory. This does not appear likely, so that the role of diamond as a high pressure mineral seems better established than ever. Incidentally, to my knowledge, no one has ever yet found coesite included in diamond.

In Fig. 9 we see a tentative phase diagram for carbon as a function of pressure and temperature. The chain line encloses the region reached experimentally by Bridgman and by Basset. The diamond-graphite equilibrium line is fairly well known at low temperatures and pressures by calculation from thermodynamic data, according to Rossini and Jessup.⁷ At higher pressures and temperatures there is indicated a broad band which corresponds to the uncertainty of the position of the equilibrium line. We have studied the growth and destruction of diamond seeds in this region from 50,000 to 110,000 atmospheres, but so far the measurement of the pressure has proved difficult enough to leave some uncertainty in the position of the line, and we seek more precise measurements before publishing our results.

Although it may be true that there is a low pressure limit below which diamond cannot be formed, even metastably, the phase diagram does not indicate any upper limit to the pressure at which diamond could be formed except that it would have to be less than the pressure at the center of the earth, some 3.6 million atmospheres.

However, some diamonds contain olivine, a basic magnesium-iron silicate. Presumably this is a very common mineral deeper in the earth. Recently Ringwood⁸ has discovered that the iron-rich form of olivine, called fayalite, can be transformed into a spinel crystal form at 55,000 atmospheres and 600° and that this spinel form can be recovered at one atmosphere. Experiments in our laboratory have confirmed this discovery, and in addition we attempted to change

(5) E. Gubelin, *J. Gemology*, III, No. 5 (1952).

(6) A. F. Williams, "The Genesis of the Diamond," Ernest Benn, London, 1932.

(7) F. D. Rossini and R. S. Jessup, *J. Research Nat. Bur. Standards*, 21, 491 (1938).

(8) A. E. Ringwood, *Nature*, 178, 1303 (1956).

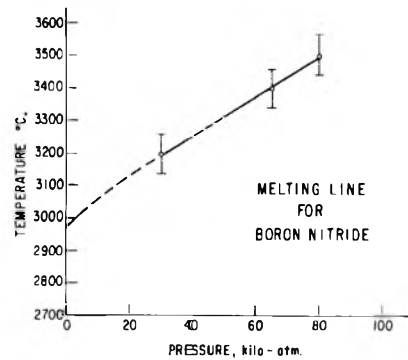


Fig. 8.

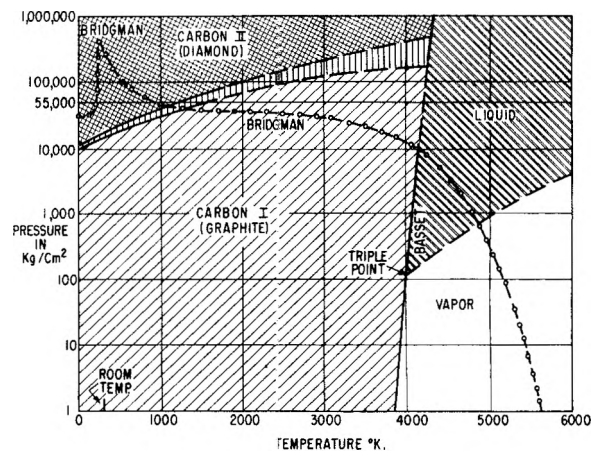


Fig. 9.

the magnesium-rich olivine called forsterite into a spinel form. But no spinel form was obtained at pressures as high as 130,000 atmospheres. When the phase diagram for the olivine-spinel system has been extended to higher pressures, we shall probably be able to set a maximum pressure limit or maximum depth of formation on those diamonds which contain inclusions of olivine. At present it is only possible to say that these diamonds could have formed at pressures as high as 130,000 atmospheres. This would correspond to a depth in the earth of about 400 km.

As mentioned earlier, certain types of garnet can occur as inclusions in diamond. The pyrope-almandine garnets are the most common of these, and such garnets are also found in the diamond-bearing blue ground of the South African diamond fields. Coes⁹ and Yoder,¹⁰ among others, have shown that many garnets require high pressure for their formation, and the pyrope-almandine garnets are among them. Thus a study of the behavior of such garnet at high pressures and temperatures might tell us more about the genesis of natural diamond and the deeper layers of the earth's crust.

A garnet which is very similar to this South African garnet is found in Gore Mountain, New York. The Gore Mountain garnet contains a little more iron and a little less magnesium than the South African garnet. The experience with garnet would indicate that the Gore Mountain garnet

(9) L. Coes, Jr., *J. Am. Ceramic Soc.*, (1955).

(10) H. S. Yoder, Jr., *Am. Min.*, 21, 342 (1955).

would hence tend to be stable at slightly lower pressures than the South African garnet.⁹

Mr. A. J. DeLai of our laboratory has recently studied the high pressure, high temperature behavior of Gore Mountain garnet. Essentially his method was to place powdered garnet in a nickel capsule and heat it to a predetermined temperature at a selected pressure. After about 5 minutes of heating the sample was chilled, the pressure was reduced, and the material in the capsule was examined under the microscope. In this way it was possible to determine whether the garnet had melted or decomposed. This garnet was found to melt and decompose *in vacuo* at 1185°. If the pressure is less than 26,000 atmospheres, this garnet cannot be melted without decomposition. The principal products of decomposition were enstatite and glass. At pressures above 26,000 atmospheres the solid and molten garnet can exist together, and the melting temperature increases with pressure. If the molten garnet at high pressure is cooled slowly from say 2000°, solid garnet forms from it. However, if the melt is quenched from too high a temperature at high pressure, enstatite and glass are formed even though the pressure is high enough for garnet to be stable. This suggests that some semblance of the solid garnet structure may exist in liquid garnet at high pressures.

It appears that well-developed crystals of garnet are rarely included in diamond; most of the garnet inclusions are irregular in shape. This would imply that the garnet was molten or nearly molten as the diamond formed around it.

In any event, the diamonds which contain garnet inclusions probably did not form at temperatures higher than about 2000°, or they would contain enstatite instead of garnet. Enstatite is a relatively rare inclusion in diamond. And because the garnet inclusions mostly appear to have been molten, the diamond often evidently formed at temperatures above about 1300°.

Now we have two high pressure minerals, garnet and diamond, one encased in the other. It is very unlikely that both were formed metastably, that is, at pressures below which either was stable. At least the garnet must have been stable. This implies that the diamonds containing garnet formed at pressures of at least 25,000 atmospheres. If in addition the diamond formed at a pressure where it was stable, then the lowest pressure possible would be about 55,000 atmospheres. Such a pressure would exist at a depth of about 150 km. beneath the surface of the earth.

Thus, it now seems even more likely that diamonds have been formed at considerable depths in the earth, and we are quite fortunate to have any of them at the surface.

The problems of the origin of natural diamonds are by no means completely solved. But you can see that we are making some progress toward understanding them. It is very likely that within a few years the diamond will prove to be a very valuable geological indicator from which we will be able to deduce much about the physical and chemical conditions which have existed and now exist in the deeper layers of the earth.

QUANTUM-MECHANICAL STUDIES ON OXIDATION POTENTIALS AND ANTIOXIDIZING ACTION OF PHENOLIC COMPOUNDS

BY TAKAYUKI FUENO, TAIKYUE REE AND HENRY EYRING

Department of Chemistry, University of Utah, Salt Lake City, Utah

Received June 5, 1959

Available data on oxidation potentials of phenolic compounds (including polyphenols) are found to be linearly related to the highest occupied molecular orbital energies for π -electrons, which are calculated on the basis of the LCAO MO (linear combination of atomic orbital molecular-orbital) theory. The oxidation potentials of nearly 180 monophenols, including some never synthesized, are predicted from the calculated values for the orbital energies. The antioxidizing action of phenolic compounds for radical chain reactions is examined theoretically, and the proposal is made that the rate-determining step for the inhibition involves an electron transfer from the phenols to the radicals. The charge-transfer stabilization energies of the transition states proposed for the primary reactions between a radical and some phenols and the degrees of charge transfer in these transition complexes are calculated by perturbation theory, assuming π -electronic interaction between the two reaction centers as the perturbation. These calculated values prove to be closely related to the antioxidizing efficiencies of the phenolic compounds.

I. Introduction

It has long been known that phenolic compounds are useful inhibitors for autoxidation of organic substances, and a large technical literature exists concerned with various kinds of inhibited autoxidation systems. Although these inhibitors are generally believed to affect the chain propagation step of the autoxidation processes by a reaction in which the inhibitor is oxidized, the mechanism of the initial step of the inhibition is still unsettled.¹

(1) C. Walling, "Free Radicals in Solution," John Wiley and Sons, Inc., New York, N. Y. 1957, pp. 430-436.

Bolland and ten Have² considered that the initial step is the abstraction of a phenolic hydrogen to yield a phenoxy (or semiquinone) radical and subsequently demonstrated that the antioxidizing efficiency of phenols parallels the oxidation-reduction potential. Recently, however, Hammond, *et al.*,³⁻⁶ have suggested, on the basis of

(2) J. L. Bolland and P. ten Have, *Disc. Faraday Soc.*, **2**, 252 (1948).

(3) C. E. Boozer and G. S. Hammond, *J. Am. Chem. Soc.*, **76**, 3861 (1954).

(4) C. E. Boozer, G. S. Hammond, C. E. Hamilton and J. N. Sea, *ibid.*, **77**, 3233 (1955).

several lines of evidence, that the inhibition reaction involves complex formation between an inhibitor and a radical.

In the present paper, the known oxidation potentials of phenols are interpreted from the molecular orbital (MO) theory of the linear combination of atomic orbitals (LCAO), and the relation between antioxidizing efficiencies and oxidation potentials⁷ of phenols is discussed on this basis. Furthermore, a possible model is proposed for the transition state of the inhibition process, and the stability of this transition state is quantitatively dealt with by perturbation theory.

II. Oxidation Potentials of Phenolic Compounds

1. Dependence of Oxidation Potential of Monophenols upon their π -Conjugating Nature.—The primary step in the oxidation of phenolic compounds in neutral media consists in the removal of one hydrogen atom from the phenolic oxygen. With respect to the mechanism, then, there is no difference between the oxidation of monophenols and the compounds of the hydroquinone type, except that the oxidation products of monophenols by the removal of hydrogen atoms are usually much less stable than those of the hydroquinone type. Fieser⁷ developed a method for measuring the potentials with a reasonable degree of accuracy even for such unstable oxidation-reduction systems. It consisted in measuring the potentials of a solution of some stable oxidation-reduction system in the presence of phenols and thereby determining the minimum potential at which the velocity of the reaction between a given phenol and the reference oxidant reaches a limiting small value. The potential was referred to as the "critical oxidation potential." Furthermore, Fieser demonstrated experimentally that the critical oxidation potential V_c bears a definite relationship to the normal oxidation potential V_0 through

$$V_0 - V_c = 0.136 \text{ v. for monophenols} \quad (1)$$

and

$$V_0 - V_c = 0.068 \text{ v. for hydroquinones}$$

Careful examination of the above reactions will lead to the possibility that the potential-determining step involves one electron transfer from phenols to the reference oxidant, followed by proton migration. Under an essentially identical assumption, several workers⁸⁻¹⁴ have shown that the reduction potentials of conjugated compounds are linearly related to their lowest vacant molecular orbital (LVMO) energies calculated by quantum-mechanical principles. Thus, it is to be expected that the relative height of the highest occupied

molecular orbital (HOMO) energy of phenols would be responsible for determining the potentials of their irreversible oxidations.

In order to examine the expected relationship for monophenols theoretically, we apply the first-order perturbation theory. Let E_j^0 be the energy of a π -electron in the j th molecular orbital, Ψ_j , of the reference hydrocarbon anion¹⁵ which has the same arrangement of atomic $p\pi$ -orbitals and the same number of π -electrons as a phenol. Then, replacement of the side chain ($-\text{CH}_2^-$) of the anion by an OH-group will change the value of E_j^0 into E_j . The first-order perturbation theory gives

$$E_j = E_j^0 + \int \Psi_j H' \Psi_j d\tau \quad (2)$$

where H' is the perturbation term of the one-electron Hamiltonian for the phenol with respect to that of the corresponding reference hydrocarbon anion. Now in the LCAO approximation

$$\Psi_j = \sum_r C_{jr} \phi_r \quad (3)$$

C_{jr} being the linear combination coefficient of atomic orbital ϕ_r in the j th molecular orbital. Putting eq. 3 into eq. 2, we obtain

$$E_j = E_j^0 + \sum_r \sum_s C_{jr} C_{js} \int \phi_r H' \phi_s d\tau \quad (4)$$

In eq. 4, the most important integral will be the coulomb term of the oxygen (X) whose atomic orbital is designated by ϕ_X . Since the HOMO's of the reference hydrocarbons are all non-bonding, the HOMO energy, E_{ho} , of phenols is, thus, approximated by

$$E_{ho} = \alpha + (C_{nX})^2 k_X \beta \quad (5)$$

where α and β are coulomb integral of a carbon atom and resonance integral of a carbon-carbon double bond, respectively, C_{nX} is the coefficient of ϕ_X in the non-bonding molecular orbital (NBMO),¹⁶ and k_X is a coulombic parameter for oxygen defined as $\int \phi_X H' \phi_X d\tau / \beta$.

For about 200 phenols, including some never synthesized, the values of $(C_{nX})^2$ were calculated by the NBMO method.¹⁶ Plots of the values of $(C_{nX})^2$ of several existing phenols against the available data for V_c give a straight line, as seen in Fig. 1. Since β is a negative quantity and k_X a positive one,¹⁷ the HOMO becomes more stable as the value of $(C_{nX})^2$ increases. Thus, the linear relationship between $(C_{nX})^2$ and V_c in Fig. 1 substantiates the expectation that, the less stable the HOMO of phenols, the more easily are they oxidized. It will be worthwhile to note that the above qualitative conclusion does not depend upon the empirical parameters α , β and k_X .

The straight line in Fig. 1 is expressed as

$$V_c = 2.807(C_{nX})^2 - 0.459 \quad (6)$$

with a correlation coefficient, $r = 0.977$.

By using eq. 6 and the values of $(C_{nX})^2$, the critical oxidation potentials, V_c , can be predicted for

(15) For example, the reference hydrocarbon anion for phenol is benzyl anion ($\text{C}_6\text{H}_5\text{CH}_2^-$).

(16) H. C. Longuet-Higgins, *J. Chem. Phys.*, **18**, 275 (1950).

(17) The parameter k_X is a measure of the electronegativity of X compared with carbon atom and is plus in sign when X is more electronegative than the carbon.

(5) G. S. Hammond, C. E. Boozer, C. E. Hamilton and J. N. Sen, *J. Am. Chem. Soc.*, **77**, 3238 (1955).

(6) C. E. Boozer, G. S. Hammond, C. E. Hamilton and C. Peterson, *ibid.*, **77**, 3380 (1955).

(7) L. F. Fieser, *ibid.*, **52**, 5204 (1930).

(8) A. Maccoll, *Nature*, **163**, 178 (1949).

(9) A. Pullman, B. Pullman and G. Berthier, *Bull. soc. chim. France*, **17**, 591 (1950).

(10) G. J. Hoijtink and J. van Schooten, *Rec. trav. chim.*, **71**, 1089 (1952).

(11) G. J. Hoijtink and J. van Schooten, *ibid.*, **72**, 391 (1953).

(12) G. J. Hoijtink and J. van Schooten, *ibid.*, **72**, 903 (1952).

(13) G. J. Hoijtink, *ibid.*, **74**, 1525 (1955).

(14) T. Fueno, K. Morokuma and J. Furukawa, *J. Chem. Soc. Japan, Pure Chem. Section*, **79**, 116 (1958).

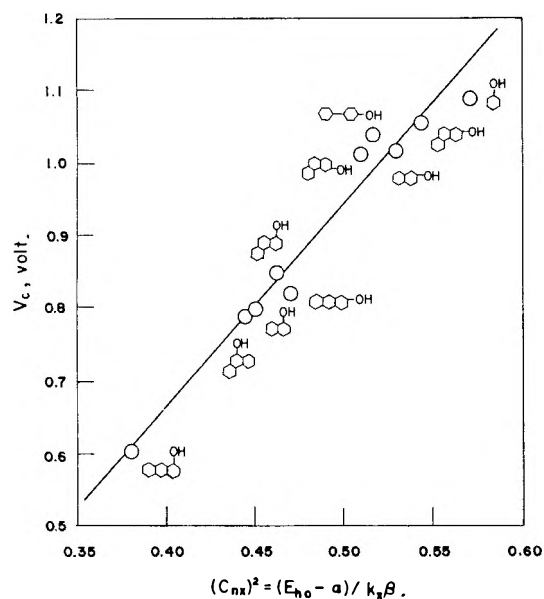


Fig. 1.—Linear relationship between critical oxidation potentials of monophenols and the HOMO energies.

various possible monophenols. In Table I the predicted values of V_c for nearly 180 possible monophenols belonging to 23 different parent alternant hydrocarbons (the number of unsaturated six-membered rings ranging from 3 to 5) are summarized.

Inspection of Table I shows that the effect of the nature of the hydrocarbon skeletons upon V_c of the corresponding phenols will be comparatively of less consequence than that of the position of terminal carbon where the hydroxyl group is linked to hydrocarbons. With several familiar

TABLE I^a
PREDICTION OF THE CRITICAL OXIDATION POTENTIALS V_c
OF MONOPHENOLS

Parent hydrocarbon	Position of the carbon atom bearing OH-group	$(C_{n\alpha})^2$	V_c , v.
Benzene	...	0.5714	(1.089)
Naphthalene	1(α)	.4500	(0.797)
	2(β)	.5294	(1.017)
Anthracene	1	.3810	(0.602)
	2	.4706	(.820)
	9	.2857	.343
Phenanthrene	1	.4630	(.848)
	2	.5435	(1.057)
	3	.5102	(1.013)
	4	.4902	0.918
Naphthacene	1	.3333	.477
	2	.4167	.711
	5	.2083	.126

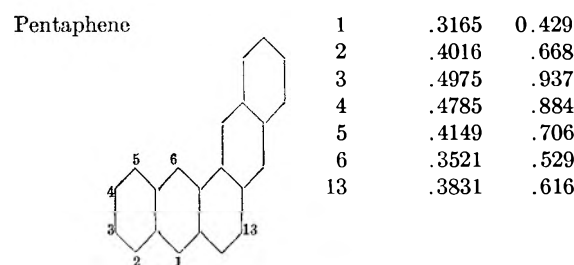
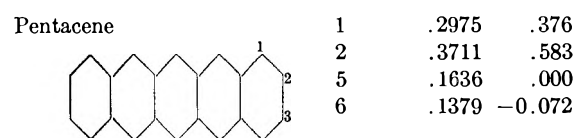
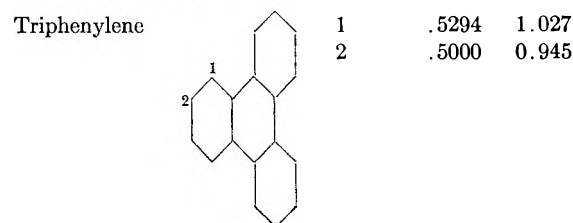
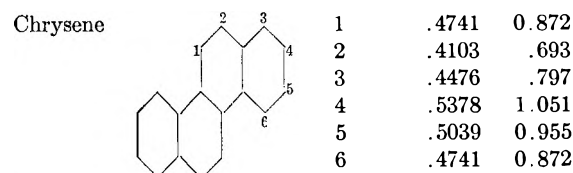
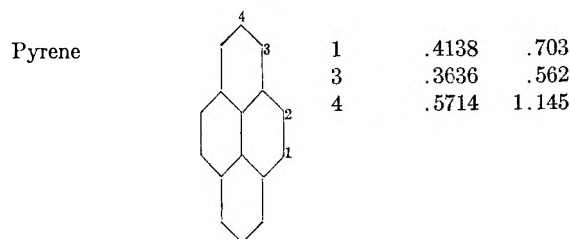
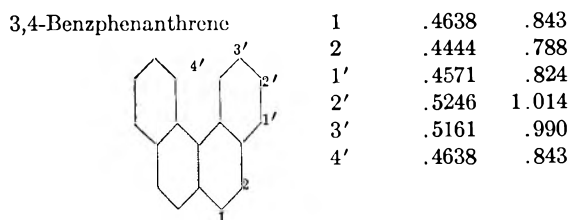
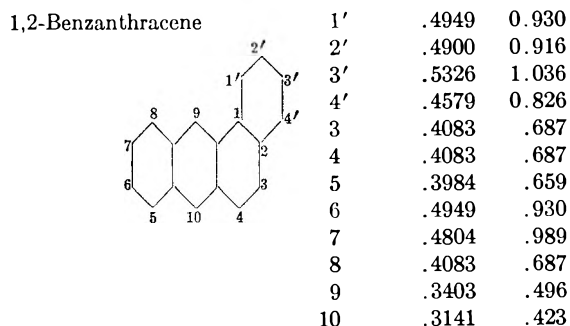
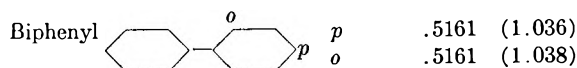


TABLE I (Continued)

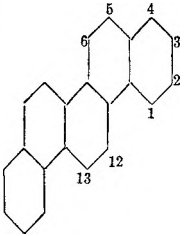
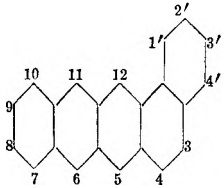
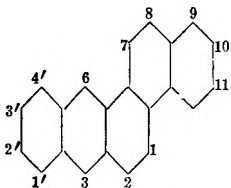
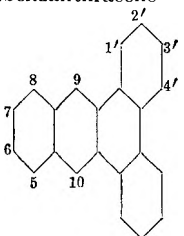
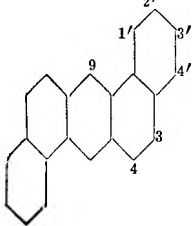
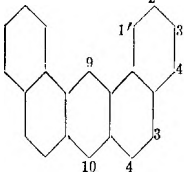
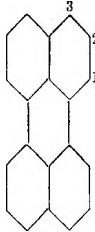
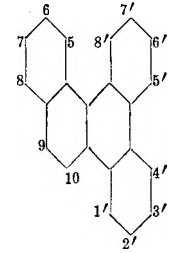
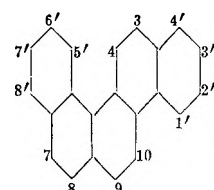
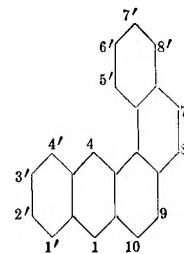
Parent hydrocarbon	Position of the carbon atom bearing OH-group	(C _{ax}) ²	V _{ox} v.				
	1	.4801	.889				
	2	.5015	.949				
	3	.5393	1.056				
	4	.4495	0.803				
	5	.4102	.692				
	6	.4633	.841				
	13	.4433	.786				
		1'	.4883	.911			
		2'	.4709	.863			
		3'	.5159	.989			
		4'	.4475	.797			
		3	.3682	.575			
		4	.3839	.619			
5		.2432	.224				
6		.2301	.187				
7		.3491	.521				
8		.4402	.777				
9		.4332	.757				
10		.3537	.534				
11	.2382	.210					
12	.2647	.284					
	1'	.3878	.630				
	2'	.4859	.905				
	3'	.4708	.863				
	4'	.3980	.658				
	1	.4291	.745				
	2	.3634	.561				
	3	.2937	.365				
	6	.3184	.435				
	7	.4821	.894				
	8	.3829	.616				
	9	.4368	.767				
	10	.5284	1.024				
11	.4959	0.933					
12	.4618	.837					
	1'	.5000	.945				
	2'	.5200	1.001				
	3'	.5200	1.001				
	4'	.5000	0.945				
	5	.4154	.718				
	6	.5000	.945				
	9	.3611	.555				
		1'	.4932	.925			
		2'	.4932	.925			
3'		.5373	1.049				
4'		.4557	0.820				
3		.4091	.689				
4		.4235	.730				
9		.3636	.562				
		1'	.4881	.911			
		2'	.4983	.940			
	3'	.5314	1.033				
	4'	.4601	0.833				
	3	.4235	.730				
	4	.4198	.719				
	9	.3902	.636				
	10	.3404	.497				
		1	.3432	.504			
		2					
3		.3080	.406				
	1'	.4851	.903				
	2'	.5297	1.028				
	3'	.5212	1.004				
	4'	.4925	0.923				
	5'	.4962	.934				
	6'	.5052	.959				
	7'	.5341	1.040				
	8'	.4712	0.864				
	5	.4558	.820				
	6	.5117	.977				
7	.5241	1.012					
8	.4465	0.794					
9	.4188	.717					
10	.4876	.910					
	1'	.4761	.877				
	2'	.5060	.961				
	3'	.5348	1.042				
	4'	.4531	0.813				
	5'	.4694	.859				
	6'	.5137	.983				
	7'	.5265	1.019				
	8'	.4592	0.830				
	3	.4225	.727				
	4	.4592	.830				
7	.4447	.789					
8	.4531	.813					
9	.4270	.740					
10	.4774	.881					
	1'	.3916	.640				
	2'	.4802	.889				
	3'	.4764	.878				
	4'	.3941	.647				
	5'	.4481	.799				
	6'	.5084	.968				
	7'	.5105	.974				
	8'	.4498	.804				
	1	.3025	.390				
	4	.3087	.408				
7	.4261	.737					
8	.4672	.852					
9	.4246	.733					
10	.3954	.651					

TABLE I (Continued)

Parent hydrocarbon	Position of the carbon atom bearing OH-group	(C_{6x}) ²	V_0 , v.
3,4,5,6-Dibenzphenanthrene	1'	.4555	.820
	2'	.5314	1.033
	3'	.5090	0.970
	4'	.4734	.870
	1	.4568	.823
	2	.4311	.751
	9	.4617	.837
	10		
	1		
	2		
1,2-Benzpyrene	1'	.4959	.933
	2'	.5193	.999
	3	.4143	.704
	4	.5576	1.106
	5	.3993	0.662
	6	.4276	.741
3,4-Benzpyrene	1'	.4500	.804
	2'	.4286	.744
	3'	.5294	1.027
	4'	.3750	0.594
	1	.3600	.552
	2	.4500	.804
	5	.2500	.243
	6	.3750	.594
	7	.3750	.594
	8	.3333	.477
9	.5625	1.120	
10	.3214	0.443	

^a The values of V_0 in parentheses are the experimental data determined by Fieser.⁷

phenols, the importance of the latter effect was qualitatively interpreted by Fieser⁷ in terms of an α -naphthol and a β -naphthol type: the phenols with the oxidizable group in the unreactive β -position to a second benzene ring differ relatively little in potential from each other and are subjected to oxidation with more difficulty than are the α -naphthol types. This trend seems to remain valid for a larger number of phenols as shown in Table I, where the phenols with predicted values of V_0 larger than 1 volt are of the β -naphthol type almost without exception.

2. Oxidation Potentials of Polyphenols.—In order to make the above-mentioned linear relation more conclusive, it is further necessary to examine whether the relation would also hold for polyphenols. Thus, the relative heights of the HOMO levels, x_{ho} , for polyphenols as well as monophenols, being defined as $E_{ho} = \alpha + x_{ho}\beta$, are calculated as the roots of the simple LCAO MO secular equations (neglecting overlap integrals). The electronegativity parameter, k_x , for the oxygen is tentatively assigned the value unity.

In Table II, the calculated values of x_{ho} are compared with the critical oxidation potentials

V_0 and the normal oxidation potentials, V_0 . All the data for V_0 are obtained by correcting Fieser's data⁷ for V_c using the relationship (1), except as otherwise noted. Comparison of x_{ho} 's should be made with the V_0 's rather than with the V_c 's since only the V_0 's can be related to the free energy changes between oxidants and reductants for both the polyphenols and the monophenols. The relationship between V_0 and x_{ho} is graphically represented in Fig. 2, where a single straight line is seen to fit the plots for polyphenols as well as those for monophenols. Thus, it is concluded that the potential-determining step for the oxidation of phenolic compounds is an electron transfer from the compounds to the relevant oxidants.

Strictly speaking, however, some factors other than the π -electronic energy difference, ΔE_π , e.g., the differences in σ -electronic energy, in entropy term and in solvation energy between reductants (phenols) and oxidants (molecular cations of the phenols) should also be taken into account. Nevertheless, the linear relationship in Fig. 2 shows that these other factors are of less significance than the π -electronic energy. This argument will be represented by the simple equation

$$\Delta F \simeq \Delta H = C + \Delta E_\pi = FV_c \quad (7)$$

where ΔF and ΔH refer, respectively, to the changes in Gibbs' free energy and in heat content accompanying the oxidation process, and C and F denote the constant energy term (corresponding to the change in σ -bond energy and solvation energy) and Faraday's constant, respectively. Since ΔE_π is nothing else than the absolute value of the HOMO energy, $\alpha + x_{ho}\beta$, of a phenol, eq. 7 can be transformed into

$$V_0 = (C - \alpha) - x_{ho}\beta \quad (8)$$

where the three constants, C , α and β , are expressed in units of electron volts. Now, statistical treatment of the data listed in Table II gives the linear equation

$$V_0 = 2.082x_{ho} + 0.245 \quad (9)$$

with a correlation coefficient $r = 0.963$. Comparison of eq. 8 and 9 gives $\beta = -2.082$ e.v. in reasonable agreement with -2.23 e.v.¹² and -2.27 e.v.¹⁴ obtained from the linear relations between polarographic reduction potentials and LVMO energies for conjugated hydrocarbons and substituted stilbenes, respectively.

It is to be expected that the calculated value of x_{ho} would also be a measure of ionization potential of phenolic compounds. However, we have not yet enough accumulated data to check this point.

III. Phenolic Compounds as Antioxidant for Radical Chain Reactions

1. Relationship between Antioxidizing Power of Phenols and their Oxidation Potential.—Some comparisons²⁰⁻²² of the effectiveness of various phenols as inhibitors in different oxidation systems are available. These comparisons have been made on the basis of the length of the induction period

(20) C. D. Lowry, G. Egloff, J. C. Morrell and C. G. Dryer, *Ind. Eng. Chem.*, **25**, 804 (1933).

(21) H. S. Olcott, *J. Am. Chem. Soc.*, **56**, 2492 (1934).

(22) K. K. Jau and H. N. Alyea, *ibid.*, **55**, 575 (1933).

(18) J. B. Conant, *Chem. Revs.*, **3**, 1 (1926).

(19) L. F. Fieser, *J. Am. Chem. Soc.*, **52**, 4915 (1930).

TABLE II
COMPARISON OF OXIDATION POTENTIALS OF PHENOLIC COMPOUNDS WITH THEIR HOMO ENERGIES

Serial no. ^a	Phenol	V_0 , ^b v.	V_0 , v.	x_{ho}	Symmetry of HOMO ^c
1	Phenol	1.089	1.225	0.5043	S
2	α -Naphthol	0.797	0.933	.3642	...
3	β -Naphthol	1.017	1.153	.4307	...
4	1-Phenanthrol	0.848	0.984	.3760	...
5	2-Phenanthrol	1.057	1.193	.4595	...
6	3-Phenanthrol	1.013	1.149	.4072	...
7	9-Phenanthrol	0.798	0.934	.3596	...
8	1-Anthrol	.602	.738	.2785	...
9	2-Anthrol	.820	.956	.3250	...
10	<i>p</i> -Hydroxybiphenyl	1.036	1.172	.4275	S
11	<i>o</i> -Hydroxybiphenyl	1.038	1.174	.4374	...
12	Resorcinol	1.043	1.179	.4450	A
13*	Hydroquinone	...	0.715 ^b	.2541	S _x A _y
14*	Catechol	0.747	.810 ^d	.2624	S
15*	Pyrogallol	.609	.676 ^d	.1912	S
16*	1,4-Naphthohydroquinone482 ^d	.1334	A
17*	1,2-Dihydroxynaphthalene564 ^e	.1468	...
18	1,3-Dihydroxynaphthalene	.753	.889	.3190	...
19*	1,5-Dihydroxynaphthalene	.673	.741	.2079	S
20	2,3-Dihydroxynaphthalene	.812	.948	.3393	S
21*	2,6-Dihydroxynaphthalene	.690	.758	.2880	S
22	2,7-Dihydroxynaphthalene	1.007	1.143	.3964	A
23	2,6-Dihydroxyphenanthrene	1.010	1.146	.4019	...
24*	3,6-Dihydroxyphenanthrene	0.832	0.900	.3157	S
25*	<i>p,p'</i> -Dihydroxybiphenyl	.882	.954 ^f	.3111	S _x A _y
26*	<i>p,p'</i> -Dihydroxystilbene	.786	.854 ^f	.2541	S _x A _y

^a The asterisk indicates that the phenol is *o*-hydroquinone type. ^b Taken from ref. 7. ^c The symmetry of the HOMO function with respect to a relevant axis of symmetry is represented, where appropriate, by the symbol S (symmetric) or A (antisymmetric). For hydroquinone, *p,p'*-dihydroxybiphenyl and *p,p'*-dihydroxystilbene, the line connecting two phenolic oxygens is chosen as the *x*-axis. ^d Taken from ref. 2. ^e Estimated from the normal oxidation-reduction potential (0.506 volt) for 1,2-naphthoquinone in 0.2 N HCl.¹⁸ (In the same medium, the potentials for 1,4-naphthoquinone and quinone are, respectively, 0.426 and 0.656 volt, which are smaller than the V_0 's by 0.056 and 0.059 volt, respectively. Thus, V_0 for 1,2-dihydroxynaphthalene is to be estimated as 0.506 + 0.058 = 0.564 volt.) ^f Taken from ref. 19.

which precedes the autoxidation of initiator-free organic substances. However, these data are not necessarily adequate for theoretical consideration since the rate of chain initiation is by no means constant in the course of the induction period.

Bolland and ten Have² made a kinetic analysis of the peroxide-initiated oxidation of ethyl linoleate in the presence of phenols (ROH) by measuring the diminution in oxidation rates due to the inhibitory action of phenols. From the results of the analysis, they established a table of dimensionless values representing relative antioxidizing efficiencies, K , of phenols, taking hydroquinone as the standard, with a value of unity (see Table III). Furthermore, they found that the value of $\log K$ increased linearly with diminishing normal oxidation potential (*i.e.*, increasing oxidizability). According to these workers, this quantitative dependence of antioxidant efficiency on the oxidizability of the phenols is interpreted by assuming that the chain termination reaction involves the transfer of a hydrogen atom from the antioxidant to the propagating radical (R'OO·), *viz.*



and, thus, the efficiency can be controlled entirely by the heat of reaction of the dissociation: $\text{ROH} \rightarrow \text{RO}\cdot + \text{H}\cdot$.

Now, let us assume that the heat of the homolytic dissociation, $\Delta H(\text{RO}-\text{H})$, of ROH is divided into two parts, *viz.*

$$\Delta H(\text{RO}-\text{H}) = \Delta H_\sigma(\text{RO}-\text{H}) + \Delta H_\pi(\text{RO}-\text{H}) \quad (11)$$

where $\Delta H_\sigma(\text{RO}-\text{H})$ and $\Delta H_\pi(\text{RO}-\text{H})$ represent the respective changes in the energies of σ - and of π -electrons accompanying the dissociation. Then, $\Delta H_\sigma(\text{RO}-\text{H})$ remains substantially constant over a series of phenolic compounds, because of the localized nature of σ -electrons in chemical bonds. The relative efficiency may, therefore, be related to the difference in the total π -electronic energy between phenols (ROH) and the corresponding phenoxy radicals (RO·). If we assume that the energy level of each occupied molecular orbital in RO· remains identical with that of the corresponding orbital in ROH, then

$$\Delta H_\pi(\text{RO}-\text{H}) = \Delta E_\pi = -E_{ho} = -(\alpha + x_{ho}\beta) \quad (12)$$

because the HOMO of RO· is occupied by one π -electron whereas that of ROH is doubly occupied. The linear dependence of $\log K$ upon x_{ho} is, thus, to be expected, provided the entropy of activation remains constant for the different phenols. In Fig. 3, the value of $\log K$ for several phenols, which were investigated by Bolland and ten Have, are plotted against x_{ho} , where it is seen that the expected linear relationship between the two quantities is actually substantiated. The linear dependence of $\log K$ upon V_0 is comprehensible if one compares eq. 8 and 12.

The above interpretation of the different antioxidizing efficiencies of phenols is, however, rather tentative; the transition state of the termination

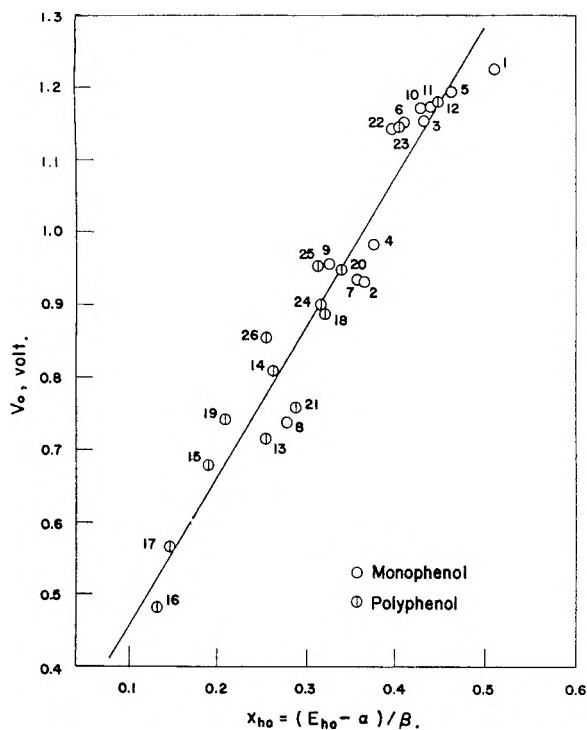


Fig. 2.—Linear relationship between normal oxidation potentials of phenolic compounds and the HOMO energies. The numbers in Figs. 2, 3 and 5 indicate the phenols shown in Table II.

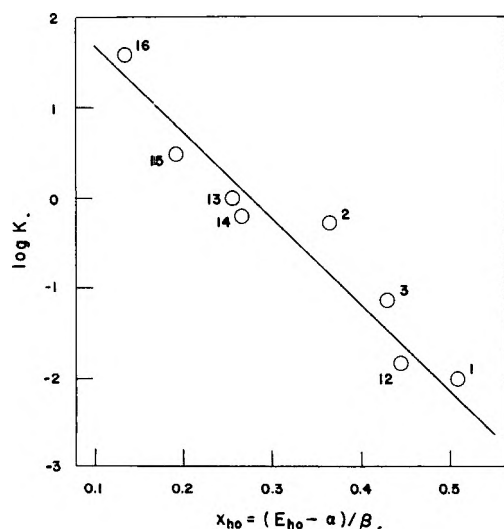
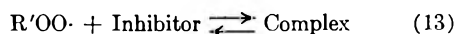


Fig. 3.—Relationship between antioxidizing efficiencies of some phenolic compounds and the HOMO energies.

reaction should be taken into consideration. This point will be discussed in a later section.

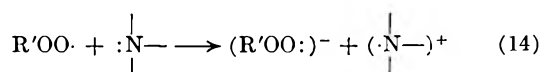
2. **Re-examination of the Antioxidation Mechanism of Phenols.**—As already described, Bolland and ten Have² concluded that the antioxidizing action of phenols is associated with the abstraction by the propagating radical of hydrogen atom attached to the phenolic oxygen. On the other hand, Hammond, *et al.*,³⁻⁶ have drawn the conclusion that this is not generally the case. They made extensive studies on the antioxidizing actions of phenols and amines toward the autoxidations of cumene and tetralin and found that the bond

dissociation between the heteroatoms and hydrogen is not a rate-determining step. As the possible evidence for this, they mentioned that N-deuterated N-methylaniline³ and diphenylamine⁵ show identical kinetics to those of the undeuterated substances and that N,N-dimethylaniline and N,N,N',N'-tetramethyl-*p*-phenylenediamine are fairly potent inhibitors despite the absence of a labile N-H function in their structures.⁵ On the basis of these observations, they suggested that the inhibition reaction involves the rate-determining step



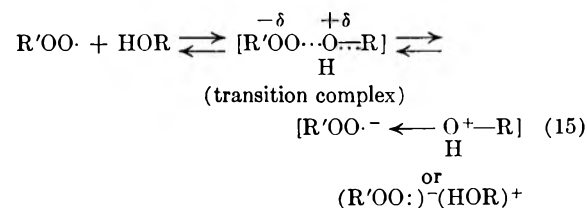
in which the complex is assumed to be a loose π -complex.⁵

Recently, an ionic mechanism of termination of the chains by amines was proposed by Pedersen,²³ who formulated it as



where the detachment of a mobile hydrogen from the amino group is not involved.

The above survey of the chain termination mechanism shows that current considerations suggest a polar (or ionic) interaction in the primary step of the reaction between the propagating radicals and the inhibitors. However, no consideration has been made of the transition state of this reaction by previous investigators. As already mentioned, the antioxidizing power of different phenols is closely related to their oxidizability, *i.e.*, the ease with which they are ionized to give the corresponding molecular cation. Thus, we assume that the rate-determining step of the termination would involve charge transfer between the attacking radical and the phenolic oxygen



and that the π -conjugation between ROH and $R'OO\cdot$ in the transition state would be responsible for the charge transfer; the stabilization energy of the transition complex directly contributes to the determination of the different antioxidizing efficiencies of phenolic compounds.

IV. Charge Transfer Between Phenols and Radicals

1. **Perturbation Theory of Charge Transfer in the Transition Complexes.**—The problem is confined to calculating, by perturbation theory, (1) the increase in total π -electron energy of the united system arising from the combination of a phenol and, for simplicity, a single atom radical and (2) the increase in π -electronic charge on the radical due to π -conjugation between the components in the transition complex. The π -electronic interaction between the radical (S) and the oxygen

(X) in phenols is considered as the perturbation. Resonance integrals for all the bonds are assumed to have the value β except for the π -bond between S and X in which the integral is denoted by γ . Overlap integrals are completely ignored.

Let us denote the m th π -MO for a phenol by

$$\Phi_m = \sum_r C_{mr} \phi_r \quad (16)$$

and the $p\pi$ -orbital for a radical, by ψ_s . Then the first-order perturbation theory²⁴ gives these new MO, Y_m , for the united system corresponding to Φ_m

$$Y_m = \Phi_m + \frac{C_{mX}\gamma}{E_m - F_n} \psi_s \quad (17)$$

where E_m and F_n are the energies of the MO, Φ_m and AO, ψ_s , respectively, and C_{mX} is a coefficient for the atomic orbital, ϕ_X , of oxygen appearing in the summation of eq. 16. Likewise, the new MO, Z_n , corresponding to ψ_s is given by

$$Z_n = \psi_s + \sum_m \frac{C_{mX}\gamma}{F_n - E_m} \Phi_m \quad (18)$$

The normalized MO functions for Y_m and Z_n are thus given by

$$Y_m' = \frac{\sum_r C_{mr} \phi_r + \frac{C_{mX}\gamma}{E_m - F_n} \psi_s}{\left[1 + \left(\frac{C_{mX}\gamma}{E_m - F_n}\right)^2\right]^{1/2}} \quad (19)$$

and

$$Z_n' = \frac{\psi_s + \sum_r \left(\sum_m \frac{C_{mX}C_{mr}\gamma}{F_n - E_m}\right) \phi_r}{\left[1 + \sum_r \left(\sum_m \frac{C_{mX}C_{mr}\gamma}{F_n - E_m}\right)^2\right]^{1/2}} \quad (20)$$

Both the first-order perturbation terms for the energies corresponding to Y_m' and Z_n' vanish. The respective energies, P_m and Q_n , of these MO's are given according to the second-order perturbation theory²⁴ as

$$P_m = E_m + \frac{(C_{mX})^2 \gamma^2}{E_m - F_n} \quad (21)$$

and

$$Q_n = F_n + \sum_m \frac{(C_{mX})^2 \gamma^2}{F_n - E_m} \quad (22)$$

Now, if we assume that the energy of the ψ_s is higher than that of the HOMO of the phenols (see Fig. 4), i.e., $F_n > (E_m)_{occ}$, then Q_n will continue to be larger than the P_m 's for occupied levels because, in eq. 21 and 22, the perturbation terms should be small compared with the E_m 's. Thus, the number of electrons occupying the MO, Y_m' , is either 0 or 2 while that in Z_n' is 1. Therefore, the increase in electron density, Δq_s , on S in the transition complex is given by

$$\Delta q_s = 2 \sum_m^{occ} \frac{\left(\frac{C_{mX}\gamma}{E_m - F_n}\right)^2}{1 + \left(\frac{C_{mX}\gamma}{E_m - F_n}\right)^2} - \frac{1}{1 + \sum_r \left(\sum_m \frac{C_{mX}C_{mr}\gamma}{F_n - E_m}\right)^2} - 1 \quad (23)$$

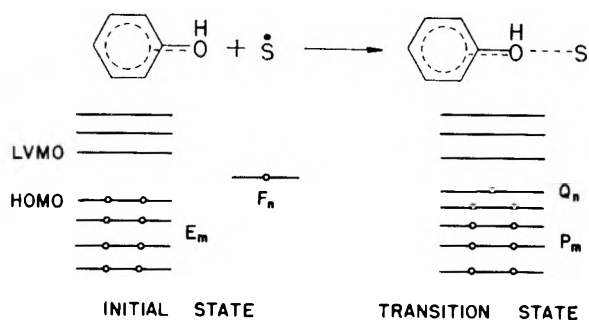


Fig. 4.—Schematic representation of the charge transfer process between phenol and a radical.

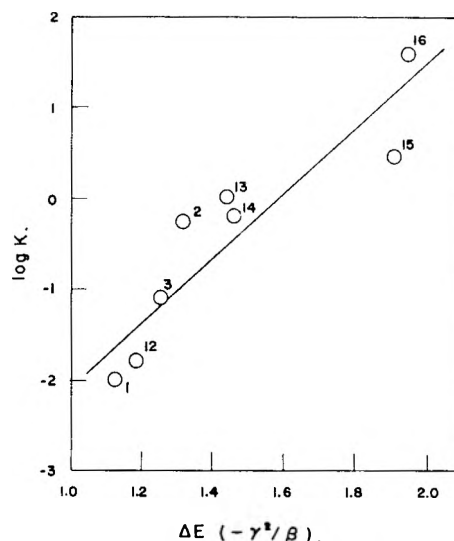


Fig. 5.—Relationship between antioxidizing efficiencies of some phenolic compounds and charge-transfer stabilization energies in the transition state.

and the stabilization energy, ΔE , of the transition complex due to charge transfer (or π -conjugation) is given by

$$\Delta E = 2 \sum_m^{occ} E_m + F_n - \left(2 \sum_m^{occ} P_m + Q_n\right) = \sum_m^{occ} \frac{(C_{mX})^2 \gamma^2}{F_n - E_m} - \sum_m^{unocc} \frac{(C_{mX})^2 \gamma^2}{F_n - E_m} \quad (24)$$

where \sum_m^{occ} and \sum_m^{unocc} denote the summations over all occupied and unoccupied levels, respectively. Introducing the conventional relations

$$E_m = \alpha + x_m \beta; F_n = \alpha + a \beta \quad (25)$$

into eq. 23 and 24, thus, gives

$$\Delta q_s = 2 \sum_m^{occ} \frac{\left(\frac{C_{mX}}{x_m - a}\right)^2 \left(\frac{\gamma}{\beta}\right)^2}{1 + \left(\frac{C_{mX}}{x_m - a}\right)^2 \left(\frac{\gamma}{\beta}\right)^2} + \frac{1}{1 + \sum_r \left(\sum_m \frac{C_{mX}C_{mr}}{x_m - a}\right)^2 \left(\frac{\gamma}{\beta}\right)^2} - 1 \quad (26)$$

and

$$\Delta E = \left[\sum_m^{occ} \frac{(C_{mX})^2}{x_m - a} - \sum_m^{unocc} \frac{(C_{mX})^2}{x_m - a} \right] \left(-\frac{\gamma^2}{\beta}\right) \quad (27)$$

2. Calculation of the ΔE and Δq_s Values.—

(24) M. J. S. Dewar, *J. Am. Chem. Soc.*, **74**, 3341 (1952).

TABLE III

DEPENDENCE OF THE ANTIOXIDIZING EFFICIENCIES OF PHENOLS UPON THE STABILITY OF THE TRANSITION STATE

Serial no.	Phenol	K^a	Δq_s	ΔE^b	q_X	f_X
16	1,4-Naphthohydroquinone	40	0.5863	1.9490	1.8262	1.323
15	Pyrogallol (central OH)	3.0	.4747	1.9141	1.8548	1.374
	Pyrogallol (side OH)		.4335	1.5870	1.8961	1.347
13	Hydroquinone	1.00	.3161	1.4438	1.8415	1.336
14	Catechol	0.63	.3132	1.4590	1.8342	1.331
2	α -Naphthol	.56	.1872	1.3184	1.8098	1.272
3	β -Naphthol	.077	.1549	1.2603	1.8141	1.295
12	Resorcinol	.016	.1307	1.1963	1.8765	1.307
1	Phenol	.010 ^c	.1153	1.1374	1.8200	1.301

^a Taken from ref. 2, unless otherwise noted. ^b In units of $-\gamma^2/\beta$. ^c Estimated from the comparative data for resorcinol and phenol as inhibitors of the thermal oxidation of sodium sulfite.²²

For several phenols investigated by Bolland and ten Have, all the molecular orbital energies x_m and the coefficients C_{mX} are calculated by the simple LCAO MO method, assuming the electronegativity parameter k_X for the phenolic oxygen as 1. By putting these calculated results into eq. 27, the values of ΔE for different phenols are obtainable in units of $-\gamma^2/\beta$, provided the value for a is given. In calculating ΔE , a is tentatively set equal to 0, *i.e.*, the electronegativity of the atom (S) bearing an odd electron in the attacking radical is assumed equal to that of carbon. The obtained values are compared with the data on relative antioxidizing efficiencies K , of the phenols in Table III, where it is seen that the larger the stabilization energy, the larger is the antioxidizing efficiency.

Figure 5 gives plots of $\log K$ against ΔE . Although the points are somewhat scattered, there does seem to be a roughly linear relationship between $\log K$ and ΔE ; the line is given by the equation

$$\log K = 3.60\Delta E - 5.52 \quad (28)$$

with the correlation coefficient, $r = 0.911$. From the slope of this line, $-\gamma^2/\beta$ is evaluated as 5.2 kcal./mole. In a foregoing section β is found to be -2.08 e.v. (*i.e.*, -48.0 kcal./mole). Hence, we find that $\gamma = -16$ kcal./mole. The value for $(\gamma/\beta)^2$, which is necessary in calculating the Δq_s by eq. 26, is thus found to have the value $(\gamma/\beta)^2 = (1/3)^2 = 0.11$.

The values of the Δq_s for the above phenols are calculated by eq. 26, using the known values for the x_m 's, the C_{mX} 's and $(\gamma/\beta)^2$. The results are listed in Table III, where it is seen that the Δq_s increases with increasing magnitude of ΔE . Since it is possible to regard the magnitude of the Δq_s as a measure of the degree of charge transfer in the transition complex, it can be concluded that, the larger the degree of charge transfer, the more stable is the transition complex. From the positive

signs of the Δq_s 's it is also concluded that the electron transfer takes place in the direction from phenols to radicals.

In pyrogallol both the Δq_s and the ΔE are larger for the complex, in which the charge transfer is assumed to take place through the central oxygen, than for the one associated with one of the side oxygens. The primary attack of the radical on pyrogallol is, therefore, considered to occur preferentially on the central oxygen in agreement with Bolland and ten Have's supposition.²

Table III also includes the π -electron density q_X and the free valence f_X for the oxygen atom in separated phenols, which were calculated from²⁵

$$q_X = 2 \sum_m^{\text{occ}} (C_{mX})^2 \quad (29)$$

and

$$f_X = \sqrt{3} - 2 \sum_m^{\text{occ}} C_{mX} C_{m r_1} \quad (30)$$

respectively, where r_1 refers to the carbon atom bearing a hydroxyl group. Comparison of these two quantities with K shows that neither of them is an index of antioxidizing efficiency of phenols. The absence of parallelism between q_X and Δq_s implies that the electrostatic force between the reaction centers is of little significance for the charge transfer from phenols to radicals; the more important factor is the ability of aromatic nuclei for π -conjugation with the radical through the oxygen atom as a reaction center.

Acknowledgment.—The authors wish to express their appreciation to the Office of Ordnance Research, United States Army, for their support of the present work under Contract No. DA-04-495-Ord-959 with the University of Utah.

(25) For example, see R. D. Brown, *Quart. Revs.*, **6**, 63 (1952), or else B. Pullman and A. Pullman, "Les Théories Electroniques de la Chimie Organique," Masson et Cie., Paris, 1952, p. 184.

HEATS OF NEUTRALIZATION AND THE STRENGTHS OF AMINES IN ACETONITRILE¹

BY EARL J. FORMAN² AND DAVID N. HUME

Contribution from the Department of Chemistry and Laboratory for Nuclear Science of the Massachusetts Institute of Technology, Cambridge, Mass.

Received June 11, 1959

Isothermal heats of neutralization at 24° of amines in acetonitrile were estimated from the initial slopes of thermometric titration curves. This technique is of particular advantage where precipitation occurs or the reaction is incomplete at the equivalence point. Heats of neutralization are shown to be a good relative measure of the strengths of aromatic amines as well as aliphatic primary and straight chain secondary amines in acetonitrile. Deviations from the correlation of aliphatic amines with the Taft equation may be accounted for by the "B-strain" hypothesis. The results may be explained in terms of a low degree of solvation of amines and ammonium ions in acetonitrile.

Introduction

Hall³ has demonstrated that the strengths of amines in aqueous solution are primarily governed by solvation effects. His study generally substantiates the hypothesis of Trotman-Dickenson⁴ who proposed that differences in strengths between primary, secondary and tertiary amines are due to differences in degrees of solvation of the N⁺-H groups of the ammonium ions. The importance of solvent effects in non-aqueous media must obviously depend on the extent and mechanism of any solvation which may take place.

The present study concerns the strengths of amines in acetonitrile. Relative strengths of bases in this solvent have been studied by Kilpatrick and Kilpatrick⁵ with indicator methods, by Fritz⁶ and by Hall,⁷ both of whom used potentiometric measurements. This communication deals with the correlations between heats of neutralization and strengths of amines in acetonitrile.

Experimental

Materials.—Acetonitrile obtained from Carbide and Carbon Chemicals Co. was used throughout. Water and other impurities were eliminated either by pre-drying over anhydrous potassium carbonate and finally distilling over phosphorus pentoxide or by shaking with type 4A Molecular Sieves (Linde Air Products Co.) for at least 15 minutes. The latter method was used for the bulk of the work and produced acetonitrile which contained less than 0.01% water according to Karl Fischer titration.

The amines were all commercial samples of the best available grade. Liquid amines were purified when necessary by distilling over sodium hydroxide. The triisobutylamine was a Kahlbaum sample that was vacuum distilled over sodium hydroxide. 1,3-Diphenylguanidine was recrystallized from toluene, ethanol, and again from toluene. Solutions, 0.02 to 0.002 *F*, were made in purified acetonitrile and protected from atmospheric moisture and carbon dioxide prior to and during titration.

Titration solutions were prepared by passing anhydrous hydrogen bromide (Matheson Co.) through a d-ying tower containing anhydrous magnesium perchlorate and silica gel, and then over the surface of dry acetonitrile which was being vigorously stirred with a magnetic stirrer. The titrant was made up to a concentration of approximately 0.1 *F*. These solutions generally developed a yellow color over a period of

an hour or two but appeared to be stable thereafter. The solutions were standardized by diluting an aliquot with water and titrating with standard sodium hydroxide to a potentiometric end-point. Frequent standardization was necessary because of the volatility of hydrogen bromide in acetonitrile solutions. The solutions decreased in strength by about 1% per day.

Apparatus and Technique.—The automatic thermometric titration method of Linde, Rogers and Hume⁸ with a modified apparatus, which included a motor-driven constant-flow buret and a more sensitive bridge circuit,⁹ was used for measuring heats of neutralization. The titration vessels were half-pint Dewar flasks capped with cork to make the system adiabatic. A thermistor (Western Electric Co. type 14B or the similar Victory Engineering Corp. type 32A1) and a small glass-covered wire heater were permanently mounted in the cap. Access for the tight-fitting buret tip and mechanical stirring were provided. Temperature changes were recorded on a 2 mv. Speedomax recorder so arranged that the unbalance potential of the recorder was essentially linear for changes up to 0.50°. The bridge circuit was capable of detecting temperature changes of 0.001°. All titrations were performed in a constant temperature room at 24 ± 0.5°.

Thermistors were calibrated over a two to three degree temperature range in order to evaluate the appropriate parameters in the thermistor equation¹⁰

$$\ln R = (B/T) + A \quad (1)$$

where *B* is the so-called material constant of the thermistor, and

$$A = \ln R_0 - (B/T_0) \quad (2)$$

The parameters *A* and *B* were evaluated by measuring the resistance of the thermistor at intervals of approximately 0.1° as determined by a Beckmann thermometer standardized against a National Bureau of Standards calibrated thermometer. The data were fitted to the first equation by the method of least squares. The temperature coefficient of resistance *a* at any temperature can be evaluated from the relationship $a = -B/T^2$.

The effective heat capacities of the Dewar flasks, stirrers, etc., were determined by adding heat electrically to known quantities of water and subtracting the known heat content of the liquid from the resulting values. These effective heat capacity values for the titration vessels were then used to determine the specific heat of a 0.05 *N* solution of aniline in acetonitrile. The experimental value (0.548 cal./g. dg. did not differ within experimental error from the literature value¹¹ for pure acetonitrile (0.541 cal./g. dg. at 25°) and therefore this latter value was used in all calculations.

Precision and Accuracy.—Keily and Hume⁹ have demonstrated excellent comparisons between results obtained by the titration method and those arrived at by classical calorimetric techniques for both heats of reactions and estimations of relative differential heat contents of mixtures. In the present work the precision of the titration technique

(1) Taken in part from the Ph.D. Thesis of Earl J. Forman, Massachusetts Institute of Technology, November, 1957. This work was supported in part by the United States Atomic Energy Commission under Contract AT(30-1)905.

(2) General Electric Co. Fellow, 1955-1956.

(3) H. K. Hall, Jr., *J. Am. Chem. Soc.*, **79**, 5441 (1957).

(4) A. F. Trotman-Dickenson, *J. Chem. Soc.*, 1293 (1949).

(5) M. Kilpatrick and M. L. Kilpatrick, *Chem. Revs.*, **13**, 131 (1933).

(6) J. S. Fritz, *Anal. Chem.*, **25**, 407 (1953).

(7) H. K. Hall, Jr., *This Journal*, **60**, 63 (1956).

(8) H. W. Linde, L. B. Rogers and D. N. Hume, *Anal. Chem.*, **25**, 404 (1953).

(9) H. J. Keily and D. N. Hume, *ibid.*, **28**, 1294 (1956).

(10) R. H. Müller and H. J. Stolten, *ibid.*, **25**, 1103 (1953).

(11) N. A. Lange, "Handbook of Chemistry," Handbook Publisher, Inc., Sandusky, Ohio, 8th Edition, 1952.

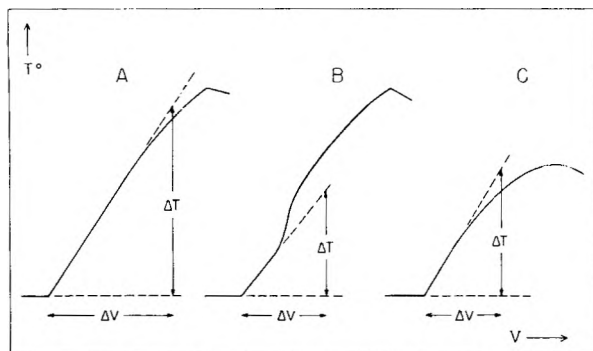


Fig. 1.—Typical curves for the thermometric titration of bases with hydrobromic acid in acetonitrile: A, product soluble; B, product insoluble but showing supersaturation; C, reaction incomplete at equivalence point.

is illustrated by the pooled standard deviation of all the thermal data, which is ± 0.4 kcal./mole.

Heats of Neutralization from Thermometric Titration Curves.—Keily and Hume⁹ have shown that good thermochemical data (heats of reaction, solution and dilution, etc.) can be obtained rapidly and simply from appropriate thermometric titration curves. For heats of neutralization, the procedure consists of determining the initial slope dT/dV of the thermometric titration curve (Fig. 1). The isothermal heat of neutralization at the initial temperature then can be calculated from the expression

$$\Delta H_{T_1} = \frac{-C_p (dT/dV)}{M} \quad (3)$$

where C_p consists of the total heat capacity of the liquid being titrated plus that of the Dewar flask, stirrers, etc., M is the molarity of the titrant solution, and dT/dV is taken to be equal to $\Delta T/\Delta V$. ΔT is measured perpendicular to the volume axis from a point on the extrapolated base line as shown in Fig. 1. Electrical heating was used to make the titrated solution isothermal with the titrant just prior to each run.

Neutralization Product Insoluble.—When the neutralization product of an acid-base titration is insoluble, the classical calorimetric determination of the heat of neutralization is in error due to the heat of formation of the precipitate. If the precipitate has moderate solubility or if supersaturation occurs before the formation of the solid phase, the initial portion of the thermometric titration curve records the true neutralization process free from interference of the precipitation process. Five of the amines discussed here—ammonia, aniline, *o*-chloroaniline, *m*-nitroaniline and *p*-toluidine—produced insoluble salts when titrated with hydrogen bromide in acetonitrile. Their true heats of neutralization, free of the heat of precipitation, were estimated from the initial slopes as outlined above.

Neutralization Reaction Incomplete.—Readily discernible end-points are not produced in the titration of *o*-chloroaniline, *m*-nitroaniline and *p*-nitroaniline with hydrogen bromide in acetonitrile indicating that the neutralization reactions are incomplete. If, however, at the start of the titration the large excess of the component being titrated is driving the reaction essentially to

completion, the initial slope technique will measure the true heat of neutralization. The correctness of this assumption may be verified by establishing that the initial slope is independent of the concentration of the substance being titrated, as implied by equation 3. In the present instance, dilutions of the above amines over a tenfold concentration range yielded heats of neutralization which were independent of dilution within the precision of the method, ± 0.4 kcal./mole. Only urea, the weakest base studied, showed a decrease in the measured heat process of 1.0 kcal./mole for a fivefold dilution of the base solution while a tenfold dilution produced a reduction of the measured heat process of 1.7 kcal./mole. (Additional evidence that the heat of neutralization is truly measured in the cases of *meta*- and *para*-nitroaniline is the fact that the values for these compounds fit the Hammett equation correlation.)

TABLE I
HEATS OF REACTION AT 24° OF AROMATIC BASES WITH HYDROGEN BROMIDE

No.	Compound	No. of detn.	$-\Delta H_{iso}$, kcal./mole	Std. dev., kcal./mole	pK_B (H ₂ O)
1	N,N-Diethylaniline	4	15.6	0.4	7.48 ¹²
2	<i>p</i> -Anisidine	3	17.7	.7	8.71 ¹³
3	Pyridine	4	14.4	.4	8.81 ¹³
4	<i>p</i> -Toluidine	4	13.7	.3	8.93 ¹³
5	N,N-Dimethylaniline	4	14.9	.8	8.94 ¹³
6	N-Methylaniline	3	13.2	.7	9.15 ¹³
7	Aniline	4	14.9	.4	9.42 ¹³
8	<i>p</i> -Chloroaniline	4	12.3	.4	10.00 ¹²
9	<i>p</i> -Bromoaniline	4	11.6	.6	10.09 ¹²
10	<i>m</i> -Chloroaniline	4	11.9	.3	10.48 ¹²
11	<i>o</i> -Chloroaniline	5	9.3	.3	11.38 ¹³
12	<i>m</i> -Nitroaniline	3	8.2	.6	11.55 ¹⁴
13	<i>p</i> -Nitroaniline	6	4.8	.7	12.89 ¹⁵

Results

In Tables I and II are assembled the experimental heats of neutralization of amines with anhydrous hydrogen bromide in acetonitrile. Along with these data are listed corresponding values for pK_B (H₂O) taken or calculated from the literature.

Aromatic Amines.—Comparison of heats of neutralization with pK_B (H₂O) in Table I shows a distinct general trend for aromatic amines, namely, that the stronger the base in water the greater the heat of neutralization in acetonitrile. In the light of Hammett's concept of substituent effects, and the wide applicability of the Hammett equation to equilibria and rates involving *meta*- and *para*-substituted compounds,^{16,17} this trend is not surprising. The plot of $-\Delta H_{iso}$ versus σ , the Hammett substituent constant for *meta*- and *para*-substituted aromatic amines (Fig. 2) shows a satisfactory correlation. The solid line in Fig. 2 was fitted by least squares and has the equation $-\Delta H_{iso} = -7.69 \sigma + 14.17$ kcal./mole.

(12) N. F. Hall, *J. Am. Chem. Soc.*, **52**, 5115 (1930).

(13) N. F. Hall and M. R. Sprinkle, *ibid.*, **54**, 3469 (1932).

(14) M. Kilpatrick and C. A. Arenberg, *ibid.*, **75**, 3812 (1953).

(15) L. P. Hammett and M. A. Paul, *ibid.*, **56**, 829 (1934).

(16) L. P. Hammett, "Physical Organic Chemistry," McGraw-Hill Book Co., New York, N. Y., 1940.

(17) H. H. Jaffe, *Chem. Revs.*, **53**, 191 (1953).

TABLE II
HEATS OF REACTION AT 24° OF NON-AROMATIC AMINES
WITH HYDROGEN BROMIDE IN ACETONITRILE

No.	Compound	No. of detn.	$-\Delta H_{\text{iso}}$, kcal./mole	Std. dev., kcal./mole	$pK_{\text{B}}(\text{H}_2\text{O})$
14	Di- <i>n</i> -butylamine	4	26.2	0.7	2.69 ¹³
15	Diethylamine	4	26.8	.5	2.98 ¹³
16	Di- <i>sec</i> -butylamine	4	24.1	.9	2.99 ³
17	Di-isopropylamine	3	24.4	.4	2.95 ¹³
18	Tri- <i>n</i> -butylamine	4	23.9	.9	3.11 ¹⁸
19	Triethylamine	4	25.2	.4	3.26 ¹³
20	Ethylamine	3	26.4	.9	3.33 ¹³
21	Isopropylamine	3	26.9	.4	3.37 ¹³
22	<i>n</i> -Butylamine	3	25.8	.3	3.39 ¹³
23	<i>n</i> -Propylamine	4	25.8	1.0	3.42 ¹³
24	<i>sec</i> -Butylamine	3	25.8	0.5	3.44 ¹³
25	<i>t</i> -Butylamine	4	25.9	.4	3.55 ¹³
26	Isobutylamine	3	25.5	.7	3.58 ¹³
27	1-Ethylpiperidine	4	24.2	.5	3.59 ¹³
28	Tri-isobutylamine	4	18.1	.1	3.68 ¹³
29	1,3-Diphenylguanidine	4	20.7	.7	4.00 ¹²
30	Trimethylamine	3	24.8	.3	4.20 ¹³
31	Ammonia	4	25.0	.3	4.24 ¹³
32	Morpholine	4	25.5	.3	5.64 ¹⁸

Since correlation with sigma constants shows $-\Delta H_{\text{iso}}$ follows a free energy function, the enthalpy values has also been compared with $pK_{\text{B}}(\text{H}_2\text{O})$ values (Fig. 3). The solid line was fitted by least squares to the data for *meta*- and *para*-substituted compounds and is described by the equation $-\Delta H_{\text{iso}} = -2.90 pK_{\text{B}}(\text{H}_2\text{O}) + 41.59 \pm 1$ kcal./mole. It is notable that with the exception of *N,N*-diethylaniline, even *ortho*- and *N*-substituted anilines fall close to the line.

The fact that enthalpy values for aromatic amines correlate reasonably well with sigma values and with aqueous pK_{B} values is interpreted as evidence that entropy effects are nearly constant in the reaction of hydrogen bromide with aromatic amines in acetonitrile. A similar correlation would also occur if the entropy changes were either zero or proportional to the free energy change for each amine. It is not felt that either of these situations is probable. In the case for constant entropy, some analogy may be drawn to the ionization of many weak acids in water, for which Pitzer¹⁹ has shown the entropies to be nearly constant.

Hall⁷ has shown that relative free energy changes (as measured by the half neutralization potentials) for the neutralization of *meta*- and *para*-substituted anilines in acetonitrile also correlate with Hammett's sigma constants as well as with the aqueous pK_{A} values. These parallel correlations make it evident, therefore, that heats of neutralization of these anilines in acetonitrile are a good relative measure of the base strengths of these compounds in this solvent.

Non-aromatic Amines.—No obvious correlation between heats of neutralization of non-aromatic amines in acetonitrile and their $pK_{\text{B}}(\text{H}_2\text{O})$ values presents itself from the data of Table II. However, the Taft equation, $\log R/R_0 = \sigma^* \rho^*$ has been used successfully to correlate the strengths of

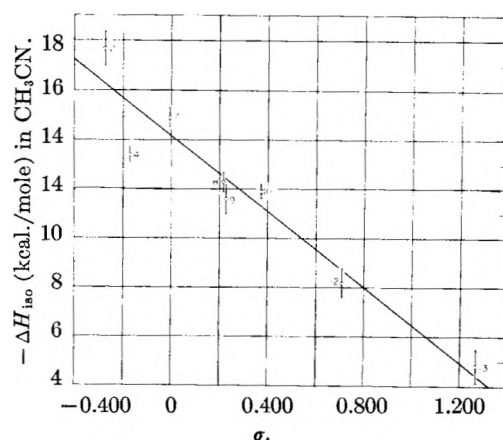


Fig. 2.— $-\Delta H_{\text{iso}}$ versus σ for *meta*- and *para*-substituted aniline in acetonitrile: 2 = *p*-anisidine, 4 = *p*-toluidine, 7 = aniline, 8 = *p*-chloroaniline, 9 = *p*-bromoaniline, 10 = *m*-chloroaniline, 12 = *m*-nitroaniline, 13 = *p*-nitroaniline.

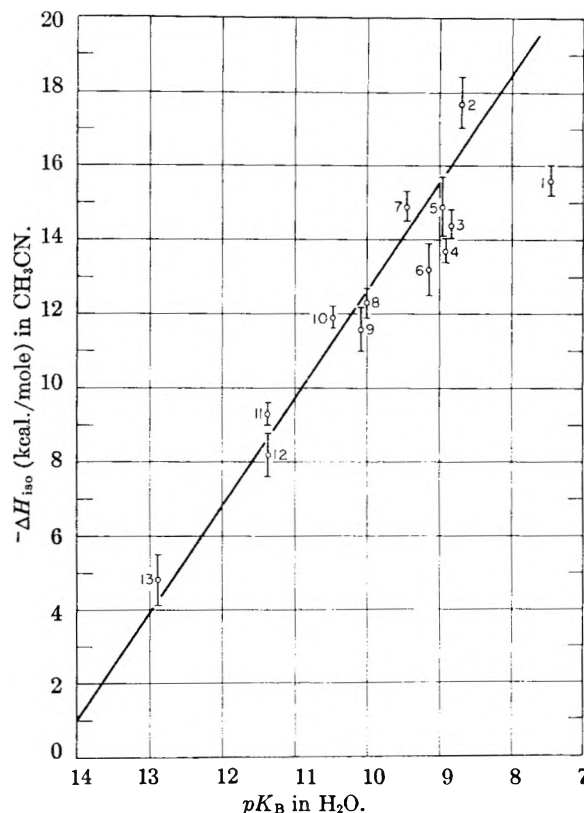


Fig. 3.— $-\Delta H_{\text{iso}}$ in acetonitrile versus pK_{B} in water for substituted anilines: 1 = *N,N*-diethylaniline, 2 = *p*-anisidine, 3 = pyridine, 4 = *p*-toluidine, 5 = *N,N*-dimethylaniline, 6 = *N*-methylaniline, 7 = aniline, 8 = *p*-chloroaniline, 9 = *p*-bromoaniline, 10 = *m*-chloroaniline, 11 = *o*-chloroaniline, 12 = *m*-nitroaniline, 13 = *p*-nitroaniline.

aliphatic amines in water⁸ as well as a large variety of rate and equilibrium data for many reactions of various aliphatic compounds.²⁰ In the Taft equation R and R_0 are rate or equilibrium constants for the substituted and reference compounds, respectively; σ^* is a constant expressing the polar effect of the substituent; and ρ^* is a constant measuring the susceptibility of a given reaction to the polar

(18) R. G. Pearson and F. V. Williams, *Chem. Revs.*, **76**, 258 (1954).

(19) K. S. Pitzer, *J. Am. Chem. Soc.*, **59**, 2365 (1937).

(20) R. W. Taft, Jr., in "Steric Effects in Organic Chemistry," M. S. Newman, editor, John Wiley and Sons, Inc., New York, N. Y., 1956.

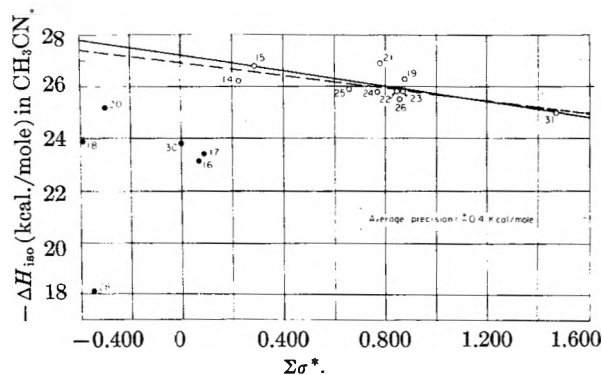


Fig. 4.— $-\Delta H_{180}$ in acetonitrile versus $\Sigma\sigma^*$ for aliphatic amines. Solid line is least squares fit for primary amines, dashed line includes primary and straight chain secondary amines: 14 = di-*n*-butylamine, 15 = diethylamine, 16 = di-*sec*-butylamine, 17 = di-isopropylamine, 18 = tri-*n*-butylamine, 19 = ethylamine, 20 = triethylamine, 21 = isopropylamine, 22 = *n*-butylamine, 23 = *n*-propylamine, 24 = *sec*-butylamine, 25 = *tert*-butylamine, 26 = isobutylamine, 28 = tri-isobutylamine, 30 = trimethylamine, 31 = ammonia.

effect. Correlations with Taft's σ^* values are taken as evidence that free energy changes govern the reaction, while deviations from a linear correlation can usually be attributed to those cases where the major factors determining the rate or equilibrium are steric factors, resonance effects or changes in the reaction mechanism within the reaction series.

The heats of neutralization for aliphatic amines are shown plotted against $\Sigma\sigma^*$ values in Fig. 4, where $\Sigma\sigma^*$ is the summed value of the individual substituents bonded to the amine nitrogen. Presumably, if a relationship between σ^* and a free energy function exists at all for a series of aliphatic amines, it has the greatest probability of existing for those compounds with the smallest steric requirements, namely, straight chain primary amines. A trial fit of the least squares correlation between straight chain primary amines and $\Sigma\sigma^*$ demonstrated that both branched chain primary amines and straight chain secondary amines fall in the same group with the straight chain primary amines. In Fig. 4 the solid line is that calculated without the straight chain secondary amines while the dotted line is that calculated by including the data for these latter bases. The equation of this latter dotted line is $-\Delta H_{180} = -1.16 \Sigma\sigma^* + 26.9 \pm 0.44$ kcal./mole.

The deviation of branched chain secondary amines as well as the tertiary amines is demonstrated in Table III in which the observed heats of neutralization for these compounds are compared with those calculated from the equation of the fit in Fig. 4. In each case the observed heat of neutralization is lower than the calculated value.

TABLE III

STERIC ENERGIES OF PROTONATED AMINES IN ACETONITRILE

Compound	$\Sigma\sigma^*$	$-\Delta H$ calcd., kcal./ mole	$-\Delta H$ obsd., kcal./ mole	Calcd. - obsd., kcal./ mole
Diisopropylamine	0.090	26.8	24.4	2.4
Di- <i>sec</i> -butylamine	.090	26.8	24.1	2.7
Trimethylamine	.000	26.9	24.8	2.1
Triethylamine	-.300	27.3	25.2	2.1
Tri- <i>n</i> -butylamine	-.390	27.4	23.9	3.5
Triisobutylamine	-.375	27.3	18.1	9.2

Solvation of Amines in Acetonitrile.—Hall's discussion of the strengths of amines³ appears to have resolved the conflict between the "B-strain" hypothesis²¹ and the solvation hypothesis of Trotman-Dickenson⁴ in favor of the latter concept for aqueous solutions. The above results in acetonitrile, however, lead to a slightly different conclusion. It is not likely that the primary and straight chain secondary amines could be correlated by a single expression if the degree of solvation for these classes differed significantly, for if the secondary amines were appreciably solvated, the steric strain produced would decrease the stability of the amine-proton bond as it apparently does for the tertiary amines and branched chain secondary amines. It is reasonable to conclude that there is little solvation of amines or ammonium ions in acetonitrile compared with that in water. In acetonitrile, as distinct from water, there seems to be no single linear free energy function that correlates tertiary amines or branched chain secondary amines. On the contrary, from the last column of Table III it can be seen that the extent of the deviations of the tertiary and branched chain secondary amines is qualitatively in the order that would be expected on the basis of the steric strain of each molecule. A small degree of solvation and rather small steric requirements seem also to account for the fact that *o*-chloroaniline, *N*-methylaniline and *N,N*-dimethylaniline fall close to the line relating the *meta*- and *para*-substituted anilines. The only major deviate in the group of anilines studied, *N,N*-diethylaniline, has the greatest steric requirements, thus making its base strength lower than predicted in acetonitrile.

Thus the "B-strain" hypothesis²¹ seems to explain these data in acetonitrile adequately. Although sufficient data are not yet available in other solvents, it seems reasonable to expect that in non-hydrogen bonding solvents, steric requirements play a greater role in determining the strengths of bases than do solvation effects.

(21) (a) H. C. Brown, D. H. McDaniel and O. Häfiger, "Determination of Organic Structures by Physical Methods," E. A. Braude and F. C. Nachod, editors, Academic Press, New York, N. Y., 1955, Chapter 14. (b) H. C. Brown, H. Bartholomay, Jr., and M. D. Taylor, *J. Am. Chem. Soc.*, **66**, 435 (1944).

AN E.M.F. INVESTIGATION OF BINARY LIQUID ALLOYS RICH IN ZINC

BY O. J. KLEPPA AND C. E. THALMAYER

*Contribution from the Institute for the Study of Metals, University of Chicago, Chicago, Illinois**Received June 18, 1959*

The liquid solutions of copper, silver, gallium, germanium, antimony and bismuth in zinc have been studied by the e.m.f. method. In the moderately dilute range the derived partial molal heats and entropies for zinc can be correlated in a semi-quantitative way with the difference in valence between solvent and solute. The heat data, even for the monovalent metals copper and zinc, are in conflict with Friedel's predictions. It is suggested that this conflict may be due to the breakdown of the free-electron model for zinc even in the liquid state.

In recent communications one of the authors^{1,2} has demonstrated that for a series of binary liquid alloys rich in the divalent metals zinc or cadmium a semi-quantitative correlation exists between the excess partial molal entropy of the solvent (Zn, Cd) and the electron concentration (valence electrons per atom) in the solution. For alloys of zinc this correlation was found to hold for its mixtures with cadmium, indium, gallium and tin, *i.e.*, for all systems for which reliable data were available. For other systems, *e.g.*, zinc-antimony and zinc-bismuth, the reported data were not comprehensive enough to permit a realistic test of the correlation. No reliable entropy data were found in the literature for liquid alloys of zinc with metals of valence lower than two. The present investigation was initiated in order to test further this entropy-valence correlation for liquid alloy systems involving zinc.

In the present communication we report new or improved thermodynamic data, obtained by the e.m.f. method, for the zinc-rich range of the liquid alloys of copper, silver, gallium, germanium, antimony and bismuth with zinc. In the case of the two systems zinc-silver and zinc-germanium we have extended our study to cover all liquid concentrations which could be handled by the e.m.f. method. The limiting factor is the volatility of zinc, which interferes somewhat with the experiments above 650° and leads to serious errors above 750-800°.

Experimental

The use of the e.m.f. cell method for the study of alloy solutions is now a standard procedure and the method will not be discussed in detail here.³ In the present investigation use was made of two different types of H-shaped cells: a sealed type made from Pyrex suitable for operation up to 650° and similar to one used by Seltz and Dunkerley,⁴ and a Vycor cell which was similar to one previously used by one of the authors.⁵ Most measurements below 650° were performed with Pyrex cells.

The LiCl-KCl-ZnCl₂ ionic melts were prepared from analytical grade reagents, which were melted down in a flow of dry HCl, degassed in vacuum and kept "on tap" over molten zinc in dry nitrogen. The metals used were all high-purity elements with total contents of metallic impurities of less than 0.05%.

The cells were filled in a stream of dry nitrogen and then placed in a 3" by 20" thermostatically controlled furnace

(±1°). In order to reduce temperature variations to a minimum, and to make sure that both legs of the cell were at the same temperature, the cells were placed inside a cylindrical metal block, made from aluminum bronze or stainless steel and of outside dimensions 3" o.d. by 4" length. Temperature measurements were by means of chromel-alumel thermocouples, located adjacent to the cell inside this metal block. The thermocouples were calibrated approximately once a week, normally at the zinc, antimony and/or aluminum points. In this way absolute temperature usually could be established to about ±1°.

All potential measurements (cell and thermocouple) were performed by means of a Leeds-Northrup type K potentiometer. For a given run below 650° the measured e.m.f. values were reproducible to better than 0.03 mv. for periods of 2-3 days. However, in most cases, reproducibility from run to run was not better than to between 0.05 and 0.1 mv., giving an uncertainty in the free energy determinations of the order of 2-5 cal./g. atom.

In each run we carried out simultaneous determinations of e.m.f. and temperature for 8-25 different temperatures, and the evaluations of E and $\Delta E/\Delta T$ were based on a graph of E vs. T . The minimum temperature range accepted for determination of $\Delta E/\Delta T$ was 25°. In some cases the electromotive force was studied over much wider ranges in temperature, up to 200°. Within the error of our measurements we were not able to find any curvature in these graphs.

At temperatures above 650°, slow drifts in the observed e.m.f. toward higher values, were noted. These drifts were due to slight losses of zinc from the electrodes through evaporation, and the "lost" zinc was deposited on the walls of the cell outside the hottest zone. In typical runs this loss was of the order of 25 mg., out of the weighed-in amounts of 3 to 5 g. of zinc. In order to reduce these losses to a minimum all runs above 650° were completed in as short a time as possible, usually in just one day. Nevertheless, as a result of these drifts the reported e.m.f. data for alloys high in germanium or silver may be as much as 0.2 to 0.3 mv. too high.

These drifts were particularly unwelcome in our attempts to obtain reliable values of $\Delta E/\Delta T$. For the few runs where this problem was present we consistently got slightly high values of $\Delta E/\Delta T$ from measurements carried out for a series of rising temperatures, and slightly low values for falling temperatures. In these cases we report below the mean of the two values as the "true" value.

Results. Comparison with Earlier Data

(a) Group I Solutes: Copper and Silver.— Due to the relatively steep rise of the liquidus for increasing amounts of copper in zinc, only 5 runs were carried out on alloys of this system, all with copper contents of 20 atomic % and less. For silver-zinc on the other hand where the liquidus rises less steeply, we studied a total of 14 different alloys, with silver contents up to 70 (80) %. The results of these experiments are summarized in Table I, and the corresponding excess thermodynamic quantities are presented graphically in Figs. 1 and 2, along with corresponding data calculated from the earlier vapor pressure studies of

(1) O. J. Kleppa, *Acta Met.*, **6**, 225, 233 (1958).

(2) O. J. Kleppa, "Thermodynamics and Properties of Liquid Solutions" in "Liquid Metals and Solidification," American Society for Metals, Cleveland, 1958.

(3) J. F. Elliott and J. Chipman, *Trans. Faraday Soc.*, **47**, 138 (1951).

(4) H. Seltz and F. J. Dunkerley, *J. Am. Chem. Soc.*, **64**, 1392 (1942).

(5) O. J. Kleppa, *ibid.*, **73**, 385 (1951).

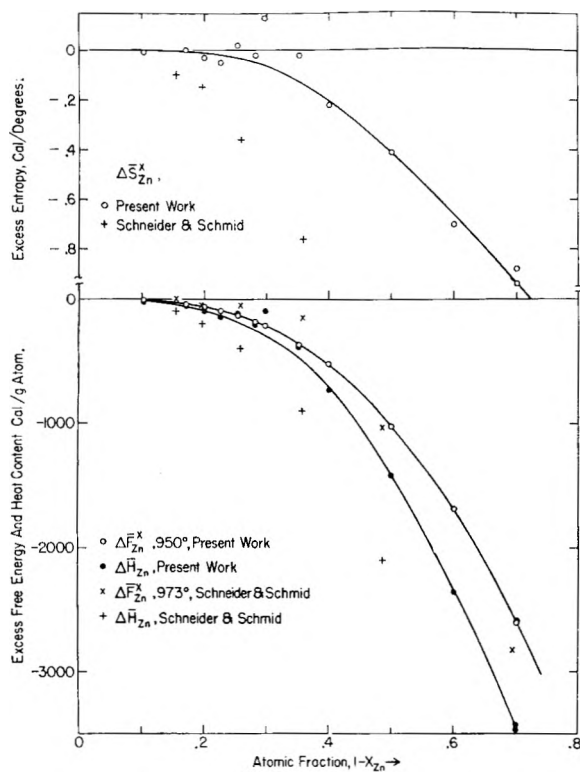


Fig. 1.—Partial molal excess thermodynamic quantities for zinc in liquid zinc-silver alloys.

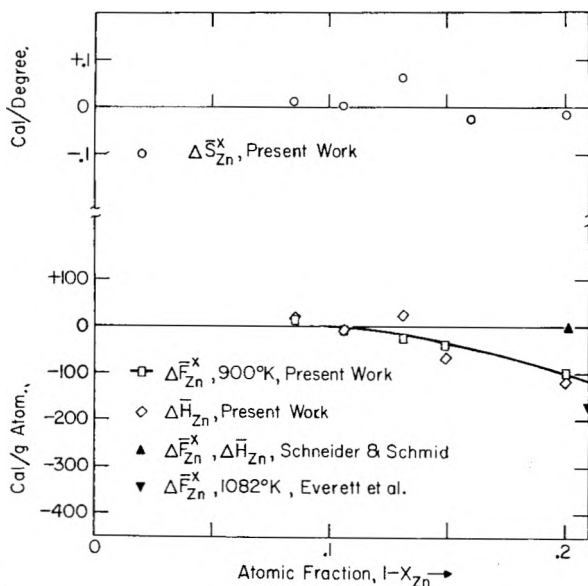


Fig. 2.—Partial molal excess thermodynamic quantities for zinc in liquid zinc-copper alloys.

Schneider and Schmid⁶ and of Everett, Jacobs and Kitchener.⁷

It will be noted that there is reasonable agreement in the case of the free energy data, while the agreement does not extend to the heat and entropy. This is hardly surprising, in view of the difficulties associated with the separation of experimental free energies into heat and entropy terms in high temperature vapor pressure studies.

(6) A. Schneider and H. Schmid, *Z. Elektrochem.*, **48**, 627 (1942).

(7) L. H. Everett, P. W. M. Jacobs and J. A. Kitchener, *Acta Met.*, **5**, 281 (1957).

(b) **Group III Solute: Gallium.**—Genta, Fiorani and Valenti⁸ have previously studied the liquid alloys of this system by the e.m.f. method. However, in recent work one of the authors noted some disagreement between the entropies obtained from e.m.f. work and corresponding values derived from a combination of calorimetric heat data with phase diagram information.¹ Therefore it was considered of interest to reinvestigate the zinc-rich part of this system by the e.m.f. method. Results obtained in 7 runs on alloys with zinc contents ranging from 96 to 60 atomic % are recorded in Table II, and the thermodynamic data are plotted along with earlier results in Fig. 3. It will be noted that the disagreement which motivated our study of this system has been removed.

TABLE I

EXPERIMENTAL E.M.F. DATA IN LIQUID ALLOYS OF ZINC-SILVER AND ZINC-COPPER

Weighed-in compn. X_{Zn}	E , ^a mv.	$\Delta E/\Delta T \times 10^3$, mv./deg.
(a) Zn-Ag, 950°K.		
0.897	(4.65)	4.45
.829	(8.64)	8.15
.800	(10.56)	8.97
.774	(12.53)	10.0
.746	(14.94)	13.1
.718	17.61	13.9
.702	19.20	18.0
.648	25.75	18.2
.600	32.26	17.2
.500	50.63	20.9
.400	74.08	24.3
.300	105.5	33
.299	105.3	31.6
200	142 (at 1110°K.)	
(b) Zn-Cu, 900°K.		
0.915	3.18	4.1
.893	4.52	4.8
.869	5.96	7.4
.841	7.56	6.7
.800	10.76	9.1

^a Data in parentheses obtained by extrapolation from lower temperatures.

(c) **Group IV Solute: Germanium.**—To the knowledge of the authors no detailed thermodynamic information on zinc-germanium alloys is recorded in the literature, apart from the phase diagram of Gebhardt.⁹ However, through the courtesy of Dr. C. D. Thurmond we were able to obtain some unpublished data from Bell Telephone Laboratories.¹⁰ In view of this scarcity of information we have studied this system in some detail. The results obtained in 21 successful runs are recorded in Table III and presented graphically in Fig. 4. Note in particular the rather extensive range in composition where the excess partial molal free energy of zinc is positive before it assumes negative values at high germanium contents. The zinc-germanium system has this

(8) V. Genta, M. Fiorani and V. Valenti, *Gazz. chim. ital.*, **85**, 103 (1955).

(9) E. Gebhardt, *Z. Metallk.*, **34**, 255 (1942).

(10) C. D. Thurmond, *et al.*, unpublished results.

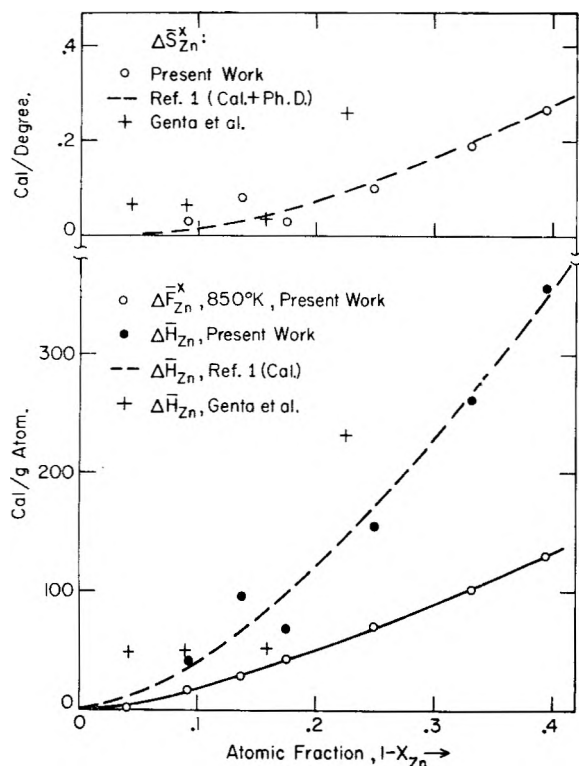


Fig. 3.—Partial molal excess thermodynamic quantities for zinc in liquid zinc-gallium alloys.

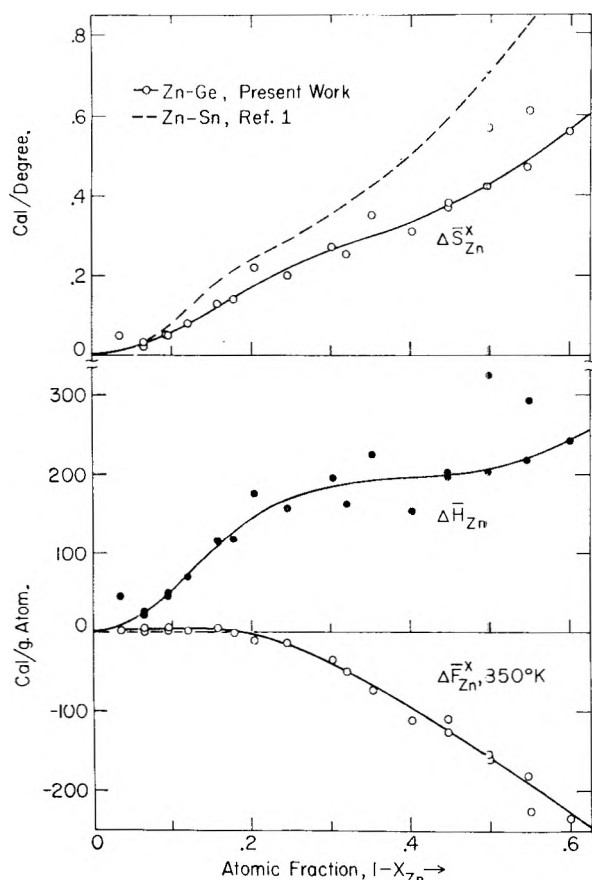


Fig. 4.—Partial molal excess thermodynamic quantities for zinc in liquid zinc-germanium alloys.

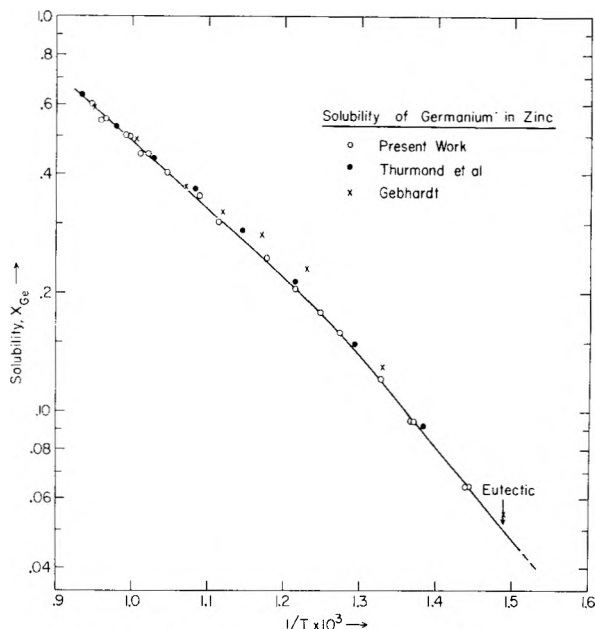


Fig. 5.—Solubility of germanium in liquid zinc.

feature in common with several other binary systems involving zinc and cadmium, for example Cd-Bi¹ and Zn-Sb.¹¹

In this system the observed e.m.f. *versus* temperature curves exhibit a very marked change in slope at the liquidus temperature. This provides a very convenient method for redetermination of the liquidus and we have included our new liquidus data in Table III. These results are plotted in Fig. 5 ($\log X_{Ge}$ vs. $1/T$) along with the earlier data of Gebhardt and the recent unpublished results of Thurmond. We note that our results are in good agreement with Thurmond's data, while Gebhardt's older results deviate somewhat more, particularly at lower temperatures.

If a solubility plot of the type given in Fig. 5 extends down to concentrations which are so low that one may assume that the laws of dilute solutions apply, and if solid solubility is small, the slope of the curve will be directly proportional to the (partial) heat of solution of the pure solid solute in the solvent.

Usually it is not safe to determine the heat of solution in this way, unless the solute concentrations are quite low.¹² In the zinc-germanium system we note that the deviations of the solutions from Raoult's law are quite small up to germanium contents of about 20 atomic %. Therefore we may be justified in adopting the mentioned evaluation procedure and we obtain from the graph a value of about 10.8 kcal. for the partial molal heat of solution of (solid) germanium in liquid alloys rich in zinc. This compares with a value of 11.1 kcal./mole obtained calorimetrically for the limiting heat of solution at 450°.¹³ The agreement must be considered satisfactory.

(d) **Group V Solute: Antimony and Bismuth.**—The binary liquid alloys of zinc with antimony and

(11) B. DeWitt and H. Seltz, *J. Am. Chem. Soc.*, **61**, 3170 (1939).
 (12) Below 1-3 atomic %, see e.g. J. F. Freedman and A. S. Nowick, *Acta Met.*, **6**, 176 (1958).
 (13) O. J. Kleppa, unpublished results.

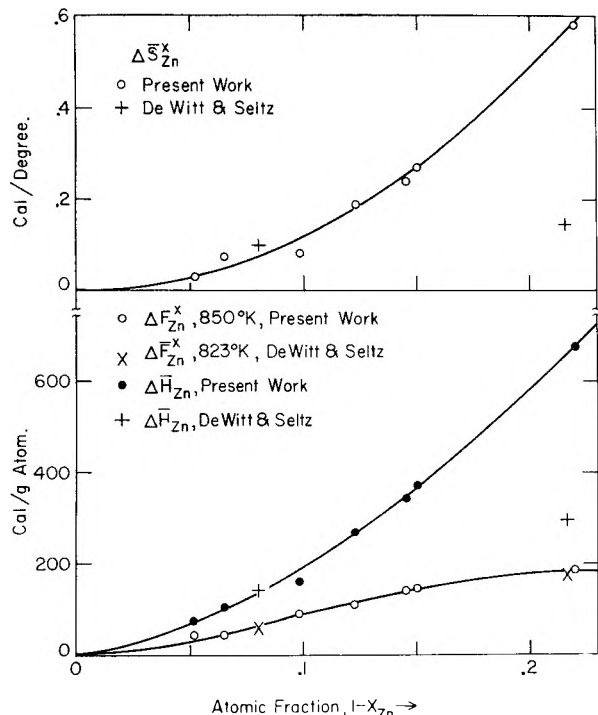


Fig. 6.—Partial molal excess thermodynamic quantities for zinc in liquid zinc-antimony alloys.

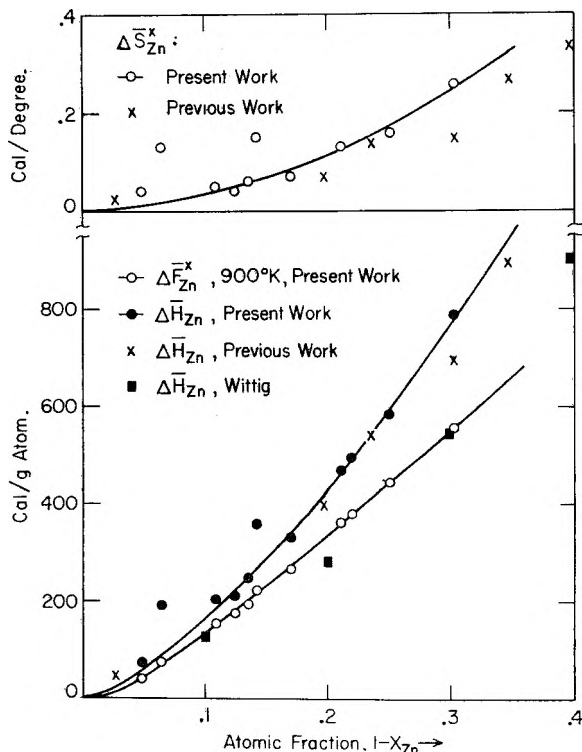


Fig. 7.—Partial molal excess thermodynamic quantities for zinc in liquid zinc-bismuth alloys.

bismuth have been studied previously by the e.m.f. method, the former system by DeWitt and Seltz,¹¹ the latter by Kleppa.¹⁴ However, in both cases the data reported for the region rich in zinc are not sufficiently comprehensive to permit a realistic

(14) O. J. Kleppa, *J. Am. Chem. Soc.*, **74**, 6052 (1952).

TABLE II
EXPERIMENTAL E.M.F. DATA IN LIQUID ALLOYS OF ZINC-GALLIUM AT 850°K.

Weighed-in compn., X_{Zn}	E , mv.	$\Delta E/\Delta T \times 10^3$, mv./deg.
0.96 ^a	1.45	...
.908	3.16	4.8
.863	4.81	8.1
.826	6.07	8.8
.751	8.97	14.6
.669	12.52	21.4
.606	15.52	27.3

^a Composition doubtful.

TABLE III
EXPERIMENTAL E.M.F. DATA IN LIQUID ZINC-GERMANIUM ALLOYS AT 850°K.

Weighed-in. compn., X_{Zn}	E , ^a mv.	$\Delta E/\Delta T \times 10^3$, mv./deg.	Liquidus temp., °C.
0.965	1.25	2.6	409
.936	2.40	3.6	420
.936	2.32	3.3	422
.906	3.55	5.3	457
.906	3.50	5.3	456
.879	4.69	7.3	480
.842	6.18	10.2	512
.822	7.18	11.5	528
.796	8.57	14.7	550
.756	10.54	16.5	577
.697	(13.97)	21.5	625
.680	(15.19)	22.0	...
.648	(17.47)	26.3	645
.597	(21.28)	29.0	684
.552	(24.12)	33.6	718
.551	(24.56)	34.0	707
.503	(28.5)	38.8	731
.500	(28.87)	42.3	737
.453	(32.92)	44.3	772
.449	(34.19)	47.8	765
.400	(38.64)	51.7	786

^a Values in parentheses obtained by extrapolation from data above the liquidus.

correlation of excess entropy with valence electron concentration. Therefore we have reinvestigated the zinc-rich solutions in these two systems. Our results are recorded in Table IV and the derived excess thermodynamic quantities are compared with earlier results in Figs. 6 (Zn-Sb) and 7 (Zn-Bi).

Our free energy data for zinc-antimony are in good agreement with those of DeWitt and Seltz, while the agreement is less satisfactory for heats and entropies. For zinc-bismuth the agreement with the earlier work is satisfactory. For the latter system there are available also some very recent calorimetric measurements by Wittig, *et al.*¹⁵ These measurements were performed at 470 and 570°, *i.e.*, at temperatures where the system still exhibits a miscibility gap (about 10 to 30 atomic % bismuth at 570°). Therefore the modest disagreement between the heats obtained in the present work and the values derived from the calorimetric results is not surprising.

(15) F. E. Wittig, E. Muller and W. Schilling, *Z. Elektrochem.*, **62**, 529 (1958).

TABLE IV
EXPERIMENTAL E.M.F. DATA IN LIQUID ALLOYS OF ZINC-ANTIMONY AND ZINC-BISMUTH

Weighted-in compn., X_{Zn}	E , mv.	$\Delta E/\Delta T \times 10^3$, m.v./deg.
(a) Zn-Sb, 850°K.		
0.948	0.99	3.0
.935	1.51	4.5
.902	1.86	6.3
.877	2.42	9.75
.854	2.74	11.9
.850	2.80	12.9
.780	5.10	23.3
(b) Zn-Bi, 900°K.		
0.952	1.11	3.0
.936	0.95	5.5
.891	1.04	5.9
.876	1.33	6.5
.865	1.45	7.6
.858	1.13	9.9
.830	1.46	9.6
.789	1.43	12.8
.780	1.46	13.6
.749	1.64	15.9
.697	2.00	21.3

Discussion

The Entropy Data.—To facilitate our discussion, we have prepared in Fig. 8 a composite graph, which gives the excess partial molal entropies of zinc plotted *versus* electron concentration.

The correlation between entropy and electron concentration referred to in the Introduction was noted originally in the alloys of zinc with cadmium, indium, gallium and tin. Among the solutes with valence higher than zinc studied in the present work we find that germanium and antimony fall reasonably well in line with these systems. However, zinc-bismuth deviates in a more significant way. Thus Fig. 8 shows that if bismuth dissolved in zinc is assumed to be pentavalent, the observed excess entropies are low, and if it is assumed trivalent, they are high compared to the other systems. It is perhaps possible that bismuth dissolved in zinc behaves as if it has a metallic valence intermediate between three and five.

In the present study we are for the first time able to survey also the excess entropy situation for solutes with valence lower than zinc. For both zinc-copper and zinc-silver, we note that the partial molal entropy of zinc remains essentially ideal until the solute concentration is 15 to 20%. For higher concentrations of silver (and probably also of copper), the excess entropy becomes negative, and follows a course which is fairly similar to the positive course followed for solutes with valence higher than two.

The positive excess entropies observed for solutes of valence higher than that of zinc cannot be explained by the lack of randomness in the mixture. On the other hand, it is conceivable that the negative excess entropies in the zinc-silver system may have this origin. Here it should be noted, however, that the quasi-chemical theory, which is most frequently invoked in attempts to estimate deviations

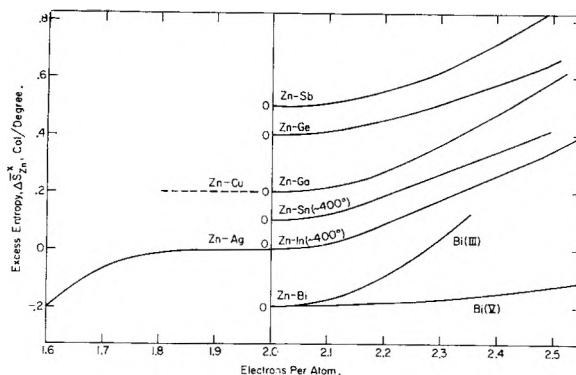


Fig. 8.—Partial molal excess entropies for zinc in zinc-rich liquid alloys. (Data for Zn-In and Zn-Sn from ref. 1. Scale on left for Zn-Ag and Zn-In only. Other curves displaced by multiple of 0.1 cal./deg.)

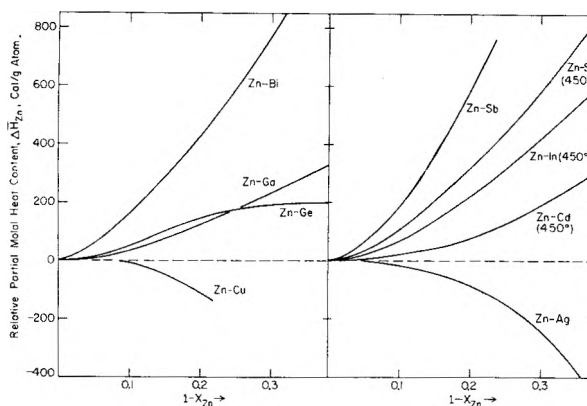


Fig. 9.—Relative partial molal heat content for zinc in zinc-rich liquid alloys. (Data for Zn-Cd, Zn-In and Zn-Sn are from ref. 1.)

from randomness in alloy systems, predicts small positive excess partial entropies of the solvent at solute concentrations below 33%.² Thus it seems probable that the entropy behavior of the zinc-silver system arises from causes other than a lack of randomness. In fact the "symmetry" of the excess entropy data around two electrons per atom at pure zinc suggests that the deviations may arise from similar factors for solutes of higher and lower valence than zinc. There is some additional support for this view in corresponding data for alloys of cadmium.¹ However, the nature and origin of these valence-entropy effects is still not clear. At present we are engaged in an experimental study of the volume changes associated with the process of mixing in liquid alloys of zinc and cadmium with metals of different valence. In this work we hope to obtain information which will permit a realistic estimate of the contribution from the volume change to the observed excess entropy of mixing.

The Heat and Free Energy Data.—It does not seem possible to correlate the observed excess free energy data with other simple physico-chemical properties characteristic of the pure elements. However, a semi-quantitative correlation is indicated between the relative partial heat contents of zinc ($\Delta\bar{H}_{Zn}$) and the difference in valence between solvent and solute. This will be evident from Fig. 9, which gives smoothed partial heat content curves for the systems studied in the pres-

ent work, along with similar data available for other alloys of zinc. It will be noted that the valence correlation is very obvious for the systematic sequence of solutes consisting of silver, cadmium, indium, tin and antimony. The observed large positive values of $\Delta\bar{H}_{Zn}$ for zinc-antimony are particularly remarkable in view of the fact that this system forms stable intermetallic compounds and that $\Delta\bar{H}_{Zn}$ assumes negative values at higher antimony contents.¹¹ The corresponding correlation for copper, gallium and germanium is less clear-cut, except possibly at very high zinc concentrations. In this range the lack of experimental precision prevents a realistic test of the correlation.

The problem of the possible influence of a difference in valence between solvent and solute on the heat (energy) of mixing in moderately dilute metallic solution has been the subject of important theoretical work by Friedel.¹⁶ Friedel points out that in the absence of a "large difference in atomic size" between solvent and solute, and of "strong chemical interaction" between them, the limiting curvature ($d^2H/dx^2_{\text{solute}}$) of the heat of mixing at low solute concentrations should be determined by the "valence factor." For solutes of valence higher than that of the solvent he predicts a *positive* curvature, for solutes of lower valence a *negative* curvature. In a given solvent the curvatures should be roughly proportional to the valence difference. As the partial heats of zinc are related in a simple way to these curvatures, we are able to test these predictions. It is immediately obvious that for the alloys of zinc covered in the present study, the observed curvatures, although on the whole roughly proportional to the valence difference, all show the opposite sign to that predicted by the Friedel theory. Analogous behavior is found also for solutes of different valence in liquid cadmium.¹ These observations are of considerable interest in view of the success of the Friedel theory in correctly predicting the curvatures both for solutions in monovalent metals such as silver and also for liquid solutions of metals of lower valence in multivalent solvents as indium and tin.¹⁷

We have attempted to find a reasonable explanation for the failure of this theory in zinc and cadmium alloys. It seems unlikely to us that this failure can be accounted for either by a "large size factor" or by "strong chemical interaction," which were the limitations suggested by Friedel. We believe instead that the explanation for the observed solution behavior may rest in the details of the electronic structure of these divalent metals.

It is well known that some of the electronic properties of *solid* zinc and cadmium show anomalies when compared with those of the neighboring mono-

valent metals such as copper and silver on the one hand and with multivalent metals such as gallium, indium and tin on the other. In the band theory of metals these anomalies are attributed to the fact that for zinc and cadmium (and for other divalent solid metals such as magnesium) the Fermi surface is located in a region of Brillouin zone overlap. It was suggested by Raynor¹⁸ that the details of this overlap may explain the low solubilities of all multivalent metals in solid zinc and cadmium, as compared to their solubilities in magnesium.

In the process of fusion the long-range periodicity of the solid crystal is lost. Thus we are no longer able to argue in a quantitative way in terms of the Brillouin zones. However, it is well known that local atomic arrangements with coordination numbers similar to those found in the solid persist in liquid metals at temperatures far above their melting points. Similarly we may expect that a considerable measure of band character should persist in the distribution of the electronic energy states. These deviations from the free electron model are most likely to occur and probably will be most pronounced in the divalent metals which have two valence electrons in their filled s-band.

We are not aware of earlier attempts to correlate the properties of solutions in liquid zinc and cadmium with possible deviations from free electron behavior in the solvent but the recognition of such deviations is far from new. The most important experimental information relating to this consists of electrical resistivity data. While the resistivity for solid metals and for most liquid metals shows the expected increase with increasing temperature, liquid zinc, cadmium and magnesium exhibit virtually no change or even a slight decrease in resistivity for a wide range in temperature.¹⁹ Mott and Jones²⁰ suggest that this may be due to an increase in the number of free electrons as the temperature is raised.

It is not known at the present time to what extent the behavior of alloys of liquid zinc and cadmium also obtains in alloys of other divalent metals. For mercury, which does not show the resistance anomaly, the available solution data differ in important respects from those observed in zinc and cadmium.^{2,13} On the other hand we have no reliable information on solutions in liquid magnesium, calcium, or in the other alkaline earth metals. An exploration of this field might prove rewarding.

Acknowledgments.—This work has been supported by the Office of Naval Research under Contract No. Nori-2121 with the University of Chicago.

(18) G. V. Raynor, *Progr. in Metal Phys.*, **1**, 1 (1949).

(19) E. Scala and W. D. Robertson, *Trans. Am. Inst. Mining Met. Engrs.*, **197**, 1141 (1953).

(20) N. F. Mott and H. Jones, "The Theory of the Properties of Metals and Alloys," Oxford University Press, New York, N. Y., 1936, p. 277.

(16) J. Friedel, *Adv. in Physics*, **3**, 446 (1954).

(17) O. J. Kleppa, *THIS JOURNAL*, **60**, 842 (1956).

THE PRESSURE-VOLUME-TEMPERATURE PROPERTIES OF PERFLUOROCYCLOBUTANE: EQUATIONS OF STATE, VIRIAL COEFFICIENTS AND INTERMOLECULAR POTENTIAL ENERGY FUNCTIONS¹

By D. R. DOUSLIN, R. T. MOORE AND GUY WADDINGTON

Contribution No. 80 from the Thermodynamics Laboratory, Petroleum Experiment Station, Bureau of Mines, U. S. Department of the Interior, Bartlesville, Okla.

Received June 22, 1959

Studies of the pressure-volume-temperature properties of perfluorocyclobutane, in the ranges 3–394 atm. and 30–350°, yielded values of gas compressibility, critical constants, vapor pressure and orthobaric liquid and vapor densities. The results were correlated by the Beattie-Bridgeman, Benedict-Webb-Rubin, and Martin-Hou equations of state and by the Stockmayer and the Kihara intermolecular potential energy functions. The merits of the several correlational methods are discussed.

The systematic investigation of physical and chemical thermodynamic properties of fluorocarbons has been a fairly recent development, initiated largely because of war-time demands for substances with exceptional physical properties. These demands are even greater today and the need for new fluorocarbon materials will remain critical in the foreseeable future. A moderate amount of information about the properties of fluorocarbons in the solid and liquid states has appeared in the literature, but little accurate information is available on the pressure-volume-temperature (P - V - T) properties in the gas state.

A comprehensive investigation of the P - V - T properties of perfluorocyclobutane was made in this Laboratory as part of a long-range program of research on fluorocarbons. As a substance of interest to theoretical chemists, and of potentially significant commercial value, perfluorocyclobutane has been the subject of several recent investigations. The molecular structure was studied by Lemaire and Livingston² to resolve questions about non-planarity of the carbon ring and the lengthening of the carbon-carbon bond distance caused by repulsion between the fluorine atoms on different carbon atoms. Masi's³ experimental results for the vapor heat capacity were significantly lower than the calculated values with a vibrational assignment based on the assumption of a planar ring structure. Furukawa, McCoskey and Reilly⁴ investigated the thermal properties in the solid and liquid states, heat of vaporization and vapor pressure. Vapor pressure data also are given by Whipple.⁵ In this paper are reported values of vapor pressure from 30° to the critical temperature, critical constants, orthobaric liquid and vapor densities, and gas compressibility in the ranges 3–394 atm. and 115.22–350°. Thus, perfluorocyclobutane is one of the relatively few fluorocarbons for which the thermodynamic properties have been determined in all three states of matter.

(1) This research was supported by the United States Air Force Office of Scientific Research of the Air Research and Development Command under contract No. CSO-680-57-4. Reproduction in whole or in part is permitted for any purpose of the United States Government.

(2) H. P. Lemaire and R. L. Livingston, *J. Chem. Phys.*, **18**, 569 (1950); *J. Am. Chem. Soc.*, **74**, 5732 (1952).

(3) J. F. Masi, *ibid.*, **75**, 5082 (1953).

(4) G. T. Furukawa, R. E. McCoskey and M. L. Reilly, *J. Research Natl. Bur. Standards*, **52**, 11 (1954) RP 2466.

(5) G. H. Whipple, *Ind. Eng. Chem.*, **44**, 1664 (1952).

Experimental

Method.—The compressibility apparatus and method were described in an earlier paper⁶ and, excepting minor differences, are similar to Beattie's.⁷ Therefore, only a brief summary of the pertinent experimental details that relate specifically to the perfluorocyclobutane measurements will be added. Before the sample was distilled into the Pyrex glass liner of the compressibility bomb it was dried by twice passing the vapor over magnesium perchlorate; then, the dissolved air was removed by an outgassing procedure (*i.e.*, freezing with liquid air, evacuating to 10^{-5} mm. or better, and melting) carried through three complete cycles. The measurements were made on a single sample that weighed 18.44855 ± 0.00020 g. and was calculated to be 0.0922243 mole.⁸ All parts of the compressibility apparatus were individually calibrated and blank-run factors were determined as described previously.^{6,7} The estimated overall error in the compressibility measurements varied from 0.03% at the lowest temperature and pressure to 0.3% at the highest temperature and pressure.

Material.—A sample of perfluorocyclobutane was supplied through the courtesy of Dr. D. E. Kvalnes and Dr. W. B. McCormack of E. I. du Pont de Nemours & Co. No impurities could be detected by infrared analysis, but a vapor-phase chromatographic analysis showed the presence of 0.2 to 0.3 mole % of a less volatile impurity. This impurity was removed by a fractional distillation performed by G. A. Spencer and R. H. Coulter, Jr., of the Branch of Production of this Station. The sample of perfluorocyclobutane used in the measurements was a center cut that had a purity of at least 99.9 mole %.

Physical Constants.—The temperature of the compressibility bomb was measured to within 0.001° with a platinum resistance thermometer that had been calibrated by the National Bureau of Standards in terms of the International Temperature Scale [$T, ^\circ\text{K.} = t, ^\circ\text{C. (Int., 1948) + 273.16$]. Measurements of the ice-point resistance of this thermometer made at the beginning and end of the experimental work showed no significant change.

The liter was chosen as the unit of volume in the equation of state correlations and in calculations of the compressibility factor, $Z = PV/RT$; but the second and third virial coefficients were calculated in volume units of cubic centimeters ($1 \text{ cm.}^3 = 0.9999720 \times 10^{-3}$ liter) to facilitate comparison with theory. Therefore, these two values of the gas constant were used as appropriate: $R = 0.0820544$ liter atm. deg.⁻¹ mole⁻¹, and $R = 82.0567$ cm.³ atm. deg.⁻¹ mole⁻¹.

Vapor Pressure.—The vapor pressure of perfluorocyclobutane was measured in the compressibility apparatus over the temperature range from 30° to the critical temperature, 115.22°. At each temperature the pressure was measured with several different fractions of sample condensed and the results were averaged to obtain the observed values of vapor pressure listed in Table I. A summary (Table II) of the

(6) D. R. Douslin, R. T. Moore, J. P. Dawson and G. Waddington, *J. Am. Chem. Soc.*, **80**, 2031 (1958).

(7) J. A. Beattie, *Proc. Am. Acad. Arts Sci.*, **69**, 389 (1934).

(8) Based upon a molecular weight of 200.040 ($C = 12.010$, $F = 19.00$), E. Wichers, *J. Am. Chem. Soc.*, **74**, 2447 (1952).

(9) F. D. Rossini, F. T. Gucker, Jr., H. L. Johnston, L. Pauling and G. W. Vinal, *ibid.*, **74**, 2699 (1952).

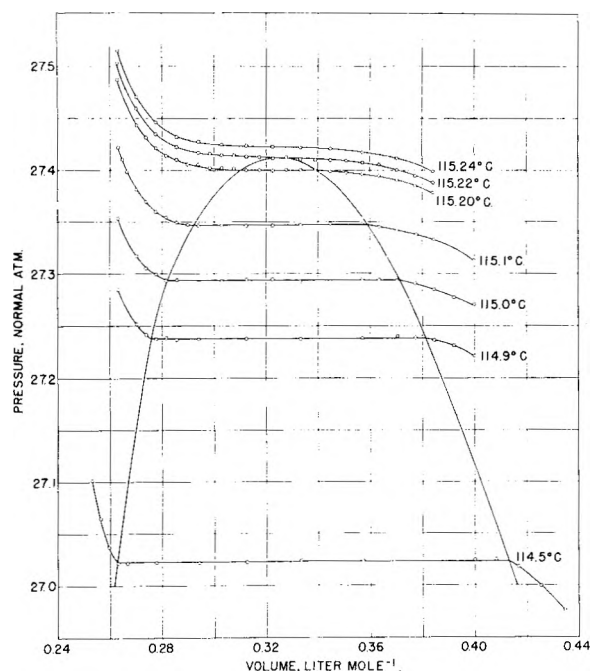


Fig. 1.—The critical region of perfluorocyclobutane.

results obtained along one isotherm typifies the precision obtained for each isotherm over the entire temperature range. The absence of any measurable increase in vapor pressure with increasing fraction condensed is a reliable indication that the sample was highly pure.

The observed vapor pressure data were correlated by the equation

$$\log P(\text{atm.}) = 11.87628 - 2025.845/T - 21.85656 \times 10^{-3} T + 2.16552 \times 10^{-5} T^2 \quad (1)$$

which is of the same form as that used by Furukawa, *et al.*,⁴ to correlate their results in the temperature range -41 to 0° . Equation 1 is in good agreement with the normal boiling point -5.99° given by Furukawa, *et al.*, and with the vapor pressure at 17° reported by Whipple.⁵

The Critical Region.—Values of the critical constants and orthobaric liquid and vapor densities (Table III) were determined from the phase boundary curve of Fig. 1, which is a plot of the compressibility data in Table IV. All pressure data inside the two-phase boundary, as well as in the single-phase gaseous and liquid regions, were corrected for the weight of the sample by a method described in a previous publication.⁶ The observed phase-boundary curve is smooth and without irregularities in the immediate region of the critical.

TABLE I
THE VAPOR PRESSURE OF PERFLUOROCYCLOBUTANE

$t, ^\circ\text{C.}$	$P, \text{ atm.}$	
	Obsd.	Obsd. - Calcd., eq. 1
-5.99^a	1.000	0.000
$+30.00$	3.607	-.008
50.00	6.394	.000
75.00	11.852	+.024
100.00	20.270	.000
114.50	27.023	-.010
114.90	27.238	-.004
115.00	27.294	-.002
115.10	27.347	-.002
115.20	27.400	-.001
115.22	27.412	.000

^a The normal boiling point was taken from ref. 4.

Compressibility.—The compressibility measurements were made at even values of both temperature and density to eliminate the need of cross-plotting the data. By this pro-

TABLE II
VARIATION OF THE VAPOR PRESSURE WITH FRACTION CONDENSED FOR THE SAMPLE OF PERFLUOROCYCLOBUTANE AT 115.00°

Fraction condensed	$P, \text{ atm.}$	Fraction condensed	$P, \text{ atm.}$
0.0112	27.294	0.5477	27.295
.0875	27.294	.6611	27.295
.1605	27.294	.7677	27.293
.2985	27.293	.8676	27.292
.4276	27.292	.9618	27.294

TABLE III
THE CRITICAL CONSTANTS AND ORTHOBARIC DENSITIES OF PERFLUOROCYCLOBUTANE

Critical constants		
$t_c, ^\circ\text{C. (Int.)}$	115.22	
$P_c, \text{ atm.}$	27.412	
$V_c, \text{ l. mole}^{-1}$	0.3248	
Orthobaric densities		
$t, ^\circ\text{C. (Int.)}$	$d, \text{ liq., g. ml.}^{-1}$	$d, \text{ vap., g. ml.}^{-1}$
30.00	1.4506	...
50.00	1.3777	...
75.00	1.2487	...
100.00	1.0501	0.2382
115.00	0.7094	.5490
115.22	0.6159	.6159

cedure, the full precision of the measurements is retained in the correlated results. The values of pressure, density and temperature in Table V are directly observed values that have not been smoothed; therefore, any small deviations of these values from a smooth curve is a measure of the precision of the results. For each isotherm beginning with the lowest, the pressure was measured first at the smallest density, 0.75 mole liter⁻¹, next at densities spaced at regular one-half unit intervals, 1.0, 1.5, 2.0, etc., up to the highest density, 7.0 mole liter⁻¹, and then the initial pressure measurement was repeated. Repetition of the initial pressure measurement for each isotherm served to check for both leakage of mercury and decomposition of the sample. The results of the second measurements at 0.75 mole liter⁻¹ in column 5 of Table V, agree with those of the initial determinations within 0.001 atm., except for the 275° isotherm, for which the deviation is 0.003 atm.

An over-all check for stability of the compound was made by observing the vapor pressure at 100° and 1.2 mole liter⁻¹ at the beginning and the end of the investigation. A difference of less than 0.001 atm. between the initial and final pressure measurement was conclusive evidence that the compound had not changed during the investigation.

The values of "observed" pressure tabulated have been corrected for the weight of the sample¹⁰ and for the partial pressure of mercury vapor¹¹ adjusted at each pressure for the Poynting effect. The correction for mercury vapor did not include that for van der Waals interaction of mercury vapor with perfluorocyclobutane, which cannot be calculated accurately at present. However, the compressibility measurements are reported in sufficient detail so that the correction can be made when a reliable method for calculating it becomes available. In any case, the inaccuracy introduced by the neglect of the mercury interaction correction is probably not great in the region of these measurements and is within the range of the over-all accuracy uncertainty stated in the Experimental Section.

Values of the compressibility factor $Z = PV/RT$ calculated from the data of Table V, are shown in Fig. 2. An isometric plot of the data of Table V on pressure and tem-

(10) The pressure equivalent of the weight of the sample varied from 0.0010 atm. at low pressure to 0.0014 at high pressure. The value varies because the shape of the top of the glass liner in the bomb is that of a hemisphere instead of a right cylinder.

(11) See reference 6 for a list of the selected values of the vapor pressure of mercury and a description of the way the mercury-vapor corrections were calculated and applied.

TABLE IV
THE COMPRESSIBILITY OF PERFLUOROCYCLOBUTANE IN THE CRITICAL REGION

Density, mole l. ⁻¹	Volume, l. mole ⁻¹	Temperature, °C. (int.)						
		114.50	114.90	115.00	115.10	115.20	115.22	115.24
2.300	0.4348	26.976						
2.350	.4255	26.999						
2.400	.4167	27.018		27.236				
2.450	.4082	27.025		27.253				
2.500	.4000	27.025	27.222	27.271	27.313			
2.550	.3922		27.231	27.277				
2.600	.3846		27.236	27.285	27.333	27.378	27.388	27.399
2.650	.3774		27.237	27.291	27.338	27.385	27.395	
2.700	.3704		27.240	27.294	27.342	27.391	27.400	27.411
2.750	.3636			27.294	27.345	27.395	27.406	
2.800	.3571	27.023	27.238	27.294	27.348	27.397	27.407	27.417
2.850	.3509					27.398	27.409	
2.900	.3448			27.293	27.348	27.399	27.410	27.421
2.950	.3390					27.401	27.410	
3.000	.3333	27.024	27.237	27.292	27.347	27.401	27.411	27.422
3.050	.3279					27.401	27.412	
3.100	.3226			27.295	27.347	27.400	27.411	27.423
3.150	.3175					27.400	27.413	
3.200	.3125	27.023	27.238	27.295	27.346	27.400	27.413	27.423
3.250	.3077					27.402	27.414	
3.300	.3030			27.293	27.346	27.402	27.414	27.425
3.350	.2985					27.402	27.416	
3.400	.2941	27.022	27.237	27.292	27.347	27.406	27.417	27.428
3.450	.2899				27.347	27.405		
3.500	.2857		27.237	27.294	27.350	27.410	27.422	27.432
3.550	.2817		27.241	27.294	27.355	27.413		
3.600	.2778	27.022	27.238	27.300	27.360	27.421	27.435	27.446
3.650	.2740		27.242	27.305	27.369	27.431		
3.700	.2703		27.252	27.317	27.382	27.443	27.459	27.471
3.750	.2667	27.021			27.399			
3.775	.2649				27.410			
3.800	.2632	27.021	27.285	27.353	27.422	27.487	27.503	27.514
3.850	.2597	27.037						
3.900	.2564	27.065						
3.950	.2532	27.101						

perature coordinates consists of lines that have negative curvature (that is, concave toward the temperature coordinate) for all densities up to 3.0 mole liter⁻¹. The 3.0 mole liter⁻¹ isometric line, which is just below the critical isometric, is nearly straight. Above the critical density the isometric lines are curved positively but become straighter above 250°.

Equations of State

Three empirical, closed equations of state for gaseous perfluorocyclobutane are presented in Table VI. The Benedict-Webb-Rubin (B-W-R)¹² equation can be used over nearly the entire range of experimental gas densities. The Beattie-Bridgeman (B-B)¹³ and Martin-Hou (M-H)¹⁴ equations are useful over more limited ranges. The B-B and the B-W-R equations have been tested extensively on aliphatic and aromatic hydrocarbons and other non-polar gases, but the more recent Martin-Hou equation has not been tested on as wide a variety of compounds.

Table V shows the differences between the calculated and the observed pressures of perfluoro-

(12) M. Benedict, G. B. Webb and L. C. Rubin, *J. Chem. Phys.*, **8**, 334 (1940); **10**, 747 (1942).

(13) J. A. Beattie and O. C. Bridgeman, *Proc. Am. Acad. Arts and Sci.*, **63**, 229 (1928).

(14) J. J. Martin and Y. C. Hou, *A.I.Ch.E. Journal*, **1**, 142 (1955).

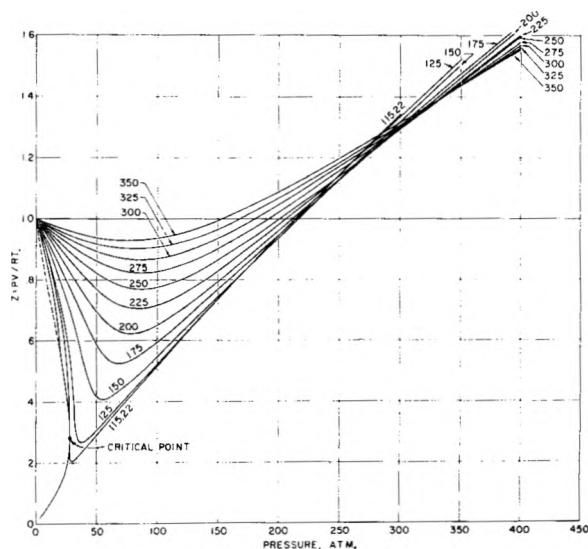


Fig. 2.—Compressibility factor for perfluorocyclobutane.

cyclobutane. Although the B-W-R equation is generally the most accurate of the three, the B-B equation is the least complicated. In the region of

TABLE V
THE COMPRESSIBILITY OF PERFLUOROCYCLOBUTANE AND THE DEVIATIONS OBTAINED WITH THE BENEDICT-WEBB-RUBIN, MARTIN-HOU, AND BEATTIE-BRIDGEMAN EQUATIONS OF STATE

t, °C. (Int.)	Obsd. Obsd. Caled.	B-W-R M-H B-B	0.75	0.75*	1.0	1.5	2.0	2.5	3.0	Density, mole liter ⁻¹					7.0					
										4.0	4.5	5.0	5.5	6.0		6.5				
100.00	Obsd.		16.171	18.942																
	Obsd.	B-W-R	+0.040	-0.014																
	Caled.	M-H	-0.024	-0.068																
115.22	Obsd.		17.549	17.550	20.978	25.175	26.911	27.367	27.411	27.422	27.691	29.542	36.222	53.724	91.858	165.323	293.450			
	Obsd.	B-W-R	+0.088	+0.024	-0.073	-0.238	-0.356	-0.238	-0.238	+0.258	+1.177	+2.801	+5.107	+6.880	+4.960	+6.344	-36.849			
	Caled.	M-H	+0.085	+0.049	+0.062	+0.044	+0.010	+0.010	+0.002	+0.000	+0.066	-0.047								
125.00	Obsd.		18.189	18.420	22.246	27.374	30.143	31.632	32.613	33.640	35.484	39.742	49.860	71.896	115.858	196.591	336.025			
	Obsd.	B-W-R	+0.039	+0.038	-0.001	-0.096	-0.218	-0.303	-0.303	-0.173	+0.526	+2.070	+4.333	+5.866	+3.469	+8.558	-37.489			
	Caled.	M-H	+0.072	+0.108	+0.172	+0.173	+0.173	+0.173	+0.173	+0.173	+0.173	+0.173	+0.173	+0.173	+0.173	+0.173	+0.173			
150	Obsd.		20.560	20.561	25.351	32.704	37.977	42.126	45.991	50.470	56.879	67.485	86.208	119.874	179.455	279.395				
	Obsd.	B-W-R	+0.017	+0.023	+0.038	+0.001	-0.159	-0.407	-0.407	-0.497	+0.008	+1.435	+3.426	+4.621	+2.219	-10.247				
	Caled.	M-H	+0.125	+0.189	+0.293	+0.252	+0.002	+0.002	+0.002	+0.002	+0.002	+0.002	+0.002	+0.002	+0.002	+0.002	+0.002			
175	Obsd.		22.646	22.646	26.355	37.523	45.527	52.412	59.448	67.801	79.178	96.313	123.839	169.084	243.386	363.045				
	Obsd.	B-W-R	+0.008	+0.008	+0.015	+0.036	+0.002	-0.162	-0.425	-0.505	+0.008	+1.365	+3.311	+4.390	+1.673	-9.775				
	Caled.	M-H	+0.162	+0.244	+0.346	+0.243	+0.097	+0.097	+0.097	+0.097	+0.097	+0.097	+0.097	+0.097	+0.097	+0.097	+0.097			
200	Obsd.		24.685	24.688	31.285	42.804	52.308	62.583	72.919	85.315	101.867	125.724	162.088	218.678	307.808					
	Obsd.	B-W-R	+0.008	+0.008	+0.016	+0.032	+0.006	-0.183	-0.425	-0.480	+0.090	+1.466	+3.423	+4.369	+1.913					
	Caled.	M-H	+0.188	+0.276	+0.360	+0.204	+0.176	+0.176	+0.176	+0.176	+0.176	+0.176	+0.176	+0.176	+0.176	+0.176	+0.176			
225	Obsd.		26.696	26.696	34.160	47.686	60.178	72.673	86.404	102.968	124.742	155.366	200.665	268.697	372.274					
	Obsd.	B-W-R	+0.019	+0.028	+0.040	-0.014	-0.189	-0.407	-0.407	-0.484	+0.109	+1.467	+3.550	+4.635	+2.433					
	Caled.	M-H	+0.203	+0.289	+0.346	+0.150	+0.243	+0.243	+0.243	+0.243	+0.243	+0.243	+0.243	+0.243	+0.243	+0.243	+0.243			
250	Obsd.		28.683	28.683	37.001	52.512	67.383	82.712	99.873	120.665	147.782	185.138	238.970	318.241						
	Obsd.	B-W-R	+0.037	+0.061	+0.078	+0.018	-0.175	-0.402	-0.402	-0.442	+0.935	+1.327	+2.498	+4.314						
	Caled.	M-H	+0.212	+0.294	+0.325	+0.100	+0.297	+0.297	+0.297	+0.297	+0.297	+0.297	+0.297	+0.297	+0.297	+0.297	+0.297			
275	Obsd.		30.648	30.651	39.804	57.283	74.520	92.696	113.327	138.444	171.012	215.364	277.995	368.311						
	Obsd.	B-W-R	+0.073	+0.102	+0.135	+0.063	-0.156	-0.433	-0.433	-0.446	+0.103	+1.420	+3.257	+4.425						
	Caled.	M-H	+0.209	+0.281	+0.285	+0.029	+0.359	+0.359	+0.359	+0.359	+0.359	+0.359	+0.359	+0.359	+0.359	+0.359	+0.359			
300	Obsd.		32.601	32.601	42.590	62.003	81.606	102.663	126.768	156.209	194.254	245.443	317.007							
	Obsd.	B-W-R	+0.116	+0.163	+0.202	+0.126	-0.137	-0.433	-0.433	-0.532	+0.013	+1.182	+3.179							
	Caled.	M-H	+0.201	+0.261	+0.217	+0.059	+0.439	+0.439	+0.439	+0.439	+0.439	+0.439	+0.439	+0.439	+0.439	+0.439	+0.439			
325	Obsd.		34.541	34.541	45.352	66.699	88.641	112.637	140.145	173.934	217.372	275.462	355.570							
	Obsd.	B-W-R	+0.165	+0.231	+0.296	+0.194	-0.108	-0.509	-0.509	-0.712	+0.369	+0.730	+2.506							
	Caled.	M-H	+0.186	+0.227	+0.143	+0.174	+0.174	+0.174	+0.174	+0.174	+0.174	+0.174	+0.174	+0.174	+0.174	+0.174	+0.174			
350	Obsd.		36.469	36.470	48.095	71.367	95.651	122.403	153.567	191.721	240.638	305.763	394.567							
	Obsd.	B-W-R	+0.220	+0.306	+0.403	+0.284	-0.081	-0.543	-0.877	-0.877	+0.673	+0.431	+2.144							
	Caled.	M-H	+0.163	+0.180	+0.052	+0.289	+0.635	+0.647	+0.647	+0.647	+0.647	+0.647	+0.647	+0.647	+0.647	+0.647	+0.647			
Av. dev., %	Obsd.		0.22	0.22	0.22	0.18	0.36	0.57	0.55	0.59	2.06	3.44	4.21	1.93	3.64	11.86				
	Obsd.	B-W-R	0.64	0.64	0.64	0.55	0.30	0.48	0.36	0.99	4.21									
	Caled.	M-H	0.27	0.32	0.31	0.21	0.58	1.37												

* Check measurements.

TABLE VI
EQUATIONS OF STATE FOR PERFLUOROCYCLOBUTANE^a

Benedict-Webb-Rubin Equation		
$P = RT/V + (B_0RT - A_0 - C_0/T^2)/V^2 + (bRT - a)/V^3 + a\alpha/V^6 + [c(1 + \gamma/V^2) \exp(-\gamma/V^2)]/V^3T^2$ (2)		
$A_0 = 6.869300$	$a = 4.632380$	$\alpha = 0.0017750$
$B_0 = 0.109250$	$b = 0.095225$	$\gamma = .0530000$
$C_0 = 1.403000 \times 10^8$	$c = .508150 \times 10^6$	$R = .0820544$
Martin-Hou Equation		
$P = RT/(V - b) + [A_2 + B_2T + C_2 \exp(-\epsilon_2.475T/T_0)]/[V - b]^2 + [A_3 + B_3T + C_3 \exp(-5.475T/T_0)]/[V - b]^3 + A_4/(V - b)^4 + B_5T/(V - b)^5$ (3)		
$A_2 = -22.256023$	$A_3 = 4.164859$	$A_4 = -0.407450$
$B_2 = 0.02198825$	$B_3 = -2.522035 \times 10^{-3}$	$B_5 = 4.954812 \times 10^{-6}$
$C_2 = -270.683570$	$C_3 = 68.185191$	$b = 0.07290$
	$R = 0.0820544$	
Beattie-Bridgeman Equation		
$P = [RT(1 - \epsilon)/V^2][V + B] - A/V^2$ (4)		
$A = A_0(1 - a/V); B = B_0(1 - b/V); \epsilon = c/VT^3$		
$A_0 = 21.5500$	$E_0 = 0.35157$	$C = 300 \times 10^4$
$a = 0.12102$	$b = .06232$	$R = 0.0820544$

^a Units: normal atm., liter mole⁻¹, °K.

negative curvature of the isometrics, the B-B equation appears to be the most practical for ordinary calculations in which an average error in pressure of up to 0.5% can be tolerated. A survey of the literature showed that the B-B and B-W-R equations of state represent the compressibility of perfluorocyclobutane with nearly the same accuracy as for hydrocarbons.

Virial Coefficients

The second and the third virial coefficients B and C in the equation

$$PV = RT[1 + B/V + C/V^2 + \dots] \quad (5)$$

were determined graphically from the compressibility data of Table V as the zero-density intercepts of the quantities $V(PV/RT - 1)$ and $[V(PV/RT - 1) - B]V$. The observed values are given in Table VII. To facilitate comparison with theory, the observed virial coefficients are given in volume units of cm.³ mole⁻¹.

TABLE VII

T , °K. (Int.)	- B , cm. ³ mole ⁻¹			$C \times 10^{-3}$, cm. ⁶ mole ⁻²
	Obsd.	Eq. 6	Eq. 17	
336.31	...	563	559	...
345.16	...	528	525	...
373.16	434	435	436	...
388.38	391	392	395	46.4
398.16	366	369	371	45.3
423.16	313	314	316	41.9
448.16	268	268	269	38.5
473.16	229	229	230	34.7
498.16	196	196	196	31.4
523.16	167	167	168	28.1
548.16	142	141	142	25.8
573.16	120	119	120	23.5
598.16	100	100	99	21.6
623.16	82	82	81	20.1
654.76	...	63	59	...
707.87	...	35	30	...
795.74	...	0	-9	...

Intermolecular Potential Energy Functions

Information about the intermolecular forces in perfluorocyclobutane was derived from the experimental values of the second virial coefficient B and the isothermal pressure derivative of vapor heat capacity, $\lim_{P \rightarrow 0} (\partial C_p / \partial P)_T = -T(d^2B/dT^2)$. The

parameters of the Stockmayer¹⁵ potential energy function were evaluated from values of both B and $\lim_{P \rightarrow 0} (\partial C_p / \partial P)_T$. Parameters of the Kihara¹⁶ equation were evaluated from values of B only. Attempts also were made to apply the Lennard-Jones 12,6 and 9,6 equations, but these equations did not provide accurate enough representation of the experimental data to obtain meaningful values of the molecular parameters.

The Stockmayer equation.—Representation of the second virial coefficient of perfluorocyclobutane by Stockmayer's equation, as presented here, is empirical to the extent that the parameter t for the orientational dipole forces is used instead to represent non-polar orientational forces. This procedure is justified by the excellent correlation of the experimental values obtained and by the similarity of the temperature dependence of the second virial coefficient for different kinds of orientational forces. The use of t as an empirical orientational parameter for fluorobenzene was discussed in a previous publication.⁶

Stockmayer's 12,6 equation for the second virial coefficient of a spherical particle with a point dipole embedded at the center

$$B = (2\pi N \sigma^3 / 3)(4/\tau)^{1/4} \left[\Gamma(3/4) - (1/4) \sum_{n=1}^{\infty} (2^n/n!) \sum_{l=0}^{\lceil n/2 \rceil} \binom{n}{2l} \Gamma[(2n - 2l - 1)/4] G_l t^{2l} \tau^{-(n+l)/2} = b_0 F(\tau, t) \right] \quad (6)$$

is based on a classical intermolecular potential energy function

(15) W. H. Stockmayer, *J. Chem. Phys.*, **9**, 398 (1941).
(16) T. Kihara, *Rev. Mod. Phys.*, **25**, 831 (1953).

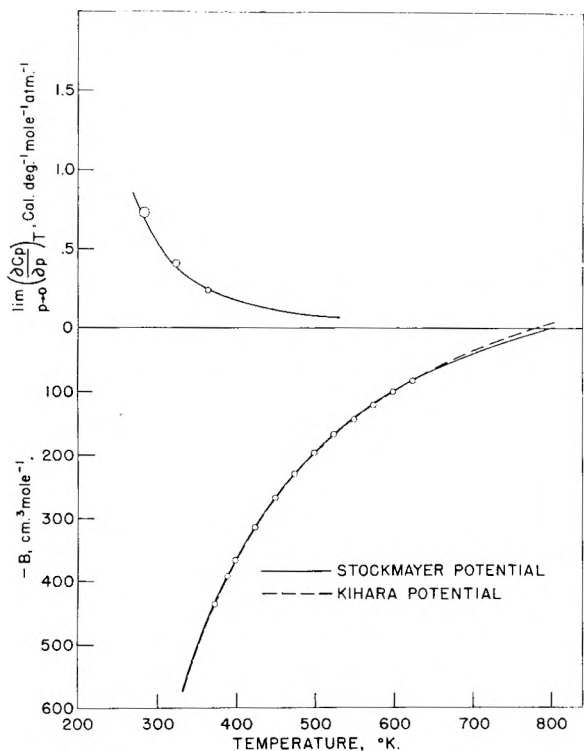


Fig. 3.—The second virial coefficient and the zero pressure limit of the isothermal pressure derivative of the vapor heat capacity of perfluorocyclobutane.

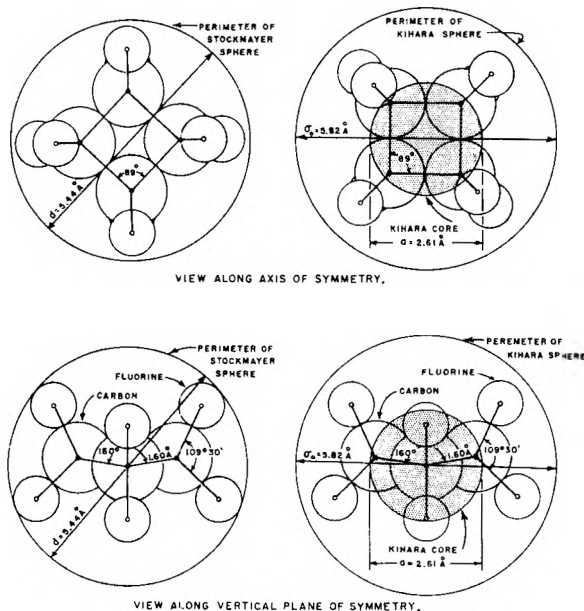


Fig. 4.—Theoretical collision and core diameters superimposed on the structural model of perfluorocyclobutane.

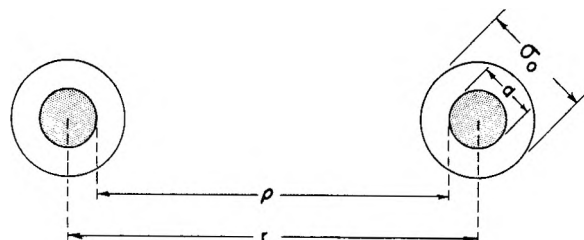


Fig. 5.—Kihara model for spherical hard-core molecules.

$$U(r) = \lambda r^{-12} - Cr^{-6} - \mu^2 gr^{-3} \quad (7)$$

where μ is the dipole moment, λ and C are constants and

$$g = 2 \cos \theta_1 \cos \theta_2 - \sin \theta_1 \sin \theta_2 \cos \varphi$$

In the expression for g , θ_1 and θ_2 are the angles between the dipole axes and the intermolecular axis, and φ is the azimuthal angle between the dipole axes. The angular dependent factors in the summation over l , eq. 6, are given by

$$G_l = (1/8\pi) \int_0^\pi \int_0^\pi \int_0^{2\pi} g^{2l} \sin \theta_1 \sin \theta_2 d\theta_1 d\theta_2 d\varphi$$

$$= (2l + 1)^{-1} \sum_{m=0}^l \binom{l}{m} [3^m (2m + 1)] \quad (8)$$

For relatively simple potential energy functions, such as the Lennard-Jones function, the adjustable parameters τ and b_0 can be defined conveniently in terms of the maximum interaction energy ϵ and the collision diameter σ by the equations

$$\tau = kT/\epsilon = 4kT\sigma^{12}/\lambda = 4kT\sigma^6/C \quad (9)$$

where k is the Boltzmann constant and

$$b_0 = 2/3\pi N\sigma^3 \quad (10)$$

When an orientational potential energy term is present, such as $-\mu^2 gr^{-3}$ in eq. 7, the maximum interaction energy and the collision diameter at zero potential energy cannot be used conveniently to define the adjustable parameters because to do so would increase greatly the complexity of eq. 6. Instead, σ was chosen as the distance between molecular centers when

$$U(r) + \mu^2 gr^{-3} = 0 \quad (11)$$

and ϵ was chosen as the value of $U(r)$ when

$$(d/dr)[U(r) + \mu^2 gr^{-3}] = 0 \quad (12)$$

Another way of expressing this choice is to say that σ and ϵ are the values of the collision diameter and maximum interaction energy in the absence of the orientational forces. Thus, σ and ϵ retain their elementary meanings as originally defined in the Lennard-Jones potential but σ no longer coincides with the distance of separation r at $U(r) = 0$, and ϵ is not the maximum interaction energy of the Stockmayer potential. Still another feature of the parameters σ and ϵ of the Stockmayer potential, which distinguishes them from the same parameters in the Lennard-Jones potential, is that they represent averages of all possible relative orientations of the molecules because they are numerically evaluated from macroscopic measurements.

In Stockmayer's derivation of eq. 6 the orientational forces were assumed to be dipolar and are expressed in terms of the parameter t

$$t = 8^{-1/2}(\mu^2/\epsilon\sigma^3) \quad (13)$$

However, in applying eq. 6 to perfluorocyclobutane each of the three potential energy parameters b_0 , τ and t was assumed to be adjustable independently without being subject to the conditions or restraints imposed by eq. 13; thus, t was used to represent the non-polar orientational forces in perfluorocyclobutane.

The three parameters were evaluated by the method of superimposed logarithmic plots, from the experimental values of B and $\lim_{p \rightarrow 0} (\partial C_p / \partial P)_T$

by use of eq. 6 and the relationship

$$\lim_{P \rightarrow 0} (\partial C_p / \partial P)_T = -T [d^2 B / dT^2] = -[b_0 / T] [d^2 F(\tau, t) / dT^2] \quad (14)$$

Values used to construct the logarithmic plots for the theoretical family of curves of the second virial coefficient function, $F(\tau, t)$ were taken from the tables of Rowlinson¹⁷ for the ranges $0.3 < \tau < 400$ ¹⁸ and $0 < t < 1.5$; and the values used to construct the logarithmic plots for the theoretical family of curves for the heat capacity function $\lim_{P \rightarrow 0} (\partial C_p / \partial P)_T$ were taken from the tables of Douslin and Waddington¹⁹ for the ranges $0.5 < \tau < 3$ and $0 < t < 1.6$. Matching of experimental curves for B and $\lim_{P \rightarrow 0} (\partial C_p / \partial P)_T$ with the corresponding theoretical curves yielded the following values of the three adjustable parameters: $b_0 = 0.2871$ liter mole⁻¹, $\epsilon/k = 177^\circ K$. and $t = 1.0$. The comparison of observed and calculated values of B and $\lim_{P \rightarrow 0} (\partial C_p / \partial P)_T$ in Fig. 3 and Tables VII and VIII show that agreement within the accuracy uncertainty of the experimental data was obtained. Further, the collision diameter²⁰ $d = 5.44 \text{ \AA}$. is nearly the same as that calculated from the elec-

tron-diffraction data of Lemaire and Livingston² as shown in Fig. 4.

The Kihara Equation.—Kihara derived a general equation¹⁶ for the second virial coefficient of hard core molecules based upon a Lennard-Jones 12, 6 intermolecular potential function. His expression for the virial coefficient is a function of the distance ρ between the surfaces of the cores instead of the distance, r , between molecular centers. In the special case of a pair of spherical molecules each having a hard core diameter a as illustrated in Fig. 5, the Kihara intermolecular potential energy function

$$U(r) = 4k\theta \{ [p\sigma_0 / (r - a)]^{12} - [p\sigma_0 / (r - a)]^6 \} \quad (15)$$

can be written in terms of r and a parameter, p , defined as the value of the ratio ρ_0 / r_0 at $U(r) = 0$. The characteristic temperature, θ , is equal to ϵ/k , and the collision diameter, σ_0 , is equal to the value of r at $U(r) = 0$.

In terms of the parameters θ , p and b_0 and the $F_s(\theta/T)$ functions given by Kihara, the second virial coefficient B is

$$B = b_0 [\sqrt{2} p^2 F_3(\theta/T) + 3\sqrt{2} p^2 (1 - p) F_2(\theta/T) + 3\sqrt{2} p (1 - p)^2 F_1(\theta/T) + \sqrt{2} (1 - p)^3] = b_0 K[\theta/T, p] \quad (16)$$

Values for $K(\theta/T, p)$ as defined by eq. 16 are given in Table IX for the ranges $0.4 < \theta/T < 2.5$ and $0.4 < p < 0.9$.

The perfluorocyclobutane molecule was assumed to be spherical enough that eq. 16 would apply. The three adjustable parameters, θ , p and b_0 , were evaluated, by the method of superimposed logarithmic plots, from the experimental values of B . The advantages of evaluating the parameters by this procedure are that the best possible representation of the experimental values of B and an independent evaluation of molecular core size are obtained. The disadvantage is, of course, that the core must be assumed to be spherical. This procedure differs from that of Kihara, who suggested that the core dimensions be evaluated from structural information.

TABLE VIII

THE ISOTHERMAL PRESSURE DERIVATIVE OF VAPOR HEAT CAPACITY OF PERFLUOROCYCLOBUTANE

$T, ^\circ K.$ (Thermo.)	$\lim_{P \rightarrow 0} (\partial C_p / \partial P)_T,$	
	cal. deg. ⁻¹ mole ⁻¹	cal. deg. ⁻¹ mole ⁻¹ Eq. 14
247.80	...	1.140
283.16	0.73	0.707
323.15	.41	.379
363.16	.24	.247
424.80143
460.20110
495.60087
531.00071

^a Evaluated graphically from the experimental values of the molal vapor heat capacity of perfluorocyclobutane given in ref. 3.

TABLE IX

THE KIHARA SECOND VIRIAL COEFFICIENT FUNCTION, $\log [K(\theta/T, p)]$, FOR SPHERICAL, HARD-CORE MOLECULES

$\log \theta/T$	p					
	0.4	0.5	0.6	0.7	0.8	0.9
+0.4	0.5898	0.7223	0.8345	0.9279	1.0086	1.0800
+ .3	.3094	.4647	.5953	.7010	.7904	.8687
+ .2	.0023	.2015	.3632	.4872	.5891	.6762
+ .1	-.4230	-.1065	.1169	.2718	.3922	.4918
0	...	-.5874	-.1812	.0356	.1874	.3061
-.1	...	-1.0136	-.6642	-.2598	-.0438	-.1075
-.2	...	-0.4626	-1.0301	-.7622	-.3281	-.1220
-.3	...	-.2826	-0.5011	-1.0097	-.8801	-.4263
-.4	...	-.1873	...	-0.5302	-.6218	-1.0177

(17) J. S. Rowlinson, *Trans. Faraday Soc.*, **45**, 974 (1949).

(18) Rowlinson's θ is designated τ so as to eliminate possible confusion with the orientational angles of the dipoles, eq. 7.

(19) D. R. Douslin and G. Waddington, *J. Chem. Phys.*, **23**, 2453 (1955).

(20) The collision diameter d is defined as the distance between molecular centers at which $U(r) = 0$. If the numerical value of the orientational parameter t is equal to 1.0, and the molecules are oriented for maximum interaction, i.e., $g = 2$, d can be calculated from σ by $(\sigma/d)^2 - (\sigma/d)^6 = \sqrt{2}$.

Calculated values of B obtained from eq. 16 with the parametric values $b_0 = 0.2483$ liter mole⁻¹, $\theta = 527^\circ K$., and $p = 0.6$ are compared with the experimental values in Table VII. The agreement is within the accuracy of the uncertainty of the experimental data. In Fig. 4, the Kihara collision and core diameters $\sigma_0 = 5.82 \text{ \AA}$. and $a = 2.61 \text{ \AA}$. are compared with the molecular model calculated

from the results of Lemaire and Livingston.² The spherical approximation for perfluorocyclobutane is moderately good.

Although the Stockmayer and the Kihara equations represent the experimental values of B

within experimental accuracy in the temperature range of the measurements, the calculated values of B begin to diverge at high temperatures and different values are calculated for the Boyle temperature, as shown in Fig. 3.

LONG CHAIN BRANCHING IN POLYSTYRENE POLYMERIZED WITH STANNIC CHLORIDE¹

BY J. T. ATKINS AND F. W. BILLMEYER, JR.²

Contribution from the Department of Chemistry, University of Delaware, Newark, Delaware

Received June 25, 1959

Long chain branching was observed in polystyrene made by ionic polymerization in carbon tetrachloride-nitrobenzene solution with stannic chloride as initiator. The weight average number of branch points per molecule was about 2 in polymer made at high conversion (80%), while branching was not detected in polymer made at 35% conversion. Branching was determined by the comparison of the intrinsic viscosity of the ionic polymerized polystyrene to that of linear free radical polymerized polystyrene of the same weight average molecular weight (\bar{M}_w). The relation between intrinsic viscosity $[\eta]$ and \bar{M}_w of linear polystyrene in the range 20,000 < \bar{M}_w < 140,000 was determined as $[\eta]_{\text{butanone}, 25^\circ} = 3.9 \times 10^{-4} \bar{M}_w^{0.56}$ dl./g.

Introduction

The formation of long chain branches through chain transfer to polymer in free radical polymerization is now widely accepted.^{3,4} Similar mechanisms have been postulated^{5,6} to occur in ionic polymerization but conclusive evidence for the presence of long chain branches in polymer prepared by an ionic mechanism has not been published.

The long chain branching mechanism proposed by Fontana involves the transfer of a hydride ion from a polymer molecule to a growing chain. The resulting tertiary carbonium ion then propagates to give a branched molecule.

Endres postulates that the transfer step proceeds by the same mechanism as Friedel-Crafts alkylation. Here the growing chain becomes attached to the polymer molecule at the point of transfer and the proton removed in the transfer step activates a monomer to initiate a new growing chain. Endres found that aromatic compounds, including cumene, act as chain transfer agents in the cationic polymerization of styrene initiated with stannic chloride. The similarity between the structures of these chain transfer agents and the repeat unit of polystyrene suggested that chain transfer to polymer might also occur. The effects of such a transfer reaction would of course be most pronounced at high conversion.

This paper presents evidence for the occurrence

of long chain branches in polystyrene prepared at high conversion by cationic polymerization initiated with stannic chloride. Branching was detected by comparing the intrinsic viscosity of the ionic polymerized polystyrene with that of linear polystyrene (prepared at low conversion in a free radical system) having the same weight average molecular weight.^{4,7}

Experimental

Ionic Polymerized Samples.—Styrene was polymerized by a carbonium ion mechanism by G. F. Endres.⁸ The polymerization was in 60/40 carbon tetrachloride/nitrobenzene solution. The initial concentration of styrene was 1.95 M , and that of the initiator, stannic chloride, was 0.023 M . Two groups of samples were studied, consisting of material polymerized to conversions below 35% and above 74%, respectively.

Free Radical Polymerized Samples.—Styrene (Matheson) was vacuum distilled through a 10'' packed column to remove inhibitor. One hundred ml. of distilled styrene was placed in a test-tube containing initiator (benzoin, recrystallized from ethanol) and chain transfer agent (carbon tetrachloride). The test-tubes were immersed in a constant temperature bath at $25 \pm 1^\circ$ and irradiated with ultraviolet light from a bank of BL-360 fluorescent lamps. A stream of Seaford grade nitrogen was bubbled slowly through the tubes during the polymerization to exclude oxygen. After a predetermined time, the contents of the tubes were poured into methanol in a Waring Blendor. The polymers were collected by filtration and twice dissolved in butanone and reprecipitated into methanol. The polymers were dried overnight at 60° under vacuum.

Molecular Weight.—Weight average molecular weight was determined by light scattering with an automatically recording photoelectric dissymmetry meter.⁹ The instrument was calibrated with solutions of the Cornell Standard Polystyrene, assuming turbidities in agreement with the so-called "high values" in the literature.¹⁰ The solvent was butanone and the refractive index gradient dn/dc was taken as 0.220 ml./g.¹¹ Mercury green light (5460 Å.) was

(1) Research performed by Joseph T. Atkins in partial fulfillment of the requirements for the degree of Master of Science. Presented at the 131st National Meeting of the American Chemical Society, Miami, Florida, April 10, 1957.

(2) Mailing address for both authors: Polychemicals Department, E. I. du Pont de Nemours & Company, Du Pont Experimental Station, Wilmington 3, Delaware.

(3) P. J. Flory, *J. Am. Chem. Soc.*, **59**, 241 (1937); **69**, 2893 (1947).
(4) F. W. Billmeyer, Jr., *ibid.*, **75**, 6118 (1953); J. K. Beasley, *ibid.*, **75**, 6123 (1953).

(5) C. M. Fontana, G. A. Kidder and R. J. Herold, *Ind. Eng. Chem.*, **44**, 1688 (1952); C. M. Fontana, R. J. Herold, E. J. Kinney and R. C. Miller, *ibid.*, **44**, 2955 (1952).

(6) C. G. Overberger and G. F. Endres, *J. Am. Chem. Soc.*, **75**, 6349 (1953); **77**, 2201 (1955); *J. Polymer Sci.*, **16**, 283 (1955).

(7) C. D. Thurmond and B. H. Zimm, *ibid.*, **8**, 477 (1952).

(8) We are indebted to Drs. Endres and Overberger, Polytechnic Institute of Brooklyn, for furnishing the samples.

(9) F. W. Billmeyer, Jr., and C. B. de Than, *J. Am. Chem. Soc.*, **77**, 4763 (1955).

(10) D. K. Carpenter and W. R. Krigbaum, *J. Chem. Phys.*, **24**, 1041 (1956).

used. Solutions were clarified by filtration through porous porcelain filters¹² with a maximum pore radius 0.6μ .

Intrinsic Viscosity.—Intrinsic viscosities were measured in butanone at 25° using Ubbelohde suspended level viscometers modified to permit successive dilutions in the viscometer. Kinetic energy corrections were negligible.

Results and Discussion

Free Radical Polystyrenes.—The free radical polystyrenes were prepared at low conversion and at a relatively low temperature, and have low molecular weights, as indicated in Table I. These conditions are extremely unfavorable for the formation of long chain branches.¹³ It was assumed without further investigation that these polymers were essentially linear.

TABLE I
MOLECULAR STRUCTURE PARAMETERS OF FREE RADICAL
POLYSTYRENES

Sample	Con- version, %	\bar{M}_w	$[\eta]_{\text{butanone}, 25^\circ}$ dl./g.
A	8	17,000	0.093
B	6	20,000	.098
C	7	30,000	.127
D ^a	<7	70,000	.205
E	3.1	79,000	.221
F	2.4	96,000	.238
G	2.7	100,000	.246
H	2.6	110,000	.256
I	2.8	114,000	.273
J	2.3	136,000	.292

^a Sample D was a 50:50 mixture of samples of C and H.

TABLE II
MOLECULAR STRUCTURE PARAMETERS OF IONIC POLYSTYRENES

Samples	Conversion %	\bar{M}_w	$[\eta]_{\text{butanone } 25^\circ}$ dl./g.	$[\eta]/[\eta]_l^b$	Long chain branching index S-F ^c	Z-K ^d
17-1	35	42,000	0.153	1.00	0	0
II-108-E	13	48,000	.167	1.00	0	0
II-108-B	13	54,000	.177	1.00	0	0
177-B-11	80	71,000	.189	0.915	1.5	2.0
II-87-B-7	74	75,000	.191	.90	1.8	2.4
115-13-13	80	79,000	.198	.91	1.7	2.2
117-A-10	82	82,000	.202	.91	1.7	2.2
117-A-8	74	83,000	.200	.89	2.1	2.7

^a Sample designations are those of G. F. Endres, Thesis, Polytechnic Institute of Brooklyn. ^b $[\eta]_l$ is the intrinsic viscosity from equation 1 of a linear polymer with the same \bar{M}_w as the ionic polystyrene. ^c Stockmayer-Fixman branching index, ref. 18. ^d Zimm-Kilb branching index, ref. 19.

The data in Table I lead to the relation

$$[\eta]_{\text{butanone}, 25^\circ} = 3.9 \times 10^{-4} \bar{M}_w^{0.55} \text{ dl./g.} \quad (1)$$

This may be compared with the relation of Outer, Carr and Zimm¹⁴ obtained for sharp fractions

$$[\eta]_{\text{butanone}, 25^\circ} = 3.9 \times 10^{-4} \bar{M}_w^{0.68} \text{ dl./g.} \quad (2)$$

covering a wide range of molecular weight. Equation 2 predicts intrinsic viscosities about 25% higher than eq. 1 in the range covered in this work. Adjustment of the constants in eq. 2 to correspond

(11) R. H. Ewart, C. P. Roe, P. Debye and J. R. McCartney, *J. Chem. Phys.*, **14**, 687 (1946); B. H. Zimm, *ibid.*, **16**, 1099 (1948); B. A. Brier, M. Halwer and R. Speiser, *J. Opt. Soc. Am.*, **40**, 768 (1950); H. J. L. Trap and J. J. Hermans, *Rec. trav. chim.*, **73**, 167 (1954).

(12) J. T. Atkins, L. T. Muus, C. W. Smith and E. T. Pieski, *J. Am. Chem. Soc.*, **79**, 5089 (1957).

(13) J. C. Bevington, C. M. Guzman and H. W. Melville, *Proc. Royal Soc. (London)*, **211A**, 453 (1954).

(14) P. Outer, C. I. Carr and B. H. Zimm, *J. Chem. Phys.*, **18**, 830 (1950).

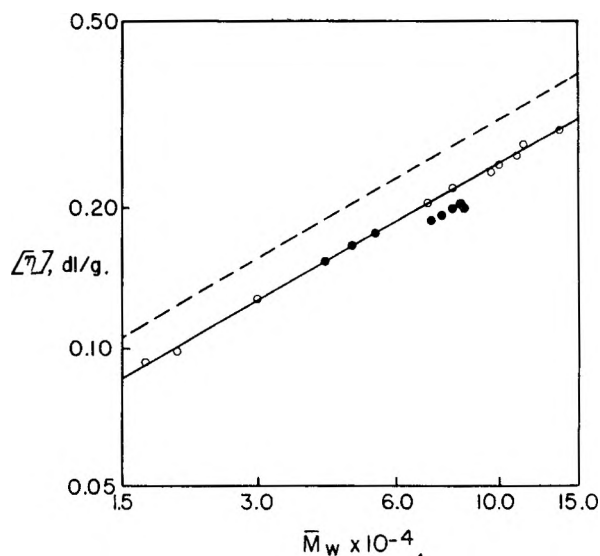


Fig. 1.—Intrinsic viscosity and weight average molecular weight of polystyrene: O, free radical polystyrene; ●, ionic polystyrene: solid line, this work; dashed line, Outer, Carr and Zimm.¹⁴

to a Flory-type molecular weight distribution with $\bar{M}_w/\bar{M}_n = 1.5$ (for termination by combination¹⁵) or $\bar{M}_w/\bar{M}_n = 2.0$ (for termination where transfer to CCl_4 is controlling) reduces the discrepancy to about 15%, comparable to the differences often observed in the determination of light scattering molecular weights and intrinsic viscosities in dif-

ferent laboratories.¹⁶ Since only the relative values of the intrinsic viscosities for free radical and ionic polystyrenes are important in this work, eq. 1 is used.

Ionic Polystyrenes.—Table II lists weight average molecular weights and intrinsic viscosities of the ionic polystyrenes. The intrinsic viscosities of the polymers made to conversions below 35% are within experimental error of those predicted by eq. 1 for linear polymers. As indicated in Fig. 1, however, the intrinsic viscosities of the ionic polymers made to conversions above 74% are significantly lower than those of the corresponding linear polymers of the same weight average molecular weight. This is characteristic of the presence of long chain branching.

(15) J. C. Bevington, H. W. Melville and R. P. Taylor, *J. Polymer Sci.*, **12**, 449 (1954).

(16) International Union of Pure and Applied Chemistry, *J. Polymer Sci.*, **10**, 129 (1953).

Estimated Amount of Branching.—Several theories¹⁷⁻¹⁹ relate the ratio of the intrinsic viscosities of branched and linear polymers to the weight average number of branch points per molecule. The theories are only approximate, however, in application to real polymer systems. Long chain

(17) B. H. Zimm and W. H. Stockmayer, *J. Chem. Phys.*, **17**, 1301 (1949).

(18) W. H. Stockmayer and M. Fixman, *Ann. N. Y. Acad. Sci.*, **57**, 334 (1953).

(19) B. H. Zimm and R. W. Kilb, *J. Polymer Sci.*, **37**, 19 (1959).

branching indices calculated from them should be considered relative measures of the amount of branching rather than representative of the true weight average number of branch points per molecule.

Table II lists long chain branching indices calculated by the relations of Stockmayer and Fixman¹⁸ and Zimm and Kilb.¹⁹ The ionic polystyrenes prepared to conversions above 74% contain of the order of two long chain branches per molecule on this basis.

DIELECTRIC CONSTANT OF LIQUID OZONE AND LIQUID OZONE-OXYGEN MIXTURES¹

BY CHARLES K. HERSH, GERALD M. PLATZ AND RAYMOND J. SWEHLA

*Chemistry and Chemical Engineering Research Division, Armour Research Foundation of Illinois Institute of Technology,
Technology Center, Chicago 16, Illinois*

Received June 29, 1969

The objective of this study was to investigate the dielectric constant of liquid ozone-oxygen mixtures as a physical property that might be useful in the analysis of these mixtures. This study was based on some preliminary measurements that showed the dielectric constants of liquid ozone and liquid oxygen at 90°K. to be 4.75 and 1.46, respectively. The data presented include the dielectric constants of liquid ozone-oxygen mixtures containing 0 to 29.8 wt. % ozone at 90°K. and of pure liquid ozone from 90 to 185°K.

Apparatus and Procedure

The dielectric constants of the liquids were determined by the conventional capacitance method. Since ozone and its solutions were the dielectrics being studied, only materials compatible with both liquid and gaseous ozone were used in the construction of the apparatus. The capacitance cell consisted of two concentric stainless steel cylinders sealed in a glass tube. Small Teflon spacers were used to maintain a 0.1-mm. gap between the cylinders. The diameter of the outer cylinder was about 2.0 cm., and the height 7.3 cm. The capacitance of this cell when empty (*in vacuo*) at 90°K. was 365 micromicrofarads ($\mu\mu\text{f.}$). Later the cell was modified so that the gap was about 3 mm., the height about 4.0 cm. and the empty capacitance 110 $\mu\mu\text{f.}$

A General Radio impedance bridge, Model 650-P1, was used to measure the capacitance (within 1%). Associated with this impedance bridge was a 1-kilocycle (kc.) oscillator-amplifier and the bridge balance was obtained by minimizing the oscillator hum.

The apparatus used to prepare the calibrating liquid ozone-oxygen mixtures was similar to the apparatus which has been used to determine various physical properties during the past several years in the Foundation laboratories, and is described in detail in the literature.² The only change was to replace the magnetic susceptibility unit with the capacitor unit.

From the appropriate capacitance measurements, the dielectric constant of liquid oxygen at 90°K. was determined to be 1.46 ± 0.01 , which agrees with the reported value of 1.46.³ These measurements indicate that corrections for dimensional changes in the cell are negligible between 90 and 298°K. A similar technique was used to obtain the dielectric constant of pure 100% liquid ozone in the temperature range of 90 to 185°K. The major change was to place the concentric cylinder capacitor in a steel pressure vessel.

Results and Discussion

Liquid Ozone-Oxygen Mixtures.—The dielectric constants of ozone-oxygen mixtures at 90°K. are given in Table I. The measurements were confined to the single phase region of 0 to 29.8 wt. % ozone. The dielectric constant of pure liquid ozone is given in Table II, which also includes the density of liquid ozone.⁴ The densities of the ozone-oxygen liquid mixtures were taken from reference 5.

TABLE I
DIELECTRIC CONSTANT OF LIQUID OZONE-OXYGEN MIXTURES AT 90°K.

—Ozone in oxygen— Wt. %	Mole %	Dielectric constant (ϵ)	Molar polarization (P_2), cc.
0	0	1.46 ± 0.01	$(P_2^0 = 3.74)$
14.9	10.5	1.82	26.352
17.6	12.5	1.90	26.296
19.2	13.7	1.93	25.642
29.8	22.1	2.20	23.774
100.0	100.0	4.75 ± 0.02	

The liquid mixture data were used to estimate the dipole moment of the ozone molecule. The treatment followed that of Daniels⁶ and LeFèvre⁷ on the infinite dilution technique and the interested

(4) R. I. Brabets and J. M. McDonough, *J. Chem. Phys.*, **27**, 880 (1957).

(5) C. K. Hersh, A. W. Berger and J. R. C. Brown, Physical Properties of Liquid Ozone-Oxygen Mixtures: Density, Viscosity and Surface Tension, "Ozone Chemistry and Technology," Advances in Chemistry Series, No. 21, 1959, p. 22.

(6) F. Daniels, J. H. Mathews and J. W. Williams, "Experimental Physical Chemistry," 4th Ed., McGraw-Hill Book Co., Inc., New York, N. Y., 1949.

(7) R. J. LeFèvre, "Dipole Moments," 3rd Ed., Methuen and Co. Ltd., London, 1953.

(1) Presented before the Division of Physical Chemistry at the 135th meeting of the American Chemical Society, Boston, Mass., 1959.

(2) C. Brown, A. W. Berger and C. K. Hersh, *J. Chem. Phys.*, **23**, 103 (1955).

(3) "International Critical Tables," Vol. VI, E. W. Washburn, editor, McGraw-Hill Book Co., New York, N. Y., 1929.

TABLE II
DIELECTRIC CONSTANT AND DENSITY OF 100% OZONE AS A
FUNCTION OF TEMPERATURE

Temp., °K.	Dielectric constant (ϵ)	Density, ^a g./cc.
90	4.75 ± 0.02	1.571
103	4.33	1.533
108	4.15	1.517
118	3.85	1.486
130	3.64	1.449
138	3.46	1.425
147	3.33	1.397
155	3.20	1.372
175	2.91	1.310
180	2.84	1.295
185	2.78	1.279

^a Reference 4.

reader is referred to these references for the derivation of the equations.

After suitable assumptions have been made, the molar polarization can be calculated from

$$P_1 = \frac{P - f_2 P_2^0}{f_1} \quad (1)$$

where P is the molar polarization, f is the mole fraction, subscript 1 indicates ozone (solute), subscript 2 indicates oxygen (solvent) and no subscript indicates the solution. As was expected, the molar polarization is a function of concentration (compare Table I). By the method of least squares, the data of Table I were extrapolated to infinite dilution to obtain a value of $P_1^0 = 28.94$ cc. The Debye modification of the Clausius-Mossotti

equation then was employed to obtain the dipole moment.

The distortion polarization, P_{1D}^0 , was estimated from the value of 7.6 cc. for the molar refraction calculated by Lewis and Smyth.⁸ These two values then were used in eq. 2

$$\mu = 0.0127 \times 10^{-18} \sqrt{(P_1^0 - P_{1D}^0)T^{\circ}K}. \quad (2)$$

where μ is the dipole moment. At 90°K. this dipole moment is 0.56 debye. The value for the dipole moment obtained from microwave spectroscopy data is 0.53 ± 0.02 debye.⁹ Lewis and Smyth⁸ give a value of 0.49 debye at 80.8°K.

Liquid Ozone.—The dielectric constant of 100% liquid ozone as a function of temperature is presented in Table II and may be represented by

$$\epsilon = \frac{346.7}{T^{\circ}K.} + 0.9378 \quad (3)$$

where ϵ is the dielectric constant. The molar polarization of liquid ozone as a function of reciprocal temperature has been computed from these data and can be represented by

$$P = \frac{529.5}{T^{\circ}K.} + 11.276 \quad (4)$$

Acknowledgments.—The present work received invaluable advice and assistance from K. Franson, C. Brown, M. J. Klein and R. I. Brabets of the Armour Research Foundation.

(8) G. L. Lewis and C. P. Smyth, *J. Am. Chem. Soc.*, **61**, 3063 (1939).

(9) R. Trambarulo, S. Ghosh, C. Burrus and W. Gordy, *J. Chem. Phys.*, **21**, 851 (1953).

NOTES

THE FORMATION OF TETRACHLOROBORATE ION IN LIQUID SULFUR DIOXIDE SOLUTION¹

By D. E. BURGE, H. FREUND AND T. H. NORRIS

Department of Chemistry, Oregon State College, Coquille, Oregon

Received January 26, 1959

The formation of salts containing the hitherto uncertain tetrachloroborate anion, BCl_4^- , has been indicated in recent reports.^{2,3} Gardner⁴ adduced the same complex in explanation of an observed great increase in the solubility of sodium chloride in liquid sulfur dioxide on addition of boron trichloride. However, in attempting further investigation of this latter system, Burg and Birnbaum⁵ have reported lately an inability to obtain stable solutions, the presence of sodium or potassium chlo-

rides strongly catalyzing the almost complete solvolysis of boron trichloride to thionyl chloride and boric oxide in a few days at room temperature.

In experiments also designed to test for tetrachloroborate ion formation in sulfur dioxide solution, we have studied conductivities of solutions to which boron trichloride and potassium chloride mixtures have been added in various proportions.⁶ In analogy to Gardner's observations we have found the initial low solubility⁷ of potassium chloride to be greatly increased by boron trichloride. To a set of liquid sulfur dioxide samples, each containing an initial large excess, solubility-wise, of potassium chloride (50 mmoles and 0.1 mmole, respectively) successively larger amounts of boron trichloride were added. The sealed tubes were kept at 0° with occasional shaking, conductances being meas-

(1) Oregon State College, Research Paper No. 355, School of Science, Department of Chemistry.

(2) M. F. Lappart, *Proc. Chem. Soc. (London)*, 121 (1957).

(3) E. L. Muetterties, *J. Am. Chem. Soc.*, **79**, 6563 (1957).

(4) D. M. Gardner, Ph.D. Thesis, University of Pennsylvania, 1955, p. 64.

(5) A. B. Burg and E. R. Birnbaum, *J. Inorg. Nucl. Chem.*, **7**, 146 (1958).

(6) A preliminary experiment showed the addition of boron trichloride to a sulfur dioxide solution of the soluble salt tetramethylammonium chloride to give only a small change in conductance. Such a result is inconclusive since, while conceivably implying the non-formation of complex, it might equally well simply indicate the molar conductance of tetramethylammonium tetrachloroborate to be approximately the same as that of the chloride.

(7) 0.013 g./100 g. solvent at 0°. I. Lauder and E. Rossiter, *Nature*, **163**, 567 (1949).

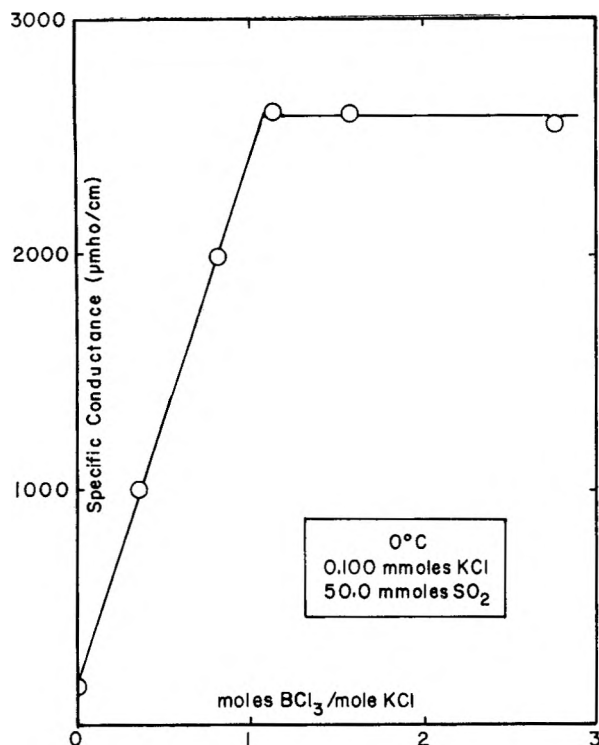


Fig. 1.—Conductances of boron trichloride-potassium chloride mixtures in liquid sulfur dioxide.

ured periodically until constant values were obtained. Dissolution required several days in all cases.

The results are shown in Fig. 1. The solution conductance increases sharply up to a 1:1 BCl_3 :KCl mole ratio, beyond which it remains constant. (In a separate experiment the specific conductance of boron trichloride alone in sulfur dioxide was shown to be unimportant compared to the values measured here.) The solubility was also observed visually, the potassium chloride dissolving completely to give a clear solution in those experiments where boron trichloride was present in excess of a 1:1 mole ratio. The results seem clearly to demonstrate a relatively stable 1:1 BCl_3 :KCl complex, soluble in sulfur dioxide and largely ionized. While the possibility of alternative explanations, as indicated by Burg and Birnbaum, such as $\text{ClSO}_2\text{BCl}_3^-$ ion formation,^{8,9} cannot be excluded without further evidence, it is tempting to suggest, at least

(8) There would seem to be no necessary relationship, one way or the other, between this argument and the quite plausibly possible occurrence in the solution of the ion $\text{ClSO}_2\text{BCl}_3^-$ in at least small concentration as an intermediate in the boron trichloride solvolysis, as postulated by Burg and Birnbaum. It is, incidentally, interesting to note that Burg and Birnbaum's interpretation of the solvolysis in terms of a basic catalysis, involving the intermediate formation of the presumably unstable ionic species SO_2Cl^- , provides further support for similar species adduced in explanation of the halide-catalyzed SO_2 - SO_2 ($\text{X} = \text{Br}$ or Cl) radiosulfur exchange reactions studied some time ago in this Laboratory.¹⁰

(9) The alternative hypothesis of a partial solvolysis to KBOCl_2 seems less inviting in view of Gardner's⁴ observation that, after evaporation of volatile material and pumping, sodium chloride could be recovered with no gain in weight. Since this solvolysis would presumably be irreversible and since boron oxychloride has been found unstable at room temperature with respect to decomposition into boric oxide and boron trichloride,¹¹ the initial formation of an ionic species reversibly dissociable on evaporation, such as BCl_4^- or possibly $\text{ClSO}_2\text{BCl}_3^-$, seems more plausible.

tentatively, that, in harmony with Gardner's postulate, the observations may possibly be related to tetrachloroborate ion formation in the solution.

The reason for the non-observance in the present research of the solvolysis found by Burg and Birnbaum is not entirely clear at present. One must assume our conditions were such as to yield a very much lower rate. In one case, at a BCl_3 :KCl ratio of 0.87, conductance readings were taken on the solution over a period of twenty days. No change was observed after the fifth day. In other cases, measurements, continued until steady conductances were found, took from three to five days. Although lower temperature (0° vs. room temperature) in our work might be a factor, it is not alone sufficient explanation, since solvolysis (though apparently slower) also was observed at -23° in the earlier work.¹² The much lower present concentrations might well be significant, the amounts of potassium chloride in the two researches being sufficient to yield respective tetrachloroborate ion concentrations of 0.03 (this research) and 2.0 molal (Burg and Birnbaum). The situation invites further investigation.

Experimental

Conductances were measured at high frequency, using electrodes external to the sealed tubes containing the solutions. After introduction of potassium chloride (reagent grade) by evaporation of standardized aqueous solutions, the tubes, sealed to the vacuum system, were baked out at 120° under high vacuum for several hours. Boron trichloride (Matheson, Coleman and Bell; fractionated *in vacuo*) and sulfur dioxide (Matheson; purified as previously described¹⁰) were introduced using standard high vacuum techniques, after which the tubes were sealed off.

The conductivity apparatus was similar in principle to that described by Kupka and Slabaugh.¹³ Rather than measure the admittance current through the cell directly, as the previous authors had done, a bridge circuit was used in which the admittance of the cell was compared to that of a similar cell containing aqueous potassium chloride. After passing through the cells, the two currents were rectified in the same way as previously and the bridge then balanced using a d.c. galvanometer and a variable resistor.

The solutions were contained in 7 mm. o.d. Pyrex tubes, specially selected to fit snugly into the coaxial brass tubing electrodes. No capillary sections were provided as in the previous work and two electrodes for each cell rather than the previous three were employed (each 5 cm. long, separated by 3 cm.). The electrodes and their associated rectification circuits were mounted rigidly on Lucite sheet, and placed in a large test-tube wrapped with aluminum foil for electrical shielding. The whole assembly was thermostated in crushed ice.

This apparatus provides a measurement proportional to the total admittance of the cell, which Reilley and McCurdy¹⁴ have shown to be in turn a monotonically increasing function of the low frequency conductance of the solution. Thus it seemed the instrument could be calibrated with standard aqueous potassium chloride solutions to determine absolute conductances (although such was not essential to the present work) rather than relative ones as usually done in high frequency measurements. To check this hypothesis, calibration curves prepared at two frequencies (to allow a wider range of measurement; 100 kc./sec.

(10) R. H. Herber, T. H. Norris and J. L. Huston, *J. Am. Chem. Soc.*, **76**, 2015 (1954); B. J. Masters and T. H. Norris, *ibid.*, **77**, 1346 (1955).

(11) J. Goubeau and H. Keller, *Z. anorg. allgem. Chem.*, **265**, 73 (1951). Burg and Birnbaum also account for their results in terms of retention of BOCl units in the non-volatile boric oxide fraction.

(12) E. R. Birnbaum, M. S. Thesis, University of Southern California, 1958, pp. 19-20.

(13) F. Kupka and W. H. Slabaugh, *Anal. Chem.*, **29**, 845 (1957).

(14) C. N. Reilley and W. H. McCurdy, Jr., *ibid.*, **25**, 86 (1953).

for specific conductances from 30 to 1000 micromhos/cm. and 1.821 mc./sec. for 200–5000 micromhos/cm.) were used to determine conductances of a series of solutions, the values then being compared with those found by conventional low frequency methods. Solutions of aluminum sulfate and acetic acid in water and of tetramethylammonium chloride in methanol were measured; the high frequency agreed within about 5% with the low frequency values over a specific conductance range 50–2000 micromhos/cm. On the basis of these preliminary experiments, the method appears valid for approximate absolute measurements over a somewhat limited range. It would be interesting to explore further the limitations of the technique as a function of frequency, dielectric constant and conductance magnitude.

Acknowledgment.—This research has been supported by the U. S. Atomic Energy Commission under Contract AT(45-1)-244.

CATALYSIS BY ION-EXCHANGE RESINS: CATALYTIC BEHAVIOR OF LOW CROSS-LINKED RESINS

BY S. L. BAFNA AND V. M. BHALE

National Chemical Laboratory, Poona, and Department of Chemistry, Holkar College, Indore, India

Received April 11, 1959

In the previous paper,¹ the study of the kinetics of acetone-iodine reaction catalyzed by cross-linked polystyrenesulfonic acid cation-exchange resins was reported. It was indicated that the velocity coefficient k reached a maximum at low concentrations, which was independent of concentration of reactants, concentration and particle size of catalyst (resin) and decreased with the decrease in the relative degree of cross-linking for the two resins used. This communication reports on the catalytic behavior of low cross-linked resins for the same reaction.

Experimental and Results

The experimental procedure, the method of calculations and the symbols used are the same as given before.¹ The resins used were Dowex-50 X1, Dowex-50 X2 and Dowex-50 X4 (Dow Chemical Co.) of -40, +60 mesh in bead form. These are sulfonated copolymers of styrene and divinylbenzene (DVB), X1, X2 and X4 indicating the % nominal DVB content, used for cross-linking. The resins were treated and finally converted into hydrogen form; the capacity of each was 5.25 meq./g. oven-dry resin. Table I briefly summarizes the results.

Catalytic behavior of cation-exchange resins of low cross-linking in the resin catalyzed acetone-iodine reaction.¹ Temp. 30.1°; 10^4 [Acetone], 5.976 mole/l.; r.p.m. (stirring), ~1050; $[I_2]_0$, the concentration of iodine when stirred with resin for 17 hours; B , meq. of replaceable hydrogen ions in the resin used/l.; t_F , the calculated time for complete reaction; k , the velocity coefficient calculated from $k_0/[Acetone]$ [Catalyst] where k_0 is the zero-order rate constant calculated from $[I_2]_0/t_F$.

TABLE I

Resin	B	$10^4[I_2]_0$ (mole/l.)	$t_F/60$, sec.	$10^4 \times k$, sec. ⁻¹ mole ⁻¹ .
Dowex-50 X1	4.294	6.45	380	11.03
	8.588	6.31	185	11.08
Dowex-50 X2	4.264	6.59	390	11.05
	8.529	6.31	186	11.09
Dowex-50 X4	4.113	6.20	380	11.06
	8.226	5.38	165	11.05

Discussion

With decrease of degree of cross-linking (d.c.) of the strong acid cation-exchange resin, the water

uptake of the resin increases² and, hence, the concentration of the resin acid solution, the resin being treated as a concentrated electrolyte solution³ (the water uptake being supposed as the solvent) should also decrease. This should imply that the velocity coefficient k should decrease as the d.c. of the resin is decreased and in the limit approach that for strong homogeneous acid-catalyzed reaction. However, the above data indicate the significant result that k has a value 2.15 times that for strong homogeneous acid,¹ and independent of d.c. for low cross-linked resins. This may be explained on the plausible assumption that for low cross-linked resins only some amount of the water uptake of the strong acid resin constitutes the concentrated electrolyte solution, this amount of water being independent of total water uptake of the resin. This may be attributed to the possible restricted migration of hydrogen ions away from the hydrocarbon skeleton of the acid resin due to electrostatic forces.

Acknowledgment.—The authors wish to thank Dr. W. V. Bhagwat and Dr. A. B. Biswas for helpful comments.

(2) B. R. Sundheim, M. H. Waxman and H. P. Gregor, *ibid.*, **57**, 974 (1953).

(3) E. Glueckauf, *Proc. Roy. Soc. (London)*, **214A**, 207 (1952); J. W. Duncan, *ibid.*, **214A**, 344 (1952).

AN APPLICATION OF VETTER'S CRITERION FOR DETERMINING HYDROGEN OVERVOLTAGE MECHANISM

BY SIGMUND SCHULDINER

U. S. Naval Research Laboratory, Washington 25, D. C.

Received March 6, 1959

A new confirmation that the hydrogen overvoltage on α -Pd-H is determined by an electrochemical desorption of hydrogen atoms can be shown from data published from this Laboratory.^{1,2}

Vetter³ showed that a distinction between the "electrochemical desorption" and "atomic combination" mechanisms of hydrogen overvoltage can be made by observing anodic polarization curves. If the atomic combination mechanism predominates, as it does on platinum,^{4,5} then a limiting current density will be observed as a sharp potential rise at an overvoltage not far removed from the open circuit potential. If the electrochemical desorption mechanism prevails then instead of a limiting anodic current density being reached in the potential range found for the atomic combination case, a Tafel slope with a b -value of 0.12 will be obtained. Figure 1 shows the anodic overvoltage curves for Pt and α -Pd-H bi-electrodes.⁶

(1) J. P. Hoare and S. Schuldiner, *J. Electrochem. Soc.*, **104**, 564 (1957).

(2) S. Schuldiner and J. P. Hoare, *ibid.*, **105**, 278 (1958).

(3) K. J. Vetter, *Z. Elektrochem.*, **59**, 435 (1955).

(4) S. Schuldiner, *J. Electrochem. Soc.*, **101**, 426 (1954).

(5) S. Schuldiner, *ibid.*, in press.

(6) η_a' is defined as the difference in potential between the open circuit reversible electrode against the polarized electrode of the same metal-solution system. Hence, the overvoltages on the Pt bi-electrode were against at Pt/H₂ reference electrode in the same solution; and the overvoltages on the α -Pd-H bi-electrode were against an α -Pd-H_{sat.}/H⁺ reference electrode⁷ in the same solution.}

(1) S. L. Bafna, *This Journal*, **59**, 1199 (1955).

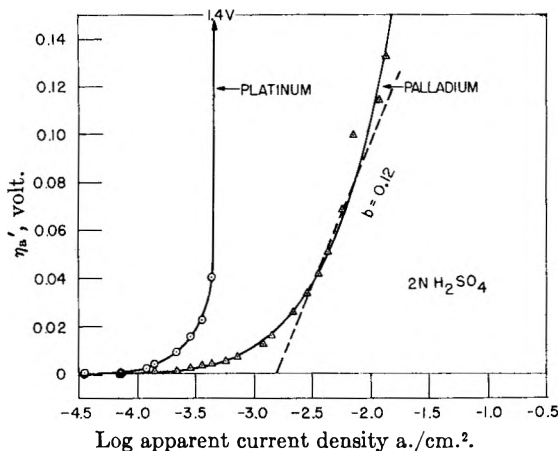


Fig. 1.—Comparison of anodic hydrogen overvoltages on α -Pd-H and Pt bielectrodes; in hydrogen stirred solutions.

The anodic curves clearly show these differences for Pt and α -Pd-H. Further confirmation can be seen from other data.^{1,2} The fact that the hydrogen diffusing through the α -Pd-H bielectrode is not the cause of the 0.12 slope can be seen from anodic polarization curves on a simple Pd anode¹ and also from data³ on atomic hydrogen overvoltage on the anode side of an α -Pd-H bielectrode in hydrogen-free solution.

(7) S. Schuldiner, G. W. Castellan and J. P. Hoare, *J. Chem. Phys.*, **28**, 16 (1958).

(8) S. Schuldiner, *J. Electrochem. Soc.*, **106**, 440 (1959).

THE STATIONARY PHASE IN PAPER CHROMATOGRAPHY

BY GEORGE H. STEWART AND HYUNG KYU SHIN

Department of Chemistry, University of Utah

Received April 23, 1959

The analysis of the partition coefficient α and the R_f value in paper chromatograms by the method of Consden, *et al.*,¹

$$\alpha = \frac{A_1}{A_s} \left(\frac{1}{R_f} - 1 \right)$$

where A_1/A_s is the ratio of the areas of cross-sections of the mobile and the stationary phase, may be corrected for the non-constant value of the concentration profile over the length of the solvent path.² The method of assigning a value to A_s requires close analysis and standardization before values of the partition coefficient may be interpreted in terms of solution theory. The ability to predict the partition coefficient by static methods would facilitate the choice of suitable solvent systems for chromatographic problems. Two pieces of information are required: (1) the cross-sectional area (or volume per unit length) of the active stationary phase and (2) the nature of the solvent in that phase.

The stationary phase may be subdivided into two distinct regions, adsorption sites and solution.³

(1) R. A. Consden, A. H. Gordon and A. J. P. Martin, *Biochem. J. (London)*, **38**, 224 (1944).

(2) R. Krulla, *Z. physik. Chem.*, **66**, 307 (1909).

(3) D. P. Burma, *Anal. Chem.*, **25**, 549 (1953), contains review of earlier work.

Partition chromatography refers to the exchange between the mobile solvent and the solution held within the cellulose fibers while adsorption chromatography deals with the bonding of solute molecules to adsorption sites (primarily hydrogen bonding to glucoside hydroxyls) on the glucoside chains. When water is the major solvent, only the strongest bases will displace it from hydrogen bonds with the cellulose⁴ and allow adsorption to compete with the partition mechanism. The occurrence of adsorption in a partition chromatogram is often signaled by tailing or ghost spots.

The analysis of adsorption kinetics and isotherms should give some insight into these questions. To this end the authors have determined rates of adsorption and adsorption isotherms for the system water and Whatman 3MM chromatographic paper.

The rates of adsorption were determined on paper samples previously dried for 48 hours *in vacuo* over P_2O_5 . Vapor pressures were achieved with sulfuric acid solutions.⁵ The rate curves (Fig. 1) indicate that adsorption is essentially complete after 24 hours. This gives a measure of the time of exposure of chromatographic papers to solvent vapors prior to use necessary to prevent water-logging and double-fronting.⁶ The values used in the isotherms, however, were taken at two weeks to allow more complete equilibration. The weight of solvent adsorbed per gram of paper, w , is a measure of the extent of the stationary phase and provides a measure of A_s in the Consden formulation. The fact that R_f values of unity are reported precludes the inclusion of dead-end capillaries exterior of the individual fibers as part of the stationary phase. The occurrence of such pools of static solvent is best considered as constituting a streamline of zero velocity in the mobile phase.

The subdivision of the adsorbed volume into a bound and a condensed phase can be made from the adsorption isotherm of Smith⁷ ($\bar{w} = \bar{w}_b - \bar{w}' \ln[1 - P/P_0]$) which allows for the swelling of the fibers and the increase in available bound sites with the percentage of moisture imbibed. The slope of the Smith plot yields the number of multilayer sites, \bar{w}' , expressed as a weight fraction, and the intercept yields the number of bound sites, \bar{w}_b , also expressed as a weight fraction. It is expected that the two quantities should be equivalent since multilayers can be formed only on water which is hydrogen bonded to the cellulosic hydroxyls. This conclusion led us to believe that the paper samples contained a residual 2% water after drying and this was confirmed by two further analyses. The isotherm below $p/p_0 = 0.4$ should be little influenced by swelling and the BET isotherm should be approached as p/p_0 approaches zero. Application of the residual moisture correction to the BET isotherm gives approximately the same number of bound sites as the Smith treatment (Table I). To check the predicted residual moisture, the

(4) F. M. Arshid, C. H. Giles and S. K. Jain, *J. Chem. Soc.*, 559 (1956).

(5) R. E. Wilson, *Ind. Eng. Chem.*, **13**, 326 (1921).

(6) H. G. Cassidy, "Fundamentals of Chromatography," Interscience Publ., Inc., New York, N. Y., 1957, p. 164 *et seq.*

(7) S. E. Smith, *J. Am. Chem. Soc.*, **69**, 646 (1947).

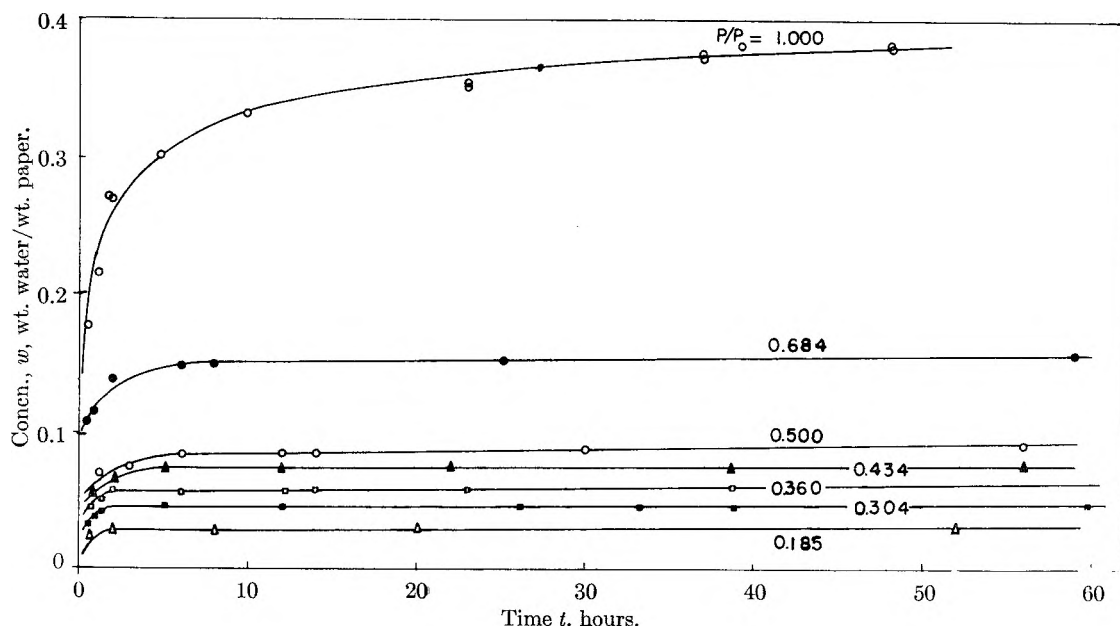


Fig. 1.—Weight of water adsorbed per gram of cellulose (W3MM) as a function of time for various relative humidities at 25°.

kinetics of drying data⁸ (Fig. 2), were extrapolated to "bone dry," analytically, and reasonable agreement with the isotherm analysis was obtained.

TABLE I

	Bound sites ^a	Multilayer sites	Residual moisture
Smith	0.046 _{corr}	0.046	0.019
BET	.044019
Drying curve018

^a Reported as grams of water per gram of paper.

The success of these treatments tempts us to determine an average capillary size. The data indicates that condensation occurs only on filled bound sites and all available bound sites (exclusive of new ones due to swelling) are filled above $p/p_0 = 0.4$. The ratio of total water to bound water should be the average number of multilayers: $w_T/w_b = 9$. This gives an average pore diameter of about 50 Å. This may be compared with electron microscope studies⁹ which give values of the order of 40 Å and with non-freezing moisture analyses¹⁰ which give maximum values ranging from 100 to 300 Å. The importance of these values is that they suggest that the kinetics of partitioning of large molecules must be governed by diffusion through a very tight labyrinth of glucoside chains necessitating the breaking of hydrogen bonds, similar to the diffusor of solvents into dry fibers.¹¹

The analysis of the adsorption isotherm by the method of Smith fails at p/p_0 values greater than 0.9. This is due in part to the limit to swelling of the cellulose fibers and in part to the approach to pure condensation energetics. It has been sug-

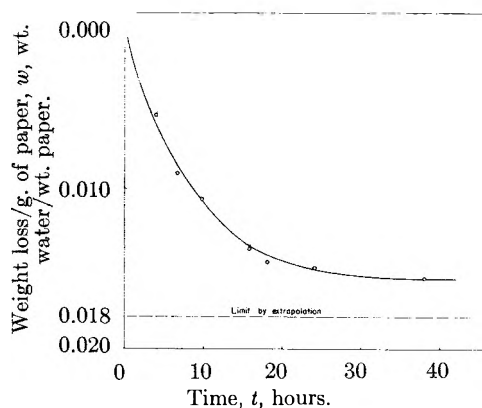


Fig. 2.—Residual moisture loss per gram of cellulose. Extrapolated by $w_{lost} = w_0(1 - e^{-k_1t})$, 100°.

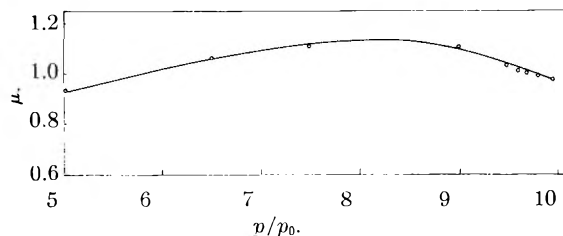


Fig. 3.—Huggins¹³ interaction parameter μ as a function of relative humidity p/p_0 , 25°.

gested that polymer solution theory is applicable in this region.¹² Consistent with the results of Simha and Rowen, the authors find that the Huggin's interaction parameter μ ¹³ has a near constant value over the range p/p_0 equal to 0.5 to 1.0 (Fig. 3).

The variety of treatments necessary to explain the adsorption isotherm of cellulose tells of the heterogeneity of the stationary phase. Martin's

(8) P. H. Hermans, "Contributions to the Physics of Cellulose Fibers," Elsevier Pub. Co., Inc., Amsterdam, 1946, p. 206.

(9) S. Asunmaa, *Svensk Papperstidn.*, **57**, 367 (1954); *C. A.*, **50**, 1299g (1956).

(10) F. C. Magne, H. J. Portas and H. Wakemar, *J. Am. Chem. Soc.*, **69**, 1896 (1947).

(11) Ref. 8, page 31.

(12) R. Simha and J. W. Rowen, *J. Am. Chem. Soc.*, **70**, 1663 (1948).

(13) M. L. Huggins, *Ann. N. Y. Acad. Sci.*, **43**, 1 (1942).

suggestion¹⁴ that it can best be approximated by a solution of polyols is still the best characterization of its average behavior in view of the applicability of polymer solution theory. With a clear definition of the size of the stationary phase, through arguments like those above, investigation of this aspect of the problem can be made. The authors hope that this note will renew interest in some of the fundamental aspects of paper chromatography.

This investigation was supported by a research grant, A-2402(Cl), from the National Institute of Health, Public Health Service.

(14) A. J. P. Martin, *Ann. Rev. Biochem.*, **19**, 517 (1950).

X-RAY ANALYSES OF THE SOLID PHASES IN THE SYSTEM LiF-ThF₄

BY L. A. HARRIS, G. D. WHITE

Ceramic Laboratory, Metallurgy Division

AND R. E. THOMA

*Reactor Chemistry Division, National Laboratory,¹
Oak Ridge, Tenn.*

Received April 25, 1959

The phase equilibrium diagram for the system LiF-ThF₄ has previously been determined at this Laboratory by R. E. Thoma, *et al.*, and shown to contain four distinct solid phases, none of which were observed to have polymorphic transformations. The reliability of these compound formulas has been established by the methods outlined in the phase equilibrium paper.² The X-ray examination of the crystalline phases and the analyses of their structure is the concern of the following paper.

Material Synthesis.—Solid-state synthesis of the four compounds was attempted in order to procure single-crystal specimens for positive structure identification and to obtain sufficient quantities of the individual phases for density determinations. Samples of powdered materials having the proper chemical compositions were thoroughly mixed, placed in nickel tubes, evacuated, sealed and positioned in a platinum-wound furnace. The samples were heated and held slightly below their melting temperatures for a period of ten days. Single crystals for Li₃ThF₇ and LiTh₂F₉ were obtained in this manner; however, materials of sufficient purity for density measurements were attained only for Li₃ThF₇ and Li₇Th₆F₃₁. Determinations of the phases formed by the above methods were based on the optical and X-ray examination of the cooled material.

X-Ray Methods.—Debye-Scherrer films were taken of all four phases using a 114.6-mm. dia. camera and Cu K α ($\lambda = 1.5418 \text{ \AA}$) radiation. Rotation, Weissenberg and precession diffraction patterns for the single-crystal samples were obtained from the Metallurgy and Ceramics X-Ray Laboratory.

X-Ray Results

Li₃ThF₇.—The data obtained from the Debye-Scherrer film for Li₃ThF₇ were indexed (Table I) and found to best fit a tetragonal unit cell whose lattice parameters are $a_0 = 6.206 \pm 0.006 \text{ \AA}$. and $c_0 = 6.470 \pm 0.002 \text{ \AA}$. and which contains two molecules with a calculated density $\rho = 5.143 \text{ g./cc}$. The observed extinctions from the Weissenberg and precession photographs are compatible with space groups P4/nmm or P4/n.

(1) Operated for the U. S. Atomic Energy Commission by the Union Carbide Corporation.

(2) R. E. Thoma, H. Insley, B. S. Landau, H. A. Friedman and W. R. Grimes, "Phase Equilibria in the Fused Salt Systems LiF-ThF₄-NaF-ThF₄," presented at meeting of the Am. Chem. Soc., Chicago, Ill., September 1958

TABLE I
INDEXED POWDER PATTERN OF Li₃ThF₇

I	sin ² θ			I	sin ² θ		
	Obsd.	Calcd.	hkl		Obsd.	Calcd.	hkl
M+	0.0142	0.0142	001	W-	0.2271	0.2272	004
S	.0295	.0296	101	W-	.2473	.2466	400
S+	.0309	.0308	110	W-	.2510	.2511	223
S	.0449	.0450	111	M+	.2571	.2571	322
M	.0617	.0616	200	W-	.2615	.2610	401
M+	.0721	.0722	102	W	.2663	.2665	303
M	.0759	.0758	201	W	.2772	.2774	330
M	.0914	.0913	211	W	.2819	.2819	312
W	.1090	W	.2892	.2884	204
M	.1233	.1233	220	W	.3087	.3082	420
S	.1338	.1339	212	W	.3195	.3187	412
M	.1378	.1375	221	W	.3283	.3281	323
M	.1428	.1432	103	W-	.3503	.3505	224
M+	.1543	.1541	310	W-	.3695	.3704	105
W+	.1582	.1586	113	W	.3814	.3813	314
M	.1687	.1683	311	W	.3892	.3898	413
M	.1898	.1894	203	W	.4012	.4007	510
W	.1956	.1955	302	W	.4156	.4149	511
W+	.2048	.2049	213	W-	.4309	.4320	215
W	.2147	.2145	321	W+	.4422	.4420	432
				W-	.4623
				W-	.4741	.4738	404
				W-	.4943	.4937	305

Li₇Th₆F₃₁.—The type compound designated M₇X₆F₃₁, where M represents an alkali atom and X a heavy atom such as uranium or thorium, has been observed by investigators of the fluoride phase equilibrium relationships at this Laboratory.²⁻⁵ In the system LiF-ThF₄, a compound with the above chemical ratio was observed and determined to be optically uniaxial.^{2a} A comparison of the Debye-Scherrer films for Li₇U₆F₃₁ and Li₇Th₆F₃₁ revealed both compounds to be isostructural. Single-crystal specimens of Li₇U₆F₃₁ which were available permitted the authors to determine the unit cell and probable space group of Li₇Th₆F₃₁ by analogy. Table II presents the powder diffraction data for the Li₇Th₆F₃₁ indexed with the help of the Weissenberg and precession photographs of Li₇U₆F₃₁. The compound has tetragonal symmetry with unit cell dimensions $a_0 = 15.10 \pm 0.002 \text{ \AA}$. and $c_0 = 6.60 \pm 0.02 \text{ \AA}$.; the calculated density is $\rho = 4.387 \text{ g./cc}$., assuming two molecules per cell. The space group I4₁/a was chosen on the basis of the systematic extinctions of reflections observed on the single-crystal photographs of Li₇U₆F₃₁.

TABLE II
INDEXED POWDER PATTERN OF Li₇Th₆F₃₁

I	sin ² θ			I	sin ² θ		
	Obsd.	Calcd.	hkl		Obsd.	Calcd.	hkl
W+	0.0162	0.0162	101	W	0.1456	0.1458	303
S	.0209	.0208	220	W	.1487	.1480	602
S	.0267	.0266	211	W	.1515	.1514	721
S	.0373	.0370	301	VW	.1562	.1562	323
S-	.0477	.0474	321	M-	.1587	.1584	622
S	.0524	.0520	420	S	.1668	.1664	800
S-	.0581	.0578	411	W	.1730	.1722	651
S	.0650	.0648	202	M	.1829	.1826	811
M	.0755	.0752	222	M	.1876	.1872	660
M	.0787	.0786	501	W	.1984	.1978	523
W	.0893	.0890	521	M	.2034	.2034	831
W	.1045	.1040	620	W	.2186	.2176	004
M	.1103	.1098	611	M-	.2317	.2312	822
M+	.1308	.1306	631	W	.2348	.2346	921
S-	.1355	.1352	640	W	.2390	.2394	633
				W	.2420	.2416	662
				W+	.2453	.2450	851

TABLE III
 INDEXED POWDER PATTERN OF LiTh_2F_9

<i>I</i>	Obsd.	$\sin^2 \theta$	Calcd.	<i>hkl</i>	<i>I</i>	Obsd.	$\sin^2 \theta$	Calcd.	<i>hkl</i>
VW	0.0096		0.0093	110	M	0.1864		0.1864	620
M	.0193		.0186	220	W	.1912		.1911	323
VS	.0376		.0373	220	W+	.2048		.2056	541
S	.0465		.0466	310	W	.2237		.2242	631
W	.0579		.0580	002	W	.2327	0.2330, 0.2320		710, 004
M	.0674		.0673	112	S	.2643		0.2656	523
M	.0748		.0746	400	S	.2690		.2693	224
M-	.0774		.0766	202	M	.2789		.2786	314
VW	.0839		.0839	330	M	.2900		.2910	712
M	.0937		.0932	420	M	.2979		.2982	800
S	.1329		.1326	402	M-	.3156		.3159	334
S	.1420		.1419	332	VW	.3271		.3283	732
S	.1491		.1491	440	W	.3802		.3811	444
S	.1542		.1538	213	VW	.3848		.3858	215
M	.1670		.1678	600	W+	.4070		.4044	305

 TABLE IV
 INDEXED POWDER PATTERN OF $\text{LiTh}_4\text{F}_{17}$

<i>I</i>	Obsd.	Calcd.	<i>hkl</i>	<i>I</i>	Obsd.	Calcd.	<i>hkl</i>
W	0.0141	0.0141	220	S	0.1468	0.1478	315
M	.0181	.0181	002	S	.1487	.1486	612
VW	.0283	.0282	220	S	.1586	.1588	630, 325
S	.0324	.0322	202, 221	S-	.1615	.1620	006
VS	.0400	.0398	003, 311	S	.1809	.1810	711
S	.0469	.0463	222	VS	.1872	.1871	720
W	.0567	.0565	400	M	.2005	.2008	505
VS	.0710	.0706	420	W	.2029	.2025	614
S	.0755	.0751	421, 313	VW	.2089	.2092	731
M	.0885	.0883	500, 422	W	.2121	.2132	624
VW	.0961	.0963	511	M	.2150	.2153	650, 525
W	.1039	.1038	304	VW	.2197	.2198	651
S	.1314	.1311	442, 601	W	.2262	.2259	800
VS	.1413	.1412	620	M	.2313	.2308	634
S	.1442	.1443	305, 540	W	.2358	.2346	207
				M	.2434	.2430	615
				W	.2483	.2487	227, 714

 TABLE V
 CRYSTALLOGRAPHIC DATA^{3,4,5} FOR PHASES IN THE SYSTEM LiF-ThF_4

Phase	Symmetry	Lattice parameters (Å.)		Space group	Density, g./cc.
		a_0	c_0		
Li_3ThF_7	Tetragonal	6.206 ± 0.006	6.470 ± 0.002	$P4/nmm$ or $P4/n$	5.143
$\text{Li}_7\text{Th}_6\text{F}_{31}$	Tetragonal	$15.10 \pm .002$	$6.60 \pm .02$	$I4/a$	4.387
LiTh_2F_9	Tetragonal	$11.307 \pm .009$	$6.399 \pm .008$	Body-centered (?)	...
$\text{LiTh}_4\text{F}_{17}$	Tetragonal	$12.984 \pm .004$	$11.46 \pm .02$

LiTh_2F_9 .—The phase LiTh_2F_9 , which was reported to be optically uniaxial,² gave reflections which were indexed (Table III) from Debye-Scherrer film and single-crystal data. The unit cell is tetragonal with lattice parameters $a_0 = 11.307 \pm 0.009$ Å. and $c_0 = 6.399 \pm 0.008$ Å. From the Weissenberg photographs the only systematic extinctions observed were those that arise from a body-centered cell.

$\text{LiTh}_4\text{F}_{17}$.—This phase was reported to be optically biaxial with a variable optic angle (2V).² The data obtained from the Debye-Scherrer films

(3) C. J. Barton, W. R. Grimes, H. Inseley, R. E. Moore and R. E. Thoma, *THIS JOURNAL*, **62**, 665 (1958).

(4) C. J. Barton, H. A. Friedman, W. R. Grimes, H. Inseley, R. E. Moore and R. E. Thoma, *J. Am. Ceram. Soc.*, **41**, 63 (1958).

(5) R. E. Thoma, H. Inseley, B. S. Landau, H. A. Friedman and W. R. Grimes, *ibid.*, **41**, 538 (1958).

were tentatively indexed (Table IV) and found to best fit a tetragonal unit cell whose lattice parameters are $a_0 = 12.984 \pm 0.004$ Å. and $c_0 = 11.46 \pm 0.02$ Å. The absence of single-crystal data allows for the possibility of error due to pseudosymmetry.

The data assembled from the X-ray analyses of the four crystalline phases in the system LiF-ThF_4 are summarized in Table V. Future detailed structure determinations are planned for all four compounds.

Acknowledgment.—The authors wish to thank H. L. Yakel, Jr., and R. M. Steele for their aid with the single-crystal determinations. Our thanks are also due to M. P. Haydon for density calculations. In addition, we are grateful for the support of other members of the Ceramic Laboratory.

HEAT AND ENTROPY OF FUSION OF MERCURIC BROMIDE¹

BY GEORGE J. JANZ AND JEROME GOODKIN

Department of Chemistry, Rensselaer Polytechnic Institute, Troy, N. Y.

Received April 8, 1959

To study the constitution of molten salt mixtures with mercuric bromide as solvent, an accurate value of the cryoscopic constant, based preferably on a calorimetrically determined heat of fusion, is essential. Beckmann,² Olivari,³ and Jander and

(1) Part II in the series: "Structure of Molten Mercuric Halides." This work was made possible in part by support received from the U. S. Air Force, Air Research and Development Command, Office of Scientific Research, under Contract No. AF-49(638)-50.

(2) E. Beckmann, *Z. anorg. Chem.*, **55**, 175 (1909).

(3) F. Olivari, *Atti Accad. Lincei*, **211**, 718 (1912).

TABLE I
HEAT EVOLVED BY MERCURIC BROMIDE IN COOLING FROM INITIAL TEMPERATURE TO 300°K.

Temp. rise calorimeter	Total	Heat evolved (cal.)		HgBr ₂ (1 mole)	Final temp. (°K.)	Enthalpy change, (cal./mole)		Initial temp. (°K.)
		Capsule alone	Sample ^a only			Cor. to 300°K.	H _T - H ₃₀₀	
2.11	1141.81	124.59	1017.22	9106.71	298.8	-23.41	9083.30	533.4
2.00	1082.28	116.86	965.42	8642.97	301.5	29.27	8672.24	522.3
1.48	800.80	111.11	689.71	6174.66	303.9	76.09	6250.75	513.9
1.99	1076.87	112.83	964.04	8630.62	303.4	64.38	8695.00	516.6
1.00	541.14	106.24	434.90	3893.46	301.5	29.27	3922.97	502.5
1.04	562.79	108.92	453.87	4063.29	302.6	50.73	4114.02	507.4
1.00	541.14	102.43	438.71	3927.57	302.4	46.82	3974.39	496.3
0.93	503.26	98.13	405.13	3626.95	301.5	29.27	3656.22	487.4
2.03	1098.51	120.82	977.61	8752.82	298.6	-23.41	8729.41	526.8
2.16	1168.86	129.27	1039.57	9306.80	300.3	5.85	9312.65	544.1

^a 40.2528 g. HgBr₂.

Brodersen⁴ reported values of 5010, 4617, and 5010 cal./mole, respectively, for the heat of fusion derived cryoscopically. Kelley^{5a} derived a value of 4020 cal./mole from the available phase diagram data in the literature. A second value, from an analysis of the available vapor pressure data, 3960 cal./mole, was recommended by Kelley^{5b} as the best value for the heat of fusion. One value for mercuric bromide obtained calorimetrically,⁶ 4614 cal./mole, differs from the above best value but insufficient information is given in this early study to account for the discrepancy. The present note reports a redetermination of the heat of fusion by the method of drop calorimetry.

Experimental

Heat of Fusion Apparatus and Accessories.—The calorimetric assembly designed to yield results with an accuracy of $\pm 2\%$ for heats of fusion in the range 2–4 kcal./mole, and the recording differential potentiometer for the temperature–time measurements were the same as described elsewhere in detail.^{7,8} For salts for which the vapor pressure is appreciable at the fusion temperature, e.g., HgBr₂, 105 mm., some modification of the platinum capsule design is necessary so that the sample can be hermetically sealed in the capsule without loss due to volatilization. It was found that a small platinum tube, 5 cm. long \times 3 mm. diameter, welded to the lid of the crucible to serve as a filling tube, proved adequate. With the modified lid soldered to the empty crucible, the sample was loaded conveniently through the platinum chimney tube, after which the upper end of the “chimney” was crimped shut and welded to give the sealed system required for the calorimetric measurements. Sample evaporation in the latter operation was prevented by cooling the “chimney” with wet cotton wool.

Mercuric Bromide.—The mercuric bromide (reagent grade) was purified by vacuum drying and resublimations as described elsewhere.⁹ The reproducibility and sharpness of the melting point, $238.1 \pm 0.1^\circ$, were taken as criteria of purity.

Results

The procedure for calibration of the calorimeter and measurement of the heat of fusion have been adequately described elsewhere.^{7,8} The data and results for a series of 10 determinations over the temperature range 210–360° to establish the en-

thalpy change for HgBr₂ above and below the melting point are summarized in Table I. The analysis of the data followed the calculations described elsewhere for the LiCl–KCl eutectic.¹⁰ From a graph of the enthalpy change *versus* temperature, the heat of fusion of HgBr₂ at its melting point (238.1°) is found to be 4280 ± 80 cal./mole from these data.

Discussion

From the heat of fusion found in the present study, 4280 ± 80 cal./mole, the values 8.4 e.u. and 32.8 deg. mole⁻¹ 1000 g.⁻¹ are found for the entropy of fusion and cryoscopic constant for HgBr₂. Insufficient details are given in the early calorimetric work of Guinchant⁶ to resolve the sources of error leading to the higher value 4.7 kcal./mole for the heat of fusion. The values based on earlier cryoscopic studies^{2–4} are indirectly derived. Organic solutes were used in the cryoscopic measurements so that some of the scatter in the values may possibly be attributed to impurities formed by thermal decompositions which may be initiated by prolonged heating of organic compounds in this temperature range. The U. S. National Bureau of Standards best value,¹¹ 3.96 kcal./mole, is based on Kelley's analysis⁵ of vapor pressure data. It would appear from the present work that the latter value, also based on an indirect method, is approximately 15% too low. The present value, 4280 ± 80 cal./mole, is recommended for adoption as the most reliable value for this parameter, being derived from direct calorimetric experiments.

Acknowledgment.—Active participation in the early phases of this work and continued interest by Cyril Solomons is gratefully acknowledged.

(10) C. Solomons, J. Goodkin, H. J. Gardner and G. J. Janz, *THIS JOURNAL*, **62**, 248 (1958).

(11) U. S. National Bureau of Standards, Circular 500, Washington, 1952.

CHEMICAL REACTIONS OF ACTIVE NITROGEN

BY HAROLD A. DEWHURST

Research Laboratory, General Electric Company, Schenectady, New York
Received April 30, 1959

The chemical reactions of active nitrogen with hydrocarbons have been studied extensively by

(4) G. Jander and K. Brodersen, *Z. anorg. allgem. Chem.*, **264**, 57 (1951).

(5) (a) K. K. Kelley, U. S. Bur. Mines Bull. 393, Washington, 1936; (b) *ibid.*, 383, Washington, 1935.

(6) M. Guinchant, *Comp. rend.*, **149**, 479 (1909).

(7) J. Goodkin, C. Solomons and G. J. Janz, *Rev. Sci. Instr.*, **29**, 105 (1958).

(8) C. Solomons and G. J. Janz, *Anal. Chem.*, **30**, 623 (1959).

(9) G. J. Janz and J. D. E. McIntyre, *Proc. N. Y. Acad. Sci.*, Conference on Molten Salts (1959).

Winkler and co-workers.¹ In general it was found that hydrogen cyanide was the major product of the active nitrogen reaction and the only one that contained nitrogen. Because of this they postulated that nitrogen atoms do not attack hydrocarbons by hydrogen atom abstraction but rather by a direct approach to the carbon atom. We have recently studied the reactions of active nitrogen with silanes and hydrocarbons and have found that significant quantities of ammonia are formed.

Experimental

The active nitrogen was produced by a condensed discharge using the apparatus described by Winkler and co-workers.² The discharge tube and reaction vessel were not poisoned. Purified Linde nitrogen was passed through a liquid nitrogen trap and then directly to the discharge tube. The nitrogen flow rate was maintained constant at 1.2×10^{-5} mole/sec. which corresponded to a pressure of 1.2 mm. The reactant flow rate was determined by pressure decrease in a calibrated volume.

The following hydrocarbons were used: purified *n*-hexane,³ Phillips research grade cyclohexane and benzene, and Phillips pure grade neopentane. The methylamine and ethylamine were Matheson C.P. and the tetramethylsilane was Dow Corning purified grade.

The amount of hydrogen cyanide formed was determined by gas liquid partition chromatography using a calibrated 2-meter didecyl phthalate column. Ammonia was identified by its characteristic infrared spectrum and determined quantitatively by its absorption at 968 cm^{-1} . Acetylene and ethylene were determined by infrared absorption at 725 and 946 cm^{-1} , respectively. Other products were studied by gas-liquid chromatography using a tetraisobutylene column.

Results and Discussion

The details of the active nitrogen reactions are given in Table I. In all cases it was found that ammonia was a significant reaction product. With neopentane and tetramethylsilane the ratio of ammonia to hydrogen cyanide was approximately 20 and 40%, respectively. The neopentane results, with the exception of the ammonia formation, are in good agreement with the results of Onyszczuk and Winkler.⁴ The reaction of active nitrogen with tetramethylsilane produced a solid deposit on the walls of the reaction vessel. Infrared examination of the deposit indicated the presence of Si-N and Si-C bonds. It is of interest that the ratio of hydrogen cyanide from neopentane and tetramethylsilane is approximately the ratio of the carbon atoms in each molecule.

The reactions with hexane, cyclohexane and benzene at high temperature and high flow rates produced approximately the same yield of hydrogen cyanide and ammonia. In addition appreciable quantities of C_2 , C_3 and C_4 products were obtained with hexane and cyclohexane whereas with benzene apparently only C_2 and C_4 products were formed. The C_4 product results for benzene shown in Table I were obtained by gas chromatography with a didecyl phthalate column. The hydrocarbon product identifications were based entirely on retention time data and therefore can only be considered as tentative identifications. After warm-up of the liquid nitrogen condensable prod-

ucts from the benzene reaction, a dark brown unidentified material was deposited.

TABLE I
ACTIVE NITROGEN REACTIONS

Reactant	Flow rate, $\times 10^7$, moles/sec.	Temp., °C.	Products					
			HCN	NH ₃	C ₂ H ₂	C ₂ H ₄	C ₃	C ₄
(CH ₃) ₄ C	40	28	1.6	0.32	0.17
	25	250	4.5	.90	0.30
(CH ₃) ₄ Si	11	28	0.7	.35
	10	250	3.2	1.2
<i>n</i> -C ₆ H ₁₄	10.2	250	4.9	1.0	1.0	1.4	0.5	0.3
<i>c</i> -C ₆ H ₁₂	14.2	250	5.8	0.7	0.6	1.5	0.5	0.3
C ₆ H ₆	14	250	4.9	0.9	1.2	0	0	(2.3)
CH ₃ NH ₂	15.5	250	5.3	4.7	0	0	0	0
C ₂ H ₅ NH ₂	3.3	250	2.0	1.3	0.35	0.11

The reaction with methylamine produced approximately equal amounts of hydrogen cyanide and ammonia. The amount of hydrogen cyanide formed was equal to the amount of methylamine reacted. Freeman and Winkler⁵ have reported that the ammonia formed is about 25% of the hydrogen cyanide formed. The reason for this discrepancy is not apparent. In the ethylamine reaction the ratio of ammonia formed to hydrogen cyanide formed was almost one-half. Small amounts of acetylene and ethylene were also formed.

The formation of significant amounts of ammonia in the reaction between active nitrogen and hydrocarbons has not been reported heretofore. It appears unlikely that ammonia is formed by a series of hydrogen atom abstraction reactions since, in the first step, imine radicals are formed which very likely disproportionate to hydrogen and nitrogen. It is also known that for hydrocarbons the first step is appreciably endothermic.¹ The combination of nitrogen atoms with hydrogen atoms is known to produce ammonia,⁶ and it is conceivable that such a mechanism could account for the ammonia observed in the active nitrogen reactions. The unified mechanism proposed by Winkler and co-workers can be adapted to account for the ammonia formation by postulating that a given fraction of the nitrogen atom-reactant complexes decompose either to an amine radical or directly to ammonia.

The author is indebted to R. S. McDonald for considerable assistance with the infrared assignments.

(5) G. R. Freeman and C. A. Winkler, *ibid.*, **59**, 780 (1955).

(6) B. Lewis, *J. Am. Chem. Soc.*, **50**, 27 (1928).

FLUID PHASES IN MUTUAL CONTACT: FURTHER EXPERIMENTAL CONSIDERATIONS

By WILLIAM FOX¹

657 Oakland Avenue, Staten Island, N. Y.

Received February 26, 1959

Presented in this communication are some fundamental physical facts regarding fluid phases in mutual contact and a description of experimental approaches which will be extended to yield a new method for the determination of absolute values of

(1) H. G. V. Evans, G. R. Freeman and C. A. Winkler, *Can. J. Chem.*, **34**, 1271 (1956).

(2) P. A. Gartaganis and C. A. Winkler, *ibid.*, **34**, 1457 (1956).

(3) H. A. Dewhurst, *THIS JOURNAL*, **62**, 15 (1958).

(4) M. Onyszczuk and C. A. Winkler, *ibid.*, **59**, 368 (1955).

(1) Faculty of Police Science, Baruch School, City College of New York, New York, N. Y. Police Department, City of New York.

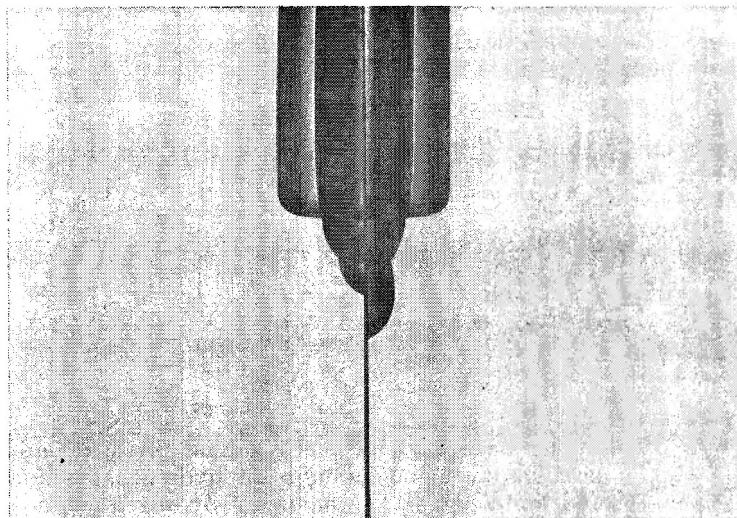


Fig. 1.

the tensions of fluid interfaces. Methods for the direct determination of relative values already have been presented.^{2,3}

Figure 1 demonstrates the case where varying masses of methylene iodide were brought into contact with the same column of air projecting into the aqueous phase. Each half of the photographic plate was exposed with a different mass of methylene iodide suspended on the same column of air. All the phases were mutually saturated. The methylene iodide had been distilled under reduced pressure and the water distilled from a block tin system. The temperature was 25°.

By directly superimposing the photographed images on another plate (*i.e.*, plate 1, Fig. 2),³ it was determined with good precision that the angle through the aqueous phase at the edge of common contact was the same in each case.

From Fig. 1 it is apparent that the magnitude of the force that can act to hold the methylene iodide on the gas phase, after equilibrium with respect to the interfaces has been established, must be at least equal to the gravitational force due to the mass of methylene iodide suspended under the conditions depicted in the right half of Fig. 1. It can therefore be concluded that the gravitational force due to the mass of methylene iodide suspended under the conditions depicted in the left half of Fig. 1 must be less than the total force that can hold it on the gas phase. It is evident from Fig. 1 that the difference between the gravitational forces due to the different masses of methylene iodide suspended in each case cannot be accounted for by the difference between the lengths of the circumferences of mutual contact.

From these experiments we may conclude that *equilibrium between the gravitational force and the force that can act to hold one fluid phase on another in the presence of a third fluid phase, after equilibrium with respect to the interfaces has been established, is not a necessary condition for equilibrium with respect to the interfaces.*

Since the gravitational force due to the mass of methylene iodide suspended in the left half of Fig. 1

must be less than the force that can hold it on the gas phase we can also conclude that the "excess" final edge force is balanced all around the circumference of contact. It is significant to note that even under the influence of the "excess" edge force the smaller drop of methylene iodide does not become extended over the gas phase but remains in a position that gives the constant, reliable, reproducible angle characteristic of the system under investigation.

These experiments also lead to an understanding of the necessary requirements for the determination of the linear force intensity, dF/dL , along the massless circumference of mutual contact, after equilibrium with respect to the interfaces has been established.

The mass of fluid phase suspended must be increased until the maximum mass that can be suspended along the circumference of mutual contact is determined. The determination of this mass and the length of the circumference of common contact will give the linear force constant operative.

The magnitude of this linear force constant can be related to the linear force constants of the interfaces concerned and thus give a new independent method for the determination of the absolute value of the tension that is manifested at the boundary limit (the edge) of each of the interfaces.

Acknowledgments.—The author wishes to thank his wife, who carefully reviewed the manuscript, and Professor Arthur W. Thomas of Columbia University, who stimulated and encouraged this research.

KINETICS OF CONSECUTIVE COMPETITIVE SECOND-ORDER REACTIONS

By P. R. WELLS¹

College of Technology and Commerce, Leicester, England

Received March 23, 1959

Due to the complex nature of the mathematical expressions obtained most treatments of consecutive competitive second-order reactions lack generality since simplifying conditions² or approximations³ are employed. The following treatment is general as far as equation 8 and is essentially equivalent to those due to Higgins and Williams,⁴ to Frost and Schwemer,⁵ to McMillan⁶ and to Riggs,⁷ but yields an expression more suitable for the present purpose

(1) Iowa State College, Ames, Iowa, U.S.A.

(2) Cf. Jen-Yuan Chien, *J. Am. Chem. Soc.*, **70**, 2256 (1948); M. Talat-Erben, *J. Chem. Phys.*, **26**, 75 (1957).

(3) Cf. C. K. Ingold, *J. Chem. Soc.*, 2170 (1931); F. H. Westheimer, W. A. Jones and R. A. Lad, *J. Chem. Phys.*, **10**, 478 (1942).

(4) H. G. Higgins and E. J. Williams, *Aust. J. Sci. Res.*, **A5**, 572 (1952).

(5) A. A. Frost and W. C. Schwemer, *J. Am. Chem. Soc.*, **74**, 1268 (1952).

(6) W. H. McMillan, *ibid.*, **79**, 4838 (1957).

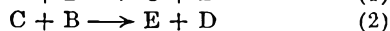
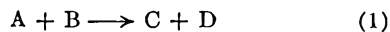
(7) N. V. Riggs, *Aust. J. Chem.*, **11**, 86 (1958).

(2) W. Fox, *J. Chem. Phys.*, **10**, 623 (1942).

(3) W. Fox, *J. Am. Chem. Soc.*, **67**, 700 (1945).

than those due to Wideqvist⁸ and to French.⁹ It is however specifically designed thereafter for the study of product composition in the case where equal equivalents of A and B are present initially.

Reaction equations 1 and 2 below



in which C and E are the products of mono- and disubstitution, respectively, lead to the differential equation

$$\frac{dE}{dt} = k_2CB \quad (3)$$

$$\frac{d(C + E)}{dt} = k_1AB \quad (4)$$

Division of (3) by (4), (elimination of t), gives

$$\frac{dE}{d(C + E)} = \frac{k_2C}{k_1A} \quad (5)$$

Making the substitutions

$$A/A_0 = a; C/A_0 = x; E/A_0 = y; x + y = z; k_2/k_1 = k$$

where the subscript 0 refers to initial concentrations, (5) becomes

$$\frac{dy}{dz} = \frac{k(z - y)}{(1 - z)} \quad (6)$$

Solution of equation 6 with the condition that $y = z = 0$ at $t = 0$ yields

$$y = 1 + \frac{k(1 - z)}{(1 - k)} - \frac{(1 - z)^k}{(1 - k)} \quad (7)$$

or

$$= 1 + \frac{ka}{(1 - k)} - \frac{a^k}{(1 - k)} \quad (8)$$

By stoichiometry, at any time

$$B_0 - B = A_0 - A + E \quad (9)$$

If $A_0 = B_0$, as in the special case under discussion, then at completion, *i.e.*, $B = 0$

$$A = E, \text{ i.e., } a = y \quad (10)$$

Hence (8) becomes

$$y^k + y(1 - 2k) \div k - 1 = 0 \quad (11)$$

Graphical solution of equation 11 gives the following values

y	k	k_1/k_2
0.01	<0.0033	>300
.02	.0067	150
.03	.0125	80
.05	.0250	40
.10	.0765	13
.25	.50	2
.32 ^a	1.0	1
.38	2.0	0.5
.45	5.5	0.2
.49	25	0.04
.495	50	0.01

^a Solution of equation 6 for $k = 1$ under the above conditions yields $\log_e y = 2 - 1/y$ which can be solved numerically for y .

Thus in order that the reaction product shall contain less than 1% of disubstitution product, the specific rate constant of the first substitution must

be greater than that of the second by at least a factor of 300, and if more than a third of the product is composed of disubstitution product then k_2 must be greater than k_1 .

It follows from these results that where one, or less than one, equivalent of a substituting reagent leads to a mixture of unchanged substrate and disubstitution product in which no monosubstitution product can be detected, as in the case of the bromination of substituted 1-naphthylamines,¹⁰ that the specific rate constant for the second substitution must exceed that of the first. Thus in the present case, since the first introduced bromo-substituent will deactivate the nucleus toward electrophilic substitution, it must be concluded that the second stage, if not the first also, cannot be a normal electrophilic substitution. The mechanistic significance of this conclusion will be discussed in a later communication.

(10) Cf. H. H. Hodgson and D. Hatbaway, *J. Chem. Soc.*, 21 (1944); H. H. Hodgson and R. Dean, *ibid.*, 822 (1950); A. Hardy, E. R. Ward and L. A. Day, *ibid.*, 1979 (1956); E. R. Ward and P. R. Wells, unpublished work.

RHODIUM(III) IN AQUEOUS SOLUTIONS

BY J. S. FORRESTER¹ AND G. H. AYRES

Contribution from the Analytical Research Laboratory of the University of Texas

Received April 4, 1959

Trivalent rhodium has strong complex-forming properties similar to chromium and cobalt. This fact explains the wealth of apparently uncorrelated facts reported for the behavior of rhodium salts in solution. Grube and Kesting² titrated solutions made by dissolving $Rh(OH)_3$ in perchloric acid; results indicated the formation of a complex, $Rh(OH)_2^+$. Perchloric acid solutions of rhodium prepared from rhodium hydroxide also have been investigated by electrophoresis and ion-exchange chromatography. Schukla³ recently has reported on these studies and postulated the existence of $Rh(H_2O)_6^{+++}$.

The preparation and X-ray powder data for solid rhodium perchlorate hexahydrate have previously been published by Ayres and Forrester.⁴ Using this salt as a starting material, aqueous solutions of rhodium(III) have now been studied under conditions relatively free from complexation.

In order to assure solutions of maximum purity, large crystals of rhodium perchlorate were dissolved in triple distilled, deaerated water. As the quantity of stock solution prepared in this manner was limited, it was decided to combine the data from three different experimental methods; potentiometric, conductimetric and spectrophotometric measurements were made on each sample.

A stock solution of rhodium(III) perchlorate, 0.00728 M , was prepared and the spectral curve recorded. This curve shows absorption maxima at 300 $m\mu$ ($a_m = 69$ g. moles⁻¹ cm.²) and 395 $m\mu$ ($a_m = 62$ g. moles⁻¹ cm.²). A 5.0-ml. aliquot of this stock solution was diluted with 25.0 ml. of water and titrated potentiometrically with 0.0316 N sodium hydroxide. After the end-point was reached, a reverse titra-

(1) Esso Research Laboratories, Esso Standard Oil Company, Baton Rouge, La.

(2) G. Grube and E. Kesting, *Z. Elektrochem.*, **39**, 955 (1933).

(3) S. K. Schukla, *J. Chromatography*, **1**, 457 (1958).

(4) G. H. Ayres and J. S. Forrester, *J. Inorg. Nucl. Chem.*, **3**, 365 (1957).

(8) S. Wideqvist, *Acta Chem. Scand.*, **4**, 1216 (1953).

(9) D. French, *J. Am. Chem. Soc.*, **72**, 4806 (1950).

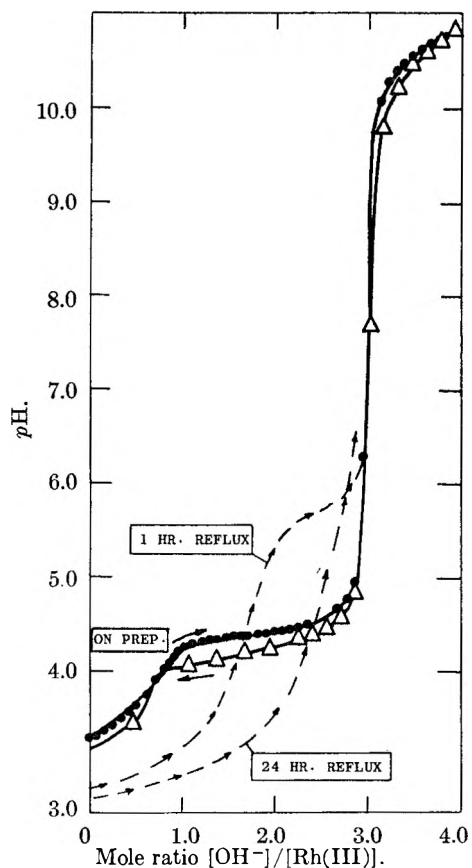
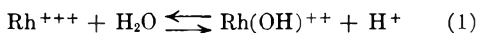


Fig. 1.—Potentiometric titrations of rhodium perchlorate.

tion was made with 0.0544 *N* perchloric acid. This last titration served to check the reversibility of the hydrolysis of the rhodium cation. A conductimetric titration then was made on an identical aliquot of the stock solution. Both titrations may be interpreted similarly.

Figure 1 illustrates the data of the potentiometric titration. The first of two changes in slope in the curve strongly suggests the titration of a hydrogen ion resulting from hydrolysis. Reaction (1) may be postulated



and from the initial *pH* of 3.29, the stability constant, *K*, for the $\text{Rh}(\text{OH})^{++}$ ion may be calculated as 3.7×10^{-4} .

Increasing the *pH* after the first end-point resulted in a turbid system. The hydrous oxide of rhodium was precipitated quantitatively when the molar ratio of hydroxyl to rhodium, $[\text{OH}^-]/[\text{Rh}^{+++}]$, reached three. This end-point was accompanied by a sharp change in the slope of the titration curve. For this reaction we may write

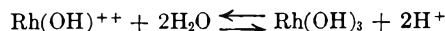


and calculate the solubility product constant for $\text{Rh}(\text{OH})_3$ ($K_{sp} = 4.8 \times 10^{-23}$).

The reversibility of the hydrolysis in the titration described previously is represented in Fig. 1 by the triangles. During these reverse titrations the hydrated rhodium showed a slight hysteresis effect as evidenced by slow attainment of equilibrium after the addition of increments of titrant. This effect appears graphically as a small displacement of the titration curves during the reverse titration. The hysteresis effect may also partially account for the displacement, along the absorbance axis, of the two spectrophotometric curves recorded before and after the titrations. In addition, this displacement is ascribed to the lower concentration of rhodium in solution and to the change in ionic strength; these effects result from addition of titrants used for the precipitation and redissolution.

Some observations were made on the state of the rhodium (III) ion after aging at room temperature and an elevated temperature. An examination of the spectral curves re-

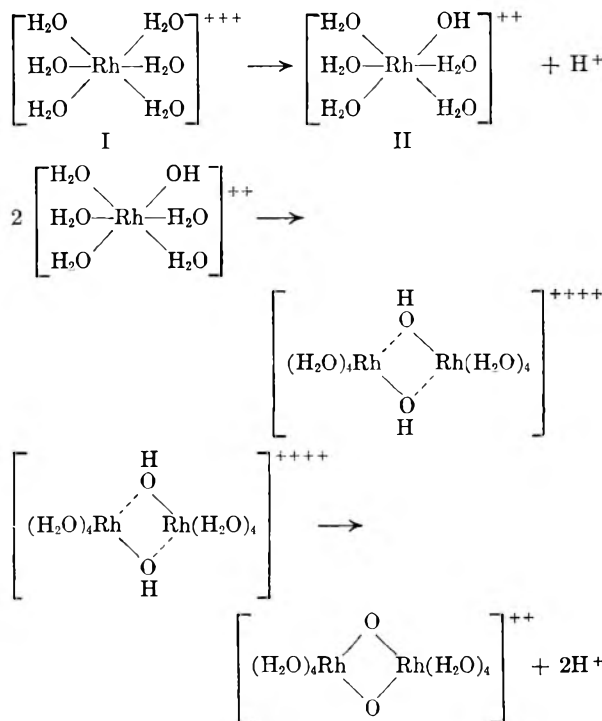
corded from the stock solution over a period of one week showed no noticeable change. Refluxing solutions for one hour and also for a 24-hour period caused pronounced changes in the spectral curves. Two solutions, refluxed for one hour and for 24 hours, respectively, also were titrated potentiometrically and conductimetrically by the procedures described previously. The dashed line in Fig. 1 again illustrates the results. The first break observed in the titration curves of freshly prepared solutions has shifted; the second break is unchanged. The formation of hydrous rhodium (III) oxide was again indicated by a visible precipitate. At first, it appears that boiling resulted in further hydrolysis of the $\text{Rh}(\text{OH})^{++}$ ion according to the equation



However, the absence of a break at $[\text{OH}^-]/[\text{Rh}^{+++}] = 1$, in the curve for the reverse titration with perchloric acid (after previous titration with sodium hydroxide), indicates that the species $\text{Rh}(\text{OH})^{++}$ is not re-formed. It may be that some dimerization or other bridging has occurred; one possibility might be $2\text{Rh}(\text{OH})^{++} \rightarrow \text{Rh}-\text{O}-\text{Rh}^{++++} + \text{H}_2\text{O}$. However, the very marked decrease in *pH* after reflux of the solution is not compatible with this explanation. Photometric curves of the refluxed solutions show a loss of spectral details, suggesting the disappearance of a single species.

Discussion

Extensive hydration and possible bridging phenomena prevent clearly defined interpretation of experimental results. Although there is good evidence for the formation of the $\text{Rh}(\text{OH})^{++}$ species, the results are not conclusive. In the titration of freshly prepared rhodium perchlorate solution with sodium hydroxide, the appearance of the first inflection point (Fig. 1) somewhat below a $[\text{OH}^-]/[\text{Rh}^{+++}]$ ratio of 1 suggests the possible formation of a dimer or even a trimer. Such a species could add more hydroxy groups for a final formation of the hydrous oxide. One might suggest the reactions



Similar species have been suggested recently for iron(III) by Hedstrom⁵ and Mulay.⁶

(5) B. O. A. Hedstrom, *Ark. Kemi*, **6**, 1 (1953).

(6) L. N. Mulay and P. W. Selwood, *J. Am. Chem. Soc.*, **77**, 2693 (1955).

The existence of a $\text{Rh}(\text{OH})^{++}$ species is contradictory to the findings of Grube and co-workers^{2,7} who postulated the formation of $\text{Rh}(\text{OH})_2\text{ClO}_4$ from titration of rhodium hydroxide with perchloric acid; no strong evidence for the $\text{Rh}(\text{OH})_2^+$ ion was found in the present study. A very slight irregularity in the titration curves of Fig. 2 and 3 may be observed at $[\text{OH}^-]/[\text{Rh}^{+++}]$ ratios of 2; however, these can hardly be noticed above the experimental scattering of the data. If $\text{Rh}(\text{OH})_2^+$ was present in the solutions, its concentration was negligible compared to the observed species.

Several strong indications for oxy or hydroxy bridges were evident during the study. In the preparation of rhodium perchlorate,⁴ extensive boiling of the solutions ultimately led to a color change from light yellow to dark brown. Crystals of rhodium perchlorate hexahydrate could not be isolated from the darkened solution. If, however, these solutions were refluxed with hydrochloric acid and the rhodium was reconverted to the chloro complex, the latter could again be destroyed with perchloric acid and the perchlorate salt recovered as rhodium(III) perchlorate hexahydrate.

(7) G. Grube and H. Autenrieth, *Z. Elektrochem.*, **44**, 296 (1938).

MOLYBDENUM DISULFIDE OF HIGH SURFACE AREA

By FRANK T. EGGERTSEN AND RICHARD M. ROBERTS

Shell Development Company, Emeryville, California

Received April 18, 1959

The surface area of molybdenum disulfide made from molybdenum trisulfide by reduction with hydrogen, or by thermal decomposition, was found to be strongly dependent on conditions of reaction. Rapid conversion of trisulfide to disulfide at 450° resulted in molybdenum disulfide of unusually high surface area, in some cases as high as 158 m.²/g., while slow conversion gave surface areas as low as 2 m.²/g.

The experiments described below were all carried out with a single preparation of molybdenum trisulfide made by a method similar to that of Yagoda and Fales.¹ A 5% solution of ammonium molybdate (81% MoO_3) at 0° was added to ten times its volume of water previously saturated with hydrogen sulfide at 0°. The resulting thiomolybdate solution, still at 0°, was acidified with 90% formic acid to a final pH of 3.0. The black sol thus formed was coagulated by heating to 50°. The mixture was digested at 50° for 30 minutes and allowed to stand overnight at room temperature. The coagulum was decanted and washed twice by decantation with 5% formic acid. It then was separated by filtration and washed on the filter with 5% formic acid and 95% ethanol. Finally, it was dried *in vacuo* for 16 hours at room temperature and 5 hours at 150°. The dried trisulfide contained 0.9% oxygen,² and had a black, glassy appearance and a conchoidal fracture. The surface area as determined by the B. E. T. method with krypton was less than 0.1 m.²/g. for a sample which was outgassed at 100°, and was 1 m.²/g. when the trisulfide was decomposed slowly by outgassing while heating to a final temperature of 500°.

Samples of this material in amounts of 0.03 to 10 g. were reduced with hydrogen while heating at 20° per minute to a final temperature of 450°. The surface area of the reduced material was found to depend greatly upon sample size.

(1) H. Yagoda and H. A. Fales, *J. Am. Chem. Soc.*, **53**, 1496 (1936).

(2) F. T. Eggertsen and R. M. Roberts, *Anal. Chem.*, **22**, 924 (1950).

Higher areas were in general obtained with larger samples. With the largest samples (10 g. or more) a fast exothermic reaction started at 350° and the temperature in the solid mass rose quickly above 400° for a brief period. It appeared that this temperature runaway was related to the surface area variations, probably because of effects on rate of reduction. It seemed likely that the temperature in small samples (0.1 g. or less) remained nearly the same as that of the hydrogen during heating and that the rate of reduction was therefore slower.

A number of experiments are described below in which the rate of reduction of small samples was controlled and varied; results are shown in Table I. The reduction was carried out in a 5-ml. glass cell having a sintered glass plate to support the sample. The same cell was employed as the adsorption cell for B. E. T. measurement of the surface area.

TABLE I

SURFACE AREAS OF MoS_2 PREPARED FROM MoS_3
Gas flow rate, 5 ml. per min., atmospheric pressure; outgassing temp. for area measurements, 500°; 30 mg. MoS_3 (< 20 mesh)

Gas	Rate of heating ^a	Final temp., °C.	Surface area, m. ² /g.
..	Untreated trisulfide	..	<0.1 (outgassed at 100°)
H ₂	Fast	450	85, 135, 158
H ₂	Slow	450	2
H ₂	Fast	400	1
H ₂	Fast	575	22
H ₂	10 min. at 300°, then dropped into H ₂ stream at 450°		31
He	Fast	450	98
He	Slow	450	4

^a Slow reduction: The sample was heated in a stream of hydrogen from room temperature to the final temperature in 25 minutes, and was held at that temperature in flowing hydrogen for two hours. Fast reduction: The sample, in a hydrogen atmosphere at room temperature, was suddenly dropped into a stream of hydrogen at the temperature shown, and was held at that temperature in flowing hydrogen for two hours.

The following points emerge from Table I.

1. Fast reduction in hydrogen at 450° produced a high surface area, while slow reduction at that temperature did not.

2. There is apparently an optimum temperature for carrying out fast reduction. Lower surface areas were obtained on rapid reduction at 575 and 400 than at 450°. Furthermore, heating at 300° in hydrogen for ten minutes, prior to rapid heating at 450°, gave a lower surface area than the 450° treatment alone. The existence of an optimum temperature implies competition between two rates: that of nucleation of MoS_2 and that of sintering of MoS_2 crystals after formation.

3. Molybdenum disulfide of high surface area also resulted from fast thermal decomposition of the trisulfide in helium at 450°.

The structure of molybdenum trisulfide has not been reported. Molybdenum disulfide has a layer structure, with weak forces between layers.³ Our sample of molybdenum trisulfide was examined by X-ray diffraction and was found to be amorphous; there were four or five broad, diffuse bands in the powder photograph. On conversion to disulfide a number of lines appeared: the first corresponded to a spacing of 11–18Å., the second (which was dif-

(3) A. F. Wells, "Structural Inorganic Chemistry," Oxford University Press, Oxford, 2nd Ed., 1950, p. 115.

fuse) to 6.5–7 Å. A faint third line was more intense in the disulfide samples of low surface area. The powder patterns of the present disulfide samples all had far fewer lines than that of molybdenite.

It was observed in the present experiments that the reduction of the trisulfide with hydrogen at about 350° was quite exothermic. From data in the literature, this reaction should be slightly endothermic at 25°, and should become slightly exothermic at higher temperatures.⁴ However, the heat of formation recorded for MoS₃(s), $\Delta H_{298.1} = -61.5$ kcal., is probably incorrect. This datum is derived from measurements of sulfur pressure over molybdenum trisulfide, under the assumption that sulfur was in equilibrium with the disulfide and trisulfide.⁵ More recently Biltz and Köcher have shown that the trisulfide is completely unstable with respect to the disulfide and sulfur, and the two sulfides are unable to exist in equilibrium.⁶ We think it probable that decomposition of the trisulfide into disulfide and sulfur is markedly exothermic.

Samoilov and Rubinshtein⁷ studied the removal of sulfur from a preparation with the empirical formula WS_{2.30} which had been obtained by partial reduction of ammonium thiotungstate in hydrogen at 400°, and had a surface area of 3 m.²/g. A progressive increase in surface area was observed on heating *in vacuo* at 200, 300 and 400°, to 19, 59 and 66 m.²/g., respectively. Surface areas on heating the preparation in nitrogen at 600, 750 and 1000° were 54, 23, and 3 m.²/g., respectively. These authors did not give details of procedure and the heating schedule, but it appears likely that the surface area of tungsten disulfide would depend on the rate of conversion of tungsten trisulfide to disulfide, since tungsten disulfide also forms a layer structure similar to that of molybdenum disulfide.

We wish to thank A. E. Smith for the results of X-ray diffraction studies and S. G. Balestrieri and B. P. Summerer for experimental assistance.

(4) K. K. Kelley, "Contributions to the Data on Theoretical Metallurgy. VII. The Thermodynamic Properties of Sulfur and Its Inorganic Compounds," U. S. Bureau of Mines Bulletin 406, U. S. Govt. Printing Off., Washington, 1937, pp. 54, 55.

(5) N. Parravano and G. Malquori, *Atti accad. Lincei*, [6] **7**, 19 (1928).

(6) W. Biltz and A. Köcher, *Z. anorg. allgem. Chem.*, **248**, 172 (1941).

(7) S. M. Samoilov and A. M. Rubinshtein, *Izvest. Akad. Nauk S.S.S.R., Otdel. Khim. Nauk*, 1158 (1957); *Bull. Acad. Sciences (USSR)*, Div. of Chem. Science (Eng. Trans.), 1185 (1957).

DEFINITION OF THE DIFFERENTIAL REACTION RATE IN AMMONIA SYNTHESIS KINETICS

By ROBERT B. ANDERSON^{1a} AND HERBERT L. TOOR^{1b}

Contribution from the Central Experiment Station, U. S. Department of the Interior, Bureau of Mines, Pittsburgh 13, Penna.

Received April 25, 1969

In ammonia synthesis kinetics the differential reaction rate has been defined in at least three

(1) (a) Branch of Coal-to-Oil Research, Bureau of Mines, Region V, 4800 Forbes Ave., Pittsburgh, Pa.; (b) Department of Chemical Engineering, Carnegie Institute of Technology, Pittsburgh 13, Pa.

ways as shown in equation 1 with $n = 1, 2$ or 3, where r is

$$r = [1/273R(1 + a)^n] da/d(1/S_0) \quad (1)$$

given as moles NH₃ produced per cc. of catalyst per hour, a the mole fraction of NH₃ at the outlet, and S_0 the inlet space velocity in volumes (S.T.P.) of feed gas per volume of catalyst space per hour. In some cases other quantities such as fraction of voids in the catalyst bed and absolute temperature are also introduced into the expression for differential reaction rate. The present paper asserts that equation 1 with $n = 2$, as derived by Uchida and Kuraishi² by the flow balance method,³ is correct. Other expressions for differential reaction rate are examined.

In the flow balance method³ for the ammonia synthesis

$$r = (1/2 \times 273R) dx/d(1/S_0) \quad (2)$$

where x is the conversion of feed, expressed as moles of N₂ + H₂ consumed per mole of feed. By substituting $x = 2a/(1 + a)$ the equation in terms of mole fraction of ammonia a is

$$r = [1/273R(1 + a)^2] da/d(1/S_0) \quad (3)$$

the equation of Uchida and Kuraishi.²

Before considering other equations, the differential reaction rate must be defined; this may be given as

$$r = (1/V_c)(dn_i/dt) \quad (4)$$

where n_i is the number of moles of species i reacted or produced in time t , per bulk volume, V_c , of catalyst.⁴ The term n_i may refer to total feed or one or more components of feed or product; however, this definition should be such as to provide a satisfactory measure of the forward progress of the reaction. For the ammonia synthesis the rate may be expressed in terms of moles of ammonia produced or moles of H₂, N₂ or N₂ + H₂ consumed.

Temkin and Pyzhev⁵ and Bokhoven, *et al.*,⁶ defined $r = dp_{\text{NH}_3}/dt$. It can be shown that $dp_{\text{NH}_3}/dt = \{(1/V_c) dn_i/dt\} RT(1 + a)^2/\phi$, where ϕ is the fraction of voids in the catalyst bed. This definition equals that of equation 4 multiplied by $RT(1 + a)^2/\phi$. Another error in the derivation of Temkin and Pyzhev, involving the subtleties of evaluating the differential reaction rate in terms of contact time, introduced an extra factor $(1 + a)$ in the denominator of the expression. The net result was equation 1 multiplied by RT/ϕ with $n = 1$.

Emmett and Kummer⁷ defined the differential

(2) H. Uchida and M. Kuraishi, *Bull. Chem. Soc. Japan*, **28**, 106 (1955); S. Kodama, K. Fukui and A. Mazume, *J. Chem. Soc. Japan (Ind. Chem. Sect.)*, **54**, 157 (1951).

(3) This method has been described by O. A. Hougen and K. M. Watson, "Chemical Process Principles," Part III, John Wiley and Sons, New York, N. Y., 1943, p. 962; *Ind. Eng. Chem.*, **35**, 529 (1943).

(4) Rate can also be defined per weight of catalyst or other extensive properties of the catalyst, if desired. As rate generally varies with position in a flow reactor, for r to be a point function, V_c must be considered to be of differential size.

(5) M. Temkin and V. Pyzhev, *Acta Physicochim. U.S.S.R.*, **12**, 327 (1940).

(6) C. Bokhoven, C. van Heerden, R. Westrick and P. Zwietering, "Catalysis," edited by P. H. Emmett, Vol. 3, Reinhold Publ. Corp., New York, N. Y., 1955, Chapter 7, pp. 325–333.

reaction rate correctly as given in equation 4, but made the same error as Temkin and Pyzhev in evaluating r by the contact time method. Emmett and Kummer obtained equation 1 with $n = 3$. Bokhoven⁶ obtained an equation similar to that of Emmett and Kummer, except that it is multiplied by RT/ϕ .

We will now show that equation 3 also results from a correct derivation in terms of contact time. The differential of contact time may be given as

$$dt = (\phi/Q')dV \quad (5)$$

where V is the volume of catalyst bed, ϕ the fraction of voids, and Q' the gas flow rate (volumes per unit time) in the increment dV at the temperature and pressure of the system. Volume dV may be taken as the catalyst space swept out in time dt by a plane that is normal to the mean flow direction and moving at the mean velocity of the gas. Then⁸

$$dt = \phi(273P/TQ)dV = \phi(Q_0/Q)(273P/TQ_0)dV \\ = \phi(1/z)(273P/T)d(1/S_0) \quad (6)$$

where Q and Q_0 are the gas flow rates under standard (S.T.P.) conditions in volume element dV and at the inlet of the bed, respectively, P is the system pressure in atmospheres, and $z = Q/Q_0$.

We now will follow a volume element of gas, occupying a volume of catalyst space dV_0 at the inlet of the bed, through the catalyst bed. If a volume change occurs, the volume of catalyst space occupied by the gaseous volume element will be $z dV_0$ after a conversion of feed x has occurred. The problem is then analogous to a variable-volume batch reactor operated at constant pressure, and the rate must be evaluated per unit volume of reactor space that is occupied. As conversion x is defined in terms of feed consumed, the change in number of moles dn_i is

$$dn_i = \phi N_i dV_0 dx = \phi(P/RT)dV_0 dx \quad (7)$$

where N_i is the moles of component i per unit volume of feed. The volume of the catalyst, $z dV_0$ (which is V_c), and the expressions for dn_i and dt are introduced into equation 4 to give

$$r = (1/V_c)dn_i/dt = (1/273R)dx/d(1/S_0) \quad (8)$$

where r is expressed as moles $H_2 + N_2$ consumed per unit volume per unit time. This expression leads directly to equations 2 and 3.

For other systems a more serious error that has been made occasionally with the contact-time approach involves using $r = dx/dt$, an expression that has the dimension time⁻¹. This definition does not agree with equation 4 and, when the system pressure is varied, has the effect of decreasing the dependence of rate on total pressure by a power of one.

Although when one considers kinetics in flowing systems for the first time the contact time approach seems familiar and obvious, the concept is difficult to formulate in terms of experimental parameters, even for relatively simple systems involving gaseous reactants and products.

(7) P. H. Emmett and J. T. Kummer, *Ind. Eng. Chem.*, **35**, 677 (1943).

(8) In these and subsequent transformations reactants and products are assumed to be ideal gases and the pressure drop through the bed is assumed to be negligible.

A generally applicable form of the equation of Hougen and Watson³ is

$$r_i = dx_i/d(W/F_i) \quad (9)$$

where x_i is the fractional conversion of reactant or reactants i , F_i is the feed rate of components designated by i in moles, S.T.P. volumes, or weight per unit time, and W is the bulk volume of catalyst or weight of catalyst. The units of r_i are those of the quantity F_i/W . The only requirement is that the components i provide an adequate measure of the forward progress of the process. Equation 9 can be used in diverse systems such as those involving liquid phases and ill-defined reactants such as broad distillation fractions of hydrocarbons. The equation is equally applicable to homogeneous reactions where W is the volume of the reactor.

Appendix.—A precise definition of differential reaction rate in terms of time may be obtained by writing equation 4 as

$$r = \phi \lim_{\Delta V \rightarrow 0} \frac{1}{\Delta V} \frac{d(C_i \Delta V)}{dt} \quad (10)$$

where C_i is the concentration of species i in the free space of bulk volume of catalyst ΔV . Replacing ΔV by $z \Delta V_0$ yields

$$r = (\phi/z)d(C_i z)/dt \quad (11)$$

Acknowledgment.—The authors are grateful to Professor P. H. Emmett for a helpful discussion and encouragement to publish this material. Professor Theodore Vermeulen also made valuable suggestions.

PHASE EQUILIBRIA OF THE BINARY SYSTEM $PuCl_3$ - KCl ¹

By ROBERT BENZ,² MILTON KAHN³ AND J. A. LEARY⁴

Contribution from the University of New Mexico, Albuquerque, New Mexico, and the Los Alamos Scientific Laboratory, Los Alamos, New Mexico

Received May 1, 1959

Interests in pyrometallurgical processing of reactor fuels have stimulated the need for physical properties of certain fused salt systems. In this paper the results of an analysis of cooling curves for $PuCl_3$ - KCl solutions at various compositions are reported.

Materials.—Plutonium(III) chloride was prepared from plutonium metal (99.9% pure) by reaction with hydrogen gas at 150° to form plutonium hydride; the hydride was subsequently converted to the chloride by reaction with hydrogen chloride at 350°. The product, plutonium(III) chloride, was vacuum distilled, cooled as large crystals and then stored in a vacuum desiccator. An analysis of the product yielded 69.14 ± 0.2% plutonium (theoretical, 69.22%) and 30.85 ± 0.5% chloride (theoretical, 30.78%). Granular potassium chloride (Mallinckrodt Analytical Reagent Grade) was dried, melted in a quartz container under an atmosphere of hydrogen chloride, cast into a stick

(1) Taken from a dissertation by R. Benz submitted in partial fulfillment of the requirements for the Degree of Doctor of Philosophy in Chemistry at the University of New Mexico.

(2) Presently on leave of absence from the Los Alamos Scientific Laboratory as a fellow at the Max Planck Institut für physikalische Chemie, Göttingen, Germany.

(3) Chemistry Department, University of New Mexico, Albuquerque, New Mexico.

(4) Los Alamos Scientific Laboratory, P. O. Box 1663, Los Alamos, New Mexico.

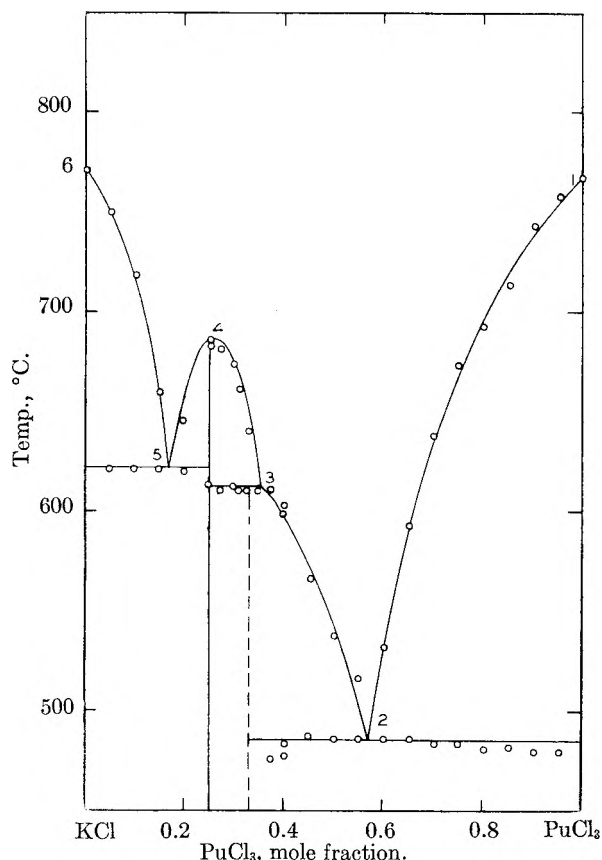


Fig. 1.—Phase diagram of the binary system PuCl_3 - KCl as determined by thermal analysis: (1) PuCl_3 melting point, $769 \pm 2^\circ$; (2) eutectic point, $486 \pm 3^\circ$ at PuCl_3 mole fraction 0.57; (3) peritectic point for the compound K_2PuCl_5 , $611 \pm 3^\circ$ at PuCl_3 mole fraction 0.35; (4) K_3PuCl_6 melting point, $685 \pm 3^\circ$; (5) eutectic point, $621 \pm 3^\circ$ at PuCl_3 mole fraction 0.17; (6) KCl melting point, $771 \pm 2^\circ$.

form by transferring the melt under vacuum into a Pyrex mold and stored in a vacuum desiccator. The melting point of the potassium chloride was determined to be $771 \pm 2^\circ$ in agreement with the reported value.⁵ Hydrogen chloride (Matheson Co.) and argon (Linde Air Products) were dried with phosphorus pentoxide.

Apparatus.—The melting chamber consisted of a 32 cm. long, 22 mm. diameter quartz test-tube with a Teflon stopper in which was mounted a 35 cm. long, 5 mm. quartz tube for the gas inlet and 35 cm. long, 3 mm. diameter quartz thermocouple well. The lower 20 cm. of the melting chamber was surrounded by graphite to ensure uniform temperatures.

A Pt-10% Rh thermocouple which checked within $\pm 0.4^\circ$ with the melting points of zinc and aluminum was employed for the temperature determinations. The thermocouple was provided with a plug-and-jack connection for the purpose of switching from a Honeywell 0-1650° recorder used to indicate the liquidus points to another thermocouple at 0° and a K-2 potentiometer used to measure the temperature at the stationary arrest points.

Procedure.—To begin an experiment the desired quantities (20 to 80 g. total) of salts in the melting chamber were melted and stirred with a stream of hydrogen chloride or argon gas. The thermocouple well projected to within 5 mm. of the bottom of the melting chamber and the volume of the solution was such that the thermocouple was immersed to a depth of 2.5 to 6.0 cm. After 0.5 hr. of stirring with the melt approximately 70° above the liquidus, the cooling curve was begun.

Although hydrogen chloride was employed in most of the experiments, identical cooling curves were obtained with argon. The accuracy of the temperature measurements at

the stationary arrest points was estimated to be within $\pm 2^\circ$. The compositions in mole fractions are based upon the weights of the added salts.

Results

The experimental results are summarized in Fig. 1. These data indicate the existence of the compound K_3PuCl_6 (melting point, $685 \pm 3^\circ$) and a second compound (peritectic point, $611 \pm 3^\circ$ at the plutonium(III) chloride mole fraction 0.35), possibly K_2PuCl_5 . The composition of the latter compound was chosen on the basis that it is the simplest compound consistent with the experimental data. The two eutectic points occur at the mole fractions 0.17 and 0.57 and the respective temperatures 621 ± 3 and $489 \pm 3^\circ$.

An attempt was made to isolate each of the two compounds by crystallization from the appropriate liquid melts. An optical study of the samples obtained in this manner indicated the presence of two different phases distinct from pure potassium chloride and pure plutonium(III) chloride.

Acknowledgments.—We wish to thank W. J. Maraman and R. D. Baker of the Los Alamos Scientific Laboratory for discussions and encouraging interests.

This work was done in the Los Alamos Scientific Laboratory. We are indebted to A. N. Morgan for the metallic plutonium, J. W. Anderson for the fabrication of the plutonium metal, C. F. Metz, G. R. Waterbury, C. T. Apel and L. A. Pulliam for chemical analyses and R. M. Douglas for inspection (optical and powder diffraction techniques) of crystals of the PuCl_3 - KCl compounds.

THE SOLUBILITY OF SILVER SULFATE IN ELECTROLYTE SOLUTIONS. PART 5. SOLUBILITY IN MAGNESIUM SULFATE SOLUTIONS¹

By M. H. LIETZKE AND R. W. STOUGHTON

Contribution from the Chemistry Division, Oak Ridge National Laboratory, Oak Ridge, Tenn.

Received June 18, 1959

Previous papers in this series have described the solubility of Ag_2SO_4 in KNO_3 ,² K_2SO_4 ,³ H_2SO_4 ⁴ and HNO_3 ⁵ solutions. It was shown in these papers that expressions of the Debye-Hückel type could be used to describe the solubility data in each system over a wide range of temperature and ionic strength. Since it seemed to be a logical extension of this solubility program to determine whether similar expressions could be used to describe the solubility of Ag_2SO_4 in polyvalent electrolyte solutions, a study has been made of the solubility of Ag_2SO_4 in 0.1, 0.5 and 1.0 *m* MgSO_4 solutions to above 150° . Again a high speed digital computer has been used in making the calculations.

(1) This paper is based upon work performed for the United States Atomic Energy Commission at the Oak Ridge National Laboratory operated by Union Carbide Corporation.

(2) M. H. Lietzke and R. W. Stoughton, *THIS JOURNAL*, **63**, 1183 (1959).

(3) M. H. Lietzke and R. W. Stoughton, *ibid.*, **63**, 1186 (1959).

(4) M. H. Lietzke and R. W. Stoughton, *ibid.*, **63**, 1188 (1959).

(5) M. H. Lietzke and R. W. Stoughton, *ibid.*, **63**, 1190 (1959).

(5) National Bureau of Standards Circular, Number 500, 1952, p. 804.

Experimental

The solubility measurements were carried out using the same technique described previously.⁶ As in the case of the KNO_3 and K_2SO_4 systems, it was fairly difficult to get a good reproducible set of data, since the solubility points were rather sluggish. The measurements were extended at each concentration of MgSO_4 to as high a temperature as possible. The upper limit was determined in each case by interference due to hydrolysis of both the Ag_2SO_4 and the MgSO_4 . It is believed, however, that the solubility data reported represent at least at the higher temperatures metastable solubility values for Ag_2SO_4 in MgSO_4 solutions, since the establishment of solubility equilibrium was more rapid than the onset of hydrolysis in the case of the points given. The measurements were reproducible to about $\pm 2^\circ$ in 0.1 *m* MgSO_4 , and to about $\pm 5^\circ$ in 0.5 and 1.0 *m* MgSO_4 solutions.

Results and Discussion

In Fig. 1 the circled points represent the experimentally observed solubilities of Ag_2SO_4 in H_2O and in 0.1, 0.5 and 1.0 *m* MgSO_4 solutions. The results in H_2O up to 100° were obtained from the work of Barre,⁷ while the values at the higher temperatures were reported in the first paper in this series.² The experimental solubility values of Ag_2SO_4 in the MgSO_4 solutions are given also in Table I.

TABLE I

THE SOLUBILITY OF Ag_2SO_4 IN MgSO_4 SOLUTIONS

MgSO_4 , <i>m</i>	<i>t</i>	s_{obsd}	s_{calcd}
0.1	25	0.0247	0.023 ($A_S = 0.82$)
	64	.0359	.036
	85	.0422	.042
	104	.0441	.045
	154	.0506	.051
	160	.0512	.052
0.5	175	.0506	.052
	64	0.0440	0.043 ($A_S = 0.77$)
	85	.0520	.052
	129	.0664	.069
	147	.0732	.076
1.0	156	.0801	.079
	64	0.0520	0.051 ($A_S = 0.72$)
	95	.0656	.069
	103	.0718	.074
	124	.0874	.087
	144	.0990	.101

On the assumption of complete dissociation of both electrolytes, the stoichiometric ionic strength *I* of the Ag_2SO_4 - MgSO_4 solutions is given at any molality *m* of MgSO_4 by

$$I = 4m + 3s \quad (1)$$

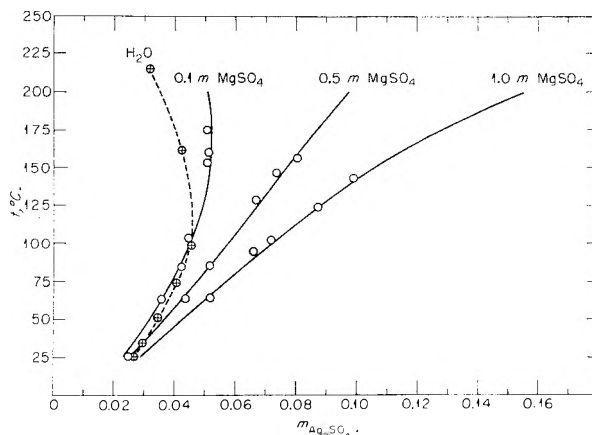
where *s* represents the molal solubility of Ag_2SO_4 in the MgSO_4 solution. As in the previous papers in this series the stoichiometric solubility product of Ag_2SO_4 on a molality basis *S* at any molality *m* of MgSO_4 was assumed to be given in terms of the solubility product in pure H_2O by a Debye-Hückel expression of the type

$$\ln S = \ln S_0 + s_T \left[\frac{\sqrt{I}}{1 + A_S \sqrt{I}} - \frac{\sqrt{I_0}}{1 + A_S \sqrt{I_0}} \right] \quad (2)$$

In this equation S_0 , the molal solubility product of

(6) M. H. Lietzke and R. W. Stoughton, *J. Am. Chem. Soc.*, **78**, 3023 (1956).

(7) M. Barre, *Ann. chim. et phys.*, [8], **24**, 211 (1911).

Fig. 1.—The solubility of Ag_2SO_4 in MgSO_4 solutions.

Ag_2SO_4 in pure H_2O , equals $4s_0^3$ at ionic strength $I_0 = 3s_0$; s_T is the appropriate Debye-Hückel limiting slope at the given temperature; and A_S is a concentration dependent but temperature independent parameter. In computing the change of s_T with temperature the equation for the variation of the dielectric constant *D* of water with temperature given by Åkerlöf and Oshry⁸ was used. At any temperature and concentration of MgSO_4 the solubility product *S* of the Ag_2SO_4 is given by

$$S = 4s^2(s + m) \quad (3)$$

In starting the calculations at each concentration of MgSO_4 the observed solubility of Ag_2SO_4 at each temperature was used to compute a value of *I*. Then using equations 2 and 3 a value of s_{calcd} (the calculated solubility of Ag_2SO_4) was obtained. This value of s_{calcd} was used to correct *I* (equation 1) and the process repeated until successive values of s_{calcd} agreed to within 0.1%. The calculations were carried out at 25° intervals from 25 to 200° at each concentration of MgSO_4 using a range of values of A_S . Then from a plot of s_{calcd} vs. A_S at each temperature and concentration of MgSO_4 it was possible to find the value of A_S which gave closest agreement with the observed solubility. It was found that the value of A_S varied little with temperature at each concentration of MgSO_4 but did show a decrease with increasing concentration of MgSO_4 . In Fig. 1 the solid lines indicate the calculated solubilities corresponding to the values of A_S averaged at each concentration of MgSO_4 . The A_S values for each concentration of MgSO_4 are: for $m = 0.1$, $A_S = 0.82$; for $m = 0.5$, $A_S = 0.77$; for $m = 1.0$, $A_S = 0.72$. The decrease in the values of A_S with concentration (and hence of the ion size parameter \bar{a} which is contained in the A_S) is consistent with an hypothesis involving smaller hydration spheres for the ions as the concentration of MgSO_4 increases.

Calculations also were performed assuming an average temperature and concentration independent value of A_S ($= 0.77$). In this case, however, the solubility values calculated at $m = 0.1$ were

(8) G. C. Åkerlöf and H. J. Oshry, *J. Am. Chem. Soc.*, **72**, 2844 (1950).

too high, while those calculated at $m = 1.0$ were too low. Hence it appears that the value of A_S must be considered concentration dependent.

It is evident that a Debye-Hückel type expression for the variation in the molality solubility product of Ag_2SO_4 with ionic strength in MgSO_4

solutions can be used to fit the solubility data over a wide range of concentration and temperature.

Acknowledgment.—The authors wish to express their appreciation to Mrs. Laura Cain Meers for performing the experimental solubility measurements.

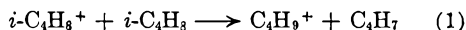
COMMUNICATION TO THE EDITOR

ON THE RADIATION-INDUCED POLYMERIZATION OF ISOBUTYLENE IN THE LIQUID PHASE

Sir:

Recent studies^{1,2} of the low temperature, radiation-induced polymerization of isobutylene have established quite conclusively that the chain propagation is not free radical, but ionic, and that the most likely initiating species is the $(\text{CH}_3)_3\text{C}^+$ ion. Free radicals are formed in the radiolysis, however, as evidenced by the disappearance of diphenylpicrylhydrazyl and other scavengers.² The natural question as to the nature of the simultaneous modes of formation of $(\text{CH}_3)_3\text{C}^+$ and free radicals in irradiated isobutylene seems to be resolved most easily by consideration of the known reaction³ of the isobutylene molecule-ion with isobutylene; that we need consider only reactions of the molecular ion of isobutylene, and not those arising from ion fragmentation processes, is supported by the results of recent calculations by Stevenson,⁴ which suggest that for the liquid-phase time interval between C_4H_8^+ formation and collision with a C_4H_8 molecule (10^{-12} second or less) such fragmentation will be negligible.

Tal'roze and Lyubimova³ showed that a reaction producing $(\text{CH}_3)_3\text{C}^+$ in isobutylene does indeed occur, *viz.*



in which, on the basis of energetic considerations of

(1) W. H. T. Davison, S. H. Pinner and R. Worrall, *Chem. and Ind.* 1274 (1957).

(2) E. Collinson, F. S. Dainton and H. A. Gillis, *THIS JOURNAL*, **63**, 909 (1959).

(3) V. L. Tal'roze and A. K. Lyubimova, *Doklady Akad. Nauk, S.S.S.R.*, **86**, 909 (1952).

(4) D. P. Stevenson, *Radiation Research*, **10**, 610 (1959).

butyl ions,⁵ C_4H_9^+ can hardly be other than tertiary, and C_4H_7 is most likely a methyl substituted allyl radical; this radical has been suggested by Collinson, Dainton and Gillis² as being present in the radiolysis. Further, the very observation of (1) in a mass spectrometer³ indicates its bimolecular specific reaction rate to be of the order of 10^{-9} cm.³-molecule⁻¹-sec.⁻¹, which means that it most likely can compete favorably with neutralization reactions. Thus, if (1) occurs without competition, every ionization event results in the formation of a polymerization initiator, $(\text{CH}_3)_3\text{C}^+$, and a free radical, C_4H_7 , with an energy yield of

$$G[(\text{CH}_3)_3\text{C}^+] = G(\text{C}_4\text{H}_7) = 100/W_{\text{C}_4\text{H}_8} \quad (2)$$

where $W_{\text{C}_4\text{H}_8}$ is the energy required to form an ion-pair in isobutylene. $W_{\text{C}_4\text{H}_8}$ is not known but, taking the measured value⁶ of $W_{\text{C}_2\text{H}_4}$ and assuming the ratios of W to ionization potential to be equal for ethylene and isobutylene, can be estimated to be 23.6 e.v. From (2), this leads to a calculated $G(\text{C}_4\text{H}_7)$ of 4.2 which is in quite good agreement with the experimental $G(-\text{DPPH})$ of 3.7 found for the disappearance of diphenylpicrylhydrazyl.² This agreement lends support to the postulate that the ion-molecule reaction, (1), known to occur in the gas phase, is of great importance in the liquid phase polymerization of isobutylene because it represents the mode of formation of the polymerization initiator.

RESEARCH AND DEVELOPMENT DIVISION
HUMBLE OIL & REFINING COMPANY

F. W. LAMPE

BAYTOWN, TEXAS

RECEIVED OCTOBER 9, 1959

(5) F. P. Lossing, P. Kebarle and J. B. Desousa, paper presented at the Institute of Petroleum Hydrocarbon Research Group and A. S. T. M. Committee E-14 Joint Conference on Mass Spectrometry, London, September, 1958.

(6) J. Weiss and W. Bernstein, *Phys. Rev.*, **103**, 1253 (1956).

Number 10 in
Advances in Chemistry Series

edited by the staff of
Industrial and Engineering Chemistry

Literature Resources for Chemical Process Industries

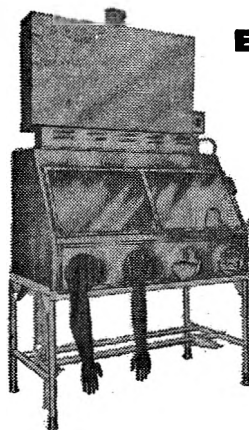
Designed To Help Both The *New*
And The *Experienced* Searcher Of
Literature Find What He Wants

Discusses various information sources with 13 articles on market research, 7 on resins and plastics, 6 on textile chemistry, 10 on the food industry, 10 on petroleum, and 13 on general topics, plus 34 pages of index.

*582 pages—paper bound—
\$7.50 per copy*

order from:

Special Issue Sales
American Chemical Society
1155 Sixteenth Street, N.W.
Washington 6, D.C.



BLICKMAN FUME HOOD

for safe
handling of
hazardous
materials

Developed originally for handling bacteria and viruses, this all-stainless steel fume hood is equipped with a micro-biological filter canister incinerator. Polished, seamless, crevice-free construction with rounded corners makes cleaning and decontamination easy and sure. Many convenience features; units 4, 5, 6 or 8 feet long, with or without stand or filter canister. Write for illustrated folder describing 22 different kinds of enclosures for safe handling of hazardous materials. S. Blickman, Inc., 9011 Gregory Avenue, Weehawken, New Jersey.

BLICKMAN SAFETY ENCLOSURES

Look for this symbol of quality



SEE US AT: Chemical Industries Show
New York Coliseum
Booth: #325
Nov. 30 thru Dec. 4, 1959

Number 18 in ADVANCES IN CHEMISTRY SERIES

edited by the staff of
**INDUSTRIAL AND ENGINEERING
CHEMISTRY**

THERMODYNAMIC PROPERTIES OF THE ELEMENTS

Tabulated values of the heat capacity, heat content, entropy, and free energy function of the solid, liquid, and gas states of the first 92 elements are given for the temperature range 298° to 3000° K. Auxiliary data include temperatures and heats of transition, melting and vaporization and vapor pressures. Published values analyzed and supplemented by estimates when experimental data are lacking. Compiled by D. R. Stull and G. C. Sinke, Dow Chemical Co.

234 pages --- hard bound --- \$5.00 per copy

order from:

Special Issues Sales
American Chemical Society
1155 Sixteenth Street, N.W.
Washington 6, D. C.

Interesting Research Positions for
CHEMISTS
AT LOCKHEED

Lockheed Missiles and Space Division has a number of important, research positions for experienced chemists at its new facilities in the Stanford Industrial Park, Palo Alto, and Sunnyvale, California. This location, on the beautiful San Francisco Peninsula, is one of the choicest living areas in the nation.

The Division is widely diversified in its work, with complete capability in more than 40 areas of science and technology—from concept to operation.

Career opportunities are available for chemists with the following background:

PHYSICAL-ORGANIC CHEMISTRY

Ph.D. required with post-doctoral experience in instrumental analytical techniques including infrared, ultra-violet and mass spectroscopy.

Experience in gas chromatography, X-ray and electron diffraction work desirable.

INORGANIC CHEMISTRY

Ph.D. with 5 years' experience in gas solid reaction kinetics, intermetallic compounds and electronic properties of matter.

ANALYTICAL CHEMISTRY

M.S. or Ph.D. with several years' experience in the development of microchemical techniques. Experience in X-ray and electron diffraction work desirable.

ELECTROCHEMISTRY

M.S. with background in corrosion effects. For work in the development of surface treatments of metals and basic work on surface reaction kinetics. Knowledge of X-ray and electron diffraction techniques desirable.

ORGANIC CHEMISTRY

M.S. or Ph.D. with background in formulation of elastomers. Should be thoroughly grounded in the molecular resistance of substances to various environments.

ORGANIC CHEMISTRY

Ph.D. with experience in reinforced plastic area. Should have ability to relate physical requirements to modifications in molecular structures.

***PHOTO CHEMISTRY**

Ph.D. with background in experimental techniques in the field of photo chemistry.

***PHYSICAL CHEMISTRY**

M.S. or Ph.D. with strong background in the theory of catalysis and experience in developing catalysts. Fundamental knowledge in solid state chemistry, physics or surface chemistry desirable.

***ELECTROCHEMISTRY**

Ph.D. required.

*For work on a high priority project in the field of energy conversion.

FOR INFORMATION regarding these positions, please write Research and Development Staff, Lockheed Missiles and Space Division, Dept. K-99, 962 West El Camino Real, Sunnyvale, California. U. S. citizenship required.

Lockheed / **MISSILES AND SPACE DIVISION**

Sunnyvale, Palo Alto, Van Nuys, Santa Cruz, Santa Maria, California
Cape Canaveral, Florida — Alamogordo, New Mexico — Hawaii